frontiers | Research Topics

Zoonotic diseases: epidemiology, multi-omics, and host-pathogen interactions, volume II

Edited by
Lei Deng, Hong Yin and Thet Aung

Published in
Frontiers in Microbiology

ISSN 1664-8714
ISBN 978-2-8325-7536-9
DOI 10.3389/978-2-8325-7536-9

Generative AI statement
Any alternative text (Alt text) provided alongside figures in the articles in this ebook has been generated by Frontiers with the support of artificial intelligence and reasonable efforts have been made to ensure accuracy, including review by the authors wherever possible. If you identify any issues, please contact us.

About Frontiers

Frontiers is more than just an open access publisher of scholarly articles: it is a pioneering approach to the world of academia, radically improving the way scholarly research is managed. The grand vision of Frontiers is a world where all people have an equal opportunity to seek, share and generate knowledge. Frontiers provides immediate and permanent online open access to all its publications, but this alone is not enough to realize our grand goals.

Frontiers journal series

The Frontiers journal series is a multi-tier and interdisciplinary set of open-access, online journals, promising a paradigm shift from the current review, selection and dissemination processes in academic publishing. All Frontiers journals are driven by researchers for researchers; therefore, they constitute a service to the scholarly community. At the same time, the *Frontiers journal series* operates on a revolutionary invention, the tiered publishing system, initially addressing specific communities of scholars, and gradually climbing up to broader public understanding, thus serving the interests of the lay society, too.

Dedication to quality

Each Frontiers article is a landmark of the highest quality, thanks to genuinely collaborative interactions between authors and review editors, who include some of the world's best academicians. Research must be certified by peers before entering a stream of knowledge that may eventually reach the public - and shape society; therefore, Frontiers only applies the most rigorous and unbiased reviews. Frontiers revolutionizes research publishing by freely delivering the most outstanding research, evaluated with no bias from both the academic and social point of view. By applying the most advanced information technologies, Frontiers is catapulting scholarly publishing into a new generation.

What are Frontiers Research Topics?

Frontiers Research Topics are very popular trademarks of the *Frontiers journals series*: they are collections of at least ten articles, all centered on a particular subject. With their unique mix of varied contributions from Original Research to Review Articles, Frontiers Research Topics unify the most influential researchers, the latest key findings and historical advances in a hot research area.

Find out more on how to host your own Frontiers Research Topic or contribute to one as an author by contacting the Frontiers editorial office: frontiersin.org/about/contact

Zoonotic diseases: epidemiology, multi-omics, and host-pathogen interactions, volume II

Topic editors

Lei Deng — Shanghai Veterinary Research Institute, Chinese Academy of Agricultural Sciences, China

Hong Yin — Lanzhou Veterinary Research Institute, Chinese Academy of Agricultural Sciences, China

Thet Aung — Singapore Eye Research Institute (SERI), Singapore

Citation

Deng, L., Yin, H., Aung, T., eds. (2026). *Zoonotic diseases: epidemiology, multi-omics, and host-pathogen interactions, volume II*. Lausanne: Frontiers Media SA.

doi: 10.3389/978-2-8325-7536-9

Table of contents

frontiers | Frontiers in Microbiology

TYPE Editorial
PUBLISHED 04 February 2026
DOI 10.3389/fmicb.2025.1764511

OPEN ACCESS

EDITED AND REVIEWED BY
Axel Cloeckaert,
Institut National de recherche pour l'agriculture, l'alimentation et l'environnement (INRAE), France

*CORRESPONDENCE
Lei Deng
✉ ldeng@shvri.ac.cn

RECEIVED 10 December 2025
REVISED 15 December 2025
ACCEPTED 15 December 2025
PUBLISHED 04 February 2026

CITATION
Aung TT, Hong Y and Deng L (2026) Editorial: Zoonotic diseases: epidemiology, multi-omics, and host-pathogen interactions, volume II. *Front. Microbiol.* 16:1764511. doi: 10.3389/fmicb.2025.1764511

Editorial: Zoonotic diseases: epidemiology, multi-omics, and host-pathogen interactions, volume II

Thet Tun Aung[1,2], Yin Hong[3] and Lei Deng[1]*

[1]Shanghai Veterinary Research Institute, Chinese Academy of Agricultural Sciences, Shanghai, China, [2]Ocular Anti-Infectives and Inflammation, Singapore Eye Research Institute, Singapore, Singapore, [3]Lanzhou Veterinary Research Institute, Chinese Academy of Agricultural Sciences, Lanzhou, China

KEYWORDS

epidemiological surveillance, host–pathogen interactions, multi-omics analysis, one health, zoonotic pathogens

Editorial on the Research Topic
Zoonotic diseases: epidemiology, multi-omics, and host-pathogen interactions, volume II

Emerging and re-emerging zoonotic pathogens

Li, Qi et al. examined *Leucobacter holotrichiae* isolated from bovine abscesses and analyzed its genomic features, identifying virulence factors, antimicrobial resistance genes, and prophage elements. Their findings expand the known host range of this previously insect-associated bacterium and provide insights into its biological characteristics. Dehong et al. investigated *Streptococcus suis* across pig farms in eastern China and described infection prevalence, serotype distribution, virulence gene profiles, and seasonal trends. They also assessed pathogenic differences among serotypes using pig infection models. Sihag et al. conducted longitudinal molecular surveillance of *Orientia tsutsugamushi* in humans, rodents, shrews, and mites. They examined circulating serotypes, analyzed genetic diversity, and reported the first detection of a TA678-like strain in Puducherry, India. Zhang, Chen et al. analyzed the occurrence of *Cryptosporidium* spp., *Giardia duodenalis*, and *Enterocytozoon bieneusi* in crab-eating macaques. They characterized age-related infection patterns, identified zoonotic genotypes, and examined subtype diversity in *C. hominis*. Li, Li et al. investigated the lung microbiota of raccoon dogs using high-throughput sequencing and viral metagenomics. They characterized a diverse assemblage of bacterial, fungal, and viral taxa, including multiple zoonotic species, illustrating the complexity of pneumonia outbreaks in these animals.

Mechanisms of pathogenesis and molecular evolution

Zhang, Yang et al. examined the role of Rab4b in the internalization of the *Glaesserella parasuis* cytolethal distending toxin (GpCDT). They analyzed Rab4b–CdtB interactions, investigated endosomal trafficking mechanisms, and identified EEA1 as a

Rab4b-dependent regulator of GpCDT uptake. Wang, Guo et al. analyzed the distribution of the deubiquitinase gene elaD across 530 *Escherichia coli* strains. They characterized its prevalence in multiple serotypes, phylogenetic groups, and sequence types and investigated evolutionary relationships using phylogenomics. Yee et al. characterized *Streptococcus pluranimalium* isolates from aborted bovine fetuses. They analyzed genome sequences, examined phylogenetic relationships, and identified mobilome-associated genes and prophage integrations.

Microbiome ecology in hosts and vectors

Akdur-Öztürk et al. investigated *Blastocystis* across humans, livestock, and environmental sources in rural Türkiye. They analyzed subtype distributions, examined host-specific patterns, and explored associations between *Blastocystis* colonization and gut microbial diversity. Wang, Yu et al. analyzed microbiome profiles in three tick species and investigated how infection with spotted fever group *Rickettsia* or *Anaplasma* influenced microbial community structure. They described pathogen-associated shifts in bacterial diversity and composition.

Host responses and immunomodulation

Bi et al. examined host angiogenic responses triggered by *Echinococcus multilocularis*. They analyzed gene expression signatures, investigated the activation of the PDGFR/PI3K/AKT/FAK pathway, and described enhanced angiogenesis in infected liver tissues. Li, Liu et al. assessed the immunogenicity of extracellular products of *Pasteurella multocida* serotype A:3. They analyzed protein components, evaluated humoral and cellular immune responses, and examined protective efficacy against multiple serotypes in mice.

Translational applications and vaccine development

Zhang, Chen et al. investigated the function of pipC in *Salmonella Enteritidis* and analyzed the phenotypic consequences of its deletion. They described reductions in environmental stress tolerance, downregulation of T3SS-associated genes, attenuation of virulence, and evaluated the ΔpipC strain as a live-attenuated vaccine candidate.

A broad conceptual foundation is outlined by Remya et al., who reviewed the epidemiology, transmission cycles, clinical manifestations, diagnostics, and public health relevance of zoonotic filariasis. Their work emphasized the interconnected nature of host, vector, and environmental factors that shape filarial disease dynamics.

Collectively, the studies in this Research Topic examined zoonotic pathogens across ecological, molecular, and immunological dimensions. By integrating epidemiology, genomics, transcriptomics, microbiome analysis, and mechanistic biology, these contributions advance the understanding of zoonotic disease emergence and host–pathogen interactions. The insights gained support the development of improved surveillance strategies, mechanistic models, and intervention tools. We thank all authors and reviewers for their contributions and hope this Research Topic stimulates further interdisciplinary research to address the expanding challenges posed by zoonotic diseases.

Author contributions

LD: Writing – review & editing, Writing – original draft. TA: Writing – review & editing, Writing – original draft. YH: Writing – review & editing, Writing – original draft.

Funding

The author(s) declared that financial support was received for this work and/or its publication. This work was supported by the Shanghai Agricultural Science and Technology Innovation Project (2025-02-08-00-12-F00031), the National Natural Science Foundation of China (32503056), the Central Public-interest Scientific Institution Basal Research Fund (2025JB05), and the Agricultural Science and Technology Innovation Program of the Chinese Academy of Agricultural Sciences (CAAS-ASTIP-2021-SHVRI).

Conflict of interest

The author(s) declared that this work was conducted in the absence of any commercial or financial relationships that could be construed as a potential conflict of interest.

Generative AI statement

The author(s) declared that generative AI was used in the creation of this manuscript. ChatGPT, v. 5, a language model developed by OpenAI in San Francisco, CA, USA, helped in language editing and proofreading.

Any alternative text (alt text) provided alongside figures in this article has been generated by Frontiers with the support of artificial intelligence and reasonable efforts have been made to ensure accuracy, including review by the authors wherever possible. If you identify any issues, please contact us.

Publisher's note

frontiers | Frontiers in Microbiology

TYPE Original Research
PUBLISHED 13 May 2025
DOI 10.3389/fmicb.2025.1589263

OPEN ACCESS

EDITED BY
Lei Deng,
Chinese Academy of Agricultural Sciences, China

REVIEWED BY
Benjamin Cull,
University of Minnesota Twin Cities, United States
Roland Eric Yessinou,
University of Abomey-Calavi, Benin
Ratree Takhampunya,
Armed Forces Research Institute of Medical Science, Thailand
Artem Rogovsky,
Michigan State University, United States

*CORRESPONDENCE
Shu-jiang Xue
✉ sjxue@ybu.edu.cn

†These authors have contributed equally to this work and share first authorship

RECEIVED 07 March 2025
ACCEPTED 22 April 2025
PUBLISHED 13 May 2025

CITATION
Wang J-q, Yu T, Qiu H-y, Ji S-w, Xu Z-q, Cui Q-c, Li H-f, Liang W-f, Feng S, Fu C-t, Gao X, Han Z-z, Tian W-n, Li J-x and Xue S-j (2025) Differential impact of spotted fever group *rickettsia* and anaplasmosis on tick microbial ecology: evidence from multi-species comparative microbiome analysis. *Front. Microbiol.* 16:1589263. doi: 10.3389/fmicb.2025.1589263

Differential impact of spotted fever group *rickettsia* and anaplasmosis on tick microbial ecology: evidence from multi-species comparative microbiome analysis

Jin-qi Wang[1†], Tian Yu[1†], Hong-yu Qiu[2†], Sheng-wei Ji[1], Zhi-qiang Xu[1], Qi-chao Cui[1], Hai-feng Li[1], Wan-feng Liang[1], Shuai Feng[2], Chen-tao Fu[2], Xu Gao[1], Zhen-zhen Han[3], Wan-nian Tian[4], Ji-xu Li[5] and Shu-jiang Xue[1*]

[1]Agricultural College of Yanbian University, Yanji, China, [2]College of Animal Science and Veterinary Medicine, Heilongjiang Bayi Agricultural University, Daqing, China, [3]Animal Health and Epidemic Prevention Center, Huludao, China, [4]College of Animal Science, Jilin Agricultural Science and Technology College, Jilin, China, [5]Yanbian Center for Disease Control and Prevention, Yanji, China

Tick-borne diseases (TBDs) pose a significant public health challenge, as their incidence is increasing due to the effects of climate change and ecological shifts. The interplay between tick-borne pathogens and the host microbiome is an emerging area of research that may elucidate the mechanisms underlying disease susceptibility and severity. To investigate the diversity of microbial communities in ticks infected with vertebrate pathogens, we analyzed the microbiomes of 142 tick specimens. The presence of *Rickettsia* and *Anaplasma* pathogens in individual samples was detected through PCR. Our study aimed to elucidate the composition and variation of microbial communities associated with three tick species, which are known vectors for various pathogens affecting both wildlife and humans. We employed high-throughput sequencing techniques to characterize the microbial diversity and conducted statistical analyses to assess the correlation between the presence of specific pathogens and the overall microbial community structure. Pathogen screening revealed an overall positivity rate of 51.9% for *Anaplasma* and 44.6% for spotted fever group *rickettsia* (SFGR). Among the three tick species (*Dermacentor silvarum*, *Haemaphysalis concinna*, and *Haemaphysalis japonica*) analyzed, *D. silvarum* (the predominant species) exhibited the highest pathogen prevalence. The results indicate significant variation in microbial diversity between tick samples, with the presence of *Anaplasma* and SFGR associated with distinct changes in the microbial community composition. These findings underscore the complex interactions between ticks and their microbial inhabitants, enriching our understanding of tick-borne diseases.

KEYWORDS

tick, *Rickettsia*, anaplasmosis, microbiota, 16S rRNA gene, microbiome analysis

1 Introduction

Ticks are hematophagous arthropods that primarily infest mammals, reptiles, and birds in the wild, causing serious disease in humans who are exposed to tick bites (Adrion et al., 2015; Duron and Gottlieb, 2020; Tokarz and Lipkin, 2021). Ticks play an essential role as vectors in the dynamics of vector-borne diseases (Simo et al., 2017). Hard ticks exhibit stage-specific feeding behavior, requiring a single prolonged blood meal per developmental instar (Wikel, 2013). During their multi-day attachment period, hard ticks engage in telmophagy, a cyclical process characterized by alternating anticoagulant saliva secretion and blood ingestion through the hypostome. During this time, pathogens are transmitted through saliva, which helps initiate infection in the host (Maldonado-Ruiz et al., 2019). Concurrently, symbiotic bacteria enter the host through the tick bite. In mice, it has been demonstrated that ticks replace the majority of the pre-existing commensal bacteria on the host's skin during blood intake (Boulanger et al., 2023), and this alteration may play an important role in transmitting pathogens. The first attempts to characterize the full tick microbiome (Andreotti et al., 2011) indicated that it is complex and of varied origin. Since then, high-throughput sequencing technologies have been utilized to further study the tick microbiome (Budachetri et al., 2014; Grandi et al., 2023; Zhang et al., 2023). Currently, *16S rRNA* genes are frequently utilized as target genes for amplicon sequencing, with the V1, V3, and V4 regions being of particular value (Sperling et al., 2017). The majority of tick-borne pathogens are of significant natural epidemiological importance, including their role in Lyme disease, anaplasmosis, rickettsiosis, and tick-borne encephalitis (Dantas-Torres et al., 2012; Madison-Antenucci et al., 2020). The microbiome plays a pivotal role in regulating various physiological processes in ticks, including immunity, nutrition, and digestion (Duron et al., 2018; Zhong et al., 2024). The environment has a significant impact on tick microbiome abundance. The prevalence of tick-borne pathogens is closely related to geographic location, climate, and other abiotic factors (Van Treuren et al., 2015).

The sampling area for this study is located on the border of China, Russia, and North Korea. This region is known for its rich biodiversity and favorable climate, which fosters the proliferation of tick communities. A substantial number of migratory birds visit the area each year, making it a potential source of pathogen transmission. This phenomenon renders the region a significant public health concern. Consequently, scientists around the world are engaged in efforts to control the spread of disease by studying the microbiomes of disease vectors (Moreira et al., 2009; Wu et al., 2019; Huang et al., 2020). Of particular importance is the elucidation of the relationship between vertebrate pathogenic infections and the arthropod microbiomes of vectors. Through the analysis of a vertical transmission model in *Rickettsia raoultii*, it has been demonstrated that interactions between rickettsiae and tick microbiome components contribute to the horizontal transmission of pathogenic rickettsiae (Du et al., 2023). In *Ixodes scapularis*, infection by anamorphs disrupts midgut microbial homeostasis, thereby facilitating the colonization by these anamorphs (Abraham et al., 2017). Conversely, the microbiome of the arthropod vector significantly influences the susceptibility of pathogens to vector-borne transmission. A substantial body of evidence has demonstrated that the gut microbial homeostasis of arthropods has a significant impact on influencing the colonization of the gut by pathogens (Gonzalez-Ceron et al., 2003; Finney et al., 2015; Gall et al., 2016; Pavanelo et al., 2020). Multiple arthropod endosymbionts show varying degrees of correlation with pathogens (Novakova et al., 2017; Budachetri et al., 2018), suggesting that the vector microbiome may have a direct influence on vectorial competence. Recently, a study conducted in the border region of Yunnan, China, discovered a mosquito gut commensal that is effective in blocking mosquito-borne viruses, representing a novel method for controlling mosquito-borne viral transmission (Zhang et al., 2024). The aforementioned evidence suggests the presence of intricate interactions between the host microbiome and pathogens. Therefore, understanding the composition of the microbiome is imperative for its rational application.

The objective of this study is to analyze the bacterial community composition of tick vectors in the region at the border of China, Russia, and North Korea in order to elucidate the distribution of tick-borne pathogens in the area and to collect fundamental data for the prevention and control of tick-borne diseases.

2 Materials and methods

2.1 Tick collection, nucleic acid preparation, and high-throughput sequencing

Ticks were collected from April to May 2022 using standard dragging methods with corduroy cloths in low-lying scrub vegetation and forest-grassland ecotones in the Yanbian Korean Autonomous Prefecture, Jilin Province, China. Collections were conducted once a month at three sampling sites, namely Yanji (43°48′N, 129°23′E), Tumen (42°58′N, 129°50′E), and Longjing (42°46′N, 129°26′E), resulting in a total of two sampling rounds at each site (Figure 1). A total of 442 questing ticks were collected, including 326 *Dermacentor silvarum*, 54 *Haemaphysalis japonica*, and 62 *Haemaphysalis concinna* (Table 1). The collected ticks were placed in 1.5 mL centrifuge tubes based on their morphological characteristics for analysis of mitochondrial 16S ribosomal DNA (16S rDNA) gene sequences and species identification (Black and Piesman, 1994; Jia et al., 2020). The ticks were then cleaned by vortexing for 30 s in a 1% bleach solution (Binetruy et al., 2019b). This was followed by three consecutive 1-min washes using sterilized, DNA-free water. After washing, the samples were dried using sterile filter paper and stored at −80°C. Sequencing was performed on 142 single-tick pools stratified by species and sex (Table 2). Personalbio Co., Ltd. managed the entire workflow, including cryogenic homogenization in lysis buffer, DNA extraction from supernatants using DNeasy Blood & Tissue Kit (Qiagen, Hilden, North Rhine-Westphalia, Germany) amplification of bacterial 16S rRNA V3–V4 regions with primers 338F (5′-ACTCCTACGGGAGGCAGCA-3′)/806R (5′-GGACTACHVGGGTWTCTAAT-3′) (Claesson et al., 2009), library preparation with TruSeq Nano Kit (Illumina, San Diego, California, CA, United States), and paired-end sequencing (2 × 250 bp) on an Illumina NovaSeq 6000 platform (Klindworth et al., 2013; Bonnet et al., 2017). Post-sequencing, DNA aliquots were transported under cold-chain conditions for subsequent pathogen PCR validation. Sequencing datasets were classified into non-infected and infected groups based on PCR validation and species metadata, with detailed stratification criteria provided in Supplementary Table S1. The remaining tick samples were individually placed in disposable zirconia

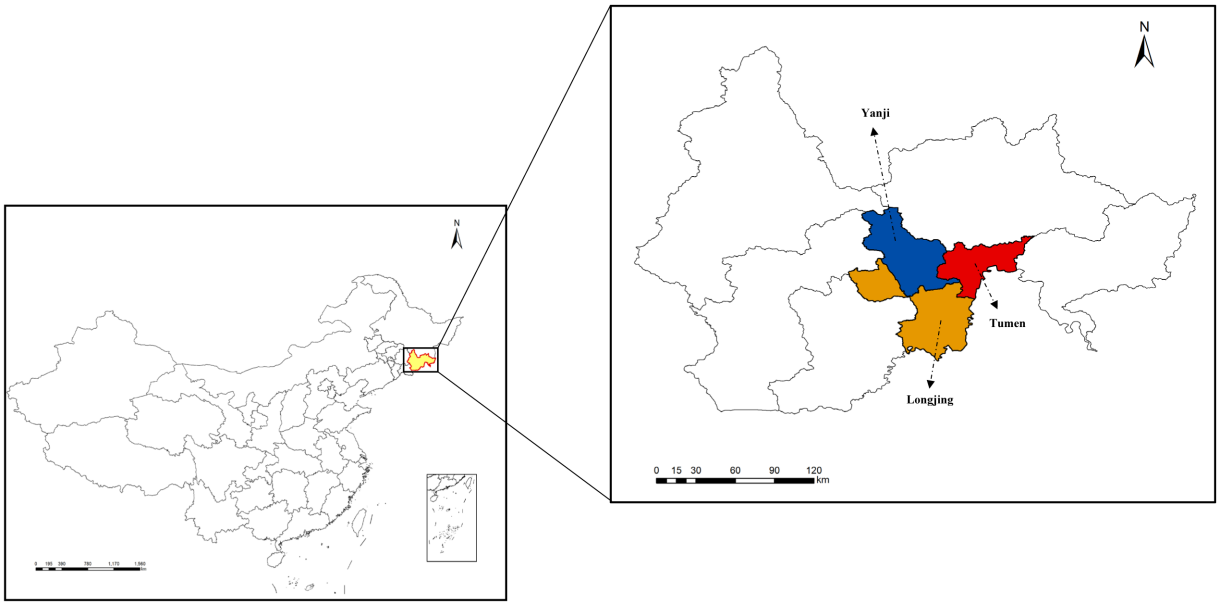

FIGURE 1
Map of the study area. Yanbian Korean Autonomous Prefecture of Jilin Province, China. Black arrows indicate the sampling locations.

TABLE 1 Number of tick samples and prevalence of tick-borne pathogens in this study.

Species	No. of males	No. of females	No. of infected (%)			
			SFG *Rickettsia*		*Anaplasma*	
			Male	Female	Male	Female
D. silvarum	149	177	48.3	55.9	61.7	66.1
H. japonica	17	37	17.6	18.9	11.7	16.2
H. concinna	39	23	33.3	17.3	23.0	17.3
Total	442		44.6		51.9	

TABLE 2 Information on tick samples for high-throughput sequencing.

Samples ID	Number	Species	Sex
DSMt 1–32	32	*D. silvarum*	Male
DSFt 33–65	33	*D. silvarum*	Female
HJMt 66–76	11	*H. japonica*	Male
HJFt 77–99	23	*H. japonica*	Female
HCMt 100–124	25	*H. concinna*	Male
HCFt 125–142	18	*H. concinna*	Female

bead grinding tubes and ground using a low-temperature tissue grinding homogenizer. The genomic DNA from ticks was then extracted using a genomic DNA extraction kit (Tiangen, China).

2.2 Bioinformatics and statistical analyses

Microbiome bioinformatics analysis was performed using QIIME2 (v2019.4) (Caporaso et al., 2010; Rai et al., 2021). Raw sequences were demultiplexed, trimmed of primers using the cutadapt plugin, and processed through the DADA2 plugin (Callahan et al., 2016) for quality filtering, denoising, merging, and chimera removal to generate a non-singleton amplicon sequence variant (ASV) table. Taxonomy was assigned to amplicon sequence variants (ASVs) using the classify-sklearn naïve Bayes taxonomy classifier in the feature-classifier plugin (Bokulich et al., 2018) against the Greengenes 13.8 Database (DeSantis et al., 2006), excluding mitochondrial, chloroplast, and unassigned sequences, along with rare ASVs (relative abundance <0.005%) (Bokulich et al., 2013). Alpha diversity metrics (ACE/Observed/Fisher's alpha/Shannon/Simpson/Chao1) were calculated on rarefied ASV tables (10,000 reads/sample) and compared across groups using the Wilcoxon rank-sum test with Benjamini–Hochberg false discovery rate correction. Beta diversity analysis based on Bray–Curtis distances revealed significant differences. For group comparisons, we performed Kruskal–Wallis tests with Benjamini–Hochberg correction (Benjamini and Hochberg, 2018) and PERMANOVA (Anderson, 2001). LEfSe analysis (Segata et al., 2011) identified differentially abundant taxa using Kruskal–Wallis screening ($p < 0.05$), LDA effect size >2.0, and all-against-all validation. Group-specific ASVs, identified via ASV-level Venn diagrams, were quantitatively compared between infected and non-infected groups using the Mann–Whitney *U*-test. Dominant phyla and genera (>1% mean abundance) were visualized in compositional bar plots (ggplot2), while the microbial community structure was illustrated through PCoA ordinations (QIIME2 View) (Asnicar et al., 2015).

2.3 Pathogen detection, phylogenetics, and prevalence analysis

The prevalence of two pathogens was detected by PCR amplification of the gene fragments of spotted fever group *rickettsia* (SFGR) (*ompA*) and *Anaplasma* spp. (16S rRNA). The sequences of the primers are shown in Supplementary Table S2. Target DNA fragments purified with a Gel Extraction Kit (Omega, Norcross, Georgia, GA, United States) were ligated into the pMD19-T vector (Takara, Japan) via TA cloning and transformed into *E. coli* DH5α competent cells (Tiangen, Beijing, China). Positive clones selected by antibiotic resistance and colony PCR underwent plasmid extraction using the Omega Plasmid Mini Kit (Omega, Norcross, Georgia, GA, United States), followed by Sanger sequencing at Jilin kumei Biotechnology Co., Ltd. The corrected sequences were then searched for similarity in the GenBank database using the National Center for Biotechnology Information (NCBI) Basic Local Alignment Search Tool (BLAST) search engine. Then, the representative sequences of the pathogens were aligned using MEGA11 software, and a phylogenetic tree was constructed using the neighbor-joining method, with the number of bootstrap replicates set to 1,000 and the Kimura's two-parameter model. Differences in pathogen positivity rates between tick species were analyzed using Pearson's chi-squared test, with statistical significance defined as a two-tailed p-value of <0.05.

3 Results

3.1 Infection of ticks with pathogens

PCR-based surveillance revealed an overall *Anaplasma* positivity rate of 51.9% (Table 1), with *D. silvarum* exhibiting a significantly higher infection prevalence than other tick species ($\chi^2 = 12.302$, df = 1, $p < 0.001$). For *D. silvarum*, female ticks demonstrated a marginally elevated positivity rate (66.1%) compared to male ticks (61.7%). Phylogenetic analysis of representative *Anaplasma* 16S rRNA sequences indicated 99.8–100% similarity to GenBank references, clustering in a monophyletic clade with *Anaplasma capra* isolates from South Korea (LC432117.1), Qinghai (MG940873.1), and Xian (MG869483.1), China (Figure 2A). Concurrently, SFGR showed an overall positivity rate of 44.6%, with the highest prevalence observed in *D. silvarum* female ticks (55.9%) and the lowest in *H. concinna* female ticks (17.3%). Comparative analysis of SFGR *ompA* gene sequences revealed 97.3–99.37% similarity to GenBank entries, with the closest phylogenetic proximity to *Rickettsia raoultii* from Yunnan Province, China (MN550901.1). These sequences formed a distinct clade that included *R. raoultii* strains from Russia (EU036986.1) and Thailand (OM281195.1) (Figure 2B).

3.2 Diversity of microbiota in ticks

To investigate the diversity of microbial communities in ticks infected with vertebrate pathogens, we analyzed the microbiomes of 142 tick specimens. The presence of *Rickettsia* and *Anaplasma* pathogens in individual samples was determined using PCR methods. Figure 3A illustrates the distribution of alpha diversity across experimental groups. There were no statistically significant differences in alpha diversity between SFGR-infected and non-infected groups across tick species (Mann–Whitney U-test, $p > 0.05$). However, *Anaplasma*-infected groups exhibited significantly higher alpha diversity indices compared to their non-infected counterparts ($p < 0.01$, Benjamini–Hochberg corrected). Notably, this trend remained consistent across all three tick species investigated. Beta diversity analysis revealed a significant divergence in the microbial community structure among the tick species (PERMANOVA, $R^2 = 0.32$, $p < 0.001$). However, congeneric *Haemaphysalis* species (*H. japonica* vs. *H. concinna*) exhibited closer clustering in the PCoA ordination based on Bray–Curtis dissimilarity (Figure 3B). Within each tick species, microbial communities showed minimal separation

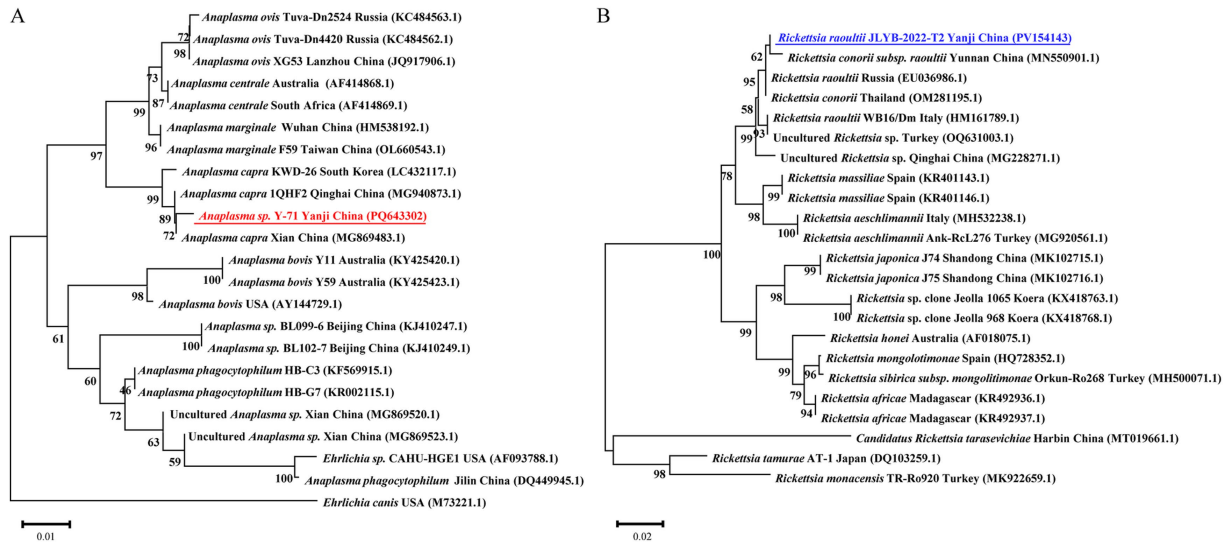

FIGURE 2
Neighbor-joining phylogenies of **(A)** *Anaplasma* spp. 16S rRNA gene sequences and **(B)** spotted fever group *rickettsia ompA*. Bootstrap support values from 1,000 replicates are indicated at branch nodes. Sequences from this study are bolded in blue (**A**; PV154143) and red (**B**; PQ643302).

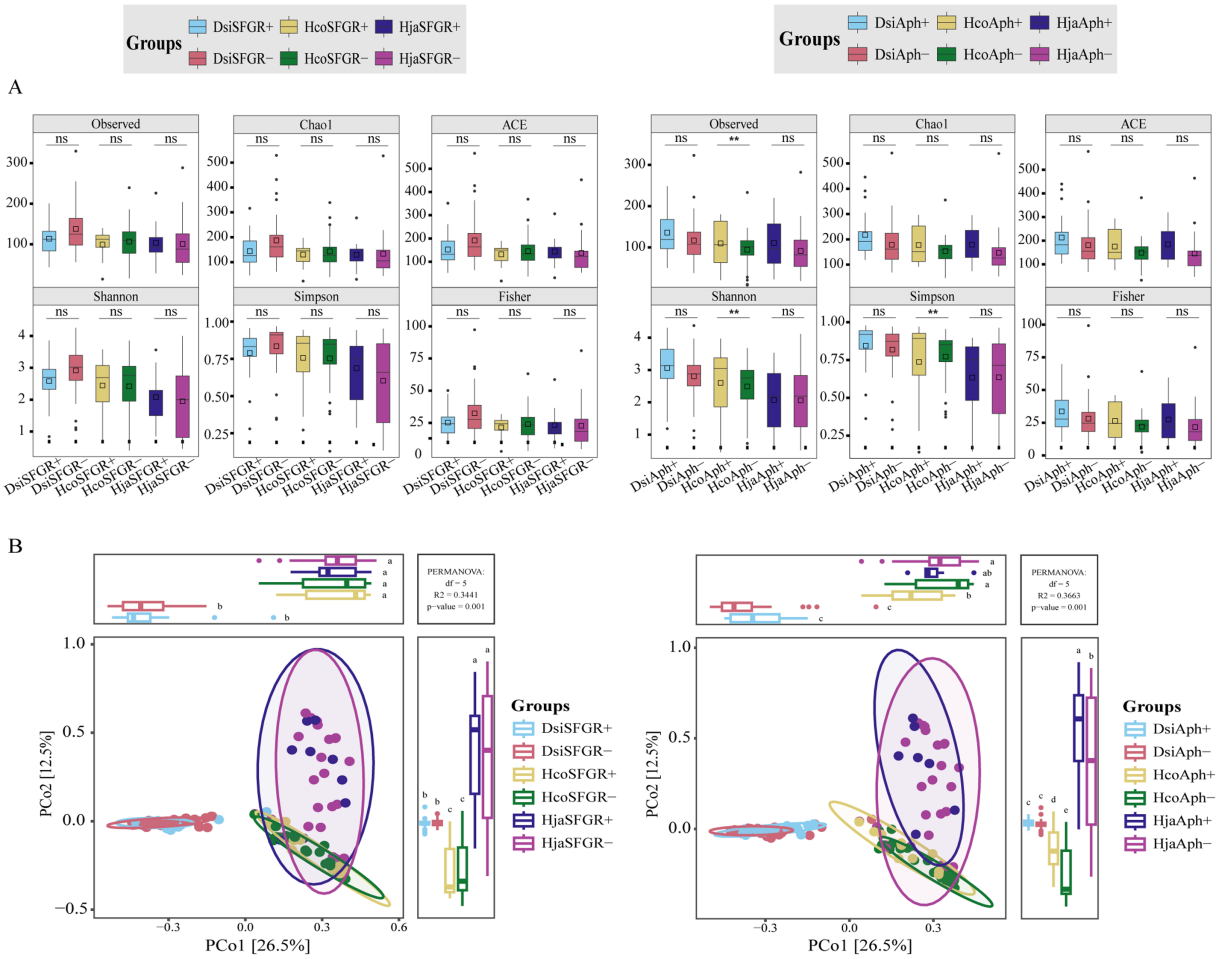

FIGURE 3
Tick microbiota diversity in pathogen-infected and uninfected groups. **(A)** α-diversity comparisons (six indices): SFGR-infected vs. SFGR-uninfected, *Anaplasma*-infected vs. *Anaplasma*-uninfected. Significance: Mann–Whitney *U*-test with Benjamini–Hochberg (**$p < 0.01$, ns: not significant). **(B)** β-diversity: Bray–Curtis PERMANOVA for each pathogen. Dsi, *Dermacentor silvarum*; Hco, *Haemaphysalis concinna*; Hja, *Haemaphysalis japonica*.

between experimental groups (infected vs. non-infected), indicating that pathogen exposure did not significantly alter β-diversity patterns (PERMANOVA, $R^2 = 0.02–0.05$, $p > 0.1$).

3.3 Composition of microbiota in ticks

Figure 4A presents an amplicon sequence variant (ASV)-level Venn diagram comparing the microbial composition across infection status groups. The analysis revealed that non-infected groups had more unique ASVs than their pathogen-infected counterparts (mean ± SEM: 1111.0 ± 78.5 vs. 410.3 ± 47.7; Mann–Whitney *U*-test, $p < 0.01$). This pattern remained consistent across all analyzed tick species, demonstrating enhanced microbial specificity in non-infected arthropods. A total of 5,954 ASVs were classified into 33 phyla, 362 families, and 804 genera. Proteobacteria, Firmicutes, Actinobacteria, and Bacteroidetes were the dominant phyla. In addition, other phyla, including Planctomycetes, TM7, Thermi, Acidobacteria, Fusobacteria, and Gemmatimonadetes, were observed. At the phylum level, Proteobacteria, Firmicutes, and Actinobacteria dominated the microbial profiles of all three tick species (Figure 4B). Notably, *D. silvarum* exhibited a significantly higher abundance of Firmicutes (18.3 ± 2.1%) than the *Haemaphysalis* species. Genus-level profiling identified Pseudomonas, Coxiella, Rhodococcus, and Carnobacterium as core taxa. A notable observation was that *Rickettsia*-infected ticks exhibited a significantly higher relative abundance of Pseudomonas compared to non-infected controls, whereas *Anaplasma*-infected ticks showed an inverse trend with reduced Pseudomonas population (Figure 4C).

3.4 Impact of microbiota on vectors

LEfSe was employed to analyze how the microbiota varied across groups of different species. The results revealed differences in bacterial community composition between each tick species. In *H. japonica*, LEfSe analysis (LDA—linear discriminant analysis, LDA score >2, $p < 0.05$) identified five significantly divergent taxonomic units at the genus level, while SFGR-infected samples exhibited specific enrichment of microbial taxa, including Brevundimonas, Clavibacter, Hyphomicrobium, Sphingopyxis, and Pediococcus. The results indicate that these taxa are potential biomarkers of infection status. Non-infected samples were

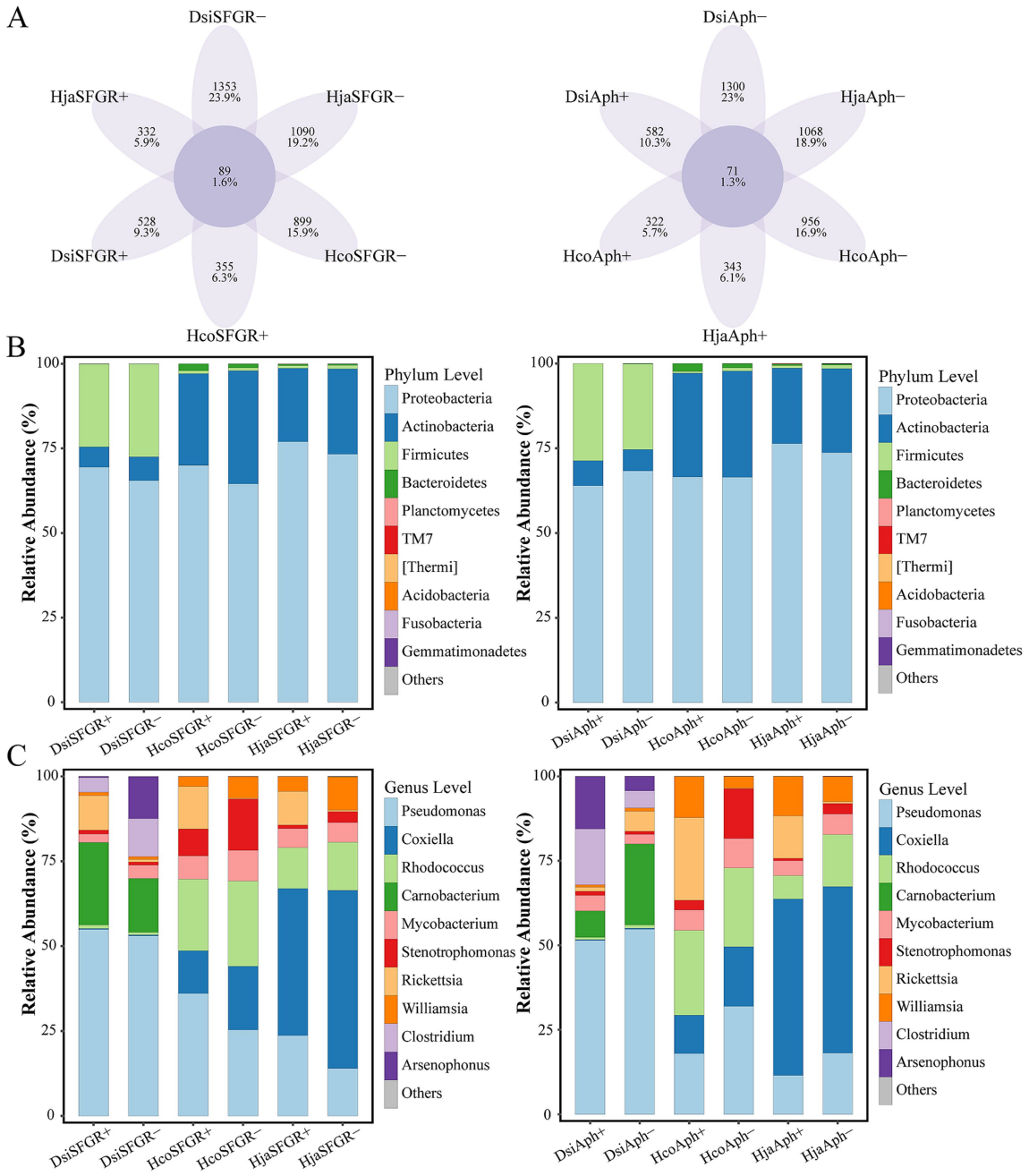

FIGURE 4
Microbial community divergence across taxonomic ranks in ticks. **(A)** Comparative analysis of unique and shared amplicon sequence variants (ASVs) between pathogen-infected and non-infected groups. **(B)** Phylum-level and **(C)** genus-level differential abundance of microbiota between infected and non-infected groups. The top 10 most abundant phyla **(B)** and genera **(C)** are displayed. Dsi, *Dermacentor silvarum*; Hco, *Haemaphysalis concinna*; Hja, *Haemaphysalis japonica*.

predominantly enriched in Caulobacteraceae, implying their antagonistic role in pathogen suppression or host homeostasis (Figure 5A). Notably, *Sphingomonas* and *Sphingopyxis* showed specific enrichment in SFGR-infected *D. silvarum* and *H. concinna*, respectively (Figures 5B–C). When grouped by the *Anaplasma* infection status, the genus of *Spirosoma* emerged as a conserved potential biomarker in both *Haemaphysalis* tick species (*H. japonica* and *H. concinna*). Notably, no significant enrichment of *Spirosoma* was detected in infected *D. silvarum* samples compared to their uninfected counterparts (Figures 5D–F).

4 Discussion

In recent years, there has been growing interest in the microbial communities associated with disease vectors. This interest stems from the understanding that bacterial interactions can influence the survival and transmission of pathogens (Wu et al., 2019; Laukaitis and Macaluso, 2021). Despite this, many arthropod-associated human diseases remain undiagnosed; furthermore, our knowledge about the prevalence, diversity, and pathogenicity of novel arthropod-borne pathogens is limited. This highlights the necessity for ongoing

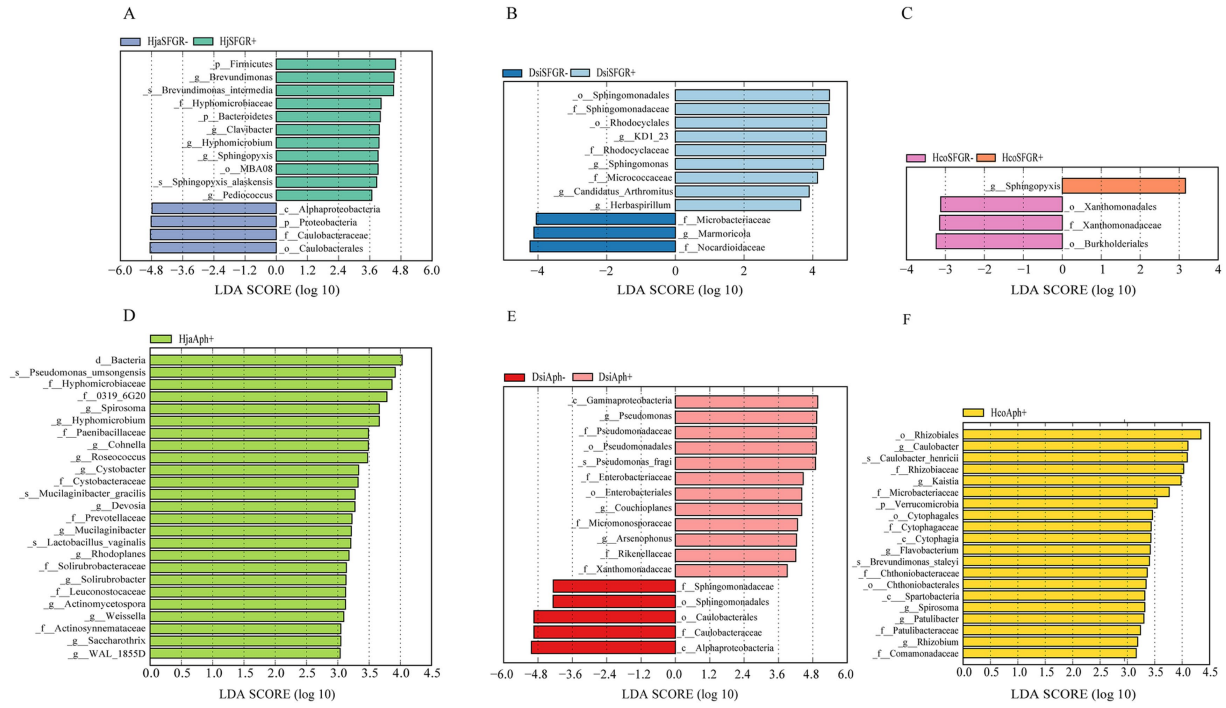

FIGURE 5
Genus-level biomarkers identified by LEfSE analysis in three tick species infected with distinct pathogens. **(A–F)** Differential genera corresponding to infection of *Haemaphysalis japonica*, *Dermacentor silvarum*, and *Haemaphysalis concinna* with spotted fever group *Rickettsia* or *Anaplasma*. *Dermacentor silvarum*; Hco, *Haemaphysalis concinna*; Hja, *Haemaphysalis japonica*.

microbiological surveillance of vectors. Differences in microbiota composition have been extensively documented in other vector arthropods, including those between vector species, sexes, organs, and different developmental stages (Muturi et al., 2017; Strand, 2018; Choubdar et al., 2021). This study focuses on the differences in microbiota between ticks with regard to two factors: species and pathogens.

Our integrated approach—PCR identification, BLAST alignment, and phylogenetic analysis—revealed two distinct pathogen species: *Anaplasma* and SFG *Rickettsia*. This finding aligns with integrated tick surveillance data from the China-Russia-North Korea border regions, which reported a 35.05% prevalence of *Anaplasma* in five tick species (Min et al., 2025), with phylogenetic clusters showing 99.2–99.7% identity to *A. capra* strains from domestic ruminants in central China (GenBank MT799937, MG869594). Three SFG *Rickettsia* genotypes were concurrently identified, including strains demonstrating 98.4–99.1% sequence homology to Siberian tick isolates (MK304548) and Turkish human clinical variants (MG920563). While these cross-jurisdictional genotypic patterns suggest potential pathogen dispersal across the Tumen River delta, conclusive validation remains constrained by the exclusive sampling of Chinese border territories in existing datasets. *A. capra* exhibits a global distribution pattern (Altay et al., 2022; Numan et al., 2023), with China being both its initial discovery site and major endemic area (Liu et al., 2012). This pathogen infects diverse hosts, including goats, sheep, cattle, and wildlife (Yang et al., 2016; Sahin et al., 2022). Since the first report of human infection in 2015 (Li et al., 2015), its pathogenicity has been confirmed by clinical manifestations such as fever, headache, fatigue, and occasional neurological involvement. *A. capra* strains from China exhibit significant genetic diversity, while retaining >99% 16S rRNA homology with East Asian isolates (Zhang et al., 2020)—a pattern consistent with our phylogenetic analyses, suggesting trans-species transmission networks (Shi et al., 2019; Altay et al., 2024). Intriguingly, South Korean surveillance detected a 17.7% prevalence in *Hydropotes inermis argyropus* (water deer) populations, along with two novel variants (Cheongju and Chungbuk isolates) (Amer et al., 2019). Of particular epidemiological significance, co-infection with *A. capra* and *R. raoultii* was identified in *H. longicornis* parasitizing wildlife hosts, highlighting the complexity of potential mixed pathogen transmission. *R. raoultii* exhibits a pan-Eurasian distribution that is strongly associated with specific tick vectors. Chinese border surveillance confirms its distribution in the analyzed region to be as follows: 32.25% prevalence in *D. silvarum* along the Sino-Russian border (Wen et al., 2014), 6.25% in *H. erinacei* at the Sino-Kazakh border (Guo et al., 2015), and 4% in *D. silvarum* from Mudanjiang, China (Wang et al., 2021). Notably, Northeast China reported two human cases presenting tender eschars without lymphadenopathy (Jia et al., 2014). In South Korea, *H. longicornis* exhibited a remarkably high *R. raoultii* infection rate of 40.9%, with dogs identified as a potential mammalian reservoir. These findings underscore the critical role of this tick species as a zoonotic transmission vector (Seo et al., 2020; Tariq et al., 2021). In Europe (including France, Spain, and Germany), *Dermacentor marginatus* and *Dermacentor reticulatus* serve as the principal vectors, with infection rates ranging from 2 to 80% across studies. Clinical cases typically present with hallmark TIBOLA/DEBONEL manifestations (Parola et al., 2009). The high genetic conservation observed across geographical isolates, as demonstrated by ≥99.4% sequence similarity in the *ompA* gene, underscores their evolutionary stability (Mediannikov et al., 2008). Both *A. capra* and *R. raoultii* demonstrate transboundary endemicity influenced by vector distribution, wildlife reservoirs, and geographic factors, necessitating enhanced multinational surveillance and clinical vigilance.

Our results revealed significant differences in the microbial composition of hematophagous ticks infected by various pathogens. This finding aligns with previous studies that have demonstrated how different pathogens can shape the microbial communities within their vectors, potentially influencing vector competence and disease transmission dynamics (Lacroux et al., 2023; Qiu et al., 2024). The intergroup analysis further elucidated the distinct microbial profiles associated with specific pathogens, suggesting that the presence of certain pathogens may drive the selection of particular microbial taxa. For instance, the dominance of specific bacterial genera in arthropods infected with pathogens such as *Plasmodium* or the dengue virus indicates a potential role for these microbes in modulating the host immune response or enhancing pathogen survival (Wu et al., 2019).

Our integrated analysis revealed that the genus *Spirosoma*—recently reclassified under Mycoplasmatota—showed significant enrichment in *Anaplasma*-infected *Haemaphysalis* ticks (LDA >2, $p < 0.05$), but was undetectable in *Anaplasma*-positive *Dermacentor* cohorts. This host-specific association suggests that the biomarker potential of *Spirosoma* for *Anaplasma* surveillance may be restricted to *Haemaphysalis* ticks. Similarly, *Sphingopyxis* enrichment was only seen in the *Haemaphysalis* species and showed no correlation with *Rickettsia* infection status in the analyzed tick populations (Oren and Garrity, 2021). This bacterium is found in various arthropods and has been extensively documented in ticks (Binetruy et al., 2019a). Spiroplasmataceae is transmitted between arthropods by maternal inheritance and horizontal transfer (Bell-Sakyi et al., 2015).

5 Conclusion

This study investigated the prevalence of SFGR and *Anaplasma* in ticks collected from the Yanbian region and examined the changes in the microbiome that occur following infection with these pathogens. The results showed that SFGR and *Anaplasma* had high positivity rates in Yanbian, whereas *D. silvarum* was the tick species with the highest prevalence of infection and the dominant tick species in the region. Notably, certain bacterial taxa were significantly enriched in infected ticks, suggesting their potential role as biomarkers of pathogen presence. The study highlights the complex interactions between tick-borne pathogens and the tick microbiome, providing insights into the ecological dynamics of pathogen transmission. The findings underscore the importance of monitoring tick microbiomes as part of integrated vector management strategies. Future research should focus on elucidating the functional roles of the identified microbial taxa in pathogen transmission and exploring their potential as targets for tick-borne disease control.

Data availability statement

The datasets presented in this study can be found in online repositories. The names of the repository/repositories and accession number(s) can be found at: https://www.ncbi.nlm.nih.gov/bioproject/PRJNA1225783.

Ethics statement

The manuscript presents research on animals that do not require ethical approval for their study.

Author contributions

J-qW: Data curation, Writing – original draft, Writing – review & editing. TY: Writing – original draft, Validation. H-yQ: Data curation, Writing – review & editing, Writing – original draft. S-wJ: Writing – review & editing, Methodology. Z-qX: Writing – review & editing, Methodology. Q-cC: Writing – review & editing, Formal analysis. H-fL: Writing – review & editing, Formal analysis. W-fL: Writing – review & editing, Formal analysis. SF: Writing – review & editing, Resources. C-tF: Writing – review & editing, Resources. XG: Writing – review & editing. Z-zH: Writing – review & editing, Data curation. W-nT: Writing – review & editing, Validation. J-xL: Writing – review & editing, Resources. S-jX: Funding acquisition, Writing – review & editing.

Funding

The author(s) declare that financial support was received for the research and/or publication of this article. This work was supported by National Natural Science Foundation of China (32360886) and Natural Science Foundation of Jilin Province (YDZJ202201ZYTS616).

Acknowledgments

We would like to express our gratitude to the staff and workers of Yanbian CDC who assisted in the collection of ticks.

Conflict of interest

The authors declare that the research was conducted in the absence of any commercial or financial relationships that could be construed as a potential conflict of interest.

Generative AI statement

The authors declare that no Gen AI was used in the creation of this manuscript.

Publisher's note

Supplementary material

The Supplementary material for this article can be found online at: https://www.frontiersin.org/articles/10.3389/fmicb.2025.1589263/full#supplementary-material

References

Abraham, N. M., Liu, L., Jutras, B. L., Yadav, A. K., Narasimhan, S., Gopalakrishnan, V., et al. (2017). Pathogen-mediated manipulation of arthropod microbiota to promote infection. *Proc. Natl. Acad. Sci. U.S.A.* 114, E781–E790. doi: 10.1073/pnas.1613422114

Adrion, E. R., Aucott, J., Lemke, K. W., and Weiner, J. P. (2015). Health care costs, utilization and patterns of care following Lyme disease. *PLoS One* 10:e0116767. doi: 10.1371/journal.pone.0116767

Altay, K., Erol, U., and Sahin, O. F. (2022). The first molecular detection of *Anaplasma capra* in domestic ruminants in the central part of Turkey, with genetic diversity and genotyping of *Anaplasma capra*. *Trop. Anim. Health Prod.* 54:129. doi: 10.1007/s11250-022-03125-7

Altay, K., Erol, U., and Sahin, O. F. (2024). *Anaplasma capra*: a new emerging tick-borne zoonotic pathogen. *Vet. Res. Commun.* 48, 1329–1340. doi: 10.1007/s11259-024-10337-9

Amer, S., Kim, S., Yun, Y., and Na, K. J. (2019). Novel variants of the newly emerged *Anaplasma capra* from Korean water deer (*Hydropotes inermis argyropus*) in South Korea. *Parasit. Vectors* 12:365. doi: 10.1186/s13071-019-3622-5

Anderson, M. J. (2001). A new method for non-parametric multivariate analysis of variance. *Austral Ecol.* 26, 32–46. doi: 10.1111/j.1442-9993.2001.01070.pp.x

Andreotti, R., Perez de Leon, A. A., Dowd, S. E., Guerrero, F. D., Bendele, K. G., and Scoles, G. A. (2011). Assessment of bacterial diversity in the cattle tick *Rhipicephalus* (*Boophilus*) microplus through tag-encoded pyrosequencing. *BMC Microbiol.* 11:6. doi: 10.1186/1471-2180-11-6

Asnicar, F., Weingart, G., Tickle, T. L., Huttenhower, C., and Segata, N. (2015). Compact graphical representation of phylogenetic data and metadata with GraPhlAn. *PeerJ* 3:e1029. doi: 10.7717/peerj.1029

Bell-Sakyi, L., Palomar, A. M., and Kazimirova, M. (2015). Isolation and propagation of a *Spiroplasma* sp. from Slovakian *Ixodes ricinus* ticks in *Ixodes* spp. cell lines. *Ticks Tick Borne Dis.* 6, 601–606. doi: 10.1016/j.ttbdis.2015.05.002

Benjamini, Y., and Hochberg, Y. (2018). Controlling the false discovery rate: a practical and powerful approach to multiple testing. *J. R. Stat. Soc. B* 57, 289–300. doi: 10.1111/j.2517-6161.1995.tb02031.x

Binetruy, F., Bailly, X., Chevillon, C., Martin, O. Y., Bernasconi, M. V., and Duron, O. (2019a). Phylogenetics of the *spiroplasma ixodetis* endosymbiont reveals past transfers between ticks and other arthropods. *Ticks Tick Borne Dis.* 10, 575–584. doi: 10.1016/j.ttbdis.2019.02.001

Binetruy, F., Dupraz, M., Buysse, M., and Duron, O. (2019b). Surface sterilization methods impact measures of internal microbial diversity in ticks. *Parasit. Vectors* 12:268. doi: 10.1186/s13071-019-3517-5

Black, W. C. T., and Piesman, J. (1994). Phylogeny of hard-and soft-tick taxa (Acari: Ixodida) based on mitochondrial 16S rDNA sequences. *Proc. Natl. Acad. Sci. U.S.A.* 91, 10034–10038. doi: 10.1073/pnas.91.21.10034

Bokulich, N. A., Kaehler, B. D., Rideout, J. R., Dillon, M., Bolyen, E., Knight, R., et al. (2018). Optimizing taxonomic classification of marker-gene amplicon sequences with QIIME 2's q2-feature-classifier plugin. *Microbiome* 6:90. doi: 10.1186/s40168-018-0470-z

Bokulich, N. A., Subramanian, S., Faith, J. J., Gevers, D., Gordon, J. I., Knight, R., et al. (2013). Quality-filtering vastly improves diversity estimates from Illumina amplicon sequencing. *Nat. Methods* 10, 57–59. doi: 10.1038/nmeth.2276

Bonnet, S. I., Binetruy, F., Hernández-Jarguín, A. M., and Duron, O. (2017). The tick microbiome: why non-pathogenic microorganisms matter in tick biology and pathogen transmission. *Front. Cell. Infect. Microbiol.* 7:236. doi: 10.3389/fcimb.2017.00236

Boulanger, N., Insonere, J. L., Van Blerk, S., Barthel, C., Serres, C., Rais, O., et al. (2023). Cross-alteration of murine skin and tick microbiome concomitant with pathogen transmission after *Ixodes ricinus* bite. *Microbiome* 11:250. doi: 10.1186/s40168-023-01696-7

Budachetri, K., Browning, R. E., Adamson, S. W., Dowd, S. E., Chao, C.-C., Ching, W.-M., et al. (2014). An insight into the microbiome of the *Amblyomma maculatum* (acari: Ixodidae). *J. Med. Entomol.* 51, 119–129. doi: 10.1603/ME12223

Budachetri, K., Kumar, D., Crispell, G., Beck, C., Dasch, G., and Karim, S. (2018). The tick endosymbiont *Candidatus* midichloria mitochondrii and selenoproteins are essential for the growth of *Rickettsia parkeri* in the Gulf Coast tick vector. *Microbiome* 6:141. doi: 10.1186/s40168-018-0524-2

Callahan, B. J., McMurdie, P. J., Rosen, M. J., Han, A. W., Johnson, A. J., and Holmes, S. P. (2016). DADA2: high-resolution sample inference from Illumina amplicon data. *Nat. Methods* 13, 581–583. doi: 10.1038/nmeth.3869

Caporaso, J. G., Kuczynski, J., Stombaugh, J., Bittinger, K., Bushman, F. D., Costello, E. K., et al. (2010). QIIME allows analysis of high-throughput community sequencing data. *Nat. Methods* 7, 335–336. doi: 10.1038/nmeth.f.303

Choubdar, N., Karimian, F., Koosha, M., and Oshaghi, M. A. (2021). An integrated overview of the bacterial flora composition of *Hyalomma anatolicum*, the main vector of CCHF. *PLoS Negl. Trop. Dis.* 15:e0009480. doi: 10.1371/journal.pntd.0009480

Claesson, M. J., O'Sullivan, O., Wang, Q., Nikkilä, J., Marchesi, J. R., Smidt, H., et al. (2009). Comparative analysis of pyrosequencing and a phylogenetic microarray for exploring microbial community structures in the human distal intestine. *PLoS One* 4:e6669. doi: 10.1371/journal.pone.0006669

Dantas-Torres, F., Chomel, B. B., and Otranto, D. (2012). Ticks and tick-borne diseases: a one health perspective. *Trends Parasitol.* 28, 437–446. doi: 10.1016/j.pt.2012.07.003

DeSantis, T. Z., Hugenholtz, P., Larsen, N., Rojas, M., Brodie, E. L., Keller, K., et al. (2006). Greengenes, a chimera-checked 16S rRNA gene database and workbench compatible with arb. *Appl. Environ. Microbiol.* 72, 5069–5072. doi: 10.1128/aem.03006-05

Du, L. F., Zhang, M. Z., Yuan, T. T., Ni, X. B., Wei, W., Cui, X. M., et al. (2023). New insights into the impact of microbiome on horizontal and vertical transmission of a tick-borne pathogen. *Microbiome* 11:50. doi: 10.1186/s40168-023-01485-2

Duron, O., and Gottlieb, Y. (2020). Convergence of nutritional symbioses in obligate blood feeders. *Trends Parasitol.* 36, 816–825. doi: 10.1016/j.pt.2020.07.007

Duron, O., Morel, O., Noel, V., Buysse, M., Binetruy, F., Lancelot, R., et al. (2018). Tick-bacteria mutualism depends on b vitamin synthesis pathways. *Curr. Biol.* 28:e1895, 1896–1902.e5. doi: 10.1016/j.cub.2018.04.038

Finney, C. A., Kamhawi, S., and Wasmuth, J. D. (2015). Does the arthropod microbiota impact the establishment of vector-borne diseases in mammalian hosts? *PLoS Pathog.* 11:e1004646. doi: 10.1371/journal.ppat.1004646

Gall, C. A., Reif, K. E., Scoles, G. A., Mason, K. L., Mousel, M., Noh, S. M., et al. (2016). The bacterial microbiome of *Dermacentor andersoni* ticks influences pathogen susceptibility. *ISME J.* 10, 1846–1855. doi: 10.1038/ismej.2015.266

Gonzalez-Ceron, L., Santillan, F., Rodriguez, M. H., Mendez, D., and Hernandez-Avila, J. E. (2003). Bacteria in midguts of field-collected *Anopheles albimanus* block plasmodium vivax sporogonic development. *J. Med. Entomol.* 40, 371–374. doi: 10.1603/0022-2585-40.3.371

Grandi, G., Chiappa, G., Ullman, K., Lindgren, P. E., Olivieri, E., Sassera, D., et al. (2023). Characterization of the bacterial microbiome of Swedish ticks through 16S rRNA amplicon sequencing of whole ticks and of individual tick organs. *Parasit. Vectors* 16:39. doi: 10.1186/s13071-022-05638-4

Guo, L. P., Mu, L. M., Xu, J., Jiang, S. H., Wang, A. D., Chen, C. F., et al. (2015). *Rickettsia raoultii* in *Haemaphysalis erinacei* from marbled polecats, China-Kazakhstan border. *Parasit. Vectors* 8:461. doi: 10.1186/s13071-015-1065-1

Huang, W., Wang, S., and Jacobs-Lorena, M. (2020). Use of microbiota to fight mosquito-borne disease. *Front. Genet.* 11:196. doi: 10.3389/fgene.2020.00196

Jia, N., Wang, J., Shi, W., Du, L., Sun, Y., Zhan, W., et al. (2020). Large-scale comparative analyses of tick genomes elucidate their genetic diversity and vector capacities. *Cell* 182, 1328–1340.e13. doi: 10.1016/j.cell.2020.07.023

Jia, N., Zheng, Y. C., Ma, L., Huo, Q. B., Ni, X. B., Jiang, B. G., et al. (2014). Human infections with *Rickettsia raoultii*, China. *Emerg. Infect. Dis.* 20, 866–868. doi: 10.3201/eid2005.130995

Klindworth, A., Pruesse, E., Schweer, T., Peplies, J., Quast, C., Horn, M., et al. (2013). Evaluation of general 16s ribosomal RNA gene PCR primers for classical and next-generation sequencing-based diversity studies. *Nucleic Acids Res.* 41:e1. doi: 10.1093/nar/gks808

Lacroux, C., Bonnet, S., Pouydebat, E., Buysse, M., Rahola, N., Rakotobe, S., et al. (2023). Survey of ticks and tick-borne pathogens in wild chimpanzee habitat in western Uganda. *Parasit. Vectors* 16:22. doi: 10.1186/s13071-022-05632-w

Laukaitis, H. J., and Macaluso, K. R. (2021). Unpacking the intricacies of *Rickettsia*-vector interactions. *Trends Parasitol.* 37, 734–746. doi: 10.1016/j.pt.2021.05.008

Li, H., Zheng, Y. C., Ma, L., Jia, N., Jiang, B. G., Jiang, R. R., et al. (2015). Human infection with a novel tick-borne *Anaplasma* species in China: a surveillance study. *Lancet Infect. Dis.* 15, 663–670. doi: 10.1016/s1473-3099(15)70051-4

Liu, Z., Ma, M., Wang, Z., Wang, J., Peng, Y., Li, Y., et al. (2012). Molecular survey and genetic identification of *Anaplasma* species in goats from central and southern China. *Appl. Environ. Microbiol.* 78, 464–470. doi: 10.1128/AEM.06848-11

Madison-Antenucci, S., Kramer, L. D., Gebhardt, L. L., and Kauffman, E. (2020). Emerging tick-borne diseases. *Clin. Microbiol. Rev.* 33:e00083. doi: 10.1128/cmr.00083-18

Maldonado-Ruiz, L. P., Montenegro-Cadena, L., Blattner, B., Menghwar, S., Zurek, L., and Londono-Renteria, B. (2019). Differential tick salivary protein profiles and human immune responses to lone star ticks (*Amblyomma americanum*) from the wild vs. a laboratory colony. *Front. Immunol.* 10:1996. doi: 10.3389/fimmu.2019.01996

Mediannikov, O., Matsumoto, K., Samoylenko, I., Drancourt, M., Roux, V., Rydkina, E., et al. (2008). *Rickettsia raoultii* sp. nov., a spotted fever group *Rickettsia* associated with *Dermacentor* ticks in Europe and Russia. *Int. J. Syst. Evol. Microbiol.* 58, 1635–1639. doi: 10.1099/ijs.0.64952-0

Min, P., Song, J., Zhao, S., Ma, Z., Meng, Y., Tang, Z., et al. (2025). Tick species, tick-borne pathogen distribution and risk factor analysis in border areas of China, Russia and North Korea. *Front. Vet. Sci.* 12:1529253. doi: 10.3389/fvets.2025.1529253

Moreira, L. A., Iturbe-Ormaetxe, I., Jeffery, J. A., Lu, G., Pyke, A. T., Hedges, L. M., et al. (2009). A wolbachia symbiont in *Aedes aegypti* limits infection with dengue, chikungunya, and plasmodium. *Cell* 139, 1268–1278. doi: 10.1016/j.cell.2009.11.042

Muturi, E. J., Ramirez, J. L., Rooney, A. P., and Kim, C. H. (2017). Comparative analysis of gut microbiota of mosquito communities in central Illinois. *PLoS Negl. Trop. Dis.* 11:e0005377. doi: 10.1371/journal.pntd.0005377

Novakova, E., Woodhams, D. C., Rodriguez-Ruano, S. M., Brucker, R. M., Leff, J. W., Maharaj, A., et al. (2017). Mosquito microbiome dynamics, a background for prevalence and seasonality of west nile virus. *Front. Microbiol.* 8:526. doi: 10.3389/fmicb.2017.00526

Numan, M., Alouffi, A., Almutairi, M. M., Tanaka, T., Ahmed, H., Akbar, H., et al. (2023). First detection of *Theileria sinensis*-like and *Anaplasma capra* in *Ixodes kashmiricus:* with notes on cox1-based phylogenetic position and new locality records. *Animals* 13:3232. doi: 10.3390/ani13203232

Oren, A., and Garrity, G. M. (2021). Valid publication of the names of forty-two phyla of prokaryotes. *Int. J. Syst. Evol. Microbiol.* 71:e005056. doi: 10.1099/ijsem.0.005056

Parola, P., Rovery, C., Rolain, J. M., Brouqui, P., Davoust, B., and Raoult, D. (2009). *Rickettsia slovaca* and *R. raoultii* in tick-borne rickettsioses. *Emerg. Infect. Dis.* 15, 1105–1108. doi: 10.3201/eid1507.081449

Pavanelo, D. B., Schroder, N. C. H., Pin Viso, N. D., Martins, L. A., Malossi, C. D., Galletti, M., et al. (2020). Comparative analysis of the midgut microbiota of two natural tick vectors of *Rickettsia rickettsii*. *Dev. Comp. Immunol.* 106:103606. doi: 10.1016/j.dci.2019.103606

Qiu, H. Y., Lv, Q. B., Wang, C. R., Ju, H., Luo, C. F., Liu, S. S., et al. (2024). Microbiota profile in organs of the horseflies (Diptera: Tabanidae) in northeastern China. *Front. Microbiol.* 15:1467875. doi: 10.3389/fmicb.2024.1467875

Rai, S. N., Qian, C., Pan, J., Rai, J. P., Song, M., Bagaitkar, J., et al. (2021). Microbiome data analysis with applications to pre-clinical studies using QIIME2: statistical considerations. *Genes Dis.* 8, 215–223. doi: 10.1016/j.gendis.2019.12.005

Sahin, O. F., Erol, U., and Altay, K. (2022). Buffaloes as new hosts for *Anaplasma capra*: molecular prevalence and phylogeny based on *gtlA*, *groEL*, and *16S rRNA* genes. *Res. Vet. Sci.* 152, 458–464. doi: 10.1016/j.rvsc.2022.09.008

Segata, N., Izard, J., Waldron, L., Gevers, D., Miropolsky, L., Garrett, W. S., et al. (2011). Metagenomic biomarker discovery and explanation. *Genome Biol.* 12:R60. doi: 10.1186/gb-2011-12-6-r60

Seo, M. G., Kwon, O. D., and Kwak, D. (2020). High prevalence of *Rickettsia raoultii* and associated pathogens in canine ticks, South Korea. *Emerg. Infect. Dis.* 26, 2530–2532. doi: 10.3201/eid2610.191649

Shi, K., Li, J., Yan, Y., Chen, Q., Wang, K., Zhou, Y., et al. (2019). Dogs as new hosts for the emerging zoonotic pathogen *Anaplasma capra* in China. *Front. Cell. Infect. Microbiol.* 9:394. doi: 10.3389/fcimb.2019.00394

Simo, L., Kazimirova, M., Richardson, J., and Bonnet, S. I. (2017). The essential role of tick salivary glands and saliva in tick feeding and pathogen transmission. *Front. Cell. Infect. Microbiol.* 7:281. doi: 10.3389/fcimb.2017.00281

Sperling, J. L., Silva-Brandao, K. L., Brandao, M. M., Lloyd, V. K., Dang, S., Davis, C. S., et al. (2017). Comparison of bacterial 16S rRNA variable regions for microbiome surveys of ticks. *Ticks Tick Borne Dis.* 8, 453–461. doi: 10.1016/j.ttbdis.2017.02.002

Strand, M. R. (2018). Composition and functional roles of the gut microbiota in mosquitoes. *Curr. Opin. Insect Sci.* 28, 59–65. doi: 10.1016/j.cois.2018.05.008

Tariq, M., Seo, J. W., Kim, D. Y., Panchali, M. J. L., Yun, N. R., Lee, Y. M., et al. (2021). First report of the molecular detection of human pathogen *Rickettsia raoultii* in ticks from the Republic of Korea. *Parasit. Vectors* 14:191. doi: 10.1186/s13071-021-04695-5

Tokarz, R., and Lipkin, W. I. (2021). Discovery and surveillance of tick-borne pathogens. *J. Med. Entomol.* 58, 1525–1535. doi: 10.1093/jme/tjaa269

Van Treuren, W., Ponnusamy, L., Brinkerhoff, R. J., Gonzalez, A., Parobek, C. M., Juliano, J. J., et al. (2015). Variation in the microbiota of Ixodes ticks with regard to geography, species, and sex. *Appl. Environ. Microbiol.* 81, 6200–6209. doi: 10.1128/AEM.01562-15

Wang, Q., Pan, Y. S., Jiang, B. G., Ye, R. Z., Chang, Q. C., Shao, H. Z., et al. (2021). Prevalence of multiple tick-borne pathogens in various tick vectors in northeastern China. *Vector Borne Zoonotic Dis.* 21, 162–171. doi: 10.1089/vbz.2020.2712

Wen, J., Jiao, D., Wang, J. H., Yao, D. H., Liu, Z. X., Zhao, G., et al. (2014). *Rickettsia raoultii*, the predominant *Rickettsia* found in *Dermacentor silvarum* ticks in China-Russia border areas. *Exp. Appl. Acarol.* 63, 579–585. doi: 10.1007/s10493-014-9792-0

Wikel, S. (2013). Ticks and tick-borne pathogens at the cutaneous interface: host defenses, tick countermeasures, and a suitable environment for pathogen establishment. *Front. Microbiol.* 4:337. doi: 10.3389/fmicb.2013.00337

Wu, P., Sun, P., Nie, K., Zhu, Y., Shi, M., Xiao, C., et al. (2019). A gut commensal bacterium promotes mosquito permissiveness to arboviruses. *Cell Host Microbe* 25:e105, 101–112.e5. doi: 10.1016/j.chom.2018.11.004

Yang, J., Liu, Z., Niu, Q., Liu, J., Han, R., Liu, G., et al. (2016). Molecular survey and characterization of a novel *Anaplasma* species closely related to *Anaplasma capra* in ticks, northwestern China. *Parasit. Vectors* 9:603. doi: 10.1186/s13071-016-1886-6

Zhang, Y., Cui, Y., Sun, Y., Jing, H., and Ning, C. (2020). Novel *Anaplasma* variants in small ruminants from central China. *Front. Vet. Sci.* 7:580007. doi: 10.3389/fvets.2020.580007

Zhang, L., Han, J., Zhou, Q., He, Z., Sun, S. W., Li, R., et al. (2023). Differential microbial composition in parasitic vs. questing ticks based on 16s next-generation sequencing. *Front. Microbiol.* 14:1264939. doi: 10.3389/fmicb.2023.1264939

Zhang, L., Wang, D., Shi, P., Li, J., Niu, J., Chen, J., et al. (2024). A naturally isolated symbiotic bacterium suppresses flavivirus transmission by *Aedes* mosquitoes. *Science* 384:eadn9524. doi: 10.1126/science.adn9524

Zhong, Z., Wang, K., and Wang, J. (2024). Tick symbiosis. *Curr. Opin. Insect Sci.* 62:101163. doi: 10.1016/j.cois.2024.101163

frontiers | Frontiers in Microbiology

TYPE Original Research
PUBLISHED 12 June 2025
DOI 10.3389/fmicb.2025.1603770

OPEN ACCESS

EDITED BY
Hong Yin,
Chinese Academy of Agricultural Sciences, China

REVIEWED BY
Hasan Faisal Hussein Kahya,
University of Mosul, Iraq
Miroslav Benić,
Croatian Veterinary Institute, Croatia

*CORRESPONDENCE
William W. L. Hsiao
✉ wwhsiao@sfu.ca

RECEIVED 01 April 2025
ACCEPTED 28 April 2025
PUBLISHED 12 June 2025

CITATION
Yee M, Trimble MJ, Ghosh K, Hughes G, Knowles D, Duan J, Raverty S, McGregor G and Hsiao WWL (2025) The genotypic characterization of *Streptococcus pluranimalium* from aborted bovine fetuses in British Columbia, Canada.
Front. Microbiol. 16:1603770.
doi: 10.3389/fmicb.2025.1603770

The genotypic characterization of *Streptococcus pluranimalium* from aborted bovine fetuses in British Columbia, Canada

Marcus Yee[1], Michael J. Trimble[1,2], Kazal Ghosh[3], Giselle Hughes[3], Daniel Knowles[3], Jun Duan[4], Stephen Raverty[3], Glenna McGregor[3] and William W. L. Hsiao[1,2]*

[1]Department of Molecular Biology and Biochemistry, Simon Fraser University, Burnaby, BC, Canada, [2]Department of Health Sciences, Simon Fraser University, Burnaby, BC, Canada, [3]Animal Health Centre, Ministry of Agriculture and Food, Government of British Columbia, Abbotsford, BC, Canada, [4]Faculty of Health Sciences, Simon Fraser University, Burnaby, BC, Canada

Introduction: Bovine abortions result in significant economic losses to dairy producers, and bacteria are among the most common causes of these abortions. In 2021, *Streptococcus pluranimalium* was isolated from a dairy abortion case for the first time in British Columbia (BC), Canada. This bacterium has previously been recovered from the reproductive tracts of dairy cattle and various other species, including humans.

Methods: Between 2021 and 2023, *S. pluranimalium* was isolated from the placenta, fetal lung, and/or fetal abomasal contents of 10 aborted dairy fetuses submitted for routine abortion diagnostics. This study was conducted to better characterize the genotype of these 10 isolates. The histopathology of the bovine abortions was examined, and the BC strains were sequenced using Nanopore technology and underwent bioinformatic analysis.

Results: The BC strains had an average genome size of 2,313,582 base pairs and an average GC content of 38.59%. Based on whole genome phylogeny, the BC strains were clustered together and distinctly separated from other publicly available strains of this species from different regions and isolation sources. Through Clusters of Orthologous Groups analysis, the BC strains contained a larger proportion of genes associated with the mobilome. Additionally, although we identified only a few antibiotic resistance genes or virulence factors (VFs) in these strains, several of these genes were located within prophage sequences.

Discussion: Although the clinical and pathological significance of these bacteria in most abortion cases remains unclear, our findings underscore the importance of continued surveillance and research into uncommon pathogens to better understand their biology and potential impact on human and animal health.

KEYWORDS

***Streptococcus pluranimalium*, bovine abortion, whole genome sequencing, antimicrobial resistance (AMR), animal health**

1 Introduction

Bovine abortions result in significant economic losses for dairy producers worldwide. Reported bovine abortion rates range from 3 to 10% and can reach up to 30% in some herds. These abortions are attributed to a variety of factors, including genetic abnormalities, pathogen exposure, nutritional conditions, iatrogenic (medications) and teratogenic compounds, and hormonal fluctuations

(Thurmond et al., 2005; Mee, 2023). Abortions are associated with various etiologic agents, including bacteria, fungi, protozoa, and viruses. Among these pathogens, infections caused by bacteria contribute significantly to morbidity, accounting for approximately 32–58% of all bovine abortion cases (Hecker et al., 2023). Pathogen exposure and invasion generally occur retrograde via the lower urogenital tract, or hematogenously through bacteremia, leading to localization in the placenta and developing fetus. These infections may be opportunistic, associated with normal commensal organisms, or result from exposure to contagious pathogens.

The dairy industry is the third largest agricultural sector in Canada (Pierre, 2017). In British Columbia (BC), particularly in the Fraser Valley, milk production plays a vital role in the regional economy. Due to the significant impact of fetal loss on dairy production, there has been an ongoing survey of bovine abortions at the Animal Health Centre (AHC) in Abbotsford, BC, to identify the causes of fetal loss. Between 2021 and 2023, a novel microbe, *Streptococcus pluranimalium,* was recovered from 10 aborted bovine fetuses. Prior to this period, this bacterium had not been identified in any bovine fetal samples submitted to the AHC. Given the limited knowledge about the natural history of this bacterium and the unknown risk of zoonotic transmission, a One Health approach was adopted to better characterize the molecular features of these isolates.

S. pluranimalium is a Gram-positive bacterium that is most closely related to *Streptococcus hyovaginalis*, *Streptococcus halotolerans*, and *Streptococcus thoraltensis* (Pan et al., 2018). The species has a broad tissue tropism and is capable of infecting a wide array of hosts, including canaries, chickens, cats, goats, and tilapia (Pan et al., 2018; Ghazvini et al., 2019). In bovine cases, *S. pluranimalium* has been linked to various diseases, such as vulvovaginitis, brain abscesses, tonsillitis, and mastitis, and reproductive issues, such as abortion (Foster et al., 2008; Twomey et al., 2012). Typically, this species transmits through blood, milk, and other infectious secretions from animals (Pan et al., 2018). There have been few reported cases of human infections, which manifested as suppurative meningitis, brain abscesses, endocarditis, and septicemia (Aryasinghe et al., 2014; Ananieva et al., 2023). Despite its wide range of potential hosts and zoonotic potential, there are few publicly available genomes of this species. As the genotype of this bacterium has not been well characterized, we performed whole-genome sequencing of 10 *S. pluranimalium* strains isolated from aborted bovine fetuses.

2 Materials and methods

2.1 Case material

The Animal Health Centre (AHC) is the provincial veterinary diagnostic laboratory for British Columbia and is accredited by the American Association of Veterinary Laboratory Diagnosticians (AAVLD). Case accessions included a range of tissue samples and whole carcasses obtained from local producers, veterinarians, and the general public. Bovine fetuses presented for necropsy underwent a standardized protocol, during which body weight and crown-to-rump length are recorded. All organ systems were examined internally and externally, and tissue samples were collected for routine bacteriology, histopathology, and other ancillary testing as deemed appropriate by a veterinary pathologist. Samples for bacteriology included the abomasal content, placenta, and lung tissues. These tissues were processed using conventional techniques, which included initial surface searing, followed by inoculation onto blood agar and MacConkey agar plates (Oxoid, ON). The samples were then incubated aerobically for up to 48 h. For any abortion cases, selective *Salmonella* culture was performed on Hektoen and XLT4 agar plates (Oxoid, ON), followed by selective enrichment in selenite broth. The colonies that grew on the agar plates were identified using biochemical tests and MALDI-TOF mass spectrometry (Bruker, ON), and the results were recorded in the proprietary veterinary information management system, VADDS&Vetstar developed by Advanced Technology Corp (Ramsey, NJ). For this study, *S. pluranimalium* isolates were archived at -20C for further analysis. The subsamples of the isolates were stored at -80C. Additional tissue samples were systematically collected for histopathological analysis, processed with an automated processor, embedded in paraffin, and sectioned at 5 *u*m. These sections were stained with hematoxylin and eosin using an automated stainer, cover-slipped, and then reviewed by board-certified veterinary pathologists. Microscopic lesions were graded on a scale from 0 (no apparent lesions) to 4 (severe lesions). A summary case report was prepared. Based on the histopathology results, ancillary diagnostic studies were conducted to screen for *Neospora caninum*, bovine viral diarrhea, *Chlamydophila abortus*, and *Ureoplasma diversum* (Hewinson et al., 1997), along with radial immunodiffusion testing for bovine IgG and IgM in select cases.

To determine the number of *S. pluranimalium* isolates recovered at the AHC, a database search covering the period from 2008 to 2024 was performed using the parameters of bovine, fetus, and abortion.

2.2 Sample extraction, library preparation, and sequencing

Bacterial isolates were recovered from freezer stocks by initial culturing on tryptic soy agar plates supplemented with 5% defibrinated sheep's blood and incubating overnight at 37°C. A single colony was picked and inoculated into tryptic soy broth supplemented with 5% defibrinated sheep's blood, and the culture was shaken overnight at 37°C. DNA extractions were performed using Qiagen's DNeasy Blood & Tissue kit (Toronto, ON), following the supplemental steps for the pretreatment of Gram-positive bacteria. The extracted DNA was then assessed for purity and concentration using gel electrophoresis, Nanodrop, and Qubit.

The samples were then prepared for sequencing on MinION, Oxford Nanopore Technologies (**ONT**) (Oxford, UK), using their Native Barcoding Kit (EXP-NBD114). This process involved repairing the DNA and performing end-preparation using the NEBNext FFPE DNA Repair Mix and the NEBNext Ultra II End Repair/dA-Tailing Module reagents (New England Biolabs, NEB; Whitby, ON). The samples were purified using AMPure XP beads, and the native barcodes were then ligated onto the fragments using Blunt/TA Ligase Master Mix (NEB). The samples were purified using AMPure XP beads, quantified, and then pooled in equimolar amounts. The ONT adapters were ligated to the barcoded pool using T4 Ligase (NEB) before being loaded onto an R10.3 flow cell, following ONT specifications. The samples were sequenced for 72 h and base-called using the MinKNOW (v22.03.6) high-accuracy base-calling model.

2.3 Sequence analysis

Raw reads had adaptors trimmed using Porechop v0.2.4 (Wick, 2018) and were quality-filtered using NanoFilt v2.8.0 (using the parameters -q 10, –l 300, –-headcrop 40) (De Coster et al., 2018). The filtered reads were

assembled using Flye v2.9.1 (Kolmogorov et al., 2019) and polished using Medaka v1.11.1 (ONT, 2024). The genomes were annotated using Bakta v1.7 (Schwengers et al., 2021), and a Maximum likelihood phylogenetic tree was created using the tool autoMLST (accessed August 23, 2022) (Alanjary et al., 2019). Genome completeness was assessed using BUSCO v5.7.1 (Simão et al., 2015). The Virulence Factor Database (accessed May 10, 2024) (Liu et al., 2022) and Abricate v1.0.0 (Seemann, 2020) were used to search for the presence of virulence factors. The Comprehensive Antibiotic Resistance Database (CARD) v3.2.9 (McArthur et al., 2013), coupled with RGI v6.0.2, was used to examine antibiotic resistance genes (ARGs). Clusters of Orthologous Groups analysis was conducted using the EggNOG-mapper v2.1.9 (Cantalapiedra et al., 2021) and EggNOG Database v5.0.2 (Huerta-Cepas et al., 2018). Plasmids were identified using Mobsuite v3.0.3 (Robertson and Nash, 2018), and phage sequences were identified using Virsorter v2.2.3 (Guo et al., 2021).

3 Results

3.1 Identification of microorganisms in aborted fetuses

Between 2008 and 2024, 382 fetuses were submitted to the AHC for diagnostic evaluation. Each case was reviewed individually, and the signalment, gross pathology, histopathology, bacteriology, and molecular results were tabulated and scored. Using MALDI-TOF mass spectrometry, *S. pluranimalium* was identified in 10 fetal samples, which then underwent further characterization. In these 10 samples, additional bacterial isolates were taxonomically identified at the species level or, if the species level could not be determined, at the genus level. Overall, 13 bacterial species and genera were isolated from the lung, stomach contents, and placenta (Supplementary Table 1). These included *S. pluranimalium* ($n = 11$), *Streptococcus uberis* ($n = 2$), the *Glutamicibacter* genus ($n = 2$), the *Staphylococcus* genus ($n = 3$), *Enterococcus saccharolyticus* ($n = 1$), the *Psychrobacter* genus ($n = 1$), the *Arthrobacter* genus ($n = 3$), *Aerococcus viridans* ($n = 1$), the *Vibrio* genus ($n = 1$), the *Acinetobacter genus* ($n = 5$), the *Corynebacterium* genus ($n = 2$), *Enterococcus faecium* ($n = 1$), and *Escherichia coli* ($n = 5$). In addition, sample BC-AHC-08 contained the fungi *Aspergillus fumigatus* and a species of *Candida*. The presence of three other pathogens—*Neospora caninum* ($n = 8$), Bovine Viral Diarrhea Virus ($n = 1$), and *Ureoplasma diversum* ($n = 1$)—was confirmed either through polymerase chain reaction or serology.

3.2 Lesion distribution

The histopathology results indicated the presence of several lesions in the aborted fetuses (Table 1), affecting various tissues including the brain, lungs, heart, muscles, kidneys, and eyes. Lesions in the eyes ($n = 6$) and placenta ($n = 7$) were the most common. Sample BC-AHC-03 exhibited the most extensive lesions, affecting six different tissues. No histopathological abnormalities were apparent in sample BC-AHC-05.

3.3 Whole-genome sequencing of *Streptococcus pluranimalium*

Among the 10 fetal samples with MALDI-TOF-confirmed *S. pluranimalium*, isolates from 9 were further characterized using molecular methods. Whole-genome sequencing was performed on one isolate from each sample, except for sample BC-AHC-09, from which two isolates were sequenced: BC-AHC-09_a isolated from the lung and BC-AHC-09_b isolated from the stomach. The BC strains had an average genome size of 2,313,582 base pairs (bp) and an average GC content of 38.59%, similar to the reference strain TH11417 (Pan et al., 2018), which has a genome size of 2,065,522 and a GC content of 38.65 (Table 2). The BC strains had an average of 15.2 contigs per assembly and an average genome completeness of 96.63%, as assigned by BUSCO.

3.4 Phylogeny

A maximum likelihood phylogenetic tree was constructed based on the analysis of core, single-copy genes present in all strains (Figure 1). The phylogenetic tree was constructed using the 10 BC genomes and 6 other publicly available genomes from the NCBI as of July 2024. The six genomes from the NCBI include TH11417 (Pan et al., 2018), 14A0014 (Rodriguez Campos et al., 2018), Colony612 (Buathong et al., 2021), SP21-2 (Xu et al., 2023), SP28 (Zhu, 2023), and SUG2384 (Holman et al., 2024). The BC strains formed a distinct clade, with strain BC-AHC-06_a being the most divergent. Strains BC-AHC-09_a and BC-AHC-09_b were isolated from the same sample but were separated on the phylogenetic tree. The publicly available strain, 14A0014, which was also recovered from a bovine abortion sample, was the most genetically distinct compared to the BC strains.

3.5 Clusters of orthologous groups

Clusters of orthologous groups (COGs) is a method of phylogenetic classification that clusters each gene into a COG ID and assigns each COG ID to a functional category. The COG analysis, supported by Fisher's exact test, revealed that the BC strains, except for strain BC-AHC-06_a, contained a significantly higher proportion of COG IDs associated with category X compared to *other S. pluranimalium* strains ($p < 0.05$) (Figure 2A). The BC strains, excluding BC-AHC-06_a, had an average of 12.5% of all COG IDs associated with category X. In comparison, strain BC-AHC-06_a had only 2.7% of its COG IDs associated with category X, which is similar to the non-BC strains that had an average of 3.2% of their COG IDs. With the exception of strain BC-AHC-06_a, many COG IDs associated with category X that were in high abundance were shared among all of the BC strains (Figure 2B).

3.6 Virulence factors

Utilizing the tool Abricate and the Virulence Factor Database, seven different virulence factors (VFs) were identified in the BC strains, encompassing four virulence classes: immune modulation, stress survival, exotoxin, and adherence (Table 3). All BC strains contained the gene cluster *rfbA*, *rfbB*, and *rfbC*, with an 80–82% nucleotide identity. The VFs *tig/ropA*, *plr/gapA*, and *eno* were also found in all BC strains, with identities of approximately 82, 89, and 90%, respectively. Strain BC-AHC-06_a contained the *SSU98_0978* virulence factor, with a nucleotide identity of 95%.

TABLE 1 Histopathological findings of aborted bovine fetuses.

Case ID	Myositis	Myocarditis	Meningoencephalitis	Placentitis	Nephritis	Pneumonia	Cholangiohepatitis	Palpebritis/conjunctivitis
BC-AHC-01	0	0	0	2	0	0	N/A	N/A
BC-AHC-02	2	4	2	2	2	0	N/A	N/A
BC-AHC-03	1	1	0	3	1	0	2	1
BC-AHC-04	0	1	0	1	1	0	1	1
BC-AHC-05	N/A	N/A	N/A	N/A	N/A	N/A	N/A	N/A
BC-AHC-06	N/A	4	N/A	1	1	0	1	1
BC-AHC-07	0	0	0	0	0	0	1	0
BC-AHC-08	0	0	0	4	0	2	0	2
BC-AHC-09	1	0	N/A	N/A	0	1	0	1

Lesions were assessed across various tissue types and were scored based on severity on a scale from 0 (no apparent lesions) to 4 (severe lesions). It is important to note that mixed bacterial or bacterial and fungal or protozoal infections likely contributed to the observed microscopic lesions.

3.7 Antimicrobial resistance genes

Utilizing the Resistance Gene Identifier tool and the Comprehensive Antibiotic Resistance Database, several genes conferring resistance to multiple antibiotics were identified using strict and perfect criteria (Figure 3). Antibiotic resistance genes (ARGs) conferring resistance to a number of antibiotics such as glycopeptides (*vanY* genes), lincosamides (*lnuC*), tetracycline (*tet(M)*), and macrolides (*mreA*) were detected (Table 2). Strains BC-AHC-08_a and BC-AHC-09_a contained the largest number of ARGs, with four each.

3.8 Plasmids

Using the tool MOB-suite, two novel plasmids were identified. The first was a 10.8 kb plasmid identified in strains BC-AHC-01_a and BC-AHC-02_a, and the second was a 5.4 kb plasmid identified in strains BC-AHC-03_a, BC-AHC-04_a, BC-AHC-08_a, and BC-AHC-09_b. Both plasmids showed the closest similarity to NSUI060 (Athey et al., 2016), a 5.6 kb *Streptococcus suis* plasmid. These *S. pluranimalium* plasmids did not contain any known virulence factors or antimicrobial resistance genes, had the MOBV relaxase type, and were classified as mobilizable.

3.9 Prophages

Using VirSorter2, a machine learning tool that predicts phage sequences based on features such as the number of hallmark viral genes, the percentage of viral genes, and the mean GC content, we identified 41 putative prophages in the BC strains (Supplementary Table 2). Their lengths ranged from 1,024 bp to 295,435 bp. Each BC strain had an average of 291,212 bp of phage sequences. In comparison, the non-BC strains Colony612 and SP28 did not contain any phage sequences. The four other non-BC strains had an average of 147,501 bp of phage sequences per strain. Strains BC-AHC-03_a and BC-AHC-09_b contained two virulence factors, tig/ropA and plr/gapA, located on a phage sequence. The *eno* virulence factor was also located on a phage sequence in strain BC-AHC-06_a. Strain BC-AHC-08_a contained a phage sequence with three ARGs: the *vanY* gene in the *vanB* cluster, *mreA*, and *lnuC*. In addition, strain BC-AHC-09_a contained one phage sequence with one ARG, *lnuC*.

4 Discussion

Bovine abortions cause significant economic losses and are frequently associated with bacterial infections. Since 2021, *S. pluranimalium*, an emerging pathogen, has been identified in a subset of aborted fetuses in BC. Notably, MALDI-TOF analysis was only implemented at the AHC in 2018; prior to this period, the biochemical tests used for bacterial identification were not capable of distinguishing this pathogen. In addition to *S. pluranimalium*, 12 other bacterial isolates were recovered from these aborted fetuses. The most common bacterial species identified were *Escherichia coli* ($n = 5$) and the *Acinetobacter* genus ($n = 5$). Evidence of exposure to the protozoan parasite, *Neospora caninum,* was also found in eight fetuses. Given the non-sterile conditions at the farm site, it is not

TABLE 2 Whole-genome sequence assembly statistics of the BC *S. pluranimalium* strains.

Strain ID	No. of contigs	Genome size (Mb)	GC (%)	N50 (Mb)	Genome completeness (%)
BC-AHC-01_a	12	2.4	38.54	1.6	98.0
BC-AHC-02_a	5	2.2	38.59	2.2	99.0
BC-AHC-03_a	13	2.1	38.68	2.1	98.0
BC-AHC-04_a	22	2.5	38.87	1.5	91.5
BC-AHC-05_a	17	2.3	38.5	2.3	95.0
BC-AHC-06_a	10	2	38.45	2	97.5
BC-AHC-07_a	31	2.4	38.59	2.3	97.7
BC-AHC-08_a	18	2.4	38.5	0.9	91.5
BC-AHC-09_a	14	2.3	38.66	2.2	90.0
BC-AHC-09_b	19	2.4	38.56	2.3	91.5
Reference TH11417 (Complete Genome)	1	2.1	38.65	2.1	98.8

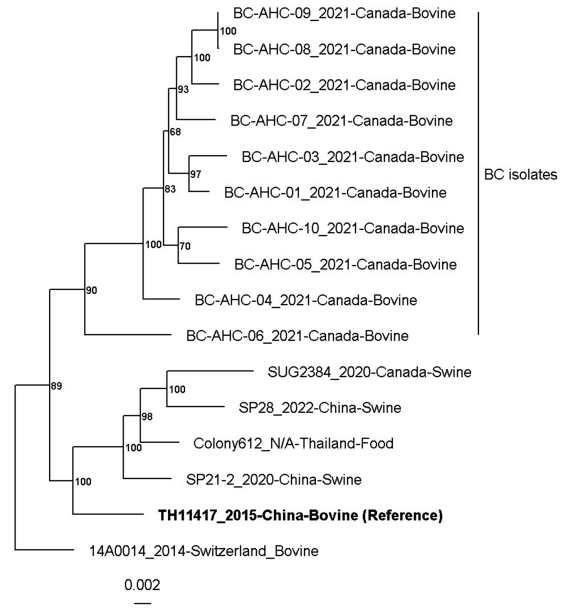

FIGURE 1
Maximum likelihood phylogenetic tree of *S. pluranimalium* strains with multilocus sequence typing analysis using the tool autoMLST.

unusual to observe a diversity of microbial isolates in the submitted case materials (Hecker et al., 2023). This situation complicates the determination of the cause of fetal death in cases of mixed infection bovine abortion (Barkallah et al., 2014). Although we cannot definitively state that *S. pluranimalium* was the cause of abortion, the discovery of this bacterium from multiple tissues with occasional active inflammation warrants further investigation.

In this study, we conducted whole-genome sequencing on 10 *S. pluranimalium* isolates, greatly increasing the number of publicly available genomes for this species (Table 2 and Supplementary Table 1). The phylogenetic analysis revealed a distinct BC clade, with strain BC-AHC-06_a being the most divergent. Strains BC-AHC-09_a and BC-AHC-09_b were both isolated from the same case, with one isolate recovered from the lung and the other from the stomach (Figure 1). These strains appeared separately on the phylogenetic tree, indicating a mixed infection of two *S. pluranimalium* strains. Interestingly, the public strain 14AA0014, which was also isolated in Canada and associated with bovine abortions, was the most distinct compared to BC strains.

In BC strains, we found a larger number of COG IDs linked to COG category X compared to the other *S. pluranimalium* strains (Figure 2B). This category is listed as the mobilome and encompasses genes associated with transposons, prophages, and plasmid replication (Galperin et al., 2014). The exception was strain BC-AHC-06_a, which was the most divergent strain on the phylogenetic tree. Analysis of the location of these COG X IDs showed that they were distributed evenly across the genomes. Although the BC strains contained more prophage sequences, as predicted by VirSorter2, and these phage sequences contained many COG category X genes, removing the phage-located COG IDs did not alter the overall trend. The BC strains, except for BC-AHC-06_a, still exhibited a significantly higher percentage of COG category X genes. Although these findings further substantiate the BC clade, differentiating the BC strains from other *S. pluranimalium* strains, further research is needed to understand the higher prevalence of genes associated with mobilizable elements in the BC strains.

Similar to other *S. pluranimalium* strains, the BC strains contained limited antimicrobial resistance genes. Several of the BC strains shared the *vanY* gene from the *vanG cluster* and the *lnuC* gene with the reference *S. pluranimalium* strain TH11417 (Figure 3) (Pan et al., 2018). The *vanY* gene confers resistance to glycopeptides, while the *lnuC* gene confers resistance to lincosamides. The BC-AHC-07_a strain contained the *tet(M)* gene, which confers resistance to tetracycline. This gene was not present in any other *S. pluranimalium* genome as of July 2024. Both BC and non-BC *S. pluranimalium* strains contained six virulence factors, indicating that these factors are likely part of the core genome for the species. These virulence genes include the gene cluster *rfbA, rfbB,* and *rfbC*. These genes are involved in capsule synthesis and are traditionally associated with O-antigen production in Gram-negative bacteria; however, they have been reported in *Streptococcus thermophilus* (Bank et al., 2022). The three other virulence factors present in all *S. pluranimalium* strains are *tig/ropA*, a trigger factor linked to stress tolerance, *plr/gapA*, a GAPDH homolog involved in host cell adherence, and *eno*, an enzyme linked to the binding of human plasminogen (Antikainen et al., 2007; Purves et al., 2010; Wu et al., 2011). BC-AHC-04_a was the only BC strain to have the virulence factor SSU98_0978, an agglutinin receptor involved in adhesion (Forsgren et al., 2010).

We also identified two novel plasmids, both showing the closest similarity to a *Streptococcus suis* plasmid from Canada (Athey et al.,

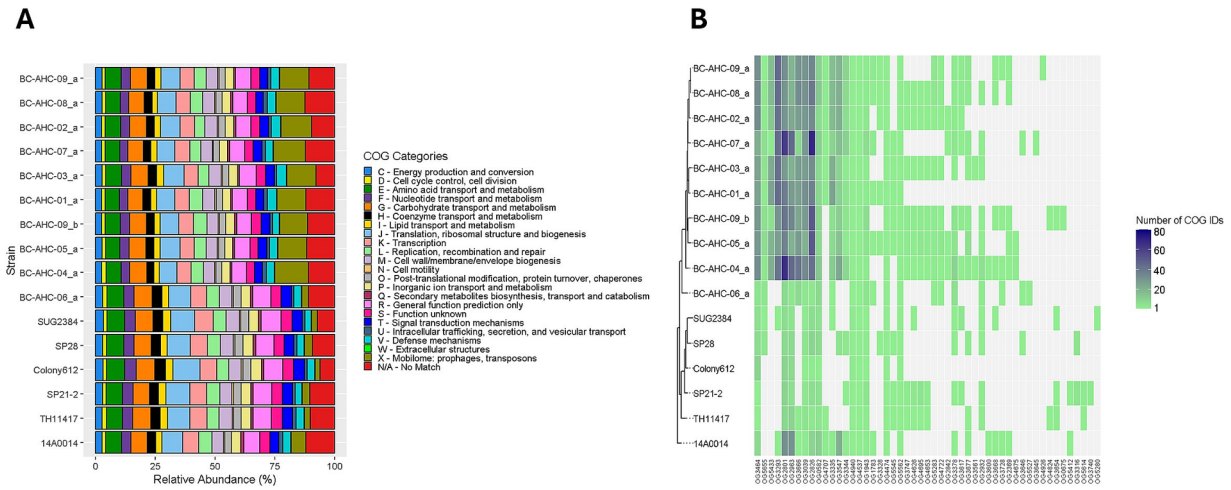

FIGURE 2
(A) Distribution of COG functional categories of each gene in *S. pluranimalium* genomes. **(B)** Heatmap showing the number of COG IDs associated with Category X in the *S. pluranimalium* genomes. COG IDs not present in a strain are colored light gray, while COG IDs present in a strain are represented by a gradient from light green to navy blue.

TABLE 3 Percent identity of virulence factors in *S. pluranimalium* strains, identified using the Virulence Factor Database.

Strains	rfbA	rfbB	rfbC	tig/ropA	plr/gapA	eno	SSU98_0978	SAG_RS09105
BC-AHC-01_a	80.6	81.06	81.82	82.4	88.97	89.82		
BC-AHC-02_a	80.6	81.06	81.82	82.24	88.27	90.05		
BC-AHC-03_a	80.6	80.87	81.82	82.4	89.26	89.82		
BC-AHC-04_a	80.48	81.06	81.48	82.4	89.17	90.13	95.46	
BC-AHC-05_a	80.48	80.79	81.48	82.24	89.07	89.9		
BC-AHC-06_a	81.06	81.16	81.48	82.24	88.77	90.13		
BC-AHC-07_a	80.6	80.98	81.48	82.17	88.27	89.9		
BC-AHC-08_a	80.71	81.06	81.48	82.24	88.27	89.9		
BC-AHC-09_a	80.71	81.06	81.48	82.24	88.27	89.9		
BC-AHC-09_b	80.48	81.16	81.82	82.17	88.97	89.9		
TH11417	80.37	81.16	81.82	82.24	89.26	90.05		
A40014	80.94	81.27	80.64	82.56	89.26	90.21		95.9
Colony612	80.71	81.06	81.45	82.4	88.87	90.21		95.86
SP-21-2	80.71	81.16	81.48	82.4	89.36	90.21		94.11
SP28	80.71	81.26	81.48	82.4	88.87	90.28		95.9
SUG2384	81.17	81.16	81.48	82.17	88.57	90.21		

A threshold of 80% identity and 80% coverage relative to a reference virulence factor was applied.

2016). The larger plasmid, measuring 10.8 kb, was found in strains BC-AHC-01_a and BC-AHC-02_a. The smaller plasmid, measuring 5.4 kb, was found in strains BC-AHC-03_a, BC-AHC-04_a, BC-AHC-09_a, and BC-AHC-09_b. Interestingly, further analysis revealed that the larger plasmid in BC-AHC-01_a and BC-AHC-02_a appeared to be an expanded version of the smaller plasmid, representing a duplication of its genetic content. No known virulence factors or antimicrobial resistance genes were found on these plasmids.

The BC strains contained a higher number of longer phage sequences compared to the other *S. pluranimalium* strains. Notably, two virulence factors, *tig/ropA* and *plr/gapA*, were identified within a phage sequence in two BC strains. In addition, another BC strain contained a phage sequence with the *eno* virulence factor. One BC strain contained a phage sequence with three ARGs: *vanY* in the *vanB* cluster, *mreA*, and *lnuC*. In contrast, another strain contained a phage sequence with *lnuC*. As these virulence factors and ARGs present on the phage sequences are potentially mobilizable, these findings highlight the need for vigilant monitoring to prevent the potential transmission of these genes from *S. pluranimalium* to other species, given its broad host tropism.

5 Conclusion

We performed whole-genome sequencing of 10 BC *S. pluranimalium* isolates, a previously unreported species in

FIGURE 3
Presence of ARGs identified using the Resistance Gene identifier tool and the Comprehensive Antibiotic Resistance Gene Database. Perfect and strict hits were used.

this region. The BC strains clustered separately from other *S. pluranimalium* strains but shared similar attributes, including a low number of detected VFs and ARGs. Overall, our findings underscore the importance of continued surveillance and research on rare and novel bacterial isolates to enhance our understanding of their biology and potential impact on human and animal health.

Data availability statement

All genome sequences generated in this study have been deposited in the GenBank database under the BioProject accession number PRJNA1251123.

Ethics statement

Ethical approval was not required for the studies involving animals in accordance with the local legislation and institutional requirements because the fetuses were submitted to the diagnostic service provided by the Animal Health Centre, Abbotsford, BC. On presenting the fetus to the Animal Health Centre, each producer or veterinarian signed a waiver included in the submission form for permission to (1) undertake and complete the requested testing and diagnostics and (2) inform the submitter that data from these investigations may be used for ongoing statistical surveillance of production animal health in British Columbia. As the fetuses comprised spontaneous abortions and were dead at the time of submission, no IACUC review was warranted. In this case series, no fetuses were actively solicited from producers and no fetuses were obtained by induced abortion of pregnant dams. Written informed consent was obtained from the owners for the participation of their animals in this study.

Author contributions

MY: Formal analysis, Software, Visualization, Writing – original draft, Writing – review & editing, Investigation. MT: Methodology, Supervision, Writing – review & editing, Investigation. KG: Conceptualization, Investigation, Methodology, Writing – review & editing, Supervision. GH: Data curation, Writing – review & editing. DK: Data curation, Writing – review & editing. JD: Data curation, Writing – review & editing. SR: Conceptualization, Investigation, Methodology, Writing – review & editing, Supervision. GM: Methodology, Writing – review & editing, Conceptualization, Investigation, Supervision. WH: Supervision, Writing – review & editing.

Funding

The author(s) declare that no financial support was received for the research and/or publication of this article.

Acknowledgments

We would like to extend our sincere thanks to the bacteriology laboratory scientists at the Animal Health Centre for conducting the bacterial cultures. We particularly thank Giselle Hughes and Daniel Knowles for their contributions to bacterial sequencing. We would also like to acknowledge Jun Duan for his role in sequence assembly. We also extend our appreciation to all submitters involved in these cases. We would like to thank the Michael Smith

Health research funding as well as the Canadian Institutes of Health Research and Canada Graduate Scholarships — Master's program.

Conflict of interest

The authors declare that the research was conducted in the absence of any commercial or financial relationships that could be construed as a potential conflict of interest.

The author(s) declared that they were an editorial board member of Frontiers, at the time of submission. This had no impact on the peer review process and the final decision.

Generative AI statement

The authors declare that no Gen AI was used in the creation of this manuscript.

Publisher's note

Supplementary material

The Supplementary material for this article can be found online at: https://www.frontiersin.org/articles/10.3389/fmicb.2025.1603770/full#supplementary-material

SUPPLEMENTARY TABLE 1
Sample metadata and Pathology.

SUPPLEMENTARY TABLE 2
Bacteriophages identified in *Streptococcus pluranimalium* strains.

References

Alanjary, M., Steinke, K., and Ziemert, N. (2019). AutoMLST: an automated web server for generating multi-locus species trees highlighting natural product potential. *Nucleic Acids Res.* 47, W276–W282. doi: 10.1093/nar/gkz282

Ananieva, M., Faustova, M., Loban, G., Avetikov, D., Tkachenko, P., Bobyr, V., et al. (2023). Biological properties of *Streptococcus pluranimalium* as the new human pathogen. Open access Macedonian. *J. Med. Sci.* 11, 53–57. doi: 10.3889/oamjms.2023.10990

Antikainen, J., Kuparinen, V., Lähteenmäki, K., and Korhonen, T. K. (2007). Enolases from gram-positive bacterial pathogens and commensal lactobacilli share functional similarity in virulence-associated traits. *FEMS Immunol. Med. Microbiol.* 51, 526–534. doi: 10.1111/j.1574-695X.2007.00330.x

Aryasinghe, L., Sabbar, S., Kazim, Y., Awan, L. M., and Khan, H. K. (2014). *Streptococcus pluranimalium*: a novel human pathogen? *Int. J. Surg. Case Rep.* 5, 1242–1246. doi: 10.1016/j.ijscr.2014.11.029

Athey, T. B., Teatero, S., Takamatsu, D., Wasserscheid, J., Dewar, K., Gottschalk, M., et al. (2016). Population structure and antimicrobial resistance profiles of *Streptococcus suis* serotype 2 sequence type 25 strains. *PLoS One* 11:e0150908. doi: 10.1371/journal.pone.0150908

Bank, N. C., Singh, V., and Rodriguez-Palacios, A. (2022). Classification of Parabacteroides distasonis and other Bacteroidetes using O-antigen virulence gene: Rfb A-typing and hypothesis for pathogenic vs. probiotic strain differentiation. *Gut Microbes* 14:1997293. doi: 10.1080/19490976.2021.1997293

Barkallah, M., Gharbi, Y., Hassena, A. B., Slima, A. B., Mallek, Z., Gautier, M., et al. (2014). Survey of infectious etiologies of bovine abortion during mid-to late gestation in dairy herds. *PLoS One* 9:e91549. doi: 10.1371/journal.pone.0091549

Buathong, R., Joyjinda, Y., Rodpan, A., Yomrat, S., Ponpinit, T., Ampoot, W., et al. (2021). "*Streptococcus pluranimalium* strain Colony 612 chromosome". (NCBI Accession No. NZ_CP078544). Available at: https://www.ncbi.nlm.nih.gov/nuccore/NZ_CP078544

Cantalapiedra, C. P., Hernández-Plaza, A., Letunic, I., Bork, P., and Huerta-Cepas, J. (2021). eggNOG-mapper v2: functional annotation, Orthology assignments, and domain prediction at the metagenomic scale. *Mol. Biol. Evol.* 38, 5825–5829. doi: 10.1093/molbev/msab293

De Coster, W., D'Hert, S., Schultz, D. T., Cruts, M., and Van Broeckhoven, C. (2018). Nano pack: visualizing and processing long-read sequencing data. *Bioinformatics* 34, 2666–2669. doi: 10.1093/bioinformatics/bty149

Forsgren, N., Lamont, R. J., and Persson, K. (2010). Two intramolecular isopeptide bonds are identified in the crystal structure of the *Streptococcus gordonii* SspB C-terminal domain. *J. Mol. Biol.* 397, 740–751. doi: 10.1016/j.jmb.2010.01.065

Foster, G., Barley, J., Howie, F., Falsen, E., Moore, E., Twomey, D. F., et al. (2008). *Streptococcus pluranimalium* in bovine reproductive disease. *Vet. Rec.* 163:638. doi: 10.1136/vr.163.21.638

Galperin, M. Y., Makarova, K. S., Wolf, Y. I., and Koonin, E. V. (2014). Expanded microbial genome coverage and improved protein family annotation in the COG database. *Nucleic Acids Res.* 43, D261–D269. doi: 10.1093/nar/gku1223

Ghazvini, K., Karbalaei, M., Kianifar, H., and Keikha, M. (2019). The first report of *Streptococcus pluranimalium* infection from Iran: a case report and literature review. *Clin Case Rep* 7, 1858–1862. doi: 10.1002/ccr3.2374

Guo, J., Bolduc, B., Zayed, A. A., Varsani, A., Dominguez-Huerta, G., Delmont, T. O., et al. (2021). VirSorter2: a multi-classifier, expert-guided approach to detect diverse DNA and RNA viruses. *Microbiome* 9:37. doi: 10.1186/s40168-020-00990-y

Hecker, Y. P., González-Ortega, S., Cano, S., Ortega-Mora, L. M., and Horcajo, P. (2023). Bovine infectious abortion: a systematic review and meta-analysis. *Front Vet Sci* 10:1249410. doi: 10.3389/fvets.2023.1249410

Hewinson, R. G., Griffiths, P. C., Bevan, B. J., Kirwan, S. E., Field, M. E., Woodward, M. J., et al. (1997). Detection of *Chlamydia psittaci* DNA in avian clinical samples by polymerase chain reaction. *Vet. Microbiol.* 54, 155–166. doi: 10.1016/s0378-1135(96)01268-0

Holman, D. B., Gzyl, K. E., and Kommadath, A. (2024). Florfenicol administration in piglets co-selects for multiple antimicrobial resistance genes. *mSystems* 9, e0125024–e0101224. doi: 10.1128/msystems.01250-24

Huerta-Cepas, J., Szklarczyk, D., Heller, D., Hernández-Plaza, A., Forslund, S. K., Cook, H., et al. (2018). eggNOG 5.0: a hierarchical, functionally and phylogenetically annotated orthology resource based on 5090 organisms and 2502 viruses. *Nucleic Acids Res.* 47, D309–D314. doi: 10.1093/nar/gky1085

Kolmogorov, M., Yuan, J., Lin, Y., and Pevzner, P. A. (2019). Assembly of long, error-prone reads using repeat graphs. *Nat. Biotechnol.* 37, 540–546. doi: 10.1038/s41587-019-0072-8

Liu, B., Zheng, D., Zhou, S., Chen, L., and Yang, J. (2022). VFDB 2022: a general classification scheme for bacterial virulence factors. *Nucleic Acids Res.* 50, D912–d917. doi: 10.1093/nar/gkab1107

McArthur, A. G., Waglechner, N., Nizam, F., Yan, A., Azad, M. A., Baylay, A. J., et al. (2013). The comprehensive antibiotic resistance database. *Antimicrob. Agents Chemother.* 57, 3348–3357. doi: 10.1128/aac.00419-13

Mee, J. F. (2023). Invited review: bovine abortion-incidence, risk factors and causes. *Reprod. Domest. Anim.* 58, 23–33. doi: 10.1111/rda.14366

ONT (2024). Medaka [Online]. Github. Available online at: https://github.com/nanoporetech/medaka (Accessed June, 2022).

Pan, Y., An, H., Fu, T., Zhao, S., Zhang, C., Xiao, G., et al. (2018). Characterization of *Streptococcus pluranimalium* from a cattle with mastitis by whole genome sequencing and functional validation. *BMC Microbiol.* 18:182. doi: 10.1186/s12866-018-1327-0

Pierre, M. S. (2017). VISTA on the Agri-food industry and the farm community Changes in Canadians' preferences for milk and dairy products. Oxford University Press: Nucleic Acids Research.

Purves, J., Cockayne, A., Moody, P. C., and Morrissey, J. A. (2010). Comparison of the regulation, metabolic functions, and roles in virulence of the glyceraldehyde-3-phosphate dehydrogenase homologues gapA and gapB in *Staphylococcus aureus*. *Infect. Immun.* 78, 5223–5232. doi: 10.1128/iai.00762-10

Robertson, J., and Nash, J. H. E. (2018). MOB-suite: software tools for clustering, reconstruction and typing of plasmids from draft assemblies. *Microb Genom* 4:e000206. doi: 10.1099/mgen.0.000206

Rodriguez Campos, S., Gobeli Brawand, S., Brodard, I., Rychener, L., and Perreten, V. (2018). "*Streptococcus pluranimalium* strain 14A0014 chromosome, complete genome". (NCBI Accession No. CP022601). Available at: https://www.ncbi.nlm.nih.gov/nuccore/CP022601

Schwengers, O., Jelonek, L., Dieckmann, M. A., Beyvers, S., Blom, J., and Goesmann, A. (2021). Bakta: rapid and standardized annotation of bacterial genomes via alignment-free sequence identification. *Microb Genom* 7:000685. doi: 10.1099/mgen.0.000685

Seemann, T. (2020). ABRicate [Online]. Github. Available online at: https://github.com/tseemann/abricate (Accessed September, 2023).

Simão, F. A., Waterhouse, R. M., Ioannidis, P., Kriventseva, E. V., and Zdobnov, E. M. (2015). BUSCO: assessing genome assembly and annotation completeness with single-copy orthologs. *Bioinformatics* 31, 3210–3212. doi: 10.1093/bioinformatics/btv351

Thurmond, M. C., Branscum, A. J., Johnson, W. O., Bedrick, E. J., and Hanson, T. E. (2005). Predicting the probability of abortion in dairy cows: a hierarchical Bayesian logistic-survival model using sequential pregnancy data. *Prev. Vet. Med.* 68, 223–239. doi: 10.1016/j.prevetmed.2005.01.008

Twomey, D. F., Carson, T., Foster, G., Koylass, M. S., and Whatmore, A. M. (2012). Phenotypic characterisation and 16S rRNA sequence analysis of veterinary isolates of *Streptococcus pluranimalium*. *Vet. J.* 192, 236–238. doi: 10.1016/j.tvjl.2011.05.007

Wick, R. (2018). Porechop [Online]. Github. Available online at: https://github.com/rrwick/Porechop (Accessed June, 2022).

Wu, T., Zhao, Z., Zhang, L., Ma, H., Lu, K., Ren, W., et al. (2011). Trigger factor of *Streptococcus suis* is involved in stress tolerance and virulence. *Microb. Pathog.* 51, 69–76. doi: 10.1016/j.micpath.2010.10.001

Xu, C. W., Zhou, X., Zhang, X. L., Zhou, Q., Qi, H. X., Li, Y. X., et al. (2023). Whole genome sequence of *Streptococcus pluranimalium* SP21-2, a porcine strain harbouring optr a and lsa (E) with chromosomal location. *J. Glob. Antimicrob. Resist.* 35, 101–103. doi: 10.1016/j.jgar.2023.09.007

Zhu, Y. (2023). *Streptococcus pluranimalium* strain SP28 chromosome, complete genome. (NCBI Accession No. CP121201). Available at: https://www.ncbi.nlm.nih.gov/nuccore/CP121201

frontiers | Frontiers in Microbiology

TYPE Original Research
PUBLISHED 24 June 2025
DOI 10.3389/fmicb.2025.1631008

OPEN ACCESS

EDITED BY
Lei Deng,
Chinese Academy of Agricultural Sciences, China

REVIEWED BY
Yuwen Dong,
University of Pennsylvania, United States
Qiangde Duan,
Yangzhou University, China
Alaa A. Ghazy,
National Research Centre (Egypt), Egypt
Chen Yuan,
Hebei Agricultural University, China

*CORRESPONDENCE
Tonglei Wu
532966952@163.com

RECEIVED 19 May 2025
ACCEPTED 03 June 2025
PUBLISHED 24 June 2025

CITATION
Zhang L, Chen Y, Yan Z, Li Y, Yang X, Chen L, Zhang Y, Chen Y, Li Y, Shi Q and Wu T (2025) PipC affects the virulence of *Salmonella enterica* serovar *Enteritidis* and its deletion strain provides effective immune protection in mice.
Front. Microbiol. 16:1631008.
doi: 10.3389/fmicb.2025.1631008

PipC affects the virulence of *Salmonella enterica* serovar *Enteritidis* and its deletion strain provides effective immune protection in mice

Lu Zhang[1], Yubin Chen[1], Zhigang Yan[2], Yuntai Li[1], Xiaowen Yang[3], Li Chen[1], Yanying Zhang[1], Yingyu Chen[4], Yonghui Li[5], Qiumei Shi[1] and Tonglei Wu[1]*

[1]Hebei Provincial Key Laboratory of Preventive Veterinary Medicine, Hebei Normal University of Science and Technology, Qinhuangdao, China, [2]Hebei Provincial Center for Livestock Breeding Improvement, Shijiazhuang, China, [3]Key Laboratory of Animal Biosafe Risk Prevention and Control (North), Ministry of Agriculture and Rural Affairs, Institute of Animal Science, Chinese Academy of Agricultural Sciences, Beijing, China, [4]College of Animal Medicine, Huazhong Agricultural University, Wuhan, China, [5]The Second Hospital of Qinhuangdao, Qinhuangdao, China

Background: Salmonellosis caused by *Salmonella* sp. is a foodborne zoonotic disease that poses a significant threat to public health security. Vaccination is a safe and effective strategy for preventing and controlling *Salmonella* infections. PipC is a chaperone protein associated with *Salmonella* invasion proteins which is crucial for bacteria to invade host cells.

Methods: In this study, a Δ*pipC* mutant strain was generated. Subsequently, we examined the environmental stress tolerance of the mutant strain through *in vitro* simulation experiments. Moreover, its virulence by employing cell and mouse infection models was investigated. Furthermore, we utilized a mouse model to further explore its potential as an attenuated live vaccine against *Salmonella enterica* serovar *Enteritidis* infection.

Results: The *Salmonella* strain C50336 with a deletion of the *pipC* gene exhibits a significant reduction in its ability to resist environmental stress and virulence. Meanwhile, the expression levels of SPI-1-related genes (*invH*, *sipA*, *sipB*, *sipC*, *sopB*, and *sopE2*) and SPI-2-related genes (*spvB*, *ssrA*, *orf245*, *ssaS*, *ssaT*, *ssaU*, *sseB*, and *sseD*) encoding the *Salmonella* type III secretion system (T3SS) were found to be decreased, leading to a significant reduction in the bacteria's invasion and intracellular survival abilities. The results of the mouse intraperitoneal challenge experiment showed that compared with the wild-type strain, the 50% lethal dose (LD_{50}) of the Δ*pipC* strain increased by 47 times, and the bacterial loads in the liver, spleen, and cecum were significantly reduced. When mice were immunized with the Δ*pipC* mutant strain, the immunized mice showed a robust immune response, with significantly increased cytokine and antibody levels in their bodies. Mice vaccinated with the Δ*pipC* mutant strain had 100% immune protection against wild-type *Salmonella* infection.

Conclusion: This study demonstrates that lack of *pipC* affects *SE* pathogenicity by decreasing its virulence both *in vitro* and *in vivo*. Vaccination of mice with Δ*pipC* conferred development of an acquired immunity and efficacious protection against experimental systemic infection. These results indicated that

the Δ*pipC* mutant strain can be used in the development of attenuated live vaccines.

KEYWORDS

***Salmonella enterica* serovar *Enteritidis*, PipC, virulence, immune protection, vaccine**

Background

Salmonella is a facultative intracellular pathogen that belongs to the Gram-negative category and exhibits a remarkable ability to infect a diverse range of animals, including humans. This broad host range not only poses a severe threat to the healthy development of the global aquaculture industry but also undermines public health safety, resulting in substantial economic losses in various aspects (Ferrari et al., 2019). Among these, *Salmonella enteritidis* (*SE*) and *Salmonella* Typhimurium are the main serotypes that infect humans, accounting for approximately 40% of human salmonellosis cases (Cao et al., 2023). The transmission routes of *SE* to humans are diverse. It can be contracted through the consumption of contaminated food products such as pork, beef, poultry, and eggs. Additionally, in areas with poor sanitation where fecal matter exposure is more likely, the risk of human infection also increases significantly. Once infected, humans may experience a series of symptoms, including abdominal pain, diarrhea, nausea, vomiting, fever, and headaches, which can greatly affect their quality of life and overall health (Guard-Petter, 2001).

Antibiotics are commonly used to treat *Salmonella* infections, but their overuse leads to environmental pollution and accelerates the rise of multidrug-resistant strains. This not only reduces treatment effectiveness but also poses a significant threat to public health. In this context, vaccination has emerged as another crucial measure for the prevention and control of *Salmonella* infections, as emphasized by Ruvalcaba-Gómez et al. (2022) and Acevedo-Villanueva et al. (2021). Given the facultative intracellular nature of *Salmonella*, strong cellular immunity plays a vital role in clearing the pathogen. As a result, attenuated live vaccines are generally considered to offer more effective immune protection compared to other types of vaccines, as demonstrated by the research of Lin et al. (2017) and Jiang et al. (2022). Moreover, previous studies have shown that attenuated live vaccines of *Salmonella* have relatively low virulence to the host. They are capable of inducing a robust and long-lasting mucosal and humoral immune response, as pointed out by Tennant and Levine (2015). This immune response can effectively reduce bacterial adhesion and colonization within the host organism.

Currently, numerous *Salmonella* gene knockout strains have been utilized as live vaccines. For instance, Zhao et al. (2024) found in 2024 that immunizing mice with a *Salmonella* strain with the *pal* gene deleted could stimulate good immune protection. Zhang et al. (2024, 2025) found that an attenuated *Salmonella enterica* vaccine with *mcpC* and *cheV* gene knockouts was able to stimulate 100% immune protection in mice. In addition, Yin et al. (2022) and Kamble and Lee (2016) also demonstrated that attenuated vaccines prepared by deleting virulence genes such as *cpxR*, *lon*, and SPI2 were effective in reducing the colonization of wild-type strains in chickens and provided good immune protection. Overall, the exploration and improvement of *Salmonella* attenuated live vaccines based on gene deletion, are of great significance for safeguarding public health and promoting the sustainable development of the aquaculture industry. *Salmonella* Pathogenicity Island 5 (SPI-5) plays a critical role in the enteropathogenicity of *Salmonella*. It encodes five proteins, namely PipA, PipB, PipC, PipD, and SopB, that are involved in mucosal secretion and inflammatory responses in the intestine. These proteins are regulated by the type III secretion systems (T3SS) encoded by SPI-1 and SPI-2 (Wang et al., 2020). Devendra H. Shah et al. reported that *sopB* and *pipB/C* are co-regulated with SPI-1 and promote host cell invasion, suggesting that *pipC* may contribute to the invasive capacity of *Salmonella* (Darwin et al., 2001; Rodríguez-Escudero et al., 2011). Previous studies have shown that deletion of SPI-5 reduces the ability of *SE* to colonize the chicken intestine (Rychlik et al., 2009; Shah et al., 2012). Furthermore, *pipC* has been implicated in the folding of key virulence factors, including the T3SS effector protein SopB. Additionally, literature reports indicate that the expression level of *pipC* is significantly reduced in macrophages compared to bacteria in the early stationary phase (ESP) under *in vitro* conditions, suggesting a potential role of *pipC* in intracellular survival within macrophages. Taken together, these findings indicate that *pipC* may influence the virulence of *SE*, though further experimental validation is required.

To further elucidate the role of *pipC* in *Salmonella* infection and its contribution to immunoprotection, this study aims to construct a *pipC* gene deletion mutant of *SE*. The effects of this gene deletion on bacterial virulence will be evaluated through both *in vitro* and *in vivo* assays, and the immunoprotective efficacy of the deletion strain will be assessed in a mouse model.

Materials and methods

Bacterial strains, plasmids and cells

The bacterial strains and plasmids used in this study are shown in Table 1. *Salmonella enterica* serovar *Enteritidis* C50336 was the wild-type strain and used for constructing the Δ*pipC* mutant. The Δ*pipC* strain in this study was constructed following the *λ*-Red recombinase gene replacement method (Datsenko and Wanner, 2000). The primer sequences used for generating and confirming mutant strains are listed in Table 2. All bacterial strains were cultured on Luria-Bertani (LB) agar plates or in LB broth with necessary antibiotics at appropriate concentrations (for example, 100 μg/mL ampicillin and 34 μg/mL chloramphenicol) (Xiong et al., 2023).

Human epithelial Caco-2 BBE cells and mouse macrophage RAW264.7 cells used in this study were provided by BeNa Culture Collection (Shanghai, China). Both cell types were cultured in DMEM

10.3389/fmicb.2025.1631008

TABLE 1 Strains and plasmids used in this study.

Strains or plasmids	Characteristics	Source
Strain		
C50336	*Salmonella enterica* serovar *Enteritidis*, wild-type	This study
Δ*pipC*:*cat*	A first recombination strain	
Δ*pipC*	A second recombination strain	
Δ*pipC* + *pipC*	Δ*pipC*-complemented strain	
Plasmids		
pKD3	Cm^R, *cat*, FRT	The Key Laboratory of Preventive Veterinary Medicine, Hebei Province
pKD46	Amp^R, encodes lambda red genes (exo, beta, gam), arabinose-inducible promoter for expression (ParaB)	
pCP20	Amp^R and Cm^R, encode FLP recombinase	
pBR322	Amp^R and Tet^R	

(Thermo Fisher Scientific Co., Ltd.) supplemented with 10% fetal bovine serum (Thermo Fisher Scientific Co., Ltd.). Antibiotics were added as necessary, such as 50 μg/mL streptomycin and 50 U/mL penicillin, or 50 μg/mL gentamicin, in an incubator with 5% CO_2.

Experimental animals and ethical statement

Kunming (KM) mice were obtained from Beijing Speifu Biotechnology Co., Ltd. Throughout the experiment, the mice were maintained in a sterile environment under standard housing conditions with an ambient temperature consistently kept at 22.0 ± 0.5°C and relative humidity maintained at 60 ± 10%. A 12-h light/dark cycle was established for the housing conditions. All animal experiments were conducted in full compliance with international ethical standards and the Experimental Animal Regulation Ordinances (HPDST 2020-17) stipulated by the Hebei Provincial Department of Science and Technology. The study protocol was reviewed and approved by the Animal Care and Use Committee of Hebei Normal University of Science and Technology.

Construction of *pipC* gene deletion and complementation strains of *SE*

The *pipC* gene deletion strain in this study was constructed using the λ homologous recombination method (Supplementary Figure 1). Briefly, the auxiliary plasmid pKD46 was introduced into C50336 through electroporation, which encodes the Gam, Exo, and Beta proteins required for λ homologous recombination. Using pKD3 as a template, the knockout fragments were amplified by P1 and P2. The knockout fragment was then introduced into C50336 containing pKD46 via electroporation, resulting in a primary recombinant strain with chloramphenicol resistance. This strain was selected using LB agar plates containing chloramphenicol and verified using primers P3 and P4. The positive strain obtained was named Δ*pipC*:*cat*. The pCP20 plasmid, which encodes the Flp recombinase, was able to excise the *cat* gene from the knockout fragment. The pCP20 plasmid was introduced into Δ*pipC*:*cat* by electroporation, resulting in a secondary recombinant strain. This strain was verified using primers P3 and P4. The positive strain obtained was named Δ*pipC*.

To construct the complement strain, the nucleic acids of C50336 were used as a template, and the complement fragment was amplified using P5 and P6. The complement fragment and pBR322 vector plasmid were digested with restriction endonucleases *BamH I* and *Sal I*, respectively. The two digested fragments were ligated using T4 DNA ligase. The recombinant vector was introduced into Δ*pipC* by electroporation and verified with P7 and P8. The positive strain was named Δ*pipC* + *pipC*.

Genetic stability testing

To determine the genetic stability of the Δ*pipC*, it was serially passaged 40 times in LB medium, every 12 h. Nucleic acids from liquid cultures are extracted every other generation and PCR verification using P3 and P4.

Growth characteristics assay

The overnight cultures of C50336, Δ*pipC*, and Δ*pipC* + *pipC* were subcultured at a 1:100 ratio into 5 mL of LB liquid medium and incubated at 37°C in a shaking incubator. Growth was determined by monitoring the absorbance of bacterial cultures at 600 nm (OD_{600} values). Growth curves were plotted based on the growth of each strain at different time points.

In vitro stress simulation experiments

Overnight cultures of C50336, Δ*pipC*, and Δ*pipC* + *pipC* were washed three times with PBS and resuspended in the original volume. The bacterial counts before stress were determined using the traditional plate count method. The bacterial suspensions were exposed to acid stress (pH 3.5), alkaline stress (pH 10.0), and heat stress (42°C) for 1 h, as well as to oxidative stress (10 mmol/L H_2O_2) for 30 min. After stress exposure, the bacterial counts were determined. The survival rate of

10.3389/fmicb.2025.1631008

TABLE 2 Primers used for the construction of the *pipC* deletion mutant and complemented strain.

Primers	Sequence (5′–3′)	Product length (bp)	Purpose
P1	TTGGCAGTCAGTAAAAGGCATTTCTTCATTAATCACATCTTGAGTCTTGAGGTAACTATtgtgtaggctggagctgcttcg	1,135	Underline: *pipC* homologous fragment; Lowercase letters: *cat* homologous fragment
P2	TTGTAAAGGGCATACGTATCGCGTTTTATCTCATTAAGAAAGTATGTTGACGTATTAAAcatatgaatatcctccttag		
P3	TTATCGCCAGAGGTGCTCAATC	554 (no recombination)/1,229 (first recombination)/246 (secondary recombination)	Identification of Δ*pipC*
P4	GCCCCTTACATTTCCACCAAAG		
P5	CGGGATCCTTGGCAGTCAGTAAAAGG	501	Underline: enzyme cleavage site
P6	GCGTCGACCCACCAAAGATTCTGGTCT		
P7	TCGCTTCGCTACTTGGAG	593	Identification of the complemented strain
P8	AAGGAGCTGACTGGGTTG		

each strain under different conditions was calculated as follows: survival rate = (post-stress bacterial count)/(initial bacterial count).

Cell culture

The human epithelial cancer cell lines Caco-2 were cultured in Dulbecco's modified Eagle medium (DMEM) supplemented with 20% fetal bovine serum (FBS) and 1% penicillin-streptomycin solution. The mouse macrophage RAW264.7 was cultured in DMEM containing 10% FBS and 1% penicillin-streptomycin solution. When the cells reached 80% confluence, the monolayers were washed three times with PBS. The cells were then seeded in 12-well tissue culture plates at a density of 1×10^6 cells/well. The plates were incubated at 37°C in an atmosphere containing 5% CO_2.

Adherence and invasion assays

To investigate the impact of *pipC* gene deletion on the adhesion and invasion ability of *SE*, the overnight cultures of C50336, Δ*pipC* and Δ*pipC* + *pipC* were washed three times with PBS and subsequently resuspended. The number of bacteria per mL of bacterial suspension (number of infected bacteria) was measured. Following the washing of confluent cell monolayers with DMEM, C50336, Δ*pipC* and Δ*pipC* + *pipC* were inoculated, respectively, onto the Caco-2 cells at a multiplicity of infection (MOI) of 100:1 and were incubated for 1 h at 37°C under 5% CO_2 (Xiong et al., 2023).

Adhesion assay

For bacterial adhesion, the cells were washed, and then incubated with PBS containing Triton X-100 (0.5%) at 37°C for 10 min. The cell lysates were serially diluted and inoculated onto LB agar for counting. The number of bacteria per mL of cell lysate (number of adherent bacteria) was measured. The adhesion rate was calculated using the formula: Adhesion rate = (number of adherent bacteria/number of infected bacteria) × 100%.

Invasion assay

For bacterial invasion, 1 h after bacterial colonization, the cells were incubated for an additional 1 h in DMEM with gentamicin (100 μg/mL), washed and incubated with PBS containing Triton X-100 (0.5%) at 37°C for 10 min. The cell lysates were serially diluted and inoculated onto LB agar for counting. The number of bacteria per mL of cell lysate (number of invading bacteria) was measured. Invasion rate = (number of invading bacteria/number of infected bacteria) × 100%.

Intracellular proliferation assay

To evaluate the survival rate of Δ*pipC* in phagocytic cells, after infecting the cells with bacteria for 2 h as described above, DMEM containing 100 μg/

mL gentamicin was added and incubated for 1 h. One group of cells was then washed and lysed with 0.5% Triton X-100, and the intracellular bacteria were counted (intracellular bacteria at 3 h). Another group of cells was washed and incubated with DMEM containing 10 μg/mL gentamicin at 37°C for 20 h. These cells were also lysed with 0.5% Triton X-100, and the intracellular bacteria were counted (intracellular bacteria at 23 h). Intracellular survival rate = (intracellular bacteria at 23 h/intracellular bacteria at 3 h) × 100%.

Assessment of bacterial virulence

A total of 75 six-week-old KM mice were randomly divided into 15 groups ($n = 5$). These groups were categorized into three sets: five groups for the Δ*pipC*, five groups for the C50336, and the remaining five groups designated as the Δ*pipC* + *pipC* group. Mice in the Δ*pipC* groups were intraperitoneally (i.p.) inoculated with Δ*pipC* containing of 1.68×10^9, 1.68×10^8, 1.68×10^7, 1.68×10^6 or 1.68×10^5 CFU/mouse, respectively. Similarly, the C50336 groups were i.p. inoculated with C50336 containing of 2×10^7, 2×10^6, 2×10^5, 2×10^4 or 2×10^3 CFU/mouse, respectivly. The Δ*pipC* + *pipC* groups were i.p. inoculated with Δ*pipC* + *pipC* containing of 2×10^7, 2×10^6, 2×10^5, 2×10^4 or 2×10^3 CFU/mouse, respectively. Five additional mice were i.p. injected with the same volume of PBS as a negative control.

The number of dead mice was recorded for 14 days and LD_{50} was calculated, which was calculated using the formula of $\log_{10}$ [50% endpoint] = A + (B × C), where A = $\log_{10}$ [infectious dose showing a mortality next below 50%], B = difference of logarithms = [50% − (mortality at infectious dose next below 50%)]/[(mortality next above 50%) − (mortality next below 50%)], and C = $\log_{10}$ [difference between serial infectious doses used in challenge studies] (Park et al., 2022; Zhang et al., 2019).

RNA extraction and qPCR

In order to further investigate the effect of *pipC* gene deletion on the virulence of *SE*, qPCR was used to measure the expression levels of virulence genes in C50336, Δ*pipC*, and Δ*pipC* + *pipC*. In short, the bacteria were cultured to the logarithmic phase and total RNA was extracted using an RNA extraction kit (Aidlab, Beijing, China). Complementary DNA (cDNA) was synthesized using a reverse transcription kit (TOYOBO, Osaka, Japan). Primers were designed by referring to previous literature (Upadhyaya et al., 2013). The primer sequences used for qPCR are listed in Table 3. Using cDNA as a template, the relative gene expression was quantified using the comparative critical threshold (Ct) method through qPCR. Data were normalized to the endogenous control (*16S rRNA*), and the level of candidate gene expression between treated and control samples were determined. The qPCR thermal cycling conditions were as follows: initial denaturation at 95°C for 10 min, followed by 40 cycles of 95°C for 15 s and 60°C for 1 min.

Bacterial colonization assay

Thirty mice were randomly divided into two groups ($n = 15$). One group was intraperitoneally injected with 1×10^4 CFU/mouse of Δ*pipC*, while the other group received an equal dose of C50336. Additionally, three mice were injected with 200 μL of PBS as a negative control. At predetermined time points (3 days, 7 days, and 14 days), five mice from each group were randomly selected and euthanized. Their spleens, livers, and cecums were collected, homogenized in PBS, and subsequently serially diluted before being evenly spread on XLT4 agar. The number of CFUs for each sample was determined 12 h later. For this animal study, all mice were anesthetized using a 20% urethane (ethyl carbamate) solution, and every effort was made to ensure humane treatment of the animals.

Vaccination schedules of oral attenuated live vaccine and sample collection

Twenty-four female KM mice, aged 8 weeks, were randomly divided into two groups ($n = 12$): an immunization group and a

TABLE 3 The qPCR primers of virulence genes.

Primers	Sequence (5′–3′)
16S-F	CCAGGGCTACACACGTGCTA
16S-R	TCTCGCGAGGTCGCTTCT
invH-F	CCCTTCCTCCGTGAGCAAA
invH-R	TGGCCAGTTGCTCTTTCTGA
orf245-F	CAGGGTAATATCGATGTGGACTACA
orf245-R	GCGGTATGTGGAAAACGAGTTT
sipA-F	CAGGGAACGGTGTGGAGGTA
sipA-R	AGACGTTTTTGGGTGTGATACGT
sipB-F	GCCACTGCTGAATCTGATCCA
sipB-R	CGAGGCGCTTGCTGATTT
ssrA-F	CGAGTATGGCTGGATCAAAACA
ssrA-R	TGTACGTATTTTTTGCGGGATGT
spvB-F	TGGGTGGGCAACAGCAA
spvB-R	GCAGGATGCCGTTACTGTCA
ssaS-F	CGCAACTTTTATGGATCGTC
ssaS-R	TGTAGCGTTTGGTCCTGTATT
sipC-F	TCTGGCAAATAATGTCACGA
sipC-R	CGCTCTGGGAAATACTACCG
sopB-F	ACCCGCCTGGAATTGTAA
sopB-R	GAAAGATTGAGCACCTCTGG
ssaT-F	TGCTTATGTCACTTACCTTTCC
ssaT-R	AATATCGTACCCATTGTCGC
ssaU-F	TATTGCGGTTTGTCTTGGC
ssaU-R	GGGATGCAGTTGCGTTCA
sseB-F	CTTATCCCAGCAAAATCCG
sseB-R	TTAGCAATCACCTCATCCATCT
sseD-F	CTTCTTCCACTCCATCTCCC
sseD-R	CGTCTGTAAAACATTGACTTGC
sopE2-F	TAACACTATCCACCCAGCACT
sopE2-R	TTAATACCGCCCTACCCTC

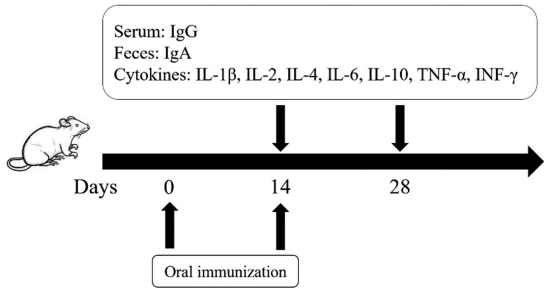

FIGURE 1
The vaccination scheme and detection protocol designed in this study.

control group. On day 0, the immunization group received an oral administration of 1×10^6 CFU of Δ*pipC*, whereas the control group was orally administered 200 μL of PBS. A booster immunization with an identical dose was given to the immunization group on day 14 dpi, while the control group received an equivalent volume of PBS.

At 14 dpi and 28 dpi, 6 mice from each group were randomly euthanized, and spleens were collected for splenic lymphocyte stimulation test and detection of cytokine expression levels. Additionally, serum and feces were collected from 3 mice for IgG and SIgA detection. The vaccination regimen of this study is shown in Figure 1.

Salmonella soluble antigen preparation

C50336 was cultivated overnight at 37°C, 180 rpm with shaking until it reached the logarithmic phase. The bacteria were centrifuged at a speed of 13,000 × g at 4°C, washed three times with PBS, and resuspended in PBS to a concentration of 1×10^{10} CFU/mL. Use SCIENTZ ultrasonic homogenizer (SCIENTZ-IID, Ningbo, China) to sonicate the cells and centrifuge the 13,000 × g sample at 4°C to granulate the fragments. The sample was sterilized through a 0.22 μm PES (polyethersulfone) filter (Merck, Darmstadt, Germany) (Ji et al., 2022).

Splenic lymphocytes stimulation test

Lymphocytes were isolated from each group of three spleen samples at 14 and 28 dpi. After Trypan blue dye exclusion testing, suspensions of splenic mononuclear cells (1×10^7 cells/well) were cultured in Roswell Park Memorial Institute 1,640 medium (RPMI-1640) supplemented with 10% FBS and 100 μg/mL penicillin-streptomycin within 96-well tissue culture plates. These cultures were then incubated with 10 μg/mL soluble antigen or without any stimulant as a negative control, under conditions of 37°C and 5% CO_2 for a duration of 72 h. Lymphocyte proliferation was measured using an MTT kit (Beyotime, Shanghai, China). The cell proliferation was expressed as the stimulation index (SI), which was calculated using the equation: SI = (OD_{570} of the antigen-stimulated cells)/(OD_{570} of the unstimulated cells) (Kang et al., 2021).

TABLE 4 The qPCR primers of cytokines.

Primers	Sequence (5′–3′)
gapdh-F	AGGTCGGTGTGAACGGATTTG
gapdh-R	TGTAGACCATGTAGTTGAGGTCA
β-actin-F	TTCAACACCCCAGCCATG
β-actin-R	CCTCGTAGATGGGCACAGT
IL-1β-F	GACTGTTTCTAATGCCTTCCC
IL-1β-R	ATGGTTTCTTGTGACCCTGA
IL-2-F	TGAGCAGGATGGAGAATTACAGG
IL-2-R	GTCCAAGTTCATCTTCTAGGCAC
IL-4-F	GGTCTCAACCCCCAGCTAGT
IL-4-R	GCCGATGATCTCTCTCAAGTGAT
IL-6-F	TAGTCCTTCCTACCCCAATTTCC
IL-6-R	TTGGTCCTTAGCCACTCCTTC
IL-10-F	CTTACTGACTGGCATGAGGATCA
IL-10-R	GCAGCTCTAGGAGCATGTGG
IFN-γ-F	ATGAACGCTACACACTGCATC
IFN-γ-R	CCATCCTTTTGCCAGTTCCTC
TNF-α-F	CCCTCACACTCAGATCATCTTCT
TNF-α-R	GCTACGACGTGGGCTACAG

The expression of cytokines in the spleen

Quantitative real-time PCR (qPCR) was employed to assess the mRNA expression levels of splenic cytokines, including IL-1β, IL-2, IL-4, IL-6, IL-10, TNF-α, and IFN-γ, at 14 and 28 days post-immunization (dpi). Total RNA was extracted from spleen tissues using Triquick Reagent (Solarbio, Beijing, China), and first-strand cDNA was synthesized with a cDNA synthesis kit (TOYOBO, Osaka, Japan). Samples were stored at −80°C until further use. qPCR was performed using the Ultra SYBR Green Mixture (CWBio, Jiangsu, China) on a Lepgen-96 Real-Time PCR System (LEpu, Lepgen-96, China). The primer sequences used for qPCR are listed in Table 4. Cytokine expression levels were normalized to the internal reference genes gapdh and β-actin, and relative expression was calculated using the $2^{-\Delta\Delta Ct}$ method (Kang et al., 2021). The thermal cycling conditions were as follows: initial denaturation at 95°C for 10 min, followed by 40 cycles of denaturation at 95°C for 15 s and annealing/extension at 60°C for 1 min.

Detection of IgG and SIgA

To examine the antibody responses, serum and feces samples were collected from 3 mice per group at 14 and 28 dpi after inoculation with the initial and booster doses of Δ*pipC*. Enzyme-linked immunosorbent assay (ELISA) was employed to quantify the serum IgG and fecal IgA (SIgA) responses against the soluble antigen derived from *SE*. For serum extraction, whole blood samples were centrifuged for 10 min at 10,000 × g at 4°C. The resultant supernatant, containing the serum, was carefully separated from the pellet and preserved at −20°C until use. To obtain the fecal supernatant, the feces samples were weighed, followed

by the addition of a 25% weight/volume (w/v) solution of fecal slurry comprised of 0.01% sodium azide, 1% protease inhibitor in PBS. The samples were homogenized by vortexing for 15 min. After centrifugation, collect the supernatant and store it at −80° C for IgA detection.

The ELISA plates were coated with *Salmonella* soluble antigen (1 μg/well) and incubated overnight at 4°C. Wells were blocked with 5% skim milk at 37°C for 2 h (200 μL/well), followed by washing three times with PBS containing 0.05% Tween-20 (PBST) (280 μL/well). Dilute the serum sample at 1:200 and add it to the well, then incubate at 4°C for 1 h (100 μL/well), and wash three times with PBST. The secondary Ab goat anti-mouse IgG-HRP diluted 1:10,000 was added (100 μL/well) (Applygen, Beijing, China). The Ab was allowed to interact with the samples for 35 min at 37°C, followed by washing three times with PBST. Add 3,3′,5,5′-tetramethylbenzidine (TMB) substrate (100 μL/well) and incubate at 37°C for 10 min. The reaction was terminated by adding 50 μL of 2 M H_2SO_4 to each well, and the absorbance was read at 450 nm in plate reader (Tecan, Shanghai, China).

For IgA, the ELISA plates were coated with 1 μg *Salmonella* soluble antigen per well and incubated overnight. Wells were blocked with 5% skim milk at 37°C for 2 h, followed by washing three times with PBST. The undiluted fecal supernatant was added to the well (100 μL/well), followed by incubated at 4°C for 1 h. The secondary Ab goat anti-mouse IgA-HRP diluted 1:10,000 was added, and the rest of the protocol was performed as described above (Emerson et al., 2022).

Immune protection assessment for the Δ*pipC*

To evaluate the immune protection of Δ*pipC*. Twenty 6-week-old female KM mice were randomly divided into 2 groups ($n = 10$), namely the vaccinated group and the unvaccinated group. The vaccinated group was orally immunized with 1×10^6 CFU/mouse of Δ*pipC*, while the unvaccinated group was orally immunized with 200 μL of PBS. In addition, another 10 mice without vaccination and challenge were used as the control group. At 14 dpi, the vaccinated mice received the same dose of Δ*pipC* for enhanced immunity. At 28 dpi, the vaccinated group and unvaccinated group were challenged with 2×10^7 CFU/mouse of C50336 by intraperitoneal injections. Deaths and clinical symptoms were recorded daily for 14 d post the challenge (dpc), and calculate the relative survival rate according to the formula: Relative survival rate = (mortality rate of the unvaccinated group − mortality rate of the vaccinated group)/mortality rate of the unvaccinated group × 100%.

Statistical analysis

Statistical analysis was conducted using GraphPad Prism 9 (GraphPad Software, CA, United States) and IBM SPSS (IBM Corporation, Armonk, NY, United States) software. Data are expressed as the mean ± standard error of the mean (SEM). All statistical analysis were two-way ANOVA and post-test. Differences between two samples were evaluated using Student's *t*-test. Significant differences are indicated with an asterisk (*), where *: $p < 0.05$, **: $0.001 < p < 0.01$, and ***: $p < 0.001$ are considered to represent statistically significant differences in mean values. ns means not significant (Kirthika et al., 2020).

Results

The Δ*pipC* and complementation strain were successfully constructed

We constructed a *pipC* gene deletion strain of *SE* by using the λ-Red homologous recombination method and constructed a complementation strain by using the pBR322 plasmid. The primers P3 and P4, P7 and P8 were used to identify Δ*pipC* and Δ *pipC* + *pipC*, respectively. As shown in Figures 2A,B, the *pipC* gene deletion strain and complementation strain have been successfully constructed.

Δ*pipC* has good genetic stability

The Δ*pipC* mutant was serially passaged 40 times in LB medium, and the presence of the *pipC* deletion was then assessed by PCR (Figure 2C). The *pipC* deletion was still detectable in the Δ*pipC* mutant strain, indicating that this strain has good genetic stability.

The *pipC* gene does not affect the growth ability of *SE*

As shown in Figure 3A, the growth characteristics of C50336, Δ*pipC* and Δ*pipC* + *pipC* in LB medium did not differ greatly. This indicated that *pipC* deletion did not influence the growth characteristics of *SE*.

The deletion of *pipC* gene weakens the resistance of *SE* to environmental stress

To investigate whether the deletion of the *pipC* gene affects the resistance of *SE* to environmental stress, the survival rates of C50336, Δ*pipC*, and Δ*pipC* + *pipC* were compared under acid stress (pH 3.5), alkaline stress (pH 10.0), oxidative stress (H_2O_2), and heat stress (42°C). The results shown in Figure 3B reveal that, compared to C50336, the survival rate of Δ*pipC* was significantly reduced under acidic, alkaline, and oxidative stress conditions, whereas no statistically significant difference was observed under heat stress conditions. Since *pipC* deletion did not affect the growth characteristics of *SE*, the reduced survival rate of the mutant strain can be attributed to the role of the *pipC* gene in enhancing resistance to acid, alkaline, and oxidative stress.

The Δ*pipC* mutant shows attenuated virulence *in vitro*

The adhesion rate and invasion rate in human epithelial Caco-2, and the intracellular survival rate in mouse macrophage RAW264.7 of Δ*pipC* and C50336 was determined. As shown in Figure 4A, the adhesion rate of bacteria was not different between C50336 and Δ*pipC* in Caco-2. However, the invasion rate in Caco-2 and the intracellular survival rate in RAW264.7 of Δ*pipC*, compared to of C50336, showed significantly reduced (Figures 4B,C). These results indicate that *SE* with *pipC* deletion shows attenuated virulence *in vitro*.

10.3389/fmicb.2025.1631008

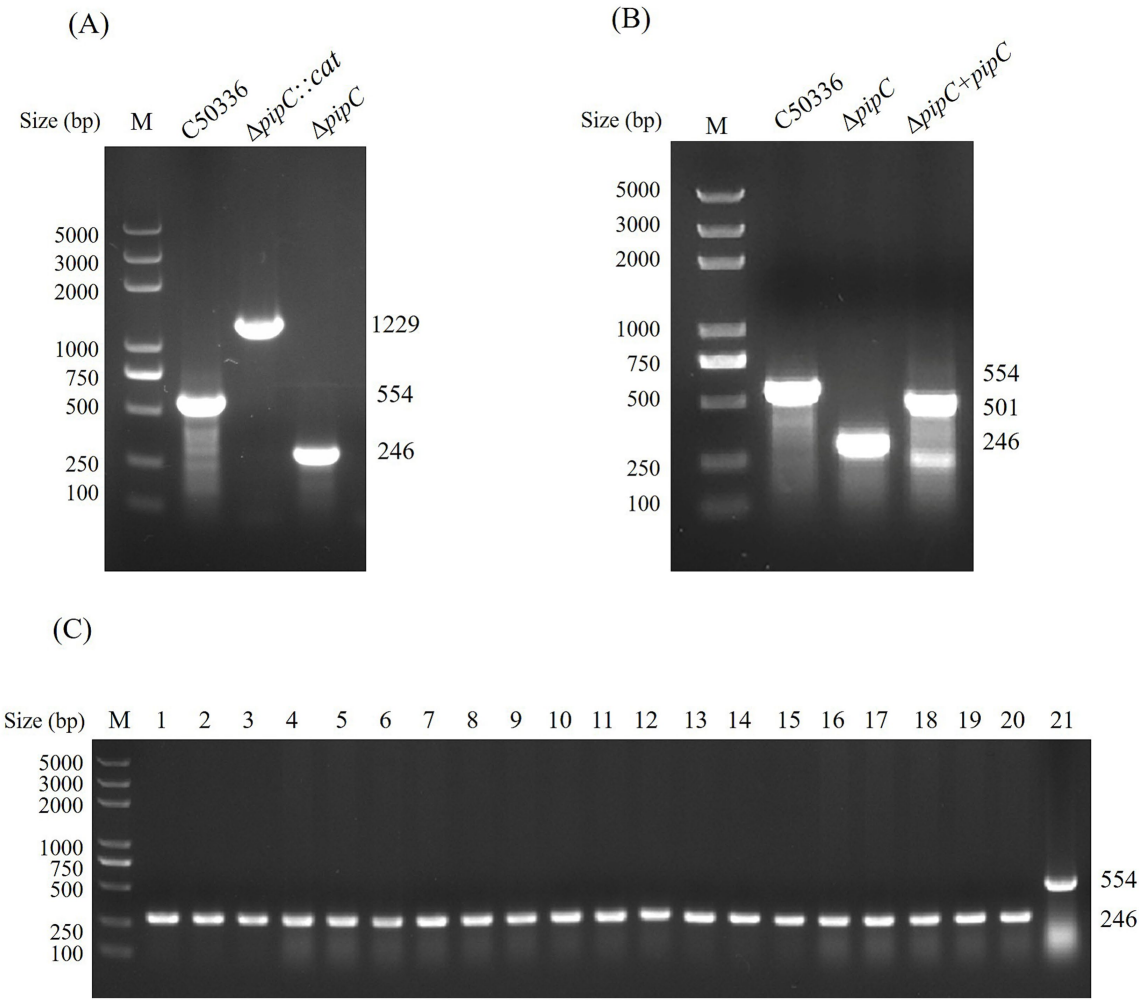

FIGURE 2
(A) PCR identification of Δ*pipC* and Δ*pipC*:*cat* mutants. The wild-type strain C50336 yields a 554 bp amplicon corresponding to the intact *pipC* gene. In contrast, the Δ*pipC* mutant produces a 246 bp fragment, while the Δ*pipC*:*cat* strain generates a 1,229 bp product. **(B)** PCR confirmation of the Δ*pipC* complemented strain. The Δ*pipC* + *pipC* strain yields a 594 bp PCR product, indicating successful complementation. **(C)** Assessment of Δ*pipC* genetic stability. Lanes 1–20 show 246 bp PCR products from sequential passages of the Δ*pipC* mutant, and lane 21 displays a 554 bp band from the wild-type C50336 strain.

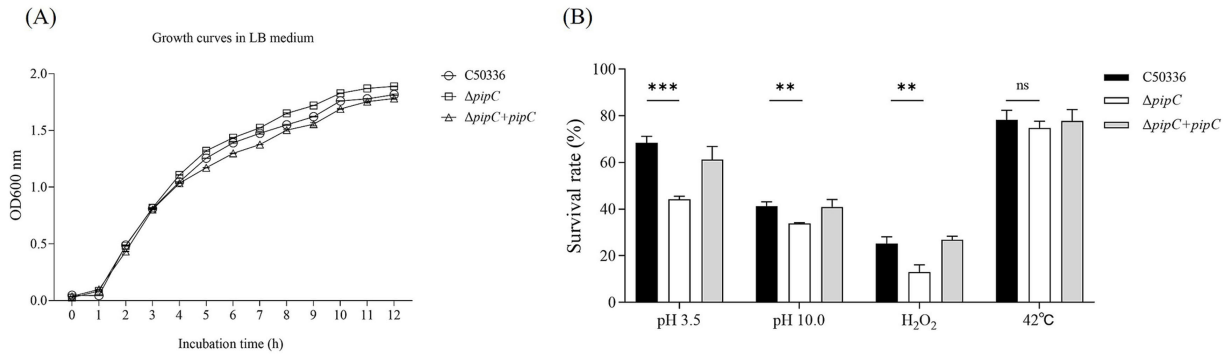

FIGURE 3
(A) Growth curves for the C50336, Δ*pipC* and Δ*pipC* + *pipC*. All strains were cultured in LB medium. **(B)** Survival rate of Δ*pipC* under different environmental stress. Data are presented as the mean ± SD of three independent replicates. Statistical significance was determined as $p < 0.01$ (**) and $p < 0.001$ (***).

10.3389/fmicb.2025.1631008

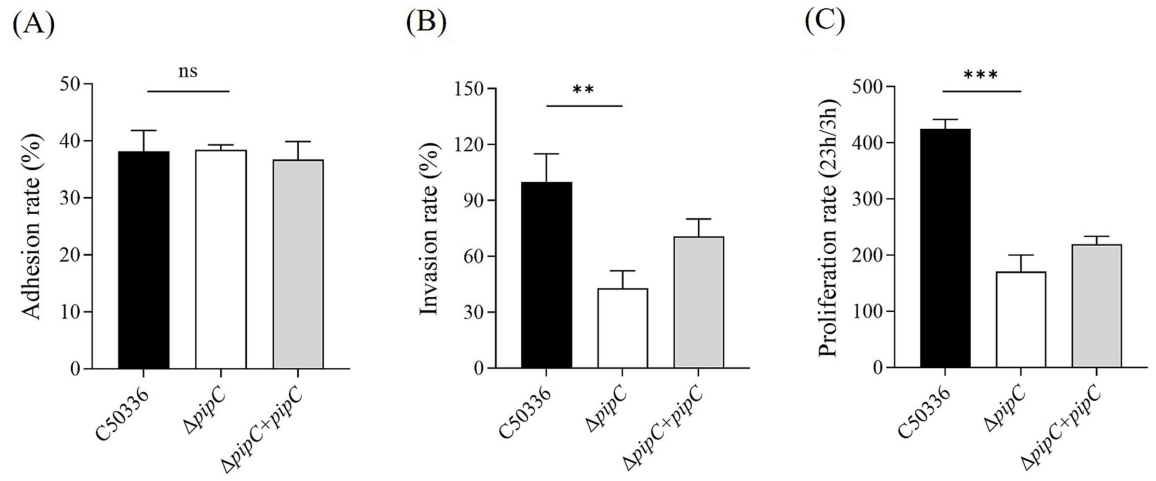

FIGURE 4
(A) Adherence and **(B)** invasion assays for C50336, Δ*pipC* and Δ*pipC* + *pipC* to Caco-2. The invasion rate of C50336 is considered to be 100%, and the invasiveness of Δ*pipC* or Δ*pipC* + *pipC* is calculated as its percentage. **(C)** Intracellular survival assay for C50336, Δ*pipC* and Δ*pipC* + *pipC* to RAW264.7. Data are presented as the mean ± SD of three independent replicates. Statistical significance was determined as $p < 0.05$ (*) and $p < 0.01$ (**).

TABLE 5 The LD_{50} of the C50336, Δ*pipC* and Δ*pipC* + *pipC* in mice.

Group	Dose (CFU/mouse)	Number of deaths/Total number of mice	LD_{50} (CFU)
C50336	2×10^7	5/5	6.32×10^5
	2×10^6	3/5	
	2×10^5	2/5	
	2×10^4	0/5	
	2×10^3	0/5	
Δ*pipC*	1.68×10^9	5/5	2.99×10^7
	1.68×10^8	4/5	
	1.68×10^7	2/5	
	1.68×10^6	0/5	
	1.68×10^5	0/5	
Δ*pipC* + *pipC*	2×10^7	5/5	1×10^6
	2×10^6	3/5	
	2×10^5	1/5	
	2×10^4	0/5	
	2×10^3	0/5	
Blank	PBS	0/5	/

The Δ*pipC* exhibits reduced virulence in a mouse model

The virulence of the Δ*pipC* and C50336 strains was evaluated in 6-week-old KM mouse after i.p. challenge. As shown in Table 5, the LD_{50} of Δ*pipC* was 2.99×10^7 CFU, which was 47-fold higher than that of the wild-type C50336 ($2.99 \times 10^7 / 6.32 \times 10^5 \approx 47$). The LD_{50} of Δ*pipC*+*pipC* is 1×10^6 CFU/mouse. The result indicated that the virulence of the Δ*pipC* was attenuated compared to the C50336.

The deletion of *pipC* results in the downregulation of multiple virulence gene expression levels in *SE*

To investigate the potential mechanism underlying the attenuation of *SE* virulence due to the deletion of the *pipC* gene, qPCR was employed to assess the expression levels of virulence factors. The results are presented in Figure 5. Compared to C50336, the expression levels of SPI-1 associated genes (*invH*, *sipA*, *sipB*, *sipC*, *sopB*, and *sopE2*) and SPI-2 associated genes (*spvB*, *ssrA*, *orf245*, *ssaS*, *ssaT*, *ssaU*,

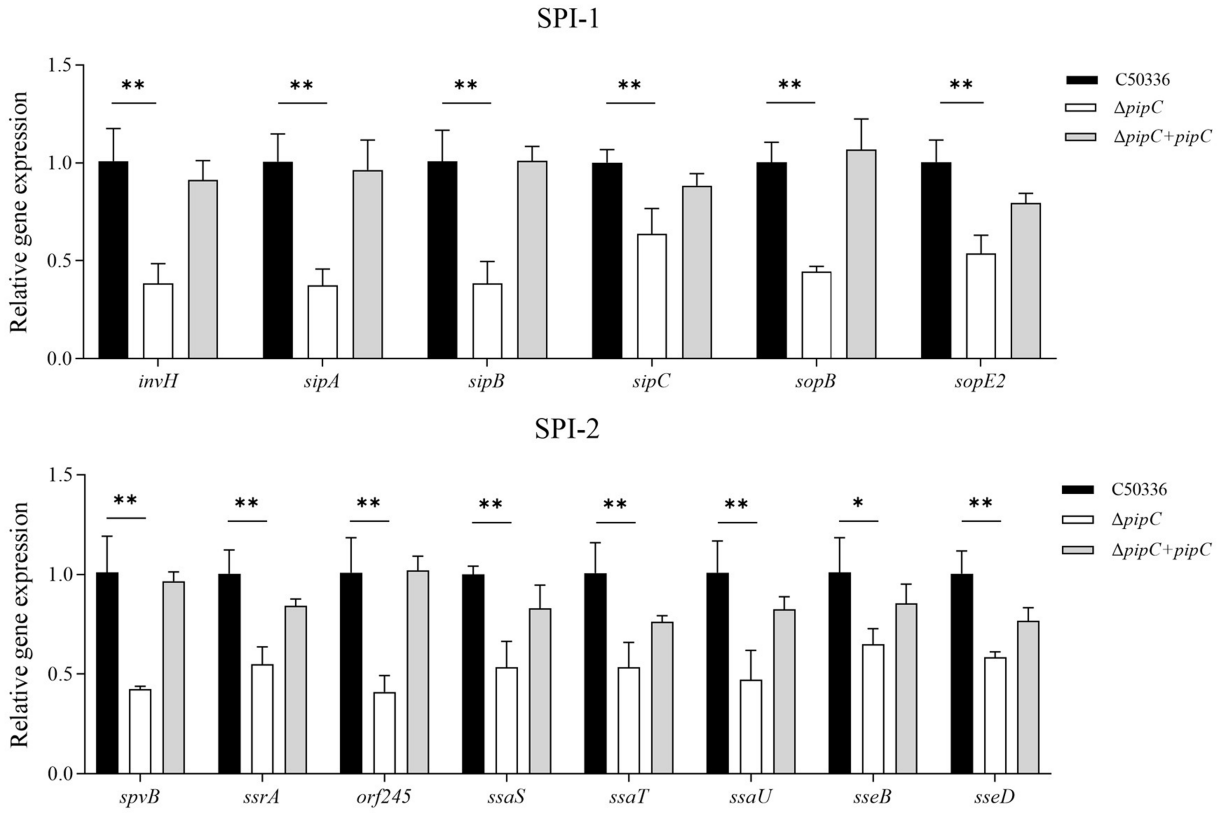

FIGURE 5
The expression level of virulence genes in C50336, Δ*pipC* and Δ*pipC* + *pipC* were detected by using qPCR, with 16*S rRNA* as the internal reference gene. Data are presented as the mean ± SD of three independent replicates. Statistical significance was determined as $p < 0.05$ (*) and $p < 0.01$ (**).

sseB, and *sseD*) in Δ*pipC* were significantly decreased. These findings suggest that *pipC* may influence the virulence of *SE* by modulating the expression levels of multiple virulence genes.

The deletion of *pipC* reduces the colonization of *SE* in organs

The results of bacteria colonization in the liver, spleen, and cecum are shown in Figure 6. All the liver, spleen and cecum samples from the blank control group were negative for *Salmonella* recovery. Bacteria could be isolated from the liver, spleen, and cecum at 3, 7, and 14 dpc. Compared to C50336, the counts of Δ*pipC* in the liver, spleen, and cecum were significantly lower at 3, 7, and 14 dpc, indicating that the colonization ability of Δ*pipC* in these organs was notably inferior to that of C50336. This suggests that the *pipC* gene can influence the colonization ability and virulence of *SE*.

Δ*pipC* can induce immune responses

To elucidate the specific immune responses to *SE* antigens following Δ*pipC* immunization, a splenic lymphocyte proliferation assay was performed using soluble antigens at 14 and 28 dpi. As shown in Figure 7A, the stimulation indices against the *SE* antigens for immunized group was 8.60 ± 0.34 at 14 dpi. Likewise, the stimulation indices against *SE* antigens for immunized group was 14.07 ± 0.51 at 28 dpi. The SI value of splenic lymphocytes in the immunized group was significantly higher than that in the control group, and the lymphocyte proliferation level further increased after enhanced immunization. These findings indicate that Δ*pipC* can induce strong specific immune responses.

To evaluate the humoral and mucosal immune responses in mice immunized with Δ*pipC*, the serum IgG and mucosal IgA responses against *SE* soluble antigens were measured by ELISA. At 14 dpi and 28 dpi, mice immunized with Δ*pipC* exhibited significantly enhanced serum IgG levels (Figure 7B) and secretory IgA (SIgA) levels (Figure 7C) compared to the control group, with further increases observed after booster immunization. These findings indicate that Δ*pipC* effectively induces robust specific humoral and mucosal immune responses, which are augmented with booster immunization.

We detected the expression of cytokines in spleen cells of immunized mice at 14 and 28 dpi. The results, shown in Figures 7D,E, revealed that at 14 dpi, the expression levels of IL-2, IL-4, IL-6, IL-10, TNF-α, and IFN-γ in the Δ*pipC* group were significantly higher than those in the control group. At 28 dpi, the expression levels of IL-2, IL-4, IL-6, IL-10, TNF-α, and IFN-γ in the Δ*pipC* group were notably higher than those in the control group. Additionally, the expression levels of IL-6 and TNF-α after the booster immunization were significantly higher than those after the primary immunization. The increased expression levels of cytokines

10.3389/fmicb.2025.1631008

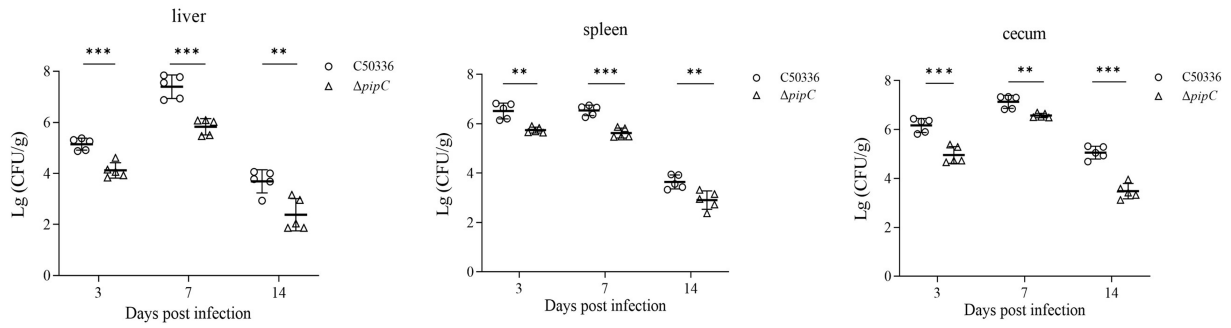

FIGURE 6
Bacterial colonization of *SE* in the liver, spleen, and cecum following challenge. Bacterial loads in these organs were quantified at the 3 dpc, 7 dpc, and 14 dpc, and results were expressed as $\log_{10}$(CFU/g). Data represents the mean ± SD from five mice. Statistical significance is indicated as $p < 0.01$ (**) and $p < 0.001$ (***).

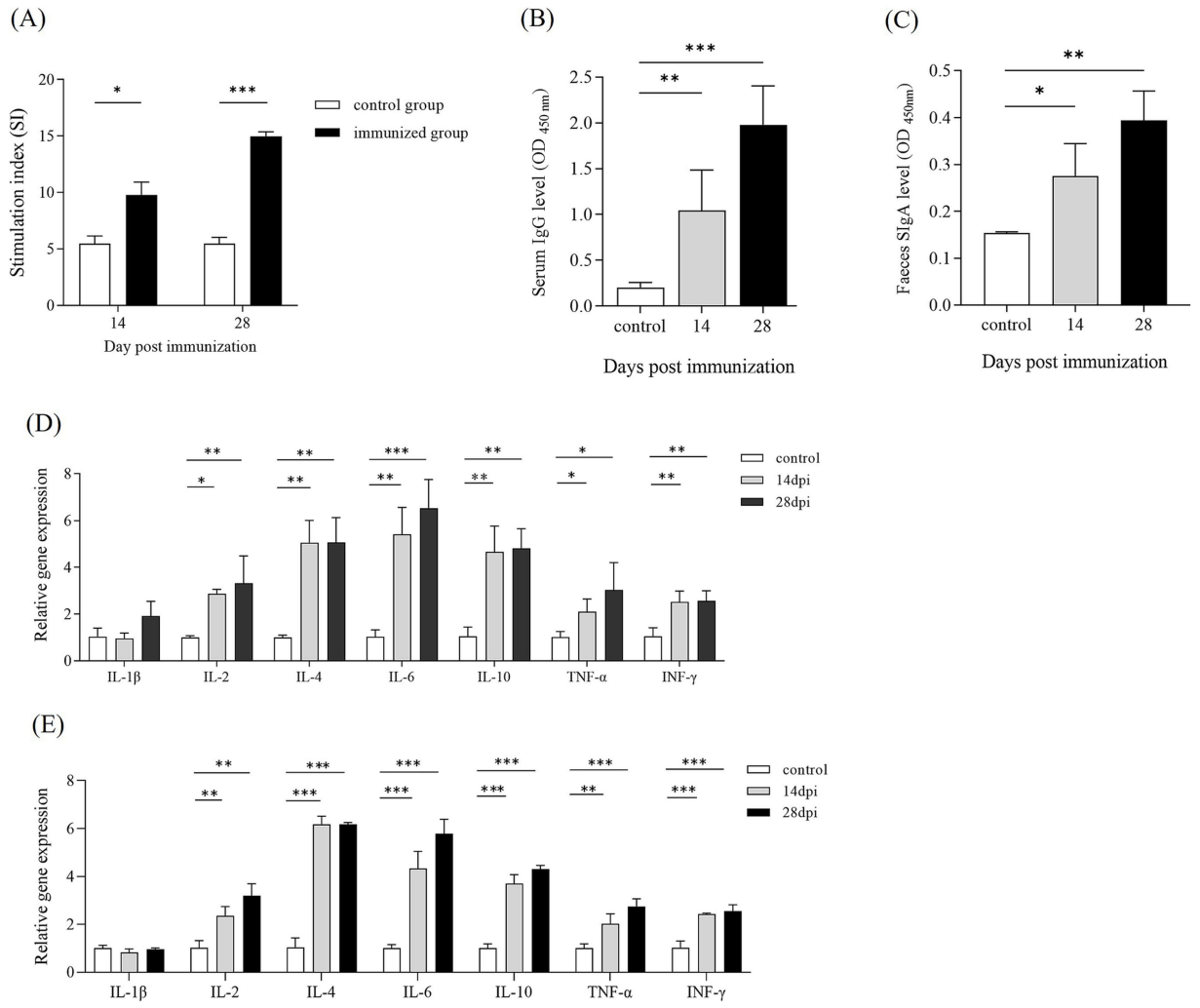

FIGURE 7
(A) The stimulation index (SI) of the splenic lymphocytes proliferation assay. Lymphocyte proliferation was measured with a MTT kit at 14 and 28 dpi. The SI was calculated using the following equation: SI = (OD_{570} of the antigen-stimulated cells)/(OD_{570} of the unstimulated cells). Data represent the mean ± SD from five mice. **(B,C)** Antibody levels in serum and feces of KM mice following immunization. Serum and fecal samples were collected from KM mice at 14 and 28 dpi. The levels of IgG in serum and IgA in feces were determined by ELISA. Data are presented as the mean ±SD from three independent replicates. **(D,E)** Cytokine expression levels in the spleen following immunization. Quantitative PCR analysis was performed to assess the mRNA expression levels of IL-1β, IL-2, IL-4, IL-6, IL-10, TNF-α, and IFN-γ at 14 and 28 dpi. The internal control gene were gapdh and β-actin, respectively. Data are presented as the mean ± SD of three independent replicates. Statistical significance was determined as $p < 0.05$ (*), $p < 0.01$ (**) and $p < 0.001$ (***).

highlight that Δ*pipC* can effectively induce a strong immune response in mice.

Immune protection by the Δ*pipC* vaccination against virulent C50336 challenge

The survival percentages in the mice vaccinated orally with the Δ*pipC* followed by the challenge with the virulent *SE* are shown in Figure 8. The vaccinated group showed no mouse deaths and a 100% survival rate; among the 10 mice in the unvaccinated group, 8 mice died after the challenge, showing a survival rate of 20%. The clinical symptoms including anorexia, chills, diarrhea, emaciation, and depression in the vaccinated group were slight and temporary after challenged compared to the unvaccinated group. Therefore, immunization with 10^6 CFU of Δ*pipC* provided full protection against *SE* challenge (see Figure 9).

Discussion

SE is a major foodborne zoonotic pathogen that poses significant economic burdens on the livestock industry and presents a serious global public health threat. The continued emergence of antimicrobial resistance (AMR), particularly multidrug resistance (MDR), in *Salmonella* has become a growing challenge worldwide. Vaccination has been recognized as an effective targeted strategy to control

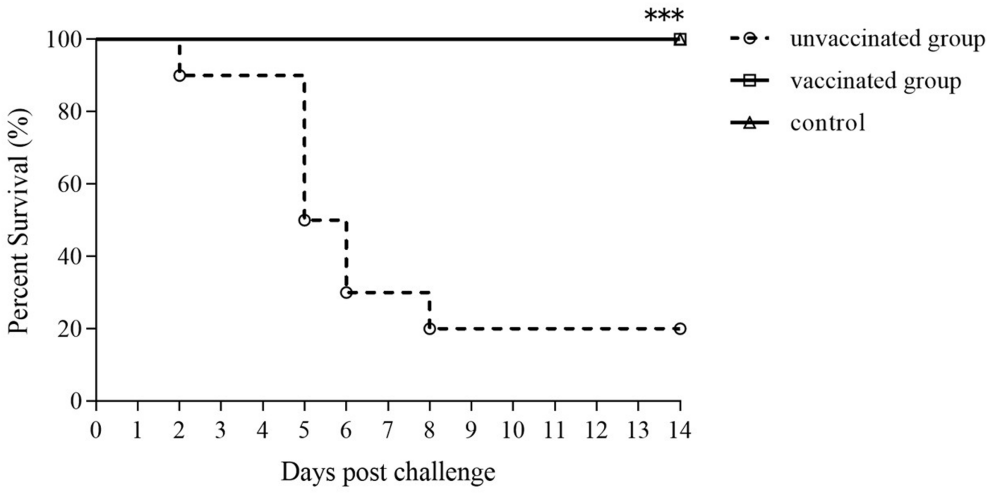

FIGURE 8
Protective efficacy of the Δ*pipC* following oral vaccination. KM mice were orally immunized with the Δ*pipC* and challenged with a lethal dose of C50336 at 28 dpi. Survival was monitored daily for 14 days after the challenge. The vaccinated group showed significantly improved survival compared to the unvaccinated group. Statistical significance was determined as $p < 0.001$ (***).

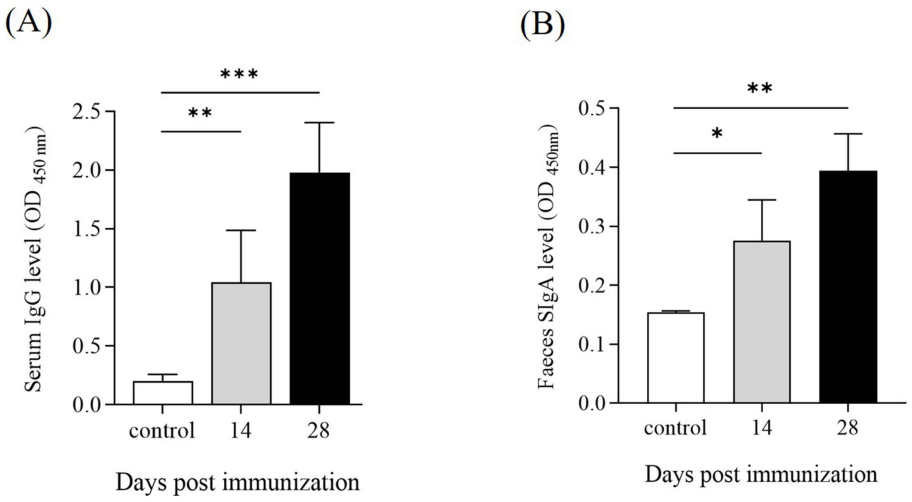

FIGURE 9
Antibody levels in serum and feces of KM mice following immunization. Serum and fecal samples were collected from KM mice at 14 and 28 days post-immunization (dpi). The levels of **(A)** IgG in serum and **(B)** IgA in feces were determined by ELISA. Data are presented as the mean ±SD from three independent replicates. Statistical significance was assessed as $p < 0.05$ (*), $p < 0.01$ (**) and $p < 0.001$ (***).

antibiotic-resistant *Salmonella* infections. Studies have demonstrated that vaccination significantly contributes to reducing infections caused by resistant strains (Bian et al., 2024).

Over the years, a variety of vaccines-including inactivated and live attenuated vaccines-have been developed to combat salmonellosis. Inactivated vaccines are considered safe but generally induce weak immunogenicity, often requiring adjuvants and booster immunizations, and mainly stimulate humoral rather than cellular immunity (Pan et al., 2024). In contrast, live attenuated vaccines represent a major advancement in vaccine technology by providing efficient and long-lasting protection. These vaccines use weakened but viable pathogens that are capable of eliciting strong immune responses without causing disease. A key advantage of live attenuated vaccines lies in their ability to closely mimic natural infections and engage both humoral and cell-mediated immune responses, thereby establishing robust and sustained protection (Nazir et al., 2025).

In recent years, the use of targeted gene deletion to attenuate virulence in *Salmonella* has become an increasingly common strategy in vaccine development (Hewawaduge et al., 2023). Given the association of *pipC* with host cell invasion and intracellular survival in macrophages, we constructed a *pipC*-deleted *SE* mutant using homologous recombination. Compared to the wild-type strain C50336, the Δ*pipC* mutant exhibited significantly reduced virulence. Immunization with the Δ*pipC* strain induced strong humoral and cellular immune responses and conferred full protection against subsequent *SE* challenge in mice.

Identification of virulence genes is essential for the rational design of live attenuated vaccines. During infection, *SE* faces various stress conditions--such as acid, alkali, and oxidative stress—both in the gastrointestinal tract and within *Salmonella*-containing vacuoles (SCVs) of epithelial and macrophage cells. Genes involved in stress responses are often linked to virulence (Pasqua et al., 2022). Our study demonstrated that deletion of *pipC* had no significant effect on the growth characteristics of *SE* under normal conditions, indicating that this gene is not essential for basic bacterial proliferation. However, the *pipC* mutant strain exhibited markedly reduced survival under acidic, alkaline, and oxidative stress conditions, suggesting that *pipC* is involved in the bacterium's ability to withstand environmental stress. These findings underscore the important role of *pipC* in stress resistance, which may, in turn, contribute to the overall virulence and persistence of *SE* in hostile environments.

Upon entering the small intestine, *Salmonella* first adheres to epithelial cells and invades host tissues via M cells located over Peyer's patches. Although macrophages within lymphoid tissues phagocytose *Salmonella*, the bacterium can evade destruction by interfering with phagosome-lysosome fusion, allowing it to survive and replicate intracellularly. Hence, adhesion to epithelial cells and intracellular survival in macrophages are crucial virulence determinants (Eakley et al., 2011). In this study, we found that the Δ*pipC* strain exhibited significantly reduced invasion of epithelial cells, consistent with findings by Shah et al. (2011). Additionally, intracellular proliferation was markedly impaired. A mouse intraperitoneal infection model showed that the LD_{50} of the Δ*pipC* strain increased 47-fold compared to the wild-type strain, indicating substantial attenuation. The SPI-1 and SPI-2 pathogenicity islands encode the Type III Secretion System (T3SS), which delivers effector proteins into host cells to facilitate cytoskeletal rearrangement and invasion. Gene expression analysis further revealed that the Δ*pipC* strain had significantly downregulated expression of several virulence-associated genes. SPI-1 genes (*invH*, *sipA*, *sipB*, *sipC*, *sopB*, and *sopE2*) and SPI-2 genes (*spvB*, *ssrA*, *orf245*, *ssaS*, *ssaT*, *ssaU*, *sseB*, and *sseD*) were all suppressed. The downregulation of these genes in the Δ*pipC* strain implies impaired T3SS function and effector protein expression, ultimately leading to reduced invasion and virulence.

Live attenuated *Salmonella* vaccines must balance attenuation, immunogenicity, and protective efficacy. An ideal vaccine strain should be non-toxic or minimally toxic. In this study, mice infected with the Δ*pipC* strain had significantly higher LD_{50} values and reduced colonization in the intestine, spleen, and liver compared to wild-type infections, confirming the attenuation of the mutant strain.

Upon entry, *SE* activates innate immunity, recruiting macrophages and monocytes, which secrete pro-inflammatory cytokines and promote inflammation. In parallel, B cells differentiate into effector cells, producing anti-inflammatory cytokines such as IL-10, which suppress inflammation and stimulate antibody production. Cytokines such as IFN-γ enhance macrophage activation and help regulate immune responses (Jan et al., 2022; Kung et al., 2022). In our study, mice immunized with the Δ*pipC* strain showed significantly higher splenic lymphocyte proliferation indices and serum antibody levels at both 14 dpi and 28 dpi compared to controls. Cytokine analysis revealed significantly increased expression of IL-2, IL-4, IL-6, IL-10, TNF-α, and IFN-γ, indicating robust activation of both humoral and cellular immune pathways. The Δ*pipC* strain provided complete protection (100%) against secondary wild-type challenge when administered orally at a dose of 1×10^6 CFU. It is important to note that we used only a single antigen concentration in our lymphocyte proliferation experiments, limiting the understanding of antigen sensitivity and cellular response thresholds. Assessment of lymphocyte response at multiple antigen concentrations should be considered in future further studies.

One of the main advantages of live attenuated vaccines over inactivated ones is their ability to stimulate both humoral and cellular immunity. Systemic dissemination of *Salmonella* promotes antigen presentation and induces specific immune responses that prevent secondary infections. Previous studies have validated the potential of gene-engineered live attenuated vaccines against *Salmonella*. Zhao et al. (2024) showed that deletion of the *pal* gene attenuated *SE* virulence, and oral immunization with 1×10^8 CFU of Δ*pal* conferred 100% protection against a 5×10^6 CFU wild-type challenge. Zhou et al. (2023) demonstrated that deletion of *rfbG* increased the LD_{50} by 56-fold. Immunizing chickens with 5×10^7 or 5×10^6 CFU of Δ*rfbG* achieved 100% survival after wild-type challenge, and significant antibody responses were observed, confirming its vaccine potential. Similarly, Pan et al. (2020) reported that the LD_{50} of *Salmonella Paratyphi A* Δ*sptP* was 1.43×10^4-fold higher than the wild-type, and oral immunization with 2×10^5 CFU conferred complete protection against challenge with 1×10^3 CFU.

In summary, our present work demonstrates that lack of *pipC* affects *SE* pathogenicity by decreasing its virulence both *in vitro* and *in vivo*. Vaccination of mice with Δ*pipC* conferred development of acquired immunity and efficacious protection against experimental systemic infection. The *pipC* mutant possesses the safety and efficacy required for use as a live attenuated vaccine. Given the potential for field applications, a more comprehensive long-term assessment of safety indicators such as fecal-shedding duration, risk of virulence re-escalation, and potential for environmental transmission is needed (Pan et al., 2020). Although the

Δ*pipC* strain exhibited attenuated virulence and genetic stability under laboratory conditions, its environmental safety and stability should still be verified by field experiments before practical application, and the applicability of target animals and the safe window of vaccine dose should be systematically evaluated.

Data availability statement

The original contributions presented in the study are included in the article/supplementary material, further inquiries can be directed to the corresponding author.

Ethics statement

The animal study was approved by Experimental Animal Regulation Ordinances defined by Hebei Provincial Department of Science and Technology HPDST2020-17. The study was conducted in accordance with the local legislation and institutional requirements.

Author contributions

LZ: Formal analysis, Writing – original draft, Methodology, Data curation. YuC: Writing – original draft, Formal analysis, Data curation, Methodology. ZY: Writing – review & editing, Funding acquisition. YuL: Methodology, Writing – original draft. XY: Methodology, Writing – original draft. LC: Writing – original draft, Software. YZ: Writing – review & editing, Funding acquisition. YiC: Writing – original draft, Software. YoL: Writing – original draft, Software. QS: Funding acquisition, Writing – review & editing. TW: Validation, Supervision, Methodology, Writing – review & editing, Investigation, Writing – original draft, Conceptualization, Funding acquisition.

Funding

The author(s) declare that financial support was received for the research and/or publication of this article. This research was funded by the National Key Research and Development Program (2023YFD1800701); Hebei Agriculture Research System (HBCT2024280205 and HBCT2024280406), and Shijiazhuang "Open Challenge" Science and Technology Project (2417908002A).

Acknowledgments

The authors thank Prof. Zhen Wang from Beijing University of Agriculture for their valuable help in our experiment.

Conflict of interest

The authors declare that the research was conducted in the absence of any commercial or financial relationships that could be construed as a potential conflict of interest.

Generative AI statement

The authors declare that no Gen AI was used in the creation of this manuscript.

Publisher's note

Supplementary material

The Supplementary material for this article can be found online at: https://www.frontiersin.org/articles/10.3389/fmicb.2025.1631008/full#supplementary-material

SUPPLEMENTARY FIGURE 1
(A) Schematic representation of a gene knockout strategy adopted from Ranallo et al. (2006). **(a)** Linear DNA substrates containing chloramphenicol cassettes are generated using PCR primers with 59 bp homology (A and B) to the gene of interest (*pipC*). Priming from pKD3 produces linear DNA substrates. **(b)** These substrates introduced into bacteria made transiently hyper-recombinogenic using Gam, Beta, Exo expressed from pKD46. **(c)** The chloramphenicol cassette is eliminated via plasmid-based expression of a yeast derived recombinase (FLP) leaving behind an ~80 bp "scar" consisting of a single FRT site. **(B)** Schematic representation of *pipC*-complemented strain construction of *SE*.

References

Acevedo-Villanueva, K. Y., Renu, S., Shanmugasundaram, R., Akerele, G. O., Gourapura, R. J., and Selvaraj, R. K. (2021). *Salmonella* chitosan nanoparticle vaccine administration is protective against *Salmonella* Enteritidis in broiler birds. *PLoS One* 16:e0259334. doi: 10.1371/journal.pone.0259334

Bian, X., Liu, Q., Chen, Y., Zhang, W., Li, M., Zhang, X., et al. (2024). Immunogenicity and cross-protective efficacy induced by delayed attenuated *Salmonella* with regulated length of lipopolysaccharide in mice. *Gut Microbes* 16:2424983. doi: 10.1080/19490976.2024.2424983

Cao, G., Zhao, S., Kuang, D., Hsu, C.-H., Yin, L., Luo, Y., et al. (2023). Geography shapes the genomics and antimicrobial resistance of *Salmonella enterica* serovar Enteritidis isolated from humans. *Sci. Rep.* 13:1331. doi: 10.1038/s41598-022-24150-4

Darwin, K. H., Robinson, L. S., and Miller, V. L. (2001). SigE is a chaperone for the *Salmonella enterica* serovar Typhimurium invasion protein SigD. *J. Bacteriol.* 183, 1452–1454. doi: 10.1128/JB.183.4.1452-1454.2001

Datsenko, K. A., and Wanner, B. L. (2000). One-step inactivation of chromosomal genes in *Escherichia coli* K-12 using PCR products. *Proc. Natl. Acad. Sci. U.S.A.* 97, 6640–6645. doi: 10.1073/pnas.120163297

Eakley, N. M., Bochsler, P. N., Gopal Reddy, P., and Fadl, A. A. (2011). Biological and virulence characteristics of the YqhC mutant of *Salmonella*. *Microbiol. Immunol.* 55, 830–840. doi: 10.1111/j.1348-0421.2011.00387.x

Emerson, L. E., Barker, H., Tran, T., Barker, S., Enslow, S., Ou, M., et al. (2022). Extracellular vesicles elicit protective immune responses against *Salmonella* infection. *J. Extracell. Vesicles* 11:e12267. doi: 10.1002/jev2.12267

Ferrari, R. G., Rosario, D. K. A., Cunha-Neto, A., Mano, S. B., Figueiredo, E. E. S., and Conte-Junior, C. A. (2019). Worldwide epidemiology of *Salmonella* serovars in animal-based foods: a meta-analysis. *Appl. Environ. Microbiol.* 85:e00591-19. doi: 10.1128/AEM.00591-19

Guard-Petter, J. (2001). The chicken, the egg and *Salmonella enteritidis*. *Environ. Microbiol.* 3, 421–430. doi: 10.1046/j.1462-2920.2001.00213.x

Hewawaduge, C., Senevirathne, A., Sivasankar, C., and Lee, J. H. (2023). The impact of lipid A modification on biofilm and related pathophysiological phenotypes, endotoxicity, immunogenicity, and protection of *Salmonella* Typhimurium. *Vet. Microbiol.* 282:109759. doi: 10.1016/j.vetmic.2023.109759

Jan, T.-R., Lin, C.-S., Wang, S.-Y., and Yang, W.-Y. (2022). Cytokines and cecal microbiome modulations conferred by a dual vaccine in *Salmonella*-infected layers. *Poult. Sci.* 102:102373. doi: 10.1016/j.psj.2022.102373

Ji, H. J., Jang, A.-Y., Song, J. Y., Ahn, K. B., Han, S. H., Bang, S. J., et al. (2022). Development of live attenuated *Salmonella* Typhimurium vaccine strain using radiation mutation enhancement technology (R-MET). *Front. Immunol.* 13:931052. doi: 10.3389/fimmu.2022.931052

Jiang, X., Chu, C., Wang, Z., Gu, J., Hong, Y., Li, Q., et al. (2022). Preclinical evaluation of OMVs as potential vaccine candidates against *Salmonella enterica* serovar Enteritidis infection. *Front. Cell. Infect. Microbiol.* 12:1037607. doi: 10.3389/fcimb.2022.1037607

Kamble, N. M., and Lee, J. H. (2016). Characterization and evaluation of a *Salmonella enterica* serotype Senftenberg mutant created by deletion of virulence-related genes for use as a live attenuated vaccine. *Clin. Vaccine Immunol.* 23, 802–812. doi: 10.1128/CVI.00233-16

Kang, X., Yang, Y., Meng, C., Wang, X., Liu, B., Geng, S., et al. (2021). Safety and protective efficacy of *Salmonella Pullorum spiC* and *rfaH* deletion rough mutant as a live attenuated DIVA vaccine candidate. *Poult. Sci.* 101:101655. doi: 10.1016/j.psj.2021.101655

Kirthika, P., Senevirathne, A., Jawalagatti, V., Park, S., and Lee, J. H. (2020). Deletion of the *lon* gene augments expression of *Salmonella* Pathogenicity Island (SPI)-1 and metal ion uptake genes leading to the accumulation of bactericidal hydroxyl radicals and host pro-inflammatory cytokine-mediated rapid intracellular clearance. *Gut Microbes* 11, 1695–1712. doi: 10.1080/19490976.2020.1777923

Kung, Y.-J., Lam, B., Tseng, S.-H., MacDonald, A., Tu, H.-F., Wang, S., et al. (2022). Localization of *Salmonella* and albumin-IL-2 to the tumor microenvironment augments anticancer T cell immunity. *J. Biomed. Sci.* 29:57. doi: 10.1186/s12929-022-00841-y

Lin, Z., Tang, P., Jiao, Y., Kang, X., Li, Q., Xu, X., et al. (2017). Immunogenicity and protective efficacy of a *Salmonella* Enteritidis *sptP* mutant as a live attenuated vaccine candidate. *BMC Vet. Res.* 13:194. doi: 10.1186/s12917-017-1115-3

Nazir, J., Manzoor, T., Saleem, A., Gani, U., Bhat, S. S., Khan, S., et al. (2025). Combatting *Salmonella*: a focus on antimicrobial resistance and the need for effective vaccination. *BMC Infect. Dis.* 25:84. doi: 10.1186/s12879-025-10478-5

Pan, J., Wei, R., Xu, P., Liu, Y., Li, C., Ding, G., et al. (2024). Progress in the application of *Salmonella* vaccines in poultry: a mini review. *Vet. Immunol. Immunopathol.* 278:110855. doi: 10.1016/j.vetimm.2024.110855

Pan, P., Zou, F., He, C., He, Q., and Yin, J. (2020). Characterization and protective efficacy of a *sptP* mutant of *Salmonella* Paratyphi A. *Immun. Inflamm. Dis.* 8, 774–781. doi: 10.1002/iid3.369

Park, S., Jung, B., Kim, E., Yoon, H., and Hahn, T.-W. (2022). Evaluation of *Salmonella* Typhimurium lacking *fruR*, *ssrAB*, or *hfq* as a prophylactic vaccine against *Salmonella* lethal infection. *Vaccine* 10:1413. doi: 10.3390/vaccines10091413

Pasqua, M., Coluccia, M., Eguchi, Y., Okajima, T., Grossi, M., Prosseda, G., et al. (2022). Roles of two-component signal transduction systems in *Shigella* virulence. *Biomol. Ther.* 12:1321. doi: 10.3390/biom12091321

Ranallo, R. T., Barnoy, S., Thakkar, S., Urick, T., and Venkatesan, M. M. (2006). Developing live *Shigella* vaccines using λ red recombineering. *FEMS Immunol. Med. Microbiol.* 47, 462–469. doi: 10.1111/j.1574-695X.2006.00118.x

Rodríguez-Escudero, I., Ferrer, N. L., Rotger, R., Cid, V. J., and Molina, M. (2011). Interaction of the *Salmonella* Typhimurium effector protein SopB with host cell Cdc42 is involved in intracellular replication. *Mol. Microbiol.* 80, 1220–1240. doi: 10.1111/j.1365-2958.2011.07639.x

Ruvalcaba-Gómez, J. M., Villagrán, Z., Valdez-Alarcón, J. J., Martínez-Núñez, M., Gomez-Godínez, L. J., Ruesga-Gutiérrez, E., et al. (2022). Non-antibiotics strategies to control *Salmonella* infection in poultry. *Animals* 12:102. doi: 10.3390/ani12010102

Rychlik, I., Karasova, D., Sebkova, A., Volf, J., Sisak, F., Havlickova, H., et al. (2009). Virulence potential of five major pathogenicity islands (SPI-1 to SPI-5) of *Salmonella enterica* serovar Enteritidis for chickens. *BMC Microbiol.* 9:268. doi: 10.1186/1471-2180-9-268

Shah, D. H., Zhou, X., Addwebi, T., Davis, M. A., Orfe, L., Call, D. R., et al. (2011). Cell invasion of poultry-associated *Salmonella enterica* serovar Enteritidis isolates is associated with pathogenicity, motility and proteins secreted by the type III secretion system. *Microbiology* 157, 1428–1445. doi: 10.1099/mic.0.044461-0

Shah, D. H., Zhou, X., Kim, H.-Y., Call, D. R., and Guard, J. (2012). Transposon mutagenesis of *Salmonella enterica* serovar Enteritidis identifies genes that contribute to invasiveness in human and chicken cells and survival in egg albumen. *Infect. Immun.* 80, 4203–4215. doi: 10.1128/IAI.00790-12

Tennant, S. M., and Levine, M. M. (2015). Live attenuated vaccines for invasive *Salmonella* infections. *Vaccine* 33, C36–C41. doi: 10.1016/j.vaccine.2015.04.029

Upadhyaya, I., Upadhyay, A., Kollanoor-Johny, A., Darre, M. J., and Venkitanarayanan, K. (2013). Effect of plant derived antimicrobials on *Salmonella Enteritidis* adhesion to and invasion of primary chicken oviduct epithelial cells *in vitro* and virulence gene expression. *Int. J. Mol. Sci.* 14, 10608–10625. doi: 10.3390/ijms140510608

Wang, M., Qazi, I. H., Wang, L., Zhou, G., and Han, H. (2020). *Salmonella* virulence and immune escape. *Microorganisms* 8:407. doi: 10.3390/microorganisms8030407

Xiong, D., Song, L., Chen, Y., Jiao, X., and Pan, Z. (2023). *Salmonella* Enteritidis activates inflammatory storm via SPI-1 and SPI-2 to promote intracellular proliferation and bacterial virulence. *Front. Cell. Infect. Microbiol.* 13:1158888. doi: 10.3389/fcimb.2023.1158888

Yin, C., Gu, J., Gu, D., Wang, Z., Ji, R., Jiao, X., et al. (2022). The *Salmonella* T3SS1 effector IpaJ is regulated by ItrA and inhibits the MAPK signaling pathway. *PLoS Pathog.* 18:e1011005. doi: 10.1371/journal.ppat.1011005

Zhang, L., Chen, L., Zhang, X., Li, Y., Zheng, Q., Li, Y., et al. (2025). The *mcpC* mutant of *Salmonella enteritidis* exhibits attenuation and confers both immunogenicity and protective efficacy in mice. *Front. Microbiol.* 16:1548920. doi: 10.3389/fmicb.2025.1548920

Zhang, X., He, L., Zhang, C., Yu, C., Yang, Y., Jia, Y., et al. (2019). The impact of *sseK2* deletion on *Salmonella enterica* serovar Typhimurium virulence *in vivo* and *in vitro*. *BMC Microbiol.* 19:182. doi: 10.1186/s12866-019-1543-2

Zhang, L., Wu, T., Wang, F., Liu, W., Zhao, G., Zhang, Y., et al. (2024). CheV enhances the virulence of *Salmonella Enteritidis*, and the Chev-deleted *Salmonella* vaccine provides immunity in mice. *BMC Vet. Res.* 20:100. doi: 10.1186/s12917-024-03951-x

Zhao, G., Duan, W., Zhang, L., Sun, W., Liu, W., Zhang, X., et al. (2024). The peptidoglycan-associated lipoprotein gene mutant elicits robust immunological defense in mice against *Salmonella enteritidis*. *Front. Microbiol.* 15:1422202. doi: 10.3389/fmicb.2024.1422202

Zhou, Y., Xiong, D., Guo, Y., Liu, Y., Kang, X., Song, H., et al. (2023). *Salmonella Enteritidis* RfbD enhances bacterial colonization and virulence through inhibiting autophagy. *Microbiol. Res.* 270:127338. doi: 10.1016/j.micres.2023.127338

frontiers | Frontiers in Microbiology

TYPE Original Research
PUBLISHED 21 July 2025
DOI 10.3389/fmicb.2025.1641632

OPEN ACCESS

EDITED BY
Hong Yin,
Chinese Academy of Agricultural Sciences, China

REVIEWED BY
Na Li,
South China Agricultural University, China
Xinan Meng,
South China Agricultural University, China

*CORRESPONDENCE
Wenchao Li
liwen303@126.com
Falei Li
fli@fynu.edu.cn

RECEIVED 05 June 2025
ACCEPTED 08 July 2025
PUBLISHED 21 July 2025

CITATION
Zhang H, Chen H, He C, Li W and Li F (2025) Distribution of human-pathogenic *Cryptosporidium* spp., *Giardia duodenalis*, and *Enterocytozoon bieneusi* in crab-eating macaques in China.
Front. Microbiol. 16:1641632.
doi: 10.3389/fmicb.2025.1641632

Distribution of human-pathogenic *Cryptosporidium* spp., *Giardia duodenalis*, and *Enterocytozoon bieneusi* in crab-eating macaques in China

Huilin Zhang[1], Huiyang Chen[1], Chaoyue He[1], Wenchao Li[2]* and Falei Li[1]*

[1]Anhui Province Key Laboratory of Embryo Development and Reproductive Regulation, College of Biological and Food Engineering, Fuyang Normal University, Fuyang, China, [2]Anhui Province Key Laboratory of Animal Nutritional Regulation and Health, College of Animal Science, Anhui Science and Technology University, Fengyang, China

Introduction: The positive rates and genetic identity of *Cryptosporidium* spp., *Giardia duodenalis* (*G. duodenalis*), and *Enterocytozoon bieneusi* (*E. bieneusi*) were unclear in crab-eating macaques in Suzhou and Beijing, China.

Methods: A total of 504 fecal samples were collected from crab-eating macaques on commercial farms in Beijing and Suzhou, China. The extracted DNA was analyzed for *Cryptosporidium* spp. and *E. bieneusi* by nested PCR and sequence analysis of the small subunit rRNA (*SSU* rRNA) gene and the internal transcribed spacer (ITS) gene, respectively. The *G. duodenalis* was detected by nested PCR targeting β-giardin (*bg*) gene, glutamate dehydrogenase (*gdh*) gene, and triosephosphate isomerase (*tpi*) gene. The *C. hominis* identified were further subtyped by nested PCR and sequence analysis of the 60 kDa glycoprotein (*gp60*) gene.

Results: All 504 fecal samples collected from crab-eating macaques, the detection rates of *Cryptosporidium* spp., *G. duodenalis*, and *E. bieneusi* were 11.9% (60/504), 5.6% (28/504), and 4.6% (23/504), respectively. The 15.1% (44/292) detection rate of *Cryptosporidium* spp. from crab-eating macaques in Suzhou was significantly higher than that in Beijing (2.8%; 6/212; $\chi^2 = 20.6$, $df = 1$, $p < 0.0001$). The detection rates of *Cryptosporidium* spp. and *G. duodenalis* were significant different between <2 months old animals and >24 months old animals ($\chi^2 = 104.7$, $df = 1$, $p < 0.0001$; $\chi^2 = 6.6$, $df = 1$, $p = 0.0104$). In contrast, there was no significant different in the detection rate of *E. bieneusi* in two age groups ($\chi^2 = 2.2$, $df = 1$, $p = 0.1360$). A total of one *Cryptosporidium* species, one *G. duodenalis* assemblage B, and 4 *E. bieneusi* genotypes have been identified, including *C. hominis* ($n = 60$), assemblage B ($n = 28$), CM1 ($n = 14$), Peru8 ($n = 5$), D ($n = 3$), and Type IV ($n = 1$). Among 60 *C. hominis* samples, five subtypes of five subtype families were successfully identified at the *gp60* gene: IbA13G4 ($n = 27$), InA26 ($n = 3$), IfA17G2R3 ($n = 3$), IiA17 ($n = 3$), and IeA11G3T3 ($n = 2$).

Discussion: The results indicate that known zoonotic *Cryptosporidium* spp., *G. duodenalis*, and *E. bieneusi* are prevalent in crab-eating macaques. The crab-

eating macaques could play a potential role in the zoonotic transmission of pathogens to humans.

KEYWORDS

Cryptosporidium spp., *Giardia duodenalis*, *Enterocytozoon bieneusi*, crab-eating macaque, zoonosis, China

1 Introduction

Cryptosporidium spp., *Giardia duodenalis* (*G. duodenalis*), and *Enterocytozoon bieneusi* (*E. bieneusi*) are common zoonotic protozoan pathogens in humans, non-human primates, and ruminants, causing moderate-to-severe diarrhea in animals (Li W. et al., 2019; Cai et al., 2021; Guo et al., 2021b). These three gastrointestinal pathogens are mainly transmitted through food-borne transmission and water-borne transmission (Xiao, 2010). In non-human primates, crab-eating macaques are very similar to humans in physiology and genetics and are used in human disease research and drug experiments (Zhang et al., 2014). In the laboratory, crab-eating macaques have close contact with humans. Therefore, these animals could become potential hosts for zoonotic *Cryptosporidium* spp., *G. duodenalis*, and *E. bieneusi*.

So far 47 *Cryptosporidium* species and more than 120 *Cryptosporidium* genotypes have been recognized in humans and animals, and most of them are host-adapted (Ryan et al., 2021). Among them, *C. hominis* has a narrower host range and mainly detect in humans and non-human primates (Huang et al., 2025). Although, *C. parvum* has a broad host range and is rarely found in non-human primates (Feng et al., 2018). More than 10 subtype families of *C. hominis* have been recognized based on sequence analysis of the 60 kDa glycoprotein (*gp60*) gene (Xiao and Feng, 2017). Among these subtype families, Ia, Ib, Ie, and Ii were only found in humans and non-human primates (Feng and Xiao, 2017). By contrast, In subtype family was only found in crab-eating macaques in Hainan (Chen et al., 2019). These subtype families of *C. hominis* differ in virulence, with subtype IbA10G2 widely distributed in both industrialized and developing countries (Bouzid et al., 2013). Subtype IbA10G2 always causes *C. hominis*-associated outbreaks in industrialized countries (Feng et al., 2018). Therefore, there is a zoonotic potential for *Cryptosporidium* spp. in crab-eating macaques.

To date, 8 *G. duodenalis* assemblages (A-H) have been recognized in humans and animals, based on sequence analysis of triosephosphate isomerase (*tpi*) gene, *β*-giardin (*bg*) gene, and glutamate dehydrogenase (*gdh*) gene (Cai et al., 2021). Among 8 assemblages, assemblages A and B were most commonly found in humans and non-human primates. In contrast, assemblage E was mainly found in ruminants and occasionally found in humans (50 cases) and non-human primates (5 cases) (Brynildsrud et al., 2018; Cai et al., 2021). Previous studies have found that non-human primates were potential hosts for *G. duodenalis* (Feng and Xiao, 2011). Therefore, there has high zoonotic potential for assemblages A, B, and E of *G. duodenalis* in crab-eating macaques.

More than 500 genotypes and 15 genetic groups of *E. bieneusi* have been recognized in humans and animals, based on sequence analysis of internal transcribed spacer (ITS) gene (Li and Xiao, 2021; Li et al., 2022; Jiang et al., 2024). Among 15 groups, Group 1 was mainly found in humans and was considered zoonotic group (Li W. et al., 2019). At least 50 genotypes of *E. bieneusi* had been found in non-human primates, and these genotypes was clustered together with Group 1 (Chen et al., 2019). Genotypes A, D, Type IV, EbpC, Peru 7, Peru 8, Peru 11, BEB6, and I of *E. bieneusi* were associated with human microsporidiosis in many countries (Santín and Fayer, 2011; Wang et al., 2013; Wang et al., 2018). Among them, genotypes Type IV, Peru 8, and macaque 3 were a common genotype in humans and most animals, however, macaque3 was only detected in non-human primates in China (Karim et al., 2014b; Karim et al., 2014c; Chen et al., 2020). Therefore, there is a zoonotic potential for *E. bieneusi* in crab-eating macaques.

In addition to Beijing and Suzhou, some studies on the occurrence of *Cryptosporidium* spp., *G. duodenalis* and *E. bieneusi* in Nonhuman primates (NHPs) have also been conducted in China (Karim et al., 2014c; Karim et al., 2014d; Ye et al., 2014; Chen et al., 2019; Guo et al., 2021a; Shu et al., 2022). The crab-eating macaque farms in Beijing and Suzhou have the same history, however the scale of animals is different. The occurrence and genetic identity of *Cryptosporidium* spp., *G. duodenalis*, and *E. bieneusi* were unclear in Suzhou and Beijing. Therefore, we examined the occurrence of three pathogens in crab-eating macaques in two cities in this study. The results of the study suggest that these three intestinal pathogens were prevalent and had high zoonotic potential in these animals.

2 Materials and methods

2.1 Samples collection

A total of 504 fecal samples were collected from crab-eating macaques on commercial farms in Beijing and Suzhou, China. These farms from lab animal companies were certified by Accreditation of Laboratory Animal Care and International Association for Assessment. The crab-eating macaques farms in Beijing and Suzhou were established in 2002. The farms in Beijing and Suzhou had 8,000 and 3,000 crab-eating macaques, respectively. These two farms mainly raised young animals (< 2 months old) and adult animals (> 24 months old) in Beijing and Suzhou, and crab-eating macaques of other ages were sent off farms and some animals were dispersed to laboratories around the world. Of these fecal samples, 292 were collected from 2 convenient age groups in Suzhou, including under 2 months animals ($n = 72$) and more than 24 months animals ($n = 227$). The 212 samples from crab-eating macaques were collected from 2 convenient age groups in Beijing, including under 2 months animals ($n = 60$) and more than 24 months animals ($n = 152$). These animals investigated were divided into 2 convenient age groups: < 2 months old ($n = 132$) and > 24 months old ($n = 379$) according to the true age information of animals at the time of sampling. Crab-eating macaques <2 months represent the juvenile stage of animals, whose immune systems are not fully developed and could be more

susceptible to pathogens. Crab-eating macaques >24 months reach sexual maturity, and their immune function is basically established, which could effectively deal with common pathogens. The room in which the animals are kept is cleaned every day. All crab-eating macaques had no obvious clinical signs during the sample collection period. These collected samples were stored in 2.5% potassium dichromate until DNA extraction.

2.2 DNA extraction

The genomic DNA of approximately 200 mg samples in crab-eating macaques were extracted using the Fast DNA Spin Kit for Soil (MP Biomedical, Santa Ana, CA, USA) as previous described (Jiang et al., 2005). The genomic DNA that had been extracted was stored at −20°C before being used in *Cryptosporidium* species, *C. hominis* subtypes, *G. duodenalis* genotypes, and *E. bieneusi* genotypes analyses.

2.3 Detection of *Cryptosporidium* spp., *G. duodenalis*, and *E. bieneusi*

The extracted DNA was analyzed for *Cryptosporidium* spp. by nested PCR and sequence analysis of the small subunit rRNA (*SSU* rRNA) gene (Xiao et al., 1999). The *C. hominis* identified were further subtyped by nested PCR and sequence analysis of the 60 kDa glycoprotein (*gp60*) gene (Alves et al., 2003). The *E. bieneusi* was detected by nested PCR targeting a 392-bp fragment of the internal transcribed spacer (ITS) of the rRNA gene (Sulaiman et al., 2003b). The *G. duodenalis* was detected by nested PCR targeting a 599-bp fragment of the glutamate dehydrogenase (*gdh*) gene, a 511-bp fragment of the *β*-giardin (*bg*) gene, and a 530-bp fragment of the triosephosphate isomerase (*tpi*) gene (Sulaiman et al., 2003a; Caccio and Ryan, 2008; Ye et al., 2014). Two replicates were used for PCR analysis of each sample with positive and negative samples. All primer sequences, cycling parameters, and expected products used are listed in Supplementary Table S1.

2.4 Sequence analysis

All positive secondary PCR products were sequenced sequenced bi-directionally in Sangon Biotech (Shanghai, China) to identify *Cryptosporidium* species, *C. hominis* subtypes, *G. duodenalis* genotypes, and *E. bieneusi* genotypes. The nucleotide sequences were assembled using ChromasPro 2.1.5.0,[1] edited using BioEdit 7.1.3.0,[2] and aligned using ClustalX 2.0.11.[3] The phylogenetic relationships of the *C. hominis* subtypes and *E. bieneusi* genotypes were analysed using maximum likelihood analysis implemented in Mega 7.0[4] based on substitution rates calculated with the general time reversible model as described (Yan et al., 2017).

1 http://technelysium.com.au/ChromasPro.html
2 https://bioedit.software.informer.com
3 http://clustal.org
4 http://www.megasoftware.net

2.5 Statistical analysis

Detection rates of *Cryptosporidium* species, *G. duodenalis*, and *E. bieneusi* were compared between different age groups and cities using the Chi-square test implemented in SPSS v.20.0 (IBM Corp., New York, NY, USA). Differences were considered significant at $p < 0.05$.

3 Results

3.1 Occurrence of *Cryptosporidium* spp. in crab-eating macaques

Of the 504 fecal samples collected from crab-eating macaques, the detection rate of *Cryptosporidium* spp. was 11.9% (60/504) in Suzhou and Beijing in present study. The 15.1% (44/292) detection rate of *Cryptosporidium* spp. from crab-eating macaques in Suzhou was significantly higher than that in Beijing (2.8%; 6/212; $\chi^2 = 20.6$, $df = 1$, $p < 0.0001$; Table 1). By age, the *Cryptosporidium* detection rates in crab-eating macaque of < 2 months and > 24 months were 32.6% (43/132) and 1.8% (7/379), respectively. The detection rate of *Cryptosporidium* spp. was significant different in two age groups ($\chi^2 = 104.7$, $df = 1$, $p < 0.0001$; Table 2).

A total of 60 *Cryptosporidium*-positive samples were successfully sequenced based on the *SSU* rRNA gene. Only one *Cryptosporidium* species was identified, namely *C. hominis* ($n = 60$). The *SSU* rRNA gene sequences of *C. hominis* generated in this study had a single nucleotide variation from the reference sequences reported from *Macaca mulatta* (GenBank: ON023862). Of the 60 *C. hominis* samples, five subtypes of five subtype families were successfully identified at the *gp60* gene: IbA13G4 ($n = 27$), InA26 ($n = 3$), IfA17G2R3 ($n = 3$), IiA17 ($n = 3$), and IeA11G3T3 ($n = 2$). The sequences from subtypes IfA17G2R3, IeA11G3T3, and IiA17 were identical to the reference sequence ON036042 from *Macaca mulatta*, AY738184 from children, and MK952706 from *Macaca fascicularis*, respectively. The sequences from subtypes IbA13G4 had TCA and TCG difference in compared to the reference sequence MK982515 from rhesus macaque. In contrast, the *gp*60 sequence of the InA26 had 9 single nucleotide polymorphisms (SNPs) compared to the reference sequence MG952711 obtained from *Macaca fascicularis*. In phylogenetic analysis of the *C. hominis* subtypes obtained from the study, emerging subtype IbA13G4 clustered with other If subtypes (Figure 1).

3.2 Occurrence of *G. duodenalis* in crab-eating macaques

In present study, the detection rate of *G. duodenalis* was 5.6% (28/504) in Suzhou and Beijing. The 8.6% (28/292) detection rate of *G. duodenalis* from crab-eating macaques in Suzhou was significantly higher than that in Beijing (0.0%; 0/212; $\chi^2 = 21.5$, $df = 1$, $p < 0.0001$; Table 1). By age, the *G. duodenalis* detection rates in crab-eating macaque of < 2 months and > 24 months were 9.8% (13/132) and 4.0% (15/379), respectively. The detection rate of *G. duodenalis* were significant different in two age groups ($\chi^2 = 6.6$, $df = 1$, $p = 0.0104$; Table 2).

10.3389/fmicb.2025.1641632

TABLE 1 Distribution of *Cryptosporidium* spp., *G. duodenalis*, and *E. bieneusi* in crab-eating macaques, China.

Location	Age (months)	No. specimens	*Cryptosporidium* spp.			*G. duodenalis*		*E. bieneusi*	
			No. positive (%)	*C. hominis* (*n*)	Subtype (*n*)	No. positive (%)	Genotype (*n*)	No. positive (%)	Genotype (*n*)
Suzhou	< 2	72	39 (54.2)	39	IbA13G4 (24); InA26 (3); IeA11G3T3 (2); IfA17G2R3 (2)	13 (18.1)	B (13)	8 (11.1)	CM1 (4); Peru8 (3); D (1)
	> 24	227	5 (2.2)	5	IbA13G4 (3); IfA17G2R3 (1)	15 (6.6)	B (15)	14 (6.2)	CM1 (10); Peru8 (2); D (2)
	Subtotal	292	44 (15.1)	44	IbA13G4 (27); InA26 (3); IeA11G3T3 (2); IfA17G2R3 (3)	28 (8.6)	B (28)	22 (7.5)	CM1 (14); Peru8 (5); D (3)
Beijing	< 2	60	4 (6.7)	4	IiA17 (2)	0 (0.0)	-	1 (1.7)	Type IV (1)
	> 24	152	2 (1.3)	2	IiA17 (1)	0 (0.0)	-	0 (0.0)	-
	Subtotal	212	6 (2.8)	6	IiA17 (3)	0 (0.0)	-	1 (0.5)	Type IV (1)
Total		504	60 (11.9)	60	IbA13G4 (27); InA26 (3); IeA11G3T3 (2); IfA17G2R3 (3); IiA17 (3)	28 (5.6)	B (28)	23 (4.6)	CM1 (14); Peru8 (5); D (3); Type IV (1)

TABLE 2 Occurrence of *Cryptosporidium* spp., *G. duodenalis*, and *E. bieneusi* in crab-eating macaques in China by age.

Age (months)	No. specimens	*Cryptosporidium* spp.			*G. duodenalis*		*E. bieneusi*	
		No. positive (%)	*C. hominis* (*n*)	Subtype (*n*)	No. positive (%)	Genotype (*n*)	No. positive (%)	Genotype (*n*)
< 2	132	43 (32.6)	43	IbA13G4 (24); InA26 (3); IeA11G3T3 (2); IfA17G2R3 (2); IiA17 (2)	13 (9.8)	B (13)	9 (6.8)	CM1 (4); Peru8 (3); D (1); Type IV (1)
> 24	379	7 (1.8)	7	IbA13G4 (3); IfA17G2R3 (1); IiA17 (1)	15 (4.0)	B (15)	14 (3.7)	CM1 (10); Peru8 (2); D (2)
Total	504	60 (11.9)	60	IbA13G4 (27); InA26 (3); IeA11G3T3 (2); IfA17G2R3 (3); IiA17 (3)	28 (5.6)	B (28)	23 (4.6)	CM1 (14); Peru8 (5); D (3); Type IV (1)

The secondary PCR products from 28 *G. duodenalis* positive samples had been successfully sequenced. Only assemblage B was identified in these positive samples in Suzhou. The obtained sequences from assemblage B samples were identical to the GenBank reference sequence MK262843 from crab-eating macaque.

3.3 Occurrence of *E. bieneusi* in crab-eating macaques

In present study, the detection rate of *E. bieneusi* was 4.6% (23/504) in Suzhou and Beijing. The 7.5% (22/292) detection rate of *E. bieneusi* from crab-eating macaques in Suzhou was

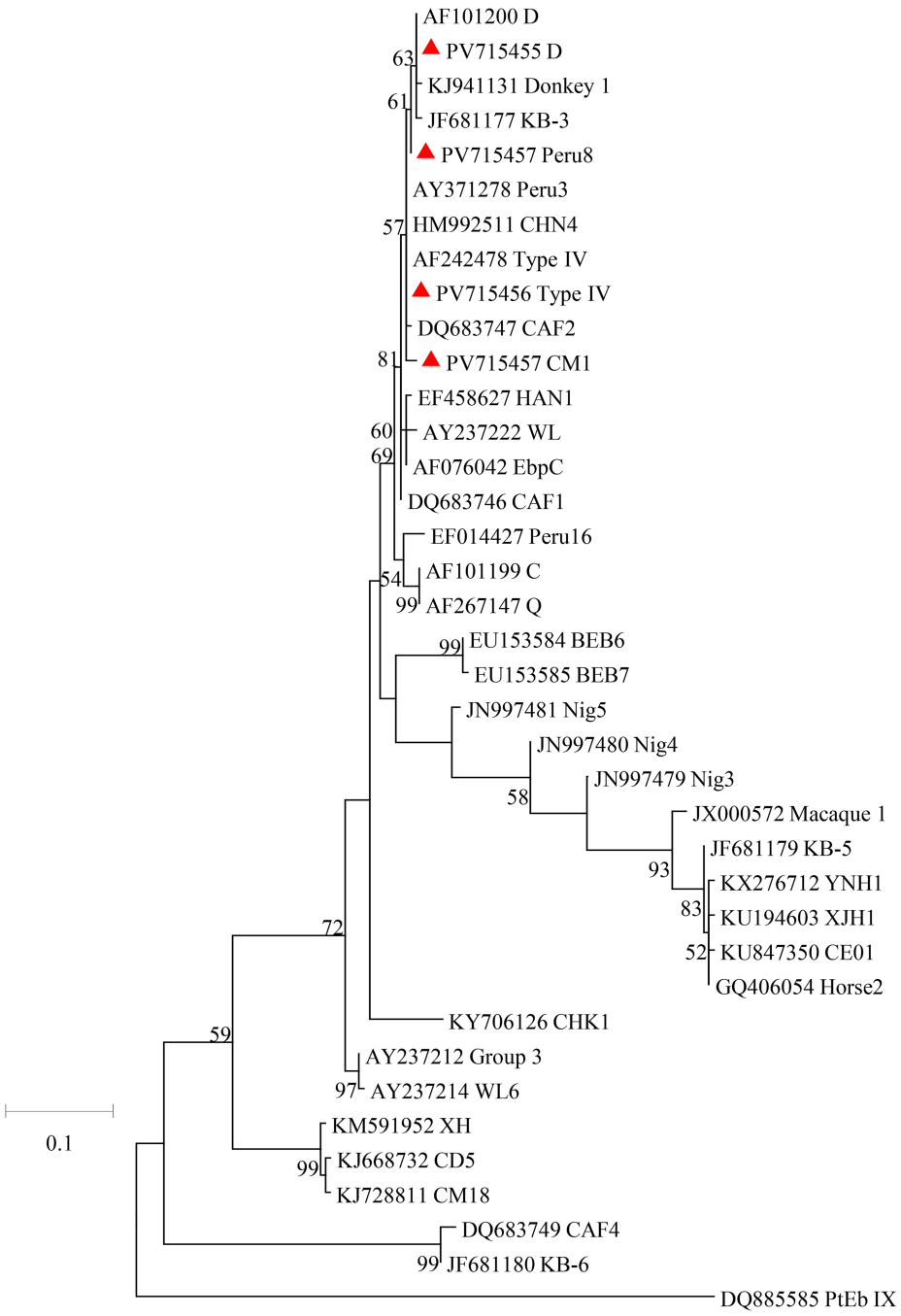

FIGURE 1
Phylogenetic relationships of *C. hominis* subtypes based on maximum likelihood analysis. The subtypes of *C. hominis* that have been identified in this study are indicated by red triangles. Bootstrap values below 50% are not shown. Bar = 0.5 substitutions per site.

significantly higher than that in Beijing (0.5%; 1/212; $\chi^2 = 14.0$, $df = 1$, $p = 0.0001$; Table 1). By age, the *E. bieneusi* detection rates in crab-eating macaque of < 2 months and > 24 months were 6.8% (9/132) and 3.7% (14/379), respectively. There were no significant different in the detection rate of *E. bieneusi* in two age groups ($\chi^2 = 2.2$, $df = 1$, $p = 0.1360$; Table 2).

The ITS products from 23 *E. bieneusi*-positive specimens from crab-eating macaques were sequenced successfully. A total of 4 known genotypes were detected, including CM1 ($n = 14$), Peru8 ($n = 5$), D ($n = 3$), and Type IV ($n = 1$). Among them, CM1 was the dominant genotype in Suzhou, while only one genotype was found in Beijing. The sequences from genotypes CM1, Peru8, D, and Type IV were identical to the reference sequence KF305581 from Rhesus macaque, JF927959 from chicken, MT895457 from amur tiger, and AF242478 from human, respectively. In the maximum likelihood analysis of the *E. bieneusi* genotypes, genotypes CM1, Peru8, D, and Type IV were clustered with Group 1 (Figure 2).

4 Discussion

The results of this study indicate that *Cryptosporidium* spp., *G. duodenalis*, and *E. bieneusi* are prevalent in crab-eating macaques in Suzhou and Beijing of Chinese cities. Altogether, the detection rates for *Cryptosporidium* spp., *G. duodenalis*, and *E. bieneusi* were 11.9, 5.6, and 4.6%, respectively. The detection rate (11.9%) in this study for *Cryptosporidium* spp. was higher than that observed in free-range monkeys conducted in Shanxi (3.0%), Yunan (0 and 0.6%), Guangxi (1.0%), and Guizhou (0.7%) of China (Karim et al., 2014d; Du et al., 2015; Gu et al., 2016; Jia et al., 2022; Shu et al., 2022). However, it is similar to the prevalence in farmed crab-eating macaques in Hainan (9.1%) (Chen et al., 2019). The high detection rate of *Cryptosporidium* spp. in this study may be due to the highly intensive farming model in crab-eating macaque farms. Further comparison with other countries, the detection rate of farmed crab-eating macaques was also higher

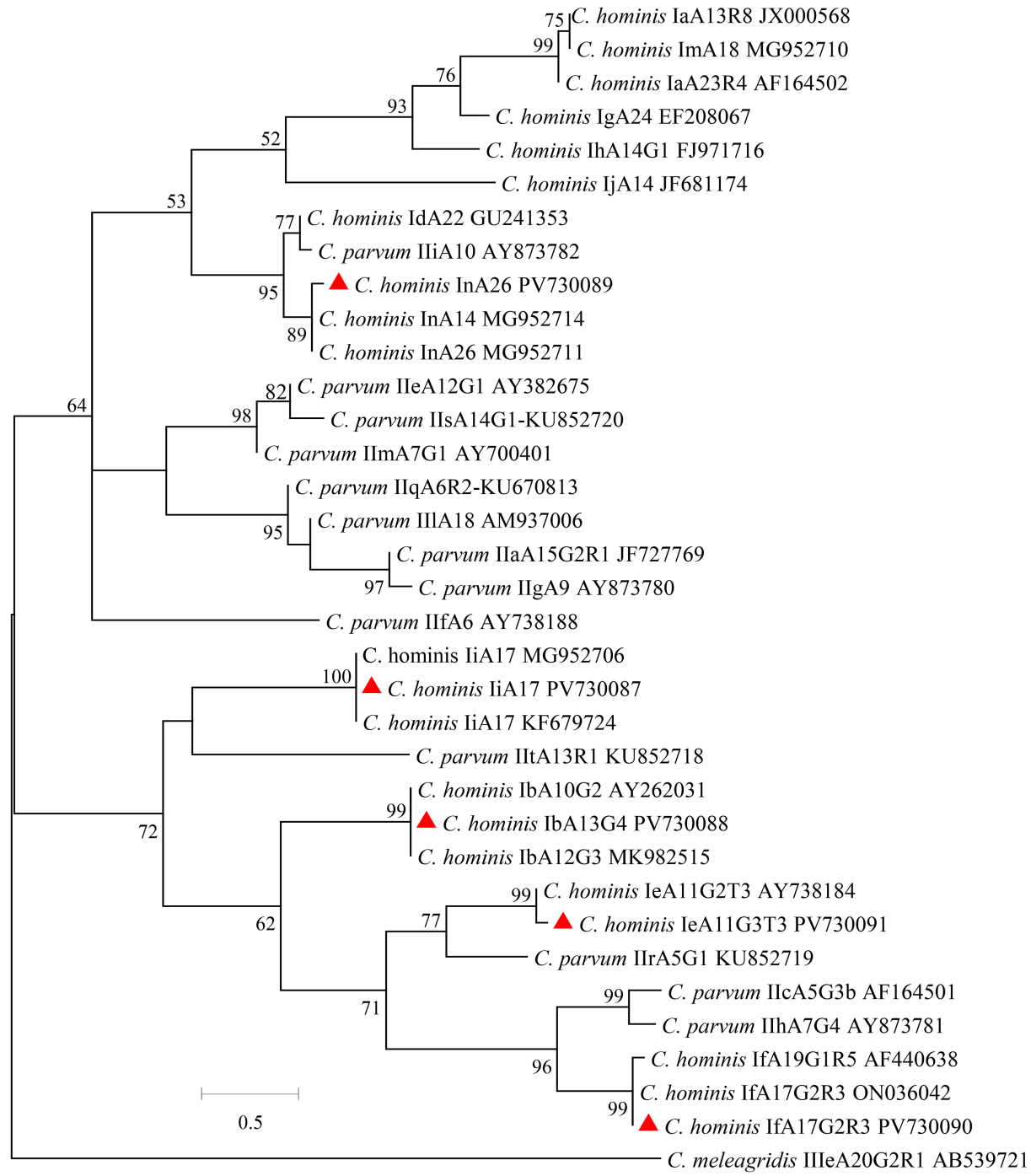

FIGURE 2
Phylogenetic relationships of *E. bieneusi* genotypes based on maximum likelihood analysis. The genotypes of *E. bieneusi* that have been identified in this study are indicated by red triangles. Bootstrap values below 50% are not shown. Bar = 0.1 substitutions per site.

than that free-range NHPs in Thailand (1.0%), Kenya (2.6%), Madagascar (4.0%), and Rwanda (4.0%) (Li et al., 2011; Sak et al., 2014; Bodager et al., 2015; Sricharern et al., 2016). Therefore, the intensive farming of animals was conducive to the transmission of *Cryptosporidium* spp. The detection rates of *G. duodenalis* (5.6%) and *E. bieneusi* (4.6%) in this study are lower than those found in NHPs in other studies, which reported detection rates ranging from 8.5 to 32.3% for *G. duodenalis* and from 11.4 to 46.2% for *E. bieneusi* (Johnston et al., 2010; Beck et al., 2011; Ye et al., 2012; Du et al., 2015; Karim et al., 2015; Zhong et al., 2017). The low detection rate of these two pathogens may be due to the high prevalence of *Cryptosporidium* limit the transmission of them. Among the two cities, the detection rates of *Cryptosporidium* spp., *G. duodenalis*, and *E. bieneusi* were higher in Suzhou, probably because of the higher stocking density on this farm. By age, the detection rates for *Cryptosporidium* spp. (32.6%), *G. duodenalis* (9.8%), and *E. bieneusi* (6.8%) in monkeys of under 2 months of age were higher than those over 2 years (1.8, 4.0%; 3.7%). Similar results have been found in other animals, including bamboo rats and horses (Li F. et al., 2019; Li et al., 2020). This may be related to the relatively low immunity of young crab-eating macaques.

The *C. hominis* subtypes found in this study belongs to highly divergent subtypes. Five subtypes of *C. hominis* were identified in crab-eating macaques in this study, namely IbA13G4 ($n = 27$), InA26 ($n = 3$), IiA17 ($n = 3$), IfA17G2R3 ($n = 3$), and IeA11G3T3 ($n = 2$). The emerging subtype IbA13G4 was dominant subtypes in this study, and was detected in crab-eating macaques for the first time. In previous studies, many outbreaks of cryptosporidiosis were caused by Ib subtype family around the world (Yang et al., 2021; Huang et al., 2025). The subtype IbA10G2 is responsible for most outbreaks of cryptosporidiosis in humans in both industrialized and developing countries (Cacciò and Chalmers, 2016; Feng et al., 2018). Furthermore, previous studies have shown that IbA12G3 induced a significantly higher intensity of oocyst and had higher parasite loads in the mouse intestine (Huang et al., 2024). Similarly, the Ie, If, and Ii subtype families are common in humans worldwide (Xiao and Feng, 2017). Among them, subtypes IeA11G3T3 and IiA17 were occasionally found in cancer patients and HIV-infected patients, they are apparently zoonotic (Sannella et al., 2019; Makipour et al., 2025). In contrast, the subtype IfA17G2R3 and InA26 were only found in rhesus monkeys in Guizhou and in crab-eating macaques in Hainan, respectively (Chen et al., 2019; Jia et al., 2022). Therefore, these two subtypes have potential zoonotic risk. In the future, we will conduct more studies to evaluate the infectivity and pathogenicity of *C. hominis* subtypes in animals.

The crab-eating macaques could be reservoirs for zoonotic assemblage B. Similar to other studies in crab-eating macaques, only assemblage B was found in this study (Karim et al., 2014d; Cai et al., 2021). Previous studies have shown that assemblage B had the broadest host range, and assemblage B was responsible for most giardiasis cases in humans (Feng and Xiao, 2011). In contrast, the assemblage A and E were occasionally found in non-human primates. A few studies had shown that the assemblage A was found in some non-human primates in China (Karim et al., 2014d; Ye et al., 2014) and other countries (Sricharern et al., 2016; Brynildsrud et al., 2018). In addition, assemblage E were found in five non-human primates (Brynildsrud et al., 2018). In present study, assemblage B was the only assemblage in the crab-eating macaques. This could have been due to the confined nature of animals in the facility, which limits the introduction of other genotypes. The common occurrence of assemblage B suggested that *G. duodenalis* from crab-eating macaques has high zoonotic potential.

Crab-eating macaques may potentially contribute to the zoonotic transmission of *E. bieneusi* genotypes to humans. In this study, 4 *E. bieneusi* genotypes were found, namely CM1 (14 specimens), Peru8 (5 specimens), D (3 specimens), and Type IV (1 specimen) and these genotypes belong to the zoonotic Group 1. Among these genotypes of *E. bieneusi*, genotypes D, Peru 8, and Type IV are mainly identified in humans, and have been frequently documented in domestic and wild animals, including non-human primates (Li W. et al., 2019; Li and Xiao, 2021; Li et al., 2022). In previous studies, the genotype CM1 has been only found in non-human primates in Guangdong, Guangxi, Yunan, and Sichuan of China and it was not found in humans (Karim et al., 2014a; Karim et al., 2014b). This is probably because only a small number of studies have been performed on human *E. bieneusi* infection in China. The common occurrence of zoonotic genotypes suggested that *E. bieneusi* from crab-eating macaques has high zoonotic potential.

5 Conclusion

This study reported the prevalence of *Cryptosporidium* spp., *G. duodenalis*, and *E. bieneusi* in crab-eating macaques in Beijing and Suzhou cities, China. The results indicate that known zoonotic *C. hominis*, Assemblage B, and *E. bieneusi* genotypes are prevalent in crab-eating macaques. Crab-eating macaques are in close contact with humans. Therefore, crab-eating macaques may play a potential role in the zoonotic transmission of pathogens to humans. Further studies are needed to monitor the molecular epidemiology of these three pathogens in farmed crab-eating macaques.

Data availability statement

The datasets presented in this study can be found in online repositories. The names of the repository/repositories and accession number(s) can be found here: https://www.ncbi.nlm.nih.gov/genbank/, PV730087-PV730091 and PV715454-PV715457.

Ethics statement

The animal studies were approved by Research Ethics Committee of the Fuyang Normal University. The studies were conducted in accordance with the local legislation and institutional requirements. Written informed consent was obtained from the owners for the participation of their animals in this study.

Author contributions

HZ: Writing – original draft, Writing – review & editing, Conceptualization. HC: Software, Writing – review & editing. CH: Software, Writing – review & editing. WL: Funding acquisition, Project administration, Writing – review & editing. FL: Funding acquisition, Project administration, Writing – review & editing.

Funding

The author(s) declare that financial support was received for the research and/or publication of this article. This work was supported by the Key Projects of Scientific Research Plan of Colleges and Universities of Anhui Province (2023AH050427), the Veterinary Science Peak Discipline Project of Anhui Science and Technology University (XK-XJGF002), the National Undergraduate Training Program for Innovation and Entrepreneurship (202410371016), the Scientific research project of Fuyang Normal University (2023KYQD0003), and the Biological and Medical Sciences of Applied Summit Nurturing Disciplines in Anhui Province (Anhui Education Secretary Department [2023]13).

Conflict of interest

The authors declare that the research was conducted in the absence of any commercial or financial relationships that could be construed as a potential conflict of interest.

Generative AI statement

The authors declare that no Gen AI was used in the creation of this manuscript.

Publisher's note

Supplementary material

The Supplementary material for this article can be found online at: https://www.frontiersin.org/articles/10.3389/fmicb.2025.1641632/full#supplementary-material

References

Alves, M., Xiao, L., Sulaiman, I., Lal, A. A., Matos, O., and Antunes, F. (2003). Subgenotype analysis of *Cryptosporidium* isolates from humans, cattle, and zoo ruminants in Portugal. *J. Clin. Microbiol.* 41, 2744–2747. doi: 10.1128/jcm.41.6.2744-2747.2003

Beck, R., Sprong, H., Bata, I., Lucinger, S., Pozio, E., and Cacciò, S. M. (2011). Prevalence and molecular typing of *Giardia* spp. in captive mammals at the zoo of Zagreb, Croatia. *Vet. Parasitol.* 175, 40–46. doi: 10.1016/j.vetpar.2010.09.026

Bodager, J. R., Parsons, M. B., Wright, P. C., Rasambainarivo, F., Roellig, D., Xiao, L., et al. (2015). Complex epidemiology and zoonotic potential for *Cryptosporidium suis* in rural Madagascar. *Vet. Parasitol.* 207, 140–143. doi: 10.1016/j.vetpar.2014.11.013

Bouzid, M., Hunter, P. R., Mcdonald, V., Elwin, K., Chalmers, R. M., and Tyler, K. M. (2013). A new heterogeneous family of telomerically encoded *Cryptosporidium* proteins. *Evol. Appl.* 6, 207–217. doi: 10.1111/j.1752-4571.2012.00277.x

Brynildsrud, O., Tysnes, K. R., Robertson, L. J., and Debenham, J. J. (2018). *Giardia duodenalis* in primates: classification and host specificity based on phylogenetic analysis of sequence data. *Zoonoses Public Health* 65, 637–647. doi: 10.1111/zph.12470

Cacciò, S. M., and Chalmers, R. M. (2016). Human cryptosporidiosis in Europe. *Clin. Microbiol. Infect.* 22, 471–480. doi: 10.1016/j.cmi.2016.04.021

Caccio, S. M., and Ryan, U. (2008). Molecular epidemiology of giardiasis. *Mol. Biochem. Parasitol.* 160, 75–80. doi: 10.1016/j.molbiopara.2008.04.006

Cai, W., Ryan, U., Xiao, L., and Feng, Y. (2021). Zoonotic giardiasis: an update. *Parasitol. Res.* 120, 4199–4218. doi: 10.1007/s00436-021-07325-2

Chen, L., Hu, S., Jiang, W., Zhao, J., Li, N., Guo, Y., et al. (2019). *Cryptosporidium parvum* and *Cryptosporidium hominis* subtypes in crab-eating macaques. *Parasit. Vectors* 12:350. doi: 10.1186/s13071-019-3604-7

Chen, L., Li, N., Guo, Y., Zhao, J., Feng, Y., and Xiao, L. (2020). Multilocus sequence typing of *Enterocytozoon bieneusi* in crab-eating macaques (*Macaca fascicularis*) in Hainan, China. *Parasit. Vectors* 13:182. doi: 10.1186/s13071-020-04046-w

Du, S. Z., Zhao, G. H., Shao, J. F., Fang, Y. Q., Tian, G. R., Zhang, L. X., et al. (2015). *Cryptosporidium* spp., *Giardia intestinalis*, and *Enterocytozoon bieneusi* in captive non-human primates in Qinling Mountains. *Korean J. Parasitol.* 53, 395–402. doi: 10.3347/kjp.2015.53.4.395

Feng, Y., Ryan, U. M., and Xiao, L. (2018). Genetic diversity and population structure of *Cryptosporidium*. *Trends Parasitol.* 34, 997–1011. doi: 10.1016/j.pt.2018.07.009

Feng, Y., and Xiao, L. (2011). Zoonotic potential and molecular epidemiology of *Giardia* species and giardiasis. *Clin. Microbiol. Rev.* 24, 110–140. doi: 10.1128/CMR.00033-10

Feng, Y., and Xiao, L. (2017). Molecular epidemiology of cryptosporidiosis in China. *Front. Microbiol.* 8:1701. doi: 10.3389/fmicb.2017.01701

Gu, Y., Wang, X., Zhou, C., Li, P., Xu, Q., Zhao, C., et al. (2016). Investigation on Cryptosporidium infections in wild animals in a zoo in Anhui Provinece. *J Zoo Wildl Med.* 47, 846–854. doi: 10.1638/2015-0301.1

Guo, Y., Li, N., Feng, Y., and Xiao, L. (2021a). Zoonotic parasites in farmed exotic animals in China: implications to public health. *Int. J. Parasitol. Parasites Wildl.* 14, 241–247. doi: 10.1016/j.ijppaw.2021.02.016

Guo, Y., Ryan, U., Feng, Y., and Xiao, L. (2021b). Emergence of zoonotic Cryptosporidium parvum in China. *Trends Parasitol.* 38, 335–343. doi: 10.1016/j.pt.2021.12.002

Huang, W., Feng, Y., and Xiao, L. (2025). Cryptosporidium hominis. *Trends Parasitol.* 29:s1471-4922(25)00095-9. doi: 10.1016/j.pt.2025.04.001

Huang, W., He, W., Huang, Y., Tang, Y., Chen, M., Sun, L., et al. (2024). Multicopy subtelomeric genes underlie animal infectivity of divergent *Cryptosporidium hominis* subtypes. *Nat. Commun.* 15:10774. doi: 10.1038/s41467-024-54995-4

Jia, R., Wen, X., Guo, Y., Xiao, L., Feng, Y., and Li, N. (2022). Decline in Cryptosporidium infection in free-ranging rhesus monkeys in a park after public health interventions. *Front. Cell. Infect. Microbiol.* 12:901766. doi: 10.3389/fcimb.2022.901766

Jiang, J., Alderisio, K. A., Singh, A., and Xiao, L. (2005). Development of procedures for direct extraction of *Cryptosporidium* DNA from water concentrates and for relief of PCR inhibitors. *Appl. Environ. Microbiol.* 71, 1135–1141. doi: 10.1128/AEM.71.3.1135-1141.2005

Jiang, S., Yu, S., Feng, Y., Zhang, L., Santin, M., Xiao, L., et al. (2024). Widespread distribution of human-infective *Enterocytozoon bieneusi* genotypes in small rodents in Northeast China and phylogeny and zoonotic implications revisited. *Acta Trop.* 253:107160. doi: 10.1016/j.actatropica.2024.107160

Johnston, A. R., Gillespie, T. R., Rwego, I. B., Mclachlan, T. L., Kent, A. D., and Goldberg, T. L. (2010). Molecular epidemiology of cross-species *Giardia duodenalis* transmission in western Uganda. *PLoS Negl. Trop. Dis.* 4:e683. doi: 10.1371/journal.pntd.0000683

Karim, M. R., Dong, H., Li, T., Yu, F., Li, D., Zhang, L., et al. (2015). Predomination and new genotypes of *Enterocytozoon bieneusi* in captive nonhuman primates in zoos in China: high genetic diversity and zoonotic significance. *PLoS One* 10:e0117991. doi: 10.1371/journal.pone.0117991

Karim, M. R., Dong, H., Yu, F., Jian, F., Zhang, L., Wang, R., et al. (2014a). Genetic diversity in *Enterocytozoon bieneusi* isolates from dogs and cats in China: host specificity and public health implications. *J. Clin. Microbiol.* 52, 3297–3302. doi: 10.1128/JCM.01352-14

Karim, M. R., Wang, R., Dong, H., Zhang, L., Li, J., Zhang, S., et al. (2014b). Genetic polymorphism and zoonotic potential of *Enterocytozoon bieneusi* from nonhuman primates in China. *Appl. Environ. Microbiol.* 80, 1893–1898. doi: 10.1128/AEM.03845-13

Karim, M. R., Wang, R., He, X., Zhang, L., Li, J., Rume, F. I., et al. (2014c). Multilocus sequence typing of *Enterocytozoon bieneusi* in nonhuman primates in China. *Vet. Parasitol.* 200, 13–23. doi: 10.1016/j.vetpar.2013.12.004

Karim, M. R., Zhang, S., Jian, F., Li, J., Zhou, C., Zhang, L., et al. (2014d). Multilocus typing of *Cryptosporidium* spp. and *Giardia duodenalis* from non-human primates in China. *Int. J. Parasitol.* 44, 1039–1047. doi: 10.1016/j.ijpara.2014.07.006

Li, W., Feng, Y., and Santin, M. (2019). Host specificity of *Enterocytozoon bieneusi* and public health implications. *Trends Parasitol.* 35, 436–451. doi: 10.1016/j.pt.2019.04.004

Li, W., Feng, Y., and Xiao, L. (2022). Enterocytozoon bieneusi. *Trends Parasitol.* 38, 95–96. doi: 10.1016/j.pt.2021.08.003

Li, W., Kiulia, N. M., Mwenda, J. M., Nyachieo, A., Taylor, M. B., Zhang, X., et al. (2011). *Cyclospora papionis*, *Cryptosporidium hominis*, and human-pathogenic *Enterocytozoon bieneusi* in captive baboons in Kenya. *J. Clin. Microbiol.* 49, 4326–4329. doi: 10.1128/JCM.05051-11

Li, F., Su, J., Chahan, B., Guo, Q., Wang, T., Yu, Z., et al. (2019). Different distribution of *Cryptosporidium* species between horses and donkeys. *Infect. Genet. Evol.* 75:103954. doi: 10.1016/j.meegid.2019.103954

Li, W., and Xiao, L. (2021). Ecological and public health significance of *Enterocytozoon bieneusi*. *One Health* 12:100209. doi: 10.1016/j.onehlt.2020.100209

Li, F., Zhang, Z., Hu, S., Zhao, W., Zhao, J., Kváč, M., et al. (2020). Common occurrence of divergent *Cryptosporidium* species and *Cryptosporidium parvum* subtypes in farmed bamboo rats (*Rhizomys sinensis*). *Parasit. Vectors* 13:149. doi: 10.1186/s13071-020-04021-5

Makipour, H., Haghighi, A., Halakou, A., Dayer, D., Bitaraf, S., Farhadi Kia, A., et al. (2025). Identifying zoonotic risks: molecular insights into *Cryptosporidium* and *Enterocytozoon bieneusi* in pediatric cancer patients in Ahvaz, 2024. *Parasitol. Res.* 124:55. doi: 10.1007/s00436-025-08500-5

Ryan, U. M., Feng, Y., Fayer, R., and Xiao, L. (2021). Taxonomy and molecular epidemiology of *Cryptosporidium* and *Giardia* – a 50 year perspective (1971-2021). *Int. J. Parasitol.* 51, 1099–1119. doi: 10.1016/j.ijpara.2021.08.007

Sak, B., Petrželková, K. J., Květoňová, D., Mynářová, A., Pomajbíková, K., Modrý, D., et al. (2014). Diversity of microsporidia, *Cryptosporidium* and *Giardia* in mountain gorillas (*Gorilla beringei beringei*) in volcanoes National Park, Rwanda. *PLoS One* 9:e109751. doi: 10.1371/journal.pone.0109751

Sannella, A. R., Suputtamongkol, Y., Wongsawat, E., and Cacciò, S. M. (2019). A retrospective molecular study of *Cryptosporidium* species and genotypes in HIV-infected patients from Thailand. *Parasit. Vectors* 12:91. doi: 10.1186/s13071-019-3348-4

Santín, M., and Fayer, R. (2011). Microsporidiosis: *Enterocytozoon bieneusi* in domesticated and wild animals. *Res. Vet. Sci.* 90, 363–371. doi: 10.1016/j.rvsc.2010.07.014

Shu, F., Song, S., Wei, Y., Li, F., Guo, Y., Feng, Y., et al. (2022). High zoonotic potential of *Cryptosporidium* spp., *Giardia duodenalis*, and *Enterocytozoon bieneusi* in wild nonhuman primates from Yunnan Province, China. *Parasit. Vectors* 15:85. doi: 10.1186/s13071-022-05217-7

Sricharern, W., Inpankaew, T., Keawmongkol, S., Supanam, J., Stich, R. W., and Jittapalapong, S. (2016). Molecular detection and prevalence of *Giardia duodenalis* and *Cryptosporidium* spp. among long-tailed macaques (*Macaca fascicularis*) in Thailand. *Infect. Genet. Evol.* 40, 310–314. doi: 10.1016/j.meegid.2016.02.004

Sulaiman, I. M., Fayer, R., Bern, C., Gilman, R. H., Trout, J. M., Schantz, P. M., et al. (2003a). Triosephosphate isomerase gene characterization and potential zoonotic transmission of *Giardia duodenalis*. *Emerg. Infect. Dis.* 9, 1444–1452. doi: 10.3201/eid0911.030084

Sulaiman, I. M., Fayer, R., Lal, A. A., Trout, J. M., Schaefer, F. W.3rd, and Xiao, L. (2003b). Molecular characterization of microsporidia indicates that wild mammals harbor host-adapted Enterocytozoon spp. as well as human-pathogenic *Enterocytozoon bieneusi*. *Appl. Environ. Microbiol.* 69, 4495–4501. doi: 10.1128/AEM.69.8.4495-4501.2003

Wang, S. S., Li, J. Q., Li, Y. H., Wang, X. W., Fan, X. C., Liu, X., et al. (2018). Novel genotypes and multilocus genotypes of *Enterocytozoon bieneusi* in pigs in northwestern China: a public health concern. *Infect. Genet. Evol.* 63, 89–94. doi: 10.1016/j.meegid.2018.05.015

Wang, L., Xiao, L., Duan, L., Ye, J., Guo, Y., Guo, M., et al. (2013). Concurrent infections of *Giardia duodenalis*, *Enterocytozoon bieneusi*, and *Clostridium difficile* in children during a cryptosporidiosis outbreak in a pediatric hospital in China. *PLoS Negl. Trop. Dis.* 7:e2437. doi: 10.1371/journal.pntd.0002437

Xiao, L. (2010). Molecular epidemiology of cryptosporidiosis: an update. *Exp. Parasitol.* 124, 80–89. doi: 10.1016/j.exppara.2009.03.018

Xiao, L., Escalante, L., Yang, C., Sulaiman, I., Escalante, A. A., Montali, R. J., et al. (1999). Phylogenetic analysis of *Cryptosporidium* parasites based on the small-subunit rRNA gene locus. *Appl. Environ. Microbiol.* 65, 1578–1583. doi: 10.1128/AEM.65.4.1578-1583.1999

Xiao, L., and Feng, Y. (2017). Molecular epidemiologic tools for waterborne pathogens *Cryptosporidium* spp. and *Giardia duodenalis*. *Food Waterborne Parasitol.* 8-9, 14–32. doi: 10.1016/j.fawpar.2017.09.002

Yan, W., Alderisio, K., Roellig, D. M., Elwin, K., Chalmers, R. M., Yang, F., et al. (2017). Subtype analysis of zoonotic pathogen *Cryptosporidium* skunk genotype. *Infect. Genet. Evol.* 55, 20–25. doi: 10.1016/j.meegid.2017.08.023

Yang, X., Guo, Y., Xiao, L., and Feng, Y. (2021). Molecular epidemiology of human cryptosporidiosis in low- and middle-income countries. *Clin. Microbiol. Rev.* 34:00087-19. doi: 10.1128/CMR.00087-19

Ye, J., Xiao, L., Li, J., Huang, W., Amer, S. E., Guo, Y., et al. (2014). Occurrence of human-pathogenic *Enterocytozoon bieneusi*, *Giardia duodenalis* and *Cryptosporidium* genotypes in laboratory macaques in Guangxi, China. *Parasitol. Int.* 63, 132–137. doi: 10.1016/j.parint.2013.10.007

Ye, J., Xiao, L., Ma, J., Guo, M., Liu, L., and Feng, Y. (2012). Anthroponotic enteric parasites in monkeys in public park, China. *Emerg. Infect. Dis.* 18, 1640–1643. doi: 10.3201/eid1810.120653

Zhang, X. L., Pang, W., Hu, X. T., Li, J. L., Yao, Y. G., and Zheng, Y. T. (2014). Experimental primates and non-human primate (NHP) models of human diseases in China: current status and progress. *Dongwuxue Yanjiu* 35, 447–464. doi: 10.13918/j.issn.2095-8137.2014.6.447

Zhong, Z., Li, W., Deng, L., Song, Y., Wu, K., Tian, Y., et al. (2017). Multilocus genotyping of *Enterocytozoon bieneusi* derived from nonhuman primates in Southwest China. *PLoS One* 12:e0176926. doi: 10.1371/journal.pone.0176926

frontiers | Frontiers in Microbiology

TYPE Original Research
PUBLISHED 29 August 2025
DOI 10.3389/fmicb.2025.1634394

OPEN ACCESS

EDITED BY
Lei Deng,
Chinese Academy of Agricultural Sciences, China

REVIEWED BY
Subbaiyan Anbazhagan,
Indian Council of Medical Research (ICMR), India
Dayakar Seetha,
Rajiv Gandhi Centre for Biotechnology, India

*CORRESPONDENCE
Srikanth Srirama
✉ dr.srikanthsrirama@gmail.com Panneer Devaraju
✉ panneeryadav82@gmail.com

RECEIVED 24 May 2025
ACCEPTED 05 August 2025
PUBLISHED 29 August 2025

CITATION
Sihag KK, Arif W, Srirama S, Chandrasek aran AK, Raveendran V, Chandrakumar AB, Kasirajan A, Thavaraj SAP, Srinivasan L, Choolayil AC, Ashokkumar M, Ramasamy A, Yellapu NK and Devaraju P (2025) A longitudinal molecular surveillance of genetic heterogeneity of *Orientia tsutsugamushi* in humans, reservoir animals, and vectors in Puducherry, India.
Front. Microbiol. 16:1634394.
doi: 10.3389/fmicb.2025.1634394

A longitudinal molecular surveillance of genetic heterogeneity of *Orientia tsutsugamushi* in humans, reservoir animals, and vectors in Puducherry, India

Krishan Kumar Sihag[1,2], Waseema Arif[1], Srikanth Srirama[1]*, Anand Kumar Chandrasekaran[3], Vinod Raveendran[4], Asayas Bosco Chandrakumar[5], Anand Kasirajan[6], Sivagamy Alias Punitha Thavaraj[7], Lakshmy Srinivasan[1], Anoop C. Choolayil[1], Mathivanan Ashokkumar[8], Amala Ramasamy[9], Nanda Kumar Yellapu[10] and Panneer Devaraju[1,2]*

[1]Unit of One Health, ICMR-Vector Control Research Centre (ICMR-VCRC), Indira Nagar, Puducherry, India, [2]ICMR-Vector Control Research Centre (ICMR-VCRC), Affiliated to Pondicherry University, Kalapet, Puducherry, India, [3]Indira Gandhi Medical College and Research Institute, Kathirkamam, Puducherry, India, [4]Sri Venkateshwaraa Medical College Hospital and Research Centre, Ariyur, Puducherry, India, [5]Sri Lakshmi Narayana Institute of Medical Science, Villianur, Puducherry, India, [6]Mahatma Gandhi Medical Advance Research Institute, Sri Balaji Vidyapeeth, Pilayarkuppam, Puducherry, India, [7]ICMR-Vector Control Research Centre (ICMR-VCRC), Indira Nagar, Puducherry, India, [8]Unit of Microbiology and Immunology, ICMR-Vector Control Research Centre (ICMR-VCRC), Indira Nagar, Puducherry, India, [9]Unit of Biostatistics and VBD Modeling, ICMR-Vector Control Research Centre (ICMR-VCRC), Indira Nagar, Puducherry, India, [10]Unit of Clinical and Molecular Medicine, ICMR-Vector Control Research Centre (ICMR-VCRC), Indira Nagar, Puducherry, India

Background: Scrub typhus (ST), is a vector borne zoonotic disease, transmitted by the larva of the trombiculid mites. The enzootic cycle of the pathogen involves rodents/shrews as the animal reservoirs and humans are the accidental dead-end host. A transposon-like activity in its major antigen 56 kDa, has led to the evolution of several serotypes/strains, and more than 40 serotypes are reported globally. Puducherry, India, is endemic to scrub, but limited data exist on local serotype distribution across hosts and vectors.

Methodology: A longitudinal molecular surveillance was conducted in Puducherry to investigate the genetic diversity of *Orientia tsutsugamushi* among humans, animal reservoirs, and vectors. Samples from febrile patients, trapped rodents/shrews, and their infesting mites were screened using real-time and nested PCR. Serotype analysis was performed by partial amplification and sequencing of the 56 kDa gene, followed by phylogenetic, pairwise genetic distance and amino acid analysis.

Result: ST infection was detected in 4.37% (95% CI: 3.05–5.71%) of human, 11.52% (95% CI: 8.6–14.4%) of rodent/shrew, and 2.36% (95% CI: 0.95–4.87%) of mite samples. Karp-like (51.72%) and Gilliam-like (41.38%) strains were predominant in both humans and animal hosts, with pairwise genetic distance (<0.1) and amino acid identity (>85%) analysis revealing a close relationship between the strains identified across the region. Notably, the only mite pool that tested positive for

the 56 kDa gene, along with a shrew, was identified to belong to the TA678-like serotype (6.90%), which has not been previously reported from Puducherry.
Conclusion: This study provides molecular evidence of the enzootic maintenance and active human transmission of *O. tsutsugamushi* in Puducherry, with multiple co-circulating serotypes. The first detection of the TA678-like strain in the region suggests the possible introduction of new strains and underscores the need to monitor for strain-specific clinical manifestations in future studies.

KEYWORDS

scrub typhus, molecular diagnostics, genetic heterogeneity, TA678-like strain, phylogenetic analysis

1 Introduction

Scrub typhus (ST) is a re-emerging rickettsial disease caused by *Orientia tsutsugamushi*, an obligate intracellular Gram-negative bacterium. It is transmitted by the bite of the chigger mites, majorly, by the trombiculid mites, e.g., *Leptotrombidium deliense*. In humans, the infection presents as an acute undifferentiated febrile illness (AUFI) with wide-ranging severity. The disease is associated with mortality rates of up to 70% (median rate 6%) in untreated cases, with over 1 billion humans at risk of acquiring the infection globally (Taylor et al., 2015). It is endemic in the Southeast Asian countries, constituting the tsutsugamushi triangle, and has recently exhibited its extension to other regions as well. Since the identification of three antigenically diverse strains of *O. tsutsugamushi* by Shishido, there have been reports of multiple strains that have caused several outbreaks (Shishido, 1962; Seetha et al., 2023). The 56 kDa gene encodes the most abundant antigen, the outer membrane protein of *O. tsutsugamushi*. The hypervariable regions in the 56 kDa gene contribute to the array of pathogenic strains (Ohashi et al., 1992). Based on the genetic diversity of the 56 kDa gene more than 40 serotypes have been reported, with their distribution changing from region to region in the tsutsugamushi triangle. The Karp and Gilliam serotypes are prevalent in Taiwan, Gilliam in China, and the Boryong in South Korea. In India Kato and Karp are dominant, while Kato, Karp, Gilliam, Kawasaki, and Kuroki types are found in Japan (Prakash, 2017). More importantly, the clinical characteristics of the disease were observed to vary with the serotype of the organism. The Karp strain is often linked to severe illness including encephalitis and multi-organ dysfunction, while strains like Boryong and Kato are generally associated with milder clinical presentations. Further, multiple ecological factors including the number of rodents, the characteristics of the habitat, the chigger index and the climatic conditions also play a critical role in the incidence of ST (Bhopdhornangkul et al., 2021; Ding et al., 2022; Chang et al., 2024; Konyak et al., 2024).

India has reported several outbreaks of ST with consistent disease burden in the past few decades. Puducherry is one among the endemic areas in the country reporting an increasing trend in the number of cases reported annually. The figures reached a maximum of 998 cases in 2022 and 984 cases in 2023. Subsequently, numerous studies were conducted to estimate the prevalence of ST in human and animal reservoirs. However, only a few have focused on the molecular characterization of the circulating serotypes of *O. tsutsugamushi* by amplification and nucleotide sequencing of the 56-kDa gene. Previous molecular studies in humans from Puducherry targeting the 56-kDa gene have reported a prevalence of 27.6 and 30% but did not determine the prevailing serotype (Patricia et al., 2017; Anitharaj et al., 2020). In the case of small mammals, Candasamy et al., did not observe any positivity for the 56-kDa gene in rodents/shrews collected from Puducherry (Candasamy et al., 2016). Recently, in household rats from Tamil Nadu, Karnataka, and Puducherry, Purushothaman et al., reported a prevalence of 55.29% by targeting the 47-kDa gene (Purushothaman et al., 2024). Notably, these studies too did not explore the serotype of the pathogen. In our previous works we observed the circulation of Karp, Kato and Kawasaki serotypes in the reservoirs and mite vectors in Puducherry (Devaraju et al., 2020; Balasubramanian et al., 2024; Eikenbary et al., 2024; Ritu et al., 2024). In continuation, the current study aimed to identify the serotype of the pathogen circulating among the patients (scrub typhus confirmed by PCR) and to establish its association with the strains circulating among the vector mites and the reservoir hosts rodents/shrews in Puducherry. Understanding the serotype distribution is crucial for refining the existing diagnostic assays, developing novel diagnostic tools, and advancing vaccine research (Koraluru et al., 2015).

2 Materials and methods

2.1 Ethical approval for study on rodent/shrews and human participants

The trapping and collection of blood and organ samples from the trapped rodents/shrews was approved by the Institutional Animal Ethics Committee (No: ICMR-VCRC/IAEC/2018/2) of ICMR-VCRC. For the use of human blood samples, the Institutional Human Ethics Committee (IHEC 1022/N/F) of ICMR-VCRC approval was obtained.

2.2 Human sample collection

All experiments on human participants were performed in accordance with the Declaration of Helsinki. Prior informed consent from human participants and/or their legal guardians were obtained before the sample collection. Blood samples were collected from patients (classified as acute undifferentiated febrile illness), with history of fever lasting between 3 to 14 days without any evident foci. The study excluded patients with severe illness precluding informed consent, those receiving immunosuppressive therapy, and individuals with a prior diagnosis of autoimmune disorders or malignancies. Additionally, patients presenting with an identifiable source of infection or an alternative cause of fever, as determined during the initial clinical

evaluation by the attending physician, were also excluded. Two milliliters of blood in EDTA vials were collected from the patients seeking medical facilities from three tertiary care centers at Puducherry [1. Sri Venkateshwaraa Medical College Hospital and Research Centre (SVMCH&RC), 2. Sri Lakshmi Narayana Institute of Medical Science (SLIMS), and 3. Indira Gandhi Medical College and Research Institute (IGMCRI)] for 19 months from August 2022 to February 2024.

2.3 Trapping and processing of rodents/shrews

ARRIVE guidelines were followed with the animal usage in this study. Rodents/shrews were trapped from 29 randomly selected study sites in and around Puducherry. The live trapping of rodents/shrews was achieved using Sherman traps, using food items made of flour ("pakoda") as bait. The rodents/shrews were trapped for a period of 1 year from January 2022 to December 2022. Traps (n = 20/site) were placed in domestic and peri-domestic areas around human habitats, vegetations and at the site of rodent/shrew burrows. The traps were set 1–2 h before the sunset and were retrieved before dawn. The positive traps were transported to the laboratory for further processing. The trapped rodents were euthanised with CO_2 as recommended by CCSEA (Committee for the Purpose of Control and Supervision of Experiments on Animals (CPCSEA), 2018) and taxonomically identified based on the morphological features (Agrawal, 2000).

From the trapped rodents/shrews, blood was collected by cardiac puncture in vials containing EDTA. Additionally, organs including the lungs, heart, brain, spleen, kidneys, liver, and small intestine were dissected and transferred to a labeled container with sterile PBS and then stored at −40°C until DNA isolation.

2.4 Ectoparasite collection from the trapped rodents/shrews

The trapped rodents/shrews were examined for the mite infestation. Using tweezers and hair brush, the mites in the pinnae, legs and fur of rodents/shrews were retrieved and stored in 70% ethanol at room temperature. Taxonomical identification based on the morphological features was carried out randomly in 2% of the mites. The taxonomically identical mites were grouped into pools (1–40 mites/pool) according to the geographical site of trapping and host.

2.5 Processing of the samples

Extraction of DNA from human and rodent/shrew blood samples was done using the DNeasy Blood and Tissue Kit (Qiagen, Hilden, Germany) following the manufacturer's instructions. DNA from the mites and rodent/shrew organ samples was extracted by phenol-chloroform method (Ritu et al., 2024). Briefly, organs and mite pools were mechanically lysed using metallic beads and a tissue lyser (Qiagen, Hilden, Germany), followed by enzymatic digestion with proteinase K and lysis buffer. DNA was extracted using phenol-chloroform-isoamyl alcohol and purified through ethanol precipitation. The final DNA pellet was air-dried and reconstituted in nuclease-free water for downstream applications.

2.6 Molecular detection of *O. tsutsugamushi*

Molecular screening of *O. tsutsugamushi* in the DNA extracted from AUFI patients, rodents/shrews and mite pools was carried out by following the published protocols using the Real-time PCR (Tantibhedhyangkul et al., 2017) and Nested PCR (Furuya et al., 1993). All oligonucleotide primers and probes used in this study were procured from Eurofins Genomics India Pvt. Ltd. (Bangalore, Karnataka). Real-time PCR targeting the 47 kDa gene was performed using primers FP: 5′-CCATCTAATACTGTACTTGAAGCAGTTGA-3′; RP: 5′-GTCCTAAATTCTCATTTAATTCTGGAGT-3′ and a TaqMan probe FAM-TCATTAAGC/ZEN/ATAACATTTAACATACCACGAC GA-IBFQ. Amplification was carried out using the Roche LightCycler® 96 system in a 10 µL reaction volume containing 2X LightCycler® 480 Probes Master (Roche Diagnostics, Mannheim, Germany), 10 pmol/µL each of forward and reverse primers, 10 pmol/µL of TaqMan probe, and template DNA. Thermal cycling conditions were: 95°C for 5 min, followed by 45 cycles of 95°C for 10 s, 60°C for 20 s, 72°C for 1 s, and a final step at 37°C for 30 s. Samples with a Ct value <40 were considered positive.

Two-step nested PCR targeting the 56 kDa type-specific antigen (TSA) gene was conducted using oligonucleotide primers N1 FP: 5′-TCAAGCTTATTGCTAGTGCAATGTCTGC-3′, N1 RP: 5′-AGGG ATCCCTGCTGCTGTGCTTGCTGCG-3′, N2 FP: 5′-GATCAAGC TTCCTCAGCCTACTATAATGCC-3′, N2 RP: 5′-CTAGGGATCC CGACAGATGCACTATTAGGC-3′ as per Furuya et al. (1993). The first-round PCR was performed in a 25 µL reaction mixture containing 2X GoTaq® Green Master Mix (Promega, Madison, WI, USA), 10 pmol/µL of each primer, 25 mM $MgCl_2$, and template DNA. The resulting amplicon was diluted 1:50 and used as the template for the second-round PCR. Thermocycling conditions for the first round were: 94°C for 5 min; 31 cycles of 94°C for 50 s, 55°C for 2 min, and 72°C for 2 min; followed by a final extension at 72°C for 7 min. The second-round PCR was carried out under the following conditions: 94°C for 5 min; 35 cycles of 94°C for 50 s, 58.8°C for 2 min, and 72°C for 2 min; followed by a final extension at 72°C for 7 min. PCR products were resolved by agarose gel electrophoresis, and the presence of a 483 bp amplicon was considered indicative of a positive result for *O. tsutsugamushi*.

2.7 Nucleotide sequencing and phylogenetic analysis

The 483 bp amplicons of 56 kDa TSA gene obtained from the nested PCR positive samples were subjected to Sanger sequencing using the Applied Biosystems Genetic Analyzer 3130XL (USA). Briefly, the PCR amplicons were purified using the NucleoSpin® Gel and PCR Clean-up kit (Macherey-Nagel, Duren, Germany) and the cycle sequencing reaction was set up using the BigDyeTM Terminator v3.1 Cycle Sequencing kit (Applied Biosystems, USA). The thermocycling conditions for the cycle sequencing PCR were: 96°C for 1 min and 25 cycles of 96°C for 10 s, 50°C for 5 s, 60°C for 4 min. The product was further purified using the NucleoSeq® kit (Macherey-Nagel, Duren, Germany), and subjected to nucleotide sequencing using the Applied Biosystems Genetic Analyzer 3130XL (USA). The quality of the Sanger sequencing results was checked using Chromas

and edited in BioEdit. Sequences with clear, sharp peaks and low background noise were selected. The low quality reads at the beginning and end of each sequence were trimmed, and only those with good quality (Phred score ≥20) were used for further analysis. These high-quality sequences were then compared with known sequences in the NCBI database using BLASTn. Only matches with 97% or higher identity were accepted for identifying the strain. Multiple sequence alignment was done using ClustalW, and the phylogenetic tree was constructed by the Maximum Likelihood method with 1,000 bootstrap replicates using the Kimura-2 parameter model in the MEGA version 11 software (Tamura et al., 2021). Additionally, a distance matrix was generated based on pairwise genetic distances between the human, animal and mite 56 kDa sequences. The time scale analysis following Bayesian phylogenetics was performed using the HKY substitution model with strict molecular clock and constant population size tree prior in the BEAST package v2.7.7. The Markov Chain Monte Carlo analyses was run with 10,00,000 steps, combined with 10% burn value and a maximum clade credibility tree was constructed with 95% highest posterior density (HPD) interval using the TreeAnnotator and visualized using Figtree v1.4.4. Further, multiple sequence alignment of the translated amino acid sequences with the full-length standard reference sequence was carried out for each serotype using BioEdit software version 7.7.1. The amino acid changes observed were presented as a table and the percentage identity was determined.

2.8 Quality control measures

DNA extraction, PCR setup, and amplification were carried out in physically separated, designated laboratory areas to minimize the risk of cross-contamination. Standard operating procedures were followed at each stage including the DNA extraction, amplification, post-amplification, and sequencing. The quality of extracted DNA was assessed by spectrophotometric analysis (A260/A280 ratio) using a Nanodrop instrument (Thermofisher, Madison, WI, USA). Each PCR run included internal positive and negative controls to monitor amplification performance. For sequencing, the post-amplification control supplied with the BigDye Terminator v3.1 Cycle Sequencing Kit (Applied Biosystems, USA) was used to confirm the reliability of reactions. All sequences generated were submitted to NCBI GenBank.

2.9 Statistical analysis

The data was entered and maintained in Microsoft Excel and analysis was performed in STATA version 18 (StataCorp, 2023). Prevalence of infection among the humans, rodents/shrews and mites were expressed as percentage with 95% Confidence interval.

3 Results

3.1 Molecular prevalence of *O. tsutsugamushi* in humans

A total of 916 blood samples from patients with AUFI were collected from three collaborating tertiary care centers in Puducherry between August 2022 and February 2024. Among these, 39 samples tested positive for the 47 kDa HtrA gene by real-time PCR, and 17 samples were positive for the 56 kDa TSA gene by nested PCR (Supplementary Figure S1). Overall, 40 patients tested positive for scrub typhus (ST) by either the 56 kDa or 47 kDa PCR assays (4.37%; 95% CI: 3.05–5.71%), and 16 patients were positive by both tests (Supplementary Table S1). The ST-positive patients (n = 40) were aged between 18 and 75 years, comprising 24 males (60%) and 15 females (37.5%); data for one patient were not available. The majority of cases (n = 24, 60%) were in the age group of 30–60 years.

3.2 Molecular prevalence of *O. tsutsugamushi* in rodents/shrews

A total of 460 rodents/shrews were captured using Sherman traps deployed across 29 study sites over the course of 1 year, from January to December 2022 of which 261 (56.73%) were male and 199 (43.26%) were female. Month-wise trap success rate ranged between 10 and 28.18% (Supplementary Table S2) whereas, area-wise trap success rate was within a range of 5–75% (Supplementary Table S3). Overall, the average trap success rate was 20.18%. Among the rodents trapped, the majority were *Suncus murinus* (n = 373, 81.08%), followed by *Rattus rattus* (n = 72, 15.65%) and *Bandicota indica* (n = 15, 3.26%) (Table 1). In the trapped animals, mite infestation was found in 39.78% (n = 183). For molecular detection of ST in trapped rodents/shrews, along with blood, seven different organs such as heart, brain, lungs, small intestine, spleen, kidney and liver were screened. In total, 58 samples—including 19 blood, 21 lungs, 5 heart, 7 liver, 2 kidney, 3 brain and 1 intestinal sample—from 45 rodents/shrews (9.78%; 95% CI: 7.07–12.5%) were tested positive for 47 kDa HtrA gene by real-time PCR. Further, 24 samples—including 9 blood, 5 lungs, 3 heart, 2 liver, 1 kidney, 2 spleen and 2 intestinal samples—from 20 rodents/shrews (4.35%; 95% CI: 2.48–6.21%) were tested positive for 56 kDa gene by nested PCR (Table 1 and Supplementary Table S4). Overall, 53 (11.52%; 95% CI: 8.6–14.4%) animals including 4 *Rattus rattus* and 49 *Suncus murinus* were identified to harbor the bacteria in blood or any other tissue either by 47 kDa or by 56 kDa PCR. In addition, 12 animals were positive for both the tests in at least one of the tissues analyzed (Supplementary Table S4).

3.3 Molecular prevalence of *O. tsutsugamushi* in chigger mites

From the animals trapped, a total of 7,465 trombiculid mites were retrieved. Of the mites identified using morphological features, the majority of them belonged to the genus *Leptotrombidium* (78.87%), including *L. insigne* (50.70%) and *L. deliense* (28.17%). The chigger index per animal was 16.23, with the highest value of 32.67 recorded in the month of June (Figure 1). Among the 296 mite pools screened for the presence of ST, 7 (2.36%; 95% CI: 0.95–4.87%) mite pools from 5 shrews were positive for ST by real-time PCR. Only one pool was tested positive for 56 kDa gene by nested PCR and was also identified to be the only sample positive for both tests (Table 1).

TABLE 1 Molecular detection of *Orientia tsutsugamushi* among infected humans, rodents/shrews, and chigger mites in and around Puducherry.

Sl. No.	Source of isolates	Total number of isolates/pools tested	Real time PCR positives	Nested PCR positives
1	Human			
	Whole blood	916	39	17
2	Rodents/shrews			
	Suncus murinus	373	42	18
	Rattus rattus	72	3	2
	Bandicota indica	15	0	0
3	Mite pools	296	7	1

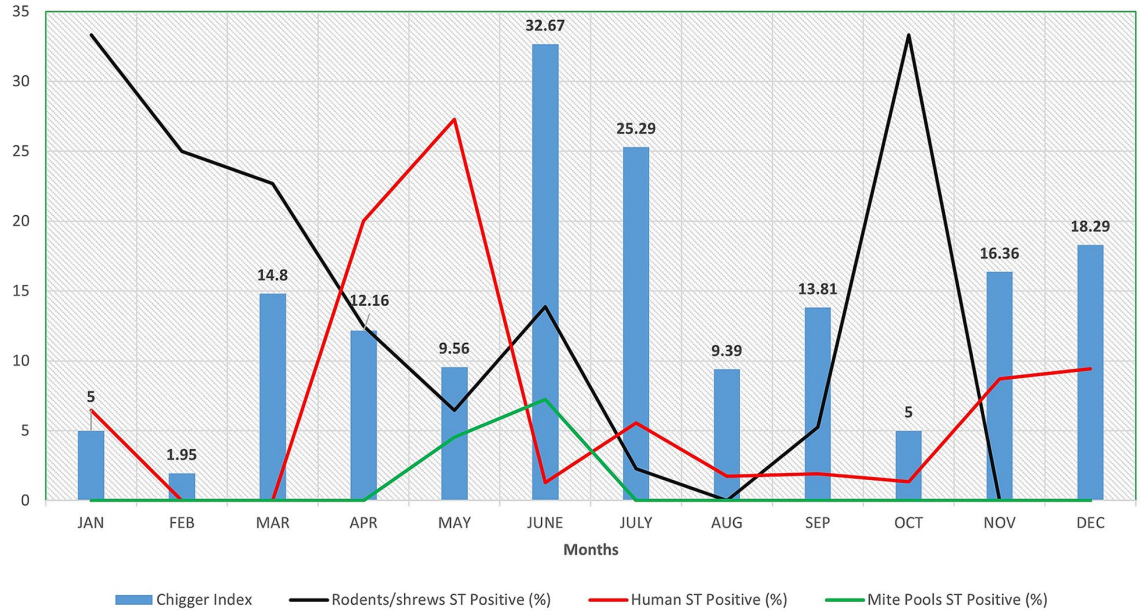

FIGURE 1
Graph depicting month wise chigger index along with scrub typhus positive (%) in rodents/shrews, humans and mite pools in and around Puducherry.

3.4 Phylogenetic analysis of *O. tsutsugamushi* strains circulating in Puducherry

Out of 42 nested PCR positive samples from humans ($n = 17$), rodents/shrews ($n = 24$) and vectors ($n = 1$), a total of 29 samples (16 human samples, 12 rodent/shrew samples, and 1 mite pool sample) yielded good quality nucleotide sequences which were subjected to genetic characterization. The sequences were analyzed and deposited in NCBI GenBank[1] with the accession numbers listed in Supplementary Table S5. In the phylogenetic analysis (Figure 2) of the human samples ($n = 16$), the predominance of Karp-like ($n = 9$; 56.25%) and Gilliam-like ($n = 7$; 43.75%) strains was observed. Similarly, the dominant serotypes observed to be enzooticaly circulated among the animal reservoirs were identified to be Karp-like ($n = 6$; 50.00%) followed by Gilliam-like ($n = 5$; 41.67%) and TA678-like ($n = 1$; 8.33%). The only mite pool that was positive for 56 kDa was identified as TA678-like serotype. Interestingly, we observed that the animal host from which the only positive mite pool was retrieved, was tested negative for ST by both the real time and nested PCR assays.

From the phylogenetic tree constructed using MEGA v. 11.0., it is notable that the strains of *O. tsutsugamushi* identified in patients, rodents/shrews and mite pools clustered into 3 groups. The pairwise genetic distance between humans and rodents/shrews/mite samples varied widely ranging from 0.03 to 0.93. Majority of the bacterial strains identified in the humans exhibited a closer genetic relatedness (distance < 0.1) with one or more of the strains circulating in rodents/shrews. The Gilliam related bacterial strain identified in a patient, with the sequence ID: PP935511, was identified to exhibit the least genetic distance (0.03) from five other strains identified in rodents/shrews (PP952072, PP952073, PP952078, OR689573 and OR689574) (Table 2). The tree constructed following the Bayesian phylogenetic exhibited the similar topology as the maximum likelihood tree. The mean evolutionary rate was determined to be 3.94×10^{-3} mutations/

1 https://www.ncbi.nlm.nih.gov/genbank/

10.3389/fmicb.2025.1634394

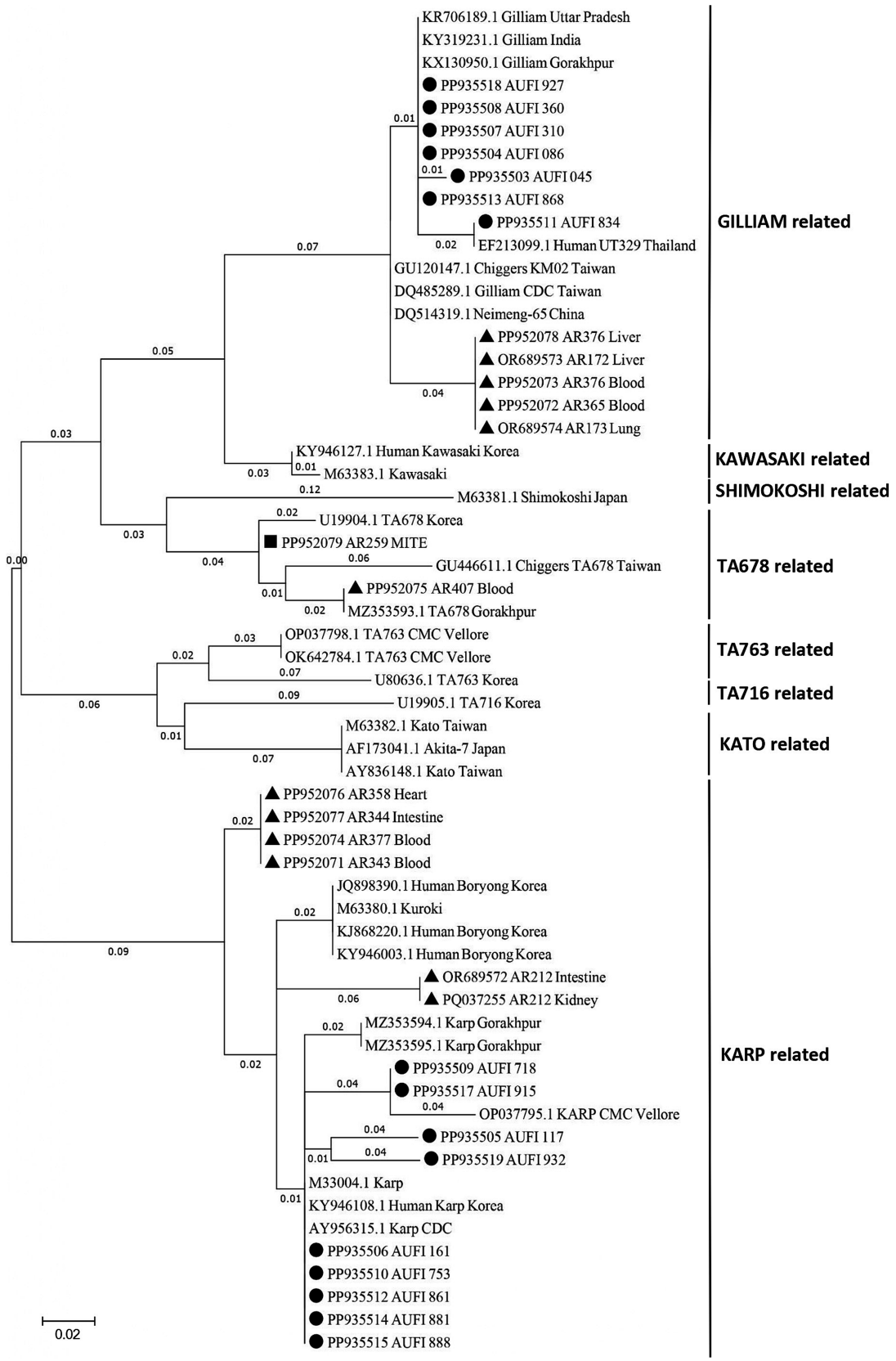

FIGURE 2
Phylogenetic analysis of *Orientia tsutsugamushi* sequences derived from animal reservoirs, humans, and chigger mites. The tree was constructed using the Maximum Likelihood method with 1,000 bootstrap replicates based on the Kimura 2-parameter model, targeting the 56-kDa type-specific antigen gene. In the current study, strains identified from rodent/shrew samples are denoted by TRIANGLES, those from human samples by CIRCLES, and those from mite samples by SQUARES.

site/year (95% HPD: 3.15×10^{-3}–4.73×10^{-3}) and the time to the most recent common ancestor (TMRCA) was estimated to be 167 years (95% HPD: 134.61–200.63 years) (Supplementary Figure S2).

A table describing the amino acid changes in each strain in comparison with the reference was constructed and included in Supplementary Table S6. Among the Gilliam-type sequences, alignment with the reference strain (accession no. DQ485289.1) revealed that the sequence PP935507 exhibited the highest amino acid identity (94.16%), while the sequence PP952078 demonstrated the lowest identity (85.58%). For the Karp-type sequences, comparison with the reference strain (accession no. AY956315.1) revealed that the sequences PP935514, and PP935515 exhibited the highest identity (98.01%) while the sequence PP935505 exhibited the lowest identity (53.13%). Similarly, the TA678-like study sequences PP952075 and PP952079 exhibited 81.88 and 95.10% identity, respectively, when aligned with the reference strain (accession no. GU446611.1). As TA678 was reported for the first time in Puducherry it was also compared with the partial sequence of the Indian isolate from Gorakhpur (accession no. MZ353593.1). The sequence PP952075 displayed 100% identity indicating no amino acid change, whereas the sequence PP952079 displayed 81.37% identity.

3.5 Seasonal trends in ST positivity in humans, animal reservoirs and mites

Among the 916 AUFI samples collected over 19 months, the ST positivity rate was highest in April (20%) and May (27.27%) (Figure 1). Among rodents/shrews trapped over a 12-month period, the highest positivity rate (33.33%) was observed in January and October. For mite pools, the highest positivity rate was recorded in June (7.25%).

4 Discussion

Scrub typhus is an endemic but frequently underdiagnosed zoonotic rickettsial disease, accounting for a significant proportion of acute undifferentiated febrile illness (AUFI) cases across multiple states in India. Outbreaks of scrub typhus are being reported over the past two decades in all the parts of the country, covering all the diverse climatic zones. As a vector-borne zoonosis, its burden is determined by the complex interactions between vector mites, animal reservoirs, and humans, the accidental hosts. Therefore, the present study aimed to investigate the genetic heterogeneity of *O. tsutsugamushi* strains across the human–animal–vector interface.

In the current study, of the 916 AUFI samples collected over 19 months from villages in and around Puducherry, ST infection was identified in 40 cases. The disease was more frequently seen in middle-aged men, likely due to occupational exposure to mite-infested environments, similar to the pattern reported in the earlier studies conducted in Kerala and Tamil Nadu (Varghese et al., 2013; Jyothi et al., 2015). The observed prevalence rate of 4.37% is considerably lower than the national prevalence of 25.3% reported in a systematic review (Devasagayam et al., 2021). The discordance observed could largely be attributed to the differences in diagnostic approaches. While the majority of studies relied on serological diagnostic tools especially IgM and IgG ELISA, we employed molecular diagnostics that enable the genetic characterization of the pathogen. PCRs are highly sensitive only during the window period of bacteremia. With the onset of adaptive immune response, the immunoglobulin levels rise, and the pathogenic load often decreases to a level undetectable by PCR. Hence, the samples collected quite later in the course of infection might have been undiagnosed by PCR, leading to the observed lower prevalence rate. In addition, the guidelines on the management of AUFI in adults, published by ICMR in 2019, insisted on the screening of patients with fever more than 5 days for ST and an optional empirical treatment with doxycycline in patients turning out to be negative in the rapid tests for dengue and malaria (ICMR guidelines on "Treatment guidelines for Antimicrobial use in common syndromes, 2019"). This in turn, could have cleared the pathogen load, hence rendering the PCR assay negative before sampling. More importantly, the study employed Real-time PCR targeting the 47 kDa gene and the Nested PCR targeting the 56 kDa gene, which were adopted from standard references. These assays have been reported to exhibit sensitivities of 75 ± 32% (range: 67.8–81.8%) and 97 ± 47% (range: 93.8–99.3%), respectively, with specificities of 100% (95.4–100%) and 100% (96.5–100%) (Kannan et al., 2020). This inherent variability in assay sensitivity, as reported in the literature, justifies the difference in the detection rates observed between the two tests in our study. This diagnostic limitation should also have contributed to the observed low prevalence estimates. Further, other factors such as the sampling bias due to case enrollment being limited to only three primary health care centers and variations in the sample collection, preservation, and transport might also have affected the positivity rate.

Rodents and shrews play a crucial role in the enzootic maintenance of *O. tsutsugamushi*, as evidenced by multiple studies (Devaraju et al., 2020; Balasubramanian et al., 2024), including the current investigation. Studies in animal models indicated that the bacteria remain detectable by PCR in multiple organs up to 84 days post-infection (Soong et al., 2016), and the viable rickettsiae have been found in rodent kidneys up to 4 months (Strickman et al., 1994). Our previous study reported a prevalence of 14.81% in rodents/shrews trapped even from areas without any reports of human cases of ST highlighting the risk of outbreak (Devaraju et al., 2020). The observed prevalence of 11.52% in this longitudinal study also reiterates the role of rodents and shrews in the enzootic maintenance of the pathogen and positive human infection confirms the transmission.

Sharma et al., reported a chigger index of 0.69 per rodent as a risk factor for ST outbreaks (Sharma, 2013). During the outbreak of ST in Himachal Pradesh (Kumar et al., 2004) and Gorakhpur (Sadanandane et al., 2021), chigger index of 2.46 and 5.3 was reported, respectively. In Puducherry, higher chigger indexes (41.1, 12.97, and 10.28 per animal) have been reported consistently in the recent past (Candasamy et al., 2016; Devaraju et al., 2020; Ritu et al., 2024). Following the same trend, in the current study a higher chigger index of 16.23 per animal was recorded. Month wise chigger index ranged from 1.95 (February) to 32.67 (June) per animal (Figure 1). Such a higher chigger index indicates a greater risk for ST outbreak during favorable climatic conditions. However, among the 296 pools of mites screened for ST, only 7 pools (2.36%) from 5 shrews (3 ST^+ and 2 ST^-) were tested positive for ST. A similar trend of low mite positivity was observed in our previous studies (Devaraju et al., 2020; Eikenbary et al., 2024) and the possible explanations include: (i) the potential DNA degradation during sample processing or storage, (ii) limitations inherent to the pooling strategy such as dilution of low-copy targets to the levels below the threshold of detection in PCR assays, (iii) the

TABLE 2 Distance matrix depicting the genetic distance between the sequences of 56 kDa antigen of *Orientia tsutsugamushi* isolated from humans, rodents, and mites in and around Puducherry.

Human samples	Animal samples												Mite
	PP952071	PP952072	PP952073	PP952074	PP952075	PP952076	PP952077	PP952078	OR689572	PQ037255	OR689573	OR689574	PP952079
PP935503	0.28	0.12	0.12	0.28	0.33	0.28	0.28	**0.09***	0.24	0.38	0.12	0.12	0.31
PP935504	0.23	**0.09***	**0.09***	0.23	0.45	0.24	0.25	**0.10***	0.24	0.33	**0.08***	**0.08***	0.33
PP935505	0.50	0.59	0.61	0.50	0.72	0.53	0.54	0.41	0.55	0.93	0.62	0.63	0.54
PP935506	**0.05***	0.30	0.30	**0.05***	0.46	**0.06***	**0.06***	0.27	**0.06***	**0.08***	0.29	0.30	0.32
PP935507	0.23	**0.08***	**0.07***	0.23	0.45	0.23	0.24	**0.09***	0.22	0.27	**0.07***	**0.07***	0.31
PP935508	0.23	**0.07***	**0.07***	0.23	0.42	0.23	0.24	**0.08***	0.24	0.34	**0.08***	**0.08***	0.31
PP935509	**0.08***	0.29	0.28	**0.08***	0.41	**0.08***	**0.08***	0.26	**0.05***	**0.06***	0.29	0.30	0.32
PP935510	**0.05***	0.30	0.30	**0.05***	0.41	**0.06***	**0.06***	0.28	**0.06***	**0.08***	0.30	0.31	0.32
PP935511	0.27	**0.03***	**0.03***	0.27	0.41	0.27	0.28	**0.03***	0.27	0.33	**0.03***	**0.03***	0.32
PP935512	**0.05***	0.30	0.30	**0.05***	0.40	**0.06***	**0.06***	0.28	**0.06***	**0.08***	0.30	0.31	0.32
PP935513	0.28	**0.06***	**0.06***	0.28	0.37	0.29	0.30	**0.03***	0.28	0.37	**0.06***	**0.06***	0.33
PP935514	**0.05***	0.30	0.30	**0.05***	0.44	**0.06***	**0.06***	0.28	**0.06***	**0.07***	0.30	0.31	0.32
PP935515	**0.05***	0.30	0.30	**0.05***	0.44	**0.06***	**0.06***	0.28	**0.06***	**0.07***	0.30	0.31	0.32
PP935517	**0.08***	0.29	0.28	**0.08***	0.43	**0.08***	**0.08***	0.26	**0.05***	**0.06***	0.28	0.29	0.32
PP935518	0.23	**0.07***	**0.07***	0.23	0.42	0.23	0.24	**0.08***	0.24	0.34	**0.08***	**0.08***	0.31
PP935519	**0.08***	0.19	0.18	**0.08***	0.25	**0.08***	**0.08***	0.18	**0.07***	0.13	0.18	0.19	0.23

Values which are highlighted using bold font and an "*" indicate close association of the pathogenic strains isolated from human and animal samples..

10.3389/fmicb.2025.1634394

possibility of genuine low infection prevalence in the sampled mite population and (iv) other biological factors such as the host specificity and variability in vector competence. To address such issues, statistical modeling to determine the optimal pool size that balances sensitivity and cost-effectiveness, development of improved extraction protocols and internal controls to monitor DNA quality and standardization of operating protocols for the molecular xenomonitoring of mites for *Orientia* infection is suggested.

Globally, more than 40 strains of *O. tsutsugamushi* have been reported including the prototype strains like Kato, Karp and Gilliam (Nallan et al., 2025). Multiple serotypes of *O. tsutsugamushi* have been reported from various regions in India, showing significant geographic diversity. The most commonly identified strains in humans include the Karp-like and Kato-like genotypes (Varghese et al., 2013, 2015). In 2017, findings from Puducherry and its surrounding border areas in Tamil Nadu revealed the presence of Karp and Gilliam prototypes along with other serotypes such as Kuroki, Boryong, and Kato in humans (Anitha et al., 2017). Following the same trend, Karp-like and Gilliam-like strains were identified as the predominant circulating serotypes in Puducherry in the current study as well. Karp strain has been associated with longer stay in the hospital, with the involvement of multiple organs compared to the Gilliam strain. Further, the molecular evolutionary rate identified by Bayesian time scale analysis aligns with that reported earlier for *O. tsutsugamushi* with the TMRCA value suggesting the long-term circulation and diversification of the pathogen (Wongprompitak et al., 2015). Thus, the study highlights the co-circulation of strains with varying degree of virulence in Puducherry and the need to establish serotype-specific clinical manifestations existing in the region.

In addition to the predominant Karp and Gilliam-like strains, the current study also reports the circulation of TA678-like strain of *O. tsutsugamushi* for the first time in Puducherry in a shrew and vector mites. Although considered a less common genotype compared to Karp, Kato, or Gilliam, TA678 has been sporadically reported across parts of Southeast Asia and India, indicating a broader geographical distribution than previously recognized. The strain has been earlier reported in rodents and mites from Gorakhpur, Uttar Pradesh, which falls in the northernmost part of the country, during ST outbreaks significantly associated with Acute Encephalitis Syndrome (AES) (Sadanandane et al., 2018, 2021). In contrast, the incidence of such AES in ST patients has been only sparsely reported in South India. The above observation suggests that this new serotype may have recently entered the region, and its impact on clinical severity and outcome have to be monitored. In addition, the presence of TA678 in vectors without corresponding human cases reflects, host-specific transmission barriers, or underdiagnosis due to limited strain-specific molecular surveillance. Continued molecular monitoring and correlation with clinical data in human cases are essential to understand its unique virulence characteristics and associated variations in the disease severity compared to the other prevalent strains.

The genetic heterogeneity among different strains of the bacterium *O. tsutsugamushi* influences its antigenicity, which in turn affects the immune response, contributing to variations in disease severity and clinical outcomes across endemic regions. This factor also affects the diagnostic efficacy of the tools, as the real-time PCR probes commonly used can detect only certain prototypes, but not all the strains (Tantibhedhyangkul et al., 2017). The Karp genotype, in particular, has been consistently linked to severe clinical manifestations such as acute respiratory distress syndrome, hepatitis, renal failure, and thrombocytopenia (Chunduru et al., 2023). The higher prevalence of Karp-like strains identified in the current study suggests an increased likelihood of the disease progressing to more severe clinical outcomes if not promptly diagnosed and treated. Accordingly, in our study we encountered fatality in two cases due to severe complications such as thrombocytopenia, acute kidney injury and myocarditis. Among them, PCR positivity for the 56 kDa gene was observed in only one, and was identified as Karp-like suggesting its potential link to severe clinical outcomes. This underscores the need for ongoing surveillance and preparedness as Karp-like strains circulate in the region.

The pairwise genetic distance analysis revealed a clear pattern of genetic clustering based on serotype, with strains of the same serotype—Karp and Gilliam—exhibiting close genetic relationships (distance <0.1), and significantly higher divergence observed between different serotypes. Among the Karp-like strains, the lowest observed genetic distance was 0.05, indicating strong relatedness between human and rodent isolates, particularly for strains such as PP935509 and PP935510, suggesting active local transmission cycles. However, the human Karp strain PP935505 (Ulundurpet, Kallakurichi district) stood out as genetically distinct, showing no close association with any rodent or mite strains. Though the patient reported to a tertiary health care center in Puducherry, his residence was geographically distant from Puducherry. This supports the likelihood of an infection acquired outside the local transmission ecosystem, accounting for its divergence. Similarly, two TA678-like strains—one from a shrew (PP952075, Madagadipet) and one from a chigger mite (PP952079, Thuthipet)—were also genetically distinct and lacked close association with each other or with any other strain, suggesting either separate introductions or independent evolution in distinct ecological niches (Figure 3). Notably, within the Gilliam group, the human strain PP935511 showed a very high degree of similarity (distance = 0.03) with five Gilliam strains from shrews across different localities (Madagadipet, Poothurai, Periyababusamudram, and Bommayarpalayam). Another human Gilliam strain, PP935503 (Suthukeny, Villianur), also shared a close genetic relationship specifically with the Poothurai shrew strain PP952078. The observed genetic similarity strongly suggests sustained zoonotic transmission within this ecological niche.

The observed variability in amino acid sequences of the strains, when aligned with the full-length reference strains, suggests that the 56 kDa TSA gene can withstand a large amount of variation, as has been previously reported for the 47 kDa HtrA gene (Jiang et al., 2013). Notably, the human Karp strain PP935505, originating from a geographically distant location, exhibited the highest genetic distance and, as expected, the lowest amino acid identity. With respect to the TA678-like serotype, the chigger-derived sequence PP952079 exhibited the highest identity with the reference sequence (GU446611.1), which was also derived from chiggers. It was also observed that the shrew-derived sequence of TA678, PP952075 exhibited the highest identity with an Indian strain (MZ353593.1) detected in a shrew from Gorakhpur. In addition, a few cluster of strains were identical with the same translated amino acid sequences (i.e.), Gilliam: PP935508 and PP935518, Karp: PP952071, PP952074 and PP952076, Karp: PP935510, PP935512, PP935514 and PP935515 and Karp: PP935509 and PP935517 reaffirming the local transmission of the strains. Future studies should aim to obtain and analyze complete genomic data to enable comprehensive mutation analysis across additional genomic regions. Given the high mutation rates in

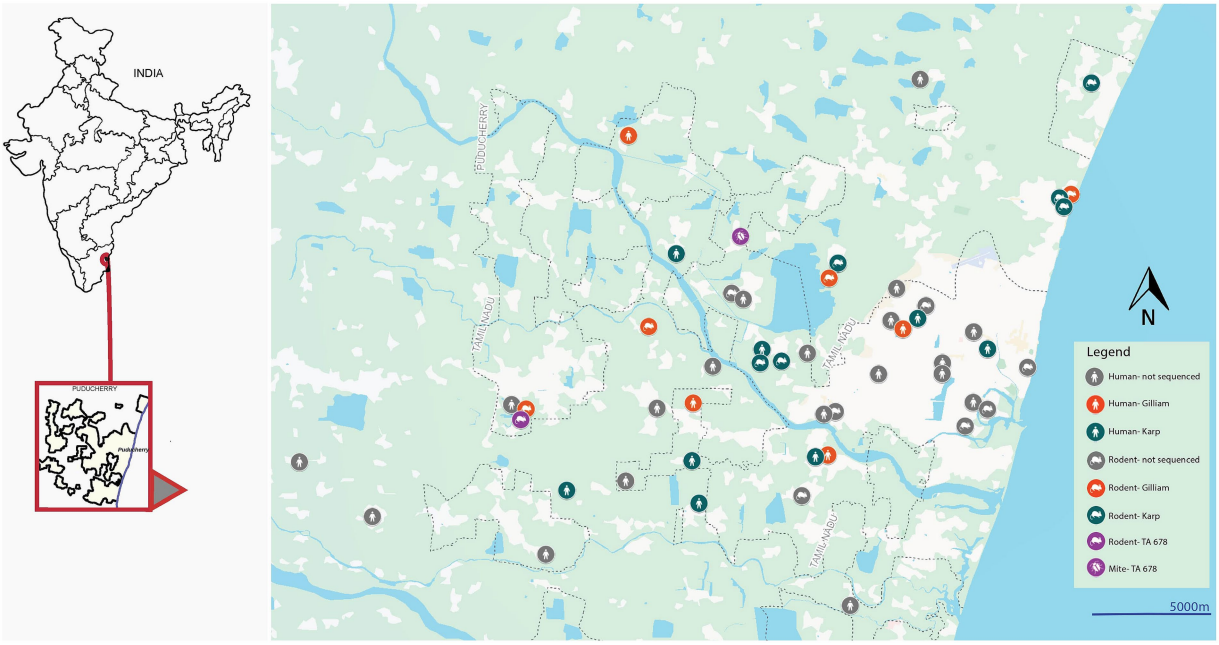

FIGURE 3
Map showing rodent/shrew, human, and chigger mite positive cases in and around Puducherry.

rickettsiae which is attributable to their short generation times and large population sizes, such investigations are essential to better understand the genetic variability and evolutionary dynamics of the pathogen.

Scrub typhus exhibits a clear seasonal pattern influenced by environmental and climatic conditions. In India, the disease is most prevalent during the post-monsoon and cooler months (October to January), though regional variations exist (Mathai et al., 2003; Candasamy et al., 2016). These seasonal changes impact the abundance and activity of vectors and reservoirs, thereby influencing transmission dynamics. In the present study from Puducherry, while rodents/shrews showed the highest ST positivity during the cooler months (October and January) aligning with the above trend, chigger mite pools peaked in June. This indicated an increased vector activity during the early monsoon and a probable lag period between detectable positivity of the pathogen in mites and rodents/shrews. In the case of humans, though a noticeable increase in the cases was observed during the cooler months (November–January), the highest ST positivity occurred during the summer, particularly in April and May. As discussed earlier, this discrepancy in the month-wise positivity in human cases reflects the under-estimation of ST positives contributed by the choice of diagnostic tests used. The major thrust of the paper was to characterize the genetic heterogeneity of the pathogens and hence, human cases were detected only by molecular tests. PCR-based detection is known to be reliable only during the acute phase of infection, when antibody titres are low and pathogen levels are still detectable. Beyond the first week of clinical symptoms, PCR sensitivity declines significantly, making it unsuitable for late-phase diagnosis. Serological tests, such as ELISA, are therefore strongly recommended for detecting cases in AUFI patients presenting with fever for more than 5 days and to better understand the seasonal changes.

A major limitation of the study was the low infection rate detected in the screening of mites. The positivity rate did not correspond with the high chigger index observed in the field. This highlights the need for improved pooling strategies for xenomonitoring of ST in mites for future studies. Another important limitation was that only 29 of the 42 positives resulted in good-quality sequences suitable for genetic characterization. This might be because of the low pathogen load, resulting in less intense amplicon bands after the PCR. To circumvent this technical issue, we therefore, recommend the use of next-generation sequencing technologies, to generate reliable sequence data even from samples with low pathogen loads, mixed infection. Further, reliability only on PCR, absence of serological data, variability in diagnostic test accuracy, empirical treatment with doxycycline and minor differences in sample collection, transport, and storage across the three primary health centers may have introduced bias in the diagnostic outcomes and should be considered as limitations.

5 Conclusion

The current study revealed the higher prevalence of the Karp-like and Gilliam-like serotypes of *O. tsutsugamushi* among the animal reservoirs, vectors and the infected humans in and around Puducherry by phylogenetic analysis. With higher intra-serotype identity, abundance of infected animal hosts around human habitations, higher chigger infestation rates (39.78%) and higher chigger index (16.23%), this study highlights the ongoing transmission of the pathogen between animal reservoirs and humans through the mites. This emphasizes the need for regular zoonotic surveillance to predict disease outbreaks and to implement effective rodent control before the onset of congenial climatic conditions favoring the disease transmission. Further, with the first report of the TA678-like serotype among the reservoirs and vectors in the region, the study highlights the potential new introductions or strain evolution and reinforce the

need for extensive molecular monitoring to track the newly emerging strains and to map their clinical significance.

Data availability statement

The datasets presented in this study can be found in online repositories. The names of the repository/repositories and accession number(s) can be found in the article/Supplementary material.

Ethics statement

The studies involving humans were approved by Institutional Human Ethics Committee, ICMR-VCRC. The studies were conducted in accordance with the local legislation and institutional requirements. Written informed consent for participation in this study was provided by the participants' legal guardians/next of kin. The animal study was approved by Institutional Animal Ethics Committee, ICMR-VCRC. The study was conducted in accordance with the local legislation and institutional requirements.

Author contributions

KS: Data curation, Formal analysis, Investigation, Methodology, Software, Writing – original draft, Writing – review & editing. WA: Data curation, Formal analysis, Investigation, Methodology, Software, Supervision, Writing – original draft, Writing – review & editing. SS: Conceptualization, Formal analysis, Funding acquisition, Project administration, Resources, Supervision, Visualization, Writing – original draft, Writing – review & editing. AnaC: Resources, Writing – review & editing. VR: Resources, Writing – review & editing. AsaC: Resources, Writing – review & editing. AK: Resources, Writing – review & editing. ST: Investigation, Methodology, Writing – review & editing. LS: Investigation, Methodology, Writing – review & editing. AnoC: Resources, Writing – original draft, Writing – review & editing. MA: Methodology, Writing – review & editing. AR: Data curation, Software, Writing – review & editing. NY: Methodology, Visualization, Software, Writing – review & editing. PD: Conceptualization, Funding acquisition, Project administration, Resources, Supervision, Validation, Visualization, Writing – original draft, Writing – review & editing.

Funding

The author(s) declare that financial support was received for the research and/or publication of this article. The study on rodents/shrews was funded by the Department of Health Research, Ministry of Health and Family Welfare, Govt. of India, New Delhi (Grant No: R.11013/57/2021-GIA/HR) funded to PD. The study on humans was funded intramurally by ICMR-VCRC (Project ID: IM2211). The APC was funded by Indian Council of Medical Research, Govt. of India, New Delhi (Grant No: VIR/16/2023/VCRC) funded to SS.

Acknowledgments

The authors acknowledge the technical support rendered by S. Rajkumar and S. Pushpa.

Conflict of interest

The authors declare that the research was conducted in the absence of any commercial or financial relationships that could be construed as a potential conflict of interest.

Generative AI statement

The authors declare that no Gen AI was used in the creation of this manuscript.

Any alternative text (alt text) provided alongside figures in this article has been generated by Frontiers with the support of artificial intelligence and reasonable efforts have been made to ensure accuracy, including review by the authors wherever possible. If you identify any issues, please contact us.

Publisher's note

Supplementary material

The Supplementary material for this article can be found online at: https://www.frontiersin.org/articles/10.3389/fmicb.2025.1634394/full#supplementary-material

References

Agrawal, V. C. (2000). Taxonomic studies on Indian Muridae and Hystricidae (Mammalia: Rodentia). Kolkata, India: Zoological Survey of India.

Anitha, P. K., Hoti, S. L., Kanungo, R., Jambulingam, P., Yasin, N., Nair, S., et al. (2017). Occurrence of *Orientia tsutsugamushi* genotypes in areas of union territory of Puducherry and Tamil Nadu state, India. *J. Emerg. Infect. Dis.* 2:124. doi: 10.4172/2472-4998.1000124

Anitharaj, V., Stephen, S., and Pratheesh, P. (2020). Scrub typhus in Puducherry, India: application of nested PCR targeting three different genes - 56 kDa, 47 kDa and groEL of *Orientia tsutsugamushi* and comparison with ST IgM ELISA. *J. Vector Borne Dis.* 57, 147–152. doi: 10.4103/0972-9062.310866

Balasubramanian, T., Sambath, U., Radja, R. D., Thangaraj, G., Devaraju, P., Srinivasan, L., et al. (2024). Pathological responses in Asian house shrews (*Suncus murinus*) to the naturally acquired *Orientia tsutsugamushi* infection. *Microorganisms* 12:748. doi: 10.3390/microorganisms12040748

Bhopdhornangkul, B., Meeyai, A. C., Wongwit, W., Limpanont, Y., Iamsirithaworn, S., Laosiritaworn, Y., et al. (2021). Non-linear effect of different humidity types on scrub typhus

occurrence in endemic provinces, Thailand. *Heliyon* 7:e06095. doi: 10.1016/j.heliyon.2021.e06095

Candasamy, S., Ayyanar, E., Paily, K., Karthikeyan, P. A., Sundararajan, A., and Purushothaman, J. (2016). Abundance & distribution of trombiculid mites & *Orientia tsutsugamushi*, the vectors & pathogen of scrub typhus in rodents & shrews collected from Puducherry & Tamil Nadu, India. *Indian J. Med. Res.* 144, 893–900. doi: 10.4103/ijmr.IJMR_1390_15

Chang, T., Min, K. D., Cho, S. I., and Kim, Y. (2024). Associations of meteorological factors and dynamics of scrub typhus incidence in South Korea: a nationwide time-series study. *Environ. Res.* 245:117994. doi: 10.1016/j.envres.2023.117994

Chunduru, K., A, R. M., Poornima, S., Hande, H. M., M, M., Varghese, G. M., et al. (2023). Clinical, laboratory, and molecular epidemiology of *Orientia tsutsugamushi* infection from southwestern India. *PLoS One* 18:e0289126. doi: 10.1371/journal.pone.0289126

Committee for the Purpose of Control and Supervision of Experiments on Animals (CPCSEA). (2018). Compendium of CPCSEA. New Delhi: Ministry of Environment, Forest and Climate Change, Government of India.

Devaraju, P., Arumugam, B., Mohan, I., Paraman, M., Ashokkumar, M., Kasinathan, G., et al. (2020). Evidence of natural infection of *Orientia tsutsugamushi* in vectors and animal hosts - risk of scrub typhus transmission to humans in Puducherry, South India. *Indian J. Public Health* 64, 27–31. doi: 10.4103/ijph.IJPH_130_19

Devasagayam, E., Dayanand, D., Kundu, D., Kamath, M. S., Kirubakaran, R., and Varghese, G. M. (2021). The burden of scrub typhus in India: a systematic review. *PLoS Negl. Trop. Dis.* 15:e0009619. doi: 10.1371/journal.pntd.0009619

Ding, F., Wang, Q., Hao, M., Maude, R. J., John Day, N. P., Lai, S., et al. (2022). Climate drives the spatiotemporal dynamics of scrub typhus in China. *Glob. Chang. Biol.* 28, 6618–6628. doi: 10.1111/gcb.16395

Eikenbary, B., Devaraju, P., Chakkravarthi, A., Sihag, K. K., Nathan, T., Thangaraj, G., et al. (2024). A molecular survey of zoonotic pathogens of public health importance in rodents/shrews and their ectoparasites trapped in Puducherry, India. *Trans. R. Soc. Trop. Med. Hyg.* 118, 616–624. doi: 10.1093/trstmh/trae033

Furuya, Y., Yoshida, Y., Katayama, T., Yamamoto, S., and Kawamura, A. (1993). Serotype-specific amplification of *Rickettsia tsutsugamushi* DNA by nested polymerase chain reaction. *J. Clin. Microbiol.* 31, 1637–1640. doi: 10.1128/jcm.31.6.1637-1640.1993

Jiang, J., Paris, D. H., Blacksell, S. D., Aukkanit, N., Newton, P. N., Phetsouvanh, R., et al. (2013). Diversity of the 47-kD HtrA nucleic acid and translated amino acid sequences from 17 recent human isolates of *Orientia*. *Vector Borne Zoonotic Dis.* 13, 367–375. doi: 10.1089/vbz.2012.1112

Jyothi, R., Sahira, H., Sathyabhama, M. C., and Bai, J. T. R. (2015). Seroprevalence of scrub typhus among febrile patients in a tertiary care hospital in Thiruvananthapuram, Kerala. *J. Acad. Ind. Res.* 3, 542–545. doi: 10.7860/NJLM/2016/21801:2159

Kannan, K., John, R., Kundu, D., Dayanand, D., Abhilash, K. P. P., Mathuram, A. J., et al. (2020). Performance of molecular and serologic tests for the diagnosis of scrub typhus. *PLoS Negl. Trop. Dis.* 14:e0008747. doi: 10.1371/journal.pntd.0008747

Konyak, B. M., Soni, M., Saikia, S., Chang, T., Gogoi, I., Khongstid, I., et al. (2024). Scrub typhus in Northeast India: epidemiology, clinical presentations, and diagnostic approaches. *Trans. R. Soc. Trop. Med. Hyg.* 118, 206–222. doi: 10.1093/trstmh/trad082

Koraluru, M., Bairy, I., Varma, M., and Vidyasagar, S. (2015). Diagnostic validation of selected serological tests for detecting scrub typhus. *Microbiol. Immunol.* 59, 371–374. doi: 10.1111/1348-0421.12268

Kumar, K., Saxena, V. K., Thomas, T. G., and Lal, S. (2004). Outbreak investigation of scrub typhus in Himachal Pradesh (India). *J. Commun. Dis.* 36, 277–283

Mathai, E., Rolain, J. M., Verghese, G. M., Abraham, O. C., Mathai, D., Mathai, M., et al. (2003). Outbreak of scrub typhus in southern India during the cooler months. *Ann. N. Y. Acad. Sci.* 990, 359–364. doi: 10.1111/j.1749-6632.2003.tb07391.x

Nallan, K., Kalidoss, B. C., Jacob, E. S., Mahadevan, S. K., Joseph, S., Ramalingam, R., et al. (2025). A novel genotype of *Orientia tsutsugamushi* in human cases of scrub typhus from southeastern India. *Microorganisms* 13:333. doi: 10.3390/microorganisms13020333

Ohashi, N., Nashimoto, H., Ikeda, H., and Tamura, A. (1992). Diversity of immunodominant 56-kDa type-specific antigen (TSA) of *Rickettsia tsutsugamushi*. Sequence and comparative analyses of the genes encoding TSA homologues from four antigenic variants. *J. Biol. Chem.* 267, 12728–12735. doi: 10.1016/S0021-9258(18)42337-X

Patricia, K. A., Hoti, S. L., Kanungo, R., Jambulingam, P., Shashikala, N., and Naik, A. C. (2017). Improving the diagnosis of scrub typhus by combining groEL based polymerase chain reaction and IgM ELISA. *J. Clin. Diagn. Res.* 11:DC27–DC31. doi: 10.7860/JCDR/2017/26523.10519

Prakash, J. A. J. (2017). Scrub typhus: risks, diagnostic issues, and management challenges. *Res. Rep. Trop. Med.* 8, 73–83. doi: 10.2147/RRTM.S105602

Purushothaman, S., Azhahianambi, P., Dharman, M., Gokula Kannan, R., Tirumurugaan, K. G., Soundararajan, C., et al. (2024). A cross sectional study on molecular prevalence of *Orientia tsutsugamushi* in household rat population of South India. *Comp. Immunol. Microbiol. Infect. Dis.* 111:102212. doi: 10.1016/j.cimid.2024.102212

Ritu, G. P., Arif, W., Sihag, K. K., Chakravarthi, A., Anthony, T. N., Srinivasan, L., et al. (2024). Comparative evaluation of different tissues and molecular techniques for the zoonotic surveillance of scrub typhus. *Vector Borne Zoonotic Dis.* 24, 299–307. doi: 10.1089/vbz.2023.0069

Sadanandane, C., Elango, A., Panneer, D., Mary, K. A., Kumar, N. P., Paily, K., et al. (2021). Seasonal abundance of *Leptotrombidium deliense*, the vector of scrub typhus, in areas reporting acute encephalitis syndrome in Gorakhpur district, Uttar Pradesh, India. *Exp. Appl. Acarol.* 84, 795–808. doi: 10.1007/s10493-021-00650-2

Sadanandane, C., Jambulingam, P., Paily, K. P., Kumar, N. P., Elango, A., Mary, K. A., et al. (2018). Occurrence of *Orientia tsutsugamushi*, the etiological agent of scrub typhus in animal hosts and mite vectors in areas reporting human cases of acute encephalitis syndrome in the Gorakhpur region of Uttar Pradesh, India. *Vector Borne Zoonotic Dis.* 18, 539–547. doi: 10.1089/vbz.2017.2246

Seetha, D., Nori, S. R. C., and Nair, R. R. (2023). Molecular-based study of scrub typhus in Kerala, South India from 2014 to 2021: a laboratory-based study. *Comp. Clin. Path.* 32, 347–356. doi: 10.1007/s00580-023-03443-8

Sharma, A. K. (2013). Entomological surveillance for rodent and their ectoparasites in scrub typhus affected areas of Meghalaya, (India). *J. Entomol. Zool. Stud.* 1, 27–29.

Shishido, A. (1962). Identification and serological classification of the causative agent of scrub typhus in Japan. *Jpn. J. Sci. Biol.* 15, 308–321.

Soong, L., Mendell, N. L., Olano, J. P., Rockx-Brouwer, D., Xu, G., Goez-Rivillas, Y., et al. (2016). An intradermal inoculation mouse model for immunological investigations of acute scrub typhus and persistent infection. *PLoS Negl. Trop. Dis.* 10:e0004884. doi: 10.1371/journal.pntd.0004884

StataCorp (2023). Stata statistical software: release 18. College station, TX: StataCorp LLC.

Strickman, D., Smith, C. D., Corcoran, K. D., Ngampochjana, M., Watcharapichat, P., Phulsuksombati, D., et al. (1994). Pathology of *Rickettsia tsutsugamushi* infection in *Bandicota savilei*, a natural host in Thailand. *Am. J. Trop. Med. Hyg.* 51, 416–423. doi: 10.4269/ajtmh.1994.51.416

Tamura, K., Stecher, G., and Kumar, S. (2021). MEGA11: molecular evolutionary genetics analysis version 11. *Mol. Biol. Evol.* 38, 3022–3027. doi: 10.1093/molbev/msab120

Tantibhedhyangkul, W., Wongsawat, E., Silpasakorn, S., Waywa, D., Saenyasiri, N., Suesuay, J., et al. (2017). Use of multiplex real-time PCR to diagnose scrub typhus. *J. Clin. Microbiol.* 55, 1377–1387. doi: 10.1128/JCM.02181-16

Taylor, A. J., Paris, D. H., and Newton, P. N. (2015). A systematic review of mortality from untreated scrub typhus (*Orientia tsutsugamushi*). *PLoS Negl. Trop. Dis.* 9:e0003971. doi: 10.1371/journal.pntd.0003971

Varghese, G. M., Janardhanan, J., Mahajan, S. K., Tariang, D., Trowbridge, P., Prakash, J. A. J., et al. (2015). Molecular epidemiology and genetic diversity of *Orientia tsutsugamushi* from patients with scrub typhus in 3 regions of India. *Emerg. Infect. Dis.* 21, 64–69. doi: 10.3201/eid2101.140580

Varghese, G. M., Janardhanan, J., Trowbridge, P., Peter, J. V., Prakash, J. A. J., Sathyendra, S., et al. (2013). Scrub typhus in South India: clinical and laboratory manifestations, genetic variability, and outcome. *Int. J. Infect. Dis.* 17, e981–e987. doi: 10.1016/j.ijid.2013.05.017

Wongprompitak, P., Duong, V., Anukool, W., Sreyrath, L., Mai, T. T., Gavotte, L., et al. (2015). *Orientia tsutsugamushi*, agent of scrub typhus, displays a single metapopulation with maintenance of ancestral haplotypes throughout continental South East Asia. *Infect. Genet. Evol.* 31, 1–8. doi: 10.1016/j.meegid.2015.01.005

frontiers | Frontiers in Microbiology

TYPE Original Research
PUBLISHED 09 September 2025
DOI 10.3389/fmicb.2025.1674831

OPEN ACCESS

EDITED BY
Lei Deng,
Chinese Academy of Agricultural Sciences, China

REVIEWED BY
Fu Lei,
Chinese Academy of Agricultural Sciences, China
Huarun Sun,
Henan Institute of Science and Technology, China

*CORRESPONDENCE
Tonglei Wu
✉ 532966952@163.com

RECEIVED 28 July 2025
ACCEPTED 21 August 2025
PUBLISHED 09 September 2025

CITATION
Li J, Liu W, Zhang X, Song Y, Chen L, Shi Q and Wu T (2025) Immunoprotective effects of extracellular products of *Pasteurella multocida* on mice.
Front. Microbiol. 16:1674831.
doi: 10.3389/fmicb.2025.1674831

Immunoprotective effects of extracellular products of *Pasteurella multocida* on mice

Jingtao Li[1,2], Wan Liu[1], Xiaoyu Zhang[1], Yang Song[1], Li Chen[1], Qiumei Shi[1] and Tonglei Wu[1]*

[1]Hebei Provincial Key Laboratory of Preventive Veterinary Medicine, Hebei Normal University of Science and Technology, Qinhuangdao, China, [2]Elanco (Sichuan) Animal Health Co., Ltd., Chengdu, China

Background: *Pasteurella multocida* (*P. multocida*) is a globally significant pathogen causing severe infections in livestock, including hemorrhagic septicemia and respiratory diseases. Current vaccines offer limited serotype-specific protection, particularly against serotype A:3, a major cause of bovine respiratory disease. Extracellular products (ECPs) of bacteria, containing secreted proteins and enzymes, have shown promise as immunogens in other pathogens, but their potential against *P. multocida* remains unclear.

Methods: Extracellular products were isolated from *P. multocida* serotype A:3 strain PmQA-1 and characterized via SDS-PAGE, mass spectrometry, and enzymatic activity assays. Pathogenicity was evaluated by determining the median lethal dose (LD_{50}) in mice. Mice were immunized with ECPs, formalin-killed cells (FKC), or a combination (FKC + ECPs), and immune responses (serum IgG, splenic lymphocyte proliferation, cytokine expression) were assessed over 28 days. Protective efficacy was tested via challenge with homologous (A:3) and heterologous (B:2, D:4) strains.

Results: Extracellular products contained 157 proteins (25–100 kDa), including immunogenic factors like transferrin-binding protein A, and exhibited stable amylase activity. The LD_{50} of ECPs in mice was 2.69 mg/mouse, inducing lesions typical of *P. multocida* infection. ECP-immunized mice showed peak IgG levels at day 21, enhanced lymphocyte proliferation, and upregulated TNF-α, IFN-γ, IL-1β, and IL-10 in key tissues. Challenge experiments demonstrated 100% survival against A:3 and B:2, and 90% against D:4, outperforming FKC and FKC + ECPs.

Conclusion: Extracellular products from *P. multocida* serotype A:3 induce robust humoral and cellular immunity, providing broad-spectrum protection against multiple serotypes. These findings support ECPs as a promising subunit vaccine candidate for controlling *P. multocida* infections in livestock.

KEYWORDS

***Pasteurella multocida*, extracellular products, vaccine, immune response, cross-protection**

1 Introduction

P. multocida is a Gram-negative bacterium commonly colonizing the upper respiratory mucosa (oropharyngeal and nasopharyngeal) of a wide range of wild and domesticated animals, including species relevant to the livestock and food production industries such as cattle, swine, poultry, rabbits, and even humans (Piorunek et al., 2023; Ryan and Feder, 2019; Wilkie et al., 2012). Under stress-inducing conditions, this typically commensal bacterium may invade host tissues, resulting in systemic or localized infections such as pneumonia, hemorrhagic septicemia (HS), atrophic rhinitis, avian cholera, cellulitis, dermonecrosis, abscesses, and meningitis (Dassanayake et al., 2025; Zhao et al., 2024).

Based on capsular composition, *P. multocida* is classified into five capsular serogroups (A, B, D, E, and F), and based on differences in lipopolysaccharide (LPS) structure, into 16 somatic serotypes (Guan et al., 2020; Gulliver et al., 2022; Megroz et al., 2016). These serogroups and serotypes differ in host specificity and disease manifestation. For instance, in cattle, *P. multocida* causes two major syndromes: hemorrhagic septicemia (HS), primarily associated with serogroup B:2 strains, and bovine respiratory disease complex (BRD), primarily caused by serogroup A:3 strains. HS is a rapidly progressing, frequently fatal septicemia, especially prevalent in Africa and Asia, with significant impact on smallholder farms. In contrast, BRD (or "shipping fever") is a multifactorial disease affecting the upper or lower respiratory tract, typically occurring in recently weaned or transported calves (Zhan et al., 2021). In China, *P. multocida* serotype D:4 strains are also frequently associated with cattle pneumonia (Sun et al., 2022).

Despite decades of vaccine deployment, *P. multocida* infections remain a persistent challenge in cattle and other livestock. Current vaccines-including inactivated whole-cell (bacterin), live attenuated, and subunit formulations-exhibit notable limitations in terms of safety, efficacy, and duration of protection. Bacterin vaccines typically confer only 4–6 months of immunity (Varshney et al., 2020), while live attenuated vaccines-mainly derived from serogroup B strains-may extend protection up to 1 year. However, both types of vaccines offer limited, serogroup-specific protection and fail to provide adequate immunity against *P. multocida* serotype A:3, the predominant strain associated with bovine respiratory disease. In recent years, substantial efforts have been made to identify alternative subunit vaccine candidates. Targets under investigation include capsular polysaccharides, lipopolysaccharides (LPS), siderophores, *P. multocida* toxin (PMT), dermonecrotic toxins, and various outer membrane proteins (OMPs) (Dabo et al., 2008; Liao et al., 2006; Pettit et al., 1993; Zhao X. et al., 2022). Among these, PlpE-a conserved, surface-exposed protein-has shown particular promise. Hatfaludi et al. (2012) identified over 70 putative surface or secreted proteins through bioinformatic analyses, but only recombinant PlpE demonstrated complete protection in challenge models. Subsequent studies reported partial protection using recombinant OmpH, PlpE, and PlpEC-OmpH fusion proteins, achieving protection rates of up to 80% (Okay et al., 2012). Furthermore, a recently identified surface lipoprotein, PmSLP, has demonstrated strong protective efficacy (75%–87.5% survival) in cattle challenged with virulent *Glaesserella parasuis (G. parasuis)* strains (Nguyen et al., 2025). Extracellular products (ECPs) are secreted metabolites produced by bacteria during growth, including various enzymes and toxins such as proteases, amylases, lipases, lecithinases, gelatinases, ureases, chitinases, DNases, and hemolysins. These factors contribute significantly to bacterial virulence by degrading host tissues, evading immune responses, and facilitating colonization (Baldissera et al., 2018; Pemberton et al., 1997; Sahu et al., 2011; Zhao Y. et al., 2022). In other pathogens-such as *Aeromonas veronii (A. veronii)*, *Vibrio vulnificus (V. vulnificus)*, and *Moritella viscosa (M. viscosa)*-ECPs have demonstrated strong immunogenicity and provided effective protection in animal models (Lee et al., 1997; MacKinnon et al., 2019; Song et al., 2018).

Given this potential, we focused on a bovine-origin *P. multocida* serotype A:3 strain (PmQA-1), commonly associated with BRD in cattle. We prepared its ECPs, evaluated enzymatic activities and pathogenicity in mice, and formulated an ECP-based subunit vaccine. Using a murine infection model, we assessed its protective efficacy against different *P. multocida* serotypes. Our results showed that although the vaccine based on ECPs provided limited cross-protection against strains of other serotypes, it granted complete (100%) protection against the challenge of homologous serotype A:3, which emphasized its potential as a candidate for a novel subunit vaccine.

2 Materials and methods

2.1 Bacterial strains

The strains PmQA-1 (serotype A:3), PmQB-1 (serotype B:2), and PmQD-1 (serotype D:4) were used in this study. All strains were cultured overnight at 37 °C in tryptic soy broth (TSB; Qingdao Hope Bio-Technology Co., Ltd., Qingdao, China) or on tryptic soy agar (TSA; Qingdao Hope Bio-Technology Co., Ltd., Qingdao, China), supplemented with 10% fetal bovine serum (FBS, Zhejiang Tianhang Biotechnology Co., Ltd., Hangzhou, China) and NAD (Beijing Bio-Lab Biotechnology Co., Ltd., Beijing, China).

2.2 Experimental animals and ethical statement

KM mice (6–8 weeks old) were purchased from SPF (Beijing, China) Biotechnology Co., Ltd. Throughout the experiment, the mice were housed under sterile conditions in individually ventilated cages, with an ambient temperature maintained at 22.0 °C ± 0.5 °C and relative humidity at 60% ± 10%. A 12-h light/dark cycle was applied. All animal procedures were conducted in strict accordance with the Experimental Animal Welfare and Ethical Regulations issued by the Hebei Provincial Department of Science and Technology (HPDST 2020-17).

2.3 Preparation of ECPs from *P. multocida* PmQA-1

A single colony of *P. multocida* PmQA-1 was inoculated into 2 L of TSB and incubated at 37 °C with shaking at 180 rpm for 36 h.

The culture was then centrifuged at 10,000 rpm for 20 min at 4 °C to collect the supernatant. The obtained supernatant was sterilized by filtration through a 0.22 μm disposable syringe filter (Merck Millipore Ltd., USA). To precipitate the extracellular proteins, ammonium sulfate was added to achieve 85% saturation and the solution was kept at 4 °C overnight. The precipitated proteins were recovered by centrifugation at 10,000 rpm for 20 min at 4 °C, and the supernatant was discarded. The resulting pellet was resuspended in 0.02 mol/L Tris-HCl buffer (pH 7.5) and dialyzed against the same buffer using dialysis tubing with a molecular weight cut-off of 3,500 Da (Beijing Solarbio Science & Technology Co., Ltd., Beijing, China). After dialysis, the ECP solution was concentrated to a final volume of 15 mL using PEG-20000 at 4 °C, and sterilized by filtration through a 0.22 μm syringe filter. To ensure sterility, an aliquot of the ECP preparation was spread onto TSA plates and incubated overnight at 37 °C. Sterile preparations were aliquoted and stored at −80 °C until use.

The total protein concentration of the ECPs was determined using a BCA Protein Assay Kit (Beijing Solarbio Science & Technology Co., Ltd., Beijing, China) following the manufacturer's instructions. Briefly, the BCA working solution was prepared by mixing BCA reagent with Cu reagent at a volume ratio of 50:1. A bovine serum albumin (BSA) standard was prepared by diluting 10 μL of stock solution with PBS to a final volume of 100 μL to yield a concentration of 0.5 mg/mL. Serial volumes (0, 2, 4, 6, 8, 12, 16, and 20 μL) of the BSA standard were added to a 96-well microplate and adjusted to 20 μL per well with PBS. ECP samples were two-fold serially diluted, and 20 μL of each dilution was added to the sample wells. Then, 200 μL of BCA working solution was added to each well and incubated at 37 °C for 15–30 min. Absorbance at 562 nm was measured using a microplate reader, and the total protein concentration was calculated based on the standard curve.

2.4 SDS-PAGE and mass spectrometry analysis of ECPs

The ECP samples were mixed with protein loading buffer and boiled for 10 min. After cooling, the samples were subjected to SDS-PAGE. Upon completion of electrophoresis, the gels were stained, destained, and photographed for record-keeping. For proteomic profiling, the ECP samples were sent to Shanghai Majorbio Bio-Pharm Technology Co., Ltd., for LC-MS/MS analysis. In brief, the ECPs were first quality-checked, then reduced and alkylated, followed by trypsin digestion. The resulting peptides were quantified, and equal amounts were analyzed by LC-MS/MS. The acquired spectra were searched using the Sequest or Mascot algorithm in Proteome Discoverer, and the identified proteins were subjected to statistical analysis.

2.5 Enzymatic activity assays of ECPs

2.5.1 Amylase activity

Tryptone Soy Agar (TSA) plates containing 2% soluble starch were prepared and sterilized by autoclaving. Wells were punched into the solidified medium, and the plates were overlaid with 0.5% sterile agar. Subsequently, 40 μL of ECPs were added to each well and incubated at 37 °C for 48 h. After incubation, iodine solution was applied around the wells. The presence of a clear hydrolytic zone indicated a positive result, while no color change indicated a negative result.

2.5.2 Urease activity

TSA medium containing 0.2% phenol red indicator was sterilized, and a sterile urea solution was added to a final concentration of 2% before pouring the plates. Wells were made and overlaid with 0.5% sterile agar. Then, 40 μL of ECPs were added to each well and incubated at 37 °C for 48 h. A pink halo around the wells indicated urease activity, while the absence of a color change indicated a negative result.

2.5.3 Protease activity

Sterilized TSA medium was supplemented with 8% skimmed milk powder and poured into plates. Wells were punched, overlaid with 0.5% sterile agar, and 40 μL of ECPs were added to each well. After incubation at 37 °C for 48 h, 10% trichloroacetic acid was dropped around the wells to stop the reaction. A clear hydrolytic zone indicated protease activity; no change indicated a negative result.

2.5.4 Lecithinase activity

TSA medium was sterilized and supplemented with 1% fresh SPF chicken egg yolk emulsion before pouring the plates. Wells were prepared and overlaid with 0.5% sterile agar. Then, 40 μL of ECPs were added and incubated at 37 °C for 48 h. The formation of an opaque, milky-white halo indicated positive phospholipase activity; absence of such a zone indicated a negative result.

2.5.5 Lipase activity

TSA plates containing 1% Tween-80 were prepared. Wells were punched and overlaid with 0.5% sterile agar, and 40 μL of ECPs were added to each well. After incubation at 37 °C for 48 h, a white, opaque halo indicated lipase activity; no change indicated a negative result.

2.5.6 Gelatinase activity

TSA medium containing 0.4% gelatin was sterilized and poured into plates. Wells were made and overlaid with 0.5% sterile agar. Then, 40 μL of ECPs were added and incubated at 37 °C for 48 h. A clear hydrolytic zone indicated gelatinase activity; absence of a zone indicated a negative result.

2.5.7 Hemolysin activity

Wells were prepared in blood agar plates (Beijing Land Bridge Technology Co., Ltd., Beijing, China) and overlaid with 0.5% sterile agar. 40 μL of ECPs were added to each well and incubated at 37 °C for 48 h. A clear, colorless hemolytic zone around the wells indicated hemolysin activity; no change indicated a negative result.

2.6 Effects of environmental physicochemical factors on ECPs enzymatic activity

A single sterile colony of *P. multocida* PmQA-1 was inoculated into 500 mL of TSB and cultured at 37 °C with shaking at 180 rpm.

To assess the effect of culture duration on enzymatic activity, 100 mL of culture was collected at 12 h, 24 h, 36 h, 48 h, and 60 h, respectively, and ECPs were prepared as described above.

To investigate the effect of temperature on ECP enzymatic activity, aliquots of the prepared ECPs were equally divided into five groups (2 mL per group). The first three groups were incubated in water baths at 20 °C, 30 °C, and 37 °C for 24 h, respectively. The fourth group was treated at 60 °C for 2 h, and the fifth group at 80 °C for 1 h. After treatment, all samples were immediately cooled on ice, and enzyme activities were measured.

To examine the effect of pH, the prepared ECPs were also equally divided into five groups (2 mL per group). The pH of each group was adjusted to 3, 5, 7, 9, or 11 using 1 mol/L HCl or 1 mol/L NaOH. Samples were maintained at room temperature for 1 h, after which the pH of all samples was readjusted to neutral (pH 7) prior to enzymatic activity assays.

2.7 Determination of LD_{50} for *P. multocida* and its ECPs

Single colonies of *P. multocida* strains PmQA-1, PmQB-1, and PmQD-1 were inoculated into TSB and cultured to the logarithmic growth phase. The bacterial cells were collected, washed with PBS, serially diluted, and plated for colony counting. Aliquots were prepared and stored at −80 °C until use.

A total of 80 female KM mice (6–8 weeks old) were randomly divided into 16 groups (n = 5 per group). Based on viable counts, groups 1–5 were intraperitoneally injected with 0.2 mL of PmQA-1 suspensions at concentrations of 1.95×10^5, 1.95×10^4, 1.95×10^3, 1.95×10^2, and 1.95×10^1 CFU/mL, respectively. Groups 6–10 received PmQB-1 at 4.87×10^5, 4.87×10^4, 4.87×10^3, 4.87×10^2, and 4.87×10^1 CFU/mL, respectively. Groups 11–15 were injected with PmQD-1 at concentrations of 1.24×10^5, 1.24×10^4, 1.24×10^3, 1.24×10^2, and 1.24×10^1 CFU/mL, respectively. Group 16 served as the negative control and received 0.2 mL of PBS.

For ECPs toxicity determination, 30 female KM mice (6–8 weeks old) were randomly assigned into six groups (n = 5 per group). Groups 1–5 were intraperitoneally injected with 0.2 mL of PmQA-1 ECPs at concentrations of 20.42, 10.21, 5.11, 2.55, and 1.28 mg/mL, respectively. Group 6 served as the control and received 0.2 mL of sterile PBS.

All mice were observed for clinical symptoms and mortality for seven days after injection. The median lethal dose (LD_{50}) was calculated using the modified Kärber method as follows:

$$LD_{50} = \log\text{-}1\{X_k - i[p-(3-P_m-P_n)/4]\}$$

where i is the logarithmic interval between consecutive doses, X_k is the logarithm of the highest dose, p is the sum of the mortality proportions for each dose group, P_m is the highest mortality proportion, and P_n is the lowest mortality proportion.

2.8 Preparation of vaccines

Based on the method described by reference (Yuan et al., 2022) and the LD_{50} results for ECPs, the ECPs were diluted to a final concentration of 13.45 mg/mL. Equal volumes of the diluted ECPs and Freund's complete adjuvant (Sigma-Aldrich Co., LLC, Missouri, USA) were thoroughly mixed and emulsified. To confirm successful emulsification, a drop of the mixture was added to water; if the droplet remained intact without dispersing, the ECP vaccine was deemed ready for use.

For the preparation of the inactivated *P. multocida* vaccine (FKC), a bacterial suspension of PmQA-1 at a concentration of 1×10^7 CFU/mL was mixed with formaldehyde to a final concentration of 0.4% and incubated at 4 °C for 24 h to achieve inactivation. The suspension was then centrifuged at 6,500 rpm for 5 min, and the supernatant was discarded. The bacterial pellet was washed three times with PBS to remove residual formaldehyde and resuspended in PBS to the original volume. Sterility was confirmed by plating an aliquot onto TSA and incubating overnight at 37 °C; absence of colony growth indicated complete inactivation. The inactivated bacterial suspension was then emulsified with an equal volume of Freund's complete adjuvant to prepare the final FKC vaccine.

To prepare the combined vaccine (FKC + ECPs), equal volumes of the ECP vaccine and the FKC vaccine were mixed thoroughly to form a homogenous emulsion.

2.9 Immunization and sample collection in mice

Twenty female KM mice (6–8 weeks old) were randomly divided into four groups (n = 5 per group) to determine the optimal safe dose for vaccination. Mice were subcutaneously immunized at multiple sites with the FKC vaccine at doses of 0.6 mL, 0.4 mL, 0.2 mL, and 0.1 mL, respectively. The animals were monitored for general health and local skin reactions. The highest safe dose was selected for subsequent immunization experiments.

For the main immunization trial, 216 female KM mice (6–8 weeks old) were randomly assigned to four groups (n = 54 per group). Immunization was performed subcutaneously at multiple sites following the procedure recommended for commercial *P. multocida* vaccines. The groups were as follows: the ECPs group received 0.2 mL of ECP vaccine; the FKC group received 0.2 mL of FKC vaccine; the FKC + ECPs group received 0.2 mL of the combined FKC + ECPs vaccine; the PBS group received 0.2 mL of sterile PBS as a control. The first immunization was designated as day 0. On day 14, a booster immunization was administered, in which the concentrations of ECPs protein and bacteria were reduced by half compared to the initial dose, while the injection volume remained the same. The booster vaccines were fully emulsified with Freund's incomplete adjuvant prior to administration.

On days 0, 7, 14, 21, and 28, three mice from each group were randomly selected for sample collection. Blood was collected by orbital enucleation, and sera were separated for cytokine assays. Liver, spleen, and lung tissues were also harvested for further analyses. Additionally, on days 0, 14, and 28, spleens from three randomly selected mice per group were collected for lymphocyte proliferation assays. The remaining 30 mice in each group were retained for subsequent challenge protection experiments.

2.10 Analysis of humoral and cellular immune responses

To prepare whole-cell proteins of PmQA-1, bacteria were cultured to the logarithmic phase and harvested by centrifugation at 12,000 rpm for 10 min. The pellet was washed three times with PBS and resuspended. Bacterial cells were disrupted using an ultrasonic homogenizer (Ningbo Scientz Biotechnology Co., Ltd., Ningbo, China) with cycles of 3 s on and 3 s off until the suspension became clear. The lysate was centrifuged at 12,000 rpm for 10 min, and the supernatant was sterilized through a 0.22 μm disposable syringe filter to obtain the whole-cell protein. The protein concentration was determined using a BCA Protein Assay Kit.

The serum IgG level was measured by indirect ELISA (iELISA). Briefly, 96-well microplates were coated with PmQA-1 whole-cell proteins at a concentration of 1000 μg/mL in carbonate buffer (0.1 mol/L, pH 9.6) with 100 μL per well and incubated at 37 °C for 4 h. Plates were washed three times with 3 mL PBS, then blocked with PBST containing 5% skimmed milk at 37 °C for 2 h. After washing, mouse sera (primary antibody) were diluted 1:50 in PBST and added at 100 μL per well, followed by incubation at 37 °C for 1 h. Plates were washed three times, then incubated with HRP-conjugated goat anti-mouse IgG (secondary antibody) diluted 1:10,000 in PBST at 100 μL per well at 37 °C for 1 h. After a final wash, 100 μL of TMB substrate was added to each well and the reaction was developed at 37 °C in the dark for 10 min. The reaction was stopped with 50 μL of 2 mol/L H_2SO_4, and absorbance was measured at 450 nm.

Lymphocyte proliferation in the spleen was assessed using the MTT assay. Mouse spleens were placed on 70 μm cell strainers and gently ground in 3 mL RPMI 1640 medium (Thermo Fisher Scientific Inc., New York, USA) to obtain single-cell suspensions. Cells were centrifuged at 1,000 rpm for 5 min, the supernatant was discarded, and the pellet was resuspended in 3 mL red blood cell lysis buffer for 10–15 min. After lysis, cells were washed three times with 5 mL RPMI 1640 and finally resuspended in complete RPMI 1640 medium supplemented with 10% FBS and 1% non-essential amino acids, adjusting the cell concentration to 1×10^7 CFU/mL. A total of 100 μL of cell suspension was added to each well of a 96-well culture plate, together with PmQA-1 whole-cell protein at a final concentration of 5 μg per well. Cells were incubated in a CO_2 incubator for 48 h. Then, 10 μL of MTT stock solution (5 mg/mL) was added per well, mixed gently, and incubated for another 4 h. After incubation, 100 μL of Formazan solvent was added per well, and plates were incubated for an additional 4 h with intermittent shaking to fully dissolve the crystals. Absorbance was measured at 570 nm using a microplate reader. The stimulation index (SI) was calculated as:

SI = (OD_{570} of protein-stimulated group - OD_{570} of medium)/(OD_{570} of non-stimulated group – OD_{570} of medium).

Gene expression levels of TNF-α, IFN-γ, IL-1β, and IL-10 in liver, spleen, and lung tissues were determined by quantitative PCR (qPCR). Total RNA was extracted using the RNAprep Pure Tissue Kit (TianGen Biotech Co., Ltd., Beijing, China), treated to remove genomic DNA, and reverse transcribed into cDNA. qPCR was performed using SYBR Green PCR Master Mix. The primer sequences are listed in Table 1. Cytokine expression levels were normalized to the internal control GAPDH and β-Actin genes and calculated using the $2^{-\Delta\Delta CT}$ method.

TABLE 1 Primers used for qPCR.

Gene	Primer sequence (5′ – 3′)
GAPDH	AGGTCGGTGTGAACGGATTTG
	TGTAGACCATGTAGTTGAGGTCA
β-Actin	TTCAACACCCCAGCCATG
	CCTCGTAGATGGGCACAGT
TNF-α	CCCTCACACTCAGATCATCTTCT
	GCTACGACGTGGGCTACAG
IFN-γ	ATGAACGCTACACACTGCATC
	CCATCCTTTTGCCAGTTCCTC
IL-10	CTTACTGACTGGCATGAGGATCA
	GCAGCTCTAGGAGCATGTGG
IL-1β	GACTGTTTCTAATGCCTTCCC
	ATGGTTTCTTGTGACCCTGA

2.11 Challenge test in immunized mice

At 28 days post-immunization, a total of 21 mice from each vaccine group (ECPs, FKC, and FKC + ECPs) and the PBS control group were randomly divided into three subgroups (n = 10 per subgroup). The mice were then intraperitoneally challenged with PmQA-1 (77.70 CFU/mouse), PmQB-1 (43.35 CFU/mouse), or PmQD-1 (4.38×10^3 CFU/mouse). The mice were monitored daily for 14 consecutive days, and mortality was recorded for each group. The relative percent survival (RPS) was calculated using the following formula:

RPS (%) = [1 - (mortality in immunized group/mortality in control group)] × 100%

2.12 Statistical analysis

Statistical analyses were conducted using SPSS version 26.0 and GraphPad Prism version 9.5.0. One-way analysis of variance (ANOVA) followed by pairwise t-tests was applied where appropriate. Data are presented as the mean ± standard error of the mean (SEM). Statistical significance was indicated as follows: $^{*}p < 0.05$, $^{**}p < 0.01$, and $^{***}p < 0.001$.

3 Results

3.1 SDS-PAGE and mass spectrometry analysis of ECPs

The protein concentration of the prepared ECPs was determined to be 20.42 g/L using the BCA method. SDS-PAGE analysis (Figure 1) revealed that the protein bands were mainly distributed between 25 and 100 kDa. Mass spectrometry analysis

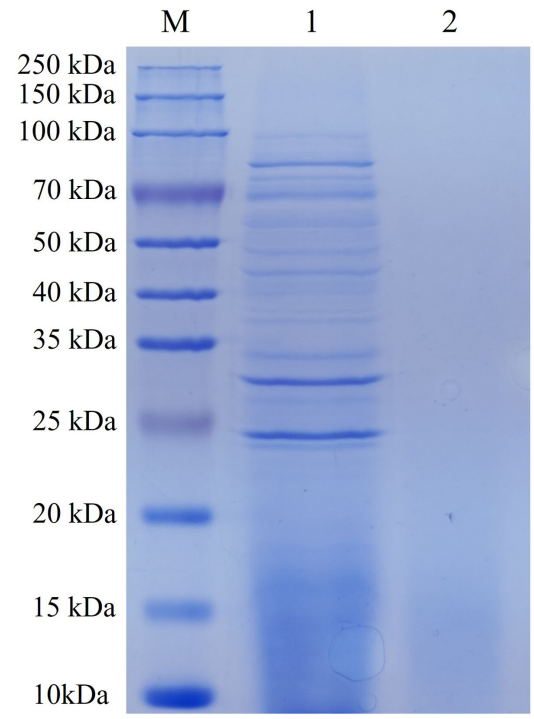

FIGURE 1
SDS-PAGE of ECPs. M, Pre-stained protein marker; 1, ECPs; 2, negative control.

(Supplementary material) identified a total of 157 proteins within the ECPs, including transferrin-binding protein A, elongation factor Tu, dihydrolipoyl dehydrogenase, pyruvate dehydrogenase E1 component, heme-binding protein A, MltA-interacting MipA protein, and metalloprotease PmbA, among others.

3.2 Amylase activity of ECPs

The enzymatic activity of the ECPs was assessed using the agar plate diffusion method. As shown in Figure 2, the ECPs exhibited amylase activity, forming clear hydrolysis zones on the agar plates, while no urease, protease, phospholipase, lipase, gelatinase, or hemolysin activities were detected.

Given the presence of amylase activity, the effects of incubation time, temperature, and pH on the amylase activity of ECPs were further investigated. As illustrated in Figure 2, amylase activity increased progressively with prolonged incubation time. Temperatures of 4 °C, 20 °C, 30 °C, and 37 °C had little effect on amylase activity; however, treatment at 60 °C resulted in reduced activity, and complete loss of activity was observed at 80 °C. Regarding pH, amylase activity increased with rising pH from 3 to 7, but showed a slight decrease as the pH increased from 7 to 11.

3.3 Determination of the LD_{50} of PmQA-1, PmQB-1, PmQD-1, and ECPs

To determine the immunization dose of ECPs and the challenge doses of *P. multocida*, mice were intraperitoneally injected with ECPs, PmQA-1, PmQB-1, and PmQD-1 to calculate their LD_{50} values. Following injection, mice in all groups except the PBS control group exhibited varying degrees of clinical symptoms, such as ruffled fur and lethargy. Necropsy of the deceased mice revealed pulmonary hemorrhage as well as splenomegaly and hepatomegaly with hemorrhage. Based on the modified Kärber method (Supplementary Table 1), the LD_{50} of ECPs was determined to be 2.69 mg/mouse, while the LD_{50} values for PmQA-1, PmQB-1, and PmQD-1 were 15.50 CFU/mouse, 8.67 CFU/mouse, and 8.76×10^2 CFU/mouse, respectively.

Accordingly, for immunization, a dose equal to half of the ECPs LD_{50} (1.35 mg/mouse) was used for subcutaneous injection. For the challenge test, a dose equivalent to five times the bacterial LD_{50} was administered intraperitoneally, resulting in final challenge doses of 77.70 CFU/mouse for PmQA-1, 43.35 CFU/mouse for PmQB-1, and 4.38×10^3 CFU/mouse for PmQD-1.

3.4 Specific IgG following immunization

Mice were immunized with different doses of the FKC and ECPs + FKC vaccine. When administered at doses of 0.6 mL and 0.4 mL, the mice exhibited noticeable adverse reactions, including lethargy and ruffled fur. Additionally, mice receiving the 0.6 mL dose developed subcutaneous abscesses and ulcers. In contrast, no obvious abnormalities were observed in mice immunized with 0.2 mL or 0.1 mL doses. Therefore, a dose of 0.2 mL FKC and ECPs + FKC was selected for subsequent immunizations.

Serum samples were collected from the mice on days 0, 7, 14, 21, and 28 post-immunization with ECPs, and the levels of specific antibodies were measured using an indirect ELISA (iELISA). As shown in Figure 3, the levels of specific IgG in the sera of the ECPs and FKC immunization groups increased continuously, peaking on day 21. Although slightly decreased by day 28, the IgG levels remained significantly higher than those in the control group. In the FKC + ECPs immunization group, the specific IgG levels continued to rise throughout the experiment, reaching their maximum on day 28. Notably, the ECPs group exhibited higher specific IgG levels than the FKC + ECPs group, which in turn showed higher levels than the FKC group alone. All immunized groups demonstrated significantly higher specific IgG levels compared to the control group. These results indicate that ECPs induced the strongest humoral immune response, followed by the FKC + ECPs combination, while FKC alone elicited the weakest response.

3.5 Analysis of splenic lymphocyte proliferation in immunized mice

Spleens were collected from mice on days 0, 14, and 28 after immunization with ECPs. The splenic lymphocyte proliferation index was determined using the MTT assay. As shown in Figure 4, the splenic lymphocyte proliferation levels in the ECPs, FKC, and FKC + ECPs immunization groups increased continuously, reaching their maximum on day 28, and were all significantly higher than those in the control group. Notably, the proliferation level in the ECPs group was higher than that in the FKC + ECPs

10.3389/fmicb.2025.1674831

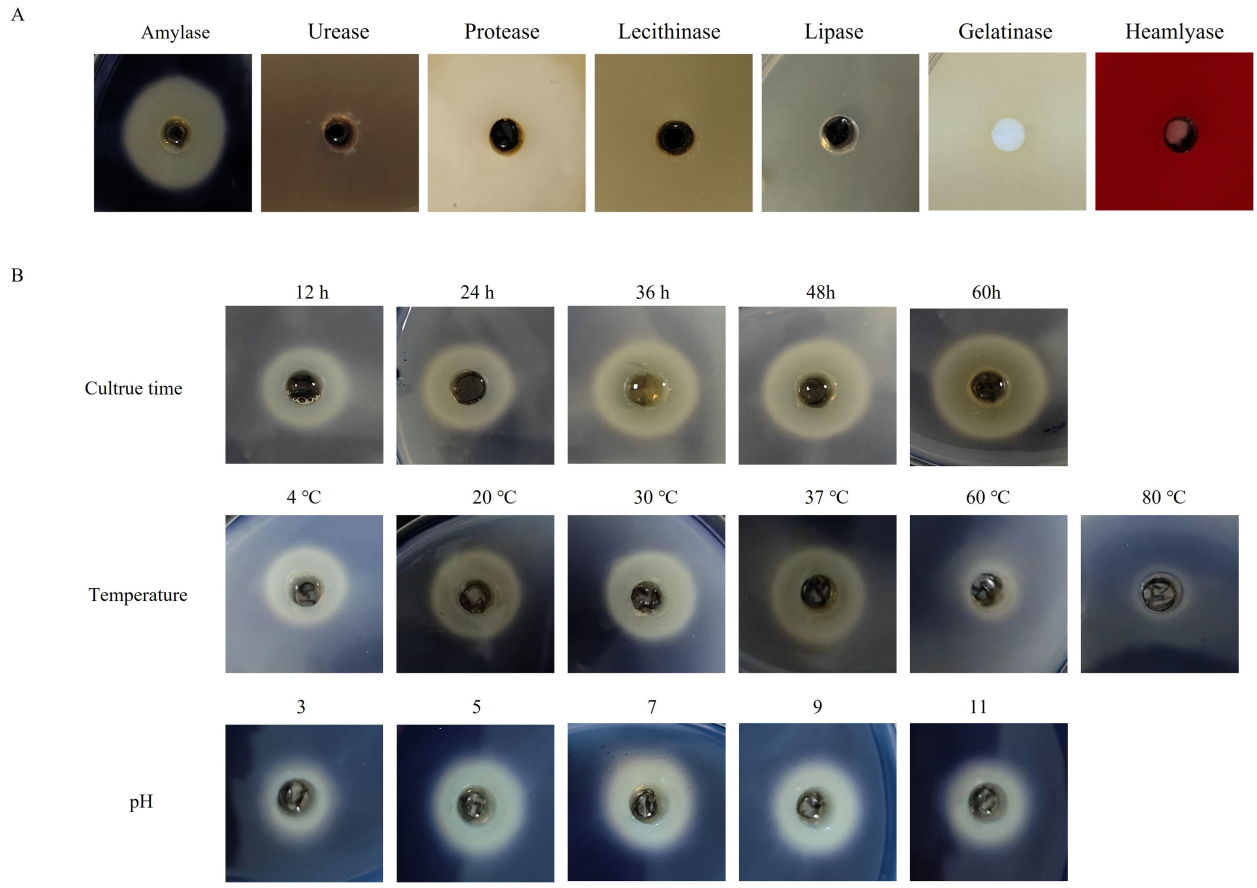

FIGURE 2
Enzymatic activity analysis of ECPs. **(A)** The prepared ECPs were applied to agar plates for the detection of amylase, urease, protease, phospholipase, lipase, gelatinase, and hemolysin activities. Plates were incubated at 37 °C for 48 h and then examined. **(B)** Effects of different culture times, temperatures, and pH values on the amylase activity of ECPs.

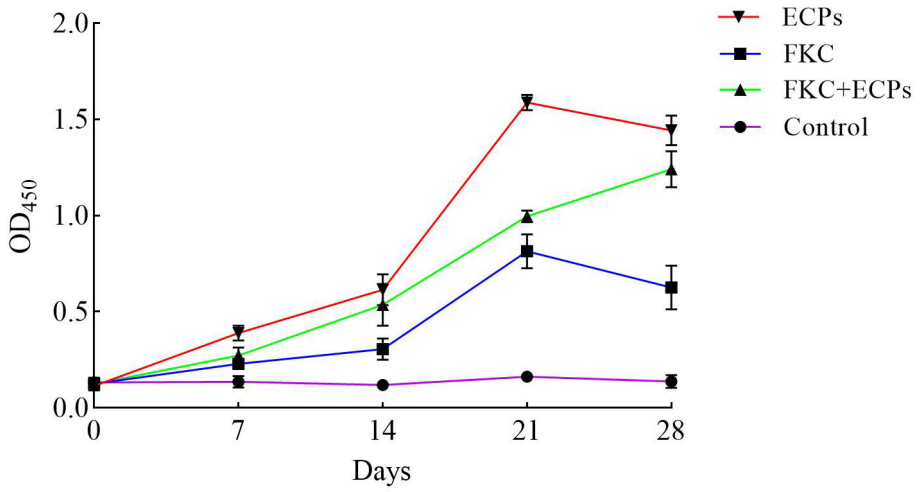

FIGURE 3
Determination of serum IgG levels in immunized mice. Mice were immunized with ECPs, FKC, or the combined FKC + ECPs vaccine. The whole-cell protein of PmQA-1 was used as the coating antigen, and serum IgG levels were measured by iELISA on days 0, 7, 14, 21, and 28 post-immunization. The PBS group received 0.2 mL of sterile PBS is the Control.

10.3389/fmicb.2025.1674831

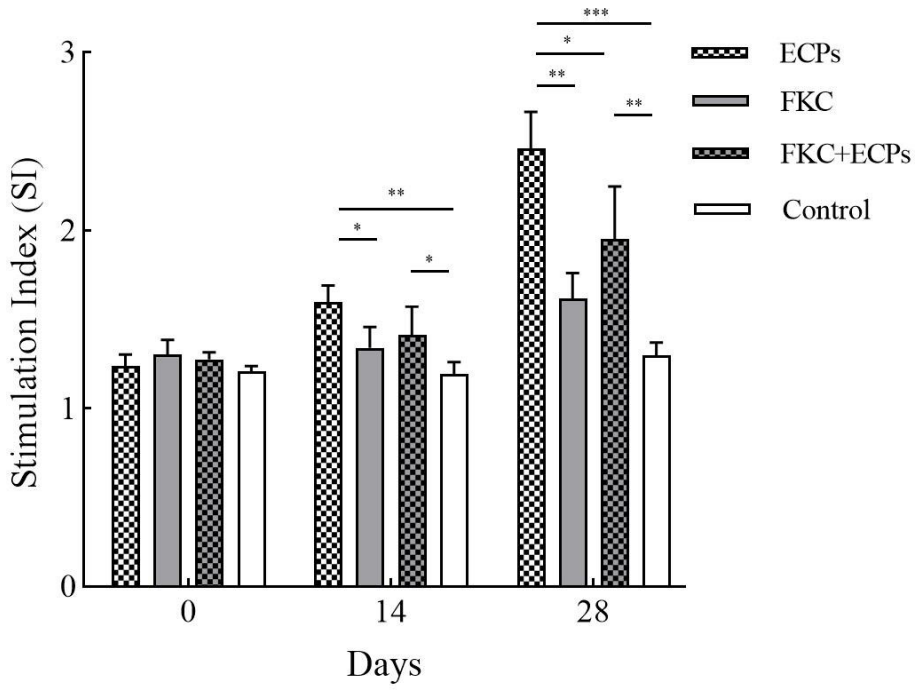

FIGURE 4
Splenic lymphocyte proliferation in immunized mice. Spleens were collected from three mice per group on days 0, 14, and 28 post-immunization. Splenic lymphocytes were isolated and adjusted to a concentration of 1×10^7 CFU/mL. A total of 100 μL of cell suspension was added to each well of a 96-well plate, with PmQA-1 whole-cell protein added at a final concentration of 5 μg per well. Cells were incubated in a CO_2 incubator for 48 h, and proliferation was assessed by measuring OD_{570} using the MTT assay. Statistical significance was indicated as follows: $^*p < 0.05$, $^{**}p < 0.01$, and $^{***}p < 0.001$.

group, which in turn was higher than that in the FKC group. These results indicate that ECPs induced the strongest cellular immune response, followed by the FKC + ECPs combination, while FKC alone elicited the weakest response.

3.6 Analysis of cytokine expression in organs of immunized mice

The expression levels of TNF-α, IFN-γ, IL-1β, and IL-10 in the liver, spleen, and lungs of immunized mice were quantified by qPCR using GAPDH (Figure 5) and β-actin (Supplementary Figure 1) as reference genes. The results showed that in the ECPs, FKC, and FKC + ECPs groups, TNF-α expression in the liver, spleen, and lungs increased continuously, reaching peak levels on day 28, except in the spleen where TNF-α peaked on day 21. In the ECPs group, IFN-γ expression in the liver, spleen, and lungs increased steadily, peaking on day 21 and slightly declining on day 28. In the FKC and FKC + ECPs groups, splenic IFN-γ expression also peaked on day 21 and then slightly decreased, whereas hepatic and pulmonary IFN-γ expression continued to rise, reaching maximum levels on day 28. For IL-1β, expression in the liver of the ECPs group increased continuously and peaked on day 28, while expression in the spleen and lungs peaked on day 21 and slightly declined by day 28. In the FKC and FKC + ECPs groups, IL-1β expression in the liver, spleen, and lungs generally increased to a maximum on day 28, except for the lungs where it peaked on day 21 and decreased slightly afterward. Regarding IL-10, expression in the spleen of the ECPs group increased continuously, peaking on day 28. In the liver and lungs, IL-10 expression peaked on day 21 and slightly declined by day 28. In the FKC group, splenic IL-10 expression peaked on day 28, hepatic expression peaked on day 21 with a slight decline at day 28, and pulmonary IL-10 expression peaked earlier on day 14 and then declined. In the FKC + ECPs group, IL-10 expression in the liver and spleen increased continuously to reach peak levels on day 28, while in the lungs, it peaked on day 21 and then slightly decreased.

Notably, cytokine expression levels (TNF-α, IFN-γ, IL-1β, and IL-10) in the liver, spleen, and lungs were consistently higher in the ECPs group than in the FKC + ECPs group, which were in turn higher than those in the FKC group.

3.7 Protective efficacy of ECPs against infections with different *P. multocida* serotypes

At 28 days post-immunization, mice were challenged intraperitoneally with PmQA-1 (Figure 6A). All mice in the PBS control groups died following intraperitoneal challenge with any of the three serotypes. No deaths were observed in the ECPs-immunized group, resulting in a relative protection rate of 100%. In the FKC + ECPs group, only one mouse died on day 2 post-challenge, corresponding to a relative protection rate of 90%. In the FKC group, three mice died in total, yielding a relative protection rate of 70%. Following challenge with PmQB-1 (Figure 6B), the

10.3389/fmicb.2025.1674831

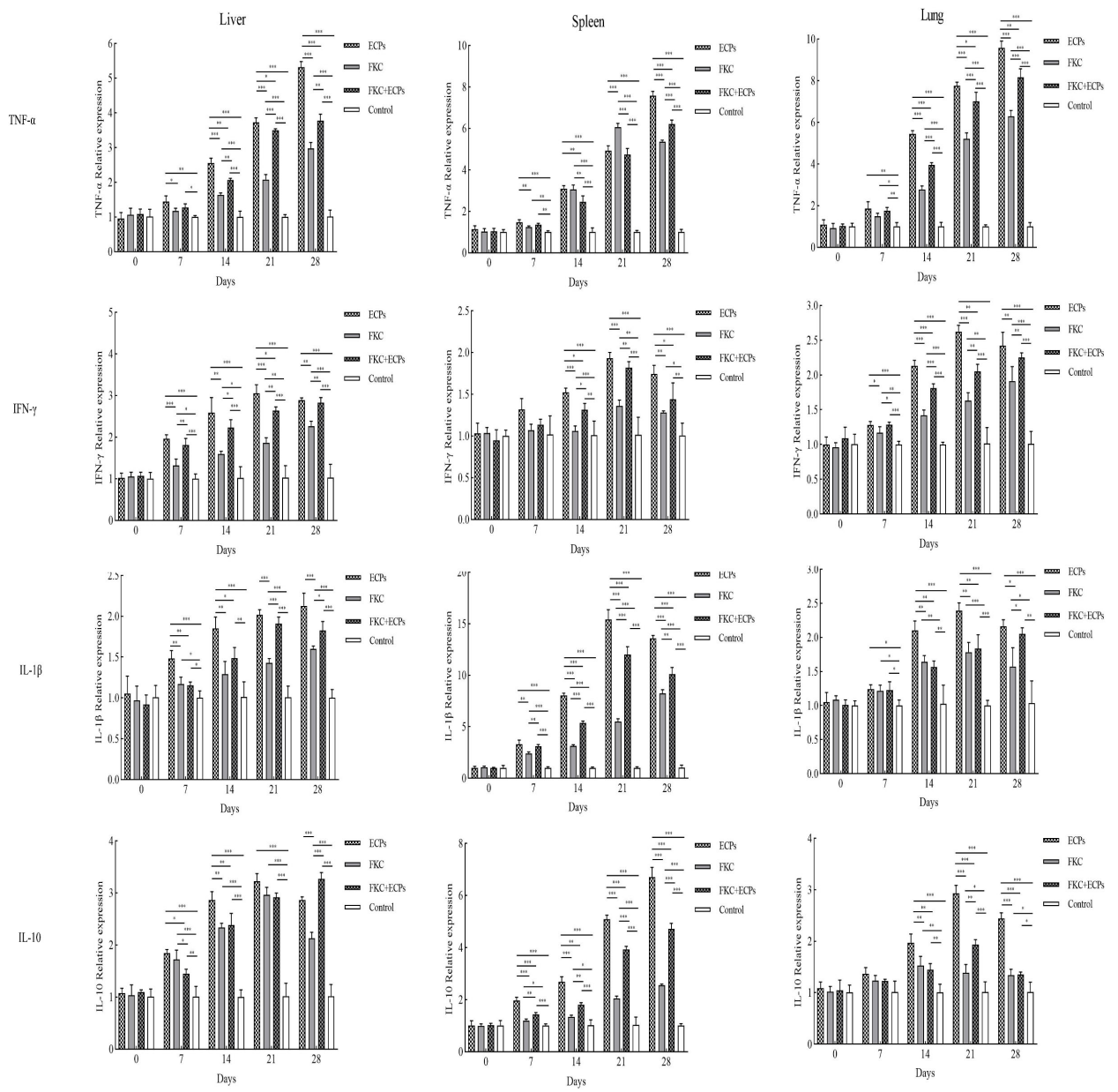

FIGURE 5
Expression levels of TNF-α, IFN-γ, IL-1β, and IL-10 in the liver, spleen, and lungs of mice immunized with ECPs, FKC, or FKC + ECPs. Cytokine expression was analyzed by qPCR using three mice per group. Data are presented as mean ± SD. Asterisks indicate significant differences compared to the negative control or among the experimental groups (*$p < 0.05$; **$p < 0.01$; ***$p < 0.001$).

ECPs group again showed no mortality, maintaining a relative protection rate of 100%. In contrast, all mice in the FKC group died by day 5 post-challenge, resulting in a relative protection rate of 0%. In the FKC + ECPs group, six mice died in total, resulting in a protection rate of 40%. When challenged with PmQD-1 (Figure 6C), one mouse in the ECPs group died on day 5 post-challenge, giving a relative protection rate of 90%. Seven mice died in the FKC group, corresponding to a relative protection rate of 30%, while three deaths were recorded in the FKC + ECPs group, resulting in a protection rate of 70%.

These findings indicate that ECPs immunization provided the highest level of protection against all tested *P. multocida* serotypes, demonstrating its strong potential as a broad-spectrum vaccine candidate against *P. multocida* infections.

4 Discussion

Due to the high infection and mortality rates of *P. multocida*, vaccination is an important measure for preventing and controlling its infection. Previous studies have demonstrated that *P. multocida* serotype A is the predominant serotype isolated from cattle and poultry. However, the commercially available vaccines for bovine *P. multocida* are mainly developed based on serotype B. Due to the fact that the cross-immune protection effect among different

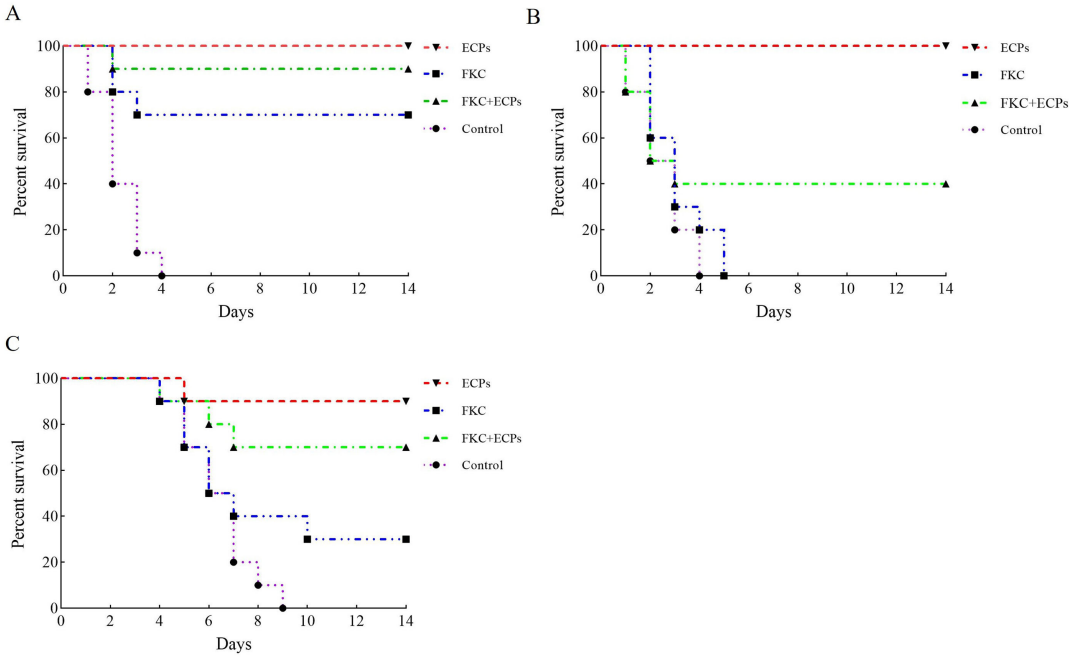

FIGURE 6
Protective efficacy of ECPs against different *P. multocida* serotypes in mice. Survival curves of mice subcutaneously immunized with extracellular products (ECPs), formalin-killed cells (FKC), or a combination of FKC + ECPs, or administered PBS as a control, and intraperitoneally challenged with *P. multocida* strains PmQA-1 **(A)**, PmQB-1 **(B)**, and PmQD-1 **(C)**.

serotypes of *P. multocida* is not satisfactory, the commercially available vaccines offer limited cross-protection against serotype A strains (Mostaan et al., 2020; Peng et al., 2016; Xiang et al., 2025). Extensive research has indicated that extracellular products (ECPs) from various pathogens contribute to bacterial pathogenicity and can also elicit strong immune responses in the host. In this study, we prepared ECPs from the *P. multocida* strain PmQA-1. Proteomic analysis revealed that the ECPs contained proteins ranging from 25 to 100 kDa, comprising at least 157 distinct proteins. Notably, these included Transferrin-binding protein A, Elongation factor Tu, Dihydrolipoyl dehydrogenase, Pyruvate dehydrogenase E1 component, Heme-binding protein A, MltA-interacting MipA protein, and Metalloprotease PmbA. Transferrin-binding protein A has been identified as a promising broad-spectrum vaccine candidate against *H. parasuis*, *Neisseria meningitidis*, and *P. multocida* serogroup B:2 (Fegan et al., 2019; Huang et al., 2013; Shivachandra et al., 2015; West et al., 2001). Similarly, Elongation factor Tu, Dihydrolipoyl dehydrogenase, Heme-binding protein, and MipA protein have all been reported to induce effective immune responses and confer protection against relevant pathogens (Devasundaram and Raja, 2017; Hays et al., 2016; Mou et al., 2020; Moustafa et al., 2024; Nagai et al., 2019; Thofte et al., 2018; Zhang et al., 2017). Additionally, studies have shown that ECPs derived from *Bacillus* spp., *V. lentus*, *Flavobacterium sasangense (F. sasangense)*, and *V. anguillarum* contain various immunogenic components capable of stimulating host immune responses and providing protection when used as vaccines (Chi et al., 2014; Santos et al., 1995; Song et al., 2018; Yuan et al., 2022). Based on these findings, we developed an ECP-based subunit vaccine and evaluated its protective efficacy against infections caused by different *P. multocida* serotypes.

Numerous studies have demonstrated that extracellular products (ECPs) carry various enzymes, including amylase, urease, protease, phospholipase, lipase, gelatinase, and hemolysin. These factors contribute to extensive tissue damage, facilitating nutrient acquisition and bacterial proliferation within the host, thereby playing a crucial role in pathogenicity (Fan et al., 2024; Zhang et al., 2014). Previous research has indicated that ECPs with proteolytic activity may suppress certain immune mechanisms by degrading immune components (Schadich and Cole, 2009; Song et al., 2018). In the present study, enzymatic activity assays revealed that the ECPs produced by PmQA-1 exhibited significant amylase activity. Amylase has been implicated as an important virulence factor in various pathogens. For example, loss of AMY1 function has been shown to reduce the ability of *Histoplasma* to kill macrophages and colonize murine lungs (Marion et al., 2006). Similarly, deletion of amyAXcc, a putative amylase-encoding gene in *Xanthomonas campestris* pv. *campestris* (*X. campestris* pv. *campestris*) 8004, resulted in complete loss of extracellular amylase activity and a marked reduction in virulence (Lin et al., 2021). To further verify the pathogenicity of ECPs, their median lethal dose (LD_{50}) was determined by intraperitoneal injection in mice. Administration of ECPs caused mortality in mice, with necropsy revealing swelling and hemorrhage in the liver, spleen, and lungs, which closely resembled the pathological changes observed in mice challenged intraperitoneally with *P. multocida*. These findings confirm the significant role of ECPs in the pathogenicity of *P. multocida*.

Specific IgG levels in serum are a key indicator for evaluating the humoral immune response induced by vaccination, while the transformation rate of splenic lymphocytes can reflect the level of cellular immune response. In this study, both the serum IgG antibody levels and splenic lymphocyte transformation rates were

significantly increased in mice immunized with ECPs, FKC, or the combination of FKC + ECPs. Notably, the ECPs-immunized group showed the highest IgG antibody titers and splenic lymphocyte transformation rates, indicating that the ECPs vaccine elicited the strongest humoral and cellular immune responses. Consistent with these findings, Zhang et al. (2014) reported that the agglutination titers of channel catfish immunized with the extracellular products (ECPs) of *A. hydrophila* increased from 2 to 4 weeks post-immunization and remained at a high level up to week seven. Similarly, Chi et al. (2014) demonstrated that the ECPs derived from three strains of intestinal autochthonous bacteria-*A. veronii* BA-1, *V. lentus* BA-2, and *F. sasangense* BA-3-significantly enhanced respiratory bursts, which are an important indicator of cellular immune mechanisms in fish, compared with the control group.

TNF-α is a pleiotropic cytokine that can activate macrophages and neutrophils to phagocytose pathogens and plays a key role in promoting inflammatory responses (Nguyen et al., 2016). IFN-γ is involved in Th1-type cellular immunity and induces cell-mediated immune responses (Kak et al., 2018). IL-1β is another important pro-inflammatory cytokine, while IL-10 participates in the regulation of cellular immunity and serves as a crucial anti-inflammatory cytokine (Weber et al., 2010). In this study, the relative expression levels of these cytokines in the liver, spleen, and lung tissues of immunized mice showed varying degrees of increase, reaching their peaks at either day 21 or day 28 post-immunization. Notably, the expression levels of cytokines in the ECPs-immunized group were higher than those in the FKC and FKC + ECPs groups across all examined tissues, indicating that ECPs immunization can elicit a stronger immune response and induce higher levels of cytokine production to protect the host. Similarly, Yuan et al. (2022) reported that crucian carp immunized with ECPs, FKC, or FKC + ECPs prepared from *A. caviae* AC-CY exhibited elevated cytokine levels in various tissues, with the ECPs group showing the most pronounced effect. This observation is consistent with the results of the present study, although the patterns of cytokine expression differed slightly.

To evaluate the protective efficacy of the vaccines, mice were intraperitoneally challenged with *P. multocida* strain PmQA-1. The results showed that immunization with ECPs conferred a relative protection rate of 100% against PmQA-1, providing robust homologous protection that was superior to that achieved by FKC + ECPs and FKC alone. These findings are consistent with previous studies on the protective effects of ECPs (Song et al., 2018; Zhang et al., 2014). Notably, the present study further demonstrated that ECPs conferred strong cross-protection, with protection rates of 100% and 87.5% against the heterologous strains PmQB-1 and PmQD-1, respectively. Similarly, Huang et al. (2013) reported that the TbpA protein, a major antigen presented in ECPs, provided cross-protection for guinea pigs against serovars 13, 4, and 14 of *G. parasuis*, for which at least 15 serovars have been identified. Given that *G. parasuis* and *P. multocida* are both members of the *Pasteurellaceae* family, the findings by Huang et al. (2013) and our study collectively indicate that ECPs and their key antigenic components hold considerable promise for the development of effective subunit vaccines with cross-serovar protection.

In summary, immunization of mice with ECPs derived from PmQA-1 significantly enhanced both humoral and cellular immune responses, increased cytokine expression levels, and provided effective cross-protection against the PmQA-1, PmQB-1, and PmQD-1 strains. These results highlight the potential of ECPs as a promising subunit vaccine candidate targeting multiple *P. multocida* serotypes. However, whether the protective efficacy and pathogenicity of ECPs are mediated by a single component or a combination of multiple components remains unclear, and further studies are needed to elucidate the underlying mechanisms and confirm their viability as vaccine candidates. In addition, it is necessary to extend the monitoring period for serum IgG levels, lymphocyte transformation rates, and cytokine expression to better understand the duration of the induced immune responses, thereby providing a more solid foundation for the development of effective subunit vaccines.

5 Conclusion

This study evaluated the immunoprotective efficacy of extracellular products (ECPs) from *Pasteurella multocida* serotype A:3 strain PmQA-1 in mice. ECPs contained 157 proteins (25–100 kDa), including transferrin-binding protein A and elongation factor Tu, with detectable amylase activity. ECPs exhibited pathogenicity (LD_{50} = 2.69 mg/mouse), inducing lesions consistent with *P. multocida* infection. ECPs vaccination triggered robust humoral immunity (peak IgG at day 21) and cellular responses (enhanced splenic lymphocyte proliferation). It also upregulated TNF-α, IFN-γ, IL-1β, and IL-10 in liver, spleen, and lungs, with peaks at days 21–28. Challenge tests showed ECPs conferred 100% protection against homologous serotype A:3 and heterologous serotype B:2, and 90% against serotype D:4, outperforming formalin-killed cell (FKC) vaccines and FKC + ECPs combinations. These results highlight ECPs as a promising broad-spectrum subunit vaccine candidate against *P. multocida* infections. One limitation of this study is that the immune protection experiments were conducted only in a murine infection model. Protective efficacy was not evaluated in livestock or poultry, which are the primary hosts of *P. multocida*. Further studies in these target animals are necessary to validate the applicability and effectiveness of the ECPs-based immunization strategy under practical field conditions.

Data availability statement

The raw data supporting the conclusions of this article will be made available by the authors, without undue reservation.

Ethics statement

The animal study was approved by the Experimental Animal Welfare and Ethical Regulations issued by the Hebei Provincial Department of Science and Technology (HPDST 2020-17). The study was conducted in accordance with the local legislation and institutional requirements.

Author contributions

JL: Data curation, Formal analysis, Methodology, Writing – original draft. WL: Data curation, Formal analysis, Methodology, Writing – original draft. XZ: Writing – original draft, Methodology. YS: Writing – original draft. LC: Writing – original draft. QS: Supervision, Writing – review & editing. TW: Funding acquisition, Supervision, Writing – review & editing.

Funding

The author(s) declare that financial support was received for the research and/or publication of this article. This work was supported by Shijiazhuang City "Unveiling and Commanding" Science and Technology Project (2417908002A) and Hebei Agriculture Research System (HBCT2025250201).

Acknowledgments

We thank Mingxing Tian from Shanghai Veterinary Research Institute, Chinese Academy of Agricultural Sciences for their valuable help in our experiment.

Conflict of interest

JL was employed by Elanco (Sichuan) Animal Health Co., Ltd.

The remaining authors declare that the research was conducted in the absence of any commercial or financial relationships that could be construed as a potential conflict of interest.

Generative AI statement

The author(s) declare that no Generative AI was used in the creation of this manuscript.

Any alternative text (alt text) provided alongside figures in this article has been generated by Frontiers with the support of artificial intelligence and reasonable efforts have been made to ensure accuracy, including review by the authors wherever possible. If you identify any issues, please contact us.

Publisher's note

Supplementary material

The Supplementary Material for this article can be found online at: https://www.frontiersin.org/articles/10.3389/fmicb.2025.1674831/full#supplementary-material

References

Baldissera, M. D., Souza, C. F., Verdi, C. M., Vizzotto, B. S., Santos, R. C. V., and Baldisserotto, B. (2018). Aeromonas caviae alters the activities of ecto-enzymes that hydrolyze adenine nucleotides in fish thrombocytes. *Microb. Pathog.* 115, 64–67. doi: 10.1016/j.micpath.2017.12.044

Chi, C., Jiang, B., Yu, X., Liu, T., Xia, L., and Wang, G. (2014). Effects of three strains of intestinal autochthonous bacteria and their extracellular products on the immune response and disease resistance of common carp, cyprinus carpio. *Fish Shellfish Immunol.* 36, 9–18. doi: 10.1016/j.fsi.2013.10.003

Dabo, S. M., Confer, A., Montelongo, M., York, P., and Wyckoff, J. H. R. (2008). Vaccination with pasteurella multocida recombinant OmpA induces strong but non-protective and deleterious th2-type immune response in mice. *Vaccine* 26, 4345–4351. doi: 10.1016/j.vaccine.2008.06.029

Dassanayake, R. P., Briggs, R. E., Kaplan, B. S., Menghwar, H., Kanipe, C., Casas, E., et al. (2025). Pasteurella multocida filamentous hemagglutinin b1 (fhab1) gene is not involved with avian fowl cholera pathogenesis in turkey poults. *BMC Vet. Res.* 21:207. doi: 10.1186/s12917-025-04668-1

Devasundaram, S., and Raja, A. (2017). Dihydrolipoamide dehydrogenase-lpd (rv0462)-specific t cell recall responses are higher in healthy household contacts of TB: A novel immunodominant antigen from m. *Tuberculosis. J. Leukoc. Biol.* 102, 135–151. doi: 10.1189/jlb.4A0916-067RR

Fan, C., Dai, W., Zhang, H., Liu, S., Lin, Z., and Xue, Q. (2024). Genomic and proteomic analyses of extracellular products reveal major virulence factors likely accounting for differences in pathogenicity to bivalves between vibrio mediterranei strains. *Animals* 14:692. doi: 10.3390/ani14050692

Fegan, J. E., Calmettes, C., Islam, E. A., Ahn, S. K., Chaudhuri, S., Yu, R., et al. (2019). Utility of hybrid transferrin binding protein antigens for protection against pathogenic neisseria species. *Front. Immunol.* 10:247. doi: 10.3389/fimmu.2019.00247

Guan, L., Zhang, L., Xue, Y., Yang, J., and Zhao, Z. (2020). Molecular pathogenesis of the hyaluronic acid capsule of pasteurella multocida. *Microb. Pathog.* 149:104380. doi: 10.1016/j.micpath.2020.104380

Gulliver, E. L., Sy, B. M., Wong, J. L., Deveson Lucas, D. S., Powell, D. R., Harper, M., et al. (2022). The role and targets of the RNA-binding protein ProQ in the gram-negative bacterial pathogen pasteurella multocida. *J. Bacteriol.* 204:e0059221. doi: 10.1128/jb.00592-21

Hatfaludi, T., Al-Hasani, K., Gong, L., Boyce, J. D., Ford, M., Wilkie, I. W., et al. (2012). Screening of 71 p. Multocida proteins for protective efficacy in a fowl cholera infection model and characterization of the protective antigen PlpE. *PLoS One* 7:e39973. doi: 10.1371/journal.pone.0039973

Hays, M. P., Kumar, A., Martinez-Becerra, F. J., and Hardwidge, P. R. (2016). Immunization with the MipA, skp, or ETEC_2479 antigens confers protection against enterotoxigenic e. Coli strains expressing different colonization factors in a mouse pulmonary challenge model. *Front. Cell. Infect. Microbiol.* 6:181. doi: 10.3389/fcimb.2016.00181

Huang, X., Li, Y., Fu, Y., Ji, Y., Lian, K., Zheng, H., et al. (2013). Cross-protective efficacy of recombinant transferrin-binding protein a of haemophilus parasuis in guinea pigs. *Clin. Vaccine Immunol.* 20, 912–919. doi: 10.1128/CVI.00621-12

Kak, G., Raza, M., and Tiwari, B. K. (2018). Interferon-gamma (IFN-gamma): Exploring its implications in infectious diseases. *Biomol. Concepts* 9, 64–79. doi: 10.1515/bmc-2018-0007

Lee, K. K., Chiang, H. T., Yii, K. C., Su, W. M., and Liu, P. C. (1997). Effects of extracellular products of vibrio vulnificus on acanthopagrus schlegeli serum components in vitro and in vivo. *Microbios* 92, 209–217.

Liao, C., Huang, C., Hsuan, S., Chen, Z., Lee, W., Liu, C., et al. (2006). Immunogenicity and efficacy of three recombinant subunit pasteurella multocida

toxin vaccines against progressive atrophic rhinitis in pigs. *Vaccine* 24, 27–35. doi: 10.1016/j.vaccine.2005.07.079

Lin, Y., Liao, Y., Huang, R., Li, A., An, S., Tang, J., et al. (2021). Extracellular amylase is required for full virulence and regulated by the global posttranscriptional regulator RsmA in xanthomonas campestris pathovar campestris. *Phytopathology* 111, 1104–1113. doi: 10.1094/PHYTO-08-20-0372-R

MacKinnon, B., Groman, D., Fast, M. D., Manning, A. J., Jones, P., and St-Hilaire, S. (2019). Atlantic salmon challenged with extracellular products from moritella viscosa. *Dis. Aquat. Org.* 133, 119–125. doi: 10.3354/dao03337

Marion, C. L., Rappleye, C. A., Engle, J. T., and Goldman, W. E. (2006). An alpha-(1,4)-amylase is essential for alpha-(1,3)-glucan production and virulence in histoplasma capsulatum. *Mol. Microbiol.* 62, 970–983. doi: 10.1111/j.1365-2958.2006.05436.x

Megroz, M., Kleifeld, O., Wright, A., Powell, D., Harrison, P., Adler, B., et al. (2016). The RNA-binding chaperone hfq is an important global regulator of gene expression in pasteurella multocida and plays a crucial role in production of a number of virulence factors, including hyaluronic acid capsule. *Infect. Immun.* 84, 1361–1370. doi: 10.1128/IAI.00122-16

Mostaan, S., Ghasemzadeh, A., Sardari, S., Shokrgozar, M. A., Nikbakht Brujeni, G., Abolhassani, M., et al. (2020). Pasteurella multocida vaccine candidates: A systematic review. *Avicenna J. Med. Biotechnol.* 12, 140–147.

Mou, Z., Barazandeh, A. F., Hamana, H., Kishi, H., Zhang, X., Jia, P., et al. (2020). Identification of a protective leishmania antigen dihydrolipoyl dehydrogenase and its responding CD4(+) t cells at clonal level. *J. Immunol.* 205, 1355–1364. doi: 10.4049/jimmunol.2000338

Moustafa, D. A., Lou, E., Schafer-Kestenman, M. E., Mateu-Borras, M., Domenech-Sanchez, A., Alberti, S., et al. (2024). *Pseudomonas aeruginosa* elongation factor-tu (EF-tu) is an immunogenic protective protein antigen. *Vaccine* 42:126476. doi: 10.1016/j.vaccine.2024.126476

Nagai, K., Domon, H., Maekawa, T., Hiyoshi, T., Tamura, H., Yonezawa, D., et al. (2019). Immunization with pneumococcal elongation factor tu enhances serotype-independent protection against streptococcus pneumoniae infection. *Vaccine* 37, 160–168. doi: 10.1016/j.vaccine.2018.11.015

Nguyen, Q. H., Lai, C. H. R., Norris, M. J., Ng, D., Shah, M., Lai, C. C., et al. (2025). A surface lipoprotein on pasteurella multocida binds complement factor i to promote immune evasion. *PLoS Pathog.* 21:e1012686. doi: 10.1371/journal.ppat.1012686

Nguyen, T. H., Maltby, S., Simpson, J. L., Eyers, F., Baines, K. J., Gibson, P. G., et al. (2016). TNF-alpha and macrophages are critical for respiratory syncytial virus-induced exacerbations in a mouse model of allergic airways disease. *J. Immunol.* 196, 3547–3558. doi: 10.4049/jimmunol.1502339

Okay, S., Ozcengiz, E., Gursel, I., and Ozcengiz, G. (2012). Immunogenicity and protective efficacy of the recombinant pasteurella lipoprotein e and outer membrane protein h from pasteurella multocida a:3 in mice. *Res. Vet. Sci.* 93, 1261–1265. doi: 10.1016/j.rvsc.2012.05.011

Pemberton, J. M., Kidd, S. P., and Schmidt, R. (1997). Secreted enzymes of aeromonas. *FEMS Microbiol. Lett.* 152, 1–10. doi: 10.1111/j.1574-6968.1997.tb10401.x

Peng, Z., Liang, W., Liu, W., Wu, B., Tang, B., Tan, C., et al. (2016). Genomic characterization of pasteurella multocida HB01, a serotype a bovine isolate from china. *Gene* 581, 85–93. doi: 10.1016/j.gene.2016.01.041

Pettit, R. K., Rimler, R. B., and Ackermann, M. R. (1993). Protection of pasteurella multocida dermonecrotic toxin-challenged rats by toxoid-induced antibody. *Vet. Microbiol.* 34, 167–173. doi: 10.1016/0378-1135(93)90170-c

Piorunek, M., Brajer-Luftmann, B., and Walkowiak, J. (2023). Pasteurella multocida infection in humans. *Pathogens* 12:1210. doi: 10.3390/pathogens12101210

Ryan, J. M., and Feder, H. M. J. (2019). Dog licks baby. Baby gets pasteurella multocida meningitis. *Lancet* 393:e41. doi: 10.1016/S0140-6736(19)30953-5

Sahu, I., Das, B. K., Marhual, N., Samanta, M., Mishra, B. K., and Eknath, A. E. (2011). Toxicity of crude extracellular products of aeromonas hydrophila on rohu, labeo rohita (ham.). *Indian J. Microbiol.* 51, 515–520. doi: 10.1007/s12088-011-0182-6

Santos, Y., Pazos, F., Bandin, I., and Toranzo, A. E. (1995). Analysis of antigens present in the extracellular products and cell surface of vibrio anguillarum serotypes o1, o2, and o3. *Appl. Environ. Microbiol.* 61, 2493–2498. doi: 10.1128/aem.61.7.2493-2498.1995

Schadich, E., and Cole, A. L. J. (2009). Inhibition of frog antimicrobial peptides by extracellular products of the bacterial pathogen aeromonas hydrophila. *Lett. Appl. Microbiol.* 49, 384–387. doi: 10.1111/j.1472-765x.2009.02677.x

Shivachandra, S. B., Yogisharadhya, R., Kumar, A., Mohanty, N. N., and Nagaleekar, V. K. (2015). Recombinant transferrin binding protein a (rTbpA) fragments of pasteurella multocida serogroup b:2 provide variable protection following homologous challenge in mouse model. *Res. Vet. Sci.* 98, 1–6. doi: 10.1016/j.rvsc.2014.11.013

Song, M., Kang, Y., Zhang, D., Chen, L., Bi, J., Zhang, H., et al. (2018). Immunogenicity of extracellular products from an inactivated vaccine against aeromonas veronii TH0426 in koi, cyprinus carpio. *Fish Shellfish Immunol.* 81, 176–181. doi: 10.1016/j.fsi.2018.07.004

Sun, Q., Yu, X., He, D., Ku, X., Hong, B., Zeng, W., et al. (2022). Investigation and analysis of etiology associated with porcine respiratory disease complex in china from 2017 to 2021. *Front. Vet. Sci.* 9:960033. doi: 10.3389/fvets.2022.960033

Thofte, O., Su, Y., Brant, M., Littorin, N., Duell, B. L., Alvarado, V., et al. (2018). EF-tu from non-typeable *haemophilus influenzae* is an immunogenic surface-exposed protein targeted by bactericidal antibodies. *Front. Immunol.* 9:2910. doi: 10.3389/fimmu.2018.02910

Varshney, R., Varshney, R., Chaturvedi, V. K., Rawat, M., Saminathan, M., Singh, V., et al. (2020). Development of novel iron-regulated pasteurella multocida b: 2 bacterin and refinement of vaccine quality in terms of minimum variation in particle size and distribution vis-a-vis critical level of iron in media. *Microb. Pathog.* 147:104375. doi: 10.1016/j.micpath.2020.104375

Weber, A., Wasiliew, P., and Kracht, M. (2010). Interleukin-1beta (IL-1beta) processing pathway. *Sci. Signal.* 3:cm2. doi: 10.1126/scisignal.3105cm2

West, D., Reddin, K., Matheson, M., Heath, R., Funnell, S., Hudson, M., et al. (2001). Recombinant *neisseria meningitidis* transferrin binding protein a protects against experimental meningococcal infection. *Infect. Immun.* 69, 1561–1567. doi: 10.1128/IAI.69.3.1561-1567.2001

Wilkie, I. W., Harper, M., Boyce, J. D., and Adler, B. (2012). Pasteurella multocida: Diseases and pathogenesis. *Curr. Top. Microbiol. Immunol.* 361, 1–22. doi: 10.1007/82_2012_216

Xiang, X., Sun, Y., Zhang, H., Wu, X., Xia, J., Han, X., et al. (2025). Evaluation of immunoprotective effects of PlpE multi-epitope protein incorporated within the aluminum hydroxide-adjuvanted inactivated vaccine against pasteurella multocida infection in chickens. *Poult. Sci.* 104:105426. doi: 10.1016/j.psj.2025.105426

Yuan, Z., Song, H., Huang, Q., Liu, J., Sun, H., Meng, X., et al. (2022). Immune enhancement effects of inactivated vaccine against extracellular products of aeromonas caviae AC-CY on crucian carp. *Fish Shellfish Immunol.* 127, 1001–1011. doi: 10.1016/j.fsi.2022.07.046

Zhan, L., Zhang, J., Zhao, B., Li, X., Zhang, X., Hu, R., et al. (2021). Genomic and transcriptomic analysis of bovine pasteurella multocida serogroup a strain reveals insights into virulence attenuation. *Front. Vet. Sci.* 8:765495. doi: 10.3389/fvets.2021.765495

Zhang, D., Pridgeon, J. W., and Klesius, P. H. (2014). Vaccination of channel catfish with extracellular products of aeromonas hydrophila provides protection against infection by the pathogen. *Fish Shellfish Immunol.* 36, 270–275. doi: 10.1016/j.fsi.2013.11.015

Zhang, X., Song, Y., Li, Y., Cai, M., Meng, Y., and Zhu, H. (2017). Immunization with streptococcal heme binding protein (shp) protects mice against group a streptococcus infection. *Adv. Exp. Med. Biol.* 973, 115–124. doi: 10.1007/5584_2016_198

Zhao, G., Tang, Y., Liu, X., Li, P., Zhang, T., Li, N., et al. (2024). Pasteurella multocida activates rassf1-hippo-yap pathway to induce pulmonary epithelial apoptosis. *Vet. Res.* 55:31. doi: 10.1186/s13567-024-01285-y

Zhao, X., Yang, F., Shen, H., Liao, Y., Zhu, D., Wang, M., et al. (2022). Immunogenicity and protection of a pasteurella multocida strain with a truncated lipopolysaccharide outer core in ducks. *Vet. Res.* 53:17. doi: 10.1186/s13567-022-01035-y

Zhao, Y., Liu, Y., Li, N., Muhammad, M., Gong, S., Ju, J., et al. (2022). Significance of broad-spectrum racemases for the viability and pathogenicity of aeromonas hydrophila. *Future Microbiol.* 17, 251–265. doi: 10.2217/fmb-2021-0112

frontiers | Frontiers in Microbiology

TYPE Original Research
PUBLISHED 17 October 2025
DOI 10.3389/fmicb.2025.1681308

OPEN ACCESS

EDITED BY
Axel Cloeckaert,
Institut National de recherche pour l'agriculture, l'alimentation et l'environnement (INRAE), France

REVIEWED BY
Wentong Cai,
Chinese Academy of Agricultural Sciences, China
Kushal Grakh,
Lala Lajpat Rai University of Veterinary and Animal Sciences, India
Xutong Xue,
Boston Children's Hospital and Harvard Medical School, United States

*CORRESPONDENCE
Shaohui Wang
✉ shwang0827@126.com

RECEIVED 07 August 2025
ACCEPTED 25 September 2025
PUBLISHED 17 October 2025

CITATION
Wang X, Guo W, Hu J, Zhang B, Qi J, Tian M, Bao Y, Deng L and Wang S (2025) The deubiquitinase ElaD is present in the majority of *Escherichia coli* strains.
Front. Microbiol. 16:1681308.
doi: 10.3389/fmicb.2025.1681308

The deubiquitinase ElaD is present in the majority of *Escherichia coli* strains

Xinyu Wang, Weiqi Guo, Jiangang Hu, Beibei Zhang, Jingjing Qi, Mingxing Tian, Yanqing Bao, Lei Deng and Shaohui Wang*

Shanghai Veterinary Research Institute, Chinese Academy of Agricultural Sciences (CAAS), Shanghai, China

Background: Pathogens employ a variety of effectors to modulate key host signaling pathways, thereby facilitating bacterial survival and enhancing pathogenicity. Despite lacking a complete ubiquitin system of their own, bacterial effectors frequently function as ubiquitin ligases or deubiquitinases (DUBs) to disrupt the eukaryotic ubiquitin machinery. DUBs have been found in a variety of bacteria, including ElaD, which has recently been recognized as a DUB in *Escherichia coli* (*E. coli*). However, the distribution and evolutionary analyses of ElaD in different *E. coli* remains largely unknown.
Methods: We retrieved and analyzed the *elaD* gene sequences of 530 *E. coli* strains. Then, molecular characterization of each strain was determined. According to all the statistical information, the distribution of *elaD* gene in *E. coli* was comprehensively investigated, and the relationship between *elaD* and *E. coli* pathotypes, serotypes, phylogenetic groups and MLSTs was analyzed. Phylogenetic tree was also constructed to analyze the evolutionary relationships between different ElaD.
Results: Our findings demonstrate that the *elaD* gene was present in 66.60% (353/530) of both pathogenic and nonpathogenic *E. coli* strains. *elaD* gene is predominantly found in the O157, O26, O139 and O8 serotypes. The majority of *elaD*-positive strains belonged to phylogenetic groups B1, A, E and D, with the predominant sequence types being ST11, ST21, ST10, ST1 and ST69. ElaD from different strains clustered in the phylogenetic tree in a correlation with O serotypes and phylogenetic groups. In addition, ElaD of some branches showed premature translation termination.
Conclusion: The widespread occurrence of the *elaD* gene among various *E. coli* strains suggests its potential significance in *E. coli*, although its precise functional role remains to be elucidated.

KEYWORDS

***Escherichia coli*, deubiquitinase, ElaD, distribution, pathotype**

Introduction

Pathogenic *Escherichia coli* (*E. coli*) capable of causing severe diseases from gastroenteritis to extraintestinal infections according to the acquisition of a mixture of comprehensive mobile genetic elements, which encode virulence factors (Frost et al., 2005; Pakbin et al., 2021). According to the different pathogenesis and lesion location, it can be divided into intestinal pathogenic *E. coli* (IPEC) and extraintestinal pathogenic *E. coli* (ExPEC) (Russo and Johnson,

2003). Among them, IPEC includes enteropathogenic *E. coli* (EPEC), Shiga toxin-producing *E. coli* (STEC), enterohaemorrhagic *E. coli* (EHEC), enterotoxigenic *E. coli* (ETEC), enteroinvasive *E. coli* (EIEC), enteroaggregative *E. coli* (EAEC), diffusely adherent *E. coli* (DAEC), as well as a new pathotype, adherent invasive *E. coli* (AIEC), which mainly causes diarrhea and intestinal diseases; newborn meningitis *E. coli* (NMEC), uropathogenic *E. coli* (UPEC), avian pathogenic *E. coli* (APEC), which can cause human urinary tract infections, neonatal meningitis, avian respiratory tract or systemic infections, are considered ExPEC (Sora et al., 2021). *E. coli* are also characterized by the serotype, phylogenetic group and MLST (multilocus sequence typing) to which they belong (Riley, 2020). Some pathogenic *E. coli* infecting humans can cause serious morbidity and mortality worldwide (Clements et al., 2012). Animal pathogenic *E. coli* (such as APEC), in addition to bringing huge economic losses to farms, may also be transmitted to humans through feces, drinking water or undercooked meat, posing a potential health threat, which has a tremendous burden on public health (Hu et al., 2022; Tapader et al., 2019).

The binding of ubiquitin molecules to eukaryotic proteins helps to regulate post-translational modifications, thus influencing and participating in the majority of cellular processes such as cell cycle, apoptosis and cell signal transduction (Kerscher et al., 2006; Song and Luo, 2019). Ubiquitination is a strictly regulated and reversible process (Liu et al., 2005). On the one hand, ubiquitin-activating enzyme, ubiquitin-conjugating enzyme and ubiquitin ligase catalyze a sophisticated three-step enzymatic cascade to add one ubiquitin (Ub) or a chain of Ubs to the substrate, which helps to complete the process of post-translational modification of proteins; on the other hand, deubiquitinases (DUBs) can remove Ub from the substrate proteins (Di Gregorio et al., 2023; Fang et al., 2023; Wolberger, 2014). DUBs are involved in counterbalancing and proofreading ubiquitin processes, as well as recycling ubiquitins (Snyder and Silva, 2021). The dynamic balance between DUBs and ubiquitin ligases is essential for many aspects of cellular processes (Komander et al., 2009; Li et al., 2023).

Increasing studies highlight bacterial pathogens also encode effectors with DUB activity (Sheedlo et al., 2015). These bacterial DUBs subvert the immune response by targeting the host's ubiquitin system, thereby contributing to bacterial survival in host cells and enhancing bacterial pathogenicity (Pruneda et al., 2016; Qiu and Luo, 2017). For example, the *Salmonella* T3SS effector SseL represents the first reported bacterial DUB within the CE family. It exhibits the ability to hydrolyze both K48- and K63-linked polyubiquitin chains. Studies have demonstrated that SseL enhances *Salmonella* intracellular survival by suppressing the NF-κB signaling pathway and inflammatory responses, cleaving polyubiquitin chains on the *Salmonella*-containing vacuole (SCV) to inhibit autophagy, and reducing host cell cytotoxicity (Geng et al., 2019; Mesquita et al., 2012; Rytkönen et al., 2007). Similarly, *Chlamydia trachomatis* effectors ChlaDUB1 and ChlaDUB2 both possess DUB activity. Beyond deubiquitinating IκBα to inhibit NF-κB activation, ChlaDUBs also stabilize the anti-apoptotic protein Mcl-1, thereby modulating host cell apoptosis (Fischer et al., 2017). *Chlamydia pneumoniae* encodes an OTU-family DUB, ChlaOTU, which reduces polyubiquitin accumulation by binding to the autophagy receptor NDP52 (Fischer et al., 2017; Schubert et al., 2020). Furthermore, the *Legionella pneumophila* effector RavD specifically cleaves M1-linked linear ubiquitin chains on the *Legionella*-containing vacuole (LCV) within infected macrophages. This process attenuates NF-κB-mediated inflammatory signaling and promotes intracellular bacterial survival (Wan et al., 2019). However, it is predicted that *E. coli* also has a DUB called ElaD. Genome comparison results showed that ElaD is only present in all IPEC, but its function is unknown (Catic et al., 2007).

Here, we comprehensively describe the distribution of *elaD* in *E. coli*, and then connect *elaD* with the pathotypes, serotypes, phylogenetic groups and MLSTs of *E. coli*. We analyze the genetic and evolutionary relationships of ElaD in different *E. coli* strains, and elucidate the importance of ElaD in *E. coli* from the perspective of genomic analysis. Our findings provide insight into the distribution of ElaD and the basis for further research.

Materials and methods

Sequence information of *Escherichia coli* strains

The whole-genome of all *E. coli* strains were accessed from the database of the National Center for Biotechnology Information,[1] from which 522 strains with known pathotypes were selected. Beside 522 strains from NCBI, we included 8 *E. coli* strains from different clinical tissue samples collected in our laboratory. These 530 strains were subjected to genome download or whole genome sequencing for bioinformatics analysis.

Determination of *elaD* distribution by bioinformatics analysis

The complete genome sequences of 530 *E. coli* strains were used to create a local BLAST database, and the distribution rate of *elaD* in the genomes of the 530 strains was investigated by running BLAST. The gene was described as present if the result match three parameters simultaneously: identity>92%, query cover>90%, and E-value = 0.

Analyses of pathotypes, serotypes, phylogenetic groups and MLSTs of *Escherichia coli* strains

To further elucidate the relationship between *elaD* distribution and *E. coli* pathotypes, serotypes, phylogenetic groups and MLSTs, each *E. coli* was determined: pathotypes were identified during the download of the *E. coli* whole-genome file by searching literatures and NCBI website details; serotypes were identified by comparison with EcOH database (Ingle et al., 2017) using ABRicate v.0.8;[2] phylogenetic groups were interfered using the Clermon Typing method in silico (Beghain et al., 2018) and sequence typing (ST) was performed with the MLST scheme of Achtman (Jolley and Maiden, 2010) using mlst v.2.11 software.[3]

1 https://www.ncbi.nlm.nih.gov
2 https://github.com/tseemann/abricate
3 https://github.com/tseemann/mlst

Phylogenomic analysis of ElaD

Based on the ElaD amino acid sequences of all 353 *E. coli* strains, phylogeny was used for sequence analysis. After using ClustalW to match sequences under default parameters, a phylogenetic tree was constructed using the neighbor-joining method with 1,000 bootstrap values in MEGA 11 software. Phylogenetic tree was annotated and visualized using the Interactive Tree of Life (iTOLs) tool. Pathotypes, serotypes, phylogenetic groups and MLSTs of *E. coli* to which ElaD belongs were displayed alongside the phylogenetic tree.

Statistical analysis

The chi-square test was used to identify differences in the prevalence of *elaD* gene of *E. coli* strains. All analyses were performed with SPSS version 16.

Results

Distribution of *elaD* genes in *Escherichia coli*

To examine the prevalence of the *elaD* sequence among *E. coli* strains, BLASTn was performed. The *elaD* gene was detected in 66.60% (353/530) of the *E. coli* strains. These *elaD* sequences shared >92% identity and were generally full length. Notably, further analysis of these *elaD* sequences revealed that 16.60% (88/530) of them matched the full-length reference gene, yet contained premature stop codons. These mutations prevent the translation of a full-length protein, suggesting that these variants are likely non-functional. Meanwhile, 2.26% (12/530) *elaD* sequences cannot encode full-length proteins but contain functionally relevant structural domains and could be considered functional. In addition, 33.40% (177/530) *E. coli* genomes did not match the *elaD* sequence at all (Figure 1). Therefore, ElaD is widely present in *E. coli* strains.

The prevalence of ElaD in various *Escherichia coli* pathotypes

In order to assign the *E. coli* strains to the different pathotypes, we summarized the details of all the strains (Table 1). As shown in Figure 2A, 13 pathotypes were identified among the 530 *E. coli* strains. 23.40% (124/530) of the strains were grouped as UPEC, 20.57% (109/530) as ETEC, 20.57% (109/530) as STEC, 11.51% (61/530) as APEC, 7.74% (41/530) as EHEC, 6.42% (34/530) as commensal *E. coli* and 4.72% (25/530) as NMEC; the remaining 27

TABLE 1 Distribution of the *elaD* gene in 530 *E. coli*.

Pathotypes	No. of strains	Total (*n* = 530)	
		No. of *elaD*-positive	No. of *elaD*-negative
IPEC	**281**	**260**	**21**
ETEC	109	103	6
STEC	109	101	8
EHEC	41	41	0
EAEC	8	8	0
EPEC	9	7	2
AIEC	4	0	4
DAEC	1	0	1
ExPEC	**215**	**76**	**139**
NMEC	25	4	21
UPEC	124	40	84
APEC	61	29	32
MPEC	3	2	1
Porcine ExPEC	2	1	1
Commensal *E. coli*	**34**	**17**	**17**
Total	**530**	**353**	**177**

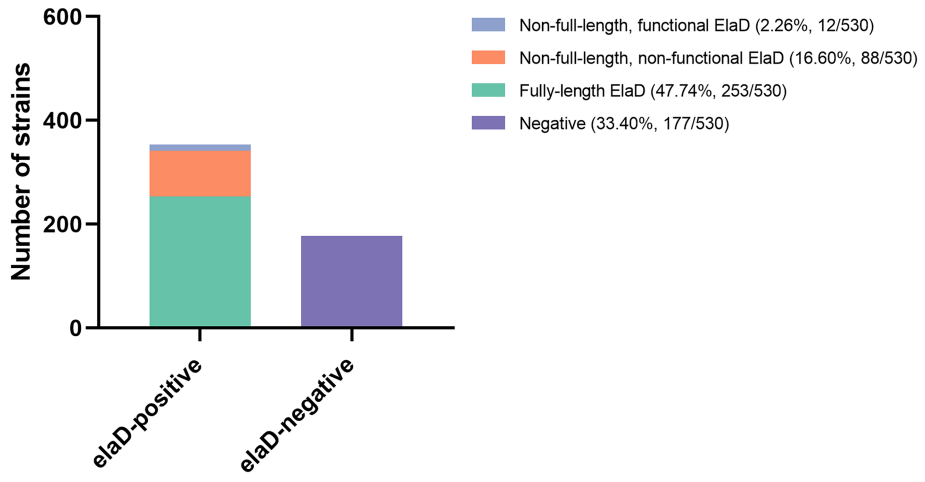

FIGURE 1
The distribution of *elaD* in *E. coli*. The distribution of the *elaD* gene in *E. coli* was confirmed using BLASTn, while the integrity of the protein encoded by the *elaD* gene was clarified by amino acid sequence analysis.

strains (5.09%), including EPEC, EAEC, AIEC, MPEC, porcine ExPEC and DAEC, accounted for only a small percentage. Next, we determined the pathotype in the *elaD*-positive *E. coli* strains. Correspondingly, of the 353 *E. coli* strains positive for *elaD*, 29.18% (103/353) were ETEC, 28.61% (101/353) STEC, 11.61% (41/353) EHEC, 11.33% (40/353) UPEC, 8.22% (29/353) APEC, 4.82% (17/353) commensal *E. coli* and 6.23% others (Figure 2B).

However, the *elaD* was present in most of the STEC (92.66%, 101/109), ETEC (94.50%, 103/109), EHEC (100.00%, 41/41), EAEC (100.00%, 8/8) and EPEC (77.78%, 7/9). A feature clearly distinguishing ExPEC from IPEC was the lower occurrence of *elaD*, which was detected in only 66.67% of MPEC (2/3), 50.00% of porcine ExPEC (1/2), 32.26% of UPEC (40/124), 47.54% of APEC (29/61) and 16.00% of NMEC (4/25). Further categorical statistics have also confirmed this viewpoint, which is that *elaD* is distributed in 92.53% (260/281) of IPEC, but only exists in 35.35% (76/215) of ExPEC. The prevalence of *elaD* in IPEC strains was significantly higher than ExPEC (92.53% vs. 35.35%, p: <0.0001). But the gene was completely absent in AIEC and DAEC strains. It even presents in the 50.00% (17/34) commensal *E. coli*, which refers to harmless members of the normal intestinal bacterial microflora in humans and animals (Figure 2C).

The prevalence of ElaD in various O serotypes

To compare the prevalence of *elaD* in various O serotypes, 530 strains were characterized using ABRicate v.0.8 software. Of these, 123 O serotypes were successfully identified, with Onovel31 (7.55%, 40/530) being the most prevalent one, followed by O157 (6.98%, 37/530), O2 (5.85%, 31/530), O6 (4.72%, 25/530), O78 (3.02%, 16/530), O1 (2.83%, 15/530), O75 (2.83%, 15/530), O139 (2.64%, 14/530), O18 (2.64%, 14/530), O26 (2.26%, 12/530), O8 (2.26%, 12/530), O111 (2.08%, 11/530) and O25 (2.08%, 11/530), while 52.26% were distributed among an additional 110 O-types (Figure 3A). elaD gene is found in the O157 (10.48%, 37/353), O139

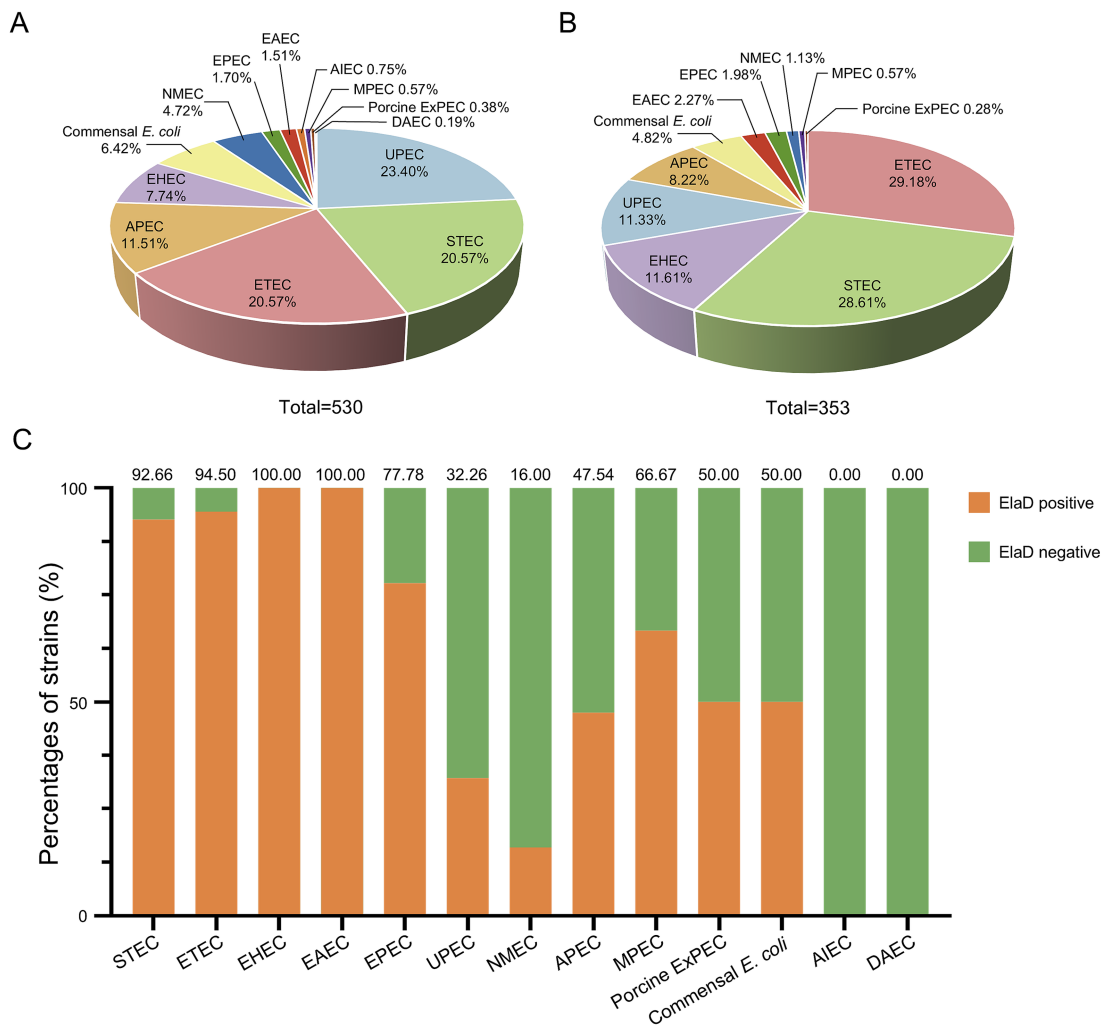

FIGURE 2
The prevalence of *elaD* in various pathotypes of *E. coli*. **(A)** The distribution of different pathotypes of all 530 *E. coli*. **(B)** The distribution of different pathotypes of 353 *elaD*-positive *E. coli* strains. **(C)** The *elaD* positivity for individual pathotypes in *elaD*-positive *E. coli* strains. The orange color represents the positive rate of *elaD* gene, while the green represents the negative rate.

(3.97%, 14/353), O26 (3.40%, 12/353), O8 (3.40%, 12/353), O78 (2.83%, 10/353), O111 (2.83%, 10/353), O104 (2.55%, 9/353), O103 (2.27%, 8/353), O115 (1.98%, 7/353), O9 (1.98%, 7/353), O113 (1.98%, 7/353), O148 (1.98%, 7/353) and strains from the other 111 O-types (Figure 3B).

The distribution of *elaD* genes for each O serotype strains are shown in Figure 3C. The *elaD* positivity rate was 100.00% across all 89 O serotypes (including O8, O9, O26, O103, O104, O113, O115, O139, O148 and O157). However, *elaD* was rarely present in all Onovel31, O75 and O18 serotype strains detected. These results suggest that there is a correlation between *E. coli elaD* and O serotypes, especially the O157, O139 and O26 serotypes.

The prevalence of ElaD in various phylogenetic groups

The distribution of the 530 collected *E. coli* strains among the phylogenetic groups was determined using the Clermon Typing method and is shown in Figure 4A. Most of the strains could be categorized into groups B1 (31.13%, 165/530) and B2 (28.87%, 153/530), while other strains belonged to groups A (14.91%, 79/530), E (9.06%, 48/530), D (7.17%, 38/530), C (3.40%, 18/530), G (2.64%, 14/530) and F (2.26%, 12/530). 3 strains (0.57%) were not assigned to any group. A comparison of the distribution of the phylogenetic groups among *elaD*-positive *E. coli* revealed that 46.74% (165/353), 20.40% (72/353), 13.60% (48/353), 10.48% (38/353), 4.82% (17/353) and 3.40% (12/353) of the *elaD*-positive strains were assigned to groups B1, A, E, D, C and F, respectively (Figure 4B).

The analyses showed a clear correlation between the distribution of the *elaD* gene in *E. coli* and the phylogenetic group. The *elaD* gene was found in all B1, E and F examined in our *E. coli* database. Notably, our results showed that *elaD* was found in none of the groups B2 and G. In addition, *elaD* gene was present in more than 90% of the A, C and D *E. coli* (Figure 4C).

The prevalence of ElaD and association of MLST

The conventional seven-gene MLST analysis revealed that the strains were relatively diverse with a total of 174 STs in the 530

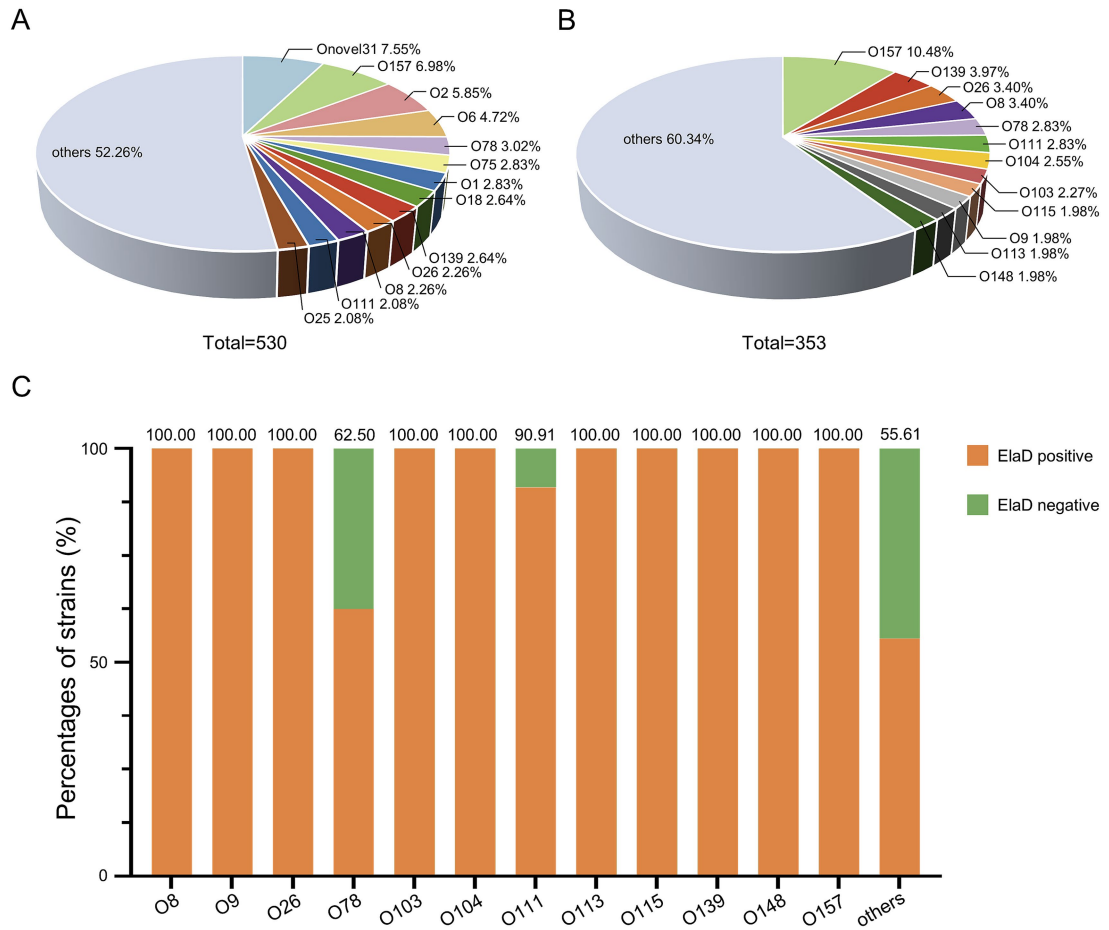

FIGURE 3
The prevalence of *elaD* in various O serotypes of *E. coli*. **(A)** The distribution of different O serotype of all 530 *E. coli*. **(B)** The distribution of different O serotype of 353 *elaD*-positive *E. coli* strains. **(C)** The *elaD* positivity for individual O serotype in *elaD*-positive *E. coli* strains. The orange color represents the positive rate of *elaD* gene, while the green represents the negative rate.

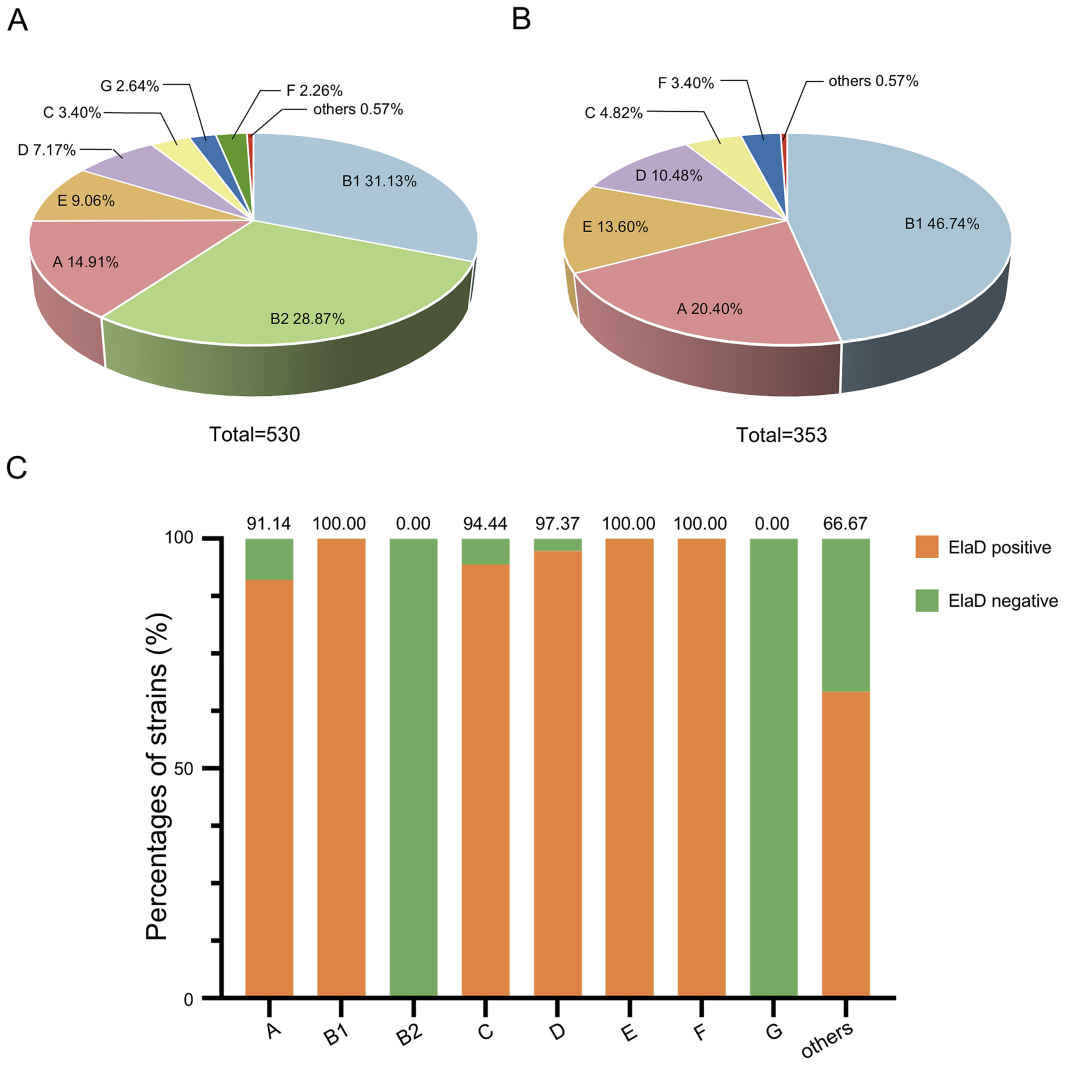

FIGURE 4
The prevalence of *elaD* in various phylogenetic groups of *E. coli*. **(A)** The distribution of different phylogenetic group of all 530 *E. coli*. **(B)** The distribution of different phylogenetic group of 353 *elaD*-positive *E. coli* strains. **(C)** The *elaD* positivity for individual phylogenetic group in *elaD*-positive *E. coli* strains. The orange color represents the positive rate of *elaD* gene, while the green represents the negative rate.

E. coli strains, among which ST131 comprised 7.74% (41/530) of the strains in this study, followed by ST95 (6.60%, 35/530), ST11 (6.60%, 35/530), ST10 (3.40%, 18/530), ST21 (2.64%, 14/530), ST1193 (2.64%, 14/530), ST1 (2.26%, 12/530), ST69 (2.08%, 11/530) and ST73 (1.89%, 10/530), while 64.15% were distributed among an additional 165 STs (Figure 5A). In contrast, the distribution of STs of 353 *elaD*-positive *E. coli* strains was 9.92% ST11 (35/353), 4.53% ST10 (18/353), 3.97% ST21 (14/353), 3.40% ST1 (12/353), 3.12% ST69 (11/353), 1.98% ST678 (7/353), 1.98% ST443 (7/353), 1.98% ST223 (7/353), 1.98% ST17 (7/353), 1.98% ST16 (7/353) and 65.16% others, which are almost the same STs mentioned earlier to predominate among 530 *E. coli* strains (Figure 5B).

The *elaD* gene was present in all tested strains of ST1, ST11, ST21, ST69, ST443 and ST678 (including most of the other STs identified), demonstrating a strong association between *elaD* and *E. coli* MLST. Surprisingly, ST73, ST95, ST127, ST131 and ST1193 *E. coli* appear to completely lack the *elaD* gene (Figure 5C).

Phylogenetic analysis of the ElaD of *Escherichia coli*

To further elucidate the distribution of the *elaD* in *E. coli*, we constructed a phylogenetic tree using the ElaD amino acid sequence of 353 strains. The pathotypes, serotypes, phylogenetic groups and MLSTs of the 353 strains were presented along with the phylogenetic tree and displayed with distinguishable colors and stripes.

The ElaD amino acid sequences of 353 strains were extensively distributed across the phylogenetic tree, of which 53 and 22 ElaD showed premature translation termination and were clustered in two regions, respectively. This phenomenon suggested that the *elaD* gene may have mutated during evolution leading to premature termination of translation. However, the remaining 13 ElaD proteins with premature translation termination were scattered in other clades. There were no major clusters of STs on the tree, except for ST11. Likewise, overlaying information on the pathotype from which these *E. coli* strains were derived revealed

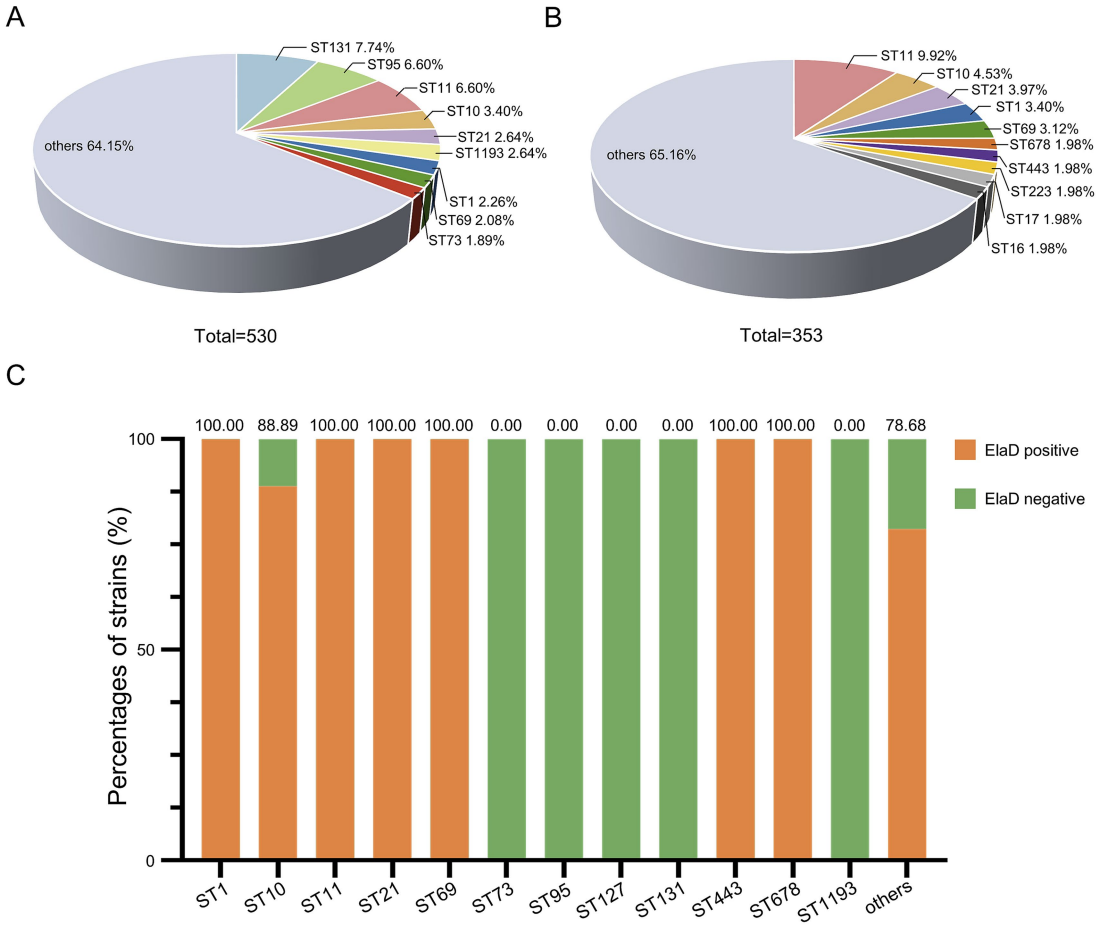

FIGURE 5
The prevalence of *elaD* in various MLSTs of *E. coli*. **(A)** The distribution of different MLSTs of all 530 *E. coli*. **(B)** The distribution of different MLSTs of 353 *elaD*-positive *E. coli* strains. **(C)** The *elaD* positivity for individual MLSTs in *elaD*-positive *E. coli* strains. The orange color represents the positive rate of *elaD* gene, while the green represents the negative rate.

no clear relevance between placement within the phylogeny and bacterial pathotype. The O antigens, such as O157, O148, O111 and O139, corresponded with the phylogenomic results to a certain extent, however, other O antigens are interspersed in the tree. Furthermore, by analyzing the correlation between the bacterial phylogenetic group and the ElaD, we found that the ElaD from the same phylogenetic group are generally on the same clade, such as A, B1 and E (Figure 6).

Discussion

Pathogenic *E. coli* can cause a wide range of diseases, from gastroenteritis and diarrhea to extraintestinal infections, threatening worldwide human health and the development of the livestock farming (Croxen and Finlay, 2010). During infection, the secretion system can deliver effectors to host cells that interfere with specific cellular and host immune responses (Green and Mecsas, 2016). A number of bacterial pathogens have been shown to encode and deliver effectors with DUB activity, which promote bacterial survival and enhance pathogenicity by targeting and disrupting the host ubiquitination system. Recently, ElaD has been identified as a DUB in *E. coli*. However, the distribution and evolution of this gene in *E. coli* remains unknown.

This study showed that 66.60% of the 530 *E. coli* strains analyzed contained the *elaD* gene. Meanwhile, the detection rate of *elaD* exceeded 70% in all five collected IPEC pathotypes—namely EHEC, STEC, ETEC, EAEC and EPEC. These pathotypes of *E. coli* can cause acute and persistent diarrhea in children, adults and other mammals (calves, piglets, etc.), and in severe cases, lead to hemorrhagic colitis or lethal hemolytic uremic syndrome, which is a health hazard (Bai et al., 2016; Kolenda et al., 2015; Kolodziejek et al., 2022). IPEC primarily relies on intestinal adhesion, colonization and the modulation of inflammatory responses to promote bacterial survival and replication, which ultimately contribute to disease development (Jesser and Levy, 2020). This process relates to various adhesins, toxins and effectors. The type III secretion system (T3SS) or *E. coli* type III secretion system 2 (ETT2) has been identified in various IPEC, which can directly deliver effectors into host cells (Gaytán et al., 2016; Wang et al., 2024). Furthermore, previous studies have compared ElaD with deubiquitinases from other bacteria in terms of evolution, structure, and function. Phylogenetic analyses indicate that *E. coli* ElaD within

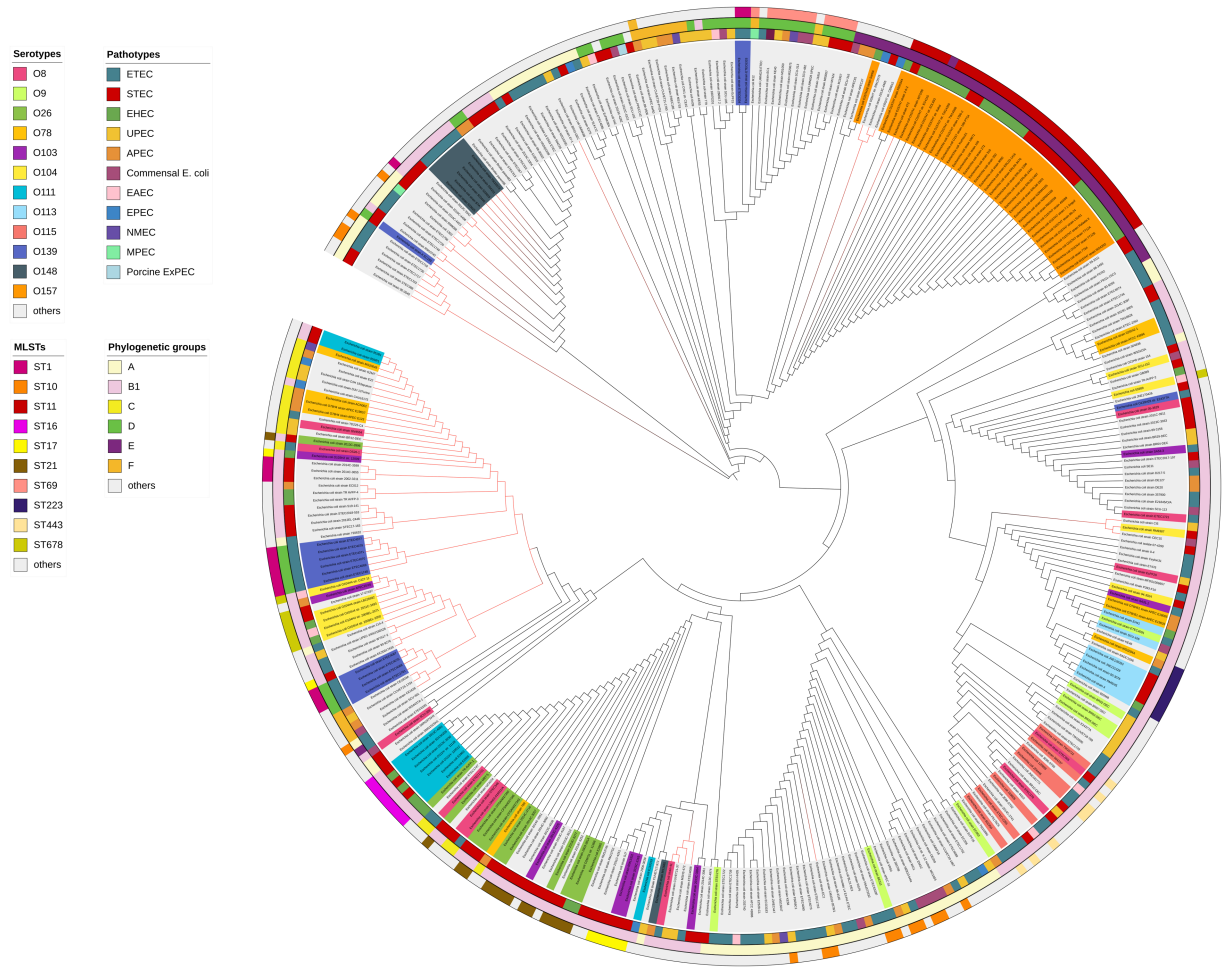

FIGURE 6
ElaD amino acid sequences based phylogenetic tree of 353 *E. coli* strains. The color range of the ring shows the names of the individual strains and their O serotypes. Then, the color strips from the innermost to the outermost represent the pathotypes, phylogenetic groups and MLSTs of *E. coli* strains, respectively. Diverse type is marked in different colors. In addition, the red branches represent the non-full-length amino acid sequence translated by the gene.

the same clade as *Legionella pneumophila* effector and *Salmonella Typhimurium* SseL, showing high sequence homology. It has been demonstrated that ElaD possesses deubiquitinating enzyme activity (Catic et al., 2007). Given that SseL has been confirmed as a T3SS effector that inhibit host inflammatory responses via its deubiquitination activity, we hypothesize that the high detection rate of *elaD* in IPEC might also indicate that the presence of *elaD* contributes to the infection process of IPEC.

A previous study showed that *elaD* was only present in commensal *E. coli* K12 and all IPEC in 16 sequenced *E. coli* strains. However, our results found that ExPEC also possessed *elaD* but its detection rate was relatively low, about 35.35%. In addition, *elaD* was also present in other commensal *E. coli*. The wide distribution of *elaD* in different pathogenic *E. coli* demonstrates its significance.

Our results revealed a high distribution of *elaD* among the O157, O139, O26, O8, O111 and O78 serotypes. These six serotypes are known to be closely associated with human and animal disease, with O157 considered to be the major serotype responsible for serious foodborne disease caused by STEC and EHEC infections worldwide, while the non-O157 serotypes, including O26 and O111, are equally important in causing outbreaks of intestinal infections (Mathusa et al., 2010; Wang et al., 2013). ETEC serotypes O8 and O139 are considered to be the main diarrheal pathogens affecting pigs below four weeks of age (Wyrsch et al., 2015). Meanwhile, O78 is the predominant serotype in APEC strains. The detection rate of the *elaD* gene was 100% for all 4 O serotypes, except for O111 (90.91%) and O78 (62.50%). The correlation between the distribution of *elaD* and bacterial serotypes also demonstrates the importance of ElaD.

A close relationship between phylogenetic group and virulence factors (VFs) of the pathogens was reported. EHEC, ETEC and STEC/EIEC and their specific VFs were found only in A, B1, C or E groups. In contrast, ExPEC strains and their VFs preferentially belonged to B2 and D group (Escobar-Páramo et al., 2004). Our study also demonstrated the relationship between the distribution of the *elaD* gene and the phylogenetic group of the pathogens. The positivity rates of *elaD* in *E. coli* was more than 90.00% in A, B1, C, D, E and F groups. Notably, in all B2 and G groups *E. coli* detected,

the *elaD* gene was absent. It further suggests the notion that the presence of the *elaD* gene on IPEC or ExPEC is correlated with its pathogenic potential.

Furthermore, the MLST results offer a crucial reference for our analysis. ST11 represents a lineage of *E. coli* that is primarily associated with the O157: H7 serotype (Pugh et al., 2023). Our findings revealed that the *elaD* gene was present in all examined ST11 *E. coli* strains, all of which belonged to the O157 serotype and the E group. This is also evidenced in the phylogenetic tree.

ST131, initially recognized for its association with the carriage of extended-spectrum β-lactamase genes, has emerged as the predominant ST among global ExPEC isolates, belonging to phylogenetic group B2 (Nicolas-Chanoine et al., 2014). Notably, the *elaD* gene was completely absent in all examined ST131 strains, which corresponds to a 100% *elaD* negativity rate within the B2 group. Likewise, ST95 strains belonging to phylogroup B2 do not carry the *elaD* gene (Xia et al., 2022). During the long-term evolution, *E. coli* genome exhibits frequent alterations by increased rates of homologous recombination or horizontal gene transfer (Mageiros et al., 2021). These genes stably gained or lost, contribute to the fitness of the group B2 strains (Touchon et al., 2009). Therefore, the absence of *elaD* in the B2 group ExPEC may reflect the loss of adaptive genes, which may be caused by environmental pressure or niche specialization. Besides, ExPEC strains usually translocate from the gut to colonization sites, evade the host's defense system (such as complement and phagocytosis) and establish persistent infection. ExPEC can even spread in bloodstream and cause fatal multisystemic infection (Biran et al., 2021). During this process, ExPEC employs various virulence factors, including adhesins, invasins, iron uptake factors, protectines, and toxins, which can cooperate and contribute to the pathogenic potential (Sora et al., 2021). Therefore, we hypothesize that the pathogenic process of these B2 group ExPEC may not primarily depend on ElaD. Further research is essential to comprehensively investigate the distribution and function of ElaD across *E. coli*.

In this study, *E. coli* strains showed a high prevalence of the *elaD* gene. Its presence correlating significantly with specific bacterial pathotypes, serotypes, phylogenetic groups, and MLSTs. Our results tentatively suggest that ElaD is strongly associated with bacterial pathogenicity, especially IPEC, but the specific regulatory mechanism by which the ElaD will act as a DUB has not yet been clarified. Further studies are still needed to evaluate the role of ElaD in the pathogenic *E. coli* to help us resolve the mechanism of *E. coli* infections and provide a reference for the prevention of *E. coli* disease and potential human and animal infections.

Data availability statement

The datasets presented in this study can be found in online repositories. The names of the repository/repositories and accession number(s) can be found in the article/Supplementary material.

Ethics statement

The manuscript presents research on bacteria isolation that does not require ethical approval.

Author contributions

XW: Data curation, Formal analysis, Investigation, Writing – original draft, Writing – review & editing. WG: Data curation, Software, Writing – review & editing. JH: Funding acquisition, Supervision, Writing – review & editing. BZ: Supervision, Writing – review & editing. JQ: Supervision, Writing – review & editing. MT: Supervision, Writing – review & editing. YB: Supervision, Writing – review & editing. LD: Supervision, Writing – review & editing. SW: Conceptualization, Funding acquisition, Project administration, Resources, Supervision, Writing – review & editing.

Funding

The author(s) declare that financial support was received for the research and/or publication of this article. This work was supported by the National Natural Science Foundation of China (32172856, 32302881), National Key Research and Development Program of China (2021YFD1800402), the Natural Science Foundation of Shanghai (22ZR1476100, 23ZR1476600), and the Agricultural Science and Technology Innovation Program (CAAS-ASTIP-2021-SHVRI-07).

Conflict of interest

The authors declare that the research was conducted in the absence of any commercial or financial relationships that could be construed as a potential conflict of interest.

Generative AI statement

The authors declare that no Gen AI was used in the creation of this manuscript.

Any alternative text (alt text) provided alongside figures in this article has been generated by Frontiers with the support of artificial intelligence and reasonable efforts have been made to ensure accuracy, including review by the authors wherever possible. If you identify any issues, please contact us.

Publisher's note

Supplementary material

The Supplementary material for this article can be found online at: https://www.frontiersin.org/articles/10.3389/fmicb.2025.1681308/full#supplementary-material

References

Bai, X., Hu, B., Xu, Y., Sun, H., Zhao, A., Ba, P., et al. (2016). Molecular and phylogenetic characterization of non-O157 Shiga toxin-producing *Escherichia coli* strains in China. *Front. Cell. Infect. Microbiol.* 6:143. doi: 10.3389/fcimb.2016.00143

Beghain, J., Bridier-Nahmias, A., Le Nagard, H., Denamur, E., and Clermont, O. (2018). ClermonTyping: an easy-to-use and accurate in silico method for *Escherichia* genus strain phylotyping. *Microb. Genom.* 4:e000192. doi: 10.1099/mgen.0.000192

Biran, D., Sura, T., Otto, A., Yair, Y., Becher, D., and Ron, E. Z. (2021). Surviving serum: the *Escherichia coli iss* gene of extraintestinal pathogenic *E. coli* is required for the synthesis of group 4 capsule. *Infect. Immun.* 89:e0031621. doi: 10.1128/iai.00316-21

Catic, A., Misaghi, S., Korbel, G. A., and Ploegh, H. L. (2007). ElaD, a deubiquitinating protease expressed by *E. coli*. *PLoS One* 2:e381. doi: 10.1371/journal.pone.0000381

Clements, A., Young, J. C., Constantinou, N., and Frankel, G. (2012). Infection strategies of enteric pathogenic *Escherichia coli*. *Gut Microbes* 3, 71–87. doi: 10.4161/gmic.19182

Croxen, M. A., and Finlay, B. B. (2010). Molecular mechanisms of *Escherichia coli* pathogenicity. *Nat. Rev. Microbiol.* 8, 26–38. doi: 10.1038/nrmicro2265

Di Gregorio, J., Appignani, M., and Flati, V. (2023). Role of the mitochondrial E3 ubiquitin ligases as possible therapeutic targets in cancer therapy. *Int. J. Mol. Sci.* 24:17176. doi: 10.3390/ijms242417176

Escobar-Páramo, P., Clermont, O., Blanc-Potard, A. B., Bui, H., Le Bouguénec, C., and Denamur, E. (2004). A specific genetic background is required for acquisition and expression of virulence factors in *Escherichia coli*. *Mol. Biol. Evol.* 21, 1085–1094. doi: 10.1093/molbev/msh118

Fang, Y. Z., Jiang, L., He, Q., Cao, J., and Yang, B. (2023). Deubiquitination complex platform: a plausible mechanism for regulating the substrate specificity of deubiquitinating enzymes. *Acta Pharm. Sin. B* 13, 2955–2962. doi: 10.1016/j.apsb.2023.02.019

Fischer, A., Harrison, K. S., Ramirez, Y., Auer, D., Chowdhury, S. R., Prusty, B. K., et al. (2017). *Chlamydia trachomatis*-containing vacuole serves as deubiquitination platform to stabilize Mcl-1 and to interfere with host defense. *eLife* 6:e21465. doi: 10.7554/eLife.21465

Frost, L. S., Leplae, R., Summers, A. O., and Toussaint, A. (2005). Mobile genetic elements: the agents of open source evolution. *Nat. Rev. Microbiol.* 3, 722–732. doi: 10.1038/nrmicro1235

Gaytán, M. O., Martínez-Santos, V. I., Soto, E., and González-Pedrajo, B. (2016). Type three secretion system in attaching and effacing pathogens. *Front. Cell. Infect. Microbiol.* 6:129. doi: 10.3389/fcimb.2016.00129

Geng, S., Wang, Y., Xue, Y., Wang, H., Cai, Y., Zhang, J., et al. (2019). The SseL protein inhibits the intracellular NF-κB pathway to enhance the virulence of *Salmonella pullorum* in a chicken model. *Microb. Pathog.* 129, 1–6. doi: 10.1016/j.micpath.2019.01.035

Green, E. R., and Mecsas, J. (2016). Bacterial secretion systems: an overview. *Microbiol. Spectr.* 4:19. doi: 10.1128/microbiolspec.VMBF-0012-2015

Hu, J., Afayibo, D. J. A., Zhang, B., Zhu, H., Yao, L., Guo, W., et al. (2022). Characteristics, pathogenic mechanism, zoonotic potential, drug resistance, and prevention of avian pathogenic *Escherichia coli* (APEC). *Front. Microbiol.* 13:1049391. doi: 10.3389/fmicb.2022.1049391

Ingle, D. J., Valcanis, M., Kuzevski, A., Tauschek, M., Inouye, M., Stinear, T., et al. (2017). Corrigendum: in silico serotyping of *E. coli* from short read data identifies limited novel O-loci but extensive diversity of O:H serotype combinations within and between pathogenic lineages. *Microb. Genom.* 3:e000109. doi: 10.1099/mgen.0.000109

Jesser, K. J., and Levy, K. (2020). Updates on defining and detecting diarrheagenic *Escherichia coli* pathotypes. *Curr. Opin. Infect. Dis.* 33, 372–380. doi: 10.1097/qco.0000000000000665

Jolley, K. A., and Maiden, M. C. (2010). BIGSdb: scalable analysis of bacterial genome variation at the population level. *BMC Bioinformatics* 11:595. doi: 10.1186/1471-2105-11-595

Kerscher, O., Felberbaum, R., and Hochstrasser, M. (2006). Modification of proteins by ubiquitin and ubiquitin-like proteins. *Annu. Rev. Cell Dev. Biol.* 22, 159–180. doi: 10.1146/annurev.cellbio.22.010605.093503

Kolenda, R., Burdukiewicz, M., and Schierack, P. (2015). A systematic review and meta-analysis of the epidemiology of pathogenic *Escherichia coli* of calves and the role of calves as reservoirs for human pathogenic *E. coli*. *Front. Cell. Infect. Microbiol.* 5:23. doi: 10.3389/fcimb.2015.00023

Kolodziejek, A. M., Minnich, S. A., and Hovde, C. J. (2022). *Escherichia coli* O157:H7 virulence factors and the ruminant reservoir. *Curr. Opin. Infect. Dis.* 35, 205–214. doi: 10.1097/qco.0000000000000834

Komander, D., Clague, M. J., and Urbé, S. (2009). Breaking the chains: structure and function of the deubiquitinases. *Nat. Rev. Mol. Cell Biol.* 10, 550–563. doi: 10.1038/nrm2731

Li, S., Song, Y., Wang, K., Liu, G., Dong, X., Yang, F., et al. (2023). USP32 deubiquitinase: cellular functions, regulatory mechanisms, and potential as a cancer therapy target. *Cell Death Discov.* 9:338. doi: 10.1038/s41420-023-01629-1

Liu, Y. C., Penninger, J., and Karin, M. (2005). Immunity by ubiquitylation: a reversible process of modification. *Nat. Rev. Immunol.* 5, 941–952. doi: 10.1038/nri1731

Mageiros, L., Méric, G., Bayliss, S. C., Pensar, J., Pascoe, B., Mourkas, E., et al. (2021). Genome evolution and the emergence of pathogenicity in avian *Escherichia coli*. *Nat. Commun.* 12:765. doi: 10.1038/s41467-021-20988-w

Mathusa, E. C., Chen, Y., Enache, E., and Hontz, L. (2010). Non-O157 Shiga toxin-producing *Escherichia coli* in foods. *J. Food Prot.* 73, 1721–1736. doi: 10.4315/0362-028x-73.9.1721

Mesquita, F. S., Thomas, M., Sachse, M., Santos, A. J., Figueira, R., and Holden, D. W. (2012). The *Salmonella* deubiquitinase SseL inhibits selective autophagy of cytosolic aggregates. *PLoS Pathog.* 8:e1002743. doi: 10.1371/journal.ppat.1002743

Nicolas-Chanoine, M. H., Bertrand, X., and Madec, J. Y. (2014). *Escherichia coli* ST131, an intriguing clonal group. *Clin. Microbiol. Rev.* 27, 543–574. doi: 10.1128/cmr.00125-13

Pakbin, B., Brück, W. M., and Rossen, J. W. A. (2021). Virulence factors of enteric pathogenic *Escherichia coli*: a review. *Int. J. Mol. Sci.* 22:9922. doi: 10.3390/ijms22189922

Pruneda, J. N., Durkin, C. H., Geurink, P. P., Ovaa, H., Santhanam, B., Holden, D. W., et al. (2016). The molecular basis for ubiquitin and ubiquitin-like specificities in bacterial effector proteases. *Mol. Cell* 63, 261–276. doi: 10.1016/j.molcel.2016.06.015

Pugh, H. L., Connor, C., Siasat, P., McNally, A., and Blair, J. M. A. (2023). *E. coli* ST11 (O157:H7) does not encode a functional AcrF efflux pump. *Microbiology* 169:001324. doi: 10.1099/mic.0.001324

Qiu, J., and Luo, Z. Q. (2017). Hijacking of the host ubiquitin network by *Legionella pneumophila*. *Front. Cell. Infect. Microbiol.* 7:487. doi: 10.3389/fcimb.2017.00487

Riley, L. W. (2020). Distinguishing pathovars from nonpathovars: *Escherichia coli*. *Microbiol. Spectr.* 8:10.1128. doi: 10.1128/microbiolspec.AME-0014-2020

Russo, T. A., and Johnson, J. R. (2003). Medical and economic impact of extraintestinal infections due to *Escherichia coli*: focus on an increasingly important endemic problem. *Microbes Infect.* 5, 449–456. doi: 10.1016/s1286-4579(03)00049-2

Rytkönen, A., Poh, J., Garmendia, J., Boyle, C., Thompson, A., Liu, M., et al. (2007). Ssel, a *Salmonella* deubiquitinase required for macrophage killing and virulence. *Proc. Natl. Acad. Sci. USA* 104, 3502–3507. doi: 10.1073/pnas.0610095104

Schubert, A. F., Nguyen, J. V., Franklin, T. G., Geurink, P. P., Roberts, C. G., Sanderson, D. J., et al. (2020). Identification and characterization of diverse OTU deubiquitinases in bacteria. *EMBO J.* 39:e105127. doi: 10.15252/embj.2020105127

Sheedlo, M. J., Qiu, J., Tan, Y., Paul, L. N., Luo, Z. Q., and Das, C. (2015). Structural basis of substrate recognition by a bacterial deubiquitinase important for dynamics of phagosome ubiquitination. *Proc. Natl. Acad. Sci. USA* 112, 15090–15095. doi: 10.1073/pnas.1514568112

Snyder, N. A., and Silva, G. M. (2021). Deubiquitinating enzymes (DUBs): regulation, homeostasis, and oxidative stress response. *J. Biol. Chem.* 297:101077. doi: 10.1016/j.jbc.2021.101077

Song, L., and Luo, Z. Q. (2019). Post-translational regulation of ubiquitin signaling. *J. Cell Biol.* 218, 1776–1786. doi: 10.1083/jcb.201902074

Sora, V. M., Meroni, G., Martino, P. A., Soggiu, A., Bonizzi, L., and Zecconi, A. (2021). Extraintestinal pathogenic *Escherichia coli*: virulence factors and antibiotic resistance. *Pathogens* 10:1355. doi: 10.3390/pathogens10111355

Tapader, R., Basu, S., and Pal, A. (2019). Secreted proteases: a new insight in the pathogenesis of extraintestinal pathogenic *Escherichia coli*. *Int. J. Med. Microbiol.* 309, 159–168. doi: 10.1016/j.ijmm.2019.03.002

Touchon, M., Hoede, C., Tenaillon, O., Barbe, V., Baeriswyl, S., Bidet, P., et al. (2009). Organised genome dynamics in the *Escherichia coli* species results in highly diverse adaptive paths. *PLoS Genet.* 5:e1000344. doi: 10.1371/journal.pgen.1000344

Wan, M., Wang, X., Huang, C., Xu, D., Wang, Z., Zhou, Y., et al. (2019). A bacterial effector deubiquitinase specifically hydrolyses linear ubiquitin chains to inhibit host inflammatory signalling. *Nat. Microbiol.* 4, 1282–1293. doi: 10.1038/s41564-019-0454-1

Wang, F., Yang, Q., Kase, J. A., Meng, J., Clotilde, L. M., Lin, A., et al. (2013). Current trends in detecting non-O157 Shiga toxin-producing *Escherichia coli* in food. *Foodborne Pathog. Dis.* 10, 665–677. doi: 10.1089/fpd.2012.1448

Wang, X., Zhu, H., Hu, J., Zhang, B., Guo, W., Wang, Z., et al. (2024). Genetic distribution, characterization, and function of *Escherichia coli* type III secretion system. *iScience* 27:109763. doi: 10.1016/j.isci.2024.109763

Wolberger, C. (2014). Mechanisms for regulating deubiquitinating enzymes. *Protein Sci.* 23, 344–353. doi: 10.1002/pro.2415

Wyrsch, E., Roy Chowdhury, P., Abraham, S., Santos, J., Darling, A. E., Charles, I. G., et al. (2015). Comparative genomic analysis of a multiple antimicrobial resistant enterotoxigenic *E. coli* O157 lineage from Australian pigs. *BMC Genomics* 16:165. doi: 10.1186/s12864-015-1382-y

Xia, F., Cheng, J., Jiang, M., Wang, Z., Wen, Z., Wang, M., et al. (2022). Genomics analysis to identify multiple genetic determinants that drive the global transmission of the pandemic ST95 lineage of extraintestinal pathogenic *Escherichia coli* (ExPEC). *Pathogens* 11:1489. doi: 10.3390/pathogens11121489

frontiers | Frontiers in Microbiology

TYPE Original Research
PUBLISHED 20 October 2025
DOI 10.3389/fmicb.2025.1677761

OPEN ACCESS

EDITED BY
Hong Yin,
Chinese Academy of Agricultural Sciences, China

REVIEWED BY
Mohamed Zeineldin,
Benha University, Egypt
Samara Beretta,
São Paulo State University, Brazil

*CORRESPONDENCE
Wanzhe Yuan
✉ yuanwanzhe@126.com
Erjun Ren
✉ renerjun2012@163.com

RECEIVED 07 August 2025
ACCEPTED 06 October 2025
PUBLISHED 20 October 2025

CITATION
Li W, Li X, Cheng J, Liu J, Liu J, Wang Y, Yuan W and Ren E (2025) Lung microbiota of raccoon dogs (*Nyctereutes procyonoides*) using high-throughput sequencing. *Front. Microbiol.* 16:1677761. doi: 10.3389/fmicb.2025.1677761

Lung microbiota of raccoon dogs (*Nyctereutes procyonoides*) using high-throughput sequencing

Wei Li[1,2], Xin Li[2], Jingran Cheng[2], Jie Liu[2], Jinjun Liu[2], Yu Wang[2], Wanzhe Yuan[1]* and Erjun Ren[2]*

[1]College of Veterinary Medicine, Hebei Agricultural University, Baoding, China, [2]Technological Innovation Center for Fur Animal Breeding of Hebei, Shijiazhuang Academy of Agriculture and Forestry Sciences, Shijiazhuang, China

Pneumonia frequently causes mass mortality in raccoon dogs, resulting in significant economic loss. Additionally, raccoon dogs carry various zoonotic pathogens. This study systematically assessed pulmonary pathogens in raccoon dogs and their potential public health implications utilizing 2bRAD microbiome sequencing (2bRAD-M) and viral metagenomics. We analyzed 30 lung tissue samples for microbial composition. Sequencing revealed Pseudomonadota, Ascomycota, and Actinobacteria as dominant phyla and *Acinetobacter*, *Escherichia*, and *Klebsiella* as predominant genera. The most abundant species were *Acinetobacter baumannii*, *Escherichia coli*, and *Klebsiella pneumoniae*. In total, 158 species across 84 genera were identified, including 49 potentially zoonotic species. Viral metagenomics revealed *Peduoviridae*, *Rountreeviridae*, and *Parvoviridae* as dominant families, with *Valbvirus ValB1MD2*, *Andhravirus andhra*, and *Amdoparvovirus carnivoran3* comprising over 80% of the viral composition. These findings highlight the pathogenic complexity of raccoon dog pneumonia and its zoonotic risks, providing crucial insights for disease control and public health management.

KEYWORDS

raccoon dog, bacterial diversity, 2bRAD-M, viral metagenomics, pathogens

1 Introduction

The raccoon dog, a basal canid species, is an omnivore with a dietary preference for animal-based feed. They are primarily fed livestock and poultry by-products such as chicken frames, duck frames, and chicken intestines. This feeding practice may not only trigger respiratory diseases in animals but also increase the risk of zoonotic pathogen transmission through cross-species transmission. China remains the world's largest producer of farmed raccoon dogs, although production has declined from a peak of approximately 16 million pelts in 2015 to about 2.49 million by 2024 (Wang, 2025). Current Chinese raccoon dog farming predominantly relies on small-scale household farming and mixed-species operations, lacking standardized management protocols, biosafety measures, or regulated feed supply chains. These systemic deficiencies increase the risk of disease transmission and compromise product quality (Yang et al., 2021). Recently, frequent pneumonia outbreaks in raccoon dogs have caused significant economic losses to farmers. This disease primarily affects the respiratory system, presenting with coughing, sneezing, and oral/nasal hemorrhage. Contributing factors include poor breeding profitability, suboptimal environmental conditions, and antibiotic misuse. Furthermore, researchers have detected multiple cross-species transmission pathogens in raccoon dogs, including norovirus (Li et al., 2021; Li et al., 2021); avian influenza viruses (H9N2 and H5N1) (Qi et al., 2009; Qian et al., 2021); SCoV-like viruses (Guan et al., 2003); and porcine circoviruses (PCV2, PCV4) (Song et al., 2019; Wang et al., 2022), as well as

bacterial pathogens such as *Escherichia, Klebsiella, Proteus, Pseudomonas,* and *Streptococcus* (Zhu et al., 2021). The transmission of these pathogens primarily originates from farmed raccoon dogs. The main routes of transmission include feeding them untreated livestock and poultry by-products or close contact with other animals in co-farming environments, leading to cross-species pathogen exchange. Some of these pathogens are zoonotic and pose substantial public health concerns.

Current studies on pulmonary microbiota rely primarily on 16S rRNA sequencing, which targets the 16S rRNA gene of microorganisms. Although it provides genus-level taxonomic resolution, it often fails to achieve precise species-level identification. Whole metagenomic sequencing (WMS) enables species-level differentiation by sequencing the entire microbial genomes, but remains cost-prohibitive and technically challenging for large-scale cohorts. Additionally, WMS typically requires substantial amounts of detectable DNA, which is difficult to obtain from low-biomass lung microbiota than from gut microbiota. To enable cost-effective, high-resolution analysis of lung microbiota, we employed 2bRAD microbiome sequencing (2bRAD-M) (Sun et al., 2022), a novel sequencing approach that uses type IIB restriction enzymes to digest microbial genomes, generating unique tags that can be mapped to species-specific 2bRAD markers. This allows accurate species-level profiling of bacteria, fungi, and archaea simultaneously, even in low-biomass samples. We analyzed the DNA virome through viral metagenomics, which involves extracting total microbial genetic material from tissues or environmental samples, followed by quality control steps (e.g., removal of rRNA, host-derived sequences, and bacterial DNA) to rapidly identify viral species composition and abundance.

Currently, there is a lack of high-throughput sequencing investigations on raccoon dog lung microbiota. In this study, we analyzed pneumonic lung tissues collected from multiple raccoon dog farms in Shijiazhuang City, Hebei Province, between 2019 and 2023 using 2bRAD-M and viral metagenomics. We aimed to compare microbial community profiles across farms, investigate the etiology of pneumonia outbreaks in these facilities, and identify potential pathogens carried by raccoon dogs, particularly major zoonotic bacterial species. This study has significant implications for the effective prevention and control of zoonotic diseases.

2 Materials and methods

2.1 Sample collection

All raccoon dogs sampled between December 2019 and September 2023 had clinical symptoms associated with pneumonia. Samples were obtained from ten different raccoon dog farms, which constitute the "groups" referenced throughout this study. Detailed information for each sample is provided in Supplementary Table S1. Disposable utensils were used during collection to avoid cross-contamination of the samples, and the samples were stored in an ultralow-temperature refrigerator at −70 °C. The experiments were approved by the Animal Welfare and Ethics Committee at Laboratory Animal Center of Hebei Agriculture University.

2.2 DNA extraction, library construction, and sequencing

The genomic DNA was extracted using the TIANamp Micro DNA Kit (Tiangen). To monitor potential contamination, both extraction and library preparation negative controls were implemented throughout the experimental process. The 2bRAD-M library was then prepared as previously described (Sun et al., 2022). Briefly, 1 pg–200 ng of DNA was digested with 4 U of BcgI (NEB) at 37 °C for 3 h. Adaptors were ligated to the digested fragments, and the products were amplified via PCR using Phusion High-Fidelity DNA Polymerase (NEB) with Illumina-compatible primers under the following conditions: 98 °C for 5 s, 60 °C for 20 s, and 72 °C for 10 s, followed by a final extension at 72 °C for 10 min. Amplified libraries were purified with the QIAquick PCR Purification Kit (Qiagen). Subsequently, 2bRAD-M sequencing was performed at Qingdao Ouyi Biotechnology Co., with individual sequencing for each sampleon an Illumina HiSeq X Ten platform (OE BioTech, China). Raw reads were filtered based on the BcgI recognition site. The taxonomic profiling was performed using the 2bRAD-M computational pipeline,[1] which relies on a unique 2bRAD tag database (2b-Tag-DB) containing species-specific BcgI-derived tags. Reads with >8% unknown bases or >20% low-quality bases ($Q \leq 20$) were discarded. Taxonomic assignment was performed using the 2bRAD-M pipeline with a custom tag database derived from 173,165 microbial genomes (Wang et al., 2023).

For viral metagenomics, a total of 30 lung tissue samples were randomly divided into three groups of 10 and equally pooled into three sequencing libraries (Libraries 1–3). This strategy ensured sufficient sequencing depth for detecting low-abundance viruses while managing costs. The pooled lung tissues were subjected to purification and concentration of virus-like particles (VLPs) through homogenization, filtration, and ultracentrifugation. Briefly, Tissue samples (1–10 g) were minced and homogenized in grinding tubes with steel beads using a tissue homogenizer under chilled conditions. The homogenate was centrifuged at 12,000 × g for 5 min to remove debris. The resulting supernatant was subjected to virus concentration using ultrafiltration devices (100 kDa MWCO, pre-equilibrated with PBS). Concentrated samples (300–500 µL) were collected by gentle pipetting after centrifugation at 4,000 × g. Genomic DNA and RNA were extracted using the QIAamp MinElute Virus Spin Kit according to the manufacturer's protocol. Total RNA was then reverse transcribed into cDNA using the QuantiTect Reverse Transcription Kit (QIAGEN). Libraries generated from both DNA and cDNA using the Illumina TruSeq Nano DNA/RNA Library Prep Kit were quantified with a Qubit 4.0 Fluorometer and subjected to paired-end sequencing on an Illumina platform. Raw reads were filtered using Fastp v0.20.0 (with the following parameters: remove reads with Q-score < 20, length < 50 bp or adapter contamination) to obtain clean reads. Using the bbmap v38.51 software suite, the clean reads were aligned to the Virus-NT database to remove rRNA, host, and bacterial sequences. The resulting clean reads were then subjected to *de novo* assembly. SPAdes v3.14.1 was used to assemble the sequencing data (Bankevich et al., 2012). Depth statistics were performed using

1 https://github.com/shihuang047/2bRAD-M

Bamsdst (v1.0.9) on the assembled scaffolds to validate the accuracy and coverage of the reads relative to the assembly results. Contigs with a length ≥500 bp were selected for depth statistics, and sliding window analysis with a window size of 200 bp was conducted and visualized. Taxonomic classification was performed on the quality-controlled sequences using Kraken2, followed by Bayesian re-estimation of species abundances with Bracken. The contigs obtained from the assembly were compared against the virus-NT database using BLAST to identify the candidate reference sequences with the closest evolutionary relationships and to determine the species classification of the aligned sequences. Whole-genome amplification and deep sequencing were performed at Shanghai Tanpu Biotechnology Co., Ltd.

2.3 2bRAD microbial database construction and relative abundance calculation

First, 173,165 microbial genomes (including those of bacteria, fungi, and archaea) were obtained from the NCBI RefSeq database. The built-in Perl scripts (GitHub: https://github.com/shihuang047/2bRAD-M) were used to sample restriction fragments from microbial genomes by each of 16 type 2B restriction enzymes. Finally, a specific taxonomic unit (without overlapping other species within the same taxonomic unit) was obtained as a species-specific 2bRAD marker to generate a 2bRAD microbial genome database. Quality-controlled 2bRAD tags from each sample were mapped to this database, and the relative abundance was calculated as previously described (Wang et al., 2023). To control the false-positive in the species identification, a G score was derived for each species identified within a sample as below, which is a geometric mean of the proportion of the species-specific markers that have been captured (by sequencing) and the number of all detected species-specific markers (by sequencing) of this species.

$$Gscore_{speciesi} = \sqrt{S_i \times t_i}$$

S: Number of reads assigned to all 2bRAD markers belonging to species i within a sample.

t: Number of all 2bRAD markers of species i sequenced within a sample.

The relative abundance data derived from 2bRAD sequencing were normalized. Specifically, the relative abundance of each species was calculated using the following formula: the average read coverage of species-specific 2bRAD markers (which serves as a proxy for the number of individuals of that species in the sample) was divided by the total read coverage across all detected species (representing the total number of individuals in the sample). To ensure robust species calls and control false positives, a G-score threshold of 5 was applied.

$$Relativeabundance_{speciesi} = \frac{S_i / T_i}{\sum_{i=1}^{n} S_i / T_i}$$

S: The number of reads assigned to all 2bRAD markers of species i in a sample.

T: The number of all theoretical 2bRAD markers of species i.

The species diversity indices were calculated without normalization/rarefaction. Instead, species abundances were scaled up by a factor of 1e6 and rounded to integers, and the diversity indices were computed at this unified depth for comparative analysis across different samples (McMurdie and Holmes, 2014).

2.4 Statistical analysis

Bacterial diversity analysis was conducted using R software. The alpha diversity across groups was compared through Kruskal-Wallis test based on the Chao1 estimator (estimating species abundance and richness), Shannon index (reflecting species richness and evenness), and Simpson index (quantifying species diversity) using the "vegan" package. The "vegan" package was also used to calculate Bray-Curtis distance and binary Jaccard distance to estimate beta diversity, which was statistically compared using permutational multivariate analysis of variance (PERMANOVA). Comparisons between groups were performed using the Kruskal-Wallis H test in IBM SPSS Statistics software (Version 19). If the test results indicated a statistically significant overall difference ($p < 0.05$), post-hoc pairwise comparisons were subsequently conducted using the built-in pairwise comparison function in SPSS with appropriate adjustment for multiple comparisons. For viral homology analysis, to elucidate phylogenetic relationships, sequences belonging to different groups of related viruses were downloaded from the GenBank database. Nucleotide sequences were aligned using MUSCLE, as implemented in MEGA-11, ModelFinder was used for model selection, and IQ-TREE was employed to construct the phylogenetic tree using the maximum likelihood (ML) method, with bootstrap support values tested using 1,000 replicates.

3 Results

3.1 Analysis of potential zoonotic bacterial pathogens

Using the "Global Pathogen Database (gcPathogen)" developed by the National Microbiology Data Center (NMDC) of the Institute of Microbiology, Chinese Academy of Sciences,[2] we identified 49 species across 24 genera with zoonotic potential out of 158 species from 84 bacterial genera (Table 1). These zoonotic bacterial genera exhibited substantial variability in prevalence and total read counts. High detection rates and abundances were observed in *Acinetobacter*, *Escherichia*, *Klebsiella*, *Ralstonia*, *Rothia*, and *Streptococcus*. The prevalence and relative abundance were calculated for species with a prevalence greater than 10/30. The results were as follows: *E. coli* had a prevalence of 30/30 and a relative abundance of 1.59–98.09%; *Acinetobacter baumannii* had a prevalence of 28/30 and a relative abundance of 0.59–60.45%; *Afipia broomeae* had a prevalence of 24/30 and a relative abundance of 0.005–3.72%; *K. pneumoniae* had a prevalence of 22/30 and a relative abundance of 0.57–62.06%; *Ralstonia pickettii* had a prevalence of 17/30 and a relative abundance of 0.033–3.32%; and *Rothia dentocariosa* had a prevalence of 11/30 and a relative abundance of 0.26–12.3%.

2 https://nmdc.cn/gcpathogen/

10.3389/fmicb.2025.1677761

TABLE 1 Composition of microorganisms with zoonotic potential in raccoon dog lungs.

Genus	Species	Prevalence rate	Relative abundance range
Actinomyces	*Actinomyces massiliensis*	2/30	0.24–0.41
	Actinomyces naeslundii	1/30	0.32
	Actinomyces oris	1/30	0.36
	Actinomyces oris E	1/30	0.25
Brevibacillus	*Brevibacillus parabrevis*	3/30	0.37–2.82
Enterococcus	*Enterococcus faecalis*	3/30	0.73–6.47
Veillonella_	*Veillonella atypica*	1/30	4.13
Cutibacterium	*Cutibacterium acnes*	6/30	0.03–1.55
Bacteroides	*Bacteroides pyogenes*	1/30	0.086
Prevotella	*Prevotella histicola*	7/30	0.29–5.72
	Prevotella jejuni	1/30	1.54
	Prevotella multiformis	1/30	0.08
	Prevotella nigrescens	2/30	0.29–0.73
	Prevotella oris	1/30	0.15
Citrobacter	*Citrobacter braakii*	1/30	0.64
Escherichia	*Escherichia coli*	30/30	1.59–98.09
	Escherichia albertii	1/30	0.03
	Escherichia fergusonii	1/30	0.01
	Escherichia marmotae	1/30	0.02
Aeromonas	*Aeromonas caviae*	1/30	1.6
	Aeromonas dhakensis	1/30	0.62
	Aeromonas media	1/30	0.18
Acinetobacter	*Acinetobacter baumannii*	28/30	0.59–60.45
	Acinetobacter guillouiae	1/30	0.17
	Acinetobacter soli	1/30	0.89
Klebsiella	*Klebsiella aerogenes*	1/30	2.07
	Klebsiella michiganensis	1/30	1.07
	Klebsiella pneumoniae	22/30	0.57–62.06
Ralstonia	*Ralstonia pickettii*	17/30	0.033–3.32
	Ralstonia pickettii B	9/30	0.004–1.23
Rothia	*Rothia dentocariosa*	11/30	0.26–12.3
	Rothia mucilaginosa A	1/30	1.14
Chlamydophila	*Chlamydophila abortus*	3/30	10.26–27.1
Streptococcus	*Streptococcus agalactiae*	1/30	6.12
	Streptococcus alactolyticus	2/30	2.08–3.47
	Streptococcus lactarius	6/30	0.22–5.54
	Streptococcus lutetiensis	1/30	8.66
	Streptococcus minor	2/30	0.23–1.38
Lactococcus	*Lactococcus garvieae*	2/30	1.87–2.48
	Lactococcus lactis	1/30	5.10
Afipia	*Afipia broomeae*	24/30	0.005–3.72
Salmonella	*Salmonella enterica*	4/30	0.02–13.47
Proteus	*Proteus mirabilis*	1/30	6.07

(Continued)

TABLE 1 (Continued)

Genus	Species	Prevalence rate	Relative abundance range
Enterobacter	*Enterobacter hormaechei A*	2/30	0.02–3.7
	Enterobacter kobei	1/30	1.1
	Enterobacter quasihormaechei	1/30	0.54
Bordetella	*Bordetella pertussis*	1/30	2.5
Pseudomonas B	*Pseudomonas B oryzihabitans*	1/30	0.45
Bacteroides	*Bacteroides pyogenes*	1/30	0.09

The information in this column is based on the "Global Pathogen Database (gcPathogen)" developed by the National Microbiology Data Center (NMDC) of the Institute of Microbiology, Chinese Academy of Sciences (https://nmdc.cn/gcpathogen/).

3.2 Fungal composition of the lung tissue

At the phylum level, Ascomycota were detected in all samples, with relative abundances ranging from 0.07 to 23.17%. Basidiomycota were observed in only one sample (0.02%). At the genus level, *Talaromyces*, *Pichia*, and *Fusarium* were identified in all samples, with relative abundances of 0.01–2.82%, 0.06–19.95%, and 0.005–1.65%, respectively. *Moesziomyces* was detected in only one sample (0.02%). At the species level, the abundance patterns of *T. rugulosus*, *P. inconspicua*, *F. oxysporum*, and *Moesziomyces antarcticus* aligned with their respective genus-level distributions.

3.3 Bacterial and fungal diversity in lung tissue samples

Numbers of 2bRAD reads before and after filtering, including raw, enzyme-digested, and clean reads, are presented in Supplementary Table S2. A total of 158 microbial species were identified across 30 samples. A Venn diagram revealed the number of species shared by different sample groups, showing that five species were common to all 30 samples: *Escherichia coli* (1.59–98.09%), *Pichia inconspicua* (0.06–19.95%), *Bradyrhizobium sp003020075* (0.04–8.31%), *Talaromyces rugulosus* (0.01–2.82%), and *Fusarium oxysporum* (0.005–1.65%) (Figure 1). Microbial α-diversity and community composition analyses are shown in Figure 2. At the phylum level, dominant taxa were Pseudomonadota (35.67–99.77%), Ascomycota (0.07–23.17%), and Actinobacteria (0–24.21%). At the genus level, the dominant genera were *Acinetobacter* (0–61.33%), *Escherichia* (1.59–98.26%), and *Klebsiella* (0–65.2%). The five most abundant species were *Acinetobacter baumannii* (0–60.45%), *E. coli* (1.59–98.09%), *Klebsiella pneumoniae* (0–62.06%), *P. inconspicua* (0.06–19.95%), and *Ralstonia sp000620465* (0–13.82%). Alpha diversity was assessed in groups with over three lung tissue samples (Groups 2, 8, 9, and 10). No significant differences were observed in the Shannon or Simpson indices among the groups, except for a significant difference in the Chao1 index between Groups 9 and 10 as well as between Groups 8 and 10 (Figure 3; Table 2).

3.4 Beta diversity of bacterial and fungal communities across farms

Beta diversity compares microbial differences across multiple groups. Permanova analysis revealed the overall microbial composition was significantly different ($p = 0.001$, $p = 0.031$) among groups based on the Binary Jaccard distance and Bray–Curtis distance (Figures 4A,B).

A statistical comparison of median differences using the Kruskal-Wallis H test was performed for Groups 2, 8, 9, and 10 at the phylum, genus, and species levels (Supplementary Table S3).

Phylum level: No significant differences were detected in Pseudomonadota, Ascomycota, Actinobacteria, Bacillota, or Chlamydiota. However, Bacteroidota showed a highly significant difference between Groups 2 and 9 ($p = 0.003$), with higher abundance in Group 2.

Genus level: No significant differences were detected among *Acinetobacter*, *Klebsiella*, or *Escherichia*. *Rothia* was significantly more abundant in Group 2 than in Group 9 ($p = 0.034$).

Species level: No significant differences were observed for *Acinetobacter baumannii*, *E. coli*, or *K. pneumoniae*. However, *Rothia sp902373285* was significantly higher in Group 2 vs. Groups 9 ($p = 0$) and 10 ($p = 0.006$). *Streptococcus lactarius* was significantly more common in Group 2 than in Group 9 ($p = 0.033$). *Alloprevotella sp905371275* was significantly elevated in Group 2 vs. Group 9 ($p = 0.005$) and Group 10 ($p = 0.035$). *Prevotella histicola* was significantly more common in Group 2 than in Group 9 ($p = 0.033$). *Lautropia mirabilis* was significantly more common in Group 2 than in Group 10 ($p = 0.024$). Compared with that in Group 9, the abundance of *Phyllobacterium calauticae* in Group 2 was significantly different ($p = 0.008$).

3.5 Viral metagenomics analysis of lung tissue

3.5.1 Raw data quality control results

Numbers of sequencing reads during virome sequencing quality control are shown in Supplementary Table S4. For Library 1, 58,512,218 raw reads were obtained, reduced to 56,042,140 reads after filtering, and further decreased to 28,021,070 reads after contaminant removal. Library 2 initially generated 75,895,168 raw reads, which were filtered to 69,573,170 reads and reduced to 34,786,585 reads after contaminant removal. Library 3 started with 65,659,632 raw reads, which were filtered to 61,543,548 reads; 30,771,774 reads were retained after contaminant removal.

3.5.2 Taxonomic annotation results at the family level

Figure 5 shows the annotation results of the sequences at the viral family level. According to Table 3, the average relative abundances of

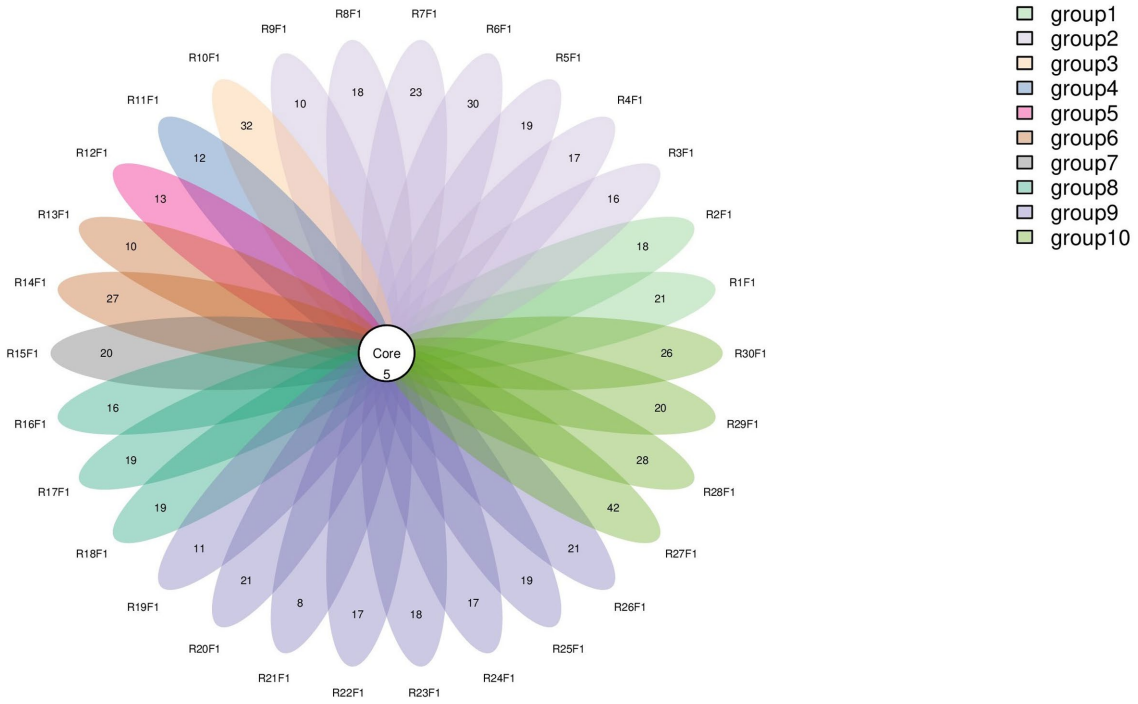

FIGURE 1
Venn diagram of species distribution. Each oval (labeled with an RF identifier) corresponds to one animal.

the top ten viral families across the three libraries were calculated as follows: *Peduoviridae* (50.4%), *Rountreeviridae* (19.44%), *Parvoviridae* (10.82%), *Poxviridae* (2.1%), *Genomoviridae* (1.92%), *Orthoherpesviridae* (1.45%), *Kyanoviridae* (1.37%), *Demerecviridae* (1.12%), *Retroviridae* (1.11%), and *Casjensviridae* (1.02%).

3.5.3 Taxonomic annotation results at the species level

Figure 6 shows the annotation results for the sequences at the viral species level. According to Table 4, the average relative abundances of the top ten viral species in the lung tissue at the species level were calculated as follows: *Valbvirus ValB1MD2* (53.92%), *Andhravirus andhra* (19.81%), *Amdoparvovirus carnivoran3* (11.19%), *Amsacta moorei entomopoxvirus* (1.81%), *Gemykibivirus rhina2* (1.26%), *Rubivirus ruteetense* (0.76%), *Cymopoleiavirus swam2* (0.75%), *Physalis rugose mosaic virus* (0.73%), *Percavirus equidgamma5* (0.63%), and *Cyvirus cyprinidallo1* (0.59%).

3.5.4 A virus belonging to the genus *Amdoparvovirus*

Amdoparvovirus sequences were detected in all three libraries. Using the Align/Assemble function of Geneious 11.1.2 in Library 3, a nearly complete *Amdoparvovirus* genome was obtained, with a length of 4,635 bp, containing three nonstructural proteins and two structural proteins. The nucleotide sequence of the genome was submitted to GenBank (accession number: PV580269). Phylogenetic analysis of NS1 and VP2 sequences, including 17 references from the five recognized *Amdoparvovirus* species within the genus *Amdoparvovirus*: *Raccoon dog amdoparvovirus*, *Skunk amdoparvovirus*; *Aleutian mink disease parvovirus* (AMDV), *Red panda amdoparvovirus*, and *Gray fox amdoparvovirus 3*, resolved five major clades. Four clades aligned with the known species, while the fifth consisted of our sequences. Notably, our samples clustered into a distinct subclade within a larger clade that includes sequences from raccoon dogs (Figures 7, 8). The assembled contigs were compared to the virus-NT database using BLAST (V2.10.0+). NCBI BLASTn analysis revealed that the NS1 nucleotide sequences of our samples shared the highest identity (97.82%) with those of the strain HS-R (GenBank no. NC_025825.1), covering a length of 1856/1923 nt, whereas the VP2 sequence showed the highest identity (98.71%) with strain SD-G1 (GenBank no. OM451163.1), covering a length of 1716/1756 nt. Strain HS-R was identified in 2013 from raccoon dog spleen tissue samples collected during a disease outbreak on a farm in Jilin Province, China (Shao XQ, et al., 2014), while strain SD-G1 was identified in 2021 from raccoon dog tissue samples collected in Hebei and Shandong Provinces, China (He et al., 2022). Compared to these strains, our sample presented 44 and 25 nucleotide sequence variations in the NS1 and VP2 regions, respectively.

3.5.5 Identification of a novel *Anelloviridae* virus in raccoon dogs

Torque Teno Virus (TTV) sequences were detected in two libraries. A nearly complete genome, designated NPTTV, was successfully assembled with a length of 2,441 bp (GenBank accession no. PV693371). The gene structure is illustrated in Figure 9 and contains two open reading frames (ORFs). Phylogenetic analysis of ORF1 revealed that the nucleotide sequences of NPTTV were grouped within a clade of tick-associated TTV isolate tick24_1 (GenBank accession: NC_076184.1) (Figure 10), BLAST results of the ORF1 sequence showed only 39 nucleotides with a similarity of 92%. Additionally, BLAST results of the 470 bp untranslated region (UTR) sequence revealed 83.76% sequence identity with the tick-associated TTV isolate tick24_1.

10.3389/fmicb.2025.1677761

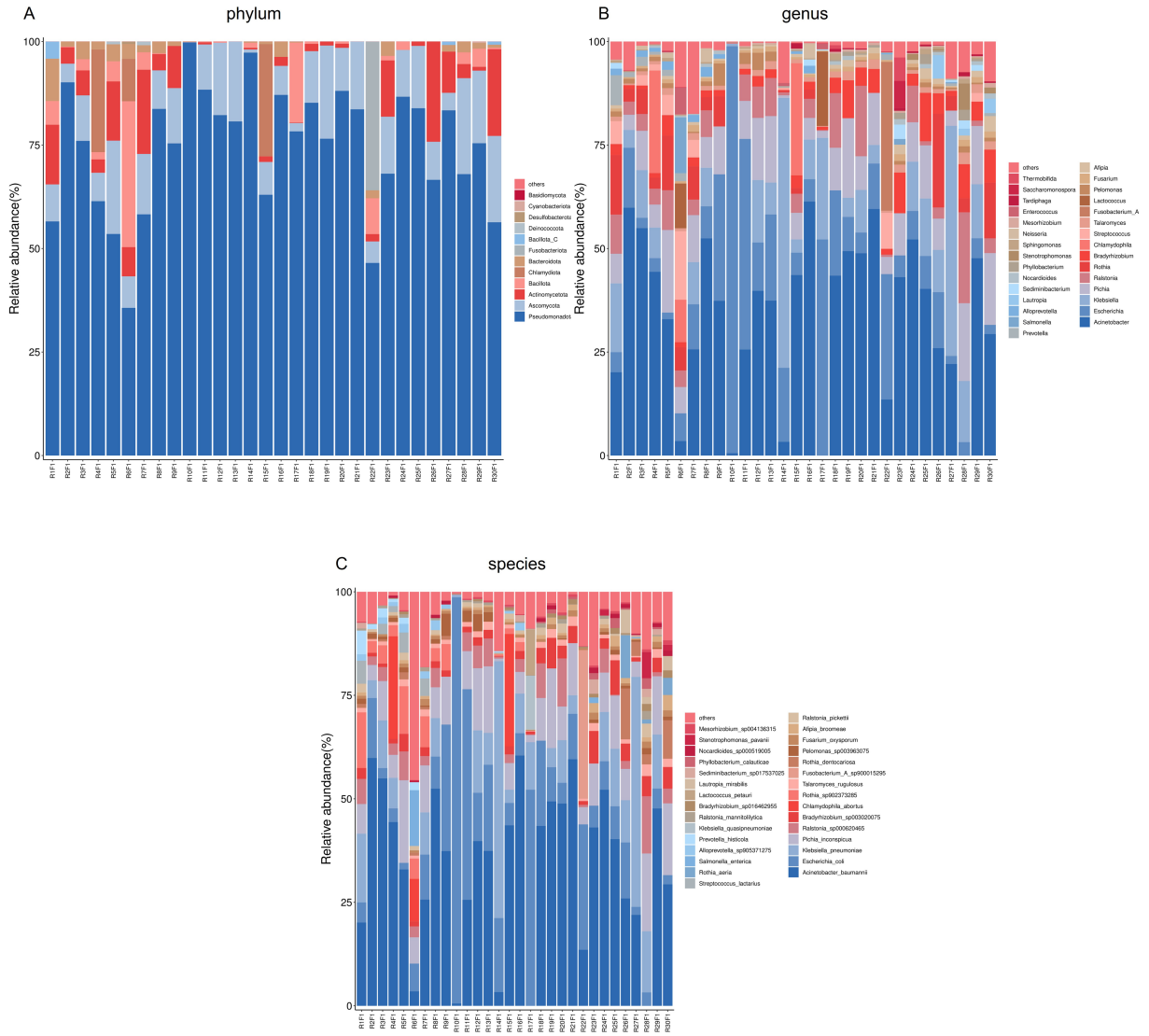

FIGURE 2
Microbial community composition of lung tissue samples. **(A)** Bar plot of phylum-level community structure across samples; **(B)** Bar plot of the top 30 genera; **(C)** Bar plot of the top 30 species.

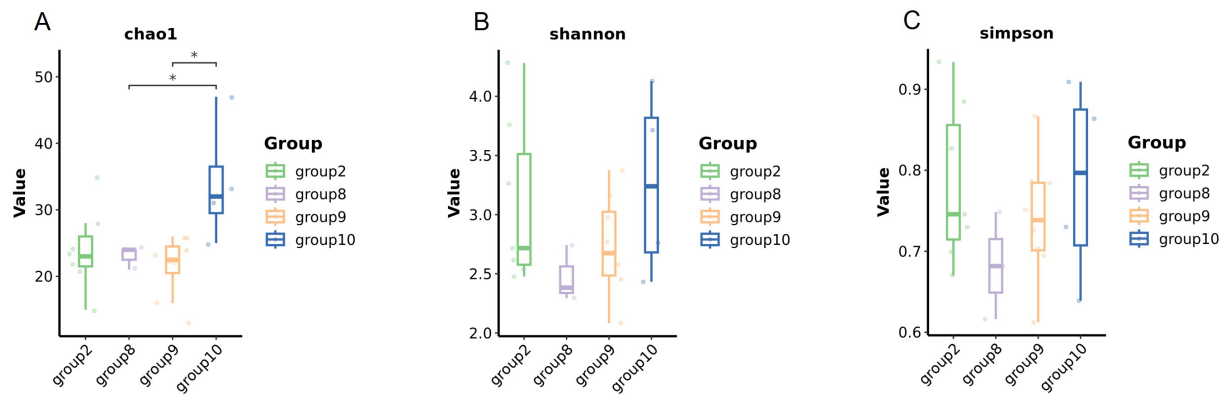

FIGURE 3
Microbial diversity of the lung tissue samples in different groups. Comparison of the alpha diversity among groups (**A** Chao1 index, **B** Shannon index, and **C** Simpson index).

10.3389/fmicb.2025.1677761

TABLE 2 Significance test of chao1, Shannon and Simpson diversity indices between different groups.

Groups		*p*-value		
		Chao1	Shannon	Simpson
2	8	1	0.18	0.27
	9	0.68	0.4	0.54
	10	0.073	0.93	1
8	9	0.92	0.28	0.28
	10	0.05	0.11	0.4
9	10	0.021*	0.46	0.57

"*"indicates a statistically significant difference ($p < 0.05$).

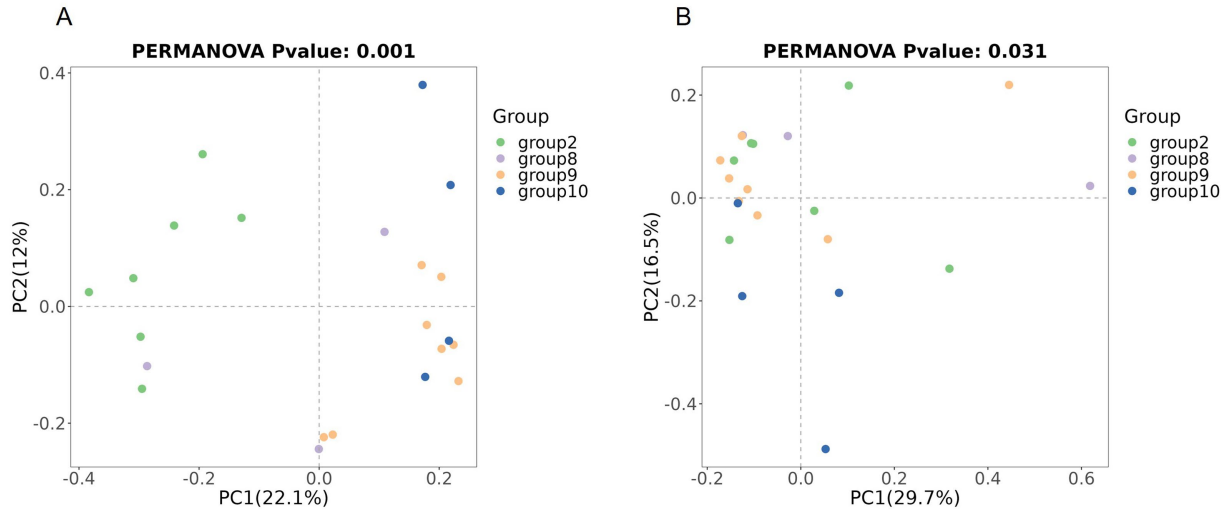

FIGURE 4
Comparison of beta diversity between the four groups based on PCoA. Comparison of the beta diversity among groups based on the Binary Jaccard distance **(A)**, and Bray–Curtis distance **(B)**.

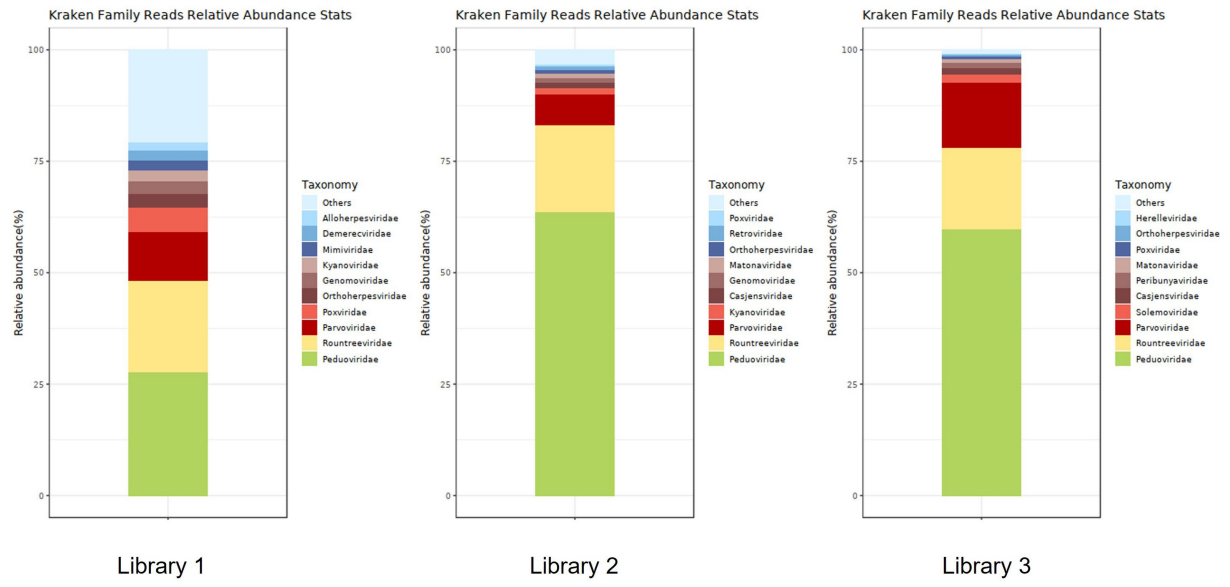

FIGURE 5
Stacked plot of annotated relative abundance at the family level of viruses in lung tissue.

10.3389/fmicb.2025.1677761

TABLE 3 Distribution of viral sequences across different viral families in lung tissue.

Name	Library 1		Library 2		Library 3	
	Reads	Fraction	Reads	Fraction	Reads	Fraction
Peduoviridae	2,862	0.27786	16,049	0.63586	5,746	0.59842
Rountreeviridae	2,116	0.20544	4,935	0.19552	1751	0.18236
Parvoviridae	1,131	0.10981	1749	0.06929	1,397	0.14549
Kyanoviridae	262	0.02544	363	0.01438	12	0.00125
Casjensviridae	65	0.00631	298	0.01181	119	0.01239
Genomoviridae	281	0.02728	283	0.01121	0	0
Matonaviridae	25	0.00243	245	0.00971	90	0.00937
Orthoherpesviridae	322	0.03126	204	0.00808	41	0.00427
Retroviridae	154	0.01495	183	0.00725	0	0
Demerecviridae	225	0.02184	16	0.00063	0	0
Alloherpesviridae	196	0.01903	62	0.00246	0	0
Mimiviridae	228	0.02214	65	0.00258	20	0.00208
Poxviridae	550	0.05340	101	0.00400	55	0.00573
Solemoviridae	43	0.00417	27	0.00107	192	0.02000
Peribunyaviridae	56	0.00544	28	0.00111	118	0.01229

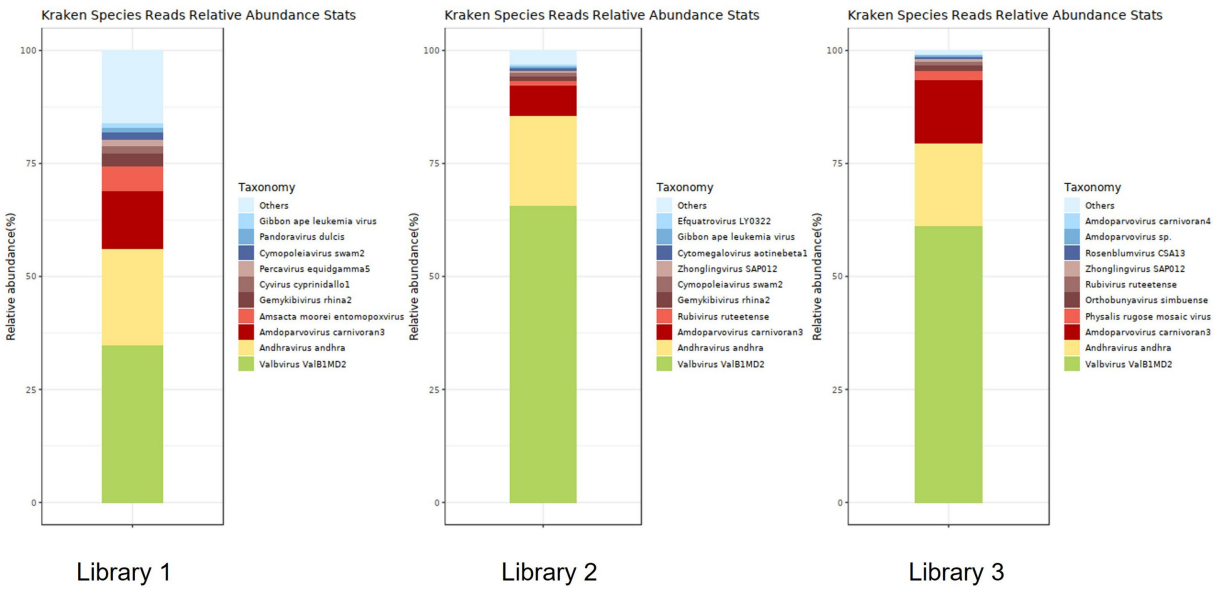

FIGURE 6
Stacked plot of annotated relative abundance of viral species levels in raccoon dog lung tissue.

3.5.6 Other viruses detected as short sequence fragments

In Library 1, we detected partial sequences with similarity to coronaviruses of SARS-CoV-2 (210 bp) with an alignment length of 103 bp. BLAST results revealed 81.55% identity with a segment of the genome of the *severe acute respiratory syndrome coronavirus 2* isolate Wuhan-Hu-1 (GenBank accession: OU471411.1). In Library 2, we identified partial sequences of raccoon dog TTV (400 bp) with an alignment length of 214 bp. BLAST analysis revealed 89.25% identity with a region of the complete genome of raccoon dog TTV 2 Raccoon dog/Japan/Rac_Fe2/2022 DNA (GenBank accession: LC743590.1). Additionally, partial sequences of *human betaherpesvirus 6* (374 bp in length) were detected in Library 2, with an alignment length of 380 bp and 81.55% identity to a segment of the *human betaherpesvirus 6* strain HP8H1 partial genome (GenBank accession: KY315527.2).

4 Discussion

Raccoon dogs are known carriers of various pathogens, yet their pulmonary microbiota remains underreported. In contrast, healthy human lungs have been reported to host Firmicutes, Proteobacteria,

TABLE 4 Distribution of viral sequences across different viral species in lung tissue.

Name	Library 1		Library 2		Library 3	
	Reads	Fraction	Reads	Fraction	Reads	Fraction
Valbvirus ValB1MD2	2,843	0.34926	16,031	0.65628	5,746	0.61212
Andhravirus andhra	1728	0.21229	4,882	0.19986	1711	0.18227
Percavirus equidgamma5	121	0.01486	25	0.00102	29	0.00309
Cyvirus cyprinidallo1	140	0.01720	11	0.00045	0	0
Amdoparvovirus carnivoran3	1,041	0.12789	1,652	0.06763	1,316	0.14019
Gemykibivirus rhina2	231	0.02838	230	0.00942	0	0
Amsacta moorei entomopoxvirus	441	0.05418	0	0	0	0
Cymopoleiavirus swam2	120	0.01474	192	0.00786	0	0
Pandoravirus dulcis	91	0.01118	39	0.00160	0	0
Rubivirus ruteetense	25	0.00307	245	0.01003	90	0.00959
Zhonglingvirus SAP012	18	0.00221	131	0.00536	49	0.00522
Physalis rugose mosaic virus	10	0.00123	16	0.00066	189	0.02013
Orthobunyavirus simbuense	28	0.00344	13	0.00053	116	0.01236

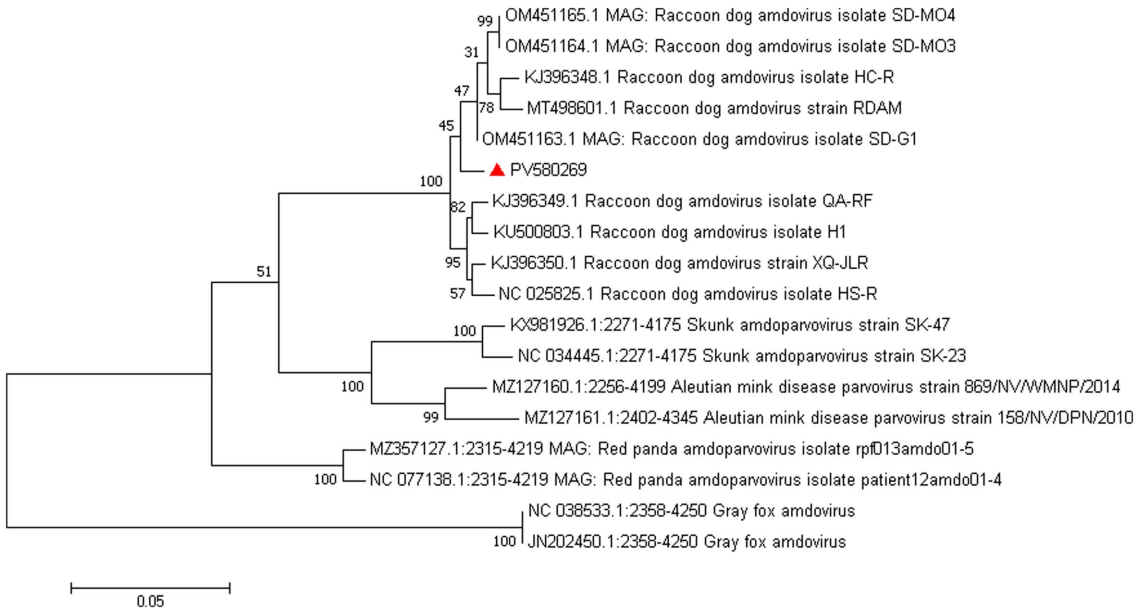

FIGURE 7
Phylogenetic tree analysis of the VP2 gene in raccoon dog *Amdoparvovirus*. The VP2 identified in this study was marked with a red triangle.

and Bacteroidetes (phylum level) and *Pseudomonas*, *Streptococcus*, *Prevotella*, *Fusobacterium*, and *Veillonella* (genus level) (Maddi et al., 2019). Fungal communities in human lungs are primarily composed of Ascomycota and Basidiomycota at the phylum level, with *Candida* and *Pichia* dominating at the genus level (Wu et al., 2022). The prevalence of Pseudomonadota and Ascomycota in raccoon dogs may reflect shared environmental exposure between humans and raccoon dogs, as backyard breeding practices often lack spatial separation between living and farming areas, increasing inhalation of airborne microorganisms. Notably, Pseudomonadota and Ascomycota are among the most common microbial taxa in the air (Sharma Ghimire et al., 2022). The composition of respiratory microbiota exhibits substantial variation among several animal species, including pigs (Huang et al., 2019; Li et al., 2021; Jiang et al., 2019), sheep (Miao et al., 2023), and dogs (Vientós-Plotts et al., 2019; Ericsson et al., 2016). Overall, the microbial profiles of raccoon dogs are similar to those of canines, with Proteobacteria and Actinobacteria as dominant phyla and *Acinetobacter* as the predominant genus, likely attributable to

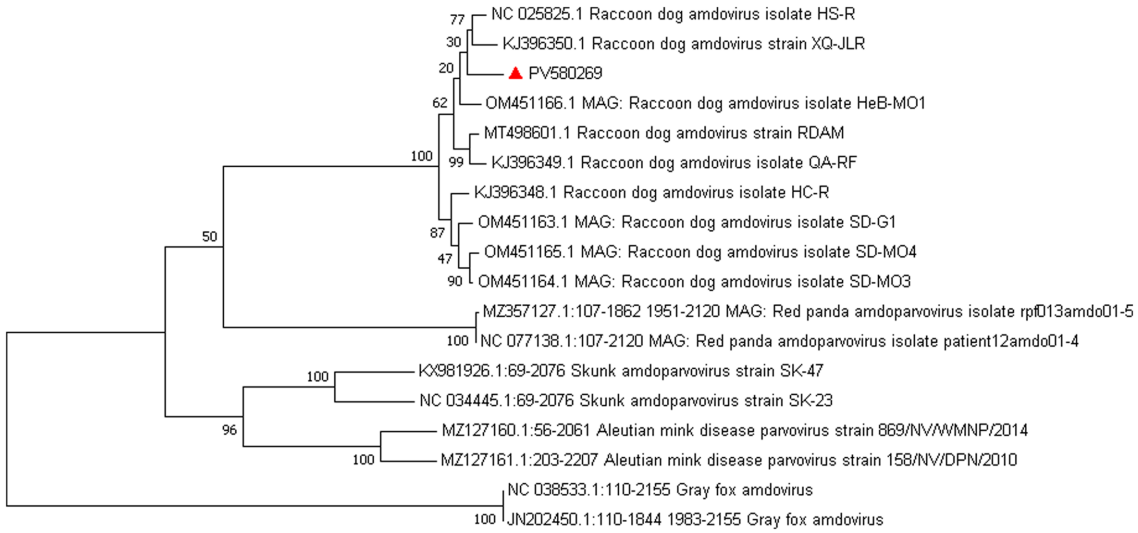

FIGURE 8
Phylogenetic tree analysis of the NS1 gene in raccoon dog *Amdoparvovirus*. The NS1 identified in this study was marked with a red triangle.

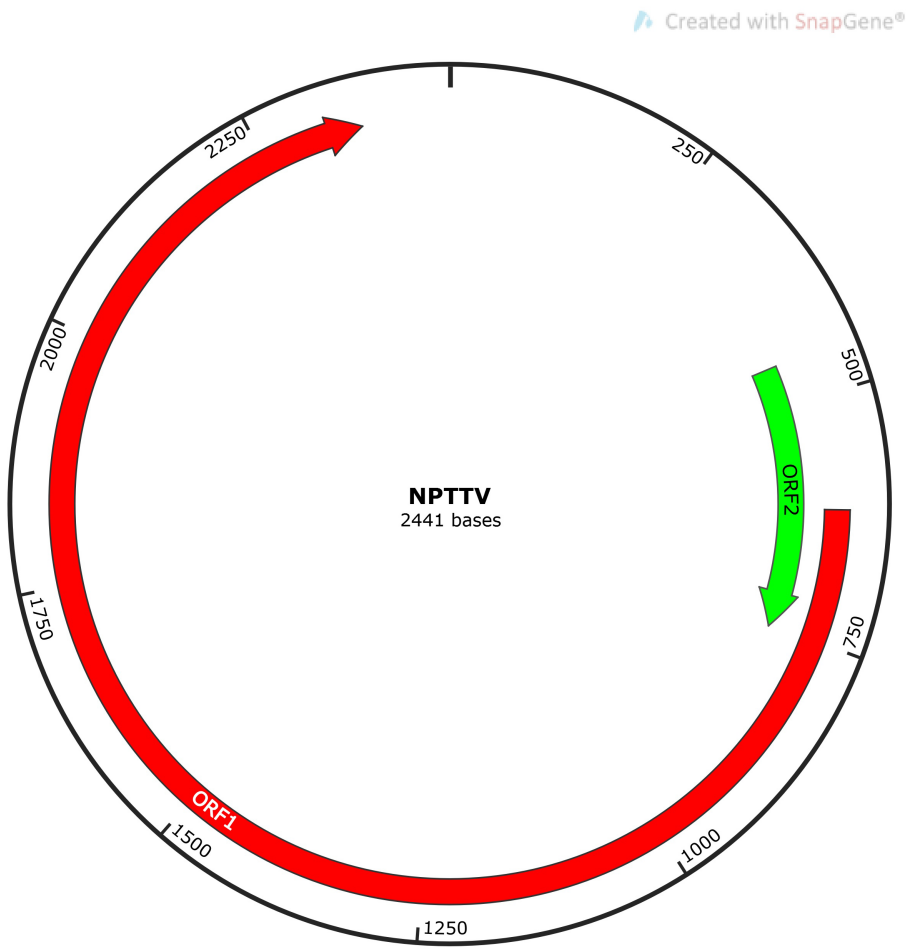

FIGURE 9
Genomic structure schematic diagram of NPTTV.

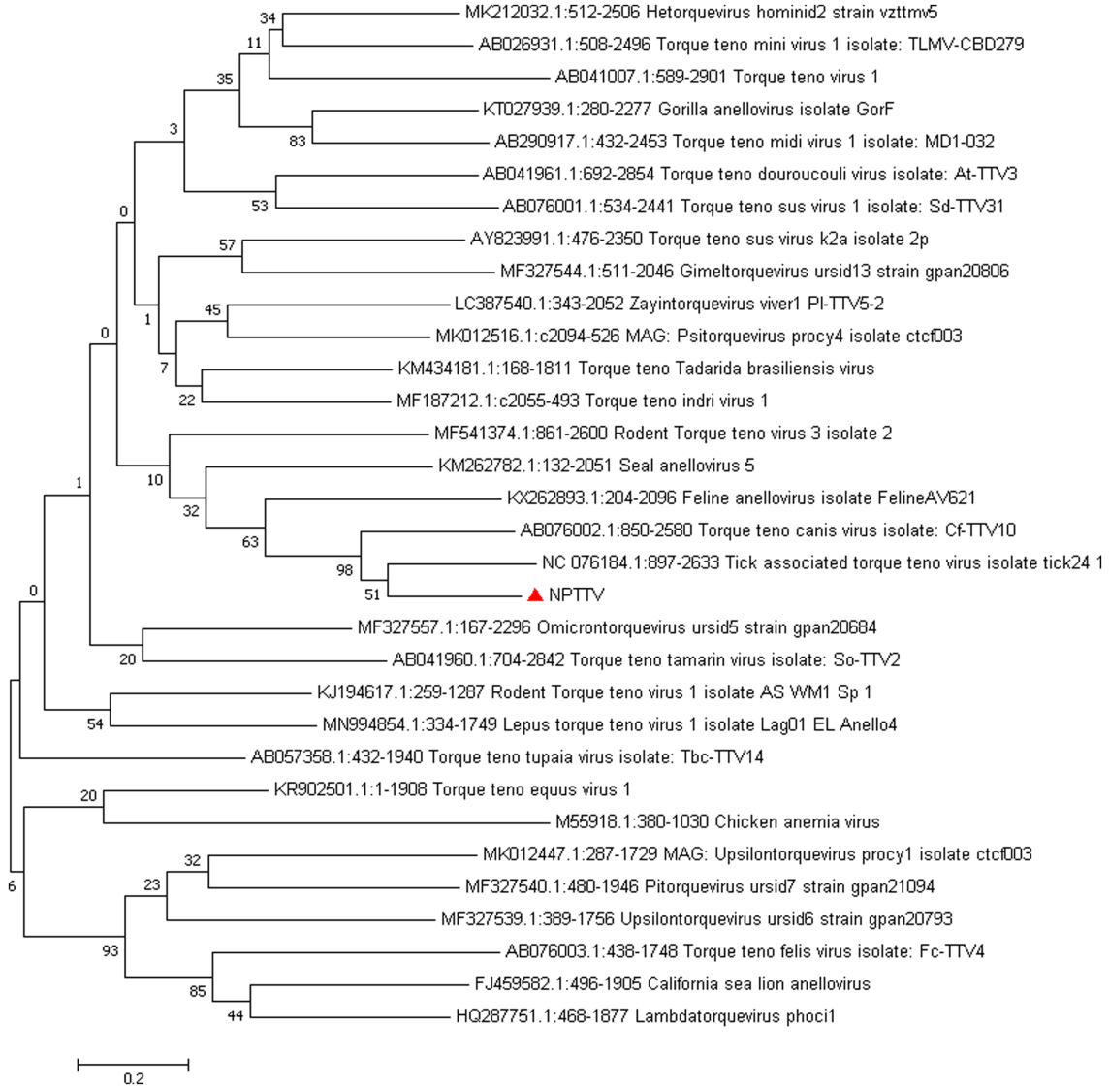

FIGURE 10
Phylogenetic tree analysis of the ORF1 gene in raccoon dog TTV. The ORF1 identified in this study was marked with a red triangle.

their taxonomic classification within the family Canidae (Fastrès et al., 2019).

In this sequencing study, we identified numerous potentially pathogenic and opportunistic bacteria in raccoon dog lungs, including 49 species across 24 genera with potential zoonotic risks. Several exhibited high relative abundance (0.01–98.09%) and prevalence (≥10/30), including *Escherichia coli* (Wang et al., 2025) (pathogenic strains can cause diarrhea, pneumonia, and more), *A. baumannii* (Al-Hassan and Al-Madboly, 2020) (a major nosocomial and opportunistic pathogen), and *Klebsiella pneumoniae* (associated with pneumonia and sepsis), *Ralstonia* species (Jin et al., 2025; Sebastian et al., 2025), *Afipia broomeae* (Brenner et al., 1991), *Rothia dentocariosa* (Zheng et al., 2024). Notably, *Bordetella pertussis*, the gram-negative causative agent of whooping cough, was detected in one tissue sample (2.5% abundance). *Salmonella enterica*, a well-known zoonotic pathogen (Chiu et al., 2004), was detected in four samples (0.02–13.47%). *Chlamydophila abortus,* identified in three samples (10.26–27.1%), is known to cause reproductive losses in livestock and flu-like symptoms such as fever, chills, headache, and myalgia in humans, with severe cases potentially progressing to respiratory diseases such as pneumonia and bronchitis (Albini et al., 2023). Six *Streptococcus* species associated with humans were detected, including *Streptococcus agalactiae* (Group B *Streptococcus*), identified in one sample (6.12%), a pathogen associated with bovine mastitis and streptococcosis in cattle and fish, respectively (Crestani et al., 2024). In humans, it poses significant risks to newborns and immunocompromised individuals, potentially causing fatal infections and long-term sequelae (Yuan et al., 2021). *Staphylococcus pseudintermedius*, detected in one sample (1.4%), is transmitted primarily to humans through close contact with dogs, and its pathogenic mechanisms resemble those of *Staphylococcus aureus* (Lynch and Helbig, 2021). These findings suggest that raccoon dogs may serve as reservoirs for multiple zoonotic pathogens, posing potential public health risks.

Using viral metagenomics, we annotated 93,579,429 reads from three sequencing libraries as viral sequences. Dominant families included

Peduoviridae, *Rountreeviridae*, and *Parvoviridae*. The most abundant viral species were *Valbvirus ValB1MD2*, *Andhravirus andhra*, and *A. carnivoran3*. These findings indicate that bacteriophages dominate the raccoon dog lung virome and may interact with prevalent bacterial hosts such as *Acinetobacter baumannii*, *E. coli*, and *K. pneumoniae*. In addition to bacteriophages, *A. carnivoran3* exhibited relatively high abundance (>80%). We also identified novel strains of raccoon dog *Amdoparvovirus* and TTV, and detected partial short genomic fragments of SARS-CoV-2, raccoon dog TTV, and human betaherpesvirus 6. However, the exceedingly short read lengths and low abundance prevent definitive confirmation of these viruses or assessment of their biological significance in raccoon dogs. These signals could potentially originate from laboratory contamination or environmental exposure rather than genuine infection. Further targeted assays would be necessary to validate their presence and significance.

Raccoon dog and arctic fox amdoparvovirus (RFAV) is an amdoparvovirus that naturally infects raccoon dogs and blue foxes, genetically distinct from Aleutian mink disease virus (AMDV) (Shao et al., 2014). Its genome is approximately 4,800 nucleotides in length and contains two large ORFs that encode structural proteins VP1 and VP2, as well as non-structural proteins NS1, NS2, and NS3. In this study, NS1 sequences showed 97.82% identity with strain HS-R (identified in 2013 in Jilin Province), while VP2 showed 98.71% identity with strain SD-G1 (identified in 2021 in Hebei and Shandong). The high homology with strains HS-R and SD-G1, which were identified in different years and provinces, confirms the circulation of this viral species in the region. The genetic stability observed across time and geography warrants further investigation.

TTV was first detected in 1997 in a patient with unexplained posttransfusion hepatitis (Nishizawa et al., 1997) and has since been identified in humans and other mammals, including nonhuman primates, livestock, and wildlife (Manzin et al., 2015). TTV is a single-stranded, negative-sense, circular DNA virus with a genome length of approximately 2.1–3.9 kb. The genome contains three ORFs encoding proteins VP1, VP2, and VP3, with structural variation across genera. Taxonomic classification of anelloviruses is based on nucleotide sequence similarity of ORF1 with cut-off values of 44 and 65%, respectively, for genus and species (Biagini et al., 2011).

In this study, BLAST analysis showed that the ORF1 sequence of NPTTV had only 39 nucleotides with 92% similarity to the tick-associated TTV isolate tick24_1, the 470 bp partial UTR sequence revealed 83.76% sequence identity with it. While the entire ORF1 sequence of NPTTV shows 42.9 and 50.3% similarity to the tick-associated TTV isolate tick24_1 and the Torque teno canis virus isolate *Cf*-TTV10, respectively. Based on the guidelines for classification for the family *Anelloviridae*, NPTTV from this study belongs to the genus *Thetatorquevirus* is a putative new species. It is likely a recombinant chimera, with its ORF1 region originating from an unknown source and its UTR region derived from a tick TTV-like ancestor.

This study offers valuable preliminary insights into pulmonary pathogens in raccoon dogs but exhibits several limitations. The absence of healthy control groups limits the interpretation of our microbiological findings. In the absence of such a comparison, it is difficult to determine whether the microorganisms that have been detected are true pathogens, part of the normal commensal flora, or environmental contaminants. Methodologically, viral metagenomics' low sensitivity may overlook low-abundance viruses. Notably, the absence of histopathological correlation and pathogen isolation means that we cannot definitively establish a causal relationship between the identified microbes and the observed pneumonia. Future studies employing histopathology, microbial culture, and *in situ* hybridization are essential to confirm the tissue tropism and pathogenic role of these microbes.

In summary, this study employed viral metagenomics and 2bRAD-M to investigate viral, bacterial, and fungal carriage in raccoon dog lung tissues. The results revealed substantial amounts of potentially pathogenic and opportunistic pathogens, underscoring raccoon dogs as potential carriers posing public health risks. Notably, a novel raccoon dog-associated TTV was identified for the first time in lung tissue.

Data availability statement

The datasets presented in this study can be found in online repositories. The names of the repository/repositories and accession number(s) can be found in the article/Supplementary material.

Ethics statement

The animal studies were approved by Animal Welfare and Ethics Committee at Laboratory Animal Center of Hebei Agriculture University. The studies were conducted in accordance with the local legislation and institutional requirements. Written informed consent was obtained from the owners for the participation of their animals in this study.

Author contributions

WL: Writing – original draft. XL: Data curation, Writing – review & editing. JC: Writing – review & editing, Methodology. JieL: Formal analysis, Writing – review & editing. JinL: Data curation, Writing – review & editing. YW: Investigation, Writing – review & editing. WY: Writing – review & editing. ER: Writing – review & editing.

Funding

The author(s) declare that financial support was received for the research and/or publication of this article. This work was supported by the Technological Innovation Center for Fur Animal Breeding of Hebei from Hebei Province in China (247790459H) and the earmarked fund for Hebei Agriculture Research System (HARS) (HBCT2024280201).

Conflict of interest

The authors declare that the research was conducted in the absence of any commercial or financial relationships that could be construed as a potential conflict of interest.

Generative AI statement

The author(s) declare that no Gen AI was used in the creation of this manuscript.

Any alternative text (alt text) provided alongside figures in this article has been generated by Frontiers with the support of artificial intelligence and reasonable efforts have been made to ensure accuracy, including review by the authors wherever possible. If you identify any issues, please contact us.

Publisher's note

All claims expressed in this article are solely those of the authors and do not necessarily represent those of their affiliated organizations, or those of the publisher, the editors and the reviewers. Any product that may be evaluated in this article, or claim that may be made by its manufacturer, is not guaranteed or endorsed by the publisher.

Supplementary material

The Supplementary material for this article can be found online at: https://www.frontiersin.org/articles/10.3389/fmicb.2025.1677761/full#supplementary-material

References

Albini, S., Marti, H., Imkamp, F., and Borel, N. (2023). Update on the zoonotic potential of Chlamydia. *Schweiz. Arch. Tierheilkd.* 165, 165–160. doi: 10.17236/sat00387

Al-Hassan, L. L., and Al-Madboly, L. A. (2020). Molecular characterisation of an Acinetobacter baumannii outbreak. *Infect. Prev. Pract.* 2:100040. doi: 10.1016/j.infpip.2020.100040

Bankevich, A., Nurk, S., Antipov, D., Gurevich, A. A., Dvorkin, M., Kulikov, A. S., et al. (2012). SPAdes: a new genome assembly algorithm and its applications to single-cell sequencing. *J. Comput. Biol.* 19, 455–477. doi: 10.1089/cmb.2012.0021

Biagini, P., et al. Family Anelloviridae. In Virus Taxonomy: Ninth Report of the International Committee on Taxonomy of Viruses, 331–341 (2011).

Brenner, D. J., Hollis, D. G., Moss, C. W., English, C. K., Hall, G. S., Vincent, J., et al. (1991). Proposal of Afipia gen. Nov., with Afipia felis sp. nov. (formerly the cat scratch disease bacillus), Afipia clevelandensis sp. nov. (formerly the Cleveland Clinic Foundation strain), Afipia broomeae sp. nov., and three unnamed genospecies. *J. Clin. Microbiol.* 29, 2450–2460. doi: 10.1128/jcm.29.11.2450-2460.1991

Chiu, C. H., Su, L. H., and Chu, C. (2004). Salmonella enterica serotype Choleraesuis: epidemiology, pathogenesis, clinical disease, and treatment. *Clin. Microbiol. Rev.* 17, 311–322. doi: 10.1128/CMR.17.2.311-322.2004

Crestani, C., Forde, T. L., Bell, J., Lycett, S. J., Oliveira, L. M. A., Pinto, T. C. A., et al. (2024). Genomic and functional determinants of host spectrum in group B Streptococcus. *PLoS Pathog.* 20:e1012400. doi: 10.1371/journal.ppat.1012400

Ericsson, A. C., Personett, A. R., Grobman, M. E., Rindt, H., and Reinero, C. R. (2016). Composition and predicted metabolic capacity of upper and lower airway microbiota of healthy dogs in relation to the fecal microbiota. *PLoS One* 11:e0154646. doi: 10.1371/journal.pone.0154646

Fastrès, A., Taminiau, B., Vangrinsven, E., Tutunaru, A. C., Moyse, E., Farnir, F., et al. (2019). Effect of an antimicrobial drug on lung microbiota in healthy dogs. *Heliyon.* 5:e02802. doi: 10.1016/j.heliyon.2019.e02802

Guan, Y., Zheng, B. J., He, Y. Q., Liu, X. L., Zhuang, Z. X., Cheung, C. L., et al. (2003). Isolation and characterization of viruses related to the SARS coronavirus from animals in southern China. *Science (New York, N.Y.)* 302, 276–278. doi: 10.1126/science.1087139

He, W. T., Hou, X., Zhao, J., Sun, J., He, H., Si, W., et al. (2022). Virome characterization of game animals in China reveals a spectrum of emerging pathogens. *Cell* 185, 1117–1129.e8. doi: 10.1016/j.cell.2022.02.014

Huang, T., Zhang, M., Tong, X., Chen, J., Yan, G., Fang, S., et al. (2019). Microbial communities in swine lungs and their association with lung lesions. *Microb. Biotechnol.* 12, 289–304. doi: 10.1111/1751-7915.13353

Jiang, N., Liu, H., Wang, P., Huang, J., Han, H., and Wang, Q. (2019). Illumina MiSeq sequencing investigation of microbiota in bronchoalveolar lavage fluid and cecum of the swine infected with PRRSV. *Curr. Microbiol.* 76, 222–230. doi: 10.1007/s00284-018-1613-y

Jin, S. S., Wang, W. Q., Jiang, Y. H., Yu, Y. T., and Wang, R. L. (2025). A comprehensive overview of Klebsiella pneumoniae: resistance dynamics, clinical manifestations, and therapeutic options. *Infect. Drug Resist.* 18, 1611–1628. doi: 10.2147/IDR.S502175

Li, J., Liu, W., Tian, F., Tu, Q., Xia, X., Liu, C., et al. (2021). First report of norovirus sequences isolated from raccoon dogs in mainland China. *Virus Res.* 305:198546. doi: 10.1016/j.virusres.2021.198546

Li, Z., Wang, X., Di, D., Pan, R., Gao, Y., Xiao, C., et al. (2021). Comparative analysis of the pulmonary microbiome in healthy and diseased pigs. *Mol. Gen. Genomics.* 296, 21–31. doi: 10.1007/s00438-020-01722-5

Lynch, S. A., and Helbig, K. J. (2021). The complex diseases of Staphylococcus pseudintermedius in canines: where to next? *Vet. Sci.* 8:11. doi: 10.3390/vetsci8010011

Maddi, A., Sabharwal, A., Violante, T., Manuballa, S., Genco, R., Patnaik, S., et al. (2019). The microbiome and lung cancer. *J. Thorac. Dis.* 11, 280–291. doi: 10.21037/jtd.2018.12.88

Manzin, A., Mallus, F., Macera, L., Maggi, F., and Blois, S. (2015). Global impact of torque Teno virus infection in wild and domesticated animals. *J. Infect. Dev. Ctries.* 9, 562–570. doi: 10.3855/jidc.6912

McMurdie, P. J., and Holmes, S. (2014). Waste not, want not: why rarefying microbiome data is inadmissible. *PLoS Comput. Biol.* 10:e1003531. doi: 10.1371/journal.pcbi.1003531

Miao, Y., Zhao, X., Lei, J., Ding, J., Feng, H., Wu, K., et al. (2023). Characterization of lung microbiomes in pneumonic Hu sheep using culture technique and 16S rRNA gene sequencing. *Animals* 13:2763. doi: 10.3390/ani13172763

Nishizawa, T., Okamoto, H., Konishi, K., Yoshizawa, H., Miyakawa, Y., and Mayumi, M. (1997). A novel DNA virus (TTV) associated with elevated transaminase levels in posttransfusion hepatitis of unknown etiology. *Biochem. Biophys. Res. Commun.* 241, 92–97. doi: 10.1006/bbrc.1997.7765

Qi, X., Li, X., Rider, P., Fan, W., Gu, H., Xu, L., et al. (2009). Molecular characterization of highly pathogenic H5N1 avian influenza a viruses isolated from raccoon dogs in China. *PLoS One* 4:e4682. doi: 10.1371/journal.pone.0004682

Qian, Z., Shou-Yu, G., Feng-Xia, Z., Peng, Y., Wen-Jian, S., Jian-Liang, L., et al. (2021). Molecular characteristics of H9N2 influenza viruses isolated from farmed raccoon dogs and arctic foxes in China. *Res. Vet. Sci.* 135, 542–546. doi: 10.1016/j.rvsc.2020.11.006

Sebastian, A., Gupta, N., Banerjee, B., Vandana, K. E., Mukhopadhyay, C., Praveen Kumar, T., et al. (2025). Ralstonia pickettii bacteremia: a retrospective review of records. *Indian J. Med. Microbiol.* 53:100786. doi: 10.1016/j.ijmmb.2024.100786

Shao, X. Q., Wen, Y. J., Ba, H. X., Zhang, X. T., Yue, Z. G., Wang, K. J., et al. (2014). Novel amdoparvovirus infecting farmed raccoon dogs and arctic foxes. *Emerg. Infect. Dis.* 20, 2085–2088. doi: 10.3201/eid2012.140289

Sharma Ghimire, P., Joshi, D. R., Tripathee, L., Chen, P., Sajjad, W., and Kang, S. (2022). Seasonal taxonomic composition of microbial communal shaping the bioaerosols milieu of the urban city of Lanzhou. *Arch. Microbiol.* 204:222. doi: 10.1007/s00203-022-02832-x

Song, T., Hao, J., Zhang, R., Tang, M., Li, W., Hui, W., et al. (2019). First detection and phylogenetic analysis of porcine circovirus type 2 in raccoon dogs. *BMC Vet. Res.* 15:107. doi: 10.1186/s12917-019-1856-2

Sun, Z., Huang, S., Zhu, P., Tzehau, L., Zhao, H., Lv, J., et al. (2022). Species-resolved sequencing of low-biomass or degraded microbiomes using 2bRAD-M. *Genome Biol.* 23:36. doi: 10.1186/s13059-021-02576-9

Vientós-Plotts, A. I., Ericsson, A. C., Rindt, H., and Reinero, C. R. (2019). Respiratory dysbiosis in canine bacterial pneumonia: standard culture vs. microbiome sequencing. *Front. Vet. Sci.* 6:354. doi: 10.3389/fvets.2019.00354

Wang, D. (2025). Statistics and market analysis of mink, fox, and raccoon dog skins produced in China in 2024. *Beijing Leather* 50, 74–76.

Wang, X., Wang, H., Zhang, J., Huang, Y., Wu, Y., Wang, Y., et al. (2025). Morphological variability of Escherichia coli colonizing human wounds: a case report. *BMC Infect. Dis.* 25:440. doi: 10.1186/s12879-025-10484-7

Wang, Y., Yan, S., Ji, Y., Yang, Y., Rui, P., Ma, Z., et al. (2022). First identification and phylogenetic analysis of porcine circovirus type 4 in fur animals in Hebei, China. *Animals* 12:3325. doi: 10.3390/ani12233325

Wang, X., Zheng, Y., Chen, X., Peng, C., Zhou, S., Shen, S., et al. (2023). 2bRAD-M reveals the difference in microbial distribution between cancerous and benign ovarian tissues. *Front. Microbiol.* 14:1231354. doi: 10.3389/fmicb.2023.1231354

Wu, X., Wei, X., Li, X., Deng, J., and Zhang, J. (2022). Diversity of fungi and bacteria in bronchoalveolar lavage fluid during development of chronic obstructive pulmonary disease. *Jpn. J. Infect. Dis.* 75, 560–568. doi: 10.7883/yoken.JJID.2022.153

Yang, S., He, Y., Chen, X., Kalim, U., Wang, Y., Yang, S., et al. (2021). Viral metagenomics reveals diverse viruses in the feces samples of raccoon dogs. *Front Vet Sci.* 8:693564. doi: 10.3389/fvets.2021.693564

Yuan, X. Y., Liu, H. Z., Liu, J. F., Sun, Y., and Song, Y. (2021). Pathogenic mechanism, detection methods and clinical significance of group B Streptococcus. *Future Microbiol.* 16, 671–685. doi: 10.2217/fmb-2020-0189

Zheng, X., Liu, F., Ma, Q., Li, J., and Ma, H. (2024). Rothia dentocariosa endocarditis with brain abscess and splenic abscess: case report and brief review. *Front. Cardiovasc Med.* 11:1370736. doi: 10.3389/fcvm.2024.1370736

Zhu, Y., Liu, J., Guo, K., Qiu, J., Cheng, Z., Liu, F., et al. (2021). Outbreak of a novel disease caused by Staphylococcus pseudintermedius in raccoon dogs (Nyctereutes procyonoides). *Transbound. Emerg. Dis.* 68, 1995–2004. doi: 10.1111/tbed.13847

frontiers | Frontiers in Microbiology

TYPE Original Research
PUBLISHED 20 October 2025
DOI 10.3389/fmicb.2025.1665966

OPEN ACCESS

EDITED BY
Lei Deng,
Chinese Academy of Agricultural Sciences, China

REVIEWED BY
Francesco Asnicar,
University of Trento, Italy
Adedolapo Aminat Rauff-Adedotun,
North-Eastern University, Nigeria

*CORRESPONDENCE
Eleni Gentekaki
✉ gentekaki.e@unic.ac.cy
Anastasios D. Tsaousis
✉ tsaousis.anastasios@gmail.com
Funda Dogruman-Al
✉ alfunda@gazi.edu.tr

RECEIVED 14 July 2025
ACCEPTED 30 September 2025
PUBLISHED 20 October 2025

CITATION
Akdur-Öztürk E, Al-Adilee YMS, Edwards W, Gentekaki E, Tsaousis AD and Dogruman-Al F (2025) *Blastocystis* across humans, animals and the environment in rural Türkiye, and relationships with the human intestinal microbiome. *Front. Microbiol.* 16:1665966. doi: 10.3389/fmicb.2025.1665966

Blastocystis across humans, animals and the environment in rural Türkiye, and relationships with the human intestinal microbiome

Eylem Akdur-Öztürk[1], Yaseen Majid Salman Al-Adilee[2,3], William Edwards[2], Eleni Gentekaki[4]*, Anastasios D. Tsaousis[2]* and Funda Dogruman-Al[5]*

[1]Department of Medical Parasitology, Faculty of Medicine, Çukurova University, Adana, Türkiye, [2]School of Natural Sciences, University of Kent, Canterbury, United Kingdom, [3]Department of Medical Microbiology, College of Medicine, Ninevah University, Mosul, Iraq, [4]Department of Veterinary Medicine, University of Nicosia School of Veterinary Medicine, Nicosia, Cyprus, [5]Division of Parasitology, Department of Microbiology, Gazi University, Ankara, Türkiye

Blastocystis is a globally prevalent intestinal protist commonly found in humans and animals, yet its role in health and disease remains ambiguous. This is a cross-sectional study of *Blastocystis* in rural Türkiye, examining 124 human, 305 livestock (cattle, sheep, goats), and 40 environmental samples using culture/microscopy, qPCR, and sequencing. We further explored associations between *Blastocystis* and population parameters, along with gut microbiota profiles. Using a combination of sequencing and microscopy, the overall prevalence was high, at 76.6% in humans, 71%–78% in livestock, and 38% in environmental samples. Subtypes ST1–ST4 were detected in humans, with ST3 being most frequent. Livestock harbored ST10 predominantly, with goats showing high carriage of ST24. Several subtypes (e.g., ST25, ST26) were recorded in livestock for the first time in Türkiye. Body mass index (BMI) was significantly associated with *Blastocystis* colonization, with lean individuals having higher carriage. Contrary to other studies, individuals with ST4 exhibited reduced bacterial diversity and altered microbial composition, suggesting subtype-specific interactions. By combining parasitology, microbiome, and environmental analysis, this study offers an overview of *Blastocystis* diversity and distribution in rural Türkiye. This work provides a foundation for future integrative research approaches to explore the ecological role of *Blastocystis* and its subtypes, potential health implications, and interactions with other microbes in rural and global contexts.

KEYWORDS

***Blastocystis*, gut microbiome, transmission dynamics, rural, microbial eukaryotes, Türkiye**

Introduction

Blastocystis is a common intestinal protist found in humans and various animals, including mammals, birds, and reptiles. It is one of the two stramenopiles known to inhabit the human gut (Hublin et al., 2021; Nguyen et al., 2023). Despite its widespread presence, its role in health and disease remains unclear, making it a subject of ongoing research (Centers for Disease Control and Prevention [CDC], 2025).

The organism exists in multiple forms–vacuolar, granular, amoeboid, cystic, and less commonly avacuolar and multivacuolar –transmitting through the fecal-oral route via cysts shed in feces (Hublin et al., 2021; Tan, 2008). *Blastocys*tis is estimated to colonize nearly one billion people globally (Stensvold and Clark, 2020) with prevalence varying from 5%–20% in developed regions to over 30% in developing areas (Tan, 2008; Khorshidvand et al., 2021). Studies of human populations across diverse geographic regions suggest that *Blastocystis* colonization is associated with distinct gut microbial profiles and higher levels of microbial diversity. It has also been associated with increases in the abundance of beneficial bacterial taxa such as *Ruminococcaceae* and *Prevotella* (Audebert et al., 2016; Beghini et al., 2017; Tito et al., 2019). This is in contrast to the reduced microbial diversity typically observed in individuals with gastrointestinal diseases such as inflammatory bowel disease. Morever, *Blastocys*tis has been reported to be associated with healthy dietary patterns, and lower rates of obesity, cardiometabolic risk, and mortality (Piperni et al., 2024). These findings suggest that *Blastocystis* may be indicative of healthy gut microbiota though the underlying mechanisms of how this might be achieved remain unknown (Audebert et al., 2016; Beghini et al., 2017; Nieves-Ramírez et al., 2018; Kodio et al., 2019; Tito et al., 2019; Alzate et al., 2020; Castañeda et al., 2020; Even et al., 2021).

Based on the diversity of *SSU* rRNA, at least 44 *Blastocystis* subtypes (STs) have been identified. Among these, 16 STs, including ST1–ST10, ST12, ST14, ST16, ST23, ST35, and ST41, have been identified in humans, with ST1–ST4 being the most frequently reported (McCain et al., 2023; Koehler et al., 2024; Santin et al., 2024). In Türkiye, *Blastocystis* prevalence ranged from 2.1 to 51% across studies, with ST3 (47.9%) as the dominant subtype (Malatyalı et al., 2023). Studies on livestock (i.e., cattle, sheep, water buffaloes, and chickens), and companion animals (i.e., dogs, cats, and horses) together with those on environmental sources indicate carriage rates of 3.65% to over 60%, but transmission dynamics remain poorly understood (Onder et al., 2021; Tavur and Önder, 2022).

Recent data suggest that there is interplay of body mass index (BMI) and *Blastocystis* colonization, with several studies reporting higher *Blastocystis* presence in lean individuals (Beghini et al., 2017; Asnicar et al., 2021; Malatyali et al., 2021; Matovelle et al., 2022), while one study found a higher *Blastocystis* prevalence in obese individuals, though the obese sample size was small (Jinatham et al., 2021). Other studies reported prevalence exceeding 40% in obese populations but the absence of lean controls limits interpretation (Caudet et al., 2022a,b).

Zoonotic transmission studies suggest that certain subtypes may spread between humans and animals, but it remains unclear whether these same strains establish colonization or are merely transient (Tsaousis et al., 2025; Abdo et al., 2021; Ruang-areerate et al., 2021; Rudzińska et al., 2022). Recent studies have reported molecular detection of *Blastocystis* in soil (Jinatham et al., 2021; Blackburn et al., 2024), with certain subtypes shared between human and environmental samples (Jinatham et al., 2021). These findings suggest soil as a transmission route, adding another layer of complexity to its transmission. Hence, an integrative approach that considers humans, animals, and the environment, is essential for shedding light to the organism's epidemiology (Tsaousis et al., 2024). The first study to investigate *Blastocystis* occurrence in this context took place in a rural community in Thailand (Jinatham et al., 2021). Nevertheless studies from diverse regions are essential to assess potential geographic or rural/urban differences. To address this gap, we conducted a study in a rural area of Türkiye. We aimed to explore diversity, distribution, and possible transmission dynamics of *Blastocystis* in humans, livestock (cattle, sheep, goats), and environmental samples from Seyhan Dam Lake in Kırıklı village using microscopy and molecular methods. Moreover, we investigated the relationship between *Blastocystis* colonization and human gut microbiota composition.

Materials and methods

This is a cross-sectional study conducted in Kırıklı village located in the Seyhan Dam Lake basin, Adana, between October and November 2023. Human, animal (cattle, sheep, and goats), and environmental (water and mud) samples were collected and analyzed using microscopy and molecular methods.

Ethics statement and research permissions

The ethics committee of Çukurova University approved this study for sample collection (approval number 49/135) and microbiome analysis (approval number 39/147). Ethical rules were according to the Declaration of Helsinki. All participants were informed about the nature of the project. Signed consent was obtained from the participants and the parents of the child participants.

For the environmental samples, research permission was obtained from the Adana Governorate and Karaisalı District Directorate of Agriculture and Forestry for the use of dam lake materials (approval number E-12757666-140.03).

Study area

This study was conducted in Kırıklı, a village with a population of 582, located in Karaisalı district of Adana province, Türkiye (37 °10′N, 35 °14′E), 35 km away from the city center (Figure 1). The village is located within the Mediterranean climate zone, characterized by hot, dry summers and mild, rainy winters. The settlement, whose residents derive their living from farming and animal husbandry, is surrounded by agricultural lands, forest patches, grazing areas and tributaries of the Seyhan Dam Lake. Seasonal animal movements are common in the areas surrounding the village. The Seyhan Dam was constructed around 70 years

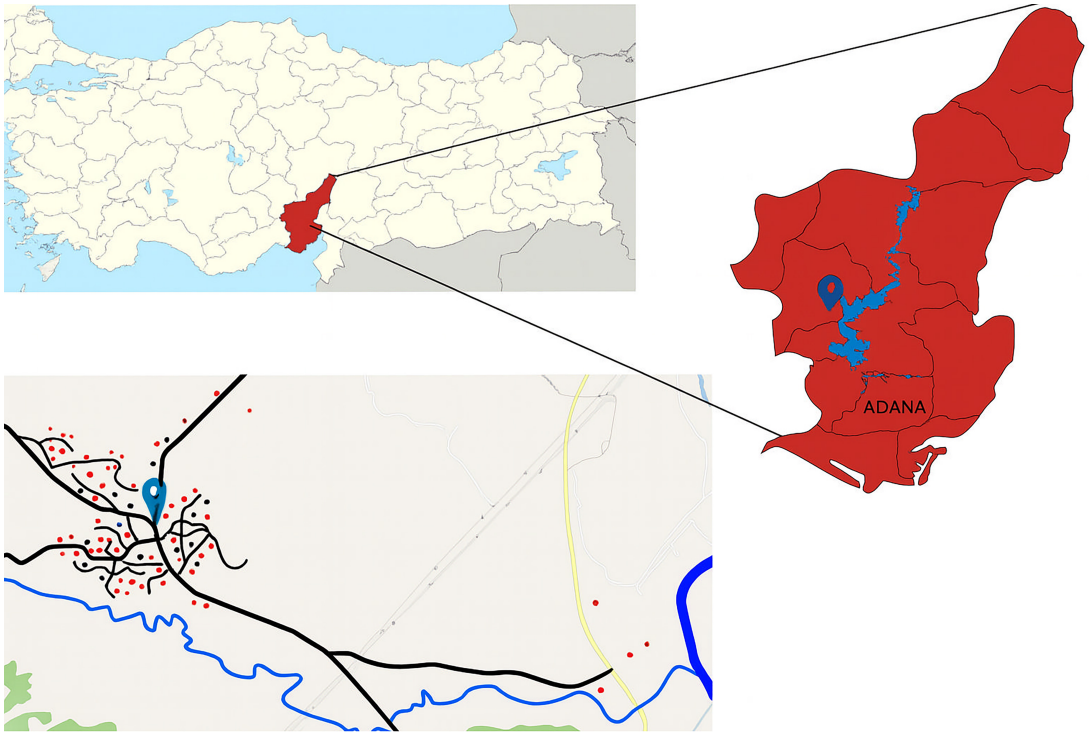

FIGURE 1
Map of Türkiye (top left), highlighting the sampling province in red. The bottom image shows sampling areas in Kırıklı Village (village's location marked with a pin). Red circles represent households where both human and animal samples were collected; black circles represent households where only human samples were collected.

ago and is located 12 km from the Kırıklı village (Supplementary Figure 1). Seyhan Dam Lake passes through the border of the village in the study area and is used to irrigate agricultural areas and animals. The water level recedes during November and December. Thus, the area becomes accessible for recreational activities, such as picnic and camping. It is also used as pasture for grazing animals, where they defecate. The area fills with water again in April and May due to snowmelt. This region was selected as a model site for the One Health approach due to its geographical location, climate, proximity to the Seyhan Lake Dam (used for livestock watering and field irrigation) substantial animal populations, rich pastures, and a population primarily engaged in agriculture and animal husbandry. Furthermore, the area has the potential to represent the human-animal-environment cycle of intestinal parasites.

Sample collection

Human, animal (cattle, sheep and goats) and environmental samples were collected and preserved in a 1:2 ratio DNA/RNA Shield™ (ZymoResearch, Freiburg, Germany) until further analysis.

Human fecal samples

The "purposive sampling method," commonly utilized in biological research and modified accordingly, was used (Işıklar, 2018) to determine the number of human samples for this study. All participants appeared to be healthy, with no cases of diarrhea or bloody stool. Samples were randomly collected from 124 participants across 64 households. Of these, 90 participants belonged to households actively engaged in animal husbandry, while the other 34 participants were from households without animals and reported not owning any animals for at least 6 months. These two groups were evaluated based on whether they were engaged in animal husbandry or not. There were no cases of diarrhea or bloody stool. Each participant was provided with a labeled, sterile fecal collection container.

Animal fecal samples

A total of 305 fecal samples were collected from 89 cattle, 151 sheep, and 65 goats belonging to the individuals participating in the study. The number of samples for each animal was calculated using the "proportional stratified sampling method" (Işıklar, 2018). Therefore, the number of animals sampled per household varied according to the household's animal population. To minimize environmental contamination, samples were collected by direct observation of the animals' defecation during morning feeding, grooming, or rest, so that only a single sample was collected from each animal. Individual samples were collected in pre-labeled containers.

Environmental samples

Twenty-four dam lake water and 16 mud samples were collected directly from the closest parts of the Seyhan Dam lake, where human activities (picnics, camping, fishing, etc.) and animal grazing occurred and from areas irrigated for livestock and agricultural use. Water samples were collected from the dam

lake, its tributaries, and from standing water in 1-liter sterile containers. These were left to stand on a flat surface at room temperature overnight (Jinatham et al., 2021), and the supernatant was drained until 50 ml of sediment was left with a manual drainage system. Then, the sediment was transferred to 15 ml tubes and centrifuged at 500 *g* for 10 min, the supernatant was drained, and the sediment remaining at the bottom was preserved in a 1:2 ratio DNA/RNA shield until further analysis. Mud samples were taken from the mentioned locations and directly preserved in a 1:2 ratio DNA/RNA shield until further analysis.

Screening of *Blastocystis*

Culture

Approximately 200 mg were taken from all fecal samples and inoculated into 2 ml of Jones' medium containing 10% horse serum (Stensvold et al., 2007; Sarzhanov et al., 2021). Similarly, sediment obtained from water and mud samples processed as described in the Environmental Samples section was also inoculated into the medium. After 48–72 h of incubation at 37 °C, culture samples were examined using a light microscope (Supplementary Figure 2) to determine whether *Blastocystis* was present.

Genomic DNA Extraction

DNA extraction was performed by taking 200 µl of a thoroughly vortexed DNA/RNA shield-sample mixture, and the PureLink™ Microbiome DNA Purification Kit (Thermo Fisher Scientific, Carlsbad, CA, USA) was used according to the manufacturer's protocol.

qPCR (Real-time PCR)

Blastocystis was identified using specific primer sequences (BL18SPPF1 _5′-AGTAGTCATACGCTCGTCTCAAA-3′ and BL 18SR2PP 5 ′-TCTTCGTTACCCGTTACTGC-3′) to amplify a conserved region of SSU rRNA gene (330 bp) by qPCR (Poirier et al., 2011). A negative control (nuclease-free water) and a positive control (genomic DNA of *Blastocystis*) were used in every qPCR run. The reaction mixtures (10 µl) contained 5 µl of Luna Taq Universal (New England Biolabs, Ipswich, MA, USA), 0.5 µl of a 10 µM primer pair, and 2 µl of template DNA. qPCR protocol included; pre-denaturation step: 95 °C for 5 min; followed by 49 cycles of denaturation step: 95 °C for 5 s, annealing step, 68 °C for 10 s, extension step: 72 °C for 15 s and final extension at 72 °C for 10 min. Reactions were set up in 96-well plates in a CFX96 Touch Real-Time PCR Detection System (Bio-Rad, United States).

Polymerase chain reaction and phylogenetic analysis

Nested PCR was performed on samples positive for *Blastocystis* by either culturing (microscopy) or qPCR methods. The primer oligonucleotide sequences of nested PCR are detailed in Supplementary Table 1. First and second-round PCR protocols were set up as follows: pre-denaturation step: 95 °C for 5 min; 30 cycles of: denaturation step: 94 °C for 1 min; annealing step: 59 °C and 50 °C (first and second-round PCR, respectively) for 1 min; extension step: 72 °C for 1 min and a final extension step: 72 °C for 10 min. DNA sequencing was performed by using internal primers for each second-round PCR-positive sample (Cologne, Germany).

The sequences obtained by Sanger sequencing were manually inspected and used as queries to perform BLAST searches for comparisons with reference gene sequences in the National Center for Biotechnology Information (NCBI). For the phylogenetic analysis, a dataset spanning *Blastocystis* diversity, as well as newly derived sequences, was constructed. To avoid redundancy, groups of highly similar sequences (% divergence <98%) were collapsed and only one or two representatives were included in the dataset. Sequences were aligned using MUSCLE v5. Ambiguous positions were removed using Trimal v1.4. Maximum likelihood analysis was performed using IQTREE (Nguyen et al., 2015).

Microbiome sequencing

High-throughput amplicon sequencing was outsourced to Novogene, following a modified version of the protocol described by Caporaso et al., 2011. One nanogram of extracted DNA was used, fragmented, and adapted for paired-end sequencing. The 16S rRNA gene was amplified using the primer pair 515F (GTGCCAGCMGCCGCGGTAA) and 907R (CCGTCAATTCCTTTGAGTTT), which targets the V3-V4 hypervariable region. Sequencing was performed on the Illumina NovaSeq platform.

Raw sequencing reads were processed using the Lotus2 pipeline (Özkurt et al., 2022). The workflow included several key steps: chimera detection and removal were conducted using Minimap2 (Li, 2018), which was also employed to identify and exclude off-target human DNA reads by performing a BLAST search against the Genome Reference Consortium Human Build 38.p14 (0 contaminated samples detected). The trimmed reads were then clustered into Amplicon Sequence Variants (ASVs) with a maximum of one nucleotide difference, using the Divisive Amplicon Denoising Algorithm 2 (DADA2) (Callahan et al., 2016). ASVs were taxonomically classified through BLAST searches against the GreenGenes2 (GG2) database (DeSantis et al., 2006).

Statistical analysis

The data obtained in this study was statistically analyzed using IBM Statistical Package for the Social Sciences (SPSS) version 29 software. A global chi-square test was used to assess whether the distributions of gender and age groups (0–18 years, 19–39 years, 40–59 years, and 60 years and above) differed significantly ($p < 0.05$). For microbiome analysis, the Shapiro-Wilk test was used to assess the normality of data distribution. Normally distributed data were analyzed using ANOVA, followed by the Tukey's HSD test for pairwise comparisons. For non-normally distributed data, the Kruskal-Wallis test was applied, followed by the Dunn test (with Bonferroni adjustment) for multiple comparisons.

Statistical analyses and data visualization were performed using R Studio 4.2.3. To account for variations in sequencing depth, data were first rarefied to 60,000 reads based on the species accumulation curve (Supplementary Figure 1). Rarefaction resulted in the exclusion of one sample. The relative abundance of each genus was then calculated for each sample, and a heatmap was generated to visualize the results. Alpha diversity was assessed using diversity indices, including Shannon and Simpson, and richness estimators including Chao1 and observed taxa, implemented in the Phyloseq

package. These indices were compared between *Blastocystis*-positive and *Blastocystis*-negative samples. To visualize microbiome composition, compositional bar plots were generated using the Microbiome package, including only taxa representing more than 1% of total reads. Principal Coordinate Analysis (PCoA) based on Bray-Curtis dissimilarity was used to visualize differences in microbial community structure between *Blastocystis*-positive and *Blastocystis*-negative samples. Samples were plotted using Bray-Curtis dissimilarity matrices. PERMANOVA (Anderson, 2017) was used to test for statistical significance of group differences. Linear Discriminant Analysis Effect Size (LEfSe) (Segata et al., 2011) was applied to identify potential biomarkers discriminating *Blastocystis*-positive from *Blastocystis*-negative samples based on relative abundance profiles.

Results

Demographic characteristics of the human participants

Of the 124 participants in the study, 58 (46.8%) were female, and 66 (53.2%) were male, with an average age of 44.7 (range between 6 and 82). Of the participants, 90 out of 124 (72.6%) are actively involved in animal husbandry, and 34 (27.4%) stated being involved in caring for any animals for at least the last 6 months. Additionally, all participants declared that they drank tap water. Body mass index (BMI) was calculated for all participants who were 19 years of age or older (*n*:109) (Geifman and Rubin, 2011). Ninety-five (87.2%) of the individuals participating in the study had a BMI above 25 and were classified as overweight or obese. The remaining participants were classified as having normal weight (18.5–24.9). There were no individuals in the study who were extremely underweight (BMI < 18.5). The distribution of sociodemographic characteristics of the participants according to the presence of *Blastocystis* is shown in Table 1. A more detailed table can be found in Supplementary Table 1.

TABLE 1 Distribution of sociodemographic characteristics of participants according to the presence of *Blastocystis*.

Characteristics		Positive (*n*%)	Negative (*n*%)	Total (%)	*p* value
Gender	Female	40 (69.0%)	18 (31.0%)	58 (46.8%)	$p \approx 0.095$ $\chi 2 \approx 2.7842$
	Male	54 (81.8%)	12 (18.2%)	66 (53.2%)	
Age group	0–18	10 (66.7%)	5 (33.3%)	15 (12.1%)	$p \approx 0.79$ $\chi^2 = 1.048$
	19–39	21 (80.8%)	5 (19.2%)	26 (21.0%)	
	40–59	45 (76.3%)	14 (23.7%)	59 (47.6%)	
	60 and above	18 (75.0%)	6 (25.0%)	24 (19.4%)	
BMI*	18.5–24.9	14 (100.0%)	0 (0.0%)	14 (12.8%)	$\mathbf{p \approx 0.032}$ $\chi^2 = 6.892$
	25.0–29.9	28 (66.7%)	14 (33.3%)	42 (38.5%)	
	≥30.0	42 (79.2%)	11 (20.8%)	53 (48.6%)	
Animal husbandry	Yes	65 (72.2%)	25 (27.8%)	90 (72.6%)	$p \approx 0.129$ $\chi^2 = 2.297$
	No	29 (85.3%)	5 (14.7%)	34 (27.4%)	

*Body mass index (BMI) is calculated for ages 19 and above. Bold values indicate statistical significance ($p < 0.05$).

Blastocystis occurrence

In this study, all sample types were investigated for the presence of *Blastocystis* using culture and qPCR. A sample was considered positive when *Blastocystis* was seen microscopically (Supplementary Figure 2) in culture or when a sequence was obtained (qPCR product or PCR product). Hence, samples positive only for microscopy were included in the prevalence calculation but not subtyping. In all cases, the vacuolar form was predominantly observed microscopically and occasionally granular and amoeboid forms. In human samples, culture positivity was 70.1% (87/124). Regarding qPCR, 111/124 samples yielded a band of the expected size, however of these only 36 samples were successfully sequenced and subtyped. 28 samples were positive by both microscopy and molecular methods. Combining the two approaches, the overall positivity rate in humans in this study was 76.6% (95/124). Positivity in the 0–18 age group was 66.7% (10/15), 80.8% (21/26) in the 19–39 group, 76.3% (45/59) in the 40–59 group and 75% (18/24) in the over 60 group. Statistical analysis showed a significant association between BMI and *Blastocystis* positivity ($p < 0.05$). Though *Blastocystis* was more prevalent among individuals with normal BMI no statistical test was performed at the subgroup level. Global chi square tests revealed no statistically significant relationships between *Blastocystis* positivity and other demographic variables such as gender, occupation, and age groups ($p > 0.05$).

In animals, 66% (200/304) were culture positive. More specifically, 65.2% (58/89) of cattle were culture positive, 66.2% (100/151) of sheep, and 64.6% (42/65) of goats. Using qPCR, 100% of the samples showed a band of the expected size. Of these, 77 were successfully sequenced and subtyped (24 cattle, 35 sheep, and 17 goats). Combining the two approaches, the positivity rate was as 71% (63/89) in cattle, 73% (110/151) in sheep, and 78% (50/64) in goats.

The environmental samples showed 37.5% (15/40) positivity solely through culture. Eleven of these were water samples, while four were mud. None of the environmental samples yielded *Blastocystis* sequences.

Blastocystis subtypes

In total, 112 sequences were subtyped from humans ($n = 36$), cattle ($n = 24$), sheep ($n = 35$) and goat ($n = 17$). In multiple instances the chromoatograms showed evidence of mixed infections, as indicated by multiple peaks. To assign subtype the criteria below were followed: reasonably good quality sequence of over 300 bp and over 98% similarity in GenBank. Subtypes were identified using a combination of phylogeny and blast against GenBank and the curated database pubmlst[1] and phylogeny (Supplementary Figure 3). In the phylogenetic analysis all subtypes were monophyletic and the new sequences placed within known subtype clades. For 18 sequences, the methodologies did not agree. In pubmlst, they were identified as belonging to one of the subtypes previously comprising ST10 (i.e., ST23, ST42-ST44), perhaps due to the short length of the sequences. In the phylogenetic tree, these

1 https://pubmlst.org/bigsdb?db=pubmlst_blastocystis_seqdef&page=sequenceQuery

TABLE 2 Distribution of Blastocystis subtypes among human and animal hosts.

Host	ST1 n (%)	ST2 n (%)	ST3 n (%)	ST4 n (%)	ST5 n (%)	ST10 n (%)	ST21 n (%)	ST24 n (%)	ST25 n (%)	ST26 n (%)	ST42 n (%)	ST43 n (%)	ST44 n (%)	Total n
Human	11 31%	11 31%	12 33%	2 6%										36
Cattle						8 33.3%			2 8.3%	3 12.5%	5 20.8%	1 4.1%	5 20.8%	24
Sheep				1 2.9%	2 5.7%	17 48.6%		5 14.3%		4 11.4%		3 8.6%	3 8.6%	35
Goat						5 29.4%	2 11.8%	7 41.2%		1 5.9%		1 5.9%	1 5.9%	17
Total	11	11	12	3	2	30	2	12	2	8	5	5	9	112

placed within the clade comprising ST10 in the past, but jumped within the clade depending on taxon sampling. Of these, 13 were from cattle, three from sheep and two from goats. These sequences were not assigned a subtype, only the clade with which they cluster.

In total, 13 subtypes were identified: ST1, ST2, ST3, ST4, ST5, ST10, ST21, ST24, ST25, ST26, ST42, ST43, and ST44. In humans, four subtypes were detected, namely ST1, ST2, ST3, and ST4. The most abundant subtype was ST3 (33%, 12/36), followed by ST1, and ST2 (each at 31%, 11/36) and ST4 (6%, 2/36). In animals, ten subtypes were detected: ST4, ST5, ST10, ST21, ST24, ST25, ST26, ST42, ST43, and ST44. In cattle, ST10 (n = 8), ST25 (n = 2), ST26 (n = 3), ST42 (n = 5), ST43 (n = 1), and ST44 (n = 5) were identified. In sheep, ST4 (n = 1), ST5 (n = 2), ST10 (n = 17), ST24 (n = 5), ST26 (n = 4), ST43 (n = 3), and ST44 (n = 3) were detected. Goat samples were positive for ST10 (n = 5), ST21 (n = 2), ST24 (n = 7), ST26 (n = 1), ST43 (n = 1), and ST44 (n = 1). Table 2 showed the distribution of *Blastocystis* subtypes among human and animal host. ST10 was the most abundant in cattle and sheep, while in goats ST24 was. ST10, ST26, ST43, and ST44 were shared by all three ruminant species (Figure 2). ST25 and ST42 were detected only in cattle, while ST21 was detected only in goats. ST24 was detected in goats and sheep, but not in cattle.

At the household level, subtype analysis was performed on more than one individual from five households, and no common subtype (ST) was identified among individuals within the same household. However, common subtypes were reported among livestock within the same household.

Microbiome analysis

Using Shannon (Figure 3A), Simpson (Figure 3B), Chao1 (Figure 3C) and observed taxa (Figure 3D), there were no significant differences in bacterial alpha diversity between *Blastocystis* positive and *Blastocystis* negative samples, as confirmed by ANOVA/Kruskal-Wallis tests. The same metrics were then

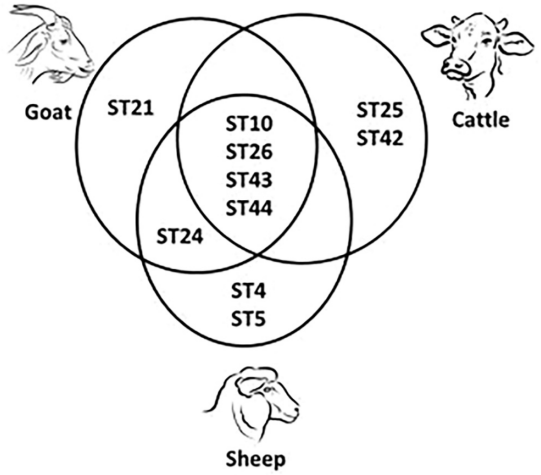

FIGURE 2
Shared and unique *Blastocystis* subtypes (ST) detected in cattle, sheep and goats.

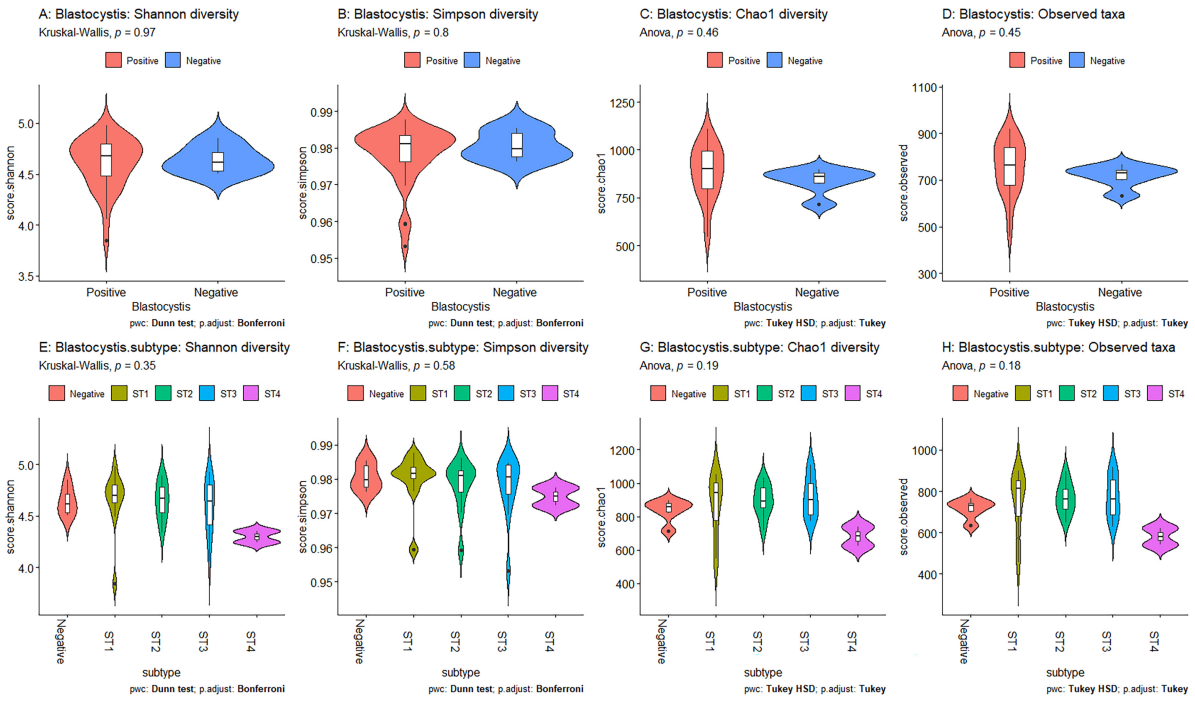

FIGURE 3
Comparisons of averaged diversity metrics by *Blastocystis* colonization status and subtype. The metrics include Shannon **(A, E)**, Simpson **(B, F)**, Chao1 **(C, G)** and Observed taxa **(D, H)**. Violin plots in panels **A–D** compare *Blastocystis*-positive (red) and *Blastocystis*-negative (blue) samples. Panels **E–H** compare diversity across *Blastocystis* subtypes (colored by subtype). Statistical testing was performed using ANOVA with Tukey's HSD for normally distributed data and Kruskal-Wallis with Dunn's test for non-normally distributed data. *P*-values > 0.05 indicate non-significance.

compared at the subtype level (ST1-ST4) (Figure 3E–H). ST1 had the highest average diversity score average across all metrics relative to the *Blastocystis* negative samples, while ST4 samples showed a trend toward lower diversity and richness, but these results were not significant. Comparison of the composition of samples grouped by *Blastocystis* presence is shown in Figure 4 (individual samples are shown in Supplementary Figure 2). At the genus level, *Blastocystis positive* samples had a higher relative abundance of *Prevotella* and *Bifidobacterium* and relatively decreased *Lachnospiraceae* (Figure 4A). When samples were grouped by subtype, ST4 had a notable reduction in *Prevotella* and a marked increase in *Bifidobacterium* along with an increase in *Agathobacter* (Figure 4B). At the phylum level, *Blastocystis positive* samples showed an increase in *Bacteroidota* and a decrease in *Proteobacteria* (Figure 4C). When the samples were grouped by *Blastocystis* subtype, ST4 showed markedly lower relative abundance of *Bacteroidota*, and an increase in Actinobacteriota (Figure 4D). To assess differences in overall bacterial community composition principal coordinate analysis (PCoA) was used based on Bray-Curtis dissimilarities (Figure 5). PERMANOVA testing indicated that the community structure differed significantly between *Blastocystis* positive and *Blastocystis* negative groups, although the effect size was small (p = 0.037, R^2 = 0.046), (Figure 5A). When samples were grouped by *Blastocystis* subtype (Figure 5B), PERMANOVA testing also revealed significant differences in community composition (p = 0.03, R^2 = 0.136), indicating a stronger effect size compared to colonization status alone. Pairwise Adonis was used to assess differences in community composition between groups. A significant difference was observed between ST3 and *Blastocystis* negative samples (Supplementary Table 2). To identify taxa associated with *Blastocystis* colonization status, Linear discriminant analysis Effect Size (LEFsE) was used. Linear discriminant analysis (LDA) scores with an absolute value of 2 were considered indicative of discriminative features. Taxa were aggregated to the genus and family levels (Figure 6). Those with high LDA scores contributed most strongly to distinguishing *Blastocystis* positive from *Blastocystis* negative samples. In total, 38 genera were identified as discriminatory for *Blastocystis* negative samples, while 13 genera were discriminatory for *Blastocystis* positive samples. At the family level, these numbers were 5 and 13, respectively.

Discussion

The current study presents the first integrative investigation of *Blastocystis* in rural Türkiye, examining human, livestock, and environmental samples to assess its prevalence, subtype distribution, and gut microbiome composition. Anthropometric data from human participants revealed a significant association between BMI and *Blastocystis* colonization in agreement with previous studies (Beghini et al., 2017; Asnicar et al., 2021; Malatyali et al., 2021; Matovelle et al., 2022), with lean individuals having the highest *Blastocystis* positivity rate. A few studies have found a high occurrence of *Blastocystis* in obese individuals (Jinatham et al., 2021; Caudet et al., 2022a,b). Nonetheless, the organism's presence has been associated with bacterial taxa linked to improved cardiometabolic health profiles (Piperni et al., 2024) and in the

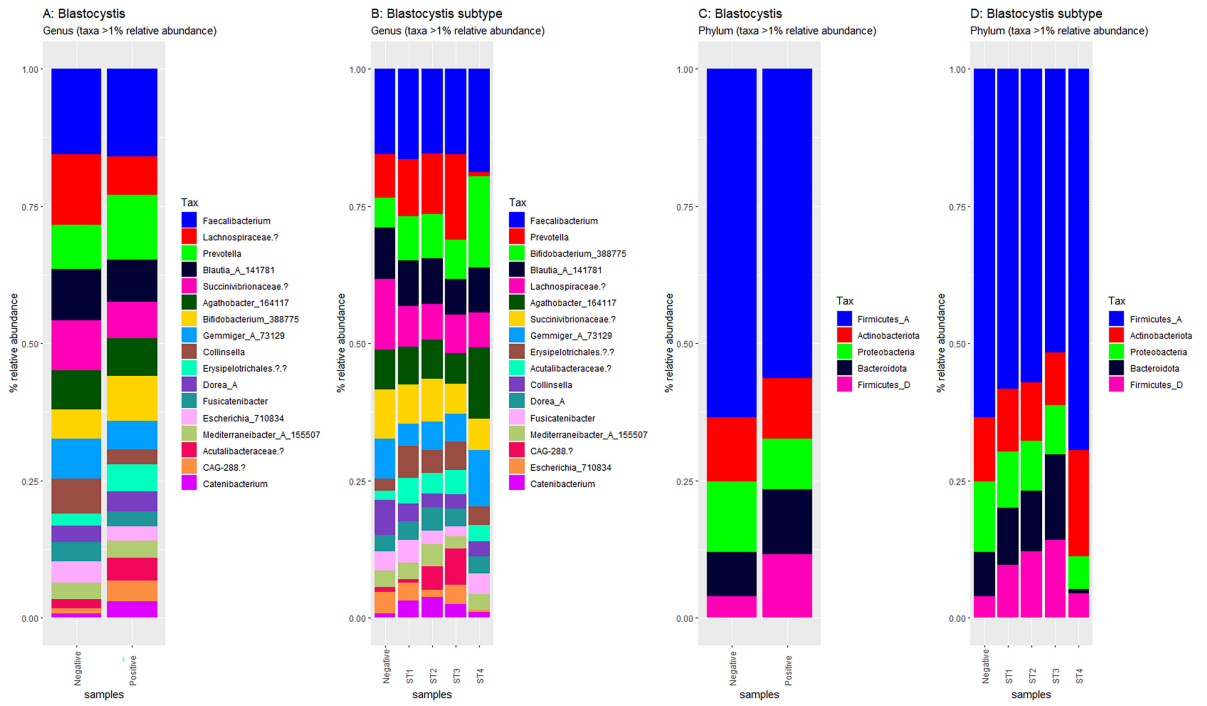

FIGURE 4
Compositional plots of the most abundant taxa in *Blastocystis*-positive and *Blastocystis*-negative samples. Relative abundances are depicted at the genus level **(A, B)** and phylum level **(C, D)**. Comparisons are by *Blastocystis* presence **(A, C)** and by subtype **(B, D)** Only taxa representing more than 1% of total reads within each sample are displayed.

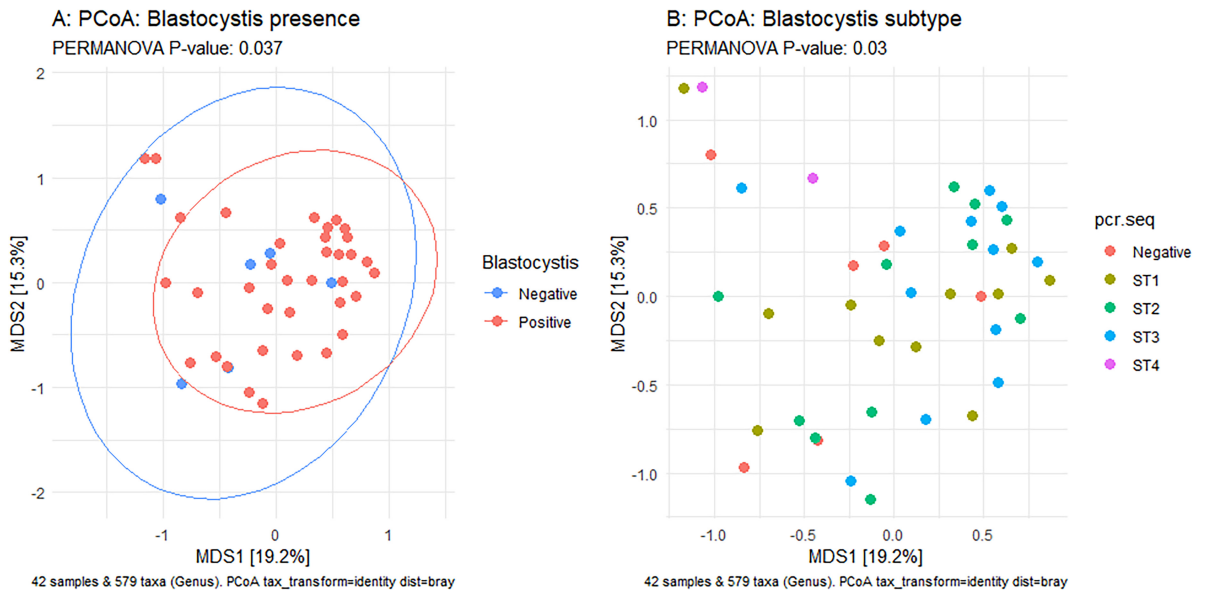

FIGURE 5
Principal Coordinates Analysis (PCoA) based on Bray-Curtis dissimilarity of samples. Left panel: Comparison of *Blastocystis*-positive (red) and *Blastocystis*-negative (blue) samples. Right panel: comparison of samples by *Blastocystis* subype. Statisitcal differences in group centroids were assessed using PERMANOVA. $P < 0.05$ indicate significance

obese with lower incidence of metabolic syndrome (Caudet et al., 2022a,b). Moreover, *Blastocystis* colonization was not associated with gut inflammation as indicated by lower fecal calprotectin levels (Nieves-Ramírez et al., 2018). Collectively, these findings support hypotheses of a beneficial role for *Blastocystis* within the gut ecosystem and warrants further exploration to understand its contributions and underlying mechanisms (Deng and Tan, 2025; Stensvold, 2025).

Our results indicate a high occurrence of *Blastocystis* across all studied host species, consistent with findings from other

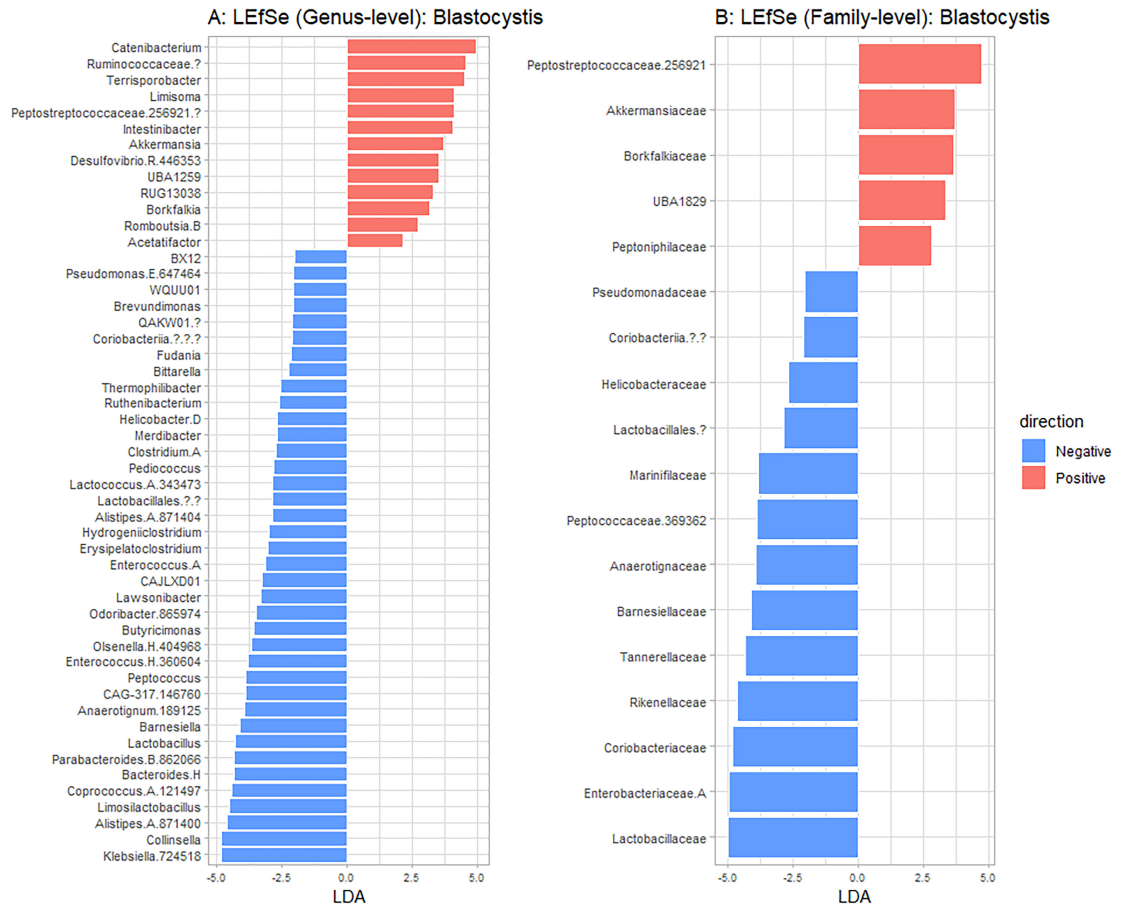

FIGURE 6
Linear discriminant analysis Effect Size (LEFsE) comparing taxa that discriminate between *Blastocystis* positive (red) and *Blastocystis* negative (blue) samples. Taxa with higher LDA scores indicate stronger discriminative power, with | LDA| > 2 being depicted. Results are shown at genus **(A)** and family **(B)** taxonomic levels.

rural communities (El Safadi et al., 2014; Jinatham et al., 2021). However, the true incidence is likely underestimated as several samples negative by microscopy were clearly *Blastocystis* positive, but had to be excluded due to poor sequencing quality. Moreover, several samples positive only by microscopy also failed amplification or sequencing. This was notably the case with the animal and environmental samples. A main issue is the lack of standardization of *Blastocystis* qPCR from environmental samples. Alternative explanations that could account for this, include potential amplification inhibition and mixed infections. Optimizing environmental DNA methodologies are essential and could significantly improve our understanding of ecological reservoirs and transmission pathways.

Overall, 13 subtypes were identified indicating high genetic diversity in the sampled area and associated hosts. Humans predominantly carried subtypes ST1, ST2, and ST3, aligning with global human-associated subtype distributions (Alfellani et al., 2013; Jiménez et al., 2022). Livestock, all of which were ruminants (cattle, sheep, and goats), carried subtypes typical of these animals (Maloney et al., 2019; Rauff-Adedotun et al., 2023; Stensvold et al., 2023; Heydarian et al., 2024; Naguib et al., 2024; Santin et al., 2024). When looking at the community and household level there was barely any sharing of subtypes between humans and their animals. This finding does not seem to match several other studies, which provide evidence that supports the zoonotic transmission of *Blastocystis*. Notably, however, the overall proportion of confirmed zoonotic cases remains low; in nearly all studies, only a small subset of humans shared identical subtypes with animals (Yoshikawa et al., 2009; Rudzińska et al., 2022; Salehi et al., 2022; McCain et al., 2023; Šejnohová et al., 2024). Hence, even though zoonotic transmission is possible, it appears to be infrequent in the studied populations. An alternative explanation might be environmental exposure. *Blastocystis* was previously detected in environmental samples, and recent studies focusing on subtyping have revealed a wide range of subtypes in such samples (Noradilah et al., 2016; Jinatham et al., 2021; Sanhueza Teneo et al., 2025). Herein, we detected *Blastocystis* in water and/or soil samples; however, sequencing failure prevented subtype identification. Collectively, these findings point toward the environment having a role in driving *Blastocystis* transmission. Nonetheless, this route remains comparatively less studied and warrants further investigation.

Blastocystis colonization has been associated with distinct gut microbial profiles characterized by increased microbial diversity and bacterial species richness (Audebert et al., 2016; Nieves-Ramírez et al., 2018; Kodio et al., 2019; Even et al., 2021; Piperni et al., 2024; Castañeda et al., 2025). Most of these studies

have considered the presence or absence of *Blastocystis*, with comparatively fewer exploring differences across subtypes (Beghini et al., 2017; Tito et al., 2019; Antonetti et al., 2024). Our analyses reveal subtypes specific structuring, indicating that individuals harboring different subtypes have distinct microbial communities consistent with previous findings. In this study, ST4 stood out as it showed a trend toward lower microbial diversity and richness in contrast to earlier studies (Beghini et al., 2017; Tito et al., 2019). Notably, in these studies, nearly all ST4-positive samples (except for two from Asia) originated from westernized populations, mainly from Europe. This suggests that ST4-microbiota associations may vary across populations or environments. Alternatively, the difference could be due to the small number of individuals with ST4 herein. Regardless, this finding highlights the need to investigate diverse populations focusing on *Blastocystis* subtype-level differences.

This study has certain limitations. First, the cross-sectional design precludes assessment of temporal relationships (Tsaousis et al., 2025). While a significant association between BMI and *Blastocystis* carriage was revealed, the test did not establish whether differences among the three BMI groups underlie that finding as other potential confounding factors (e.g., diet, co-existing diseases) were not considered.

Conclusion

This study not only bridges a knowledge gap by characterizing *Blastocystis* subtype diversity in humans and livestock within a rural Turkish setting but also spearheads a model for integrated One Health investigations in the region. By combining classical parasitological, and microbiome analyses, we demonstrate the feasibility and value of this type of framework. These findings lay the groundwork for future longitudinal and comparative research both within Türkiye and in similar rural communities globally. Additional multidisciplinary collaborative studies will be instrumental in redefining our understanding of intestinal protists–not solely as pathogens, but as complex microbial players in host health and environmental ecosystems (Tsaousis et al., 2024).

Data availability statement

The Blastocystis sequences presented in this study can be found in NCBI under the accession numbers PX444604-PX444713. The raw microbiome data presented in this study can be found under the accession number PRJNA1291457 in the same database.

Ethics statement

The studies involving humans were approved by Research Ethics Committee of Çukurova University Faculty of Medicine, Adana, Türkiye. The studies were conducted in accordance with the local legislation and institutional requirements. The participants provided their written informed consent to participate in this study.

Author contributions

EA-Ö: Conceptualization, Formal analysis, Funding acquisition, Investigation, Writing – original draft. YA-A: Data curation, Investigation, Methodology, Writing – original draft. WE: Data curation, Formal analysis, Methodology, Writing – original draft. EG: Investigation, Supervision, Validation, Writing – review & editing. AT: Conceptualization, Data curation, Funding acquisition, Project administration, Resources, Supervision, Validation, Visualization, Writing – review & editing. FD-A: Conceptualization, Funding acquisition, Project administration, Resources, Visualization, Writing – original draft.

Funding

The author(s) declare that financial support was received for the research and/or publication of this article. This study was supported within the scope of the Scientific and Technological Research Council of Türkiye (TÜBİTAK) 1002 Quick Support Program (project no: 123S965), CA21105 - *Blastocystis* under One Health (OneHealthBlastocystis) and South Coast Biosciences Doctoral Training Partnership SoCoBio DTP BBSRC BB/T008768/1 to W.J.S.E.

Acknowledgments

We would like to thank the village veterinarians Nadir Öztürk and Hacer Güneş for their help in collecting animal materials, the village doctor Mustafa Yaşar Yılmaz and the village nurse Raşide Çam for their help in collecting human materials, and all the Kırıklı villagers for their support.

Conflict of interest

The authors declare that the research was conducted in the absence of any commercial or financial relationships that could be construed as a potential conflict of interest.

The handling editor LD declared a past co-authorship with the author AT.

Generative AI statement

The author(s) declare that no Generative AI was used in the creation of this manuscript.

Any alternative text (alt text) provided alongside figures in this article has been generated by Frontiers with the support of artificial intelligence and reasonable efforts have been made to ensure accuracy, including review by the authors wherever possible. If you identify any issues, please contact us.

Publisher's note

Supplementary material

The Supplementary Material for this article can be found online at: https://www.frontiersin.org/articles/10.3389/fmicb.2025.1665966/full#supplementary-material

SUPPLEMENTARY FIGURE 1
Field photographs of the sampling area.

SUPPLEMENTARY FIGURE 2
Blastocystis cells observed in culture.

SUPPLEMENTARY FIGURE 3
Maximum likelihood phylogeny of *Blastocystis* sequences.

SUPPLEMENTARY FIGURE 4
Rarefaction curves of 16S sequencing samples. The total number of sequencing reads is shown on the X-axis, and the taxa detected at the corresponding sequencing are displayed on the Y-**axis.**

SUPPLEMENTARY FIGURE 5
Compositional bar plots showing the most abundant taxa in *Blastocystis*-positive and negative samples. Each bar represents an individual sample. Taxa were aggregated to Genus **(A,B)** and phylum **(C,D)** level. Samples have been grouped by *Blastocystis* colonization status **(A,C)** or *Blastocystis* subtype **(B,D)**. Only taxa representing more than 1% of the total reads within each sample are displayed.

References

Abdo, S. M., El-Adawy, H., Farag, H. F., El-Taweel, H. A., Elhadad, H., and El-Badry, A. A. M. (2021). Detection and molecular identification of Blastocystis isolates from humans and cattle in northern Egypt. *J. Parasitic Dis.* 45, 738–745. doi: 10.1007/s12639-021-01354-5

Alfellani, M. A., Taner-Mulla, D., Jacob, A. S., Imeede, C. A., Yoshikawa, H., Stensvold, C. R., et al. (2013). Genetic diversity of blastocystis in livestock and zoo animals. *Protist* 164, 497–509. doi: 10.1016/j.protis.2013.05.003

Alzate, J. F., Toro-Londoño, M., Cabarcas, F., Garcia-Montoya, G., and Galvan-Diaz, A. (2020). Contrasting microbiota profiles observed in children carrying either Blastocystis spp. or the commensal amoebas Entamoeba coli or Endolimax nana. *Sci. Rep.* 10:15354. doi: 10.1038/s41598-020-72286-y

Anderson, M. J. (2017). "Permutational multivariate analysis of variance (PERMANOVA)," in *Wiley StatsRef: Statistics Reference Online*, eds N. Balakrishnan, T. Colton, and B. Everitt (Hoboken, NJ: Wiley), 1–15. doi: 10.1002/9781118445112.stat07841

Antonetti, L., Berrilli, F., Di Cristanziano, V., Farowski, F., Daeumer, M., Eberhardt, K. A., et al. (2024). Investigation of gut microbiota composition in humans carrying blastocystis subtypes 1 and 2 and Entamoeba hartmanni. *Gut Pathog.* 16:72. doi: 10.1186/s13099-024-00661-5

Asnicar, F., Berry, S. E., Valdes, A. M., Nguyen, L. H., Piccinno, G., Drew, D. A., et al. (2021). Microbiome connections with host metabolism and habitual diet from 1,098 deeply phenotyped individuals. *Nat. Med.* 27, 321–332. doi: 10.1038/s41591-020-01183-8

Audebert, C., Even, G., Cian, A., Blastocystis Investigation, Group, Loywick, A., et al. (2016). Colonization with the enteric protozoa Blastocystis is associated with increased diversity of human gut bacterial microbiota. *Sci. Rep.* 6:25255. doi: 10.1038/srep25255

Beghini, F., Pasolli, E., Truong, T. D., Putignani, L., Cacciò, S. M., and Segata, N. (2017). Large-scale comparative metagenomics of Blastocystis, a common member of the human gut microbiome. *ISME J.* 11, 2848–2863. doi: 10.1038/ismej.2017.139

Blackburn, C. C., Yan, S. M., McCormick, D., Herrera, L. N., Iordanov, R. B., Bailey, M. D., et al. (2024). Parasitic contamination of soil in the Southern United States. *Am. J. Trop. Med. Hyg.* 111, 506–514. doi: 10.4269/ajtmh.24-0075

Callahan, B. J., McMurdie, P. J., Rosen, M. J., Han, A. W., Johnson, A. J. A., and Holmes, S. P. (2016). DADA2: High-resolution sample inference from Illumina amplicon data. *Nat. Methods* 13, 581–583. doi: 10.1038/nmeth.3869

Caporaso, J. G., Lauber, C. L., Walters, W. A., Berg-Lyons, D., Lozupone, C. A., Turnbaugh, P. J., et al. (2011). Global patterns of 16S rRNA diversity at a depth of millions of sequences per sample. *Proc. Natl. Acad. Sci. U S A.* 108, 4516–4522. doi: 10.1073/pnas.1000080107

Castañeda, S., Muñoz, M., Villamizar, X., Hernández, P. C., Vásquez, L. R., Tito, R. Y., et al. (2020). Microbiota characterization in Blastocystis-colonized and Blastocystis-free school-age children from Colombia. *Parasit Vectors* 13:521. doi: 10.1186/s13071-020-04392-9

Castañeda, S., Tomiak, J., Andersen, L. O. B., Acosta, C. P., Vasquez-A, L. R., Stensvold, C. R., et al. (2025). Impact of Blastocystis carriage and colonization intensity on gut microbiota composition in a non-westernized rural population from Colombia. *PLoS Negl. Trop. Dis.* 19:e0013111. doi: 10.1371/journal.pntd.0013111

Caudet, J., Trelis, M., Cifre, S., Soriano, J. M., and Merino-Torres, J. F. (2022a). Presence and significance of intestinal unicellular parasites in a morbidly obese population. *Int. J. Obes.* 46, 220–227. doi: 10.1038/s41366-021-00980-6

Caudet, J., Trelis, M., Cifre, S., Soriano, J. M., Rico, H., and Merino-Torres, J. F. (2022b). Interplay between intestinal bacterial communities and unicellular parasites in a morbidly obese population: A neglected trinomial. *Nutrients* 14:3211. doi: 10.3390/nu14153211

Centers for Disease Control and Prevention [CDC]. (2025). *Blastocystis*. Available online at: https://www.cdc.gov/blastocystis/about/?CDC_AAref_Val=https://www.cdc.gov/parasites/blastocystis/index.html (accessed October 7, 2025).

Deng, L., and Tan, K. S. W. (2025). Unveiling the hidden ally: Blastocystis links healthier diets and cardiometabolic benefits. *Signal Transduct. Target Ther.* 10:77. doi: 10.1038/s41392-025-02146-6

DeSantis, T. Z., Hugenholtz, P., Larsen, N., Rojas, M., Brodie, E. L., Keller, K., et al. (2006). Greengenes, a chimera-checked 16S rRNA gene database and workbench compatible with ARB. *Appl. Environ. Microbiol.* 72, 5069–5072. doi: 10.1128/AEM.03006-05

El Safadi, D., Gaayeb, L., Meloni, D., Cian, A., Poirier, P., Wawrzyniak, I., et al. (2014). Children of senegal river basin show the highest prevalence of Blastocystis sp. ever observed worldwide. *BMC Infect. Dis.* 14:164. doi: 10.1186/1471-2334-14-164

Even, G., Lokmer, A., Rodrigues, J., Audebert, C., Viscogliosi, E., Ségurel, L., et al. (2021). Changes in the human gut microbiota associated with colonization by blastocystis sp. and Entamoeba spp. in non-industrialized populations. *Front. Cell. Infect. Microbiol.* 11:533528. doi: 10.3389/fcimb.2021.533528

Geifman, N., and Rubin, E. (2011). Towards an age-phenome knowledge-base. *BMC Bioinformatics* 12:229. doi: 10.1186/1471-2105-12-229

Heydarian, M., Manouchehri Naeini, K., Kheiri, S., and Abdizadeh, R. (2024). Prevalence and subtyping of Blastocystis sp. in ruminants in Southwestern. *Iran. Sci. Rep.* 14:20254. doi: 10.1038/s41598-024-70907-4

Hublin, J. S. Y., Maloney, J. G., and Santin, M. (2021). Blastocystis in domesticated and wild mammals and birds. *Res. Vet. Sci.* 135, 260–282. doi: 10.1016/j.rvsc.2020.09.031

Işıklar, E. (2018). *Özmen ahmet and Şeniş berat fethi [Özmen ahmet and Şeniş berat fethi]*. Eskişehir: Anadolu Üniversitesi. Turkish.

Jiménez, P., Muñoz, M., and Ramírez, J. D. (2022). An update on the distribution of Blastocystis subtypes in the Americas. *Heliyon* 8:e12592. doi: 10.1016/j.heliyon.2022.e12592

Jinatham, V., Maxamhud, S., Popluechai, S., Tsaousis, A. D., and Gentekaki, E. (2021). Blastocystis one health approach in a rural community of Northern Thailand: Prevalence, subtypes and novel transmission routes. *Front. Microbiol.* 12:746340. doi: 10.3389/fmicb.2021.746340

Khorshidvand, Z., Khazaei, S., Amiri, M. R., Taherkhani, H., and Mirzaei, A. (2021). Worldwide prevalence of emerging parasite Blastocystis in immunocompromised patients: A systematic review and meta-analysis. *Microb. Pathog.* 152:104615. doi: 10.1016/j.micpath.2020.104615

Kodio, A., Coulibaly, D., Koné, A. K., Konaté, S., Doumbo, S., Guindo, A., et al. (2019). Blastocystis colonization is associated with increased diversity and altered gut bacterial communities in healthy malian children. *Microorganisms* 7:649. doi: 10.3390/microorganisms7120649

Koehler, A. V., Herath, H. M. P. D., Hall, R. S., Wilcox, S., and Gasser, R. B. (2024). Marked genetic diversity within Blastocystis in Australian wildlife revealed using a next generation sequencing–phylogenetic approach. *Int. J. Parasitol. Parasites Wildl* 23:100902. doi: 10.1016/j.ijppaw.2023.100902

Li, H. (2018). Minimap2: Pairwise alignment for nucleotide sequences. *Bioinformatics* 34, 3094–3100. doi: 10.1093/bioinformatics/bty191

Malatyalı, E., Ertabaklar, H., and Ertuğ, S. (2023). Subtype distribution of blastocystis in Türkiye. *Turkiye Parazitoloji Dergisi.* 47, 184–189. doi: 10.4274/tpd.galenos.2023.79188

Malatyali, E., Tilekliogl u, E., Yildiz, I., Unsal, O., Demirag, S., Hatice, E., et al. (2021). Investigation of the relationship between obesity and Blastocystis infection in an adult population in Aydin, Turkey. *Ann. Parasitol.* 67, 249–255. doi: 10.17420/ap6702.336

Maloney, J. G., Lombard, J. E., Urie, N. J., Shivley, C. B., and Santin, M. (2019). Zoonotic and genetically diverse subtypes of Blastocystis in US pre-weaned dairy heifer calves. *Parasitol. Res.* 118, 575–582. doi: 10.1007/s00436-018-6149-3

Matovelle, C., Tejedor, M. T., Monteagudo, L. V., Beltrán, A., and Quílez, J. (2022). Prevalence and associated factors of Blastocystis sp. infection in patients with gastrointestinal symptoms in Spain: A case-control study. *Trop. Med. Infect. Dis.* 7:226. doi: 10.3390/tropicalmed7090226

McCain, A., Gruneck, L., Popluechai, S., Tsaousis, A. D., and Gentekaki, E. (2023). Circulation and colonisation of Blastocystis subtypes in schoolchildren of various ethnicities in rural northern Thailand. *Epidemiol. Infect.* 151:e77. doi: 10.1017/S0950268823000596

Naguib, D., Gantois, N., Desramaut, J., Dominguez, R. G., Arafat, N., Atwa, S. M., et al. (2024). Large-scale molecular epidemiological survey of Blastocystis sp. among herbivores in Egypt and assessment of potential zoonotic risk. *Microorganisms* 12:1286. doi: 10.3390/microorganisms12071286

Nguyen, L. D. N., Gantois, N., Hoang, T. T., Do, B. T., Desramaut, J., Naguib, D., et al. (2023). First epidemiological survey on the prevalence and subtypes distribution of the enteric parasite Blastocystis sp. in Vietnam. *Microorganisms* 11:731. doi: 10.3390/microorganisms11030731

Nguyen, L. T., Schmidt, H. A., von Haeseler, A., and Minh, B. Q. (2015). IQ-TREE: A fast and effective stochastic algorithm for estimating maximum likelihood phylogenies. *Mol. Biol. Evol.* 32, 268–274. doi: 10.1093/molbev/msu300

Nieves-Ramírez, M. E., Partida-Rodríguez, O., Laforest-Lapointe, I., Reynolds, L. A., Brown, E. M., Valdez-Salazar, A., et al. (2018). Asymptomatic intestinal colonization with protist *Blastocystis* is strongly associated with distinct microbiome ecological Patterns. *mSystems* 3:e00007-18. doi: 10.1128/mSystems.00007-18

Noradilah, S. A., Lee, I. L., Anuar, T. S., Salleh, F. M., Manap, S. N. A. A., Mohtar, N. S. H. M., et al. (2016). Occurrence of Blastocystis sp. in water catchments at Malay villages and Aboriginal settlement during wet and dry seasons in Peninsular Malaysia. *PeerJ* 2016:e2541. doi: 10.7717/peerj.2541

Onder, Z., Yildirim, A., Pekmezci, D., Duzlu, O., Pekmezci, G. Z., Ciloglu, A., et al. (2021). Molecular identification and subtype distribution of Blastocystis sp. in farm and pet animals in Turkey. *Acta Trop.* 220:105939. doi: 10.1016/j.actatropica.2021.105939

Özkurt, E., Fritscher, J., Soranzo, N., Ng, D. Y. K., Davey, R. P., Bahram, M., et al. (2022). LotuS2: An ultrafast and highly accurate tool for amplicon sequencing analysis. *Microbiome* 10:176. doi: 10.1186/s40168-022-01365-1

Piperni, E., Nguyen, L. H., Manghi, P., Kim, H., Pasolli, E., Andreu-Sánchez, S., et al. (2024). Intestinal Blastocystis is linked to healthier diets and more favorable cardiometabolic outcomes in 56,989 individuals from 32 countries. *Cell* 187, 4554–4570.e18. doi: 10.1016/j.cell.2024.06.018

Poirier, P., Wawrzyniak, I., Albert, A., El Alaoui, H., Delbac, F., and Livrelli, V. (2011). Development and evaluation of a real-time PCR assay for detection and quantification of Blastocystis parasites in human stool samples: Prospective study of patients with hematological malignancies. *J. Clin. Microbiol.* 49, 975–983. doi: 10.1128/JCM.01392-10

Rauff-Adedotun, A. A., Lee, I. L., Abd Talib, N., Shaari, N., Yahaya, Z. S., and Meor Termizi, F. H. (2023). Prevalence, potential risk factors and genetic diversity of Blastocystis in ruminant livestock animals from Penang, Malaysia. *Parasitol. Res.* 122, 2193–2205. doi: 10.1007/s00436-023-07920-5

Ruang-areerate, T., Piyaraj, P., Suwannahitatorn, P., Ruang-areerate, P., Thita, T., Naaglor, T., et al. (2021). Zoonotic transmission of blastocystis subtype 1 among people in Eastern communities of thailand: Organic fertilizer from pig feces as a potential source. *Microbiol. Spectr.* 9, 362–321. doi: 10.1128/spectrum.00362-21

Rudzińska, M., Kowalewska, B., Kurpas, M., and Szostakowska, B. (2022). Rare occurrence of blastocystis in pet animals and their owners in the pomeranian voivodeship in poland in the light of literature data. *J. Clin. Med.* 11:2975. doi: 10.3390/jcm11112975

Salehi, R., Rostami, A., Mirjalali, H., Stensvold, C. R., and Haghighi, A. (2022). Genetic characterization of Blastocystis from poultry, livestock animals and humans in the southwest region of Iran—Zoonotic implications. *Transbound. Emerg. Dis.* 69, 1178–1185. doi: 10.1111/tbed.14078

Sanhueza Teneo, D., Chesnais, C. B., Manzano, J., Moll, M. P., Téllez, A., and Valenzuela-Nieto, G. (2025). Waterborne transmission driving the prevalence of Blastocystis sp. in Los Ríos Region, Southern Chile. *Microorganisms* 13:1549. doi: 10.3390/microorganisms13071549

Santin, M., Figueiredo, A., Molokin, A., George, N. S., Köster, P. C., Dashti, A., et al. (2024). Division of blastocystis ST10 into three new subtypes: ST42-ST44. *J. Eukaryotic Microbiol.* 71:e12998. doi: 10.1111/jeu.12998

Sarzhanov, F., Dogruman-Al, F., Santin, M., Maloney, J. G., Gureser, A. S., Karasartova, D., et al. (2021). Investigation of neglected protists blastocystis sp. And Dientamoeba fragilis in immunocompetent and immunodeficient diarrheal patients using both conventional and molecular methods. *PLoS Negl. Trop. Dis.* 15:e0009779. doi: 10.1371/JOURNAL.PNTD.0009779

Segata, N., Izard, J., Waldron, L., Gevers, D., Miropolsky, L., Garrett, W. S., et al. (2011). Metagenomic biomarker discovery and explanation. *Genome Biol.* 12:R60. doi: 10.1186/gb-2011-12-6-r60

Šejnohová, A., Koutenská, M., Jirkù, M., Brožová, K., Pavlíèková, Z., Kadlecová, O., et al. (2024). A cross-sectional survey of Blastocystis sp. and Dientamoeba fragilis in non-human primates and their caregivers in Czech zoos. *One Health* 19:100862. doi: 10.1016/j.onehlt.2024.100862

Stensvold, C. R. (2025). Blastocystis in stool: Friend, foe or both? *J. Travel Med.* 32:taaf011. doi: 10.1093/jtm/taaf011

Stensvold, C. R., and Clark, C. G. (2020). Pre-empting pandora's box: Blastocystis subtypes revisited. *Trends Parasitol.* 36, 229–232. doi: 10.1016/j.pt.2019.12.009

Stensvold, C. R., Arendrup, M. C., Jespersgaard, C., Mølbak, K., and Nielsen, H. V. (2007). Detecting Blastocystis using parasitologic and DNA-based methods: A comparative study. *Diagn. Microbiol. Infect. Dis.* 59, 303–307. doi: 10.1016/j.diagmicrobio.2007.06.003

Stensvold, C. R., Berg, R. P. K. D., Maloney, J. G., Molokin, A., and Santin, M. (2023). Molecular characterization of Blastocystis and entamoeba of muskoxen and sheep in Greenland. *Int. J. Parasitol.* 53, 673–685. doi: 10.1016/j.ijpara.2023.05.005

Tan, K. S. W. (2008). New insights on classification, identification, and clinical relevance of *Blastocystis* spp. *Clin. Microbiol. Rev.* 21, 639–665. doi: 10.1128/cMR.00022-08

Tavur, A., and Önder, Z. (2022). Molecular prevalence and phylogenetic characterization of blastocystis in cattle in Kayseri Province, Turkey. *Kocatepe Vet. J.* 15, 1–6. doi: 10.30607/kvj.996557

Tito, R. Y., Chaffron, S., Caenepeel, C., Lima-Mendez, G., Wang, J., Vieira-Silva, S., et al. (2019). Population-level analysis of Blastocystis subtype prevalence and variation in the human gut microbiota. *Gut* 68, 1180–1189. doi: 10.1136/gutjnl-2018-316106

Tsaousis, A. D., Gentekaki, E., and Stensvold, C. R. (2024). Advancing research on Blastocystis through a one health approach. *Open Res. Eur.* 4:145. doi: 10.12688/openreseurope.18046.1

Tsaousis, A. D., Shaw, D., Jirku, K., Carmena, D., and Gentekaki, E. (2025). Rethinking Blastocystis: Ubiquity and cyclical abundance in the human gut. *Trends Parasitol.* doi: 10.1016/j.pt.2025.08.009 Online ahead of print.

Yoshikawa, H., Wu, Z., Pandey, K., Pandey, B. D., Sherchand, J. B., Yanagi, T., et al. (2009). Molecular characterization of Blastocystis isolates from children and rhesus monkeys in Kathmandu, Nepal. *Vet. Parasitol.* 160, 295–300. doi: 10.1016/j.vetpar.2008.11.029

frontiers | Frontiers in Microbiology

TYPE Original Research
PUBLISHED 31 October 2025
DOI 10.3389/fmicb.2025.1660176

OPEN ACCESS

EDITED BY
Hong Yin,
Chinese Academy of Agricultural Sciences, China

REVIEWED BY
Saixiang Feng,
South China Agricultural University, China
Huixing Lin,
Nanjing Agricultural University, China

*CORRESPONDENCE
Yiping Wen
✉ wyp@sicau.edu.cn

†These authors have contributed equally to this work

RECEIVED 17 July 2025
ACCEPTED 09 September 2025
PUBLISHED 31 October 2025

CITATION
Zhang Y, Yang Z, Du S, Zhao Q, Huang X, Wu R, Wang Y, Yan Q, Cao S and Wen Y (2025) Host factor Rab4b mediates internalization and intoxication of 3D4/21 cells by the active subunit of the *Glaesserella parasuis* cytolethal distending toxin via influencing EEA1 expression. *Front. Microbiol.* 16:1660176. doi: 10.3389/fmicb.2025.1660176

Host factor Rab4b mediates internalization and intoxication of 3D4/21 cells by the active subunit of the *Glaesserella parasuis* cytolethal distending toxin via influencing EEA1 expression

Yiwen Zhang[1†], Zhen Yang[2†], Senyan Du[1], Qin Zhao[1], Xiaobo Huang[1], Rui Wu[1], Yiping Wang[1], Qigui Yan[1], Sanjie Cao[1] and Yiping Wen[1*]

[1]Research Center for Swine Diseases, College of Veterinary Medicine, Sichuan Agricultural University, Chengdu, China, [2]Chongqing Academy of Animal Sciences, Chongqing, China

Background: The cytolethal distending toxin (CDT), a significant exotoxin, is closely linked to the pathogenicity of *Glaesserella parasuis* (GPS), but its pathogenic not yet fully elucidated. Previously, we identified Rab4b as a potential host factor contributing to the cytotoxicity of *Gp*CDT through a whole-genome CRISPR/Cas9 screen technology, and subsequently confirmed its association with *Gp*CDT cytotoxicity in PK-15 cells.
Aims: In this study, our data first indicated that Rab4b could interact with the active subunit of the *Glaesserella parasuis* cytolethal distending toxin.
Methods: Investigating the relationship between Rab4b and *Gp*CDT subunits as confirmed by coimmunoprecipitation assay. Next, the porcine alveolar macrophage cell line 3D4/21 was used to establish an infected cell model. Using CRISPR/Cas9 gene editing, we established Rab4b and EEA1-expression-deficient 3D4/21 cell lines. 3D4/21 cells, Rab4b-KO cells and EEA1-KO cells were treated with *Gp*CDT. Cell Counting Kit-8 (CCK-8) assay was used to detect cell viability. Western blotting and qRT-PCR were used to measure the expression of related proteins and genes, and cell morphology observation and indirect immunofluorescence were performed to evaluate the *Gp*CDT-mediated cytotoxicity. Then utilise transcriptome sequencing analysis to investigate its specific mechanisms.
Result: In this study, our data first indicated that Rab4b could interact with the active subunit of the *Gp*CDT. Next, we demonstrated that Rab4b also influences *Gp*CDT-induced cytotoxicity and vesicle trafficking in 3D4/21 cells. To investigate the Rab4b-mediated cytotoxicity of *Gp*CDT in 3D4/21 cells, we screened for EEA1, a gene critical in this process, by transcriptome sequencing analysis. 3D4/21 cells exposed to *Gp*CDT exhibit upregulated EEA1 expression, an event that is lost in the absence of Rab4b. Using CRISPR/Cas9 gene editing, we established EEA1 expression-deficient 3D4/21 cell lines that fail to internalize GpCdtB, resulting in resistance to GpCDT-induced toxic effects.
Conclusions: We suggest that Rab4b facilitates the cellular uptake of *Gp*CDTby upregulating EEA1 protein expression, thereby facilitating the vesicular transport of *Gp*CDT in 3D4/21 cells. Our findings may provide new insights into the pathogenicity of *Gp*CDT and lay the experimental foundation for a deeper understanding of the role of Rab4b proteins

KEYWORDS

Glaesserella parasuis, Rab4b, *Gp*CDT, EEA1, vesicle trafficking

1 Introduction

Glaesserella parasuis (formerly known as *Haemophilus parasuis*) is a commensal microorganism of the upper respiratory tract of swine and the causative agent of *Glässer*'s disease (Costa-Hurtado et al., 2020), which is characterized by fibrinous polyserositis, plasmacytosis, meningitis, and arthritis (Brockmeier et al., 2013; Mao et al., 2023; Ni et al., 2020). Cytolethal distending toxins (*Gp*CDT) are a class of thermally unstable genotoxins produced by Gram-negative pathogens, which are secreted by a variety of bacteria, including *Actinobacillus actinomycetemcomitans*, *Haemophilus ducreyi*, *Escherichia coli*, and *Campylobacter jejuni* (Pons et al., 2019; Scuron et al., 2016). The complete CDT consists of three subunits: CdtA, CdtB, and CdtC, they are encoded by consecutive genes within a single manipulator (Gargi et al., 2012). The CdtA and CdtC subunits work together to form the "B component," which facilitates the binding and transport of the "catalytically active a component," CdtB, which then binds and translates into the host cell. This is similar to the classical "A-B" functional structure of many intracellularly acting bacterial exotoxins (Dixon et al., 2015; Pons et al., 2019; Shenker et al., 2016). CDT was the first toxin protein identified in bacteria capable of damaging the nuclear DNA of target cells (Dixon et al., 2015). Crossing the cell membrane and reaching the target cell's nucleus is a key step in its DNA-damaging action. Like many bacterial toxins, CdtA and CdtC act as binding components, attaching to cholesterol- and sphingomyelin-rich membrane microdomains (also known as lipid rafts), thereby enhancing the delivery of CdtB into the cell (Chen et al., 2020; Dixon et al., 2015; Yeh et al., 2020). The host cell absorbs and binds *Gp*CDT in the extracellular environment, which triggers the DNA damage response and stops the cell cycle from progressing, eventually causing DNA damage (Boesze-Battaglia et al., 2020; Huhn et al., 2022; Kailoo et al., 2021).

The Rab protein family is the largest group of small GTPases within the Ras superfamily, comprising over 60 members in the human genome (Spano and Galan, 2018). Multiple Rabs can exist on a single intracellular compartment, each occupying its own unique "microstructural domain" (Brumell and Scidmore, 2007; Jordens et al., 2005). A distinct Rab protein mediates each step of the endocytosis pathway. Activated Rab5 co-mediates with Rab4 the transport of extracellular macromolecules from the plasma membrane to early endosomes, acting as a marker for these endosomes (Kalin et al., 2016; Somsel Rodman and Wandinger-Ness, 2000). Rab4b, as a subtype of Rab4, is a key protein involved in vesicle trafficking and is mainly localised in lattice-encapsulated vesicles, early endosomes, and circulating endosomes and is an important regulator of cellular endocytosis and cycling processes (He et al., 2002; Krawczyk et al., 2007; Pereira-Leal and Seabra, 2001; Perrin et al., 2013). In 1999, scholars first examined the presence of Rab4b protein in human umbilical vein endothelial cells. Subsequently, Rab4b was also detected to be upregulated in hepatocellular carcinoma and intrahepatic cholangiocarcinoma (Perrin et al., 2013). Rab4b was also detected in mouse adipocytes (3T3-L1), lung, and myocardial tissue (Kaddai et al., 2009).

Early endosomal antigen 1 (EEA1) is a cytosolic protein that specifically binds to early endosomal membranes, where it plays a crucial role in the tethering process leading to homotypic endosome fusion (Bergeland et al., 2008). EEA1 is a long coiled-coil homodimer with 17–20% homology to myosin. It contains calmodulin-binding IQ (isoleucine and glutamine) motifs associated with these proteins, which are involved in cellular uptake functions, promote the formation of vesicles encapsulating toxin proteins (Mu et al., 1995), and control the transport of vesicles to the early endosomes and then fuse with early endosomes (Fouraux et al., 2004; Mishra et al., 2010; Rubino et al., 2000). Rab5 can regulate the production of lattice protein-encapsulated vesicles, and EEA1, an effector protein of Rab5, has been shown to undergo a conformational change on vesicles upon binding to Rab5-GTP and to provide the mechanical force necessary to disengage vesicles from the cell membrane and bring them closer to the early endosomes or other vesicles (Adams and Wayne Vogl, 2017; Mills et al., 1998; Simonsen et al., 1998; Stenmark et al., 1996). The C-terminal FYVE structural domain of the EEA1 protein binds to abundant PI3P on early endosomes and promotes vesicle fusion with early endosomes (Rubino et al., 2000). EEA1 regulates numerous biological events through its effects on cellular uptake functions.

The CRISPR/Cas9 gene editing technology can induce random or targeted gene mutations, leading to the loss of protein function. The affected regions include the coding and non-coding regions of the gene. CRISPR/Cas9 technology has become the most extensively examined gene editing technology in recent years due to its simple design, low cost, high efficiency, and ease of operation, which can also achieve simultaneous editing of multiple loci. It can also be carried out without using plasmids, thereby saving the trouble caused by plasmids. CRISPR/Cas9 has shown great potential in studying genes and genomic functions in microorganisms, plants, animals, and humans (Bergeland et al., 2008). CRISPR/Cas9 can systematically screen out host proteins that directly or indirectly participate in the cytotoxicity of *Gp*CDT, including toxin receptors on the cell membrane and interacting/non-interacting proteins within the cell (Hesping and Boddey, 2024; Hu and Wang, 2024; Schoellkopf et al., 2022). In the early stage, we utilized the CRISPR/Cas9 technology to identify host proteins involved in the cytotoxicity of *Gp*CDT. We successfully identified multiple host proteins, including the host protein Rab4b. Considering Rab4b's significance in cell membrane transport, we investigated its potential involvement in the cytotoxicity of 3D4/21, which *Gp*CDT produces.

2 Materials and methods

2.1 Cell lines, plasmids, and antibodies

3D4/21 cells were cultured in a complete medium of RPMI-1640 (Gibco, Carlsbad, CA, United States). Human embryo kidney (HEK-293T) cells were grown in DMEM (Gibco, Carlsbad, CA, United States). Both cells required the addition of 10% fetal bovine serum (Gibco, Carlsbad, CA, United States). They were subcultured upon reaching 90% confluence and incubated in a 37 °C incubator

TABLE 1 Bacterial strains and plasmids used in this study.

Strain or plasmid	Relevant characteristics	Source
BL21(DE3)	*E. coli* str. B F⁻ ompT gal dcm lon hsdSB(rB⁻mB⁻) λ (DE3 [lacI lacUV5-T7p07 ind1 sam7 nin5]) [malB+]K-12(λS)	Biomed
pET-*cdtA*	A 624 bp cdtA CDS in pET-32a (+)	Laboratory collection
pET-*cdtB*	A 768 bp cdtB CDS in pET-32a (+)	Laboratory collection
pET-*cdtC*	A 471 bp cdtC CDS in pET-32a (+)	Laboratory collection
pMD2.G	Lentivirus envelope plasmid	Laboratory collection
pSPAX2	Lentivirus envelope plasmid	Laboratory collection
pLentiCRISPR V2	sgRNA[a] carrier plasmid	Laboratory collection
pEGFP-N1-Rab4b	Overexpression plasmid	Laboratory collection
pcDNA-3.1-Flag-Rab4b	Overexpression plasmid	Laboratory collection

containing 5% CO_2. The bacterial strains and plasmids used in this study are listed in Table 1. All strains were grown in broth with shaking at 180 rpm at 37 °C.

Antibodies for caspase-3 (ab32351), EEA1 (ab109110), Rab5 (ab218624), and RCAS1 (ab200348) were purchased from Abcam (Cambridge, Cambridgeshire, Britain). Antibodies for Flag (66008-4-Ig), and His (66005-1-IG) were from Proteintech Group (Wuhan, Hubei, China). Na^+/K^+-ATPase (P06685) and γH2AX (9718T) were purchased from Cell Signaling Technology (Danver, MA, United States). β-actin (High Dilution) (AC026) and the secondary antibodies including HRP Goat Anti-Mouse IgG (H + L) (AS003), HRP Goat Anti-Rabbit IgG (H + L) (AS014), Alexa Fluor 488-conjugated Goat anti-Rabbit IgG (H + L) (AS053) and Alexa Fluor 594-conjugated Goat anti-Rabbit IgG (H + L) (AS039) were bought from Abclonal (Wuhan, Hubei, China). Cell Plasma Membrane Staining Kit with DiI (Red Fluorescence) (C1991S) was bought from Beyotime (Shanghai, China).

A previous report has been published on the production of Rab4b antiserum. Simply put, Rab4b antiserum was produced by immunizing mice with the C-terminal peptide of Rab4b conjugated to KLH (Zhang et al., 2024).

2.2 Preparation of recombinant *Gp*CDT protein and mouse antiserum

Construction and expression of plasmids containing *cdtA*, *cdtB*, and *cdtC* genes have been reported previously. In brief, the constructed plasmids were transformed into Rosetta (DE3) pLysS. Recombinant clones were induced with 0.2 mM IPTG for 12 h at 25 °C to achieve optimal expression. These three His-tag fusion recombinant proteins were purified by Ni affinity chromatography (Bio-Rad, Hercules, CA, United States) and then confirmed by SDS-PAGE electrophoresis. In this study, the three subunits were reconstituted as a holotoxin at 4 °C overnight.

The expression of anti-*Gp*CdtA, anti-*Gp*CdtB, and anti-*Gp*CdtC antisera was also as previously described. Each mouse was immunized subcutaneously on days 0, 14, and 21 with 0.1 mg of *Gp*CdtA, *Gp*CdtB, or *Gp*CdtC (200 μL) and 20 μL of water adjuvant Montanide Gel 01 (SEPPIC, France). Twenty-eight days later, blood was collected from the mice and left at 4 °C overnight. The serum was then collected and stored in the refrigerator (Yang et al., 2023).

2.3 Coimmunoprecipitation assay

HEK-293T cells at 50% confluence in 6-well plates were cotransfected with pcDNA-3.1-Flag-Rab4b. At 36 h post-transfection, the cells were incubated with 10 μg/mL *Gp*CDT for 30 min. Then, coimmunoprecipitation assays were performed using Protein A/G Magnetic Beads (MedChemExpress, United States). Western blot analysis was performed using antisera against *Gp*CdtA, *Gp*CdtB, and *Gp*CdtC.

To analyze the interaction between *Gp*CDT subunits and the host protein Rab4b, HEK-293T cells were seeded into 6-well culture plates and transfected with the corresponding expression plasmid. Transfected cells were harvested at 48 h post-transfection and lysed in cell lysis buffer containing one mM protease inhibitor. After centrifugation at 14,000 g for 10 min, the lysate supernatant was incubated with 2.5 μg of His-*Gp*CDT subunits for 4 h with gentle rocking at 4 °C. It was then incubated overnight with mouse monoclonal antibodies (mAbs) against the Flag or His tag, also with gentle rocking at 4 °C. Protein A/G Magnetic Beads washed with cell lysate were added to the supernatants and incubated with gentle rocking for 4 h at 4 °C. The beads were washed four times with cold cell lysate and then boiled in SDS loading buffer for 10 min, followed by Western blot analysis.

2.4 Rab4b and EEA1 knockout

The Rab4b and EEA1 small guide RNA (sgRNA) were inserted into the lentiCRISPR-V2 plasmid (Table 2). Using Lipofectamine 3000, the latter were transfected into HEK-293T cells. After a 40-h incubation, the lentivirus-containing supernatants were harvested. 3D42/1 cells were infected with the harvested lentiviruses by incubation for 24 h, and 8 μg/mL puromycin was added to the screen, followed by Rab4b and EEA1 knockout screening for stable Rab4b and EEA1 knockout ("Rab4b-KO" and "EEA1-KO") cells.

2.5 Western blotting

After cells were infected with *Gp*CDT, they were lysed in RIPA buffer (Proteintech, Wuhan, China) and centrifuged. The supernatant was then collected for Western blotting. Samples were then moved to PVDF membranes after being separated on 12.5% SDS-PAGE. The membranes

TABLE 2 Primers used in this study.

Gene	Primer direction	Sequence (5′–3′)	Size (bp)
Rab4b-sgRNA	Forward	CACCGTGACGCGGAGTTATTACCG	24
	Reverse	AAACCGGTAATAACTCCGCGTCAC	
Rab4b-KO	Forward	CACAATCGGCGTGGAGTT	176
	Reverse	AGTTGTAAGTCTCCCGGCTGT	
EEA1	Forward	AACGAGGCGAAACGTACCAT	140
	Reverse	ACTGCGATTTCCCCCGTAAG	
EEA1-sgRNA	Forward	CACCTTACATGAATACCAACCACG	24
	Reverse	AAACCGTGGTTGGTATTCATGTAA	
EEA1-KO	Forward	GATGACCGCATTAAACGAAAAC	112
	Reverse	AGCACTTTTCTCAAGACTTCGG	

were blocked with 5% nonfat dry milk before the primary antibody was incubated. Then, the membranes were treated with a second antibody after being washed with PBS. The Clarity Max Enhanced Chemiluminescence (ECL) (Bio-Rad, Hercules, CA, United States) was added to membranes and captured by ImageJ software (National Institutes of Health).

2.6 Quantitative real-time PCR

Using the UNIQ-10 column total RNA purification kit (Sangon, China), RNA was extracted from 3D4/21 cells that had been treated with *Gp*CDT. The PrimeScript TM RT kit with gDNA Eraser (Takara, Japan) was used to conduct a two-step RT-PCR. Using SYBR premix EX Taq™ II (Tli RNaseH Plus; Takara, Japan), transcripts were analyzed by qRT-PCR. The $2^{-\Delta\Delta CT}$ method was used to quantify gene expression, and results are presented relative to expression of β-actin. Table 2 lists the primer sequences that were employed.

2.7 Microscopy imaging

Cells were seeded in 6-well tissue culture plates (5×10^5 cells per well). After *Gp*CDT exposure for 48 h, static bright field images of cells were captured using light microscopy (Olympus America, Center Valley, PA).

2.8 Cell viability assay

For detecting cell viability, cells were pre-seeded into 96-well plates and treated with *Gp*CDT (10 μg/mL) for 0, 12, 24, 36, 48, and 60 h. A routine CCK-8 assay was used to examine cell viability according to the manufacturer's protocol.

2.9 Indirect immunofluorescence

In 6-well plates, cells were grown to around 90% confluence. Purified *Gp*CDT (10 μg/mL) was then added to each well, and the cells were incubated for 12 and 24 h at 37 °C. Following three PBS washes, the cells were fixed with 4% paraformaldehyde for 15 min before being rinsed with PBS once more. After that, cells were blocked for an hour at 37 °C in a BSA (3%) solution. Anti-H2AX primary antibody (1:1,000; Abcam, MA, United States) was incubated with cells overnight at 4 °C. Samples were then incubated at 37 °C for 1 h in the dark with fluorescein isothiocyanate (FITC)-conjugated goat anti-mouse IgG (Proteintech, Beijing, China). To identify the nuclei, DAPI (Beyotime, Shanghai, China) was utilized.

Trafficking studies were performed as follows. Cells were inoculated in 6-well plates and incubated with 10 μg/mL *Gp*CDT for 30 min at 4 °C to promote binding, followed by incubation at 37 °C for 45 min to stimulate uptake. Cells were subsequently immunostained for *Gp*CdtB and intracellular markers.

2.10 Statistical analysis

Statistical analyses were performed using GraphPad Prism version 8.0 (CA, United States). Statistical significance was assessed using Student's *t*-test, one-way ANOVA, or two-way ANOVA. Significant differences between groups are indicated by $^{*}p < 0.05$, $^{**}p < 0.01$, $^{***}p < 0.001$, and $^{****}p < 0.0001$.

3 Results

3.1 Interaction analysis of Rab4b and *Gp*CDT subunits

We previously demonstrated that Rab4b has the potential for a direct interaction with *Gp*CDT (Zhang et al., 2024). The *Gp*CDT subunits have molecular masses of approximately 42 kDa (*Gp*CdtA), 47 kDa (*Gp*CdtB), and 36 kDa (*Gp*CdtC) (Yang et al., 2023). To further understand how Rab4b controls sorting events in the early endosomes of the *Gp*CDT subunit, the present study aimed to investigate the possible role of Rab4b in this process using a coimmunoprecipitation assay. HEK-293T cells were transfected with expression plasmids to overexpress Flag-Rab4b. The expression of this construct was confirmed by Western blotting (Figure 1A). In addition, co-IP was performed with anti-*Gp*CdtA antiserum, anti-*Gp*CdtB antiserum, anti-*Gp*CdtC antiserum, anti-Flag mAb, or anti-His mAb to capture protein complexes. As shown in Figure 1B, anti-*Gp*CdtA and anti-*Gp*CdtC antisera did not result in imprint bands, but *Gp*CdtB could be observed in the IP samples by using anti-*Gp*CdtB antisera. In the next series of experiments, we incubated Rab4b directly with the *Gp*CdtA, *Gp*CdtB, and *Gp*CdtC subunits. Coimmunoprecipitations, performed using anti-His and anti-Flag mAb, showed that Rab4b coimmunoprecipitated with *Gp*CdtB (Figure 1C) but not with *Gp*CdtA and *Gp*CdtC (Figures 1D,E). These results suggested that Rab4b can interact with the *Gp*CdtB.

3.2 Rab4b influences *Gp*CDT from *Glaesserella parasuis*-induced cytotoxicity and vesicle trafficking in 3D4/21 cells

We used the CRISPR/Cas9 gene editing method to knock out Rab4b (see the Methods section). qRT-PCR and Western blotting results confirmed that Rab4b mRNA (Figure 2A) and protein

10.3389/fmicb.2025.1660176

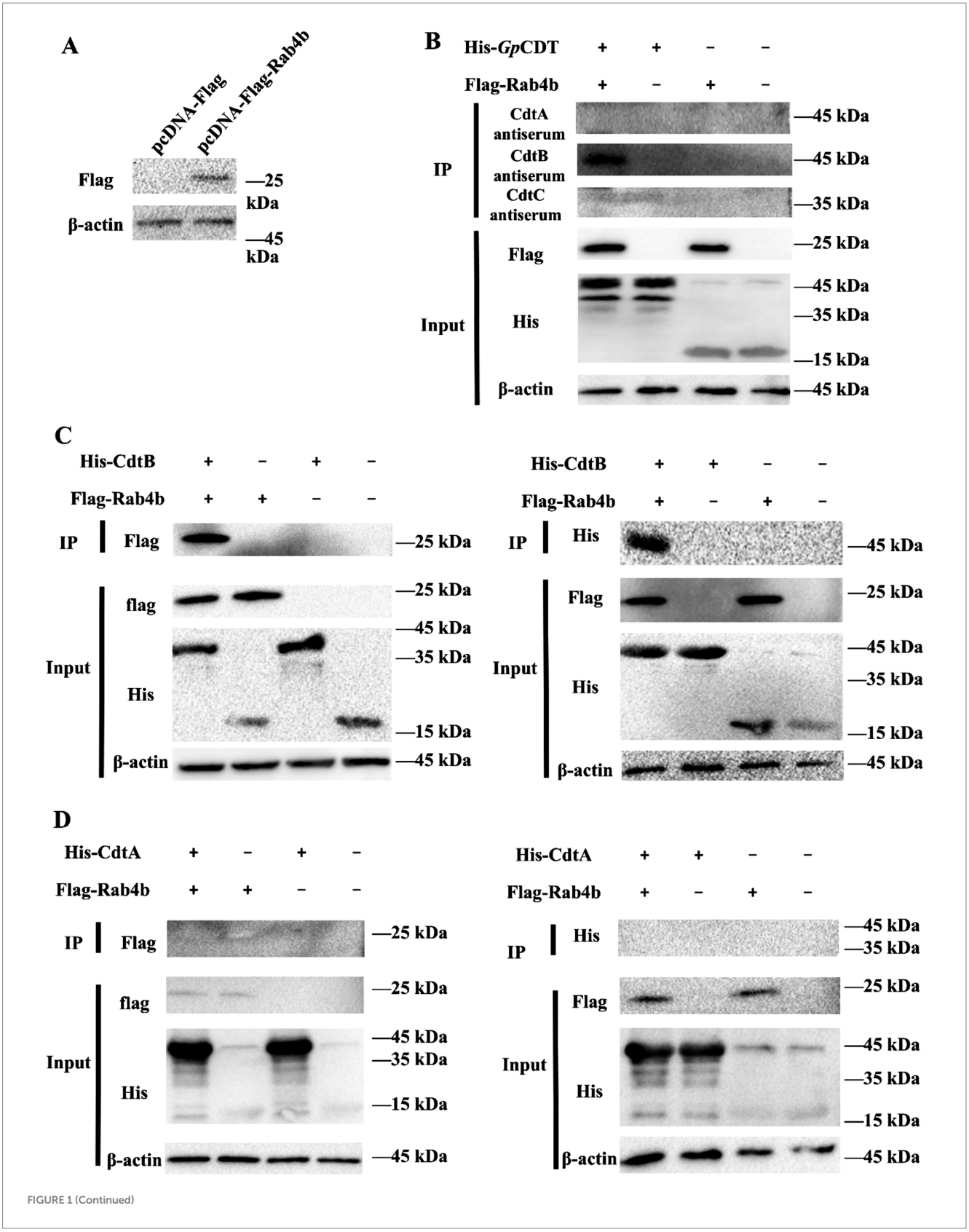

FIGURE 1 (Continued)

(Figure 2B) were knocked out entirely in Rab4b-KO cells. Next, we examined the morphology of 3D4/21 cells and Rab4b-KO cells after treatment with *Gp*CDT. Knockout of Rab4b resulted in significantly exhibited less cell distention after 48 h of *Gp*CDT treatment (Figure 2C). Furthermore, Rab4b-KO cells demonstrated a considerable improvement in cell viability after *Gp*CDT treatment (Figure 2D). Moreover, as shown in Figure 2E, *Gp*CDT treatments for 24 h increased the number of gH2AX foci, a marker for DNA damage

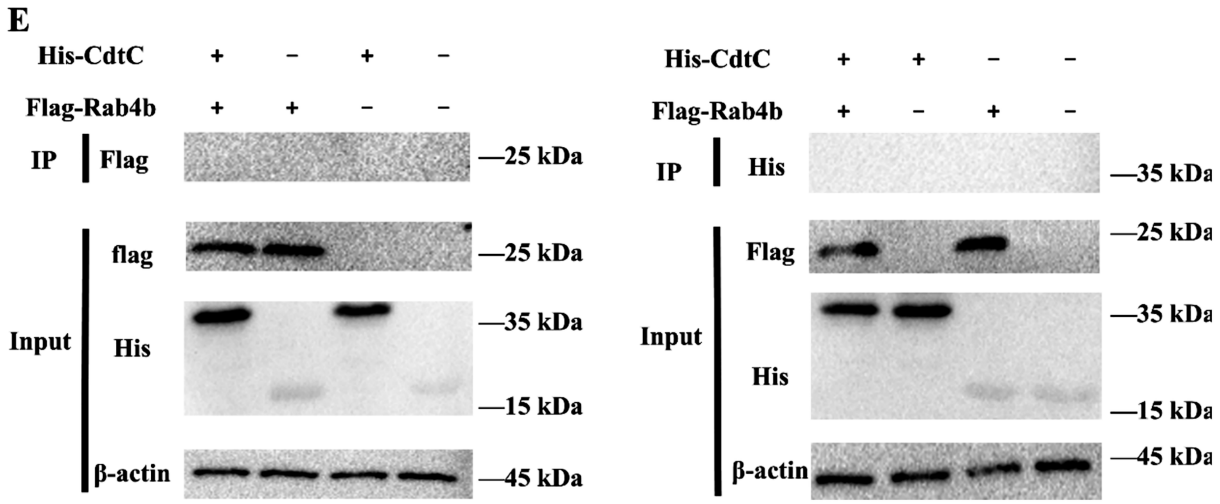

FIGURE 1
The interaction of Rab4b and CTD subunits was detected by coimmunoprecipitation. **(A)** Expression of the Rab4b gene on HEK-293T cells was detected by Western blot. **(B)** Immunoblot of host factor Rab4b recombinant protein from transfected HEK 293T cells and His-*Gp*CDT protein precipitated using anti-*Gp*CdtA, anti-*Gp*CdtB, and anti-*Gp*CdtC antisera. **(C–E)** Interactions between host factor Rab4b and His-*Gp*CdtA were analyzed by using anti-Flag mAb or anti-His mAb.

signaling, in 3D4/21 cells, when compared with Rab4b-KO cells. Moreover, in control 3D4/21 cells, *Gp*CDT treatment induced caspase-3 cleavages (Figure 2F). These results indicate that Rab4b is necessary for *Gp*CDT-induced cytotoxicity against the 3D4/21 cells.

Early endosomes and sorting endosomes, which are located where the endocytic and exocytic pathways converge, have been important hubs for membrane trafficking. We first demonstrated that in the presence of Rab4b, 3D4/21 cells took up *Gp*CDT inwards (Figure 2G). Once internalized, CdtB first reaches the early endosomes. Rab4b, located in the early endosomes, then exerts its function of controlling early endosome sorting, regulating the translocation of internalized *Gp*CdtB to the Golgi apparatus and endoplasmic reticulum (ER) in a retrograde manner in several cell types. 3D4/21 cells treated with *Gp*CDT display fluorescence of *Gp*CdtB (green), which co-localises with early lysosomes and the Golgi apparatus (red). This indicates that CdtB transport from early endosomes (Rab5+) to the Golgi apparatus (RCAS1+) also occurs in 3D4/21 cells (Figure 2H). Noteworthy is that we examined the vesicle trafficking of *Gp*CDT in Rab4b-KO cells to investigate the impact of Rab4b on this process. The results revealed that in Rab4b-KO cells, the red fluorescence of *Gp*CdtB did not colocalize with the green fluorescence of Rab5 and RCAS1 (Figure 2I), indicating that *Gp*CDT failed to reach the early endosome after Rab4b knockout. In summary, these findings show that Rab4b influences vesicle trafficking in *Gp*CDT.

3.3 Using comparative transcriptomic analysis, EEA1 was found to be a crucial gene for Rab4b-mediated internalization and intoxication of 3D4/21 cells by the active subunit of the *Glaesserella parasuis* cytolethal distending toxin

To explore the role of Rab4b after *Gp*CDT treatment, we conducted a comparative transcriptomic study on Rab4b-KO cells and 3D42/1 cells incubated with purified *Gp*CDT for 12 h. Following quality control, all samples had Q20 and Q30 percentages of clean data greater than 97 and 93%, respectively. Each sample's clean readings had a GC content ranging from 51.63 to 53.34% (Supplementary Tables S1). Transcriptome analysis revealed 1,420 differentially expressed genes (DEGs) after 12 h in the Rab4b-KO group compared with the 3D4/21 control group. Of these genes, 483 were upregulated and 937 were downregulated (Figure 3A). Six genes with elevated transcription levels and six with downregulated transcription levels were arbitrarily chosen for relative fluorescence measurement to corroborate the transcriptome sequencing results (Supplementary Tables S2). As shown in Figure 3B, the expression of most of the selected DEGs generated by RNA sequencing was consistent with the levels obtained using qRT-PCR. In addition, the correlation between the expression levels of the selected DEGs obtained using RNA sequencing and qRT-PCR was analyzed by calculating Pearson's correlation coefficient. The results revealed that Pearson's correlation coefficient was 0.3331, confirming that the data generated by RNA sequencing were reliable.

KEGG pathway analysis and GO categorization were applied to the DEGs. According to the GO analysis, the most prevalent categories were leukocyte migration, the G-protein-coupled receptor signaling pathway, the extracellular space, the cell surface, and chemokine activity (Figure 3C). KEGG analysis revealed that the significantly enriched pathways were associated with cytokines and cytokine receptors and pathways involved in lipid metabolism and atherosclerosis (Figure 3D). GO and KEGG enrichment analyses suggested that Rab4b influences several biological functions in 3D4/21 cells infected with *Gp*CDT. Rab4b is associated with the endocytosis pathway in the KEGG signaling pathway, which is closely related to cell vesicle trafficking. Fourteen DEGs were identified in the endocytosis pathway (Figure 3E), and only EEA1, like Rab4b, is located in the early endosomes, which can mediate early endosome fusion, as well as the capture of vesicles derived from clathrin-coated

10.3389/fmicb.2025.1660176

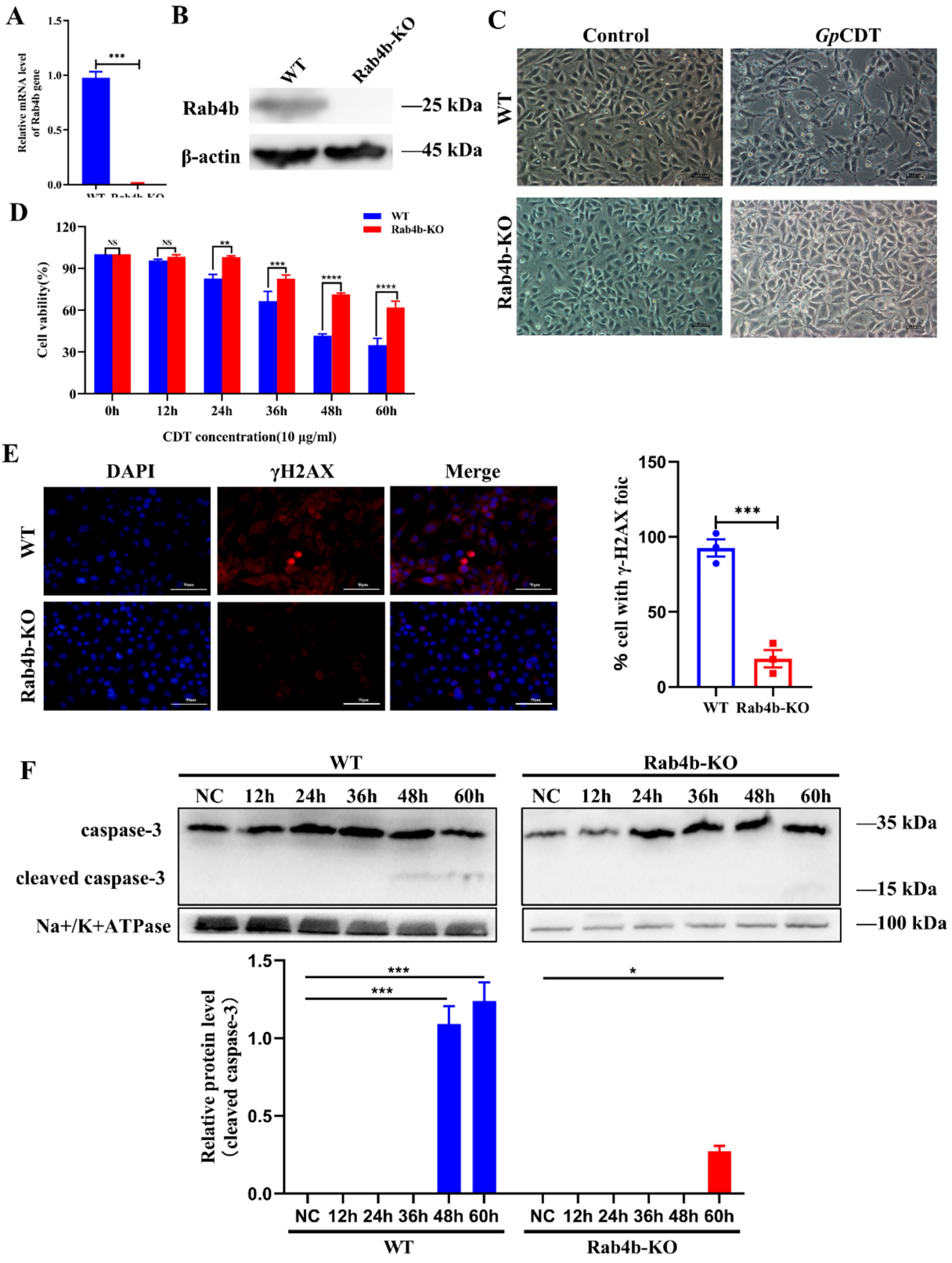

FIGURE 2 (Continued)

10.3389/fmicb.2025.1660176

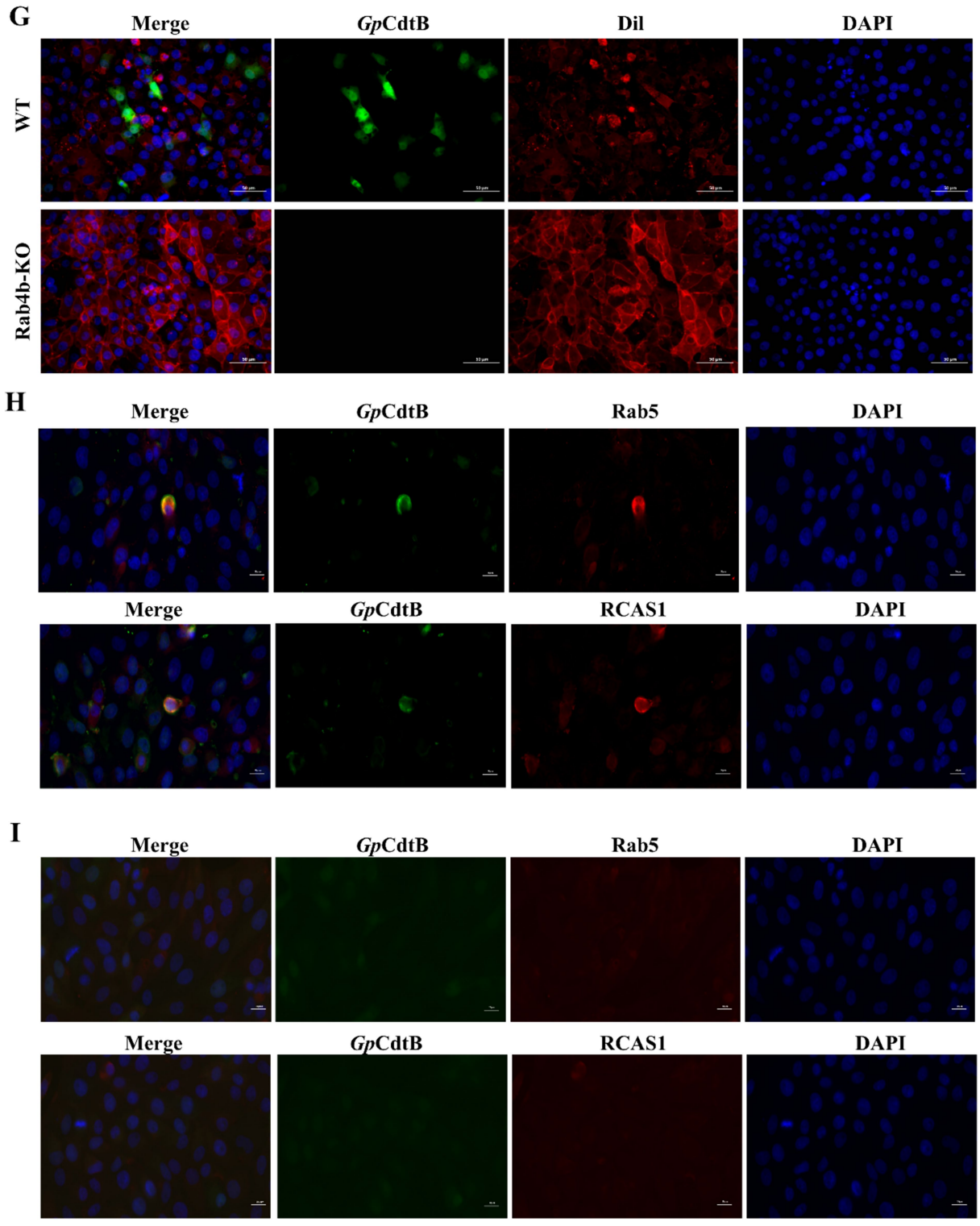

FIGURE 2
Knockout of Rab4b weakened *Gp*CDT-induced cytotoxicity and vesicle trafficking in 3D4/21 cells. **(A)** Detection of Rab4b gene mRNA level by qRT-PCR. **(B)** Western blot analysis comparing Rab4b protein expression level in3D4/21 and Rab4b-KO cells. **(C)** Typical morphology of 3D4/21 cells and Rab4b-KO cells treated with 10 μg/mL *Gp*CDT. Scale bar 100 μm. **(D)** Cell viability after 10 μg/mL *Gp*CDT exposure for varying durations (0, 12, 24, 36, 48, and 60 h) (* means $p < 0.05$, ** means $p < 0.01$, *** means $p < 0.001$, **** means $p < 0.001$, and ns means $p > 0.05$). **(E)** The DNA damage signature, as indicated by γH2AX, was detected using immunofluorescence microscopy with a bar graph quantifying γH2AX foci. Scale bar 50 μm. **(G)** The entry of *Gp*CDT into 3D4/21 cells and Rab4b-KO cells was detected by indirect immunofluorescence: *Gp*CDT B (green) and DiI (red). Scale bar 50 μm. **(H,I)** For the trafficking study, the indirect immunofluorescence results for the 3D4/21 and Rab4b-KO cells were obtained after treatment with *Gp*CDT. Green fluorescence indicates the *Gp*CdtB, and red fluorescence indicates the organelle marker. Rab5 is an early endosomal marker, and RCAS1 is a marker of the Golgi apparatus. Scale bar 20 μm.

10.3389/fmicb.2025.1660176

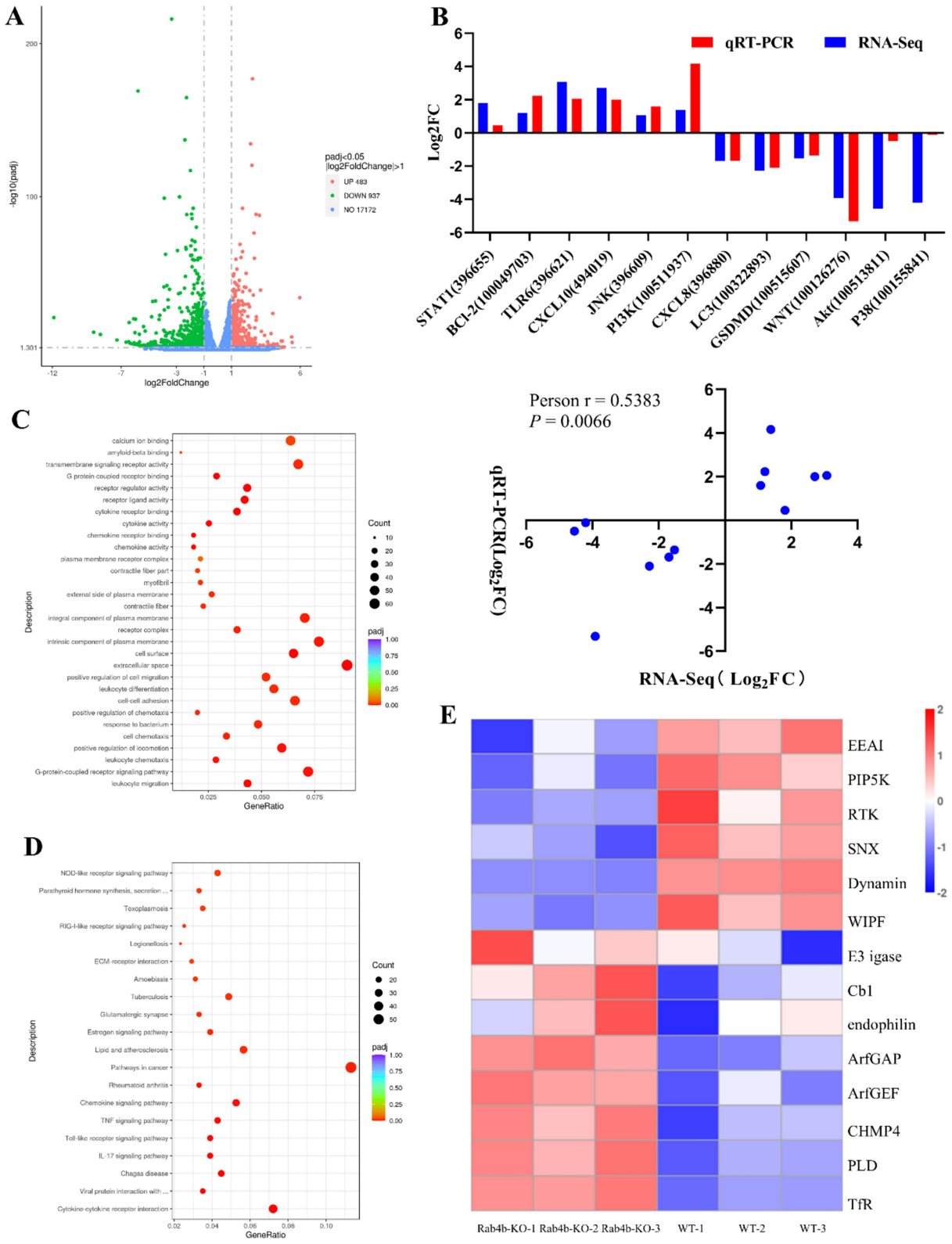

FIGURE 3
Comparative transcriptomic analysis (Rab4b-KO vs. 3D4/21 Cells). **(A)** The differentially expressed genes (DEGs) in Rab4b-KO and 3D42/1 cells infected with *Gp*CDT were analyzed via volcano plots. Red dots indicate DEGs that are upregulated, green dots indicate downregulated DEGs, and blue dots indicate genes that do not significantly differ. **(B)** DEGs were selected randomly for qRT-PCR analysis, and the expression levels of those DEGs were estimated using the $2^{-\Delta\Delta CT}$ method. The correlation between DEG expression levels, as determined by RNA sequencing and qRT-PCR, was analyzed using Pearson's correlation analysis. **(C)** Bubble map of the top 20 most enriched GO terms. **(D)** Histograms of the top 20 most enriched signaling pathways. **(E)** A heat map that shows the expression of endocytosis pathway-related genes.

10.3389/fmicb.2025.1660176

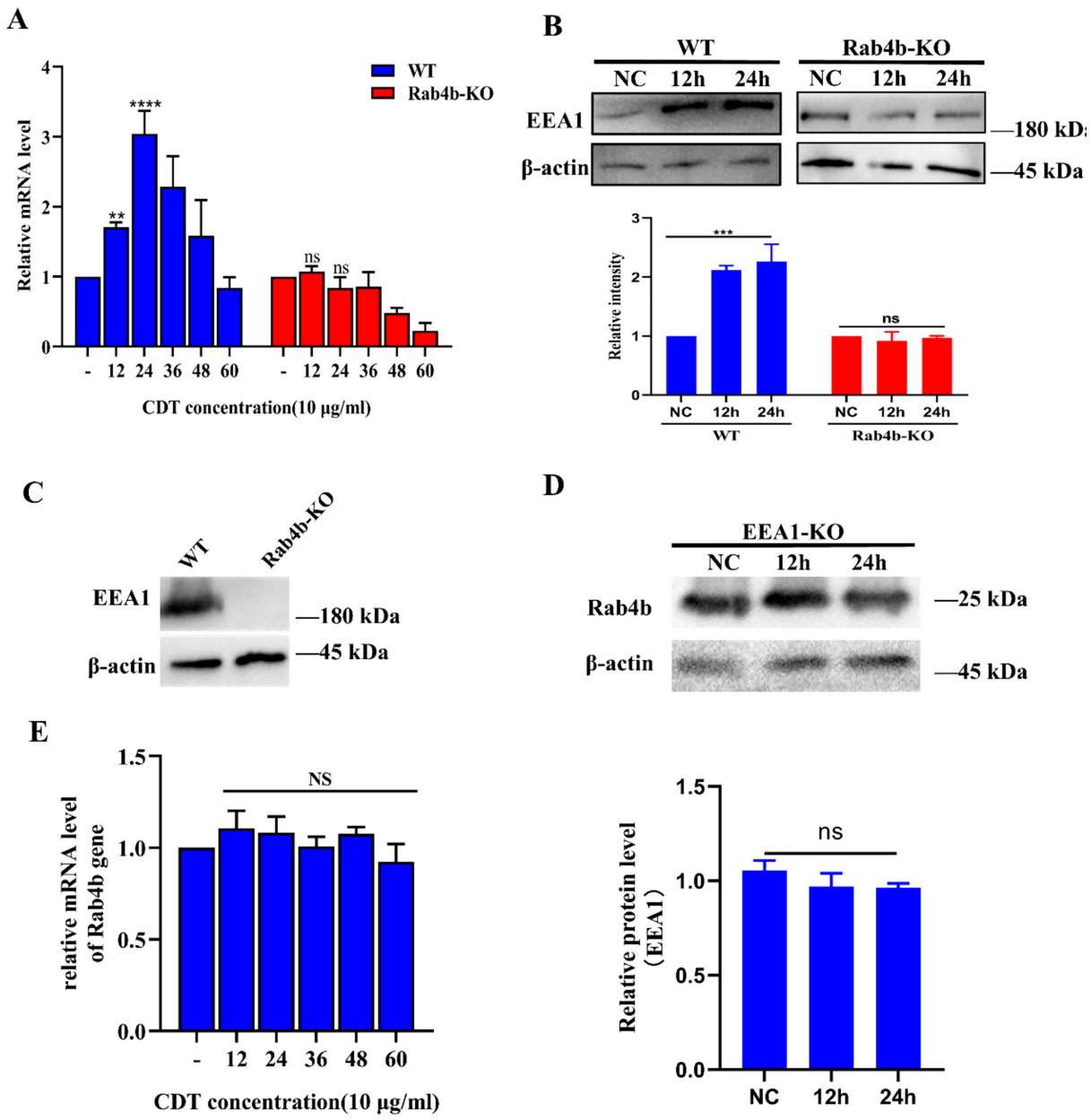

FIGURE 4
Effect of Rab4b on EEA1 expression in 3D4/21 cells after treatment with *Gp*CDT. **(A)** The mRNA level of EEA1 in *Gp*CDT-treated 3D4/21 and Rab4b-KO cells was measured via qRT-PCR (* means $p < 0.05$, ** means $p < 0.01$, *** means $p < 0.001$, **** means $p < 0.001$, and ns means $p > 0.05$). **(B)** The protein expression level of EEA1 in *Gp*CDT-treated 3D4/21 and Rab4b-KO cells was analyzed by Western blotting. **(C)** The efficiency of EEA1 protein knockout was confirmed by Western blot analysis. **(D)** The expression level of the Rab4b protein in *Gp*CDT-treated EEA1-KO cells was analyzed by Western blotting. **(E)** Detect the mRNA level of Rab4b by qRT-PCR in EEA1-KO cells after *Gp*CDT treatment (* means $p < 0.05$, ** means $p < 0.01$, *** means $p < 0.001$, **** means $p < 0.001$, and ns means $p > 0.05$).

pits by early endosomes. EEA1 may be an important protein involved in Rab4b-mediated *Gp*CDT cytotoxicity and vesicle trafficking.

3.4 After *Gp*CDT treatment, Rab4b can upregulate the expression of EEA1 in 3D4/21 cells

In this study, transcriptomic sequencing revealed that the expression level of EEA1 changed significantly after 12 h of cell infection with *Gp*CDT. The expression levels of EEA1 in 3D4/21 and Rab4b-KO cells, as detected by qRT-PCR and Western blot, after *Gp*CDT treatment. The results showed that the mRNA level of EEA1 increased after *Gp*CDT treatment in WT cells. After the elimination of Rab4b, the mRNA level of EEA1 did not change significantly (Figure 4A). Western blotting results also revealed that the EEA1 protein level increased after 24 h of treatment of 3D4/21 cells with *Gp*CDT, whereas the EEA1 protein level did not change significantly after Rab4b knockout (Figure 4B).

The EEA1 knockout cells were subsequently constructed via CRISPR/Cas9 technology. The western blot results showed that

10.3389/fmicb.2025.1660176

the expression level of the EEA1 protein in EEA1-KO cells was knocked out compared with WT cells, indicating that the EEA1 knockout ("EEA1-KO") cells were successfully constructed (Figure 4C). Subsequently, using Western blotting and qRT-PCR, the Rab4b mRNA levels in EEA1-KO cells treated with *Gp*CDT were determined. These results confirmed that when EEA1 was knocked out, Rab4b mRNA and protein levels did not alter considerably (Figures 4D,E). These findings suggested that in *Gp*CDT-treated cells, EEA1 did not affect Rab4b transcription levels.

3.5 The effect of EEA1 on the Rab4b mediates internalization and intoxication of 3D4/21 cells by the *Gp*CDT

It has been confirmed that knockout of Rab4b can inhibit the expression of the EEA1 protein after *Gp*CDT treatment. The following steps were taken to confirm whether the EEA1 protein influences Rab4b-mediated *Gp*CDT-induced cytotoxicity and vesicle trafficking in 3D4/21 cells. Using indirect immunofluorescence, we were able to identify the fluorescence of *Gp*CdtB and get insight into the uptake of

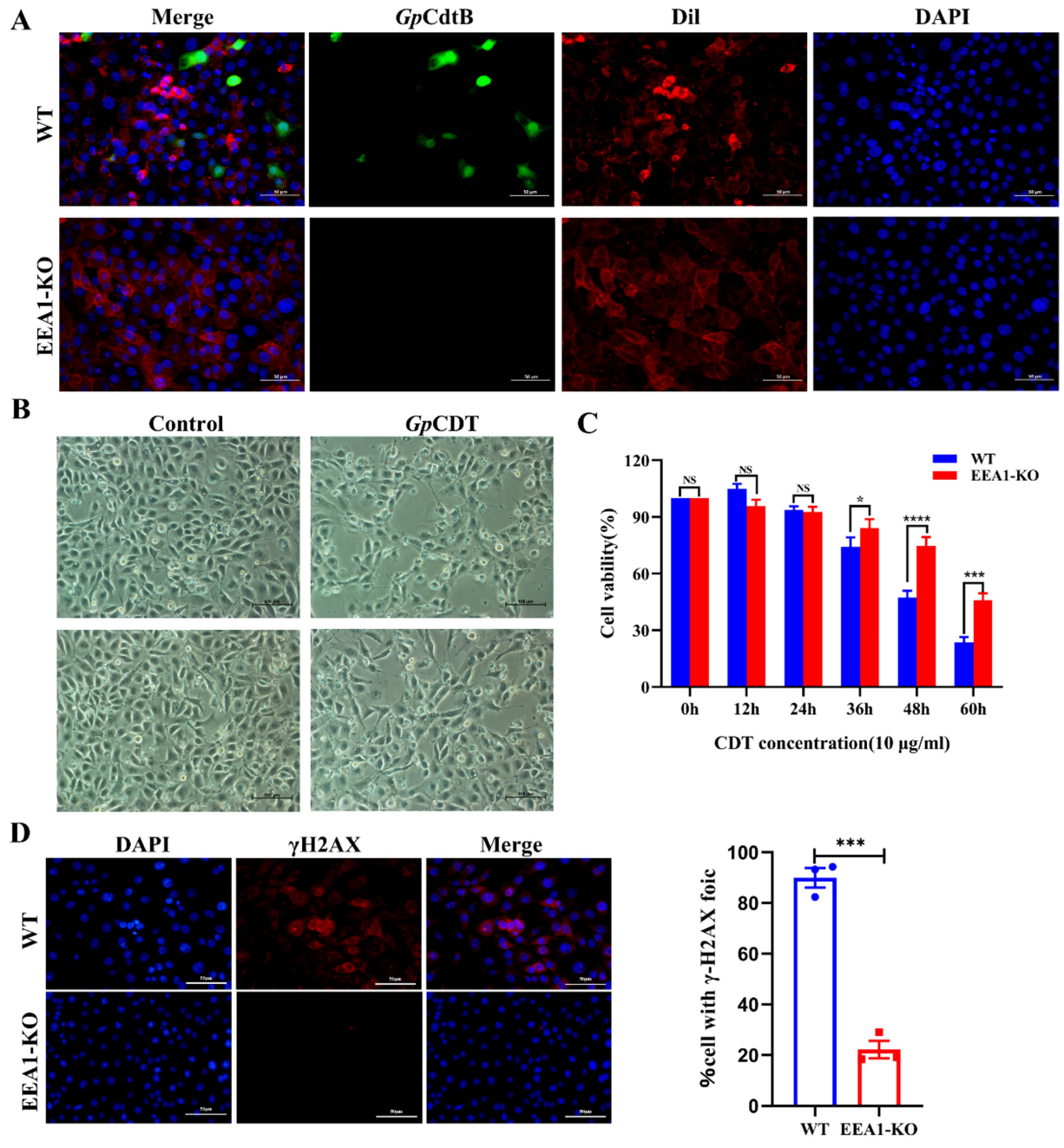

FIGURE 5 (Continued)

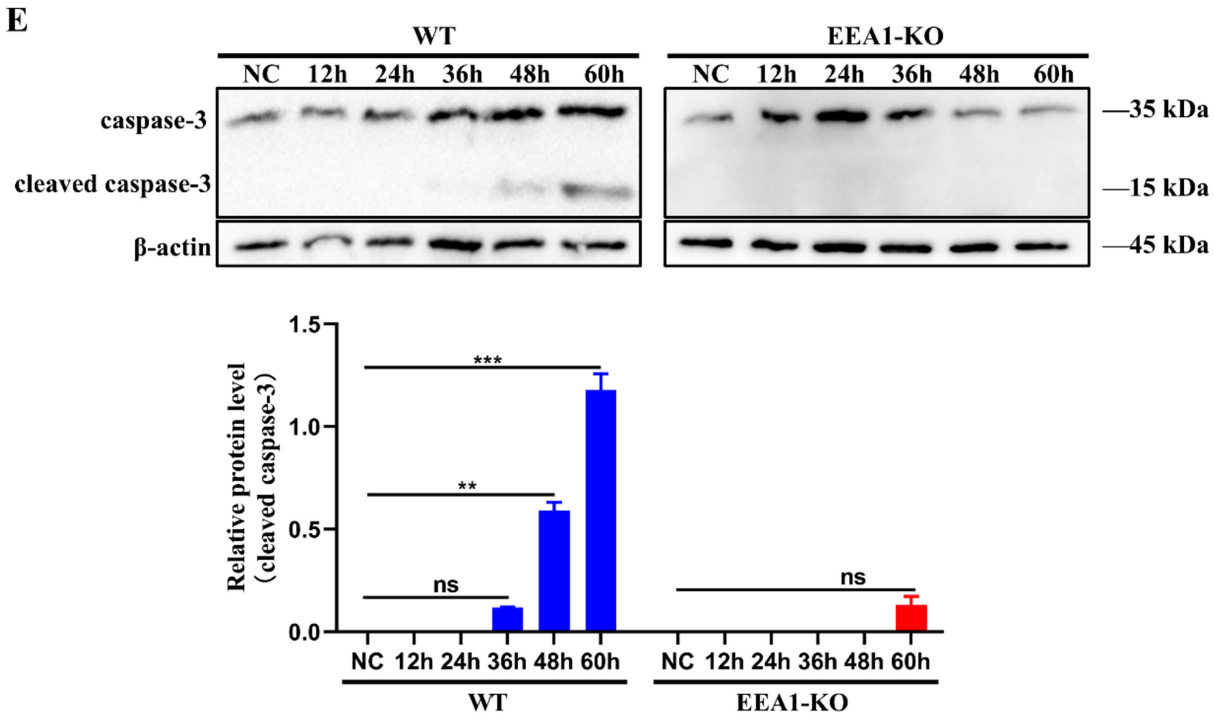

FIGURE 5
In 3D4/21 cells, the Rab4b-mediated cytotoxicity and vesicle trafficking of *Gp*CDT can be influenced by EEA1. **(A)** The entry of *Gp*CDT into 3D4/21 cells and EEA1-KO cells was detected by indirect immunofluorescence. *Gp*CdtB (green) and DiI (red). Scale bar 50 μm. **(B)** Observed the typical morphology of 3D4/21 cells and EEA1-KO cells after *Gp*CDT treatment for 48 h. Scale bar 100 μm. **(C)** CCK-8 was used to determine the survival rates of 3D4/21 and EEA1-KO cells treated with 10 μg/mL *Gp*CDT at different time points (* means $p < 0.05$, ** means $p < 0.01$, *** means $p < 0.001$, **** means $p < 0.001$, and ns means $p > 0.05$). **(D)** 3D4/21 cells and EEA1-KO cells cells were exposed to *Gp*CDT for 24 h, and analyzed by immunofluorescence microscopy with antibodies directed against γH2AX (red) and DAPI (blue), alongside a bar graph showing the percentage of cells with γH2AX foci. Scale bar 50 μm. **(E)** Cleaved caspase-3 levels were detected in 3D4/21 and EEA1-KO cells treated with *Gp*CDT using Western blotting ($n = 3$).

*Gp*CDT by cells following EEA1 deletion. The findings showed that *Gp*CdtB fluorescence was not seen in EEA1-KO cells (Figure 5A). Next, observe the morphological changes that occur as a result of exposure to *Gp*CDT. EEA1-KO cells were more resistant to *Gp*CDT and exhibited less cell distention (Figure 5B). Meanwhile, the study of the EEA1 effect on cell survival rate showed that the survival rate of EEA1-KO cells treated with *Gp*CDT was greater than that of WT cells (Figure 5C). Similarly, we demonstrated that *Gp*CDT reduced the number of γH2AX foci in EEA1-KO cells compared to 3D4/21 cells, a marker for DNA damage signaling (Figure 5D). Western blotting was used to detect the activation level of caspase-3, a key apoptotic factor, after *Gp*CDT treatment. The results showed that the cleaved caspase-3 bands appeared at 48 h after *Gp*CDT treatment, while the caspase-3 cleavage bands appeared at 60 h in EEA1-KO cells (Figure 5E). Overall, the experimental data support our hypothesis that EEA1 affects the Rab4b-mediated internalization and intoxication of 3D4/21 cells by the *Gp*CDT.

4 Discussion

The present study investigated the role of Rab4b in mitigating the toxic effects of *Gp*CDT on cells by modulating the vesicle trafficking process of *Gp*CDT and identified key genes involved in this process through transcriptome sequencing analysis. The following are our work's three main conclusions: (i) Rab4b interacts with the active subunit of *Gp*CDT and influences *Gp*CDT-induced cytotoxicity in 3D4/21 cells; (ii) Rab4b promotes the uptake of *Gp*CDT by cells through the upregulation of EEA1 protein expression and promotes subsequent vesicle trafficking.

Existing studies have reported that Rab4b is involved in various intracellular functions. Antigen-presenting cells APC enhance their antigen-presenting capacity by increasing Rab4b-mediated endosomal recycling, informing studies to improve immune cell recognition (Krawczyk et al., 2007). In 3T3-L1 preadipocytes, Rab4b, together with Rab4a and Rab8a, mediates the recycling of the glucose transporter protein GLUT4 (Chen et al., 2012). It has also been demonstrated that Rab4b is involved in regulating endosomal circulation, which is essential for maintaining the spine and recirculating neurotransmitter receptors. At the same time, the neuron-specific effector of Rab4b, GRIP-associated protein-1 (GRASP-1), is a key component in coordinating the maturation of circulating endosomes in dendrites (Hoogenraad et al., 2010). This study not only further confirmed the impact of Rab4b on the cytotoxicity of *Gp*CDT but also conducted an initial exploration into the role of Rab4b within the vesicle trafficking of *Gp*CDT.

CdtB as an active subunit can induce significant cytotoxic and inflammatory responses in a wide range of cells, like THP-1 human macrophages (Chen et al., 2020), Human colorectal cancer cell line HCT116 cells, Human colonic epithelial cell line FHC cells (Gu et al., 2022), and Newborn pig tracheal epithelial cells (Yang et al., 2023). In this study, we first verified the connection between Rab4b and *Gp*CdtB, and first characterize the effects of Rab4b on *Gp*CDT-induced cytotoxicity in 3D4/21 cells. Furthermore, we employed

indirect immunofluorescence to investigate the effect of Rab4b on *Gp*CDT vesicle trafficking in 3D4/21 cells. After cellular uptake, *Gp*CDT colocalized with early endosomes and the Golgi apparatus. Nevertheless, *Gp*CDT did not colocalize with the Golgi apparatus in Rab4b-KO cells. Thus, it is confirmed that the Rab4b protein interacts directly with *Gp*CDT, affecting its vesicle trafficking.

To further explore the mechanism by which Rab4b mediates *Gp*CDT vesicle trafficking, we performed transcriptomic analysis on 3D4/21 and Rab4b-KO cells after they were treated with *Gp*CDT. Through transcriptome sequencing, we found that the expression of 14 genes in the endocytosis pathway, in which Rab4b is located, was significantly altered, and only EEA1 was localized in early endosomes, similar to Rab4b. However, there are some functional differences between Rab4b and EEA1 (Jovic et al., 2010). Rab4b has been confirmed to participate in early endosomal sorting and endosomal circulation. EEA1, as an effector protein of Rab5, plays an important role in forming vesicles. It is a tethering molecule that provides directionality to vesicular transport from the plasma membrane to early endosomes (Adams and Wayne Vogl, 2017; McCaffrey et al., 2001; Rubino et al., 2000). Our study demonstrated that Rab4b can affect the expression of EEA1 in cells. After 3D4/21 cells were treated with *Gp*CDT, the level of the EEA1 protein changed significantly. However, Rab4b expression was not affected when EEA1 was knocked down. Moreover, the knockout of EEA1 inhibited the vesicle trafficking of *Gp*CDT and the uptake of *Gp*CDT by cells. We also tested the cellular uptake of *Gp*CDT in Rab4b-KO cells and reported that Rab4b knockout inhibited the uptake of *Gp*CDT by cells; however, green fluorescence of *GpCDT B* was still observed in Rab4b-KO cells. We speculated that the inhibition of *Gp*CDT uptake by Rab4b-KO cells was weaker than that by EEA1-KO cells because the knockout of Rab4b resulted in no upregulation of EEA1 expression in *Gp*CDT-treated cells, rather than a direct reduction in the expression of EEA1. Therefore, after binding to the cell membrane, *Gp*CDT can be separated from the cell membrane to form vesicles under the action of EEA1 and can be transported to early endosomes through vesicles. Subsequently, Rab4b mediates endosomal sorting in early endosomes, transports *Gp*CtdB to the Golgi apparatus, and circulates the *Gp*CDT receptor to the cell membrane. The knockout of Rab4b prevents the upregulation of the EEA1 protein, inhibits the formation of vesicles in which cells take up *Gp*CDT, and hinders the fusion of vesicles containing *Gp*CDT with early endosomes. Moreover, the Rab4b-mediated vesicle trafficking function is eliminated, resulting in a weakened toxic effect of *Gp*CDT on cells. Rab5 and its effector EEA1 mediate the delivery of internalized cargo molecules to the early endosomes. Cargoes can then be sorted at early endosomes.

Rab4b and EEA1 have been shown to assist bacterial infection. For example, *Clostridium difficile* binary toxins first bind to lipoprotein receptors (LSRs) stimulated by lipolysis on cell membranes (Hemmasi et al., 2015) and are then encased by clathrin to form vesicles that enter the cell and reach the early endosome (Papatheodorou et al., 2010). The interaction between EEA1 and Rab5 can regulate the occurrence of this process (Semerdjieva et al., 2008). Postentrant *Clostridium difficile* binary toxins are retrogradely transported from the endoplasmic reticulum through the Golgi apparatus via Rab4b-mediated vesicle trafficking into the cytoplasm (Schmidt et al., 2015), where they exert their toxic effects in the cytoplasm. In addition, *Pasteurella multocida* toxin (PMT) binds to low-density lipoprotein (LDL) receptor-associated protein 1 (LRP-1) on the cell membrane. It enters the cell (Schoellkopf et al., 2022), after which the vesicles coated with PMT fuse with early endosomes. Finally, the cells reach late endosomes, expand in the region, and then insert and translocate across the vesicle. The transfer of the catalytic domain into the cytoplasm is also influenced by EEA1 and Rab4b (Kubatzky, 2022; Repella et al., 2011). Additionally, Rab4b and EEA1 also play a crucial role in the virus's infection. For example, during the process of Japanese Encephalitis Virus (JEV) entry, Rab4b and EEA1 play a crucial role in facilitating transport to early endosomes (Miao et al., 2025). Based on the cellular uptake and vesicle trafficking processes of *Clostridium difficile* binary toxins and *Pasteurella multicida* toxin, we hypothesized that *GpCDT* first binds to the receptor on the cell membrane to form a complex. Then EEA1 promotes the uptake of this complex by cells, leading to the formation of vesicles and their subsequent delivery to early endosomes. The complex subsequently disintegrates, and *GpCDT* interacts with Rab4b. The receptor of *GpCDT* returns to the cell membrane through early endosome sorting and binds to the next *Gp*CDT.

In summary, we conducted a systematic study to investigate the mechanism by which Rab4b contributes to the cytotoxicity of *Gp*CDT in 3D4/21 cells. Our findings demonstrate that Rab4b is essential for the transport of *Gp*CDT to endosomes. The mechanisms we identified contribute to a deeper understanding of how *Gp*CDT utilizes the Rab4b protein to facilitate infection, and may aid in the development of new strategies to control bacterial infections.

5 Conclusion

In conclusion, our investigation revealed, for the first time, that the host factor Rab4b enables the cellular uptake process of *Gp*CDT by upregulating EEA1 protein expression, thereby promoting the vesicle trafficking of *Gp*CDT in 3D4/21 cells and ultimately leading to the active subunit of *Gp*CDT-induced cytotoxicity. However, a limitation of this study is the lack of research on *Gp*CDT receptors and how RAB4B interacts with other Rab proteins to facilitate the transition of *Gp*CDT from early endosomes to late endosomes. In the future, we will continue to study the above issues.

Data availability statement

The data presented in the study are deposited in the SRA database, accession number PRJNA1332541.

Ethics statement

Specific pathogen-free C57/BL6 mice were utilized for in vivo experiments. All animal experimental protocols were approved by the Animal Ethics Committee of Sichuan Agricultural University and were carried out accordingly.

Author contributions

YZ: Methodology, Supervision, Investigation, Data curation, Writing – review & editing, Software, Resources, Writing – original draft, Formal analysis, Visualization, Validation. ZY: Formal analysis, Writing – original draft, Software, Data curation, Methodology, Visualization, Validation, Investigation, Writing – review & editing, Supervision. SD: Writing – review & editing, Supervision. QZ: Supervision,

Writing – review & editing. XH: Supervision, Writing – review & editing. RW: Supervision, Writing – review & editing. YWa: Supervision, Writing – review & editing. QY: Writing – review & editing, Supervision. SC: Supervision, Writing – review & editing. YWe: Conceptualization, Funding acquisition, Writing – review & editing.

Funding

The author(s) declare that financial support was received for the research and/or publication of this article. This work was funded by the Key R&D support Plan of Chengdu Science and Technology Bureau (No. 2022-YF05-00817-SN).

Acknowledgments

We would like to express our sincere gratitude for their support.

Conflict of interest

The authors declare that the research was conducted in the absence of any commercial or financial relationships that could be construed as a potential conflict of interest.

Generative AI statement

The authors declare that no Gen AI was used in the creation of this manuscript.

Any alternative text (alt text) provided alongside figures in this article has been generated by Frontiers with the support of artificial intelligence and reasonable efforts have been made to ensure accuracy, including review by the authors wherever possible. If you identify any issues, please contact us.

Publisher's note

Supplementary material

The Supplementary material for this article can be found online at: https://www.frontiersin.org/articles/10.3389/fmicb.2025.1660176/full#supplementary-material

References

Adams, A., and Wayne Vogl, A. (2017). High resolution localization of Rab5, EEA1, and Nectin-3 to tubulobulbar complexes in the rat testis. *Anat. Rec.* 300, 1160–1170. doi: 10.1002/ar.23563

Bergeland, T., Haugen, L., Landsverk, O. J., Stenmark, H., and Bakke, O. (2008). Cell-cycle-dependent binding kinetics for the early endosomal tethering factor EEA1. *EMBO Rep.* 9, 171–178. doi: 10.1038/sj.embor.7401152

Boesze-Battaglia, K., Dhingra, A., Walker, L. M., Zekavat, A., and Shenker, B. J. (2020). Internalization and intoxication of human macrophages by the active subunit of the *Aggregatibacter actinomycetemcomitans* cytolethal distending toxin is dependent upon cellugyrin (synaptogyrin-2). *Front. Immunol.* 11:1262. doi: 10.3389/fimmu.2020.01262

Brockmeier, S. L., Loving, C. L., Mullins, M. A., Register, K. B., Nicholson, T. L., Wiseman, B. S., et al. (2013). Virulence, transmission, and heterologous protection of four isolates of *Haemophilus parasuis*. *Clin. Vaccine Immunol.* 20, 1466–1472. doi: 10.1128/cvi.00168-13

Brumell, J. H., and Scidmore, M. A. (2007). Manipulation of rab GTPase function by intracellular bacterial pathogens. *Microbiol. Mol. Biol. Rev.* 71, 636–652. doi: 10.1128/mmbr.00023-07

Chen, Y., Wang, Y., Zhang, J., Deng, Y., Jiang, L., and Song, E. (2012). Rab10 and myosin-Va mediate insulin-stimulated GLUT4 storage vesicle translocation in adipocytes. *J Cell Biol* 198:545–60.

Chen, M. X., Chen, Y., Fu, R., Mao, G. Q., Liu, S. Y., and Shen, T. B. (2020). Rab5a promotes cytolethal distending toxin B-induced cytotoxicity and inflammation. *Infect. Immun.* 88:e00132-20. doi: 10.1128/iai.00132-20

Costa-Hurtado, M., Barba-Vidal, E., Maldonado, J., and Aragon, V. (2020). Update on Glasser's disease: how to control the disease under restrictive use of antimicrobials. *Vet. Microbiol.* 242:108595. doi: 10.1016/j.vetmic.2020.108595

Dixon, S. D., Huynh, M. M., Tamilselvam, B., Spiegelman, L. M., Son, S. B., Eshraghi, A., et al. (2015). Distinct roles for CdtA and CdtC during intoxication by cytolethal distending toxins. *PLoS One* 10:e0143977. doi: 10.1371/journal.pone.0143977

Fouraux, M. A., Deneka, M., Ivan, V., van der Heijden, A., Raymackers, J., van Suylekom, D., et al. (2004). Rabip4′ is an effector of rab5 and rab4 and regulates transport through early endosomes. *Mol. Biol. Cell* 15, 611–624. doi: 10.1091/mbc.e03-05-0343

Gargi, A., Reno, M., and Blanke, S. R. (2012). Bacterial toxin modulation of the eukaryotic cell cycle: are all cytolethal distending toxins created equally? *Front. Cell. Infect. Microbiol.* 2:124. doi: 10.3389/fcimb.2012.00124

Gu, J., Lin, Y., Wang, Z., Pan, Q., Cai, G., He, Q., et al. (2022). *Campylobacter jejuni* cytolethal distending toxin induces GSDME-dependent pyroptosis in colonic epithelial cells. *Front. Cell. Infect. Microbiol.* 12:853204. doi: 10.3389/fcimb.2022.853204

He, H., Dai, F., Yu, L., She, X., Zhao, Y., Jiang, J., et al. (2002). Identification and characterization of nine novel human small GTPases showing variable expressions in liver cancer tissues. *Gene Expr.* 10, 231–242. doi: 10.3727/000000002783992406

Hemmasi, S., Czulkies, B. A., Schorch, B., Veit, A., Aktories, K., and Papatheodorou, P. (2015). Interaction of the *Clostridium difficile* binary toxin CDT and its host cell receptor, lipolysis-stimulated lipoprotein receptor (LSR). *J. Biol. Chem.* 290, 14031–14044. doi: 10.1074/jbc.M115.650523

Hesping, E., and Boddey, J. A. (2024). Whole-genome CRISPR screens to understand apicomplexan-host interactions. *Mol. Microbiol.* 121, 717–726. doi: 10.1111/mmi.15221

Hoogenraad, C. C., Popa, I., Futai, K., Martinez-Sanchez, E., Wulf, P. S., van Vlijmen, T., et al. (2010). Neuron specific Rab4 effector GRASP-1 coordinates membrane specialization and maturation of recycling endosomes. *PLoS Biol.* 8:e1000283. doi: 10.1371/journal.pbio.1000283

Hu, X., and Wang, Y. (2024). Protocol to identify receptors of secreted proteins through CRISPR-Cas9 whole-genome screening technology. *STAR Protoc.* 5:103315. doi: 10.1016/j.xpro.2024.103315

Huhn, G. R. 3rd, Sparkes, C., Silva, I., Reyes, C., Perez, G., Khondker, F., et al. (2022). Acid-induced disassembly of the *Haemophilus ducreyi* cytolethal distending toxin. *Biochem. Biophys. Res. Commun.* 636, 57–63. doi: 10.1016/j.bbrc.2022.10.068

Jordens, I., Marsman, M., Kuijl, C., and Neefjes, J. (2005). Rab proteins, connecting transport and vesicle fusion. *Traffic* 6, 1070–1077. doi: 10.1111/j.1600-0854.2005.00336.x

Jovic, M., Sharma, M., Rahajeng, J., and Caplan, S. (2010). The early endosome: a busy sorting station for proteins at the crossroads. *Histol. Histopathol.* 25, 99–112. doi: 10.14670/hh-25.99

Kaddai, V., Gonzalez, T., Keslair, F., Gremeaux, T., Bonnafous, S., Gugenheim, J., et al. (2009). Rab4b is a small GTPase involved in the control of the glucose transporter GLUT4 localization in adipocyte. *PLoS One* 4:e5257. doi: 10.1371/journal.pone.0005257

Kailoo, S., Shreya, and Kumar, Y. (2021). Cytolethal distending toxin: from genotoxin to a potential biomarker and anti-tumor target. *World J. Microbiol. Biotechnol.* 37:150. doi: 10.1007/s11274-021-03117-z

Kalin, S., Buser, D. P., and Spiess, M. (2016). A fresh look at the function of Rabaptin5 on endosomes. *Small GTPases* 7, 34–37. doi: 10.1080/21541248.2016.1140616

Krawczyk, M., Leimgruber, E., Seguin-Estevez, Q., Dunand-Sauthier, I., Barras, E., and Reith, W. (2007). Expression of RAB4B, a protein governing endocytic recycling, is co-regulated with MHC class II genes. *Nucleic Acids Res.* 35, 595–605. doi: 10.1093/nar/gkl980

Kubatzky, K. F. (2022). *Pasteurella multocida* toxin—lessons learned from a mitogenic toxin. *Front. Immunol.* 13:1058905. doi: 10.3389/fimmu.2022.1058905

Mao, W., Wang, Z., Wen, S., Lin, Y., Gu, J., Sun, J., et al. (2023). LRRC8A promotes *Glaesserella parasuis* cytolethal distending toxin-induced p53-dependent apoptosis in NPTr cells. *Virulence* 14:2287339. doi: 10.1080/21505594.2023.2287339

McCaffrey, M. W., Bielli, A., Cantalupo, G., Mora, S., Roberti, V., Santillo, M., et al. (2001). Rab4 affects both recycling and degradative endosomal trafficking. *FEBS Lett.* 495, 21–30. doi: 10.1016/s0014-5793(01)02359-6

Miao, C., Zhao, Q., Zhang, Y. T., Luo, S. Q., Han, X., Wen, Y., et al. (2025). RAB4B and Japanese encephalitis virus E protein interaction is essential for viral entry in early endosomes. *Int. J. Biol. Macromol.* 306:141452. doi: 10.1016/j.ijbiomac.2025.141452

Mills, I. G., Jones, A. T., and Clague, M. J. (1998). Involvement of the endosomal autoantigen EEA1 in homotypic fusion of early endosomes. *Curr. Biol.* 8, 881–884. doi: 10.1016/s0960-9822(07)00351-x

Mishra, A., Eathiraj, S., Corvera, S., and Lambright, D. G. (2010). Structural basis for Rab GTPase recognition and endosome tethering by the C2H2 zinc finger of early endosomal autoantigen 1 (EEA1). *Proc. Natl. Acad. Sci. U.S.A.* 107, 10866–10871. doi: 10.1073/pnas.1000843107

Mu, F. T., Callaghan, J. M., Steele-Mortimer, O., Stenmark, H., Parton, R. G., Campbell, P. L., et al. (1995). EEA1, an early endosome-associated protein. EEA1 is a conserved alpha-helical peripheral membrane protein flanked by cysteine "fingers" and contains a calmodulin-binding IQ motif. *J. Biol. Chem.* 270, 13503–13511. doi: 10.1074/jbc.270.22.13503

Ni, H. B., Gong, Q. L., Zhao, Q., Li, X. Y., and Zhang, X. X. (2020). Prevalence of *Haemophilus parasuis* "*Glaesserella parasuis*" in pigs in China: a systematic review and meta-analysis. *Prev. Vet. Med.* 182:105083. doi: 10.1016/j.prevetmed.2020.105083

Papatheodorou, P., Zamboglou, C., Genisyuerek, S., Guttenberg, G., and Aktories, K. (2010). Clostridial glucosylating toxins enter cells via clathrin-mediated endocytosis. *PLoS One* 5:e10673. doi: 10.1371/journal.pone.0010673

Pereira-Leal, J. B., and Seabra, M. C. (2001). Evolution of the Rab family of small GTP-binding proteins. *J. Mol. Biol.* 313, 889–901. doi: 10.1006/jmbi.2001.5072

Perrin, L., Lacas-Gervais, S., Gilleron, J., Ceppo, F., Prodon, F., Benmerah, A., et al. (2013). Rab4b controls an early endosome sorting event by interacting with the gamma-subunit of the clathrin adaptor complex 1. *J. Cell Sci.* 126, 4950–4962. doi: 10.1242/jcs.130575

Pons, B. J., Vignard, J., and Mirey, G. (2019). Cytolethal distending toxin subunit B: a review of structure-function relationship. *Toxins* 11:595. doi: 10.3390/toxins11100595

Repella, T. L., Ho, M., Chong, T. P., Bannai, Y., and Wilson, B. A. (2011). Arf6-dependent intracellular trafficking of *Pasteurella multocida* toxin and pH-dependent translocation from late endosomes. *Toxins* 3, 218–241. doi: 10.3390/toxins3030218

Rubino, M., Miaczynska, M., Lippe, R., and Zerial, M. (2000). Selective membrane recruitment of EEA1 suggests a role in directional transport of clathrin-coated vesicles to early endosomes. *J. Biol. Chem.* 275, 3745–3748. doi: 10.1074/jbc.275.6.3745

Schmidt, G., Papatheodorou, P., and Aktories, K. (2015). Novel receptors for bacterial protein toxins. *Curr. Opin. Microbiol.* 23, 55–61. doi: 10.1016/j.mib.2014.11.003

Schoellkopf, J., Mueller, T., Hippchen, L., Mueller, T., Reuten, R., Backofen, R., et al. (2022). Genome wide CRISPR screen for *Pasteurella multocida* toxin (PMT) binding proteins reveals LDL receptor related protein 1 (LRP1) as crucial cellular receptor. *PLoS Pathog.* 18:e1010781. doi: 10.1371/journal.ppat.1010781

Scuron, M. D., Boesze-Battaglia, K., Dlakic, M., and Shenker, B. J. (2016). The cytolethal distending toxin contributes to microbial virulence and disease pathogenesis by acting as a tri-perditious toxin. *Front. Cell. Infect. Microbiol.* 6:168. doi: 10.3389/fcimb.2016.00168

Semerdjieva, S., Shortt, B., Maxwell, E., Singh, S., Fonarev, P., Hansen, J., et al. (2008). Coordinated regulation of AP2 uncoating from clathrin-coated vesicles by rab5 and hRME-6. *J. Cell Biol.* 183, 499–511. doi: 10.1083/jcb.200806016

Shenker, B. J., Boesze-Battaglia, K., Scuron, M. D., Walker, L. P., Zekavat, A., and Dlakic, M. (2016). The toxicity of the *Aggregatibacter actinomycetemcomitans* cytolethal distending toxin correlates with its phosphatidylinositol-3,4,5-triphosphate phosphatase activity. *Cell. Microbiol.* 18, 223–243. doi: 10.1111/cmi.12497

Simonsen, A., Lippé, R., Christoforidis, S., Gaullier, J. M., Brech, A., Callaghan, J., et al. (1998). EEA1 links PI(3)K function to Rab5 regulation of endosome fusion. *Nature* 394, 494–498. doi: 10.1038/28879

Somsel Rodman, J., and Wandinger-Ness, A. (2000). Rab GTPases coordinate endocytosis. *J. Cell Sci.* 113, 183–192. doi: 10.1242/jcs.113.2.183

Spano, S., and Galan, J. E. (2018). Taking control: hijacking of Rab GTPases by intracellular bacterial pathogens. *Small GTPases* 9, 182–191. doi: 10.1080/21541248.2017.1336192

Stenmark, H., Aasland, R., Toh, B. H., and D'Arrigo, A. (1996). Endosomal localization of the autoantigen EEA1 is mediated by a zinc-binding FYVE finger. *J. Biol. Chem.* 271, 24048–24054. doi: 10.1074/jbc.271.39.24048

Yang, Z., Zhang, Y., Du, S., Zhao, Q., Huang, X., Wu, R., et al. (2023). Upregulation of occludin by cytolethal distending toxin facilitates *Glaesserella parasuis* adhesion to respiratory tract cells. *Infect. Immun.* 91:e0035123. doi: 10.1128/iai.00351-23

Yeh, J. Y., Lin, H. J., Kuo, C. J., Feng, C. L., Chou, C. H., Lin, C. D., et al. (2020). *Campylobacter jejuni* cytolethal distending toxin C exploits lipid rafts to mitigate *Helicobacter pylori*-induced pathogenesis. *Front. Cell Dev. Biol.* 8:617419. doi: 10.3389/fcell.2020.617419

Zhang, Y., Yang, Z., Dai, K., Hu, B., Xu, S., Wang, Y., et al. (2024). Rab4b promotes cytolethal distending toxin from *Glaesserella parasuis*-induced cytotoxicity in PK-15 cells. *Toxins* 16:407. doi: 10.3390/toxins16090407

frontiers | Frontiers in Microbiology

TYPE Review
PUBLISHED 14 November 2025
DOI 10.3389/fmicb.2025.1700645

OPEN ACCESS

EDITED BY
Lei Deng,
Chinese Academy of Agricultural Sciences, China

REVIEWED BY
Sunny Doodu Mante,
African Filariasis Morbidity Project, Ghana
Kokouvi Kassegne,
Shanghai Jiao Tong University, China

*CORRESPONDENCE
Prasanta Saini
✉ prasantasaini09@gmail.com

RECEIVED 07 September 2025
ACCEPTED 29 October 2025
PUBLISHED 14 November 2025

CITATION
M R, Rahi M and Saini P (2025) Zoonotic filariasis and its public health significance: a comprehensive literature review. *Front. Microbiol.* 16:1700645. doi: 10.3389/fmicb.2025.1700645

Zoonotic filariasis and its public health significance: a comprehensive literature review

Remya M., Manju Rahi and Prasanta Saini*

ICMR-Vector Control Research Centre, Puducherry, India

Animal filariasis, a group of vector-borne parasitic infections, is a widely significant yet often underreported complex disease affecting a broad range of domestic and wild animals across tropical and subtropical regions. This comprehensive literature review aims to compile current knowledge on its epidemiology, pathogenesis, diagnosis, economic impact, and zoonotic implications to support improved control strategies. This review was conducted using databases such as PubMed, Scopus, and Google Scholar to collect data on filarial species, their vectors, hosts, clinical manifestations, diagnostic methods, and control measures across different geographical regions. Disease is caused by filarial nematodes belonging to order Spirurida, family Onchocercidae, which include species such as *Setaria, Dirofilaria, Onchocerca, Stephanofilaria, and Parafilaria*. This disease transmission primarily depends on blood sucking arthropod vectors, such as mosquitoes, blackflies, and biting midges. Distribution and involvement of these vectors influenced by environmental conditions, host availability, and regional factors. The lifecycle of all members of Onchocercidae family uniformly exhibit a similar pattern. Clinical manifestations vary depending on the host and parasites, can cause a mild to severe conditions including peritonitis, dermatitis as skin nodules, ocular infections, neurological disorders and cardiopulmonary complications. Worms have been detected in various tissues, including subcutaneous tissues, lymphatics, eye, heart, lungs, and central nervous system. Zoonotic infections have involved species from genera such as *Setaria*, *Dirofilaria*, *Onchocerca*, *Brugia*, *Dipetalonema*, *Loaina*, and *Meningonema*. Diagnosis of filarial infections relies on conventional methods like blood smears and skin scrapings, along with advanced molecular and serological assays for enhanced sensitivity and species identification. Control strategies include routine prophylactic treatment, vector control, and increased awareness among livestock farmers and pet owners. Filariasis in livestock causes economic losses through reduced productivity, fertility, hide quality, and treatment costs and meat condemnation. It also leads to higher management expenses, trade barriers, and decreased agricultural efficiency, particularly in endemic regions. A comprehensive understanding of intricate interactions among filarial parasites, mosquito vectors and vertebrate hosts is crucial for formulating effective prevention and control strategies. So, integrated control programs and one health approach, driven by interdisciplinary research and public health collaboration, are crucial to addressing this challenge and mitigating its zoonotic potential.

KEYWORDS

filariasis, zoonosis, setariasis, dirofilariasis, onchocerciasis

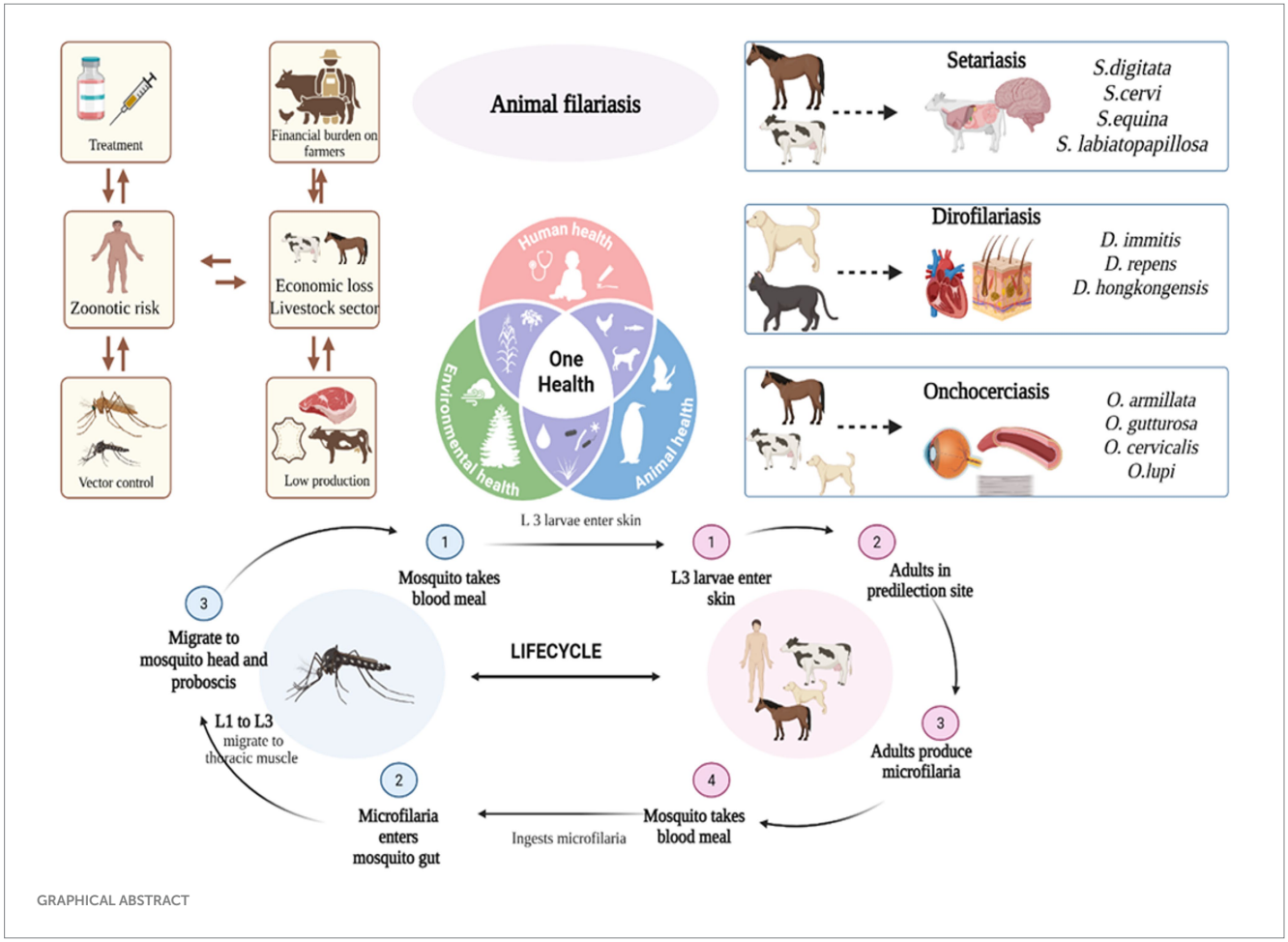

GRAPHICAL ABSTRACT

Introduction

Filariasis is an arthropod-borne zoonotic disease caused by various species of filarial nematodes, transmitted by the bites of infected blood-sucking arthropods such as mosquitoes, ticks, sandflies, and black flies. Mosquito belonging to various genera, like *Aedes, Anopheles, Armigeres, Culex, Mansonia* and *Ochlerotatus* are involved in the transmission of filariasis (Orihel and Eberhard, 1998; Foster and Walker, 2019). Mainly, *Culex, Aedes* and *Anopheles* are primary carriers for Dirofilariasis and Setariasis. Black flies (*Simulium* spp.) are known to transmit Onchocerciasis, especially in livestock and wildlife. Biting midges (Culicoides) contribute to transmission of *Onchocerca*, *Setaria* and *Stephanofilaria* species in cattle. Additionally, horseflies (*Tabanus* spp.) can serve as mechanical or biological vectors for *Parafilaria* and some *Setaria* species. Therefore, tropical and subtropical areas are where these diseases are most common. It is essential to comprehend the complex interactions among filarial parasites, vertebrate hosts, and mosquito vectors in order to evaluate the risks of disease transmission and create efficient preventative and control measures (Siriyasatien et al., 2023).

The order Spirurida, superfamily Filarioidea comprises relatively long and thin worms, primarily belonging to three families: Filariidae, Setariidae, and Onchocercidae (Soulsby, 1982). Among these *Dirofilaria* spp., *Setaria* spp., *Onchocerca* spp. pose a major threat to both animals as well as humans, while *Stephanofilaria* spp. and *Parabovicola* spp. have been reported to cause minor infections in animals. In their definitive vertebrate hosts, filarial nematodes generate moving microfilariae (mf) to be their first-stage larvae (L1). Microfilarial larvae, enclosed in a thin, flexible membrane, enter the bloodstream or lymphatic tissue of host. From there, they are ingested by mosquitoes, which serve as intermediate hosts and biological vectors. These microfilariae then develop into third-stage larvae (L3) within blood-feeding arthropods (Orihel and Eberhard, 1998; Otranto and Deplazes, 2019). In blood-feeding arthropods, these microfilariae subsequently mature into third-stage larvae (L3) (Otranto and Deplazes, 2019). When the mosquito feeds on a new host, L3 larvae proceed to proboscis inside the mosquito and escape. The microfilariae then complete their development within the final host. Notably, microfilariae can survive in the host for several weeks after the death of the adult worm, and can also be transmitted to uninfected hosts (Soulsby, 1982). Animal filariasis exhibits different predilection sites different hosts, affecting various body systems, including heart, lungs, subcutaneous tissues, eyes, lymphatic system, and central nervous system. Adult worms typically reside in connective tissues, lymphatic channels, internal cavities, and blood vessels of host animals (Chatterjee and Nutman, 2015). Moreover, filarial parasites are found in various vertebrates, but only those in mammals can be transmitted to humans, posing a zoonotic risk (Anderson, 2000). So, the symptoms of filariasis vary depending on the location of adult and larval nematodes, with infection severity linked to parasite species and abundance (Magnis et al., 2013). Although these infections are widespread across tropical and subtropical regions, they remain

neglected and underreported in veterinary and public health sectors. The disease causes substantial economic losses through reduced animal productivity, reproductive failure, and increased mortality, while zoonotic transmission continues to emerge as a growing health concern.

Zoonotic filariasis, caused by animal derived filarial infections in humans, is distributed world-wide. First report in modern literature over a century ago, both in number of cases and number of implicated parasitic species have steadily increased. So, recently, a wide range of filarial species pose a significant risk to humans as well. Although, Humans are mainly affected by lymphatic filariasis such as *Wuchereria bancrofti* as well as to a lower degree, *Brugia malayi* and *Brugia timori*, which seriously impair the health of almost 68 million people in 73 countries. In humans, a number of filarial parasites have been found, including *Wuchereria, Brugia, Dirofilaria, Onchocerca, Dipetalonema, Loaina*, and *Meningonema* (Ramaiah and Ottesen, 2014). Animal filariasis also poses a significant threat to human health, notably through onchocerciasis caused by *Onchocerca volvulus*, parasite responsible for river blindness. This disease affects approximately 40 million humans, primarily from Africa (Taylor et al., 2010; Tekle et al., 2016). Another form of animal filariasis, particularly that caused by *Dirofilaria repens*, is more common in males and children (Pampiglione et al., 1995). Epidemiology of these infections is primarily impacted by human activity and environmental factors associated with parasite vectors; incidence rates are higher in regions with longer mosquito breeding seasons and higher levels of outdoor exposure, whether for work or pleasure. So, close contact between humans and animals heightens the risk of zoonotic disease transmission and newly emerging zoonotic diseases represent a major threat to public health and significantly disrupts socioeconomic stability (McArthur, 2019). Several methods are typically used to diagnose filarial infections, such as separating adult worms and then identifying them morphologically, observing circulating microfilariae morphologically using direct wet smears, stained blood smears, modified Knott's technique, and Wylie's filtration technique (Irwin and Jefferies, 2004). Recombinant antigen-based assays and molecular techniques enhance diagnostic sensitivity and specificity while also increasing diagnostic accuracy. Additionally, histochemical or immuno-histochemical staining (IHC) of blood microfilariae has been used as a diagnostic technique detecting filarial infections (Ananda et al., 2006). Numerous genes have been described according to their potential for therapeutic targeting, including their protein products. Moreover, molecular diagnostic techniques are being used more and more for surveillance and research (Casiraghi et al., 2006; Rishniw et al., 2006). Although wide-spectrum anthelmintics are frequently used to treat and manage filarial infections, there remains a pressing need for new antifilarial therapies that can specifically target and eliminate adult parasites (Hoerauf, 2008). Despite being one of the most serious issues facing public health world-wide, resulting in fatalities in livestock, humans and wildlife, as well as significant economic losses, vectors pose direct impacts such as bites, irritation, psychological stress, and discomfort during feeding. Additionally, they serve as carriers of various diseases and incur substantial costs for their control. Implementing vector control through the modern approach of integrated Pest management offers the most effective solution, as it not only enhances control efficiency but also helps mitigate issues related to acaricide resistance and reduces the environmental risks posed by harmful chemical use. Furthermore, these disease affects the productivity, health, and reproductive performance of infected animals, resulting in reduced milk yield, weight loss, poor growth rates, decreased work capacity, and increased mortality. These outcomes directly impact livestock producers, industries, and national economies. Indirectly, the presence of the disease may necessitate changes in farming practices and labour allocation, ultimately reducing household income and food security (Perumal et al., 2016). Despite decades of research on human lymphatic filariasis, the epidemiological patterns, host–vector relationships, and cross-species transmission dynamics of animal-derived filarial infections are poorly understood. Most available data are fragmented, region-specific, and lack integration under a One Health framework. Furthermore, limited molecular and surveillance studies constrain our ability to monitor emerging zoonotic strains and design evidence-based control measures. To address these gaps, this study investigates the increasing occurrence of zoonotic filarial infections in humans and animals, emphasizing their clinical manifestations, economic impact, and ecological determinants. Although several studies have explored the epidemiology and control of filariasis, limited attention has been given to the zoonotic potential of animal filarial infections and their role in sustaining transmission in endemic regions. By consolidating current evidence, the review aims to identify research gaps and inform integrated control strategies under a one health framework.

Therefore, insights gained from studies on the interactions between filarial parasites and mosquito vectors are crucial for assessing disease transmission risks and guiding effective mosquito control strategies in endemic regions. In the present study, we investigate the rise in humans and animal zoonotic filarial infections, emphasizing their potential to cause clinical symptoms such as peritonitis, dermatitis, ocular complications, skin nodules, cardiopulmonary diseases and epilepsy. These findings highlight the critical need for one health strategies to detect and manage the emerging infections effectively. The objective is to highlight the current knowledge by conducting a thorough examination of the economic impact of zoonotic diseases on different species, adopting a one Health approach that highlights the intricate relationships between human, animal, and environmental wellbeing.

Materials and methods

A comprehensive literature review was conducted to explore the zoonotic filariasis and its public health significance mainly dealing seteriasis, dirofilariasis and onchocerciasis. This review synthesizes current knowledge on the epidemiology, pathogenesis, diagnosis, economic impact, and zoonotic implications of animal filariasis. We conducted a database search of PubMed, Scopus, Web of Science, and Google Scholar, retrieving articles from their inception through April 2025. The search keywords included animal filariasis, zoonotic filariasis, seteriasis, onchocerciasis, dirofilariasis, impacts of filariasis in livestock sector. The inclusion criteria consisted of English-language, peer-reviewed articles that offered cutting-edge perspectives on animal filariasis, encompassing epidemiology, pathogenesis, diagnosis, economic burden, and zoonotic significance mainly on seteriasis, dirofilariasis and onchocerciasis. The exclusion criteria included human lymphatic filariasis and animal filarial diseases other than setariasis, onchocerciasis, and dirofilariasis. Through critical

analysis of selected articles, we examined the progression, technical aspects, challenges, and future directions of zoonotic animal filariasis. Our findings underscore the need for a One Health approach, integrating interdisciplinary research and public health partnerships to effectively control zoonotic risk.

Animal filariasis

Setaria, Dirofilaria, and *Onchocerca* are key genera in animal filariasis, characterized by distinct epidemiological patterns and transmission dynamics. The disease cycle is vector-borne, involving arthropods such as mosquitoes, blackflies, and biting midges, which transmit infective larvae to vertebrate hosts. Beyond their impact on animal health and productivity, certain filarial species exhibit zoonotic potential, posing significant public health concerns. This section provides a comprehensive overview of these genera, focusing on their life cycles, pathology, and implications for public health.

Setariasis

Setaria is a type of nematode that often lives free within peritoneal cavity of ungulates. It is a member of family Setariidae and order Spirurida, is transmitted by biting insects like flies (*Haematobia, Simulium*) and mosquitoes (*Aedes, Anopheles, Culex, and Mansonia*) (Soulsby, 1982; Azari-Hamidian et al., 2019). There are 43 known species of nematodes in the genus *Setaria*, that inhabit the abdominal cavity of artiodactyl animals, including cattle, sheep, horses, and pigs, with a global distribution as enlisted in Table 1 (Laaksonen et al., 2009). Three of these, *S. digitata*, *S. cervi* and *S. labitopapillosa* have been reported from India, six from Europe, and five from America.

TABLE 1 Different species of *Setaria*, their predilection sites, and associated clinical signs.

Species	Host	Predilection site	Clinical signs	References
S. digitata	Cattle Buffalo	Peritoneal cavity	Fibrinous peritonitis (mild insignificant)	Bazargani et al. (2008), Tamilmahan et al. (2013), Davoodi (2015), Abdullah et al. (2021), Lee et al. (2021), and Hanafiah et al. (2023)
	Goat Sheep	CNS	Cerebrospinal nematoidosis Lumbar paralysis Death	
	Horse	CNS Eye	Equine neurological ataxia Lacrimation, Photophobia Corneal opacity Conjunctivitis Loss of vision	
	Human	Eye Lungs Urinary bladder Skin	Abscess formation Allergy responses Enlarged lymph node Lung inflammation Eye lesions, Eosinophilic granulomatous lesions (in urinary bladder)	
S. labiatopapillosa	Cattle	Peritoneal cavity	Fibrinous peritonitis (mild insignificant)	Sundar and D'Souza (2015)
	Sheep Goat Horses Human	Eye & CNS	Ocular pathology, Neurological diseases, Death	
S. equina	Horses, Cattle, Buffalo	Sub conjunctiva	Eye infection	Devi et al. (2020)
S. cervi	Cattle Buffalo Deer	Peritoneal cavity CNS	Peritonitis Nervous lesions	Sundar and D'Souza (2015).
S. marshalli	Cattle Buffalo	Peritoneal cavity	Peritonitis	Tung et al. (2003)
S. tundra	Reindeer, Cattle and buffalo	Peritoneal cavity	Peritonitis	Lanková et al. (2021)

Adult worms (about 5 to 10 cm) reside freely within abdominal cavity, while their microfilaria (190 μm in length) circulate in blood of definitive host. Each setaria species has a specific host preference; for example, *S. equina* predominantly infects horses, while *S. digitata* and *S. labiatopapillosa* are found in ruminants (Davoodi, 2015). In addition, *S. cervi*, *S. equina S. tundra, S. marshalli, S. leichungwingi* and *S. nelsoni* are also found in cattle (Sundar and D'Souza, 2015). These parasites predominantly inhabit in peritoneal cavities, particularly in both domestic and wild animals (Gomez-Puerta and Mayor, 2017; Mrifag et al., 2021). In Asia, *S. digitata, S. labiatopapillosa*, and *S. marshalli* are the most common nematodes observed in cattle (Khedri et al., 2014). Moreover, *S. digitata* and *S. labiatopapillosa* parasites can accidently infect humans. Also, *S equina* originating from horses and donkeys, has been responsible for rare zoonotic transmissions, occasionally causing to subconjunctival eye infections (Nabie et al., 2017; Ţălu et al., 2012).

Setariasis, also referred to as setariosis, is a disease brought on by *Setaria* nematodes. In tropical areas where mosquito vectors are common, setariasis poses a serious risk to vulnerable animals. The life cycle begins when mosquitoes ingest microfilariae while mosquitoes feeding on the blood of infected host. After which, in 2 to 3 weeks, the mosquitoes mature into infectious larvae (L3). Additionally, L3 larvae are spread by infected mosquitoes to other hosts during subsequent blood meals, where they develop into adult nematodes over a period of 8–10 months (Perumal et al., 2016). Among the various species, *S. digitata* is the most widely recognized and is prevalent across Asia, with several reports of its occurrence in India (Chaithra et al., 2024). It is particularly notable for being a common cause of cerebrospinal nematodiasis (CSN) or neurological ataxia in equines (Lee et al., 2021). When *S. digitata* infections occur in its usual hosts, for example cattle and buffaloes, they often only result in moderate fibrinous peritonitis and are generally benign. However, immature worms migrate to odd places, including the central nervous system, when infectious L3 larvae are unintentionally transferred to aberrant hosts like goats, sheep, or horses, which may result in severe neurological consequences (Bazargani et al., 2008). Typical symptoms in infected goats often exhibit paralysis of one or both forelimbs or hind limbs, lumbar region paralysis, incoordination, and a swaying gait, which can progress to death (Bazargani et al., 2008). In horses, primary migration of *Setaria* infection often involves ocular migration, where the parasites migrate to either single/both eyes (Radwan et al., 2016). Infected horses may exhibit various ocular symptoms, including blindness, conjunctivitis, corneal opacity, excessive lacrimation, and photophobia, especially if treatment is postponed (Tamilmahan et al., 2013). In addition to animal infections, zoonotic cases of *S. digitata* have been reported in humans, resulting in abscess formation, allergic reactions, lymphadenopathy, ocular lesions, and pulmonary inflammation (Rodrigo et al., 2014). It may also lead to eosinophilic granulomatous lesions in the urinary bladder. Given these findings, *S. digitata* should be regarded as a significant health threat to animals, with serious economic consequences for livestock owners. Therefore, further epidemiological studies are essential, particularly focusing on both natural and aberrant hosts (Yu et al., 2021). *Setaria equina* is present in all part of the world and commonly seen in equines. This worm is found in the peritoneal cavity and sometimes in the scrotum. It has also been recorded from the pleural cavity and lung of horses and from the eye of horse and cattle. The infection rate is high and 50% horses are affected in endemic areas. *S. equina* is found not only in the peritoneal cavity but also in the scrotum, pleural cavity, lungs, and eyes of horses (Devi et al., 2020).

The main pathogenic effects of *Setaria* spp. is the induction of various degrees of fibrinous peritonitis, mostly as a result of discomfort from mature worms living in the peritoneal cavity (Rhee et al., 1994). Although mature *S. digitata* parasites may persist in their typical host for as long as 18 months without suffering significant harm, migrating larvae can often invade other organs and produce pathological lesions. Nevertheless, they may have detrimental effects in unexpected places, like the central nervous system, nerves, eyes, and even the foetus of pregnant animals, which might cause serious impairment, paralysis, and death in a matter of days. In aberrant hosts, the main pathological conditions included ocular setariasis, cerebrospinal nematodiasis, and lumbar paralysis, this may result in blindness, neurological conditions, paralysis, corneal opacity, and eventually death (Tamilmahan et al., 2013; Abdullah et al., 2021). However, these parasites exhibit unpredictable migration patterns, often affecting the eyes and sometimes other organs like the CNS, urinary bladder, and reproductive system, as well as the liver, heart, and fetus in pregnant hosts (Yu et al., 2021). Several studies have reported that this filarial parasite can infiltrate horses' and cattle's eyes and cause blindness (Tamilmahan et al., 2013). Congenital infection has also been reported in animals, where the parasite penetrates the placenta, migrates to the fetus, enters the foetal bloodstream, and develops into adult worms (Kim et al., 2002; Schuster et al., 2019). Additionally, instances in cattle have been reported symptoms such as eye swelling, corneal damages, corneal cloudiness, and even blindness (Hanafiah et al., 2023). In horses, ocular setariosis is marked by the migration of parasite within anterior chamber of eye, often resulting in varying degrees of corneal opacity, including excessive lacrimation, photophobia, conjunctivitis and, in severe cases, partial or complete vision loss (Rafee and Amarpal, 2016). Interestingly, this parasite has been observed in multiple organs, including heart, lungs, spleen, kidneys, uterus, oviduct, ovaries, and urinary bladder. Also, it has been detected in the contents of the rumen, reticulum, and abomasum (Mandal and Ray, 1994). The effects of host–parasite interactions and predilections are shown in Figure 1.

The morphological identification of *Setaria* species, including *S. digitata*, *S. equina*, *S. labiatopapillosa*, and *S. cervi*, is often challenging due to their close morphological similarities (Maharana et al., 2020). To overcome this limitation, a nucleic acid-based detection approach was employed. Gel electrophoresis revealed a distinct 209 bp amplicon, and BLAST analysis of the corresponding genetic sequence confirmed the species as *S. digitata*, showing 99% similarity to isolates previously reported from cattle and buffaloes in Sri Lanka and China. This molecular identification was further substantiated by phylogenetic analysis, which clustered the isolate within the *S. digitata* clade (Yu et al., 2021).

Dirofilariasis

Dirofilariasis is a zoonotic helminthic disease caused by *Dirofilaria* species, transmitted through mosquito vectors, and has a worldwide distribution, impacting both human and animal health. As summarized in Table 2, the disease predominantly affects domestic dogs, cats, and various wild mammals, highlighting its significance in both veterinary and public health contexts (Day, 2011; McCall et al.,

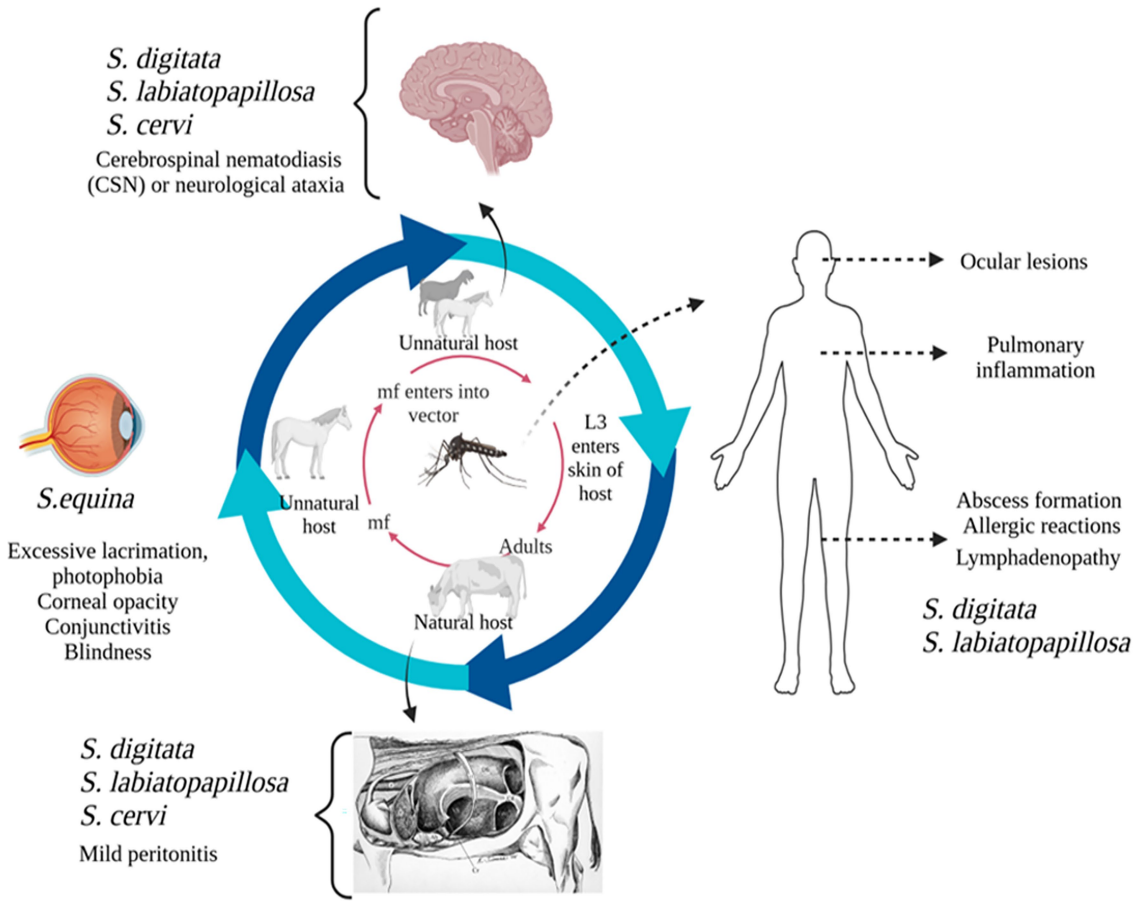

FIGURE 1
Diagrammatic representation of *Setaria* species and their predilection sites in natural and unnatural hosts.

TABLE 2 Different species of *Dirofilaria*, their predilection sites, and associated clinical signs.

Species	Host	Predilection site	Clinical signs	References
D. immitis	Dog Cat & wild felids Ferrets Monkeys	Pulmonary arteries Right ventricle	Right ventricular hypertrophy Pulmonary lesions (coughing, persistent expiratory lung sounds)	Day (2011), McCall et al. (2008), and Sevimli et al. (2007)
	Human	Pulmonary artery	Pulmonary nodules	
D. repens	Dog Cat	Subcutaneous tissue Subconjunctiva	Subcutaneous nodules	Petry et al. (2015), Genchi et al. (2010), and Albanese et al. (2013)
	Human	Subcutaneous tissue Subconjunctiva orbital zone Eyelids Intra vitreous tissues	Subcutaneous nodules Ocular lesions	
D. hongkongnesis	Dog Cat	Subcutaneous tissue	Subcutaneous nodules	Kwok et al. (2016), Luk et al. (2021), and Manathunga et al. (2024)
	Humans	Subcutaneous tissue Subconjunctiva	Subcutaneous nodules Ocular lesions	

2008). Infected animals commonly exhibit signs associated with cardiopulmonary system, in addition to subcutaneous, ocular, and dermatological symptoms. The adult worms primarily inhabit pulmonary arteries, where they release microfilariae into bloodstream. Mosquitoes, such as *Culex pipiens*, *Aedes albopictus*, *Anopheles maculipennis*, and *Coquilletidia richiardii*, acquire these microfilariae

while feeding. After developing into infectious L3 larvae within the mosquito's hemocoel, the larvae go to the mouthparts of the mosquito. After being spread by a mosquito bite, L3 larvae move to the pulmonary arteries and develop into adult worms. In mammalian host, larvae progress from L3 to L4 within somatic tissues over 3–12 days, then travel to the pulmonary arteries and right ventricle. In these locations, they undergo a final moult to L5 immature adults, which later develop into mature heartworms (Hoch and Strickland, 2008). In contrast to *D. immitis*, L4 larvae of *D. repens* do not migrate but moult and mature into an adult within the subcutaneous tissues.

In dog populations, both *D. immitis and D. repens* are common. However, *D. repens* poses a more substantial threat to humans due to its greater ability to survive and persist in both hosts and vectors compared to *D. immitis*. *D. immitis* heartworm infections are frequently observed in dogs between the ages of 5 and 6 years, with a higher incidence in male dogs. Additionally, cases of subcutaneous dirofilariasis have been documented in dog populations in India (Song et al., 2003; Traversa et al., 2010). Although other animals, such as domestic cats, ferrets, monkeys, and wild canids, are also prone to *D. immitis* infection, the associated risk factors for these species have not been extensively investigated (Venco et al., 2015; Bowman et al., 2016; Alsarraf et al., 2023). Also, Infection caused by *D. repens* are more commonly reported in males and children (Simón et al., 2012). Moreover, *Dirofilaria hongkongensis*, initially reported in China, is a direct cause of dirofilariasis in human beings and dogs (To et al., 2012). A rigid genetic connection among *D. hongkongensis* and other *Dirofilaria* species that infect humans and animals, including dogs and jackals, is revealed by phylogenetic analysis, which may indicate that their clinical presentations are comparable (Saini et al., 2024). Furthermore, various wildlife-associated *Dirofilaria* species are also reported, such as *D. ursi, D. striata, D. tenuis, D. spectans*, and *D. magnilarvata* have been implicated in dirofilariasis cases of humans (Simón et al., 2022; Perles et al., 2024). Many hosts, such as foxes, dogs, cats, and other mammals, get infected by these parasites.

D. immitis, a zoonotic filarial nematode, generally resides in the pulmonary arteries and, in severe cases, may extend to the right ventricle of the heart, leading to significant cardiovascular pathology in dogs and other canids. It can cause significant pathology in multiple organs, including the lungs, heart, liver, and kidneys, with the most severe changes observed in the pulmonary arteries, right ventricle, and kidneys. Clinical signs progress from mild symptoms such as persistent cough and elevated body temperature to more severe manifestations, including dyspnea, generalized weakness, ascites due to right ventricular failure, and potentially life-threatening complications such as cachexia, respiratory distress, and sudden death. Severe chronic pulmonary arterial disease caused by *D. immitis* infection can result in right ventricular hypertrophy due to increased pressure load on the heart. Electrocardiographic abnormalities, such as P pulmonale, are frequently observed, and various arrhythmias, including atrial premature beats and atrial fibrillation, may develop as a consequence of the disease's impact on cardiac function (Sevimli et al., 2007). The presence of persistent expiratory lung sounds, even in the absence of coughing, is a potential indicator of heartworm disease. Sometimes laboratory findings on complete blood count (CBC) may include eosinophilia, thrombocytopenia, and neutrophilia, which should prompt consideration of *D. immitis* infection in their definitive host (Bendas et al., 2022).

In most canine cases of *D. repens* infection, condition is subclinical or presents with nonspecific symptoms, resulting in many infections going undiagnosed. Through the muscular connective fascia and subcutaneous tissue, the infectious larvae develop into adults and settle down there permanently. Interestingly, *D. repens* does not initiate an inflammatory response or form a connective tissue capsule around the living parasite, which can be seen moving actively beneath connective serous layers. As a result, the infection often goes unnoticed due to the lack of clear clinical signs (Petry et al., 2015; Genchi et al., 2010). Occasionally, skin conditions such as itching, conjunctivitis, eye irritation, swelling, and parasite-containing subcutaneous nodules are all noticeable (Albanese et al., 2013). Infections with *D. hongkongensis* have also been documented to produce subcutaneous nodules resembling those produced by *D. repens* (Manathunga et al., 2024). According to Tarello (2011), the subcutaneous nodules caused by *D. hongkongensis* are predominantly located in the posterior body regions, such as the scrotal and mammary areas, similar to the anatomical distribution of *D. repens* lesions. Approximately 85% of *D. repens*-related dermatological lesions are observed in the lumbosacral region, hind limbs, and perianal area (Tarello, 2011).

Canine dirofilariasis is a neglected zoonotic disease with significant implications for human health, as accidental infection can lead to pulmonary, subcutaneous, and ocular manifestations, potentially mimicking more severe conditions such as malignancies. Humans serve as incidental hosts for *D. repens* and *D. immitis*. Despite the rarity of human infections, *D. immitis* is usually linked to pulmonary lesions, which frequently appear as radiological coin type lesions in lungs (Foroulis et al., 2005; Theis, 2005). Individuals residing in endemic regions are at increased risk of infection through mosquito vectors, which facilitate the development of the parasite in subcutaneous tissues, mucosal membranes, and the subconjunctival space near the site of the mosquito bite. Additionally, some cases have reported the presence of tumor-like lesions in the lungs (Leccia et al., 2012). Rare instances of *D. immitis* and *D. repens* larvae have been documented in atypical sites, including mesentery, eye, spermatic cord, cerebral arteries and liver (Theis, 2005; Kim et al., 2002). Similarly, *D. hongkongensis* has also been identified in ocular (Kwok et al., 2016) and subcutaneous forms (Luk et al., 2021) in humans as illustrated in Figure 2. Given zoonotic nature of dirofilariasis and its significant clinical implications underscore the importance of early diagnosis, prevention through vector control measures, and targeted treatment strategies to mitigate the disease's impact on both veterinary and human health. For the disease to be controlled and prevented, as related to other vector-borne infections, precise understanding of natural reservoir and vectors is essential.

Diagnosis of dirofilariasis relies on a combination of traditional and modern diagnostic techniques aimed at detecting the parasite in both humans and animals. Microscopic methods, such as Knott's test and blood smear examinations using Giemsa or hematoxylin and eosin (H&E) stains, are employed to identify microfilariae in blood samples. Serological assays, including ELISA, indirect fluorescent antibody (IFA) tests, and immunochromatographic tests (ICT), are used to detect specific antibodies or antigens associated with *Dirofilaria* infection. Radiographic and imaging techniques, such as chest X-rays and ultrasonography, help visualize adult worms, particularly in pulmonary or subcutaneous lesions. In certain cases, necropsy and histopathological examination of tissues allow for

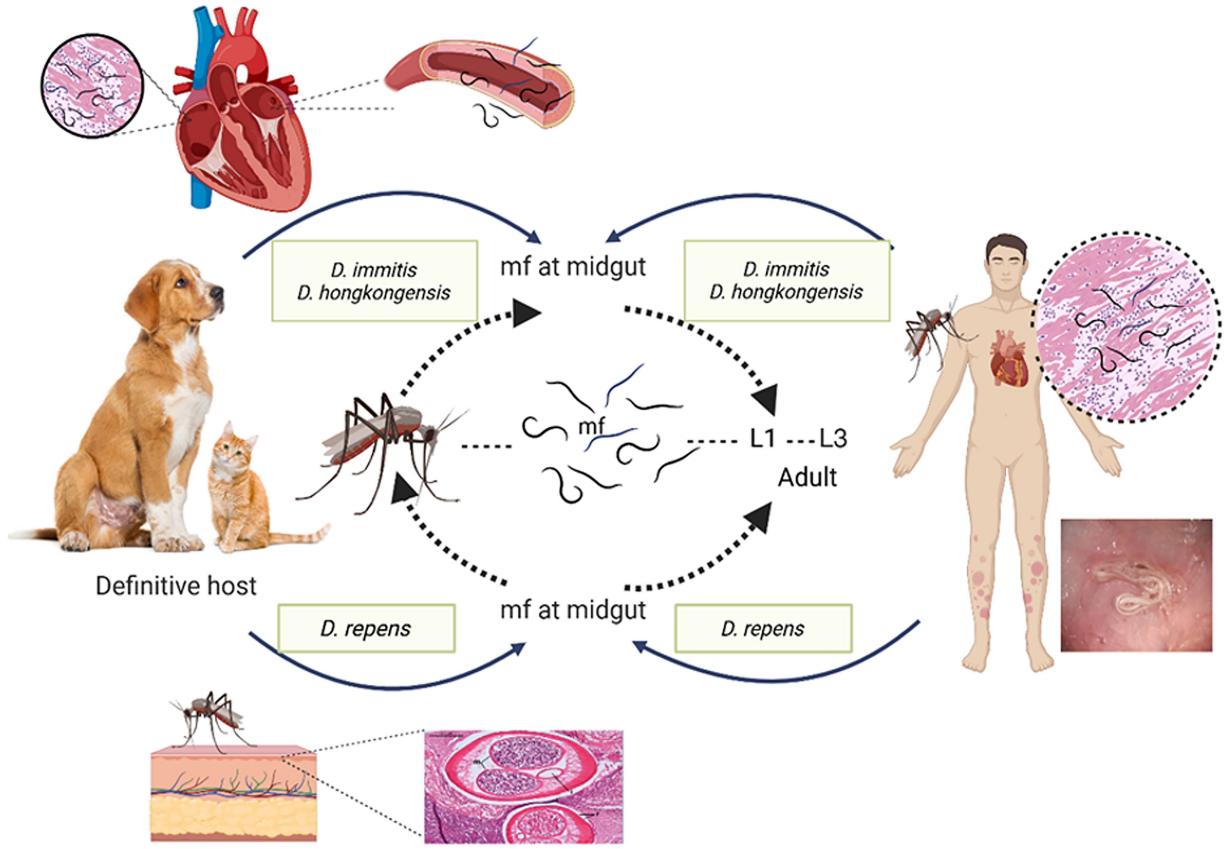

FIGURE 2
Diagrammatic representation of *Dirofilaria* species and different host range and clinical symptoms.

definitive identification of adult parasites. This integrated, multi-modal diagnostic approach enhances the accuracy and reliability of dirofilariasis detection (Trancoso et al., 2020; Pękacz et al., 2022). Molecular diagnosis of dirofilariasis primarily employs the polymerase chain reaction (PCR), a highly sensitive and specific technique for detecting *Dirofilaria* DNA in clinical and experimental samples. By amplifying species-specific gene sequences, PCR provides superior accuracy compared to conventional diagnostic methods (Obradovic et al., 2013). Commonly targeted genes include the internal transcribed spacer (ITS) regions, cytochrome c oxidase subunit 1 (cox1), and 12S ribosomal RNA (12S rRNA), which facilitate precise species identification and phylogenetic analysis. In addition, advanced molecular platforms such as next-generation sequencing (NGS), loop-mediated isothermal amplification (LAMP), digital PCR (dPCR), and digital microfluidics have been increasingly applied. These technologies integrate molecular amplification with high-resolution imaging and computational analysis, offering rapid, reliable, and quantitative detection of *Dirofilaria* species (Aththanayaka et al., 2024). These advancements collectively strengthen diagnostic and healthcare practices, underscoring the importance of continued collaboration in research, standardization of diagnostic protocols, and effective implementation strategies. Such integrated efforts are essential to improving the accuracy of detection, guiding timely interventions, and ultimately enhancing the overall management and control of dirofilariasis.

Onchocerciasis

There are around 30 species in the genus *Onchocerca*, which primarily parasitic to ungulates and are widely distributed throughout the world (Lefoulon et al., 2017). Moreover, *Onchocerca* spp. exhibits a highly specific host range (Rommel and Boch, 2000), with strong affinity for particular ungulates like bovines and equines as described in Table 3. Besides, these are also reported in canids, felids, and humans. Although primarily zoonotic, certain Onchocerca species, notably *Onchocerca volvulus*, have been identified as significant human pathogens, causing onchocerciasis in humans (Lefoulon et al., 2017). Transmission of Onchocerca nematodes occurs via arthropod vectors, primarily blackflies of genera *Simulium* and, in some cases, *Culicoides*, which serve as intermediate hosts and facilitate its lifecycle (Taylor and Muller, 1979). The lifecycle of all *Onchocerca* species is indirect, involving a dual host system such as an intermediate host (arthropod vectors, such as blackflies) and a definitive host (vertebrates, including animals and humans), where the parasites undergo progressive maturation and development (Rommel and Boch, 2000). Adult Onchocerca parasites exhibit a prolonged lifespan, persisting for 10–15 years within the host, where they reside and reproduce within fibrous nodules known as onchocercomas. These nodules are predominantly located in subcutaneous tissues but can also be found in various connective tissues, including ligaments, tendons, perimysial sheaths, and cartilage (Mather and Treuting, 2012).

TABLE 3 Different species of *Onchocerca*, their predilection sites, and associated clinical signs.

Species	Host	Predilection site	Clinical signs	References
O. armillata	Cattle buffaloes, dromedaries, goats	tunica intima of the aorta	Acute aortitis Eosinophilic inflammation to chronic granulomatous, Calcifying and fibrosing aortitis,	Neary et al. (2010), Sazmand and Joachim (2017)
O. gutturosa	Cattle, camels, dromedaries, horses, humans	Cervical ligaments	Subcutaneous nodules	Bino Sundar et al. (2017) and and Cambra-Pellejà et al. (2020)
O. volvulus	Humans	Skin, Eye	Skin irritation Blindness	Lefoulon et al. (2017)
O. cervicalis	Horses, ponies, humans, donkeys	Skin Cervical ligaments	Skin nodules Impaired function of ligaments blindness	Dagnaw et al. (2016)
O. lupi	Wolf, Dogs, Cats, Humans	Occular tissues	Conjunctivitis, Exophthalmos, Periorbital swelling, Photophobia, Lacrimation,	Egyed et al. (2001), Sréter and Széll (2008), and Otranto et al. (2015)

Bovine onchocerciasis remains a relatively neglected disease, despite its widespread distribution in temperate and tropical regions largely due to its frequently asymptomatic or subclinical presentation, which can obscure its impact on cattle health and productivity (Rabeya Begam et al., 2015). In *O. armillata* infections in cattle, adult parasitic nodules are primarily located in the tunica intima of aorta, marking a unique predilection site compared to other *Onchocerca* species (Neary et al., 2010). In contrast to *O. armillata*, other onchocerca species infecting cattle, as *O. dukei*, *O. ochengi*, and *O. gutturosa*, exhibit a predilection for cervical ligaments, thoracic connective tissues and ventral connective tissues, highlighting species-specific tissue tropism (Neary et al., 2010; Sazmand and Joachim, 2017). *O. armillata* infections result in a range of pathological changes in the bovine aorta, from acute aortitis with necrosis and eosinophilic inflammation to chronic granulomatous, calcifying, and fibrosing aortitis, primarily affecting the media and adventitia, with potential intimal and endothelial damage and thrombosis (Mather and Treuting, 2012). *O. armillata* infections can lead to severe complications, including aneurysm formation and potential rupture due to aortitis. While adult worms may elicit a minimal host response, microfilariae can cause significant clinical disease through inflammatory reactions as they migrate and die in tissues (Mather and Treuting, 2012).

In horses, *Onchocerca* infections frequently present as asymptomatic subcutaneous nodules that may remain undetected by owners. Nevertheless, in some cases, these infections can progress to cause dermatitis, ligamentous dysfunction, and ocular complications, including blindness (Lia et al., 2017). Adult *Onchocerca* parasites exhibit a predilection for specific anatomical locations, primarily residing within the ligamentum nuchae of equine hosts, where they form characteristic coiled aggregates. Additionally, they may localize within flexor tendon and fetlock suspensory ligament connective tissues, to produce that affect tissue function (Cambra-Pellejà et al., 2020). Among these, *O. cervicalis* is a prevalent species within the onchocerca genus, primarily infecting equine hosts, including horses, donkeys, and mules, and contributing to the burden of onchocerciasis in these animals. In addition to *O. cervicalis*, other Onchocerca species, including *O. reticulata* and *O. raillieti*, have been identified in equine hosts, but with lower prevalence rates. Female filarial nematodes release large numbers of microfilariae, which localize in the dermal layer after migrating through connective tissues, with common sites including the ventral abdomen, thoracic region, withers, neck, and facial areas (Dagnaw et al., 2016).

In canines, the localization of *Onchocerca* species may occasionally resemble that observed in other hosts. However, a reported case of an *Onchocerca* nodule protruding into the tracheal lumen led to severe respiratory distress, including coughing, dyspnea, suffocation, and eventual death (Papaioannou et al., 2004). Canine onchocerciasis is regarded as an atypical infection in which *O. lienalis*, a bovine parasite, accidently infects a canine host and localizes in an ectopic site (Eberhard et al., 2000; Zarfoss et al., 2005). *O. lupi* is a parasitic nematode that predominantly infects dogs but can also affect cats (Otranto et al., 2015). In definitive hosts, adult *O. lupi* worms exhibit a specific tissue tropism, localizing within the connective tissues of ocular structures, including the subconjunctiva, conjunctiva, eyelids, and nictitating membrane, where they reside on the sclera until reaching sexual maturity (Egyed et al., 2001; Sréter and Széll, 2008). These worms are characteristically coiled and confined within distinct nodules in connective tissue. Occasionally, this exhibits aberrant migration to atypical sites, including the laryngeal soft tissues in dogs (Alho et al., 2016) and spinal cord in humans (Chen et al., 2015; Dudley et al., 2015). Both acute and chronic ocular diseases are possible manifestations of canine onchocerciasis. Clinical symptoms of acute infections include ocular discharge, pain, lacrimation, periorbital oedema, conjunctivitis, exophthalmos, and photophobia; these symptoms usually appear without development of granulomas or cysts surrounding adult parasites (Eberhard et al., 2000; Egyed et al., 2002).

The rising prevalence of *Onchocerca* species in both wildlife and domestic animals, alongside habitat expansion driven by climate change and urbanization, has been identified as an important factor in amplifying human-parasite interactions, thereby increasing the risk of zoonotic transmission (Uni et al., 2015). Zoonotic *Onchocerca* infections in humans, although rare, can lead to clinical manifestations such as dermatitis and ocular complications, with some cases also associated with epilepsy (Gumisiriza et al., 2020). Generally, prevalence of onchocerciasis is higher in adults than in juveniles due to the prolonged prepatent

period of the infection (Boijsen et al., 2017). Among this, *O. volvulus* is the primary pathogenic species affecting humans, typically manifests as a pruritic skin disease and can also lead to a range of visual impairments, with untreated cases potentially progressing to irreversible blindness (Brattig et al., 2021). Adult *O. volvulus* worms are typically encapsulated within subcutaneous nodules under skin, whereas microfilariae exhibit a specific distribution pattern in the dermal tissues, predominantly localizing on the hips, shoulders, and lower body regions (Rodríguez-Pérez et al., 2011). Additionally, major public health threat of *O. volvulus* occurs in conjunction with its Wolbachia endosymbiont, is a causative agent of river blindness, a major cause of vision loss worldwide. Mass ivermectin administration effectively reduces microfilarial loads and pathology, but its inability to target adult worms, which can live for over a decade, poses a challenge for disease control.

Onchocerca species exhibit host specificity, establishing patent infections primarily in closely related species, with microfilariae localizing in skin, subcutaneous tissues, and ocular structures in definitive hosts are shown in Figure 3. *Onchocerca* evolution suggests, co-speciation between parasites and hosts is not predominant mechanism for speciation. Rather, there is evidence that sympatric speciation mostly happens as a result of site movement and host switching (Morales-Hojas et al., 2006; Krueger et al., 2007). Typical host switching in *Onchocerca* is exemplified by species like *O. volvulus* (humans), *O. dewittei* (wild boars), and *O. fasciata* (camels), while site shift speciation is seen in *O. gutturosa* (cattle) and *O. lienalis* (cattle). *O. Lupi*, a parasite of dogs, illustrates a combination of both host switching and site shifting in its evolutionary history. So, understanding the mechanisms of speciation and host adaptation in *Onchocerca* is crucial for developing more effective control and management strategies for these parasitic infections.

Diagnosis of onchocerciasis remains challenging due to the inherent limitations of existing diagnostic methods. Although dermatological examination and nodule palpation are non-invasive and practical for field use, they often lack sufficient specificity and sensitivity. In contrast, invasive diagnostic approaches, including skin snip microscopy, quantitative PCR (qPCR), and loop-mediated isothermal amplification (LAMP), provide greater accuracy but require trained personnel and laboratory infrastructure, limiting their application in endemic settings (Hotterbeekx et al., 2020). Among molecular techniques, qPCR assays have demonstrated high sensitivity by targeting parasite-specific DNA sequences such as O-150, actin, and mitochondrial genes. Despite significant progress in global elimination programs, the final phase of onchocerciasis control demands diagnostics that are more specific, sensitive, and scalable. The development of innovative tools that can be integrated into local surveillance programs, accommodate coendemic infections,

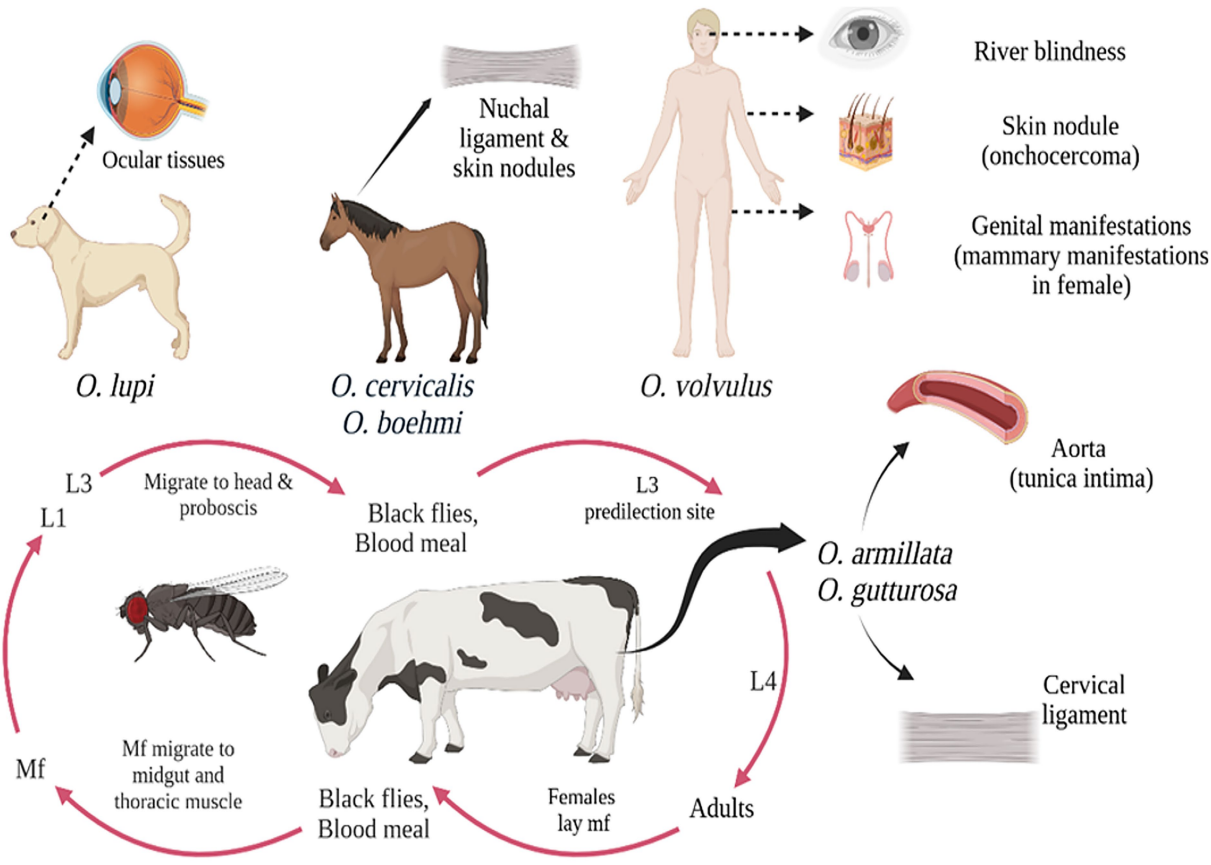

FIGURE 3
Diagramatic representation of *Onchocerca* species and different host range and clinical symptoms.

and align with WHO performance benchmarks is critical. With the deployment of robust diagnostic strategies and sustained global commitment, achieving the 2030 elimination goals remains an attainable target, underscoring the central role of diagnostics in this effort (Lubbers et al., 2025).

Economic losses in livestock and pet sector

Vector-borne zoonotic diseases have a profound impact on global health and economies, contributing to considerable morbidity, mortality, and economic losses in human and animal populations. These diseases pose a major threat to livestock, resulting substantial financial burdens on producers and the agricultural sector, thereby impeding socio-economic development (Perumal et al., 2016). Filarial infections in livestock result in clinical manifestations such as lethargy, growth retardation, and decreased feed efficiency, ultimately compromising productivity and yields. Severe cases can lead to significant reduction in livestock population, directly affecting farm profitability. The economic impact is further exacerbated by diagnostic, treatment, and management costs, as well as increased management expenses, trade restrictions, and reduced labour efficiency, culminating in substantial economic losses for farmers and the agricultural sector.

Climate change is expected to impact the distribution, frequency, and severity of infectious diseases by altering the ecosystems of disease vectors. Rising temperatures can enable vectors to expand their range, potentially introducing diseases to new areas. This can affect the transmission of diseases like lymphatic filariasis and onchocerciasis, which are influenced by changes in mosquito and black fly populations. Climate-induced changes in landscape patterns, such as flooding and desertification, can also alter the distribution of disease vectors, impacting disease transmission dynamics. The growing threat of climate change to public health and the livestock sector necessitates timely and coordinated action to protect vulnerable populations and mitigate economic impacts.

In tropical areas, setariosis is a serious hazard to vulnerable animals. The widespread distribution and economic impact of *Setaria* spp. have established them as major parasitic concerns, particularly in atypical animal hosts. This disease contributes to substantial economic losses in livestock production by adversely affecting animal health, reducing productivity, and increasing mortality rates. In cattle, *S. digitata* is primarily non-pathogenic when localized in the peritoneal cavity. However, the migration of immature worms can lead to neurological disorders, peritonitis, tissue damage, and reproductive complications, negatively impacting overall health and productivity. In sheep and goats, cerebrospinal nematodiasis manifests as symptoms like incoordination, hindlimb paralysis, and recumbency, often resulting in death (Dehkordi et al., 2015). Additionally, ocular infections and organ damage further contribute to disease severity in affected animals. These health impacts lead to considerable economic losses in livestock industry, as they reduce milk and meat production, increase mortality rates, and impose financial burdens on the agricultural sector through diminished productivity and higher veterinary expenses. This filarial parasite has been documented to invade the ocular structures of horses, resulting in blindness (Shin et al., 2017), which contributes to significant financial losses equine industry because of its negative impacts on animal health, performance, and management expenses. Vision impairment compromises coordination and responsiveness, diminishing horse's reliability for work and increasing the risk of accidents. Horses experiencing partial or complete blindness are less marketable, leading to a significant reduction in their commercial value. Additionally, the breeding potential of affected horses is adversely impacted, thereby reducing long-term economic gains for breeders.

Human cases of dirofilariasis have clearly been on the rise in recent years, most likely as a result of enhanced transmission from prolonged exposure periods, growing mosquito populations, and climate change (Darchenkova et al., 2009). *D. immitis* infection causes heartworm disease, which has serious clinical effects on dogs and financial ramifications for pet owners. The disease's cost is determined by dividing the costs into three categories: opportunity cost of treatment, treatment cost, and preventative cost (heartworm medicine). As the condition spreads geographically, its prevalence rises in regions where it is already present, and pet care standards increase globally, heartworm expenditures are expected to rise in the future (Klug and Drake, 2022).

Dirofilariasis poses a significant threat to health and survival of pet animals while also negatively impacting their overall welfare and imposing both financial and emotional burdens on pet owners. This disease primarily targets the cardiovascular and respiratory systems, often resulting in pulmonary hypertension, heart failure, and potential multi-organ dysfunction (Darchenkova et al., 2009). Beyond its physiological effects, dirofilariasis greatly diminishes the overall health and standard of living of impacted animals. Affected pets frequently exhibit symptoms such as lethargy, respiratory distress, and decreased endurance, which restrict their ability to participate in normal activities, including exercise and playing.

Onchocerciasis is a debilitating filarial disease with profound socio-economic consequences, particularly in tropical regions where vector flies flourish, have a favourable environmental condition throughout the year. Recognized by the World Health Organization as a significant impediment to socio-economic development since the 1980s, the disease severely impacts productivity and disrupts social and reproductive aspects of life due to blindness and other debilitating complications. Onchocerciasis continues to pose a considerable burden in resource-poor settings, exacerbating physical disability and social stigma, which in turn diminish the quality of life for affected individuals and impact land productivity (Moya Alonso et al., 2009). In livestock, *Onchocerca* species, such as *O. gutturosa*, pose substantial economic challenges by compromising meat quality, rendering affected portions of cattle carcasses unsuitable for human consumption, and adversely affecting the meat export sector (Bino Sundar et al., 2017; Cambra-Pellejà et al., 2020). To mitigate these effects, increased research efforts are necessary, particularly in understanding the vectors responsible for transmission and their ecological dynamics, to facilitate the development of effective control strategies. Given the proven success and cost-effectiveness of existing control programs,

prioritizing the development of innovative tools and strategies to reinforce these efforts is essential for achieving disease eradication. As filarial worm infections become increasingly prevalent due to climate change and rising mosquito populations, prioritizing awareness and preventive measures is crucial. Enhancing public education on disease prevention, making preventive treatments more accessible, and promoting routine veterinary check-ups can help reduce both the financial and emotional strain on the livestock and agricultural industries.

Prevention and control up to this era and future aspects

Filarial nematode infections are a significant cause of morbidity in both animals and humans. Current control methods rely on routine injection of microfilaricidal medications, which target larval stages of parasite, which disrupt the lifecycle of parasite and help reduce clinical manifestations (Addiss and Mackenzie, 2004). However, there is a critical demand for novel antifilarial treatments that specifically target and eliminate adult parasites (Hoerauf, 2008). Existing treatments rely on broad-spectrum anthelmintics such as macrolactones, levamisole, and benzimidazoles, which target both adult worms and microfilariae, highlighting the need for more targeted and effective therapies.

Due to the strong predilection of *Setaria* species for ocular tissues in equines, surgical removal remains the preferred treatment over anthelmintic therapy. By taking this strategy, the infestation will be resolved quickly and there will not be any serious intraocular immune-mediated reactions related to dead parasite, which could cause problems like tissue necrosis, structural eye degeneration, elevated intraocular pressure, or even globe rupture. Although it has been demonstrated that pharmacological treatment with diethylcarbamazine (DEC) at 20 mg/kg intramuscular (IM) effectively clears microfilaremia, multiple doses are necessary, and the drug is ineffective against adult parasites living in ocular tissues (Peng et al., 2019). Topical ophthalmic treatments and anti-inflammatory therapy are also advised to reduce clinical symptoms and encourage healing. Ivermectin (300 µg/kg) administered subcutaneously once has been shown to be an effective treatment for *S. digitata* induced microfilariasis. Despite this, resolution of microfilaremia occurs only 7 days post-treatment, with adult eyeworms being eliminated 15 days post-treatment. Complete resolution of ocular symptoms has been observed approximately 90 days following treatment (Muhammad and Saqib, 2007). Given the detrimental effects of ocular *Setaria* infections on equine health and the associated economic burden on owners, preventive strategies are crucial.

Heartworm disease, caused by *D. immitis*, is a dangerous and potentially fatal aliments affecting both dogs and cats. The medical management of persistent heartworm infection is complex, expensive, and associated with significant risks. In order to eradicate symbiotic bacterium *Wolbachia*, which has been demonstrated to be essential to *D. immitis* survival and reproduction, the main method is to employ arsenical medication melarsomine, frequently followed by a month-long course of doxycycline. Currently, only drug registered for adulticidal therapy in canine heartworm infections is an arsenical drug (melarsomine). The standard protocol consists of two intramuscular injections of melarsomine (2.5 mg/kg) administered 24 h apart, achieving approximately 90% efficacy in eliminating adult worms. An alternative three-dose protocol, consisting of a single initial dose followed by two additional injections 30 days later (24 h apart), has demonstrated improved efficacy, eliminating up to 98% of adult worms. This staged approach reduces the overall parasite burden and lowers the risk of severe pulmonary thromboembolism (American Heartworm Society, 2012). Macrocyclic lactones (MLs), such as ivermectin, milbemycin, moxidectin, and selamectin, are widely used for heartworm prevention. While ivermectin has demonstrated partial adulticidal activity when administered at 6–12 mg/kg monthly for 16 months, it completely eradicate adult worms within 30 months (McCall et al., 2008). However, prolonged ML therapy is not recommended treatment due to the risk of continued disease progression, thromboembolism, and potential worsening of clinical signs (Venco et al., 2004). Doxycycline has emerged as a promising adjunct therapy due to its macrofilaricidal effects on *D. immitis*. The elimination of *Wolbachia* reduces inflammation and decreases microfilarial burden. A combination of doxycycline (10 mg/kg/day for discontinuous cycles) and ivermectin (6 µg/kg weekly) has been shown to accelerate microfilarial clearance and improve adulticidal efficacy compared to either drug alone (Bazzocchi et al., 2008). Historically, heartworm prevention relied on daily administration of diethylcarbamazine (DEC) during mosquito season. Prophylaxis has been transformed by the introduction of macrocyclic lactones, such as selamectin, moxidectin, milbemycin, and ivermectin. These agents interrupt larval development within the first 2 months post-infection, providing effective monthly or even less frequent administration schedules. The long-term use of available heartworm treatments has raised concerns about emerging drug resistance. Evidence of resistance to MLs has been reported in various veterinary parasitic diseases, emphasizing the need for novel therapeutic strategies (Noack et al., 2021).

The primary approach to treating and controlling onchocerciasis relies on ivermectin, which is highly effective against the microfilarial stage of *O. volvulus* but has limited impact on long-lived adult worms residing in tissues. With onchocerciasis now designated for elimination, there is a pressing need for new treatments, particularly those with macrofilaricidal properties (Gokool et al., 2024). As there is no available vaccine, the current strategy for preventing and eliminating onchocerciasis depends on mass drug administration (MDA) programs. These programs involve large-scale distribution of ivermectin, either once or twice a year, without requiring prior diagnosis or direct supervision by healthcare providers (WHO, 2023). Ivermectin, a macrocyclic lactone, acts exclusively on microfilariae by eliminating them and inhibiting the release of new larvae from female worm's uterus, temporarily suppressing reproduction. This dual mechanism can reduce skin microfilarial loads by up to 99% within 2 months of treatment (Basáñez et al., 2008). To effectively reduce filarial transmission, treatment must continue throughout the reproductive lifespan of adult worms, which can survive for up to 15 years. However, absence of drugs capable of directly killing adult worms remains a major limitation to the success of these programs. Additionally, concerns are emerging regarding potential ivermectin resistance in *Onchocerca* parasites, as similar resistance

has already been observed in veterinary nematodes. Given urgent need to identify macrofilaricidal drugs, drug repurposing has been explored as a strategy to accelerate the development of new treatments for filariasis. This approach is not new, as several currently used antifilarial drugs including ivermectin, diethylcarbamazine, moxidectin, and doxycycline were originally developed for veterinary or other medical applications before being adapted for human use (Tagboto and Orish, 2022).

Effective vector management is crucial in controlling the spread of animal filariasis, which is transmitted by mosquitoes, black flies, and biting midges. Integrated vector management is a comprehensive strategy that utilizes multiple resources to enhance vector control. It integrates different interventions aimed at one or more diseases and employs a range of approaches, including environmental, mechanical, biological, chemical, and innovative technologies. Successful implementation depends on evidence-based decisions, coordination among sectors, strong advocacy, community participation, appropriate legislation, and capacity development (Handbook for Integrated Vector Management in the Americas, 2019). Preventing mosquito exposure is essential in minimizing the risk of filarial disease transmission. Environmental changes, including deforestation, urbanization, and irrigation, combined with socio-economic shifts, can enhance mosquito migration and dispersal via wind and water, facilitating the transmission and spread of diseases to previously non-endemic regions (Wilson et al., 2020). So, a comprehensive strategy involves environmental management, chemical control, and targeted interventions are needed. Among this, integrated mosquito management is a comprehensive approach aimed at keeping mosquito populations below levels that pose a risk to public health, thereby reducing disease transmission and, under certain conditions, achieving local elimination. This strategy is guided by four core principles. First, it emphasizes understanding the relationship between mosquito breeding patterns and environmental factors that influence their proliferation. Second, it promotes the implementation of environmental management practices to reduce or eliminate breeding sites. Third, it focuses on targeting specific mosquito species known to transmit diseases, ensuring that control efforts are species-specific and effective. Lastly, the approach prioritizes controlling mosquito population density rather than pursuing complete eradication, recognizing the ecological balance and sustainability of interventions (Zhao and Xue, 2022). Eliminating stagnant water around farms, kennels, and pastures is essential to disrupt mosquito breeding, while regular cleaning and maintenance of water troughs and drainage systems help prevent larval development. Housing livestock in well-ventilated stables equipped with insect-proof screens can significantly reduce vector entry, and the use of high-velocity fans further deters flying insects. Chemical control measures, such as applying pyrethroid-based insecticides in animal shelters and resting sites, effectively eliminate adult mosquitoes and flies. Additionally, use of larvicides like temephos and methoprene in water sources disrupts the mosquito life cycle. It has been shown that using pesticides and pour-on insecticides, like deltamethrin, is ineffective, presumably because of their brief residual activity, particularly during rainy season (Laaksonen et al., 2009). So, to maintain sufficient protection against vector exposure, its efficacy could be increased with frequent and repeated applications. Periodic fogging in high-risk areas, along with targeted insecticide spraying in cattle farms and kennels, further suppresses vector populations. Implementing these integrated control measures is essential to minimizing vector densities and reducing the risk of animal filariasis transmission. Advancing knowledge on the epidemiology, pathogenesis, diagnosis, economic impact, and zoonotic significance of animal filariasis is critical for developing effective control and prevention strategies. Implementation of the one health approach requires active collaboration among veterinary, public health, and environmental health sectors. In endemic regions, veterinary services conduct surveys for filariasis in various animal species, including dogs, cats, sheep, cattle, and horses. This integrated framework is critical for the prevention, surveillance, and control of zoonotic diseases. Without such collaboration, disease control efforts are likely to be inefficient, and the risk of outbreaks and zoonotic transmission remains high. However, routine, ongoing interdisciplinary coordination remains limited in many regions. Strengthening such collaboration through one health platforms is essential for effective prevention and control of zoonotic and vector-borne diseases.

Conclusion

Filariasis poses a significant health threat to both humans and animals, with considerable medical, veterinary, and economic implications, affecting millions worldwide. The genetic diversity of filarial parasites can lead to varied phenotypic expressions, influencing host–parasite interactions. Effective control and elimination strategies primarily target mosquito vectors and potential reservoir hosts. The application of molecular techniques for parasite identification is crucial in developing effective strategies for managing emerging filarial infections. Comprehensive data on filariasis, including its geographic distribution, interaction with hosts and vectors, and effects on veterinary and human health, is necessary for focused interventions. Advancements in research methodologies are necessary to enhance disease detection, assess infection status, and identify more effective therapeutic targets. Currently, treatment largely depends on chemotherapy-based approaches, highlighting the need for intensified vaccine research to either prevent filarial infections or interrupt transmission. For the successful implementation of vector control measures, detailed investigations into the life cycle of filarial nematodes, particularly their developmental stages within mosquito vectors, are imperative. Understanding these key biological processes could facilitate the identification of novel intervention targets, contributing to more effective disease management strategies.

Animal filariasis, attributable to filarial nematodes such as *Setaria*, *Dirofilaria*, and *Onchocerca* species, remains a significant concern in veterinary medicine, particularly in tropical and subtropical regions. These parasitic infections not only induce considerable morbidity in domestic animals but also contribute to decreased productivity, reproductive impairments, and deterioration in hide and meat quality, collectively imposing substantial economic burdens on the livestock sector. Beyond veterinary concerns, several filarial species possess notably zoonotic potential, imposing a threat to public health and highlights the need for a one health approach to mitigate these infections. Despite being largely neglected in many parts of the world, filarial infections continue to spread due to factors such as insufficient vector control, climate change, and global animal trade. Effective control of filariasis relies on timely diagnosis, appropriate therapeutic interventions, and comprehensive management strategies encompassing vector control and prophylactic measures. However, persistent challenges in disease surveillance, diagnostic accuracy, and

vaccine development continue to hinder progress in mitigating the spread of filarial infections. Addressing the burden of animal filariasis need a multidisciplinary approach involving veterinarians, public health professionals, entomologists, and researchers. Increased awareness, enhanced research funding, and the implementation of coordinated control strategies will be vital in reducing the burden of animal filariasis and preventing its spillover to human populations. The findings provide a foundation for future quantitative studies assessing infection prevalence, vector competence, and transmission dynamics.

Author contributions

RM: Data curation, Investigation, Methodology, Software, Writing – original draft, Writing – review & editing. MR: Funding acquisition, Writing – review & editing. PS: Conceptualization, Funding acquisition, Investigation, Supervision, Validation, Visualization, Writing – original draft, Writing – review & editing.

Funding

The author(s) declare that financial support was received for the research and/or publication of this article. The article processing charge for this manuscript was supported by extramural funding from the Indian Council of Medical Research, New Delhi (No. 6/9-7(271)/KA/2021-ECD-II).

Conflict of interest

The authors declare that the research was conducted in the absence of any commercial or financial relationships that could be construed as a potential conflict of interest.

Generative AI statement

The authors declare that no Gen AI was used in the creation of this manuscript.

Any alternative text (alt text) provided alongside figures in this article has been generated by Frontiers with the support of artificial intelligence and reasonable efforts have been made to ensure accuracy, including review by the authors wherever possible. If you identify any issues, please contact us.

Publisher's note

References

Abdullah, H. H. A. M., Amanzougaghene, N., Dahmana, H., Louni, M., Raoult, D., and Mediannikov, O. (2021). Multiple vector-borne pathogens of domestic animals in Egypt. *PLoS Negl. Trop. Dis.* 15:e0009767. doi: 10.1371/journal.pntd.0009767

Addiss, D. G., and Mackenzie, C. (2004). Lymphatic filariasis – clinical management. *Am. J. Trop. Med. Hyg.* 71, 12–15.

Albanese, F., Abramo, F., Braglia, C., Caporali, C., Venco, L., Vercelli, A., et al. (2013). Nodular lesions due to infestation by *Dirofilaria repens* in dogs from Italy. *Vet. Dermatol.* 24, 255–e56. doi: 10.1111/vde.12009

Alho, A. M., Cruz, L., Coelho, A., Martinho, F., Mansinho, M., Annoscia, G., et al. (2016). Aberrant laryngeal location of Onchocerca lupi in a dog. *Parasitol. Int.* 65, 218–220. doi: 10.1016/j.parint.2015.12.010

Alsarraf, M., Dwużnik-Szarek, D., Hildebrand, J., Mierzejewska, E. J., Kloch, A., Kot, K., et al. (2023). Occurrence of Dirofilaria repens in wild carnivores in Poland. *Parasitol. Res.* 122, 1229–1237. doi: 10.1007/s00436-023-07823-5

American Heartworm Society (2012). Curret canine guidelines for the diagnosis, prevention, and management of heartworm (Dirofilaria immitis) infection in dogs. Wilmington, DE: American Heartworm Society.

Ananda, K. J., D'Souza, P. E., and Jagannath, M. S. (2006). Methods for identification of microfilaria of *Dirofilaria repens* and *Dipetalonema reconditum*. *J. Vet. Parasitol.* 20, 45–47.

Anderson, R. C. (2000). Nematode parasites of vertebrates: Their development and transmission. London: CABI Pub.

Aththanayaka, A. M. M. T. B., Dayananda, B. S. W. M. T. B., Ranasinghe, H. A. K., and Amarasinghe, L. D. (2024). Evolution of dirofilariasis diagnostic techniques from traditional morphological analysis to molecular-based techniques: a comprehensive review. *Front. Parasitol.* 3:1427449. doi: 10.3389/fpara.2024.1427449

Azari-Hamidian, S., Norouzi, B., and Harbach, R. E. (2019). A detailed review of the mosquitoes (Diptera: Culicidae) of Iran and their medical and veterinary importance. *Acta Trop.* 194, 106–122. doi: 10.1016/j.actatropica.2019.03.019

Basáñez, M.-G., Pion, S. D., Boakes, E., Filipe, J. A., Churcher, T. S., and Boussinesq, M. (2008). Effect of single-dose ivermectin on *Onchocerca volvulus*: a systematic review and meta-analysis. *Lancet Infect. Dis.* 8, 310–322. doi: 10.1016/S1473-3099(08)70099-9

Bazargani, T., Eslami, A., Gholami, G. R., Molai, A., Ghafari-Charati, J., Dawoodi, J., et al. (2008). Cerebrospinal nematodiasis of cattle, sheep and goats in Iran. *Iran. J. Parasitol.* 3, 16–20.

Bazzocchi, C., Mortarino, M., Grandi, G., Kramer, L. H., Genchi, C., Bandi, C., et al. (2008). Combined ivermectin and doxycycline treatment has microfilaricidal and adulticidal activity against Dirofilaria immitis in experimentally infected dogs. *Int. J. Parasitol.* 38, 1401–1410. doi: 10.1016/j.ijpara.2008.03.002

Bendas, A. J. R., Alberigi, B., Galardo, S., Labarthe, N., and Almeida, F. M. D. (2022). Clinical and blood count findings in dogs naturally infected with Dirofilaria immiti. *Brazilian Journal of Veterinary Medicine* 44:e001922. doi: 10.29374/2527-2179.bjvm001922

Bino Sundar, S. T., Dhivya, B., Jyothimol, G., Anandaraja, R., Ramesh, P., Balachandran, C., et al. (2017). Incidence of Onchocerca gibsoni in subcutaneous nodules of cross bred Jersey cows: case report. *J. Parasit. Dis.* 41, 473–475. doi: 10.1007/s12639-016-0831-0

Boijsen, B., Uhlhorn, H., Ågren, E., and Höglund, J. (2017). Nodular onchocercosis in red deer (*Cervus elaphus*) in Sweden. *Int. J. Parasitol. Parasites Wildlife* 6, 340–343. doi: 10.1016/j.ijppaw.2017.09.003

Bowman, D. D., Liu, Y., McMahan, C. S., Nordone, S. K., Yabsley, M. J., and Lund, R. B. (2016). Forecasting United States heartworm Dirofilaria immitis prevalence in dogs. *Parasit. Vectors* 9:540. doi: 10.1186/s13071-016-1804-y

Brattig, N. W., Cheke, R. A., and Garms, R. (2021). Onchocerciasis (river blindness) – more than a century of research and control. *Acta Trop.* 218:105677. doi: 10.1016/j.actatropica.2020.105677

Cambra-Pellejà, M., Gandasegui, J., Balaña-Fouce, R., Muñoz, J., and Martínez-Valladares, M. (2020). Zoonotic implications of onchocerca species on human health. *Pathogens* 9:761. doi: 10.3390/pathogens9090761

Casiraghi, M., Bazzocchi, C., Mortarino, M., Ottina, E., and Genchi, C. (2006). A simple molecular method for discriminating common filarial nematodes of dogs (*Canis familiaris*). *Vet. Parasitol.* 141, 368–372. doi: 10.1016/j.vetpar.2006.06.006

Chaithra, S. N., Gopinathan, A., Singh, K., Kumar, A., Arya, M., Tiwari, V. K., et al. (2024). Management of ocular setariasis in equine: a report of 15 cases. *Explor. Anim. Med. Res.* 14, 66–69. doi: 10.52635/eamr/14(S1)66-69

Chatterjee, S., and Nutman, T. B. (2015). "Filarial nematodes" in Manual of clinical microbiology. eds. J. H. Jorgensen, K. C. Carroll, G. Funke and M. A. Pfaller (London: ASM Press), 2461–2470.

Chen, T., Moon, K., deMello, D. E., Feiz-Erfan, I., Theodore, N., and Bhardwaj, R. D. (2015). Case report of an epidural cervical Onchocerca lupi infection in a 13-year-old boy. *J. Neurosurg. Pediatr.* 16, 217–221. doi: 10.3171/2014.12.PEDS14462

Dagnaw, M., Zemene, M., Getaneh, G., and Tibenu, S. (2016). A review on equine onchocerchiasis. *Afr. J. Basic Appl. Sci.* 8, 27–33.

Darchenkova, N. N., and Supriaga, V G, null, Guzeeva, M. V., Morozov, E. N., Zhukova, L. A., and Sergiev, V. P. (2009). [Prevalence of human dirofilariasis in Russia]. Med. Parazitol. Parazit. Bolezn., 2, 3–7.

Davoodi, J. (2015). Prevalence of setariosis in small and large ruminant in Miyaneh City, northwest of Iran. *Sci. J. Vet. Adv.* 3, 1–5. doi: 10.14196/SJVA.V3I1.1145

Day, M. J. (2011). One health: the importance of companion animal vector-borne diseases. *Parasit. Vectors* 4:49. doi: 10.1186/1756-3305-4-49

Dehkordi, Z. S., Heidari, H., and Halajian, A. (2015). Case report of adult *Setaria digitata* in sheep, Hamedan province, Iran. *Comp. Clin. Pathol.* 24, 185–187. doi: 10.1007/s00580-014-1912-z

Devi, A., Sudan, V., and Shanker, D. (2020). Phylogenetic characterization of Setaria equina and its association with other filarids. *Parasitol. Res.* 119, 4267–4270. doi: 10.1007/s00436-020-06917-8

Dudley, R. W. R., Smith, C., Dishop, M., Mirsky, D., Handler, M. H., and Rao, S. (2015). A cervical spine mass caused by Onchocerca lupi. *Lancet* 386:1372. doi: 10.1016/S0140-6736(14)62255-8

Eberhard, M. L., Ortega, Y., Dial, S., Schiller, C. A., Sears, A. W., and Greiner, E. (2000). Ocular Onchocerca infections in two dogs in western United States. *Vet. Parasitol.* 90, 333–338. doi: 10.1016/S0304-4017(00)00252-1

Egyed, Z., Sréter, T., Széll, Z., Beszteri, B., Oravecz, O., Márialigeti, K., et al. (2001). Morphologic and genetic characterization of Onchocerca lupi infecting dogs. *Vet. Parasitol.* 102, 309–319. doi: 10.1016/S0304-4017(01)00541-6

Egyed, Z., Sréter, T., Széll, Z., Nyirő, G., Dobos-Kovács, M., Márialigeti, K., et al. (2002). Electron microscopic and molecular identification of Wolbachia endosymbionts from Onchocerca lupi: implications for therapy. *Vet. Parasitol.* 106, 75–82. doi: 10.1016/S0304-4017(02)00029-8

Foroulis, C. N., Khaldi, L., Desimonas, N., and Kalafati, G. (2005). Pulmonary dirofilariasis mimicking lung tumor with chest wall and mediastinal invasion. *Thorac. Cardiovasc. Surg.* 53, 173–175. doi: 10.1055/s-2004-830567

Foster, W. A., and Walker, E. D. (2019). "Mosquitoes (Culicidae)" in Medical and veterinary entomology. eds. G. R. Mullen and L. A. Durden (Amsterdam: Elsevier), 261–325.

Genchi, M., Pengo, G., and Genchi, C. (2010). Efficacy of moxidectin microsphere sustained release formulation for the prevention of subcutaneous filarial (Dirofilaria repens) infection in dogs. *Vet. Parasitol.* 170, 167–169. doi: 10.1016/j.vetpar.2010.01.034

Gokool, S., Townson, S., Freeman, A., Siemienski-Kleyn, J., Zubrzycki, J., Tagboto, S., et al. (2024). Onchocerciasis drug discovery: in vitro evaluation of fda-approved drugs against onchocerca gutturosa in Gambia. *Pharmaceutics* 16:210. doi: 10.3390/pharmaceutics16020210

Gomez-Puerta, L. A., and Mayor, P. (2017). Congenital filariasis caused by setaria bidentata (Nematoda: Filarioidea) in the red brocket deer (*mazama americana*). *J. Parasitol.* 103, 123–126. doi: 10.1645/16-86

Gumisiriza, N., Mubiru, F., Siewe Fodjo, J. N., Mbonye Kayitale, M., Hotterbeekx, A., Idro, R., et al. (2020). Prevalence and incidence of nodding syndrome and other forms of epilepsy in onchocerciasis-endemic areas in northern Uganda after the implementation of onchocerciasis control measures. *Infect. Dis. Poverty* 9:12. doi: 10.1186/s40249-020-0628-3

Handbook for Integrated Vector Management in the Americas (2019). PAHO/WHO | Pan American health organization. Geneva: WHO.

Hanafiah, M., Athaillah, F., Helmi, T. Z., and Sutriana, A. (2023). Morphology of Setaria spp. (Setariidae; Nematoda) in Aceh cattle, Indonesia. *Biodiversitas* 24. doi: 10.13057/biodiv/d240754

Hoch, H., and Strickland, K. (2008). Canine and feline dirofilariasis: life cycle, pathophysiology, and diagnosis. *Compendium* 30:133.

Hoerauf, A. (2008). Filariasis: new drugs and new opportunities for lymphatic filariasis and onchocerciasis. *Curr. Opin. Infect. Dis.* 21, 673–681. doi: 10.1097/QCO.0b013e328315cde7

Hotterbeekx, A., Perneel, J., Mandro, M., Abhafule, G., Siewe Fodjo, J. N., Dusabimana, A., et al. (2020). Comparison of diagnostic tests for Onchocerca volvulus in the Democratic Republic of Congo. *Pathogens* 9:435. doi: 10.3390/pathogens9060435

Irwin, P. J., and Jefferies, R. (2004). Arthropod-transmitted diseases of companion animals in Southeast Asia. *Trends Parasitol.* 20, 27–34. doi: 10.1016/j.pt.2003.11.004

Khedri, J., Radfar, M. H., Borji, H., and Azizzadeh, M. (2014). An epidemiological survey of setaria in the abdominal cavities of Iranian sistani and Brahman cattle in the southeastern of Iran. *Iran. J. Parasitol.* 9, 249–253

Kim, M. K., Kim, C. H., Yeom, B. W., Park, S. H., Choi, S. Y., and Choi, J. S. (2002). The first human case of hepatic dirofilariasis. *J. Korean Med. Sci.* 17:686. doi: 10.3346/jkms.2002.17.5.686

Klug, D., and Drake, J. (2022). "Global economics of heartworm disease" in Human and Animal Filariases. eds. R. Kaminsky and T. G. Geary (New York, NY: Wiley), 329–343.

Krueger, A., Fischer, P., and Morales-Hojas, R. (2007). Molecular phylogeny of the filaria genus Onchocerca with special emphasis on Afrotropical human and bovine parasites. *Acta Trop.* 101, 1–14. doi: 10.1016/j.actatropica.2006.11.004

Kwok, R. P. W., Chow, P. P. C., Lam, J. K. M., Fok, A. C., Jhanji, V., Wong, V. W. Y., et al. (2016). Human ocular dirofilariasis in Hong Kong. *Optom. Vis. Sci.* 93, 545–548. doi: 10.1097/OPX.0000000000000770

Laaksonen, S., Solismaa, M., Kortet, R., Kuusela, J., and Oksanen, A. (2009). Vectors and transmission dynamics for Setaria tundra (Filarioidea; onchocercidae), a parasite of reindeer in Finland. *Parasit. Vectors* 2:3. doi: 10.1186/1756-3305-2-3

Lanková, S., Vejl, P., Melounová, M., Čílová, D., Vadlejch, J., Miklisová, D., et al. (2021). *Setaria cervi* (Filarioidea, Onchocercidae) undressing in ungulates: altered morphology of developmental stages, their molecular detection and complete sequence *cox* 1 gene. *Parasitology* 148, 598–611. doi: 10.1017/S0031182020002449

Leccia, N., Patouraux, S., Carpentier, X., Boissy, C., Giudice, P. D., Parks, S., et al. (2012). Pseudo-tumor of the scrotum, a rare clinical presentation of dirofilariasis: a report of two autochtonous cases due to Dirofilaria repens. *Pathogens Global Health* 106, 370–372. doi: 10.1179/2047773212Y.0000000029

Lee, H., Hwang, H., Ro, Y., Kim, J.-H., Lee, K., Choi, E., et al. (2021). *Setaria digitata* was the main cause of equine neurological ataxia in Korea: 50 cases(2015–2016). *J. Vet. Med. Sci.* 83, 869–875. doi: 10.1292/jvms.20-0741

Lefoulon, E., Giannelli, A., Makepeace, B. L., Mutafchiev, Y., Townson, S., Uni, S., et al. (2017). Whence river blindness? The domestication of mammals and host-parasite co-evolution in the nematode genus Onchocerca. *Int. J. Parasitol.* 47, 457–470. doi: 10.1016/j.ijpara.2016.12.009

Lia, R. P., Mutafchiev, Y., Veneziano, V., Giannelli, A., Abramo, F., Santoro, M., et al. (2017). Filarial infection caused by Onchocerca boehmi (Supperer, 1953) in a horse from Italy. *Parasitol. Res.* 116, 191–198. doi: 10.1007/s00436-016-5277-x

Lubbers, C., Amaral, L.-J., Colebunders, R., Brattig, N., and Hadermann, A. (2025). The last mile in onchocerciasis elimination: diagnostic challenges. *Trends Parasitol.* 41, 894–908. doi: 10.1016/j.pt.2025.08.006

Luk, B. W., Cheung, C., and Chan, Y. (2021). Anaphylaxis after surgical excision of subcutaneous infection with parasitic Dirofilaria: a case report. *Hong Kong Med. J.* 27, 297–299. doi: 10.12809/hkmj208675

Magnis, J., Lorentz, S., Guardone, L., Grimm, F., Magi, M., Naucke, T. J., et al. (2013). Morphometric analyses of canine blood microfilariae isolated by the Knott's test enables Dirofilaria immitis and *D. repens* species-specific and Acanthocheilonema (Syn. Dipetalonema) genus-specific diagnosis. *Parasit. Vectors* 6:48. doi: 10.1186/1756-3305-6-48

Maharana, B. R., Potliya, S., Ganguly, A., Bisla, R. S., Mishra, C., and Ganguly, I. (2020). First report of the isolation and phylogenetic characterization of equine Setaria digitata from India based on mitochondrial COI, 12S rDNA, and nuclear ITS2 sequence data. *Parasitol. Res.* 119, 473–481. doi: 10.1007/s00436-019-06587-1

Manathunga, T., Tse, M., Perles, L., Beugnet, F., Barrs, V., and Otranto, D. (2024). Zoonotic Dirofilaria sp. "Hongkongensis" in subcutaneous nodules from dogs and cats, Hong Kong SAR. *Parasit. Vectors* 17:469. doi: 10.1186/s13071-024-06544-7

Mandal, S. C., and Ray, S. (1994). Note on uncommon occurrence of *Setaria labiatopapillosa*. *Indian Vet. J.* 71:726.

Mather, C., and Treuting, P. (2012). Onchocerca armillata contamination of a bovine pericardial xenograft in a human patient with repaired tetralogy of Fallot. *Cardiovasc. Pathol.* 21, e35–e38. doi: 10.1016/j.carpath.2011.07.004

McArthur, D. B. (2019). Emerging infectious diseases. *Nurs. Clin. N. Am.* 54, 297–311. doi: 10.1016/j.cnur.2019.02.006

McCall, J. W., Genchi, C., Kramer, L. H., Guerrero, J., and Venco, L. (2008). Chapter 4 heartworm disease in animals and humans. *Adv. Parasitol.* 66, 193–285. doi: 10.1016/S0065-308X(08)00204-2

Morales-Hojas, R., Cheke, R. A., and Post, R. J. (2006). Molecular systematics of five *Onchocerca* species (Nematoda: Filarioidea) including the human parasite, *O. Volvulus*, suggest sympatric speciation. *J. Helminthol.* 80, 281–290. doi: 10.1079/JOH2006331

Moya Alonso, L., Murdoch, M. E., and Jofre-Bonet, M. (2009). Psycho-social and economic evaluation of onchocerciasis: a literature review. *Soc. Med.* 4, 8–31. doi: 10.71164/socialmedicine.v4i1.2009.280

Mrifag, R., Lemrabott, M. A., El Kharrim, K., Belghyti, D., and Basco, L. K. (2021). Setaria labiatopapillosa (Filarioidea, nematoda) in Moroccan cattle: atypical localization and morphological characterization of females and microfilariae by light and scanning electron microscopy. *Parasitol. Res.* 120, 911–918. doi: 10.1007/s00436-020-06966-z

Muhammad, G., and Saqib, M. (2007). Successful treatment of ocular equine microfilariasis (*Setaria* species) with ivermectin. *Vet. Rec.* 160:25.

Nabie, R., Spotin, A., and Rouhani, S. (2017). Subconjunctival setariasis due to Setaria equina infection; a case report and a literature review. *Parasitol. Int.* 66, 930–932. doi: 10.1016/j.parint.2016.10.017

Neary, J. M., Trees, A. J., Ekale, D. D., Tanya, V. N., Hetzel, U., and Makepeace, B. L. (2010). Onchocerca armillata contains the endosymbiotic bacterium Wolbachia and elicits a limited inflammatory response. *Vet. Parasitol.* 174, 267–276. doi: 10.1016/j.vetpar.2010.08.031

Noack, S., Harrington, J., Carithers, D. S., Kaminsky, R., and Selzer, P. M. (2021). Heartworm disease - overview, intervention, and industry perspective. *Int. J. Parasitol. Drugs Drug Resist.* 16, 65–89. doi: 10.1016/j.ijpddr.2021.03.004

Obradovic, J., Jurisic, V., Tosic, N., Mrdjanovic, J., Perin, B., Pavlovic, S., et al. (2013). Optimization of PCR conditions for amplification of GC-rich EGFR promoter sequence. *J. Clin. Lab. Anal.* 27, 487–493. doi: 10.1002/jcla.2013.27.issue-6

Orihel, T. C., and Eberhard, M. L. (1998). Zoonotic filariasis. *Clin. Microbiol. Rev.* 11, 366–381. doi: 10.1128/CMR.11.2.366

Otranto, D., and Deplazes, P. (2019). Zoonotic nematodes of wild carnivores. *Int. J. Parasitol. Parasites Wildlife* 9, 370–383. doi: 10.1016/j.ijppaw.2018.12.011

Otranto, D., Giannelli, A., Scotty Trumble, N., Chavkin, M., Kennard, G., Latrofa, M., et al. (2015). Clinical case presentation and a review of the literature of canine onchocercosis by Onchocerca lupi in the United States. *Parasit. Vectors* 8:89. doi: 10.1186/s13071-015-0699-3

Pampiglione, S., Canestri Trotti, G., and Rivasi, F. (1995). Human dirofilariasis due to *Dirofilaria* (*Nochtiella*) repens: a review of world literature. *Parassitologia* 37, 149–193.

Papaioannou, N., Psalla, D., Papadopoulos, E., Adamama-Moraitou, K. K., Petanidis, T., Rallis, T., et al. (2004). Obstructive, granulomatous tracheitis caused by *Onchocerca* sp. in a dog. *J. Veterinary Med. Ser. A* 51, 354–357. doi: 10.1111/j.1439-0442.2004.00660.x

Pękacz, M., Basałaj, K., Kalinowska, A., Klockiewicz, M., Stopka, D., Bąska, P., et al. (2022). Selection of new diagnostic markers for Dirofilaria repens infections with the use of phage display technology. *Sci. Rep.* 12:2288. doi: 10.1038/s41598-022-06116-8

Peng, T. L., Armiladiana, M. M., Ruhil, H. H., Maizan, M., and Choong, S. S. (2019). First report of equine Setaria digitata (Von linstow 1906) infestation in Malaysia. *Vet. Parasitol. Reg. Stu. Rep.* 17:100310. doi: 10.1016/j.vprsr.2019.100310

Perles, L., Dantas-Torres, F., Krücken, J., Morchón, R., Walochnik, J., and Otranto, D. (2024). Zoonotic dirofilariases: one, no one, or more than one parasite. *Trends Parasitol.* 40, 257–270. doi: 10.1016/j.pt.2023.12.007

Perumal, A. N. I., Gunawardene, Y. I. N. S., and Dassanayake, R. S. (2016). Setaria digitata in advancing our knowledge of human lymphatic filariasis. *J. Helminthol.* 90, 129–138. doi: 10.1017/S0022149X15000309

Petry, G., Genchi, M., Schmidt, H., Schaper, R., Lawrenz, B., and Genchi, C. (2015). Evaluation of the adulticidal efficacy of imidacloprid 10%/moxidectin 2. 5%(W/v) spot-on(advocate®, advantage® multi) against dirofilaria repens in experimentally infected dogs. *Parasitol. Res.* 114, 131–144. doi: 10.1007/s00436-015-4519-7

Rabeya Begam, R. B., Saidul Islam, S. I., Munmi Saikia, M. S., Aditi Kalita, A. K., Bulbul, K. H., Joken Bam, J. B., et al. (2015, 2015). Prevalence of aortic onchocerciasis in cattle of Assam. *Vet. Pract.* 16, 225–227.

Radwan, A. M., Ahmed, N. E., Elakabawy, L. M., Ramadan, M. Y., and Elmadawy, R. S. (2016). Prevalence and pathogenesis of some filarial nematodes infecting donkeys in Egypt. *Veterinary World* 9, 888–892. doi: 10.14202/vetworld.2016.888-892

Rafee, M. A., and Amarpal, A. (2016). Equine ocular setariasis and its management. *J. Exp. Biol. Agric. Sci.* 4, S139–S143. doi: 10.18006/2016

Ramaiah, K. D., and Ottesen, E. A. (2014). Progress and impact of 13 years of the global programme to eliminate lymphatic filariasis on reducing the burden of filarial disease. *PLoS Negl. Trop. Dis.* 8:e3319. doi: 10.1371/journal.pntd.0003319

Rhee, J. K., Choi, E. Y., Park, B. K., and Jang, B. G. (1994). Application of scanning electron microscopy in assessing the prevalence of some Setaria species in Korean cattle. *Korean J. Parasitol.* 32, 1–6. doi: 10.3347/kjp.1994.32.1.1

Rishniw, M., Barr, S. C., Simpson, K. W., Frongillo, M. F., Franz, M., and Dominguez Alpizar, J. L. (2006). Discrimination between six species of canine microfilariae by a single polymerase chain reaction. *Vet. Parasitol.* 135:303. doi: 10.1016/j.vetpar.2005.10.013

Rodrigo, W. W., Dassanayake, R. S., Weerasena, S. J., and Silva Gunawardene, Y. I. (2014). Novel parasitic nematode-specific protein of bovine filarial parasite *Setaria digitata* displays conserved gene structure and ubiquitous expression. *Trop. Biomed.* 31, 514–524.

Rodríguez-Pérez, M. A., Unnasch, T. R., and Real-Najarro, O. (2011). Assessment and monitoring of onchocerciasis in Latin America. *Adv. Parasitol.* 77, 175–226.

Rommel, M., and Boch, J. (2000). Veterinärmedizinische Parasitologie: 100 Tabellen. Parey: Georg Thieme Verlag.

Saini, P., Haritha, H. A., Sivalaxmi, B., Ajithlal, P. M., Fathima, P. A., Shah, H. K., et al. (2024). Molecular prevalence of *Dirofilaria* sp. Hongkongensis, among the dog population in Thiruvananthapuram, India. *Res. Vet. Sci.* 180:105399. doi: 10.1016/j.rvsc.2024.105399

Sazmand, A., and Joachim, A. (2017). Parasitic diseases of camels in Iran (1931–2017) – a literature review. *Parasite* 24:21. doi: 10.1051/parasite/2017024

Sevimli, F. K., Kozan, E., Bülbül, A., Birdane, F. M., Köse, M., and Sevimli, A. (2007). Dirofilaria immitis infection in dogs: unusually located and unusual findings. *Parasitol. Res.* 101, 1487–1494. doi: 10.1007/s00436-007-0665-x

Schuster, R. K., Wibbelt, G., Maio, E., Wernery, U., and Sivakumar, S. (2019). Diaplacental infection of a bactrian camel (Camelus bactrianus) with the filarial worm Dipetalonema evansi: A case report. *J. Camel Pract. Res.* 26:231. doi: 10.5958/2277-8934.2019.00036.5

Shin, J., Ahn, K.-S., Suh, G.-H., Kim, H.-J., Jeong, H.-S., Kim, B.-S., et al. (2017). First blindness cases of horses infected with setaria digitata (Nematoda: Filarioidea) in the Republic of Korea. *Korean J. Parasitol.* 55, 667–671. doi: 10.3347/kjp.2017.55.6.667

Simón, F., Diosdado, A., Siles-Lucas, M., Kartashev, V., and González-Miguel, J. (2022). Human dirofilariosis in the 21st century: a scoping review of clinical cases reported in the literature. *Transbound. Emerg. Dis.* 69, 2424–2439. doi: 10.1111/tbed.14210

Simón, F., Siles-Lucas, M., Morchón, R., González-Miguel, J., Mellado, I., Carretón, E., et al. (2012). Human and animal dirofilariasis: the emergence of a zoonotic mosaic. *Clin. Microbiol. Rev.* 25, 507–544. doi: 10.1128/CMR.00012-12

Siriyasatien, P., Intayot, P., Sawaswong, V., Preativatanyou, K., Wacharapluesadee, S., Boonserm, R., et al. (2023). Description of potential vectors of zoonotic filarial nematodes, Brugia pahangi, Setaria digitata, and Setaria labiatopapillosa in Thai mosquitoes. *Heliyon* 9:e13255. doi: 10.1016/j.heliyon.2023.e13255

Song, K. H., Lee, S. E., Hayasaki, M., Shiramizu, K., Kim, D. H., and Cho, K. W. (2003). Seroprevalence of canine dirofilariosis in South Korea. *Vet. Parasitol.* 114, 231–236. doi: 10.1016/S0304-4017(03)00137-7

Soulsby, E. J. L. (1982). Helminths, arthropods and protozoa of domesticated animals. *7th* Edn. India: Elsevier India Pvt. Ltd.

Sréter, T., and Széll, Z. (2008). Onchocercosis: a newly recognized disease in dogs. *Vet. Parasitol.* 151, 1–13. doi: 10.1016/j.vetpar.2007.09.008

Sundar, S. T. B., and D'Souza, P. E. (2015). Morphological characterization of Setaria worms collected from cattle. *J. Parasit. Dis.* 39, 572–576. doi: 10.1007/s12639-013-0399-x

Tagboto, S., and Orish, V. (2022). Drug development for onchocerciasis-the past, the present and the future. *Front. Trop. Dis.* 3:953061. doi: 10.3389/fitd.2022.953061

Ţălu, S., Ştefănuţ, A., Mihalca, A., and Coroiu, Z. (2012). Subconjunctival infestation with *Setaria*. *Helminthologia* 49, 119–121. doi: 10.2478/s11687-012-0024-z

Tamilmahan, P., Zama, M., Pathak, R., Muneeswaran, N., and Karthik, K. (2013). A retrospective study of ocular occurences in domestic animals: 799 cases. *Vet. World* 6:274. doi: 10.5455/vetworld.2013.274-276

Tarello, W. (2011). Clinical aspects of dermatitis associated with dirofilaria repens in pets: a review of 100 canine and 31 feline cases (1990–2010) and a report of a new clinic case imported from Italy to Dubai. *J. Parasitol. Res.* 2011, 1–7. doi: 10.1155/2011/578385

Taylor, M. J., Hoerauf, A., and Bockarie, M. (2010). Lymphatic filariasis and onchocerciasis. *Lancet* 376, 1175–1185. doi: 10.1016/S0140-6736(10)60586-7

Taylor, A. E. R., and Muller, R. (1979). Problems in the identification of parasites and their vectors: Symposia of the british society for parasitology. London: Blackwell.

Tekle, A. H., Zouré, H. G. M., Noma, M., Boussinesq, M., Coffeng, L. E., Stolk, W. A., et al. (2016). Progress towards onchocerciasis elimination in the participating countries of the African Programme for onchocerciasis control: epidemiological evaluation results. *Infect. Dis. Poverty* 5:66. doi: 10.1186/s40249-016-0160-7

Theis, J. H. (2005). Public health aspects of dirofilariasis in the United States. *Vet. Parasitol.* 133, 157–180. doi: 10.1016/j.vetpar.2005.04.007

To, K. K. W., Wong, S. S. Y., Poon, R. W. S., Trendell-Smith, N. J., Ngan, A. H. Y., Lam, J. W. K., et al. (2012). A novel *dirofilaria* species causing human and canine infections in Hong Kong. *J. Clin. Microbiol.* 50, 3534–3541. doi: 10.1128/JCM.01590-12

Trancoso, T. A. L., Lima, N. D. C., Barbosa, A. S., Leles, D., Fonseca, A. B. M., Labarthe, N. V., et al. (2020). Detection of *Dirofilaria immitis* using microscopic, serological and molecular techniques among dogs in Cabo Frio, RJ, Brazil. *Rev. Bras. Parasitol. Vet.* 29:e017219. doi: 10.1590/s1984-29612020009

Traversa, D., Aste, G., Milillo, P., Capelli, G., Pampurini, F., Tunesi, C., et al. (2010). Autochthonous foci of canine and feline infections by *Dirofilaria immitis* and *Dirofilaria repens* in Central Italy. *Vet. Parasitol.* 169:128. doi: 10.1016/j.vetpar.2009.12.034

Tung, K.-C., Lai, C.-H., Ooi, H.-K., Yang, C.-H., and Wang, J.-S. (2003). Cerebrospinal Setariosis with *Setaria marshalli* and *Setaria digitata* infection in cattle. *J. Vet. Med. Sci.* 65, 977–983. doi: 10.1292/jvms.65.977

Uni, S., Fukuda, M., Otsuka, Y., Hiramatsu, N., Yokobayashi, K., Takahashi, H., et al. (2015). New zoonotic cases of *Onchocerca dewittei japonica* (Nematoda: Onchocercidae) in Honshu, Japan. *Parasit. Vectors* 8:59. doi: 10.1186/s13071-015-0655-2

Venco, L., Marchesotti, F., and Manzocchi, S. (2015). Feline heartworm disease: a 'Rubik's-cube-like' diagnostic and therapeutic challenge. *J. Vet. Cardiol.* 17, S190–S201. doi: 10.1016/j.jvc.2015.08.004

Venco, L., McCall, J. W., Guerrero, J., and Genchi, C. (2004). Efficacy of long-term monthly administration of ivermectin on the progress of naturally acquired heartworm infections in dogs. *Vet. Parasitol.* 124, 259–268. doi: 10.1016/j.vetpar.2004.06.024

WHO. (2023). Available online at: https://www.who.int/health-topics/neglected-tropical-diseases#tab=tab_1 (accessed October 15, 2023).

Wilson, A. L., Courtenay, O., Kelly-Hope, L. A., Scott, T. W., Takken, W., Torr, S. J., et al. (2020). The importance of vector control for the control and elimination of vector-borne diseases. *PLoS Negl. Trop. Dis.* 14:e0007831. doi: 10.1371/journal.pntd.0007831

Yu, F., Liu, B., Chen, S., Yi, Z., Liu, X., Zhu, Y., et al. (2021). First molecular confirmation of equine ocular setaria digitata in China. *Vet. Sci.* 8:55. doi: 10.3390/vetsci8040055

Zarfoss, M. K., Dubielzig, R. R., Eberhard, M. L., and Schmidt, K. S. (2005). Canine ocular onchocerciasis in the United States: two new cases and a review of the literature. *Vet. Ophthalmol.* 8, 51–57. doi: 10.1111/j.1463-5224.2005.00348.x

Zhao, T.-Y., and Xue, R.-D. (2022). Integrated mosquito management in rice field in China. *Wetl. Ecol. Manag.* 30, 963–973. doi: 10.1007/s11273-021-09840-6

frontiers | Frontiers in Microbiology

TYPE Original Research
PUBLISHED 17 November 2025
DOI 10.3389/fmicb.2025.1686956

OPEN ACCESS

EDITED BY
Axel Cloeckaert,
Institut National de recherche pour l'agriculture, l'alimentation et l'environnement (INRAE), France

REVIEWED BY
Xuenong Luo,
Chinese Academy of Agricultural Sciences, China
Şule Haskoloğlu,
Ankara University, Türkiye

*CORRESPONDENCE
Guodong Lü
✉ lgd_xj@xjmu.edu.cn
Tuerganaili Aji
✉ tuergan78@sina.com
Renyong Lin
✉ renyonglin@xjmu.edu.cn

†These authors have contributed equally to this work

RECEIVED 16 August 2025
ACCEPTED 27 October 2025
PUBLISHED 17 November 2025

CITATION
Bi X, Yang N, Ke Y, Xue J, Zhang X, Liu H, Chu J, Li L, Shao Y, Lü G, Aji T and Lin R (2025) Host angiogenic reprogramming by *Echinococcus multilocularis* protoscoleces protein via PDGFR/PI3K/AKT cascade. *Front. Microbiol.* 16:1686956. doi: 10.3389/fmicb.2025.1686956

Host angiogenic reprogramming by *Echinococcus multilocularis* protoscoleces protein via PDGFR/PI3K/AKT cascade

Xiaojuan Bi[1†], Ning Yang[1†], Ying Ke[1†], Junlong Xue[1], Xue Zhang[1], Hui Liu[1], Jin Chu[1], Liang Li[1], Yingmei Shao[2], Guodong Lü[1]*, Tuerganaili Aji[2]* and Renyong Lin[1]*

[1]State Key Laboratory of Pathogenesis, Prevention, and Treatment of Central Asian High Incidence Diseases, Clinical Medical Research Institute, The First Affiliated Hospital of Xinjiang Medical University, Urumqi, Xinjiang, China, [2]Department of Hepatic Hydatid and Hepatobiliary Surgery, Digestive and Vascular Surgery Centre, The First Affiliated Hospital of Xinjiang Medical University, Urumqi, China

Background: Alveolar echinococcosis (AE) is a globally present zoonotic disease caused by *Echinococcus multilocularis* (*E. multilocularis*) infection, characterized by the formation of tumor-like growths primarily in the liver, with the potential to spread to other organs. Similar to tumors, *E. multilocularis* infection is accompanied by pathological angiogenesis, suggesting that the implementation of anti-angiogenic therapeutic strategies may also have promising applications in the treatment of AE. However, the mechanism of angiogenesis in AE remains unclear and has not been fully elucidated.

Results: In this study, we discovered that angiogenesis related genes are significantly up-regulated in the mouse model of *E. multilocularis* infection and pathological angiogenesis around the lesion was significantly increased at 10–12 weeks after infection compared to the control group. Interventions utilizing a range of inhibitors at the *in vitro* level, including the PDGFR-β inhibitor AG1296, the PI3K inhibitor LY294002, the AKT inhibitor MK2206, and the FAK inhibitor Y15, demonstrated that *E. multilocularis* protoscoleces protein (EmP) induces angiogenesis through PDGFR/PI3K/AKT/FAK signaling pathway.

Conclusion: Our findings provide new perspectives on how *E. multilocularis* infection triggers pathological angiogenesis in the host liver, and may provide a novel anti-angiogenic therapeutic strategy against *E. multilocularis* infection.

KEYWORDS

***Echinococcus multilocularis*, pathological angiogenesis, human umbilical vein endothelial cells, PDGF-BB, PDGFR**

Highlights

- Angiogenesis related genes are significantly up-regulated in the liver surrounding the lesion in *E. multilocularis* infected mice.
- *E. multilocularis* protoscoleces protein (EmP) induces pathological angiogenesis via the PDGFR/PI3K/AKT/FAK signaling pathway *in vitro*.

1 Introduction

Alveolar echinococcosis (AE) is a parasitic zoonotic disease distributed in both developing and developed Northern Hemisphere countries, with an estimated 17,400 new infections per year, most of which occur in China (Casulli et al., 2019). AE is caused by the larval stage (metacestode) of the tapeworm *E. multilocularis*. The eggs are ingested orally and hatch in the host's gastrointestinal tract, releasing an oncosphere which penetrates the epithelium in the small intestine and gains access to the inner organs, especially the liver. In the liver, the oncosphere undergoes metamorphosis into the metacestode. AE is characterized by the progressing infiltrative proliferation of the parasite, mimicking a malignancy (Herz and Brehm, 2021). The continuous growth of metacestodes erodes blood vessels and bile ducts in the liver tissue of intermediate hosts, leading to organ failure. Mortality in untreated or inadequately treated AE patients is more than 90% within 10 to 15 years of diagnosis (Yang et al., 2022). In recent years, significant progress has been made in the prevention, diagnosis and treatment of echinococcosis. However, considering the toxicity and inefficiency exhibited by presently accessible medications, insufficiency of surgical approaches, as well as the difficulties in controlling and preventing the condition, it is imperative to promptly explore novel therapeutic pathways and targets (Wen et al., 2019).

Large animals necessitate a circulatory system to facilitate the distribution of essential substances such as oxygen, nutrients, hormones, and growth factors throughout the entire body, while also facilitating the elimination of waste products including carbon dioxide, lactic acid, and urea. This vital function is carried out by the blood vascular system (Dennis et al., 2011). Similarly, parasites, as relatively large pathogens, they have high requirements comparable requirements in order to effectively establish themselves within their parasitized host. Throughout the development of various parasites that reside in tissues or blood vessels, it becomes evident that there are both direct and indirect interactions with the host's blood vascular systems (Dennis et al., 2011). To date, a variety of parasites have been identified that may have the ability to initiate or promote the growth of new blood vessels in the host (Andrade and Santana, 2010; El-Dardiry et al., 2021). Angiogenesis has been observed in the vicinity of lesions in canines and rodents infected with *E. multilocularis*. The emergence of these newly formed blood vessels may be important in the provision of nutritional factors, serves as potential mediators of signals governing host-parasite interactions, and potentially contributes to the development of metastasis (Weiss et al., 2010; Stadelmann et al., 2010; Perez Rodriguez et al., 2023). Nevertheless, the mechanism of angiogenesis caused by *E. multilocularis* infection remains unclear and has not been fully elucidated.

Pathological angiogenesis is intrinsically related to the progression of chronic liver diseases such as liver fibrosis and hepatocellular carcinoma (Bocca et al., 2015). Considering that angiogenesis is a crucial process for tumor growth and metastasis, the implementation of anti-angiogenic therapy represents a promising anti-cancer strategy with the objective of depriving tumors of essential nutrients and oxygen supply through the decrease of the vascular network and the avoidance of new blood vessels formation (Kountouras et al., 2005). As mentioned above, akin to tumors, parasitic infections are also commonly accompanied by pathological angiogenesis, especially in AE, also called "worm cancer." Consequently, the implementation of anti-angiogenic therapeutic strategies may have promising therapeutic applications in the treatment of AE. In a recent study, Jiang et al. (2023) found that sunitinib malate (SU11248) treatment markedly reduced vascular endothelial growth factor A (VEGFA) induced angiogenesis and significantly inhibited the growth of multilocular tapeworms in *E. multilocularis* infected mice. This study preliminarily reveals the promise of anti-angiogenesis strategies in the treatment of AE.

Presently, the majority of anti-angiogenic agents approved for cancer treatment rely on targeting vascular endothelial growth factor (VEGF) actions, given that VEGF signaling is widely acknowledged as the principal promoter of angiogenesis (Lopes-Coelho et al., 2021). However, there are many pathways that regulate angiogenesis, and when one of these processes is blocked, others may play alternative roles, leading to the fact that therapeutic strategies targeting VEGF are not always effective (Vimalraj, 2022). Combining alternative effector factors that target the angiogenic pathway may be a potential solution for anti-angiogenic therapies. Malignant tumors including ovarian cancer (OC), non-small cell lung cancer (NSCLC), and hepatocellular carcinoma (HCC) are known to have tumor vascularization that is connected to over-stimulation of platelet-derived growth factor (PDGF) signaling, either alone or in conjunction with VEGFA (Levitzki, 2004). In AE patients, our previous study has demonstrated that the expression of PDGF-BB and platelet derived growth factor receptor beta (PDGFR-β) was significantly higher in the close liver tissue (CLT) compared to distant liver tissue (DLT) (Ke et al., 2022). In addition, serum PDGF-BB levels were significantly lower in patients with AE, especially in patients with high-activity lesions, compared with healthy subjects. This finding suggests that serum PDGF-BB levels may serve as a straightforward, non-invasive, and expeditious biomarker for evaluating the metabolic activity of lesions in AE patients (Ke et al., 2022). However, the underlying mechanisms of altered PDGF signaling expression in AE remain elusive.

In this study, we analyzed the role of PDGF signaling-mediated angiogenesis in *E. multilocularis* infected mice. We confirmed that pathological angiogenesis surrounding the lesion was observed at 10–12 weeks post-infection in *E. multilocularis* infected mice. Mechanistically, we found that *E. multilocularis* protoscoleces protein (EmP) induces angiogenesis through PDGFR/phosphatidylinositol 3-kinase (PI3K)/AKT Serine/Threonine Kinase (AKT)/Focal Adhesion Kinase (FAK)

Abbreviations: AE, Alveolar echinococcosis; AKT, AKT Serine/Threonine Kinase; AOD, Average Optical Density; α-SMA, α-smooth muscle actin; CL, Close liver tissue; DLT, Distant liver tissue; *E. multilocularis*, *Echinococcus multilocularis*; EmP, *E. multilocularis* protoscoleces protein; FAK, Focal Adhesion Kinase; H&E, Hematoxylin & eosin; HUVECs, Human umbilical vein endothelial cells; IHC, Immunohistochemistry; PAS, Periodic Acid-Schiff; PCNA, Proliferating cell nuclear antigen; PDGF, Platelet-derived growth factor; PDGFR-β, Platelet derived growth factor receptor beta; PI3K, Phosphatidylinositol 3-kinase; PSCs, Protoscoleces; qRT-PCR, Quantitative real-time PCR; *S. mansoni*, *Schistosoma mansoni*; *T. spiralis*, *Trichinella spiralis*; VEGF, Vascular endothelial growth factor.

signaling pathway similar to PDGF-BB *in vitro*. Our study elucidated the underlying mechanism of pathological angiogenesis in AE, which is mediated by PDGF signaling. This finding lays a fundamental basis for the potential implementation of anti-angiogenic therapeutic approaches in the treatment of AE.

2 Materials and methods

2.1 Establishment of *E. multilocularis* infection models

Thirty female C57BL/6 mice (weighing about 18–20 g, Beijing Vital River Laboratory Animal Technology Co. Ltd, Beijing, China) were randomly assigned to five groups of five animals each: a sham-operated group (Sham group) and four groups representing different time points post-infection with *E. multilocularis* (2 weeks, 4 weeks, 10 weeks, and 12 weeks groups). Mice in *E. multilocularis* infection groups were inoculated with protoscoleces suspended in normal saline (3,000 PSCs/mouse in 200 μl normal saline) via the hepatic portal vein, as previously described (Yang et al., 2022), while mice in the sham operation group were injected with equivalent amount of normal saline. Briefly, protoscoleces were obtained from intraperitoneal lesions maintained in Mongolian gerbils, washed several times using PBS, counted under a microscope, and adjusted to the appropriate concentrations before injection. Mice were kept pathogen-free at 20–24 °C under a 12 h light/dark cycle. Before the experiment, mice had free access to a regular diet and water for 1 week. At the end of the infection period, mice were anesthetized with 4% isoflurane and maintained with 1% isoflurane (RWD, Shenzhen, Cat# 20072102). Before collecting the mouse samples, we euthanized the mice using an overdose of anesthetic. The animal experiments were approved by the Institutional regulations of Ethical Committee of the First Affiliated Hospital of Xinjiang Medical University (No. K202110-18). The study was carried out in compliance with ARRLVE guidelines.

2.2 Histopathological and immunohistochemical analyses

Liver samples were harvested from mice and divided into two parts, one part was processed for histopathological assessment while the other part was promptly cryopreserved in liquid nitrogen for RNA extraction. For histopathological analyses, samples were fixed in 4% paraformaldehyde for 48 h and embedded in paraffin. Hematoxylin & eosin (H&E), Periodic Acid-Schiff (PAS) and immunohistochemistry (IHC) staining were performed on serial sections (4 μm thick). In addition, liver fibrosis in mice was assessed using Sirius red staining as previously described (Yang et al., 2022). The H&E, PAS, Sirius red and IHC stained sections were imaged by light microscopy (BX43, Olympus, Japan), the result of Sirius red and IHC staining were quantitatively analyzed using the Image-Pro Plus software (Version 6.0.0.260, Media Cybernetics, USA). Differences in protein expression or fibrosis levels in each group were determined using the Average Optical Density (AOD = integrated optical density/area) of positive reactions. Three to five fields per section were randomly selected and analyzed at highpowerfield (400× magnification). Antibodies used for immunohistochemical staining are presented in Supplementary Table S1.

2.3 Quantitative real-time PCR (qRT-PCR) analysis

Total RNA was extracted from liver tissues preserved in liquid nitrogen sing the TRIzol reagent (Invitrogen). Purified total RNA was quantified using Nanodrop ND2000 (NanoDrop Technologies, Wilmington, DE, USA) and reverse-transcribed using a PrimeScript RT reagent Kit (RR047A, Takara, Japan). Then, 2 μl of cDNA was mixed with 18 μl of Master Mix (miScript SYBR Green PCR Kit, 218073, Germany, Qiagen) after which RT-PCR was performed using the CFX96 Touch System (BioRad, Hercules, CA, USA). The 2−ΔΔCt method was used to calculate relative mRNA expressions which were normalized to the housekeeping gene *GAPDH* (human) or *ACTB* (mouse) (Yang et al., 2022). The primer sequences used for qRT-PCR are presented in Supplementary Table S2.

2.4 Cell culturing

In order to clarify whether the *E. multilocularis* has an angiogenesis-inducing effect *in vitro*, the human umbilical vein endothelial cells (HUVECs) cell line was purchased from the Cellverse Co., Ltd. (iCell-h110, Shanghai, China), and utilized this cell line for our *in vitro* experimentation. Cells were cultured in RPMI-1640 supplemented with 10% FBS and 1% Penicillin-Streptomycin (Gibco). The cells were grown in a humidified incubator at 37 °C with 5% CO_2. The culture medium was refreshed every day.

2.5 *E. multilocularis* PSC protein (EmP) preparation and inhibitors intervention

EmP refers to the crude extract of proteins derived from *Echinococcus multilocularis* protoscoleces. For protein preparation, *E. multilocularis* PSC were collected from intraperitoneal lesions maintained in BALB/c mice. PSC were ruptured by sonication (30 s pulses of 30% power with 10 s intervals in triplicate). The lysates were left overnight on a rocker at 4 °C and centrifuged at 12,000 × g for 15 min at 4 °C. The supernatant was sterilely filtered (0.45 μm) and protein concentration was quantified using the BCA Protein Assay Kit (Thermo Fisher Scientific, USA). For *in vitro* experiments, EmP (5μg/ml) or recombinant human PDGF-BB (Peprotech, 50 ng/ml) were added into medium in the lower well of the transwell chambers. PDGFR-β inhibitor AG1296, PI3K inhibitor LY294002, Akt inhibitor MK2206, and FAK inhibitor Y15 were used under the standard protocols (Selleckchem, Germany). For *in vitro* experiments, HUVECs were pretreated with PDGFR-β

inhibitor AG1296 (10 μM), PI3K inhibitor LY294002 (10 μM), Akt inhibitor MK2206 (10 μM) and FAK inhibitor Y15 (10 μM) were added into medium for 1 h, respectively. After inhibitor treatment, the cells were seeded in the upper well of the transwell chambers (three replicates per group).

2.6 Cell viability assay

HUVECs were seeded in 24 well plates (2×10^4/well) and evaluated at 1–4 days after seeding. CCK8 solution (10 μl, Dojindo, Japan) was added to the medium per well according to the manufacturer's instructions and incubated with the cells for 3 h at 37 °C and 5% CO_2. After incubation, the absorbance of the solution was measured at a wavelength of 450 nm (Multiskan MK3, Thermo, USA).

2.7 Transwell migration and tube formation assay

Transwell migration assay was performed in 96-well Transwell plates (Corning) with 8-μm pore filters. HUVECs were seeded in the upper chambers (2×10^4/well) and then incubated with or without EmP or PDGF-BB in the lower chambers for 3 h. At the end of incubation, HUVECs were fixed with 10% formaldehyde and stained with crystal violet (Sigma-Aldrich) for 15 min sequentially. After gently washing three times by PBS for 5 min each time, cells that migrated through the membrane to the lower chambers were counted by light microscopy (BX43, Olympus, Japan) at 200× magnification. Tube formation assay was performed in 96-well Transwell plates (Matrigel was polymerized 45 min at 37 °C). HUVECs were seeded in the upper chambers (2×10^4/well) and then incubated with or without EmP or PDGF-BB in the lower chambers for 3 h. After incubation at 37 °C, pseudocapillary formation was pseudocapillary formation was imaged by light microscopy (BX43, Olympus, Japan). The parameters of pseudocapillary formation by HUVECs were measured by ImageJ with the Angiogenesis Analyzer plugin. The cumulative pseudocapillary length, the numbers of mesh and major junction were quantified in this study (Guan et al., 2020).

2.8 Statistical analysis

Statistical analyses were performed using the SPSS statistical software package version 20.0 (SPSS, Inc, Chicago, IL, USA) and GraphPad Prism (version 7.0d for MacOS X, USA, GraphPad Software, San Diego, California, USA). Significance was determined with the two-tailed Student's *t*-test for comparison of two groups. Significance between multiple groups was determined by one-way ANOVA followed by Tukey's *post hoc* test. $^*P < 0.05$ was the threshold for significance. Error bars represent ± standard error of the mean (SEM).

3 Results

3.1 Increased expression of PDGF-BB/PDGFR-β and angiogenesis around liver lesions in *Echinococcosis multilocularis* infected mice

In our prior investigation, it was observed that the mRNA and protein expression levels of PDGF-BB and PDGFR-β exhibited a noteworthy increase in the close to the lesion (CLT) group when compared to the distal to the lesion (DLT) group among AE patients (Ke et al., 2022). The PDGF family is composed of polypeptide homodimers of PDGF-A, B, C, and D, as well as the heterodimer PDGF-AB. These ligands bind to PDGFR and tyrosine kinase receptors, triggering pathways that exhibit similarities or identical characteristics to those induced by VEGF. Activation of PDGF signaling is associated with growth, survival and angiogenesis of various cells (Su et al., 2020). Therefore, we hypothesized that PDGF-BB is involved in hepatic angiogenesis in alveolar echinococcosis and proceeded to conduct an investigation on this matter.

The *E. multilocularis* infection mouse model was established to investigate the mechanism of angiogenesis in alveolar echinococcosis. Animals were sacrificed at 2-, 4-, 10- and 12-weeks post-infection, respectively. With the prolongation of infection, the lesion volume gradually increased and normal liver tissue is constantly being eroded (Supplementary Figure S1A). PAS staining showed the laminated layer of the metacestode (Supplementary Figure S1B). The results of Sirius red staining and α-SMA immunohistochemical staining demonstrated a progressive increase in the extent of fibrosis as the duration of infection prolonged. Additionally, significant destruction of the hepatic architecture was observed, particularly during the later stages of infection (10 to 12 weeks) (Supplementary Figures S1C–F).

To clarify whether angiogenesis was present in the livers of *E. multilocularis* infected mice, we examined the expression of angiogenesis-related genes in the liver. A notable augmentation in angiogenesis surrounding the lesion was observed at 10–12 weeks post-infection, as evidenced by immunohistochemical staining of CD31, in contrast to the sham operation group. In addition, the angiogenesis observed at 2–4 weeks post-infection was also increased in comparison to the sham operation group, but there was no statistical significance (Figures 1A, B). Furthermore, the result of qRT-PCR analysis and immunohistochemical staining showed that the expression of PDGF-BB and PDGFR-β were significantly elevated at 10–12 weeks post-infection (Figures 1C–F). qRT-PCR analysis also showed that the angiogenesis-related genes, Angpt1 (Ezaki et al., 2024), Id1 (Guo et al., 2023), and Lyve1 (Lu et al., 2023), were significantly upregulated at 10 weeks post-infection, and Pecam1 (Zhang et al., 2024) was significantly upregulated at 10–12 weeks post-infection. As an antagonistic gene of *Angpt1*, the mRNA level of Angpt2 (Ezaki et al., 2024) was significantly down-regulated at 10–12 weeks post-infection, indicating elevated angiogenesis (Figures 1G–K).

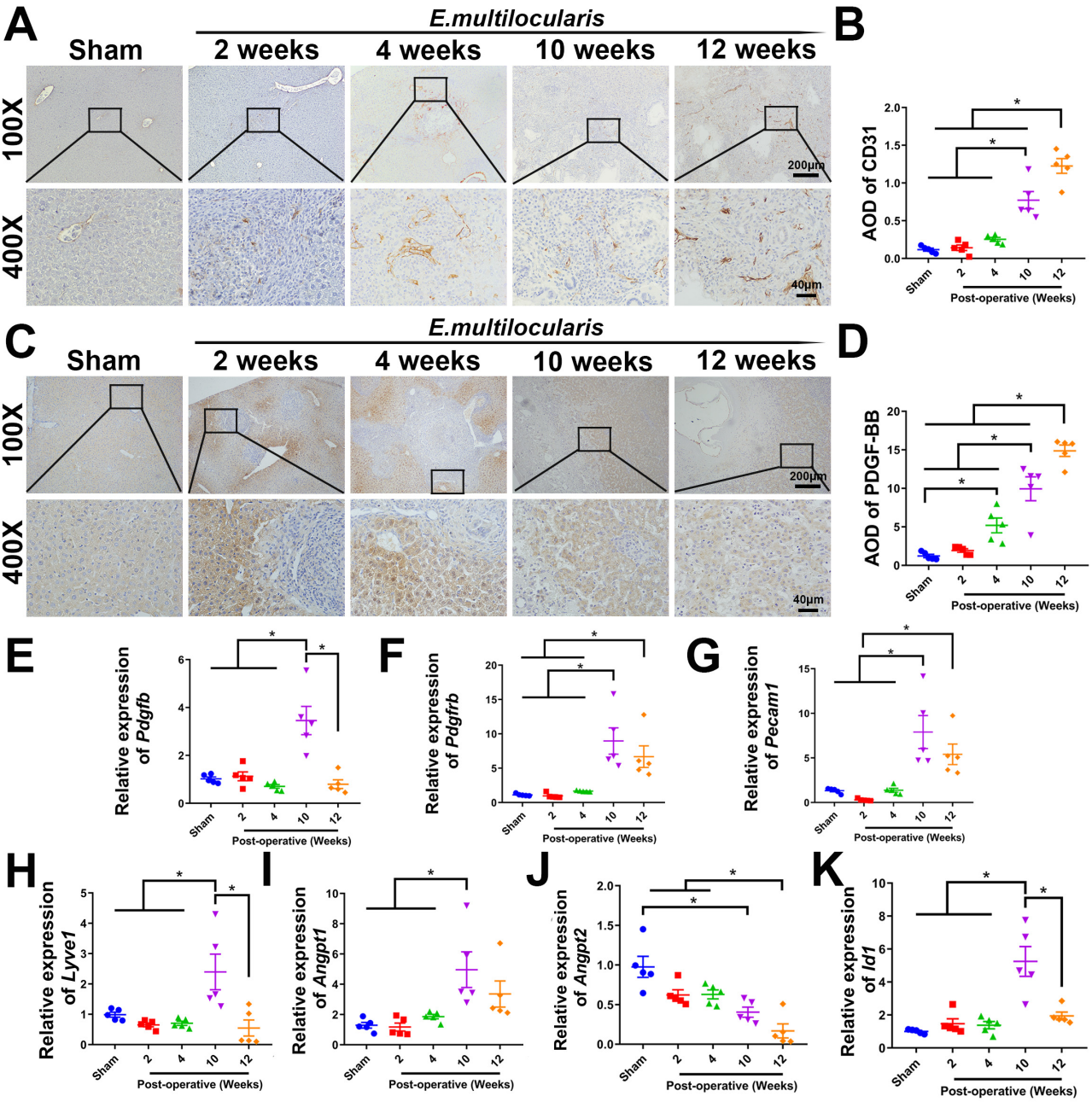

FIGURE 1
Increased hepatic angiogenesis in *E. multilocularis* infected mice. **(A, B)** Immunohistochemical staining of CD31. **(C, D)** Immunohistochemical staining of PDGF-BB. Quantitative real-time PCR detection of *Pdgfb*. **(E, F)** Quantitative real-time PCR detection of *Pdgfb* and *Pdgfrb*. **(G–K)** Quantitative real-time PCR detection of *Pecam1*, *Lyve1*, *Angpt1*, *Angpt2*, and *Id1* genes expression. All data are presented as mean ± SEM. $^*P < 0.05$, $n = 5$.

3.2 EmP exhibits a PDGF-like pro-angiogenic function *in vitro*

The results of CCK-8 assay showed that the proliferative ability of HUVECs was significantly enhanced after treatment with PDGF-BB or EmP, where PDGF-BB showed dose-dependent within a certain range. Specifically, the proliferation of HUVECs was significantly increased when treated with EmP at 5 μg/ml or PDGF-BB at 50 ng/ml (Figures 2A, B). In addition, the expression of proliferating cell nuclear antigen (PCNA) also demonstrated that stimulation with 5 μg/ml EmP for 24 h significantly promoted the proliferation of HUVECs (Figure 2C). Interestingly, we found that EmP at 5 μg/ml can promote the expression of PDGFR-β in HUVECs cells like PDGF-BB, which may partly explain the pro-angiogenic function of EmP (Figure 2D).

To further evaluate the angiogenic effects of EmP on HUVECs, we conducted the migration assay and tube formation assay. The migration assay displayed that the migratory ability of the

10.3389/fmicb.2025.1686956

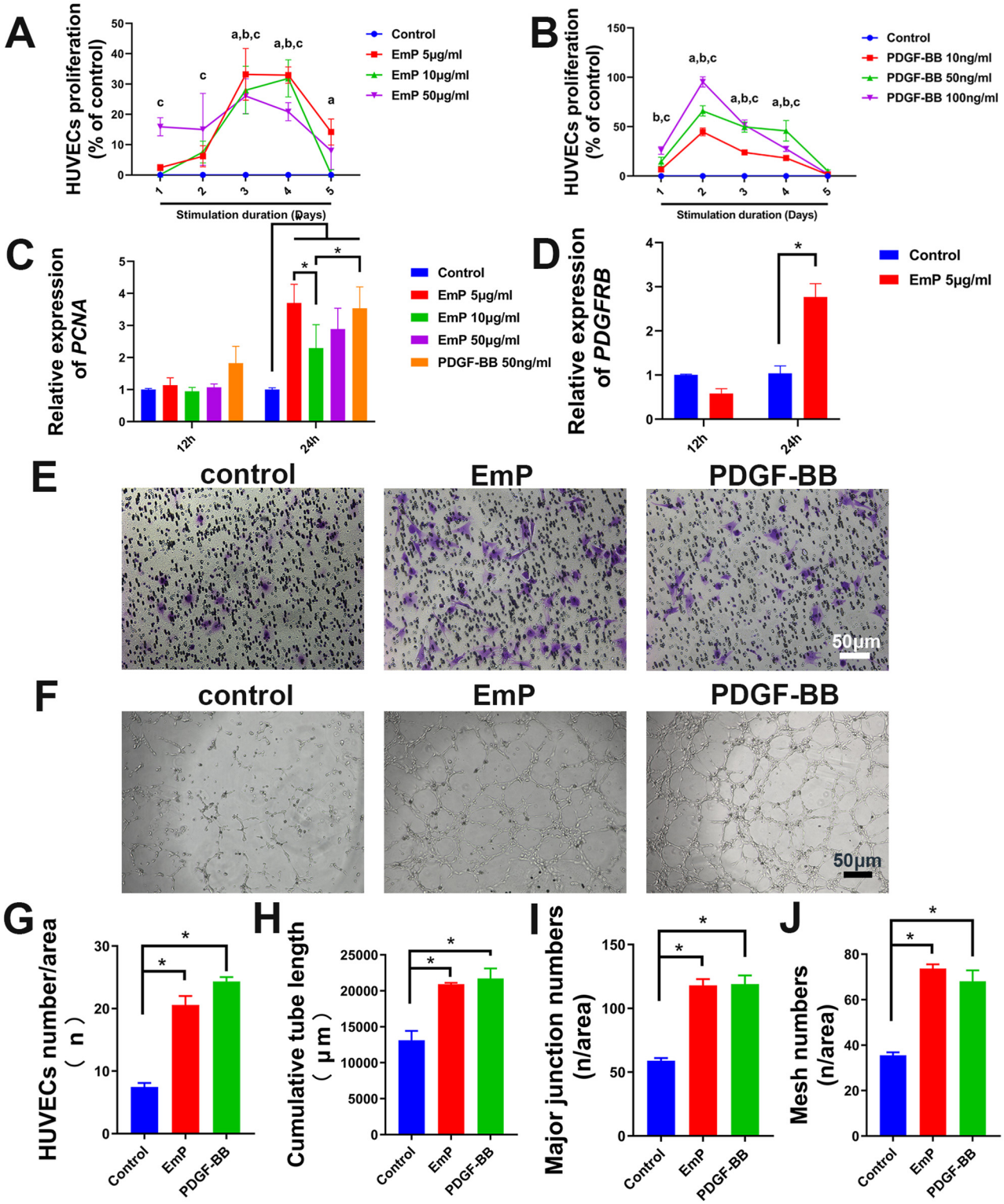

FIGURE 2
EmP significantly enhances the pseudocapillary formation ability of HUVECs in vitro. **(A)** Effect of EmP on the proliferation of HUVECs detected by CCK8 assay. $^{a}P < 0.05$, Emp 5 ug/ml compared with Control, $^{b}P < 0.05$, Emp 10 ug/ml compared with Control, $^{c}P < 0.05$, Emp 15 ug/ml compared with Control. **(B)** Effect of PDGF-BB on the proliferation of HUVECs detected by CCK8 assay. $^{a}P < 0.05$, PDGF-BB 10 ng/ml compared with Control, $^{b}P < 0.05$, PDGF-BB 50 ng/ml compared with Control, $^{c}P < 0.05$, PDGF-BB 100 ng/ml compared with Control. **(C)** Quantitative real-time PCR detection of PCNA after EmP and PDGF-BB stimulation. **(D)** Quantitative real-time PCR detection of PDGFRB after 679 EmP stimulation. **(E)** Representative images of transwell migration assay. **(F)** Representative images of pseudocapillary formation assay. **(G)** HUVECs counting results of transwell migration assay. **(H)** Counting results of the cumulative pseudocapillary length in HUVECs cells. **(I)** Counting results of the major junction numbers in HUVECs cells. **(J)** Counting results of the mesh numbers in HUVECs cells. Experiments were repeated three times and all data are presented as mean ± SEM. $^{*}P < 0.05$. n = counts.

HUVECs in the both PDGF-BB-treatment or EmP treatment groups were significantly enhanced compared with the control group (Figures 2E, F). The tube formation assay showed that the EmP, functions similar to PDGF-BB, significantly increased the cumulative tube length, major junction numbers and mesh numbers in HUVECs cells, indicating that EmP can significantly enhanced the tube formation ability of HUVECs *in vitro* (Figures 2G–J).

3.3 EmP induces angiogenesis through PDGFR/PI3K/AKT/FAK signaling pathway similar to PDGF-BB

To further investigate the mechanism by which EmP promotes angiogenesis, we cultured HUVECs with or without EmP and examined PI3K signaling pathways, which known to play an important role in cell migration, cell growth, and invasion (Glaviano et al., 2023). We intervened the phosphorylation of PDGFR-β and other downstream kinases on HUVECs using inhibitors, and the results showed that independent inhibition of each component of PDGFR signaling pathway, was sufficient to block EmP or PDGF-BB induced HUVECs migration and pseudocapillary formation (Figures 3A–D). In addition, administration of inhibitors alone did not significantly affect the migration and pseudocapillary formation of HUVECs and there were no statistical differences between groups (Figures 4A–E). Taken together, the results suggest that EmP induced angiogenesis is dependent on the PDGFR/PI3K/AKT/FAK signaling pathway similar to PDGF-BB (Figure 5).

4 Discussion

Accumulating evidence indicates that parasites can increase survival within host by regulating host's angiogenesis. In *Schistosoma mansoni* (*S. mansoni*), the angiogenesis is induced by inflammation or released ovular antigens, which promote the activation and proliferation of endothelial cells (Francisco et al., 2022). Specifically, in *S. mansoni* infected mice, serum VEGF levels and the expression of Heme oxygenase-1 were progressively increased, which may serve as new indicators of progression of *S. mansoni* associated angiogenesis (Huwait et al., 2021). Bevacizumab has a promising protective effect against the *Schistosoma* induced angiogenesis. A regression in the vascular activity and microvascular density was observed in the infected mice following the administration of bevacizumab (Hasby Saad and El-Anwar, 2020). Furthermore, Paeoniflorin, an herbal extract derived from paeony, exhibits anti-angiogenic effects and also significantly reduces the mean egg count/gram stool, worm burden and egg count/gram liver tissue in *S. mansoni* infected mice (Abd El-Aal and Abdelbary, 2019). In trichinellosis, the *Trichinella spiralis* (*T. spiralis*) is capable of inducing angiogenesis and attracting highly permeable blood vessels to the surface of its collagenous capsule. This process facilitates the acquisition of nutrients and disposal of waste, thereby sustaining a prolonged host-parasite association (Rayia et al., 2022). Treatment with bevacizumab exhibited anti-angiogenic activities during the muscular phase of infection through down-regulating the expression of VEGF and CD31 (Rayia et al., 2022; Fadil et al., 2022). Similarity, zinc oxide nanoparticles decrease adult counts in the intestine and larval deposition in muscle through suppress the expression of VEGF induced by *T. spiralis* (Ashoush and Soliman, 2023). Unexceptionally, therapeutic strategies based on anti-angiogenesis strategies have also been applied to a variety of parasitic diseases such as chagas disease (Vellasco et al., 2022), malaria (Park et al., 2019), heartworm disease (Zueva et al., 2020; Machado et al., 2023), and neurocysticercosis (Carmen-Orozco et al., 2019), etc. Based on the aforementioned information, we pose the following scientific questions: Does echinococcosis exhibit similarities on angiogenesis to the aforementioned parasitic diseases? Can anti-angiogenesis strategies be equally applicable in the treatment of echinococcosis?

With the development of bioinformatics, multi-omics technology has been gradually applied in the study of echinococcosis. Consistent with our study, it has been demonstrated that the invasive growth of *E. multilocularis* is accompanied by notable angiogenesis and the expression of CD31 (Qing et al., 2019). Besides, through transcriptomic analysis, Yimingjiang et al. (2023) similarly found that angiogenesis-related genes *ADAM12, APLN, TWIST1, SPP1, RSPO3*, and *FOXC2* were elevated in the CLT group. The proteomic analysis revealed exosomes derived from *E. multilocularis* protoscoleces can be involved in focal adhesion and potentially promote angiogenesis. Increased angiogenesis was observed and the expression of several angiogenesis-regulated molecules, including VEGF, MMP9, MCP-1, SDF-1, and serpin E1 were increased in livers of *E. multilocularis* infected mice (Liu et al., 2023). These results suggest that angiogenesis is a possible mechanism underlying the tumor-like biological behavior observed during *E multilocularis* infection. Clinically, CT perfusion imaging with microvessels density reflected different situation of angiogenesis around lesions, indicating the presence of blood perfusion at the periphery of the lesion (Wang et al., 2011). All of the above studies suggest that anti-angiogenic therapeutic strategies are also promising in the treatment of AE. However, further validation of angiogenesis-regulated genes expression in the liver of AE patients is needed to clarify the reliability of therapeutic targets.

In many pathological conditions, developmental angiogenic processes are recapitulated, including but not limited to atherosclerosis, arthritis, psoriasis, endometriosis, and obesity, especially in various tumors. Thus, pathological angiogenesis presents new challenges yet new opportunities for the design of vascular-directed therapies (Dudley and Griffioen, 2023). Currently, the majority of approved agents for anti-angiogenic treatment primarily focus on the modulation of VEGF effects. Bevacizumab, the first VEGF-targeted agent approved by the Food and Drug Administration for cancer treatment, has been made accessible for cancer therapy (Kopetz et al., 2010). In *E. multilocularis* infection, elevated expression of VEGFA and VEGFR2 in the liver may mediate angiogenesis in *Echinococcus multilocularis* infection (Jiang et al., 2020). Furthermore, the administration of SU11248 markedly reduced neovascular formation and substantially inhibited *E. multilocularis* metacestode growth in mice. Moreover, SU11248 treatment also reduced the expression of VEGFA, VEGFR2, and p-VEGFR2 significantly

10.3389/fmicb.2025.1686956

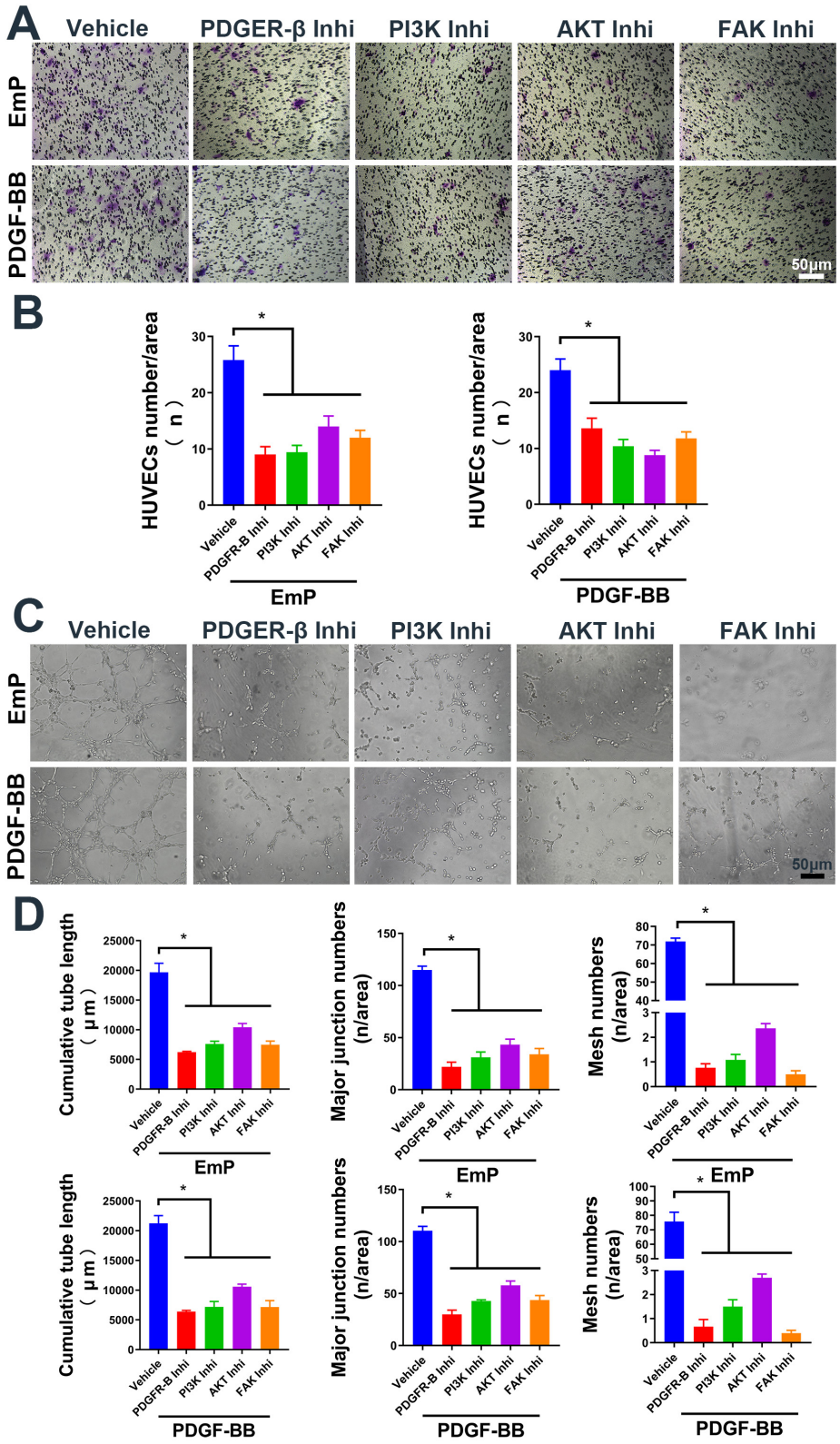

FIGURE 3
EmP promote HUVECs migration and pseudocapillary formation through PDGFR/PI3K/AKT/FAK pathway. **(A)** Representative images of transwell migration assay in HUVECs with inhibitor intervention. **(B)** HUVECs counting results of transwell migration assay with inhibitor intervention. **(C)** Representative images of pseudocapillary formation assay in HUVECs with inhibitor intervention. **(D)** Counting results of the cumulative pseudocapillary length, major junction numbers and mesh numbers in HUVECs with inhibitor intervention and co-treatment with EmP or PDGF-BB. Experiments were repeated three times and all data are presented as mean ± SEM. *$P < 0.05$. Inhi, inhibitor.

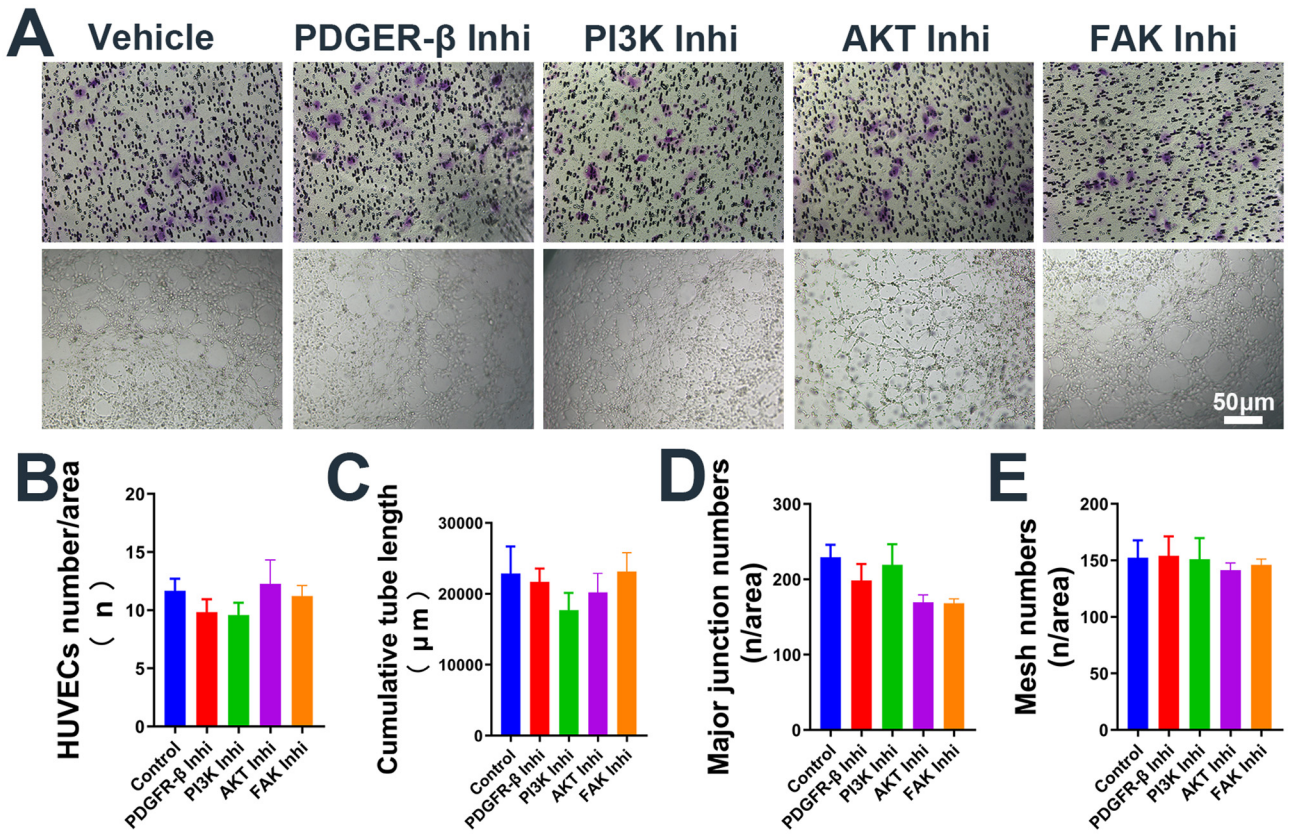

FIGURE 4
Administration of inhibitors alone the use of inhibitors alone does not affect the migration and pseudocapillary formation of HUVECs. **(A)** Representative images of transwell migration assay (Top) and pseudocapillary formation assay (Bottom) in HUVECs with inhibitor alone. **(B)** HUVECs counting results of transwell migration assay with inhibitor alone. **(C)** Counting results of the cumulative pseudocapillary length in HUVECs with inhibitor alone. **(D)** Counting results of the major junction numbers in HUVECs with inhibitor alone. **(E)** Counting results of the mesh numbers in HUVECs with inhibitor alone. Experiments were repeated three times and all data are presented as mean ± SEM. Inhi, inhibitor. n = counts.

(Jiang et al., 2023). However, compensatory mechanisms of other angiogenic mediators may be account for the resistance observed in patients when the VEGF signaling pathway is blocked. Therefore, targeting multiple effectors of angiogenic pathways simultaneously could potentially be an effective approach for anti-angiogenic therapies (Lopes-Coelho et al., 2021).

In addition to VEGF, PDGF-BB is a chemotactic and mitogenic factor within the PDGF family, which plays a crucial role in facilitating the migration, proliferation, and differentiation of diverse mesenchymal cell populations, including endothelial progenitor cells and mesenchymal stem cells, thereby promoting the processes of angiogenesis and osteogenesis (Andrae et al., 2008; Peng et al., 2020). PDGFs and their corresponding receptors, PDGFRα and PDGFRβ, exhibit expression in a diverse range of malignant tumors, such as non-small cell lung cancer (NSCLC), gastrointestinal stromal tumor (GIST), pancreatic cancer, breast cancer, ovarian carcinoma and hepatocellular carcinoma (Pandey et al., 2023). The findings obtained from employing various antibodies and inhibitors, including MOR8457 (Kuai et al., 2015), 1-NaPP1 (Tsioumpekou et al., 2020), CP-673451 (Yang et al., 2018), among others (Zou et al., 2022), indicate that targeting the PDGF/PDGFR signaling pathway represents a promising strategy for the treatment of cancer via regulating blood vessel regeneration. During osteoarthritis development, it was observed that the expression of PDGFR-β, primarily in the $CD31^{hi}Emcn^{hi}$ endothelium, was significantly increased in subchondral bones obtained from patients with osteoarthritis as well as in rodent models. PDGFR-β deletion specifically in endothelial cells reduced the number of H-type vessels, improvement in subchondral bone degradation, and mitigation of cartilage degeneration (Cui et al., 2022). Furthermore, PDGFR-β was increased in methionine-choline-deficient and high-fat (MCDHF)-induced liver injury in mice with a positive correlation to fibrosis and angiogenesis-related genes. The inhibition of liver fibrogenesis and angiogenesis is achieved by miR-26b-5p through its direct targeting of PDGFR-β, which may represent an effective therapeutic strategy for liver fibrosis (Yang et al., 2019). Our previous study also confirmed that the mRNA and protein expression levels of PDGF-BB and PDGFR-β exhibited a noteworthy increase in the CLT group when compared to the DLT group in AE patients (Ke et al., 2022). In this study, we further demonstrated that the expression of both PDGF-BB and PDGFR-β were significantly upregulated in *E. multilocularis* infected mice. The use of PDGFR-β inhibitor can block the pro-angiogenesis effect of EmP and PDGF-BB in HUVECs. These results suggest that PDGF-BB/PDGFR signaling are involved in the host's pathological angiogenesis, and blocking

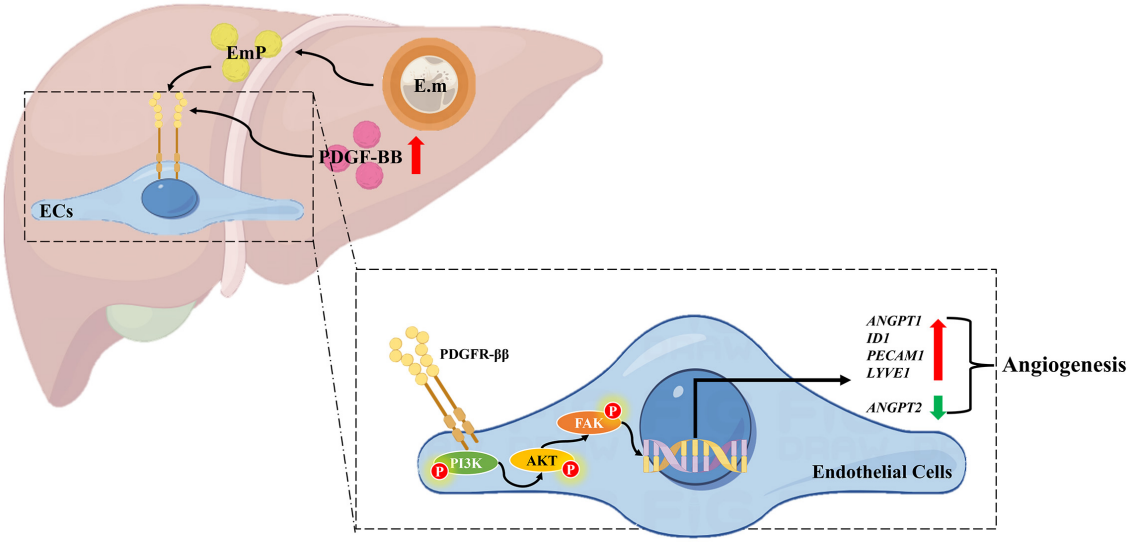

FIGURE 5
Schematic diagram of pro-angiogenesis mechanism in *Echinococcus multilocularis* infection. On the one hand, *Echinococcus multilocularis* infection directly upregulates PDGF-BB expression in the host liver, thereby stimulating angiogenesis through the activation of the PDGFR/PI3K/AKT/FAK signaling pathway. On the other hand, the secretion of EmP also contributes to angiogenesis by acting on the PDGFR/PI3K/AKT/FAK signaling pathway. The pathological angiogenesis in the peri-lesion area provides nutrients for the growth and development of the parasite, thus facilitating parasitism. E.m, *E. multilocularis* infection; EmP, *E. multilocularis* protoscoleces protein.

this signaling is expected to be a new approach for the treatment of AE.

The activation of the PDGF/PDGFR signaling pathway has been observed to be associated with angiogenesis through the regulation of multiple downstream pathways, such as PI3K/AKT pathway and Notch pathway (Zou et al., 2022). The activation of PI3K/AKT pathway plays a pivotal role in enhancing tumor angiogenesis, as evidenced by the numerous anti-vascular regeneration drugs that have been developed to specifically target this signaling pathway (Liu et al., 2019). Studies have demonstrated a significant positive correlation between the expression level of PI3K/AKT pathway and the formation of endothelial cell proliferation and survival in angiogenic experiments conducted using roxarsone (Zhu et al., 2013; Wang et al., 2016). In addition, in ischemic stroke rats, catalpol treatment significantly increased the expression of VEGF through up-regulating PI3K/AKT signaling and subsequently increasing FAK and Paxillin (Wang et al., 2022). Here, we provide evidence that EmP or PDGF-BB can induce phosphorylation of PI3K/AKT through up-regulating PDGFR-β, subsequently facilitating cell migration and pseudocapillary formation in HUVECs. The administration of PI3K/AKT inhibitors effectively impeded this process. FAK, a non-receptor protein tyrosine kinase, has been observed to be overexpressed in various types of cancer cells and peripheral vascular cells of solid tumors (Shiau et al., 2021; Arora et al., 2022). Previous studies have indicated that FAK plays a role in regulating tumor angiogenesis (Shiau et al., 2021; Zhang et al., 2023; Cai et al., 2019). In this study, the application of FAK inhibitors has been observed to impede the pro-angiogenesis impact of EmP and PDGF-BB, while having no discernible impact on the activation status of the PI3K/AKT pathway. This suggests that FAK, as a downstream element of the PI3K/AKT pathway, plays a role in promoting angiogenic activity. Taken together, these results suggest that blocking the PI3K/AKT/FAK pathway has the potential to inhibit angiogenesis and may be an effective treatment for AE patients.

However, many questions remain unanswered. Firstly, the angiogenesis-related genes, which were upregulated in *E. multilocularis* infected mice needs to be further verified in AE patients. Our previous study only demonstrated that PDGF-BB and PDGFR-β were highly expressed in the CLT group of AE patients, and validation of other angiogenesis-related genes will be our next move. Secondly, we found in this study that EmP has a pro-angiogenesis regenerative effect and mechanism similar to that of PDGF-BB, whether it is because *E. multilocularis* itself secretes PDGF-BB-like protein. This has not been clearly demonstrated by existing studies and needs to be confirmed by further studies on *E. multilocularis* secretome (Huang et al., 2017; Wang et al., 2015; Ahn et al., 2015, 2017). Thirdly, in the present study we performed a series of signaling pathway blockades on HUVECs *in vitro*, and preliminarily demonstrated that blocking the PDGFR/PI3K/AKT/FAK pathways could inhibit pathological angiogenesis. However, whether blockade of this pathway is equally effective *in vivo* is still unknown and needs to be confirmed by further studies.

5 Conclusion

In conclusion, our study confirms that the increased expression of PDGF-BB and PDGFR-β in *E. multilocularis* infected mice is associated with peri-lesion pathological angiogenesis. EmP has the capability to stimulate angiogenesis through the PDGFR/PI3K/AKT/FAK signaling pathway *in vitro*. The results of our study indicate that inhibiting PDGF signaling could potentially

serve as an effective anti-angiogenic therapeutic strategy for the treatment of AE patients.

Data availability statement

The original contributions presented in the study are included in the article/Supplementary material, further inquiries can be directed to the corresponding authors.

Ethics statement

The animal study was approved by Ethical Committee of the First Affiliated Hospital of Xinjiang Medical University. The study was conducted in accordance with the local legislation and institutional requirements.

Author contributions

XB: Conceptualization, Project administration, Methodology, Writing – original draft, Funding acquisition, Resources, Formal analysis. NY: Methodology, Data curation, Writing – original draft, Formal analysis. YK: Methodology, Formal analysis, Writing – original draft, Data curation. JX: Methodology, Data curation, Writing – original draft. XZ: Methodology, Data curation, Writing – original draft. HL: Writing – original draft, Methodology, Data curation. JC: Data curation, Writing – original draft. LL: Writing – original draft, Data curation. YS: Resources, Investigation, Writing – review & editing. GL: Data curation, Project administration, Conceptualization, Resources, Writing – review & editing, Supervision, Funding acquisition, Formal analysis. TA: Writing – review & editing, Investigation, Resources. RL: Investigation, Supervision, Funding acquisition, Conceptualization, Formal analysis, Writing – review & editing, Project administration, Writing – original draft.

Funding

The author(s) declare that financial support was received for the research and/or publication of this article. This work was supported by National Natural Science Foundation of China (82060371 for RL, 82060373 and 82273977 for GL, 32060223 for XB), Xinjiang Tianshan Project (2022TSYCLJ0032 for RL, 2022TSYCCX0111 for GL), Key Program of Xinjiang Natural Science Foundation (2022D01D59 for RL), and Xinjiang Natural Science Foundation for Distinguished Young Scholars (2022D01E66 for GL, 2022D01E67 for XB). The funders had no role in study design, data collection and analysis, decision to publish, or preparation of the manuscript.

Conflict of interest

The authors declare that the research was conducted in the absence of any commercial or financial relationships that could be construed as a potential conflict of interest.

Generative AI statement

The author(s) declare that no Gen AI was used in the creation of this manuscript.

Any alternative text (alt text) provided alongside figures in this article has been generated by Frontiers with the support of artificial intelligence and reasonable efforts have been made to ensure accuracy, including review by the authors wherever possible. If you identify any issues, please contact us.

Publisher's note

Supplementary material

The Supplementary Material for this article can be found online at: https://www.frontiersin.org/articles/10.3389/fmicb.2025.1686956/full#supplementary-material

References

Abd El-Aal, N. F., and Abdelbary, E. H. (2019). Paeoniflorin in experimental BALB/c mansoniasis: a novel anti-angiogenic therapy. *Exp. Parasitol.* 197, 85–92. doi: 10.1016/j.exppara.2018.11.002

Ahn, C. S., Han, X., Bae, Y. A., Ma, X., Kim, J. T., Cai, H., et al. (2015). Alteration of immunoproteome profile of *Echinococcus granulosus* hydatid fluid with progression of cystic echinococcosis. *Parasit Vectors* 8:10. doi: 10.1186/s13071-014-0610-7

Ahn, C. S., Kim, J. G., Han, X., Kang, I., and Kong, Y. (2017). Comparison of *Echinococcus multilocularis* and *Echinococcus granulosus* hydatid fluid proteome provides molecular strategies for specialized host-parasite interactions. *Oncotarget* 8, 97009–97024. doi: 10.18632/oncotarget.20761

Andrade, Z. A., and Santana, T. S. (2010). Angiogenesis and schistosomiasis. *Mem. Inst. Oswaldo Cruz.* 105, 436–439. doi: 10.1590/S0074-02762010000400013

Andrae, J., Gallini, R., and Betsholtz, C. (2008). Role of platelet-derived growth factors in physiology and medicine. *Genes Dev.* 22, 1276–1312. doi: 10.1101/gad.1653708

Arora, A., Kivelä, A. M., Wang, L., Minkeviciene, R., Taskinen, J. H., Zhang, B., et al. (2022). Protrudin regulates FAK activation endothelial cell migration and angiogenesis. *Cell Mol. Life Sci.* 79:220. doi: 10.1007/s00018-022-04251-z

Ashoush, S. E., and Soliman, E. K. (2023). Antihelminthic and antiangiogenic effects of zinc oxide nanoparticles on intestinal and muscular phases of trichinellosis. *J. Helminthol.* 97:e56. doi: 10.1017/S0022149X23000421

Bocca, C., Novo, E., Miglietta, A., and Parola, M. (2015). Angiogenesis and fibrogenesis in chronic liver diseases. *Cell. Mol. Gastroenterol. Hepatol.* 1, 477–488. doi: 10.1016/j.jcmgh.2015.06.011

Cai, H., Gong, L., Liu, J., Zhou, Q., and Zheng, Z. (2019). Diosgenin inhibits tumor angiogenesis through regulating GRP78-mediated HIF-1α and VEGF/VEGFR signaling pathways. *Pharmazie* 74, 680–684. doi: 10.1691/ph.2019/9526

Carmen-Orozco, R. P., Dávila-Villacorta, D. G., Cauna, Y., Bernal-Teran, E. G., Bitterfeld, L., Sutherland, G. L., et al. (2019). Blood-brain barrier disruption and angiogenesis in a rat model for neurocysticercosis. *J. Neurosci. Res.* 97, 137–148. doi: 10.1002/jnr.24335

Casulli, A., Barth, T. F. E., and Tamarozzi, F. (2019). *Echinococcus multilocularis*. *Trends Parasitol.* 35, 738–739. doi: 10.1016/j.pt.2019.05.005

Cui, Z., Wu, H., Xiao, Y., Xu, T., Jia, J., Lin, H., et al. (2022). Endothelial PDGF-BB/PDGF-β signaling promotes osteoarthritis by enhancing angiogenesis-dependent abnormal subchondral bone formation. *Bone Res.* 10:58. doi: 10.1038/s41413-022-00229-6

Dennis, R. D., Schubert, U., and Bauer, C. (2011). Angiogenesis and parasitic helminth-associated neovascularization. *Parasitology* 138, 426–439. doi: 10.1017/S0031182010001642

Dudley, A. C., and Griffioen, A. W. (2023). Pathological angiogenesis: mechanisms and therapeutic strategies. *Angiogenesis* 26, 313–347. doi: 10.1007/s10456-023-09876-7

El-Dardiry, M. A., Abdel-Aal, A. A., Abdeltawab, M. S. A., El-Sherbini, M., Hassan, M. A., Abdel-Aal, A. A., et al. (2021). Effect of mast cell stabilization on angiogenesis in primary and secondary experimental *Trichinella spiralis* infection. *Parasit Vectors* 14:567. doi: 10.1186/s13071-021-05075-9

Ezaki, T., Tanaka, T., Tamura, R., Ohara, K., Yamamoto, Y., Takei, J., et al. (2024). Status of alternative angiogenic pathways in glioblastoma resected under and after bevacizumab treatment. *Brain Tumor Pathol.* 41, 61–72. doi: 10.1007/s10014-024-00481-0

Fadil, K. H. A., Mahmoud, E. M., El-Ahl, S. A. H. S., Abd-Elaal, A. A., El-Shafaey, A. A. M., Badr, M. S. E. D. Z., et al. (2022). Investigation of the effect of the calcium channel blocker, verapamil, on the parasite burden, inflammatory response and angiogenesis in experimental *Trichinella spiralis* infection in mice. *Food Waterborne Parasitol.* 26:e00144. doi: 10.1016/j.fawpar.2022.e00144

Francisco, J. S., Terra, M., Klein, G. C. T., Dias de Oliveira, B., and Pelajo-Machado, M. (2022). The hepatic extramedullary hematopoiesis during experimental murine Schistosomiasis mansoni. *Front. Immunol.* 13:955034. doi: 10.3389/fimmu.2022.955034

Glaviano, A., Foo, A. S. C., Lam, H. Y., Yap, K. C. H., Jacot, W., Jones, R. H., et al. (2023). PI3K/AKT/mTOR signaling transduction pathway and targeted therapies in cancer. *Mol. Cancer* 22:138. doi: 10.1186/s12943-023-01827-6

Guan, J. T., Li, X. X., Peng, D. W., Zhang, W. M., Qu, J., Lu, F., et al. (2020). MicroRNA-18a-5p administration suppresses retinal neovascularization by targeting FGF1 and HIF1A. *Front. Pharmacol.* 11:276. doi: 10.3389/fphar.2020.00276

Guo, X., Niu, Y., Han, W., Han, X., Chen, Q., Tian, S., et al. (2023). The ALK1-Smad1/5-ID1 pathway participates in tumour angiogenesis induced by low-dose photodynamic therapy. *Int. J. Oncol.* 62:55. doi: 10.3892/ijo.2023.5503

Hasby Saad, M. A., and El-Anwar, N. (2020). Bevacizumab as a potential anti-angiogenic therapy in schistosomiasis: a double-edged, but adjustable weapon. *Parasite Immunol* 42:e12724. doi: 10.1111/pim.12724

Herz, M., and Brehm, K. (2021). Serotonin stimulates *Echinococcus multilocularis* larval development. *Parasit Vectors* 14:14. doi: 10.1186/s13071-020-04533-0

Huang, F., Dang, Z., Zhang, H., Yagi, K., Kim, K., Joseph, M., et al. (2017). Comparative study on secretome and transmembranome of immature and mature metacestodes of *Echinococcus multilocularis*. *Vet. Parasitol.* 245, 153–159. doi: 10.1016/j.vetpar.2017.05.006

Huwait, E. A., Al-Ghamdi, M. A., Ghattas, M. H., Hinnis, A. R., El-Maaty, D. A. A., Abo-Elmatty, D. M., et al. (2021). Role of heme oxygenase-1, cytokines, and vascular endothelial growth factor in murine *Schistosoma mansoni*. *Int. J. Health Sci.* 15, 22–28.

Jiang, H., Wang, X., Guo, L., Tan, X., Gui, X., Liao, Z., et al. (2023). Effect of sunitinib against *Echinococcus multilocularis* through inhibition of VEGFA-induced angiogenesis. *Parasit Vectors* 16:407. doi: 10.1186/s13071-023-05999-4

Jiang, H.-j., Gui, X.-w., Guo, L.-j., Yang, X.-f., Wang, X.-y., Chen, X.-l., et al. (2020). Expression and angiogenic effect of VEGFA/VEGFR2 in mice hepatic metacestode tissue of *Echinococcus multilocularis*. *Chin. J. Parasitol. Parasitic Dis.* 38, 673–681. doi: 10.12140/j.issn.1000-7423.2020.06.001

Ke, Y., Bi, X., Yang, N., Chu, J., Li, X., Ma, W., et al. (2022). Serum platelet-derived growth factor-BB levels as a potential biomarker in assessing the metabolic activity of lesions in alveolar echinococcosis patients. *Acta Trop.* 227:106290. doi: 10.1016/j.actatropica.2021.106290

Kopetz, S., Hoff, P. M., Morris, J. S., Wolff, R. A., Eng, C., Glover, K. Y., et al. (2010). Phase II trial of infusional fluorouracil, irinotecan, and bevacizumab for metastatic colorectal cancer: efficacy and circulating angiogenic biomarkers associated with therapeutic resistance. *J. Clin. Oncol.* 28, 453–459. doi: 10.1200/JCO.2009.24.8252

Kountouras, J., Zavos, C., and Chatzopoulos, D. (2005). Apoptotic and anti-angiogenic strategies in liver and gastrointestinal malignancies. *J. Surg. Oncol.* 90, 249–259. doi: 10.1002/jso.20254

Kuai, J., Lidia, M., Jon, B., Michael, C., Gregory, J. C., Shinji, O., et al. (2015). Characterization of binding mode of action of a blocking anti-platelet-derived growth factor (PDGF)-B monoclonal antibody, MOR8457, reveals conformational flexibility and avidity needed for PDGF-BB to bind PDGF receptor-beta. *Biochemistry* 54, 1918–1929. doi: 10.1021/bi5015425

Levitzki, A. (2004). PDGF receptor kinase inhibitors for the treatment of PDGF driven diseases. *Cytokine Growth Factor Rev.* 15, 229–235. doi: 10.1016/j.cytogfr.2004.03.010

Liu, C., Cao, J., Zhang, H., Field, M. C., and Yin, J. (2023). Extracellular vesicles secreted by *Echinococcus multilocularis*: important players in angiogenesis promotion. *Microbes Infect.* 25:105147. doi: 10.1016/j.micinf.2023.105147

Liu, X. F., Li, J. W., Chen, H. Z., Sun, Z. Y., Shi, G. X., Zhu, J. M., et al. (2019). Yanghe Huayan decoction inhibits the capability of trans-endothelium and angiogenesis of HER2+ breast cancer via pAkt signaling. *Biosci. Rep.* 39:BSR20181260. doi: 10.1042/BSR20181260

Lopes-Coelho, F., Martins, F., Pereira, S. A., and Serpa, J. (2021). Anti-angiogenic therapy: current challenges and future perspectives. *Int. J. Mol. Sci.* 22:3765. doi: 10.3390/ijms22073765

Lu, J. H., Hsia, K., Su, C. K., Pan, Y. H., Ma, H., Chiou, S. H., et al. (2023). A novel dressing composed of adipose stem cells, and decellularized Wharton's jelly facilitated wound, healing and relieved lymphedema by enhancing angiogenesis and lymphangiogenesis in a rat model. *J. Funct. Biomater.* 14:104. doi: 10.3390/jfb14020104

Machado, C. D. C., Alarcón-Torrecillas, C., Pericacho, M., Rodríguez-Escolar, I., Carretón, E., Montoya-Alonso, J. A., et al. (2023). Involvement of the excretory/secretory and surface-associated antigens of Dirofilaria immitis adult worms in the angiogenic response in an in-vitro endothelial cell model. *Vet. Parasitol.* 318:109939. doi: 10.1016/j.vetpar.2023.109939

Pandey, P., Khan, F., Upadhyay, T. K., Seungjoon, M., Park, M. N., and Kim, B. (2023). New insights about the PDGF/PDGF, R signaling pathway as a promising target to develop cancer therapeutic strategies. *Biomed. Pharmacother.* 161:114491. doi: 10.1016/j.biopha.2023.114491

Park, M. K., Ko, E. J., Jeon, K. Y., Kim, H., Jo, J. O., Baek, K. W., et al. (2019). Induction of angiogenesis by malarial infection through hypoxia dependent manner. *Korean J. Parasitol.* 57, 117–125. doi: 10.3347/kjp.2019.57.2.117

Peng, Y., Wu, S., Li, Y., and Crane, J. L. (2020). Type H blood vessels in bone modeling and remodeling. *Theranostics* 10, 426–436. doi: 10.7150/thno.34126

Perez Rodriguez, M. D. P., Alarcón-Torrecillas, C., Pericacho, M., Rodríguez-Escolar, I., Carretón, E., and Morchón, R. (2023). Effect of somatic antigens of Dirofilaria repens adult worms on angiogenesis, cell proliferation and migration and pseudo-capillary formation in human endothelial cells. *Parasit Vectors* 16:105. doi: 10.1186/s13071-023-05726-z

Qing, Z., Xiong-feng, Y., Huan-huan, H., Hui-jiao, J., Xiao-yi, W., Lin-lin L., et al. (2019). Correlation between angiogenesis and disease progression of hepatic Echinococcus multilocularis in C57BL/6 mice. *Chin. J. Parasitol Parasitic Dis.* 37, 302–310. doi: 10.12140/j.issn.1000-7423.2019.03.011

Rayia, D. A., Othman, A., Harras, S., Helal, D., Dawood, L., and Soliman, S. (2022). Bevacizumab: a new take on therapy of muscle phase of *Trichinella spiralis* infection. *Acta Trop.* 230:106409. doi: 10.1016/j.actatropica.2022.106409

Shiau, J. P., Wu, C.-C., Chang, S.-J., Pan, M.-R., Liu, W., Ou-Yang, F., et al. (2021). FAK regulates VEGFR expression and promotes angiogenesis in triple-negative breast cancer. *Biomedicines* 9:1789. doi: 10.3390/biomedicines9121789

Stadelmann, B., Spiliotis, M., Müller, J., Scholl, S., Müller, N., Gottstein, B., et al. (2010). *Echinococcus multilocularis* phosphoglucose isomerase (EmPGI): a glycolytic enzyme involved in metacestode growth and parasite-host cell interactions. *Int. J. Parasitol.* 40, 1563–1574. doi: 10.1016/j.ijpara.2010.05.009

Su, W., Liu, G., Liu, X., Zhou, Y., Sun, Q., Zhen, G., et al. (2020). Angiogenesis stimulated by elevated PDGF-BB in subchondral bone contributes to osteoarthritis development. *JCI Insight* 5:e135446. doi: 10.1172/jci.insight.135446

Tsioumpekou, M., Cunha, S. I., Ma, H., Åhgren, A., Cedervall, J., Olsson, A. K., et al. (2020). Specific targeting of PDGFRbeta in the stroma inhibits growth and angiogenesis in tumors with high PDGF-BB expression. *Theranostics* 10, 1122–1135. doi: 10.7150/thno.37851

Vellasco, L., Svensjö, E., Bulant, C. A., Blanco, P. J., Nogueira, F., Domont, G., et al. (2022). Sheltered in stromal tissue cells *Trypanosoma cruzi* orchestrates inflammatory neovascularization via activation of the mast cell chymase pathway. *Pathogens* 11:187. doi: 10.3390/pathogens11020187

Vimalraj, S. A. (2022). A concise review of VEGF, PDGF, FGF, Notch, angiopoietin, and HGF signalling in tumor angiogenesis with a focus on alternative approaches and future directions. *Int. J. Biol. Macromol.* 221, 1428–1438. doi: 10.1016/j.ijbiomac.2022.09.129

Wang, H. J., Ran, H. F., Yin, Y., Xu, X. G., Jiang, B. X., Yu, S. Q., et al. (2022). Catalpol improves impaired neurovascular unit in ischemic stroke rats via enhancing VEGF-PI3K/AKT and VEGF-MEK1/2/ERK1/2 signaling. *Acta Pharmacol. Sin.* 43, 1670–1685. doi: 10.1038/s41401-021-00803-4

Wang, J., Ren, B., Liu, W.-Y., Wen, H., Qing, S., Xie, W.-D., et al. (2011). The correlation of CT perfusion imaging with microvessel density and vascular endothelial growth factor in hepatic alveolar echinococcosis. *Chin. J. Radiol.* 45, 1036–1039. doi: 10.3760/CMA.J.ISSN.1005-1201.2011.11.010

Wang, S., Wei, W., and Cai, X. (2015). Genome-wide analysis of excretory/secretory proteins in Echinococcus multilocularis: insights into functional characteristics of the tapeworm secretome. *Parasit Vectors* 8:666. doi: 10.1186/s13071-015-1282-7

Wang, Y., Yin, D., Xu, C., Wang, K., Zheng, L., and Zhang, Y. (2016). Roxarsone induces angiogenesis via PI3K/Akt signaling. *Cell Biosci.* 6:54. doi: 10.1186/s13578-016-0119-1

Weiss, A. T., Bauer, C., and Kohler, K. (2010). Canine alveolar echinococcosis: morphology and inflammatory response. *J. Comp. Pathol.* 143, 233–238. doi: 10.1016/j.jcpa.2010.03.004

Wen, H., Vuitton, L., Tuxun, T., Li, J., Vuitton, D. A., Zhang, W., et al. (2019). Echinococcosis: advances in the 21st century. *Clin. Microbiol. Rev.* 32:e00075–18. doi: 10.1128/CMR.00075-18

Yang, L., Dong, C., Yang, J., Yang, L., Chang, N., Qi, C., et al. (2019). MicroRNA-26b-5p inhibits mouse liver fibrogenesis and angiogenesis by targeting PDGF receptor-beta. *Mol. Ther. Nucleic Acids* 16, 206–217. doi: 10.1016/j.omtn.2019.02.014

Yang, N., Ma, W., Ke, Y., Liu, H., Chu, J., Sun, L., et al. (2022). Transplantation of adipose-derived stem cells ameliorates Echinococcus multilocularis-induced liver fibrosis in mice. *PLoS Negl. Trop. Dis.* 16:e0010175. doi: 10.1371/journal.pntd.0010175

Yang, Y., Deng, Y., Chen, X., Zhang, J., Chen, Y., Li, H., et al. (2018). Inhibition of PDGFR by CP-673451 induces apoptosis and increases cisplatin cytotoxicity in NSCLC cells via inhibiting the Nrf2-mediated defense mechanism. *Toxicol. Lett.* 295, 88–98. doi: 10.1016/j.toxlet.2018.05.033

Yimingjiang, M., Aini, A., Tuergan, T., and Zhang, W. (2023). Differential gene expression profiling in alveolar echinococcosis identifies potential biomarkers associated with angiogenesis. *Open Forum Infect. Dis.*10:ofad031. doi: 10.1093/ofid/ofad031

Zhang, J., Li, W., Wang, W., Chen, Q., Xu, Z., Deng, M., et al. (2023). Dual roles of FAK in tumor angiogenesis: a review focused on pericyte FAK. *Eur. J. Pharmacol.* 947:175694. doi: 10.1016/j.ejphar.2023.175694

Zhang, J., Xu, L., Ye, J., Xu, C., Wu, B., Wu, J., et al. (2024). Identification of core genes of craniopharyngioma angiogenesis based on single-cell nuclear transcriptome sequencing. *Cell Mol. Biol.* 70, 136–141. doi: 10.14715/cmb/2024.70.3.20

Zhu, J., Cui, W., Liu, X., Ying, J., Hu, C., and Zhang, Y. (2013). In vitro and ex vivo angiogenic effects of roxarsone on rat endothelial cells. *Toxicol. Lett.* 223, 175–182. doi: 10.1016/j.toxlet.2013.09.003

Zou, X., Tang, X. Y., Qu, Z. Y., Sun, Z. W., Ji, C. F., Li, Y. J., et al. (2022). Targeting the PDGF/PDGFR signaling pathway for cancer therapy: a review. *Int. J. Biol. Macromol.* 202, 539–557. doi: 10.1016/j.ijbiomac.2022.01.113

Zueva, T., Morchón, R., Carretón, E., Ollauri-Ibáñez, C., Pericacho, M., Rodríguez-Barbero, A., et al. (2020). Angiogenesis in cardiopulmonary dirofilariosis: does the Wolbachia surface protein have a pro- or anti-angiogenic effect? *J. Helminthol.* 94:e162. doi: 10.1017/S0022149X20000450

frontiers | Frontiers in Microbiology

TYPE Original Research
PUBLISHED 11 December 2025
DOI 10.3389/fmicb.2025.1716137

OPEN ACCESS

EDITED BY
Lei Deng,
Chinese Academy of Agricultural Sciences, China

REVIEWED BY
Anna Kopf,
Technical University Dresden, Germany
Pavel A. Andriyanov,
Federal Research Center of Virology and Microbiology, Russia
Antonio Norberg,
FAMESC BJI, Brazil

*CORRESPONDENCE
Chen Cheng Xiao
✉ 305639447@qq.com
Ya Yin Qi
✉ 75997921@qq.com

RECEIVED 02 October 2025
REVISED 15 November 2025
ACCEPTED 24 November 2025
PUBLISHED 11 December 2025

CITATION
Li YJ, Qi BR, Cao SZ, Zhang RZ, Jiao LL, Zhou M, Cai JC, Du MY, Li KS, Xiao CC and Qi YY (2025) Host range expansion of *Leucobacter holotrichiae*: first evidence of mammalian infection and comparative genomic insights.
Front. Microbiol. 16:1716137.
doi: 10.3389/fmicb.2025.1716137

Host range expansion of *Leucobacter holotrichiae*: first evidence of mammalian infection and comparative genomic insights

Yong Jian Li, Bo Rui Qi, Shu Zhu Cao, Run Ze Zhang, Long Ling Jiao, Ming Zhou, Jin Chun Cai, Meng Ying Du, Ke Shuang Li, Chen Cheng Xiao* and Ya Yin Qi*

College of Animal Science and Technology, Shihezi University, Shihezi, Xinjiang, China

Leucobacter holotrichiae has previously been identified exclusively in insect hosts, with no reports of its presence in mammals. This study is the first to report the isolation of three *L. holotrichiae* strains (LH23001, LH23002, and LH23003) from mixed cultures of bovine actinomycotic abscesses in a large-scale dairy farm in Xinjiang, China. Phenotypic analysis revealed that these Gram-positive bacilli are non-spore-forming, non-flagellated, non-hemolytic, non-motile, and capable of biofilm formation. The isolates formed transparent membranous white colonies on modified Gao's medium and could grow in BHI liquid medium containing 9% NaCl. Phylogenetic analysis based on 16S rRNA gene sequences and average nucleotide identity (ANI) further confirmed that these strains are most closely related to *L. holotrichiae*, with all strains exhibiting strong biofilm-forming ability. Intraperitoneal infection experiments in mice showed that infection induced pathological changes in multiple tissues: vacuolar degeneration of cardiomyocytes, mild steatosis of hepatocytes, focal necrosis of a small number of lymphocytes in the white pulp of the spleen, extensive granulocyte infiltration in the alveolar walls of lung tissue, and mild edema of renal tubular epithelial cells in the renal cortex. Whole-genome sequencing results indicated that the genome size of these strains ranges from 3.63 to 3.68 Mb with a GC content of 66.8–67.2%. They carry multiple antimicrobial resistance genes and virulence factors, and five complete prophages were predicted. Functional annotation results showed that the strains have annotated information in databases including NR, GO, eggNOG, Swiss-Prot, CAZy, CARD, and VFDB. This study expands the known host range of *L. holotrichiae*, systematically analyzes its biological characteristics and genomic features, and provides a theoretical basis for future research on this bacterium.

KEYWORDS

***Leucobacter holotrichiae*, isolation and identification, microbiological characterization, antimicrobial susceptibility, biofilm formation, murine infection model, bovine actinomycosis, whole-genome sequencing**

Introduction

The genus *Leucobacter*, a member of the family *Microbacteriaceae* within the phylum Actinobacteria (Takeuchi et al., 1996), comprises Gram-positive, non-spore-forming bacteria with high GC content. Species within this genus are typically isolated from diverse environmental habitats (Sturm et al., 2011), including soil (Zhu et al., 2022), fermented seafood (Shin et al., 2011), Skin (Boxberger et al., 2023), plant rhizospheres (Li et al., 2024), and the intestinal tracts of insects (Hyun et al., 2021), and are generally regarded as non-pathogenic or commensal organisms. Since its initial description from the gut of *Holotrichia oblita* larvae, *Leucobacter holotrichiae* has been exclusively associated with invertebrate hosts (Zhu et al., 2016). To date, no reports have documented its presence in vertebrates or its involvement in mammalian disease.

In recent years, the ecological and pathogenic boundaries of environmental actinobacteria have become increasingly ambiguous (Poullain and Nuismer, 2012; Barber and Fitzgerald, 2024). Members of genera once considered strictly saprophytic are now being detected in clinical and veterinary settings. This shift is driven in part by global changes in microbiome composition, antimicrobial usage, host immune status, and environmental pressures—factors that collectively contribute to the emergence of cryptic or opportunistic pathogens (Berendonk et al., 2015). In this context, this study is the first to successfully isolate this bacterium from bovine actinomycotic abscesses, marking its ecological niche expansion from insects to mammals. This finding not only confirms the evolutionary trend of pathogenic potential in environmental actinomycetes but also highlights the need to re-evaluate the host adaptation range and pathogenic mechanisms of such microorganisms (Wani et al., 2022; Combs et al., 2023; Duar et al., 2017).

In veterinary medicine, actinomycosis is a chronic suppurative infection characterized by firm abscesses and granulomatous inflammation (Brook, 2008; Figueiredo et al., 2013). While *Actinomyces bovis* has traditionally been considered the primary causative agent in cattle, emerging evidence underscores the contribution of polymicrobial communities and secondary colonizers to disease persistence and progression (Duar et al., 2017). Bovine abscesses have been documented in several cases as polymicrobial infections; however, the isolation of *L. holotrichiae* from bovine actinomycotic lesions reported here is the first of its kind. This study focuses specifically on the isolation and identification of *L. holotrichiae* and aims to elucidate its potential role in such mixed infections. The isolation of *L. holotrichiae* from actinomycotic lesions in dairy cattle thus represents a notable intersection of environmental microbiology and veterinary infectious disease, meriting further in-depth investigation.

In this study, we report the isolation and comprehensive characterization of three *L. holotrichiae* strains from actinomycotic abscesses in dairy cattle in Xinjiang, China. To assess their biological behavior and potential for mammalian infection, we conducted an integrated series of phenotypic, microbiological, and genomic analyses. These included biochemical profiling, antimicrobial susceptibility testing, biofilm formation assays, experimental infection in a murine model, and whole-genome sequencing with comparative annotation. Through this multifaceted approach, we aimed to (i) validate the taxonomic identity of the isolates, (ii) evaluate their capacity to colonize and disseminate within a mammalian host, and (iii) elucidate the genomic features that may facilitate their apparent host range expansion. The results demonstrate that *L. holotrichiae*, as a potential opportunistic pathogen, resides in the suppurative lesions of mammals (cattle), significantly expanding its known host range from insects to livestock. This study systematically analyzed the bacterium's biological phenotypes, pathogenic potential, and genomic basis, revealing key pathogenicity-related traits including environmental tolerance, biofilm formation, and partial resistance to antibiotics. This finding provides new empirical evidence for the notion that the ecological and pathogenic boundaries of environmental actinobacteria are increasingly blurred.

Materials and methods

Bacterial isolation and identification

Purulent samples were aseptically collected from mandibular actinomycotic abscesses of three adult Holstein dairy cows with chronic swelling and suppuration in Xinjiang, China, during routine veterinary inspections in 2023. Each sample was streaked onto brain heart infusion (BHI) agar plates and incubated aerobically at 37 °C for 24–48 h. Colonies with similar morphology—dry, pale-yellow, and slightly rough—were selected and sub-cultured to purity. For molecular identification, genomic DNA was extracted from pure cultures using a commercial bacterial genomic DNA extraction kit (Tiangen, China), following the manufacturer's protocol. The nearly full-length 16S rRNA gene was amplified using universal primers 27F (5'-AGAGTTTGATCCTGGCTCAG-3′) and 1492R (5'-GGTTACC TTGTTACGACTT-3′) (Greisen et al., 1994). PCR was carried out in a 25 μL reaction volume with an initial denaturation at 94 °C for 5 min, followed by 30 cycles of 94 °C for 30 s, 55 °C for 30 s, and 72 °C for 90 s, and a final extension at 72 °C for 7 min. Amplicons were verified by 1% agarose gel electrophoresis and submitted for bidirectional Sanger sequencing (Sangon Biotech, China). The obtained sequences were analyzed using the NCBI BLASTn tool to identify closely related taxa. Phylogenetic trees were constructed using the neighbor-joining method with 1,000 bootstrap replications in MEGA 11 software. All three isolates (designated LH23001, LH23002, and LH23003) exhibited 99.7–99.9% identity with *Leucobacter holotrichiae* (KJ_461711.1) (Zhu et al., 2016), confirming their taxonomic affiliation.

Morphological, biochemical, and physiological characterization

Colonial morphology was assessed after aerobic incubation of isolates on BHI agar plates at 37 °C for 24 h. Colony color, texture, elevation, and margin were recorded. Cellular morphology was observed using Gram staining under a light microscope (1,000× magnification). All isolates were Gram-positive, rod-shaped, and non-spore-forming. Motility was evaluated using a semi-solid motility medium (0.4% agar supplemented with 5% fetal bovine serum). Each isolate was stab-inoculated and incubated at 37 °C for 24–48 h. The absence of radial diffusion from the inoculation site indicated non-motility. Catalase activity was determined by adding 3% hydrogen peroxide to freshly cultured bacterial cells on a glass slide.

The appearance of rapid bubble formation was interpreted as a positive reaction. Oxidase activity was tested using oxidase reagent strips (bioMérieux, France), with color change to deep purple within 30 s indicating a positive result. Carbohydrate utilization profiles were evaluated using the API 50 CH system (bioMérieux, France). Bacterial suspensions were prepared in API 50 CHL medium to a turbidity equivalent of McFarland 2.0, and inoculated into microtubes. Strips were incubated at 37 °C for 48 h and color changes were used to assess fermentation patterns according to the manufacturer's instructions. Enzymatic activity was assessed with the API ZYM system (bioMérieux, France). Suspensions of each isolate were inoculated into wells containing chromogenic enzyme substrates. Reactions were monitored at 4 h and 24 h intervals. All biochemical and enzymatic tests were conducted in triplicate for validation and reproducibility.

Antibiotic susceptibility testing

Antimicrobial susceptibility of the three *L. holotrichiae* isolates (LH23001, LH23002, and LH23003) was evaluated using the standard disk diffusion method (Kirby–Bauer) on Mueller-Hinton agar (Oxoid, United Kingdom), following the Clinical and Laboratory Standards Institute (CLSI) guidelines (M100, 2023). Overnight cultures were adjusted to a turbidity equivalent to 0.5 McFarland standard and uniformly spread onto agar plates using sterile swabs. Commercial antibiotic disks (Hangwei, China) were placed onto the inoculated plates, including the following agents: ampicillin (10 μg), amoxicillin–clavulanate (20/10 μg), ceftiofur (30 μg), streptomycin (10 μg), tetracycline (30 μg), gentamicin (10 μg), florfenicol (30 μg), ciprofloxacin (5 μg), enrofloxacin (5 μg), sulfamethoxazole-trimethoprim (23.75/1.25 μg), and erythromycin (15 μg). Plates were incubated at 37 °C for 18–24 h, and the diameters of inhibition zones were measured in millimeters. The interpretation of the results was mainly based on the criteria for aerobic actinomycetes in CLSI document M24. For antibiotics not covered in M24, we refer to the general recommendations for rare bacteria in the CLSI document M45 and determine the results as Susceptible (S), moderately Susceptible (I) or resistant (R) (Abbey and Deak, 2019). All susceptibility tests were performed in triplicate to ensure consistency.

Biofilm formation assay

The ability of *L. holotrichiae* isolates to form biofilms was assessed using the crystal violet microtiter plate assay. Overnight cultures of LH23001, LH23002, and LH23003 were diluted 1:100 in fresh brain heart infusion (BHI) broth and 200 μL of each suspension was inoculated into sterile, flat-bottom 96-well polystyrene microplates (Corning, United States). Each strain was tested in eight technical replicates. *Staphylococcus aureus* ATCC 6538 and uninoculated BHI medium were used as positive and negative controls, respectively. The plates were incubated aerobically at 37 °C for 24 h without agitation. After incubation, wells were gently washed three times with sterile phosphate-buffered saline (PBS, pH 7.4) to remove planktonic cells. Attached biofilms were fixed with 200 μL of 99% methanol for 15 min, air-dried, and stained with 0.1% crystal violet solution for 15 min. Excess dye was rinsed off with distilled water, and the retained stain was solubilized with 200 μL of 33% glacial acetic acid. The optical density (OD) was measured at 595 nm using a microplate reader (BioTek, United States). Based on OD values, biofilm-forming capacity was classified as follows: $OD \leq ODc$, no biofilm (−); $ODc < OD \leq 2 \times ODc$, weak (+); $2 \times ODc < OD \leq 4 \times ODc$, moderate (++); $OD > 4 \times ODc$, strong (+++), where ODc represents the cut-off value calculated as the mean OD of the negative control plus three standard deviations. Each assay was repeated three times independently to ensure reproducibility.

Animal infection model

To evaluate the pathogenic potential of *L. holotrichiae* isolates *in vivo*, a murine peritoneal infection model was established. Six-week-old female BALB/c mice ($n = 18$, specific-pathogen-free) were purchased from Beijing Vital River Laboratory Animal Technology Co., Ltd. and maintained under controlled conditions with *ad libitum* access to food and water. All procedures were approved by the Animal Ethics Committee of [Shihezi University], under protocol number [A2025-906]. Each bacterial isolate (LH23001, LH23002, and LH23003) was cultured overnight in BHI broth, washed, and resuspended in sterile PBS. Groups of six mice were intraperitoneal injected with 0.2 mL bacterial suspension containing 1×10^7 CFU. A negative control group received sterile PBS alone. Mice were monitored daily for clinical signs including lethargy, weight loss, and local inflammation at the injection site. At 120 h post-inoculation, all mice were euthanized by CO_2 asphyxiation. Gross pathological examination was performed, and visceral organ tissues were collected for histological analysis. The tissue was fixed in 10% neutral buffered formalin, embedded in paraffin, sliced 5 μm, and stained with hematoxylin and eosin (H&E). Each internal organ has different injuries. No clinical abnormalities or tissue lesions were observed in the PBS-injected controls.

Whole-genome sequencing and annotation

Genomic DNA was extracted from overnight cultures of *Leucobacter holotrichiae* isolates LH23001, LH23002, and LH23003 using the TIANamp Bacteria DNA Kit (Tiangen Biotech, China), following the manufacturer's instructions. DNA quality and concentration were assessed by agarose gel electrophoresis and a NanoDrop spectrophotometer (Thermo Fisher Scientific, United States). Whole-genome sequencing was performed on the Illumina NovaSeq 6,000 platform (Novogene, China), generating paired-end reads with an average insert size of 350 bp. Raw reads were quality-trimmed using Trimmomatic v0.39, and *de novo* genome assembly was conducted using SPAdes v3.15.3. Genome completeness and contamination were evaluated using CheckM v1.1.6. Gene prediction and functional annotation were performed using the NCBI Prokaryotic Genome Annotation Pipeline (PGAP) and Prokka v1.14.6 (Simpson et al., 2009; Xu et al., 2020; Besemer and Borodovsky, 2005; Lowe and Eddy, 1997; Lagesen et al., 2007). Protein-coding sequences were further annotated using multiple public databases, including COG (Clusters of Orthologous Groups), KEGG (Kyoto Encyclopedia

of Genes and Genomes), VFDB (Virulence Factor Database), and CARD (Comprehensive Antibiotic Resistance Database). The circular genome map was visualized using CGView. The original sequencing genome sequences of strains LH23001, LH23002 and LH23003 have been deposited in the gene bank GenBank, and their accession numbers are, respectively, SAMN51023674, SAMN51023675, SAMN51023676. The complete genome assembly sequence is currently under review at NCBI, and the temporary accession number is SAMN52852392, SAMN52852393, SAMN52852394.

Statistical analysis

All quantitative data are presented as mean ± standard deviation (SD) from at least three independent experiments. Statistical analyses were performed using GraphPad Prism version 9.5 (GraphPad Software, United States). Comparisons between multiple groups were conducted using one-way analysis of variance (ANOVA) followed by Tukey's multiple comparisons test. For two-group comparisons, unpaired two-tailed Student's *t*-tests were used. Differences were considered statistically significant at $p < 0.05$. For biofilm formation assays, OD values were compared across isolates using ANOVA. For antimicrobial susceptibility tests, zone diameters were analyzed descriptively and categorized based on CLSI guidelines, without inferential statistics. Histological severity scores from the animal infection model were semi-quantitatively evaluated but not statistically compared due to limited sample size. All statistical methods applied were pre-specified and consistent across replicates. Figures were generated using GraphPad Prism and Adobe Illustrator 2023 for final layout and annotation.

Results

Clinical and epidemiological findings

From April to July 2023, a total of 37 adult Holstein cows from three large farms in Changji, Xinjiang, China, presented with localized submandibular or mandibular swelling (Figure 1A). The clinical symptoms were confined to the affected area, with no obvious systemic signs such as fever or depression. Physical examination revealed that the swellings were solid, poorly defined,

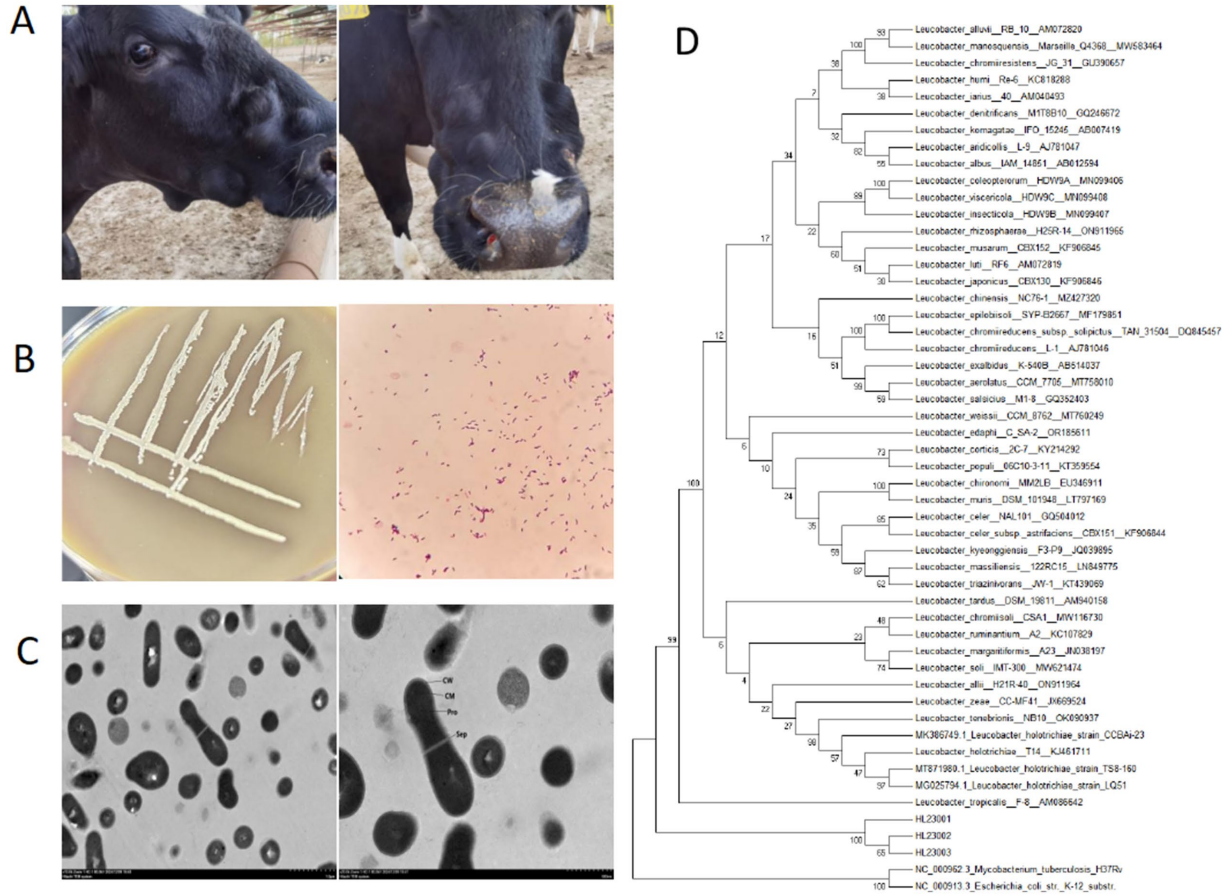

FIGURE 1
Isolation and identification of *Leucobacter holotrichiae*. Clinical presentation, colony morphology, and phylogenetic identification of *Leucobacter holotrichiae* **(A)** Submandibular actinomycotic abscess in dairy cattle. **(B)** Colony morphology in pure culture (blood agar medium) and gram staining morphology under light microscope (1000×). **(C)** Scanning electron microscope images (10,000×, 20,000×). **(D)** Neighbor-joining phylogenetic tree based on nearly full-length 16S rRNA sequences, showing the relationship of isolates LH23001, LH23002, and LH23003 to related *Leucobacter* species. Bootstrap values (50%) from 1,000 replicates are indicated at the nodes.

and had limited mobility. Among the affected cattle, 24 cases exhibited purulent exudate upon pressure or puncture. A total of 19 pus samples were collected using sterile syringes and submitted for laboratory analysis. Generally, the purulent material appeared as a viscous, yellow-white liquid, sometimes containing visible particles. The samples were inoculated onto blood agar and brain heart infusion (BHI) agar plates and cultured at 37 °C for 24 h. Bacterial colonies grew well under aerobic conditions and displayed mixed morphology. In the primary culture of the original samples, several distinct colony types were observed simultaneously on BHI agar, indicating a polymicrobial community within the abscesses. Preliminary 16S rRNA sequencing analysis of these different colonies identified other bacteria, including *Actinomyces lingnae*, *Staphylococcus aureus*, and *Corynebacterium pyogenes*. These microorganisms are common commensals or environmental flora on cattle skin or mucosa but are also known to have pathogenic potential. Among the mixed colonies, three isolates (designated LH23001, LH23002, and LH23003), obtained from different individual cows across the three farms, formed pale yellow, dry, and rough colonies that were distinct from others. Based on preliminary morphological characteristics and Gram staining, these isolates were tentatively classified as *Actinobacteria*. Conventional phenotypic and biochemical tests could not identify these microorganisms using commercial identification systems. 16S rRNA gene sequencing showed that the isolates shared over 99.8% identity with *L. holotrichiae* (Figure 1D). This species was previously known to colonize the intestinal tract of insects but has not been reported in mammalian infections. As this is the first isolation and identification of *L. holotrichiae* from a mammalian host, this study focuses on a detailed characterization of the strain to elucidate its biological features and potential pathogenic significance. This discovery also raises questions regarding its host range, environmental transmission, and pathogenic potential in vertebrates.

Phenotypic and biochemical characteristics of isolates

The three isolates, designated LH23001, LH23002, and LH23003, displayed consistent colony morphology. After 24 h of aerobic incubation at 37 °C on blood agar or BHI agar, colonies appeared dry, yellowish, wrinkled, and with rough surfaces, approximately 1–2 mm in diameter (Figure 1B) and were non-motile (Figure 2A). Transmission electron microscopy (Figure 1C) field of view showed that the bacterial morphology was mostly oval or short rod-shaped. No hemolytic activity was observed. Gram staining revealed that all isolates were Gram-positive short rods, arranged singly or in pairs, and non-spore-forming. Acid-fast staining was negative. All three isolates were catalase-positive and oxidase-negative. Biochemical identification was performed using the API Coryne test system (bioMérieux, France). Results showed that the strains were positive for pyrazinamidase, β-glucosidase, and glucose fermentation, and negative for urease, nitrate reduction, and gelatin hydrolysis. The API profile numbers did not match any known species in the system, yielding low discrimination scores. In terms of growth conditions, the isolates grew well in BHI broth supplemented with 5% fetal bovine serum (FBS) and tolerated NaCl concentrations up to 9% (Figure 2B). No growth was observed at 10% NaCl or under anaerobic conditions (Figure 2C). The isolates could grow in the environment of pH5-pH8, and the optimal growth pH was pH7 (Figure 2D). Based on their morphological and biochemical profiles, the isolates did not correspond to common bovine pathogens. Their colony features and API results suggested affiliation with high-GC Gram-positive actinobacteria, supporting the initial classification under the genus *Leucobacter*.

Antibiotic susceptibility profiles

The antibiotic susceptibility profiles of *L. holotrichiae* strains LH23001, LH23002, and LH23003 were determined using the standard Kirby-Bauer disk diffusion method on Mueller-Hinton agar plates, incubated at 37 °C for 24 h under aerobic conditions. Results were interpreted based on Clinical and Laboratory Standards Institute (CLSI) guidelines where available: All three strains were Susceptible to commonly used β-lactam antibiotics, including penicillin (10 units), ampicillin (10 μg) and cefotaxime (30 μg), and their inhibition zone diameters were greater than 20 mm. It was also susceptible to tetracycline (30 μg), gentamicin (10 μg), enrofloxacin (5 μg), norfloxacin (10 μg) and chloramphenicol (30 μg). It showed moderate sensitivity to erythromycin (15 μg), and its inhibition zone diameter was between 16 and 20 mm. All strains were resistant to Benzylpenicillin (10 μg), Furazolidone (10 μg), Bacitracin (10 μg) and Clindamycin (2 μg), and the inhibition zone diameter was less than 13 mm. Antibiotic sensitivity is summarized in Table 1. These strains showed a consistent pattern, suggesting that they are inherently resistant mechanisms rather than acquired mutations.

Biofilm-forming capacity

To assess their capacity to form biofilms, the three *L. holotrichiae* isolates (LH23001, LH23002, and LH23003) were cultured in 96-well polystyrene microtiter plates using BHI broth supplemented with 1% glucose. After 24 h of static incubation at 37 °C, adherent cells were stained with 0.1% crystal violet and quantified by measuring absorbance at 595 nm. All three isolates demonstrated the ability to form biofilms, with strain LH23001 exhibiting the highest OD < sub > 595</sub > value (1.21 ± 0.11), followed by LH23002 (0.96 ± 0.09) and LH23003 (0.63 ± 0.08). Based on standard classification criteria, LH23001 and LH23002 were categorized as moderate biofilm producers, while LH23003 exhibited weak biofilm-forming ability. One-way analysis of variance showed that there were significant statistical differences in biofilm formation ability among different isolates ($p < 0.01$), indicating that not all *Leucobacter* isolates have the same ability to form biofilm *in vitro*. From a biological point of view, this variation is very important because it means that some strains may have a stronger potential to colonize and persist on the host surface. The formation of biofilm is a key virulence factor of bacterial pathogenicity, which is related to the increased tolerance to antimicrobial therapy and the increased difficulty of immune system clearance. Specifically, the strong biofilm-forming ability of *L. holotrichiae* may help it establish and maintain chronic infection in primary abscess samples and mouse models.

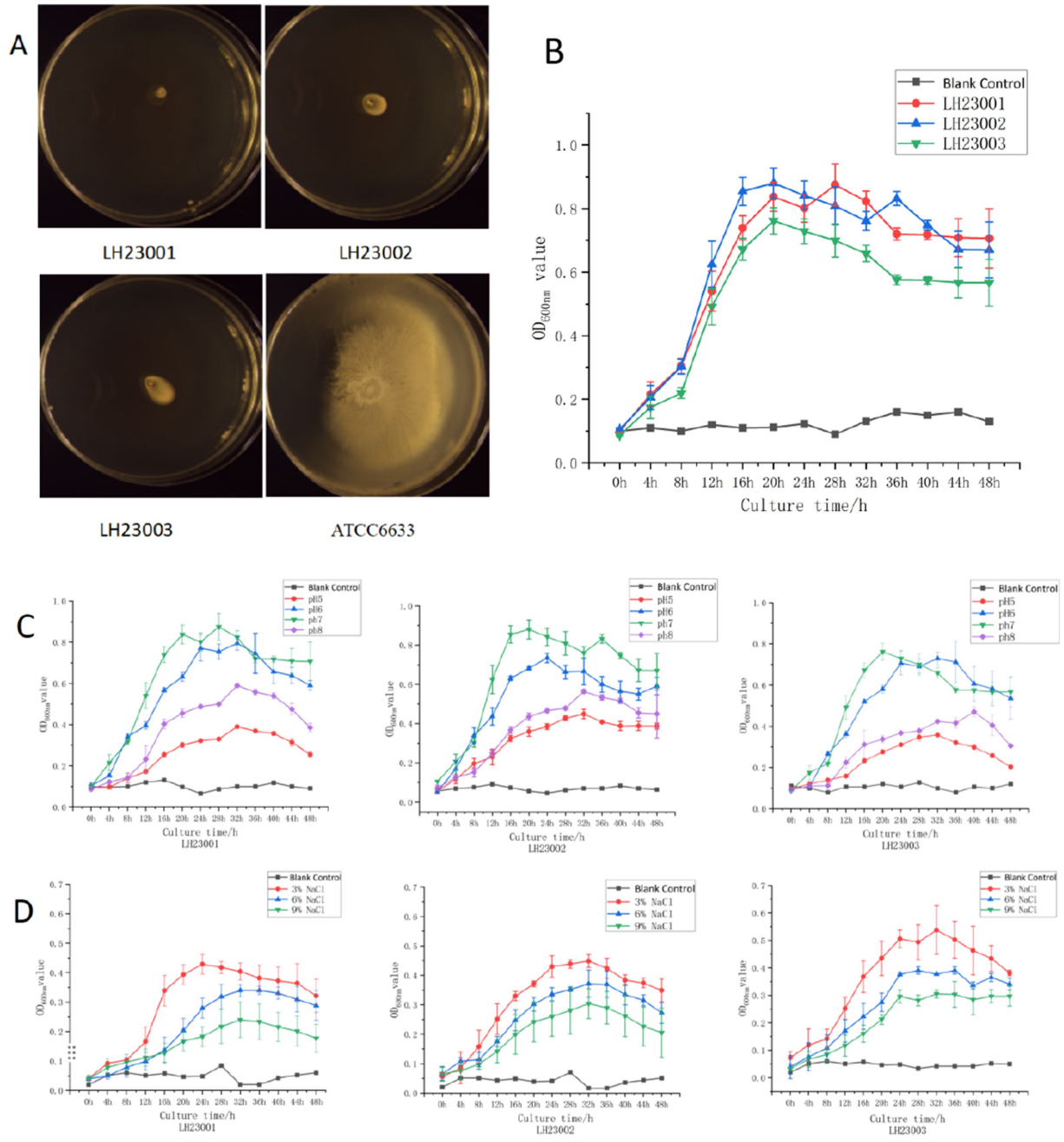

FIGURE 2
Phenotypic and physiological characteristics. Phenotypic and physiological characteristics of *L. holotrichiae* isolates. **(A)** Results of motility test of *L. holotrichiae* isolates. **(B)** Growth curve in BHI broth at 37 °C. **(C)** Growth curves in BHI broth at different pH concentrations. **(D)** Growth curves in BHI broth at different NaCl concentrations. Data represent the mean ± standard deviation of three independent experiments.

Pathogenicity in mice

To evaluate the virulence potential of *L. holotrichiae* isolates in a mammalian host, an intraperitoneal infection model was established using female BALB/c mice (6–8 weeks old, $n = 5$ per group). Each mouse was inoculated with 0.2 mL of bacterial suspension containing 1×10^7 CFU of strains LH23001, LH23002, or LH23003, respectively. Control mice received sterile PBS. Throughout the 120 h observation period, infected mice exhibited transient signs of ruffled fur and decreased activity, particularly in the LH23001 group. No mortality was observed in any group. On 72 h post-infection, animals were euthanized for gross pathological and histological evaluation. Necropsy revealed visible fibrinous exudates and turbid ascites in the abdominal cavity of mice infected with LH23001 and LH23002, whereas the LH23003 group showed only mild peritoneal congestion. No lesions were observed in the control group. Histopathological examination (H&E staining) of liver, spleen, and kidney tissues showed inflammatory infiltration, hepatocellular vacuolation, and splenic red pulp expansion in LH23001- and LH23002-infected mice. Lesions were

TABLE 1 Antimicrobial susceptibility testing results for *Leucobacter holotrichiae* Strain.

Antibiotic	CLSI standard (S≥; I; R≤)	Inhibitory zone diameter/mm			Interpretation		
		Strain LH23001	Strain LH23002	Strain LH23003	Strain LH23001	Strain LH23002	Strain LH23003
Cefixime	≥19; 16–18; ≤15	27.6 ± 0.4	26.1 ± 0.3	27.3 ± 0.4	S	S	S
Amoxicillin	≥20; –; ≤19	28.4 ± 0.7	26.3 ± 0.5	24.3 ± 0.2	S	S	S
Neomycin	≥17; 14–16; ≤13	18.2 ± 0.3	16.0 ± 0.2	18.0 ± 0.3	S	I	S
Tetracycline	≥19; 16–18; ≤15	27.8 ± 0.6	26.0 ± 0.4	25.1 ± 0.2	S	S	S
Vancomycin	≥17; 15–16; ≤14	23.6 ± 0.5	22.8 ± 0.4	22.9 ± 0.3	S	S	S
Enrofloxacin	≥22; 19–21; ≤18	26.4 ± 0.2	26.0 ± 0.5	25.5 ± 0.7	S	S	S
Ofloxacin	≥16; 13–15; ≤12	22.2 ± 0.5	23.1 ± 0.3	21.3 ± 0.5	S	S	S
Roxithromycin	≥18; 14–17; ≤13	17.2 ± 0.5	16.8 ± 0.2	16.9 ± 0.4	I	I	I
Benzylpenicillin	≥32; 29–31; ≤28	6.0 ± 0.1	6.0 ± 0.1	6.0 ± 0.1	R	R	R
Furazolidone	≥16; 13–15; ≤12	12.1 ± 0.2	10.6 ± 0.2	11.8 ± 0.1	I	R	R
Bacitracin	≥13; 11–12; ≤10	6.0 ± 0.1	6.0 ± 0.1	6.0 ± 0.1	R	R	R
Clindamycin	≥19; 16–18; ≤15	6.0 ± 0.1	6.0 ± 0.1	6.0 ± 0.1	R	R	R

S, susceptible; I, intermediate; R, resistant.

milder in the LH23003 group. Representative micrographs are shown in Figure 3.

Genomic features of the isolates

Whole-genome sequencing of *L. holotrichiae* strains LH23001, LH23002, and LH23003 was conducted on the Illumina NovaSeq platform. Quality assessment results of the genomic sequencing data are summarized in Table 2. The assembled genomes range in size from 3.63 to 3.68 megabases, with GC contents between 66.8 and 67.2%, and N50 values ranging from 85,000 to 96,000 base pairs. Gene prediction identified 3,200 to 3,280 coding sequences (CDS), including genes involved in oxidative stress resistance (e.g., catalase and superoxide dismutase), metal ion transport, and biofilm regulation. All three genomes contain genes encoding multidrug efflux pumps as well as various virulence-associated factors. Additionally, five active prophages were predicted. Comparative genomic analysis revealed an average nucleotide identity (ANI) greater than 99.6%, supporting a close genetic relationship among the isolates. BLAST analysis of the 16S rRNA gene and whole-genome sequences further confirmed their classification as *L. holotrichiae*, showing over 99.4% sequence identity with the reference strains TS8-160 (GenBank: MT871980.1) and LQ51 (GenBank: MG025794.1) (Figure 4).

Comparative genomic and functional note

The KEGG database annotation mapped 2,637 genes to 23 distinct pathways. The analysis demonstrated that *Leucobacter holotrichiae* possesses a pronounced genetic predisposition toward metabolic functions, with 2,163 genes (82.02% of KEGG-annotated genes) participating in diverse metabolic pathways. Amino acid metabolism constituted the most represented category (234 genes), followed by carbohydrate metabolism (196 genes) and metabolism of cofactors and vitamins (111 genes). This considerable gene repertoire underscores the organism's substantial metabolic versatility.

The GO database annotation categorized 1,461 genes into functional classifications. Within the molecular function domain, catalytic activity and binding represented the most prevalent functional assignments. Cellular components were predominantly characterized by fundamental cellular architecture, while biological processes were chiefly represented by metabolic processes, cellular processes, and growth as the three most abundant annotations (Table 3).

CAZy database analysis revealed 71 annotated genes, encompassing the following enzyme classes: auxiliary activities (5), carbohydrate esterases (13), glycoside hydrolases (17), and glycosyl transferases (36).

Comprehensive analysis using the Virulence Factor Database (VFDB) and the Comprehensive Antibiotic Resistance Database (CARD) detected 4 categories encompassing 8 resistance genes (Table 4). VFDB annotation identified 3 functional gene categories comprising 10 genes (Table 5), primarily implicated in bacterial metabolism, metal ion acquisition and homeostasis, immune evasion mechanisms, antioxidant defense and stress adaptation, alongside pathogenicity mechanisms associated with metabolic and structural functions.

Discussion

This study presents the first confirmed isolation of *L. holotrichiae* from a mammalian host, marking a notable expansion in the known ecological and host range of this species. Previously described exclusively from insect gastrointestinal environments, *L. holotrichiae* was generally considered a harmless environmental commensal with no reported pathogenicity in vertebrates. Our identification of three independent strains from actinomycotic abscesses in cattle challenges this assumption and

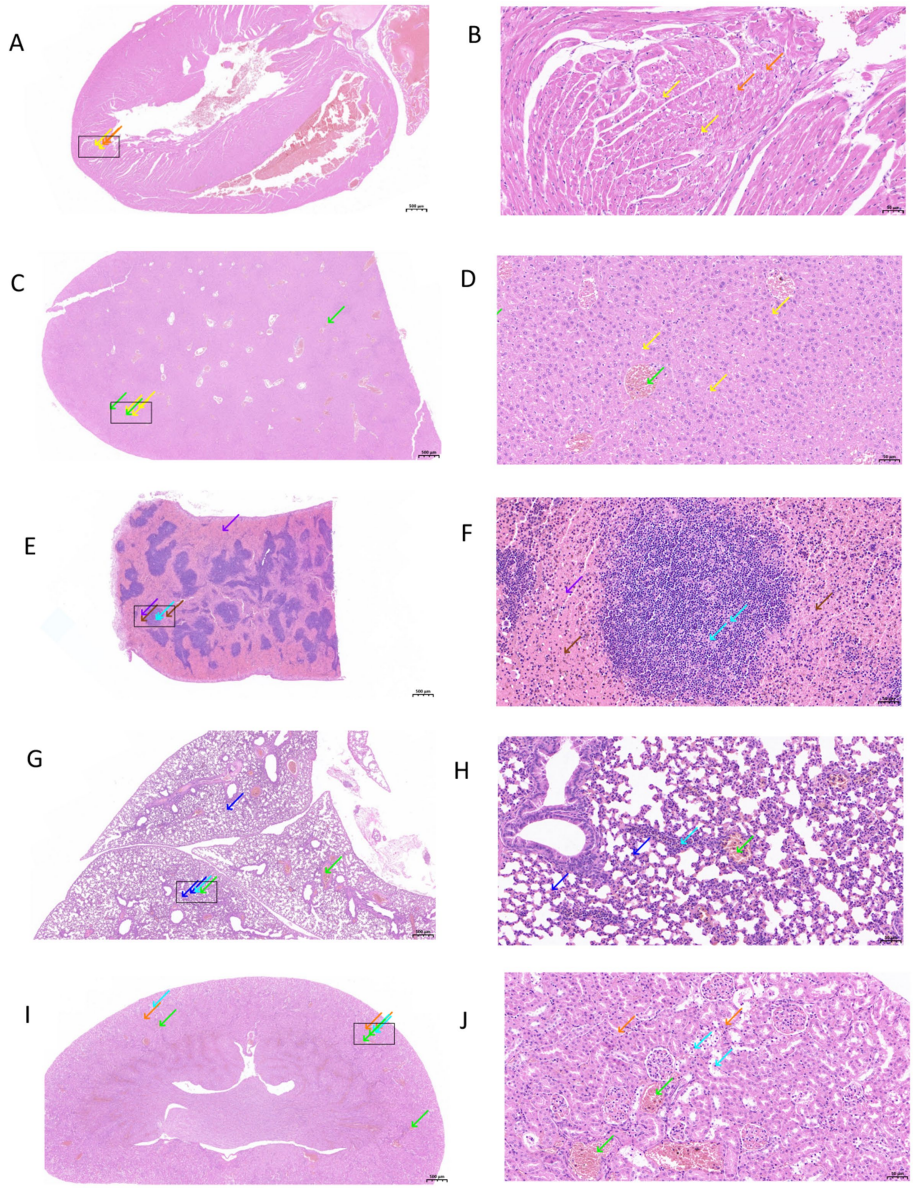

FIGURE 3
Pathogenicity in mice. Experimental infection of BALB/c mice with *L. holotrichiae*. **(A)** Histopathological changes in cardiac tissue (H&E staining, scale bar = 500 μm). The boxed area is the magnified region shown in **(B)**. **(B)** High-power field with a 50 μm scale bar in the same case. A small amount of myocardial cell vacuolar degeneration (yellow arrow), small vacuoles in the cytoplasm, and a small amount of myocardial cell edema (orange arrow) were observed. **(C)** Histopathological changes in liver tissue (H&E staining, scale bar = 500 μm). The boxed area is the magnified region shown in **(D)**. **(D)** High-power field with a 50 μm scale bar in the same case. Mild steatosis (yellow arrows) was observed in liver tissue cells, and small round vacuoles were seen in the cytoplasm. There was no obvious expansion or extrusion of hepatic sinus; more central vein and portal vein congestion (green arrow). **(E)** Histopathological changes in spleen tissue (H&E staining, scale bar = 500 μm). The boxed area is the magnified region shown in **(F)**. **(F)** High-power field with a 50 μm scale bar in the same case. It can be seen that a small amount of lymphocyte punctate necrosis (blue arrows) can be seen in the white pulp of the spleen tissue, and the nucleus is pyknosis and deep staining; a large range of red pulp congestion (purple arrow), red pulp visible amount of brown pigment deposition (brown arrow). **(G)** Histopathological changes in lung tissue (H&E staining, scale bar = 500 μm). The boxed area is the magnified region shown in **(H)**. **(H)** High-power field with a 50 μm scale bar in the same case. A large number of granulocyte infiltration (blue arrow) was seen in the alveolar wall of the lung tissue, and the alveolar wall was slightly thickened and the alveolar septum was widened. Interstitial visible more vascular lumen filled with granulocytes (cyan arrow), more vascular congestion (green arrow). **(I)** Histopathological changes in kidney tissue (H&E staining, scale bar = 500 μm). The boxed area is the magnified region shown in **(J)**. **(J)** High-power field with a 50 μm scale bar in the same case. It can be seen that there was more mild edema of renal tubular epithelial cells (orange arrows) in the cortex of renal tissue, loose and lightly stained cytoplasm, more necrosis and shedding of renal tubular epithelial cells (blue arrows), and pyknosis and deep staining of nucleus. Interstitial no obvious hyperplasia, more vascular congestion (green arrow).

highlights its potential role as an opportunistic pathogen. By combining clinical, microbiological, animal model, and genomic data, we provide compelling evidence that *L. holotrichiae* is not merely a transient contaminant, but a biologically competent organism capable of surviving—and possibly persisting—in vertebrate tissue. These findings contribute to the growing

recognition that traditionally non-pathogenic actinobacteria may possess latent virulence traits and represent a previously underappreciated component of the emerging pathogen landscape in veterinary medicine.

The detection of *L. holotrichiae* in a vertebrate host is consistent with a broader trend in which environmental actinobacteria, once considered benign, are increasingly recognized as opportunistic pathogens under specific ecological or immunological conditions (Hyun et al., 2021; Zhu et al., 2016; Clark and Hodgkin, 2015). Similar shifts have been documented in related genera such as *Corynebacterium*, *Rhodococcus*, and *Gordonia*, many of which now occupy dual roles as both environmental saprophytes and conditional pathogens (Chen and Williamson, 2011). The expansion of this cognition is partly due to the wide application of high-throughput identification technology represented by next-generation sequencing, which enables us to more accurately identify the unusual or difficult-to-culture microorganisms in infected lesions. Therefore, the first appearance of L. holotrichiae in mammalian lesions may reflect its ecological expansion as a potential emerging pathogen, or it may be due to the improvement of detection ability to make it 'visible'. Its ability to form moderate biofilms, tolerate oxidative and osmotic stress, and persist in murine tissues suggests that it is equipped with baseline traits necessary for survival in vertebrate niches (Zhu et al., 2022). Further genomic analysis revealed the genetic basis of host interactions such as adhesion-related genes, sorting enzyme homologs, and iron uptake systems, which are often considered to be part of the conditional pathogenic mechanism (Donlan and Costerton, 2002; Alekshun and Levy, 2007).

Genome analysis showed that the core metabolic framework of *L. holotrichiae* was particularly prominent, and a large number of genes were involved in the metabolic processes of amino acids, carbohydrates and cofactors. The enrichment of some key amino acid biosynthesis genes may contribute to its survival and reproduction in a nutrient-rich host environment (Tamakoshi et al., 1998; Zhang et al., 2012). In addition, there are diverse iron acquisition systems in the genes, indicating that they have the potential to reduce nutritional dependence and respond to the host's 'nutritional immunity' (Alekshun and Levy, 2007; Rodriguez and Smith, 2006). In addition, the annotation of carbohydrate active enzyme (CAZyme) reveals its strong glycosylation ability, which is mainly reflected in the significant advantages of glycosyltransferases (GTs) (36/71, 50.7%). This enzyme system plays a key role in the biosynthesis of cell wall polysaccharides (such as peptidoglycan and lipopolysaccharide), indicating that its cell envelope integrity may be enhanced (Srivastava and Ghosh, 2025; Scaletti et al., 2023). These intrinsic metabolic plasticity, efficient nutrient acquisition mechanisms and enhanced physical barriers together constitute the genetic basis, which may together give *L. holotrichiae* a strong ability to maintain a competitive advantage in harsh environments such as bovine abscesses.

Although the pathogenic potential of *L. holotrichiae* remains to be fully elucidated, genomic analysis has identified homologs of multiple key virulence-associated genes, suggesting its capacity for host interaction and persistent colonization. It harbors a high-affinity iron acquisition system, including *irtA, irtB,* and *fxuB*, which may enable the bacterium to compete for essential iron in the host environment (Rodriguez and Smith, 2006; Ryndak et al., 2010). Additionally, genes such as *zmp1* and *ctpV* reveal its potential mechanisms of host damage and defense (Liang et al., 2021). Global regulatory systems, including *phoP* and *regX3*, may allow the bacterium to sense host-derived signals and adjust its gene expression accordingly (Zwir et al., 2005; Parish, 2003). Furthermore, the presence of *hspX* and *katG* indicates its ability to resist oxidative stress and other environmental pressures encountered during infection (Nono et al., 2025). The coexistence of these genetic traits, encompassing nutrient acquisition, immune regulation, stress response, and regulatory adaptation, suggests that *L. holotrichiae* is genetically equipped with tools facilitating its survival in mammalian hosts.

Genomic analysis further revealed that *L. holotrichiae* carries multiple antimicrobial resistance genes, indicating potential resistance to various drug classes. Bioinformatics predictions identified genes associated with resistance to fluoroquinolones

TABLE 2 Sequencing data statistics table.

Sample ID	Raw data (Mb)	Clean data (Mb)	Clean data Q20 (%)	Clean data Q30 (%)	Clean data GC (%)
LH23001	1311.5	1,138	97.21	92.49	67.43
LH23002	1,286	1117.2	97.25	92.57	67.87
LH23003	1080.6	950	97.34	92.85	68.14

TABLE 3 Statistical table of assembly results.

Sample ID	LH23001	LH23002	LH23003
Gene num	3,010	3,011	3,011
Gene total length	2,924,466	2,924,220	2,924,559
Gene average length	971.	971.	971.
Gene density genes per kb	0.923	0.923	0.924
GC content in gene region	69.3%	69.3%	69.3%
Gene/Geonme	89.7%	89.7%	89.7%
plus Gene num	1,346	1,351	1,332
minus Gene num	1,664	1,660	1,679
tRNA	48	48	48
5S rRNA	1	1	1
16S rRNA	1	1	1
23S rRNA	1	1	1

TABLE 4 Drug resistance gene prediction results.

Primary mechanism	Sub-category	ARO name	Identity %	Coverage %
Antibiotic inactivation	Enzymatic modification	*novA*	*87.5*	94.6
	ABC transporter	*macB*	*81.0*	88.3
		oleC	*86.2*	92.8
	MFS transporter	*tetA*	*81.3*	95.2
Target protection	Ribosomal RNA methylation	*Erm*	*86.8*	90.5
Regulatory genes	Two-component system	*vanS*	*86.3*	94.5
		vanR	*81.3*	84.4
		vanO	*90.5*	94.0

10.3389/fmicb.2025.1716137

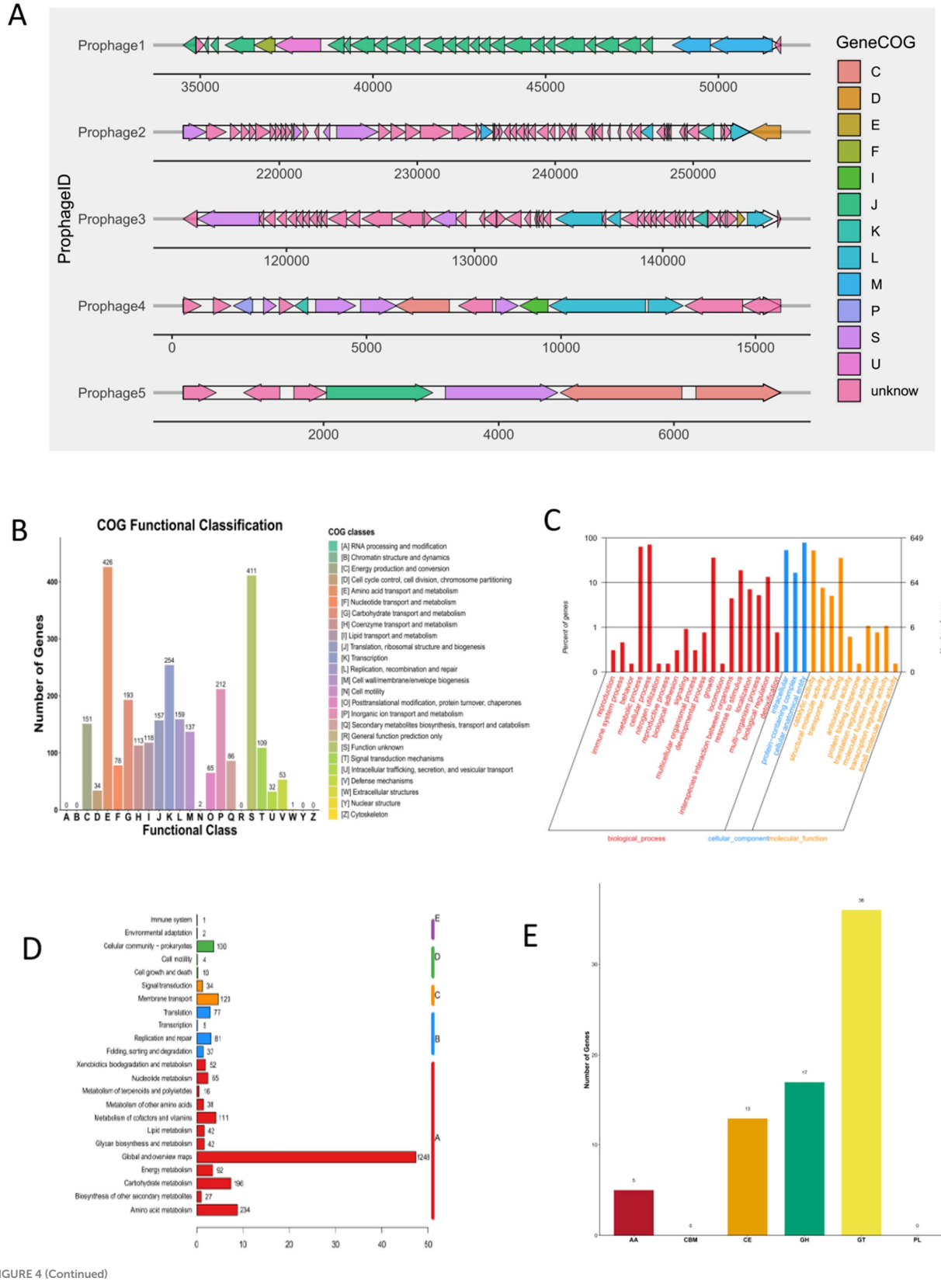

FIGURE 4 (Continued)

(*novA*), macrolides (*Erm, macB, oleC*), tetracyclines (*tetA*), and glycopeptides (*vanS, vanR, vanO*). A significant discrepancy exists between the bacterium's resistance genotype and phenotype, posing additional challenges for clinical drug use. On one hand, the clindamycin-resistant phenotype is fully consistent with the Erm resistance gene it carries, validating the predictive value of genotype

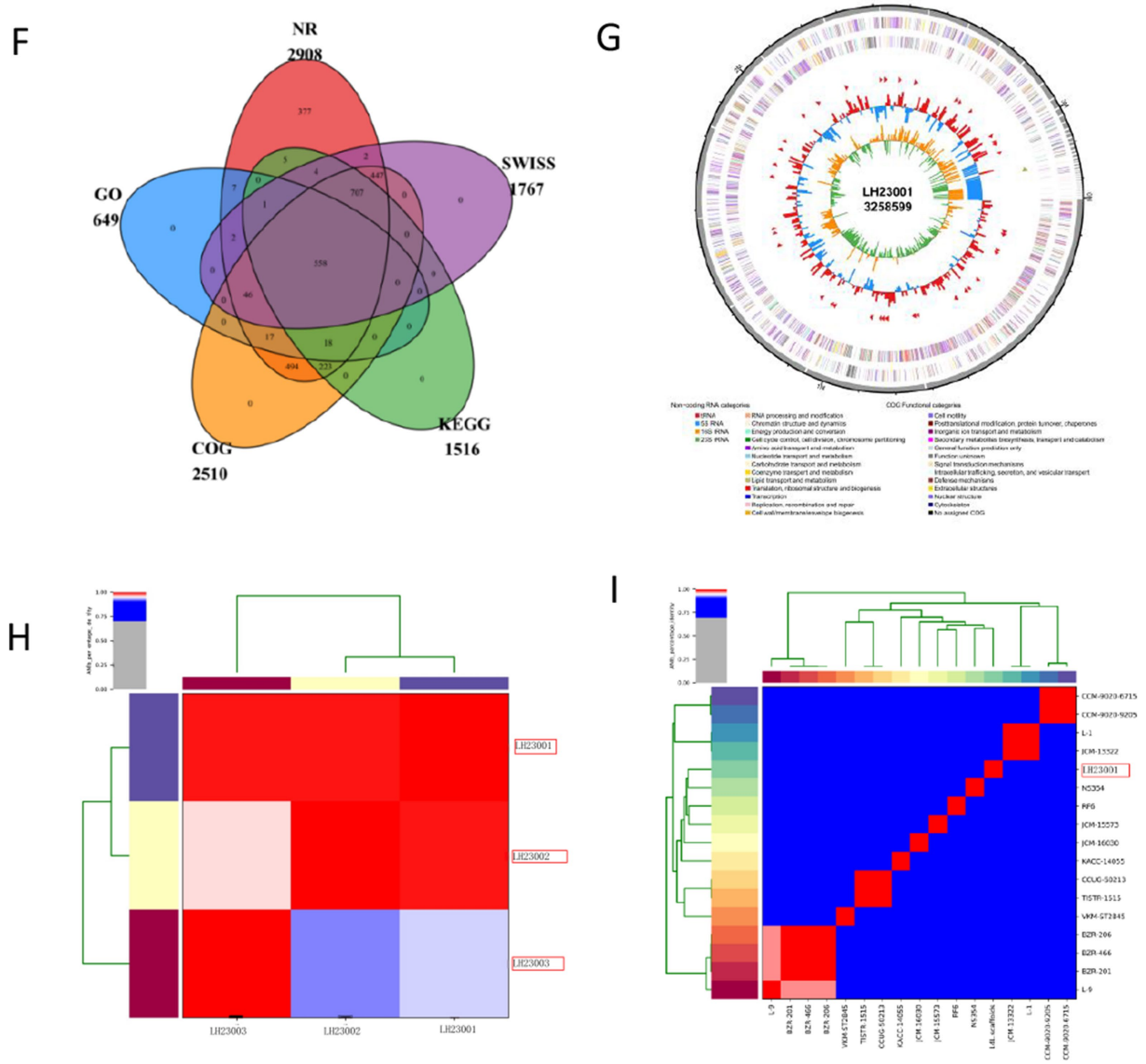

FIGURE 4
Genomic features and functional note. Genomic characteristics of *L. holotrichiae* isolates **(A)** Prophage prediction results. **(B)** Distribution of genes in different COG functional categories. **(C)** KEGG metabolic pathway annotation statistics. **(D)** GO database annotation diagram. **(E)** Annotated CAZy statistical chart. **(F)** Venn diagram of annotation results from five databases. **(G)** Circular genome map of strain LH23001 showing coding sequences (CDS), tRNAs, rRNAs, GC content, and GC skew. **(H)** The average nucleotide identity (ANI) among the three strains. **(I)** The average nucleotide identity (ANI) between the isolates and the reference species of the *Leucobacter*.

for phenotype. On the other hand, despite harboring the *tetA* tetracycline efflux pump gene and glycopeptide resistance-related genes (*vanS, vanR, vanO*), the bacterium remains susceptible to tetracyclines and glycopeptides. This genotype–phenotype inconsistency may stem from complex factors at multiple biological and technical levels (Diarmaid and Andersson, 2017). At the genetic regulatory level, resistance genes may exhibit low basal expression levels or be in a state of transcriptional silencing, with their full activation often relying on induction by specific environmental signals (Fojo, 2007). At the gene function level, the gene sequences identified by bioinformatics predictions may contain nonsense or frameshift mutations in key functional domains, or the function of their expression products may depend on specific cofactors or genetic backgrounds, thereby preventing the formation of fully active resistance proteins. Therefore, the resistance genotype revealed by genomic data should be regarded as a potential resistance risk that may be activated under specific conditions (Ju et al., 2025).

The recovery of *L. holotrichiae* from actinomycotic abscesses in dairy cattle also prompts a re-evaluation of the microbial landscape underlying chronic suppurative infections. During the isolation process, we also isolated various other microorganisms, including *Actinomyces lingnae*, *Staphylococcus aureus*, and *Corynebacterium pyogenes*. Bovine actinomycosis has historically been attributed to *Actinomyces bovis* as a primary pathogen (Ishikawa et al., 2000;

TABLE 5 Virulence gene prediction results.

VF class	Virulence factors	Related genes	Identity %	Coverage %
Copper uptake	Copper exporter	*ctpV*	82.0	94.6
Iron uptake	ABC transporter	*irtA*	90.1	94.4
		irtB	86.0	97.4
	Exochelin (smegmatis)	*fxuB*	81.2	83.8
	ABC transporter (Corynebacterium)	*fagA*	80.3	94.0
Protease	Zn++ metalloprotease	*zmp1*	84.0	95.2
Regulation	PhoP/R	*phoP*	82.4	86.2
	RegX3	*regX3*	86.3	92.3
	Alpha-crystallin	*hspX*	80.2	94.7
	Catalase-peroxidase	*katG*	82.0	89.6

Bauer et al., 2006); however, increasing evidence suggests that polymicrobial interactions and secondary colonizers may significantly contribute to lesion development, persistence, and immune evasion (Szafrański et al., 2017; Routray et al., 2025). The ability of *L. holotrichiae* to persist in purulent lesions, resist multiple antibiotics, and form biofilms suggests that it may act as a co-pathogen or opportunistic invader that exacerbates the chronicity of infection (Penttinen et al., 2016; Kaushik et al., 2020). Its detection in multiple independent samples from distinct anatomical sites strengthens the case for its biological relevance rather than incidental presence. While its precise role in disease pathogenesis remains to be fully elucidated, these findings warrant broader microbial profiling of similar abscesses in cattle and other livestock species. Recognizing atypical taxa such as *L. holotrichiae* as contributors to chronic infections may improve diagnostic sensitivity and inform more effective therapeutic strategies in veterinary practice.

While this study provides the first insights into the genomic characteristics and pathogenic potential of *L. holotrichiae*, several limitations should be acknowledged. First, there are a variety of cultures in the sample, and the isolation of *L. holotrichiae* does not prove that the bacteria are the main pathogenic bacteria. Second, due to the limited number of available strains, genomic analysis is limited and comprehensive pan-genomic analysis cannot be performed. Our conclusions primarily rely on bioinformatic predictions and homology-based comparisons. Although we identified various gene homologs associated with virulence and antimicrobial resistance, it is important to note that some of these may represent conserved physiological components rather than specific pathogenicity determinants. Moreover, the functional significance of these genetic characteristics remains speculative. Additionally, although the mouse infection model used here provides preliminary evidence for *in vivo* colonization, it does not fully replicate the natural infection route, tissue specificity, or host-specific immune response of cattle. Employing stricter thresholds for sequence identity and coverage in future studies would enhance the specificity of such predictions. Second, the functional implications of these genomic features remain speculative, as they have not been functionally validated through molecular experiments such as targeted mutagenesis or transcriptomic analysis. Furthermore, while the murine infection model used here provided preliminary evidence of *in vivo* colonization, it does not fully recapitulate the natural routes of infection, tissue tropism, or host-specific immune responses in cattle. Therefore, the assessment of its pathogenic potential and ecological role remains provisional. Future investigations should expand epidemiological surveillance, incorporate a greater diversity of isolates to decipher genomic plasticity, and employ integrated approaches—including functional genetics, *in vivo* gene expression analysis, and CRISPR-based functional assays—to elucidate the mechanistic basis of its pathogenicity and define the roles of key genes in the adaptation and virulence of *L. holotrichiae*.

Conclusion

This study is the first to isolate and identify the species *Leucobacter holotrichiae* from mixed cultures of bovine actinomycotic abscesses. This finding significantly expands the known host range of this species and suggests its potential role as a novel opportunistic pathogen. Through an integrated approach combining microbiological phenotypic characterization, a murine infection model, and whole-genome sequencing, we demonstrated that this bacterium is capable of colonizing and persisting in a mammalian host. Key attributes supporting this capability include robust biofilm formation, broad stress tolerance, and a genetic repertoire harboring various features potentially involved in host interaction, such as adhesion, iron acquisition, and cell envelope fortification systems. It is crucial to emphasize that this bacterium was isolated from a polymicrobial abscess context. Therefore, the precise pathogenic role of *L. holotrichiae* in bovine actinomycosis—whether it acts as a primary pathogen, a co-pathogen, or a secondary colonizer—remains to be fully elucidated. In conclusion, our research broadens the understanding of the ecological diversity within the genus *Leucobacter* and underscores the importance of ongoing surveillance of environmental actinobacteria. Under specific conditions, such microorganisms may cross species barriers and emerge as potential sources of infection in veterinary medicine and even public health. Future investigations employing functional genomics, epidemiological surveys, and polymicrobial infection models are warranted to definitively establish the pathogenicity of *L. holotrichiae* and decipher its true transmission cycle in nature.

Data availability statement

The datasets presented in this study can be found in online repositories. The names of the repository/repositories and accession number(s) can be found in the article/supplementary material.

Ethics statement

The animal study was approved by Shihezi University Bioethics Committee. The study was conducted in accordance with the local legislation and institutional requirements.

Author contributions

YL: Data curation, Investigation, Methodology, Project administration, Software, Validation, Writing – original draft, Writing – review & editing. BQ: Conceptualization, Data curation, Formal analysis, Writing – review & editing. SC: Writing – review & editing. RZ: Investigation, Validation, Writing – original draft. LJ: Formal analysis, Investigation, Writing – original draft. MZ: Project administration, Supervision, Writing – original draft. JC: Writing – original draft. MD: Validation, Writing – review & editing. KL: Writing – review & editing. CX: Methodology, Supervision, Visualization, Writing – review & editing. YQ: Funding acquisition, Resources, Visualization, Writing – review & editing.

Funding

The author(s) declare that financial support was received for the research and/or publication of this article. This research was supported by the National Natural Science Foundation of China (Grant nos. 32460898 and 31760737); the Key Core Technology Research Project of Xinjiang Production and Construction Corps Agriculture (Grant no. 2023AA310); and the Tianshan Talent Program (Grant no. 2024D14009, "Three Rural Backbone Talent - 2024 - 97").

Conflict of interest

The authors declare that the research was conducted in the absence of any commercial or financial relationships that could be construed as a potential conflict of interest.

Generative AI statement

The authors declare that no Gen AI was used in the creation of this manuscript.

Any alternative text (alt text) provided alongside figures in this article has been generated by Frontiers with the support of artificial intelligence and reasonable efforts have been made to ensure accuracy, including review by the authors wherever possible. If you identify any issues, please contact us.

Publisher's note

References

Abbey, T. C., and Deak, E. (2019). What's new from the CLSI subcommittee on antimicrobial susceptibility testing M100, 29th edition. *Clin. Microbiol. Newsl.* 41, 203–209. doi: 10.1016/j.clinmicnews.2019.11.002

Alekshun, M. N., and Levy, S. B. (2007). Molecular mechanisms of antibacterial multidrug resistance. *Cell* 128, 1037–1050. doi: 10.1016/j.cell.2007.03.004

Barber, M. F., and Fitzgerald, J. R. (2024). Mechanisms of host adaptation by bacterial pathogens. *FEMS Microbiol. Rev.* 48:fuae017. doi: 10.1093/femsre/fuae019

Bauer, P., Sultan, S., and Atienza, P. (2006). Perianal actinomycosis: diagnostic and management considerations. *Gastroenterol. Clin. Biol.* 30, 29–32. doi: 10.1016/s0399-8320(06)73070-9

Berendonk, T. U., Manaia, C. M., Merlin, C., Fatta-Kassinos, D., Cytryn, E., Walsh, F., et al. (2015). Tackling antibiotic resistance: the environmental framework. *Nat. Rev. Microbiol.* 13, 310–317. doi: 10.1038/nrmicro3439

Besemer, J., and Borodovsky, M. (2005). GeneMark: web software for gene finding in prokaryotes, eukaryotes and viruses. *Nucleic Acids Res.* 33, W451–W454. doi: 10.1093/nar/gki487

Boxberger, M., Magnien, S., Antezack, A., Rolland, C., Makoa Meng, M., Lo, C. I., et al. (2023). *Leucobacter manosquensis* sp. nov.—a novel bacterial species isolated from healthy human skin. *Microorganisms* 11:2535. doi: 10.3390/microorganisms11102535 IF: 4.2 Q2

Brook, I. (2008). Actinomycosis: diagnosis and management. *South. Med. J.* 101, 1019–1023. doi: 10.1097/SMJ.0b013e3181864c1f

Chen, S. H., and Williamson, P. R. (2011). Lessons from cryptococcal laccase: from environmental saprophyte to pathogen. *Curr. Fungal Infect. Rep.* 5:233. doi: 10.1007/s12281-011-0069-3

Clark, L. C., and Hodgkin, J. (2015). *Leucobacter musarum* subsp. *musarum* sp. nov., subsp. nov., *Leucobacter musarum* subsp. *japonicus* subsp. nov., and *Leucobacter celer* subsp. *astrifaciens* subsp. nov., three nematopathogenic bacteria isolated from *Caenorhabditis*, with an emended description of *Leucobacter celer*. *Int. J. Syst. Evol. Microbiol.* 65, 3977–3984. doi: 10.1099/ijsem.0.000523

Combs, M. A., Tufts, D. M., Adams, B., Lin, Y. P., Kolokotronis, S. O., and Diuk-Wasser, M. A. (2023). Host adaptation drives genetic diversity in a vector-borne disease system. *PNAS Nexus.* 2:pgad247. doi: 10.1093/pnasnexus/pgad234

Diarmaid, H., and Andersson, D. I. (2017). Environmental and genetic modulation of the phenotypic expression of antibiotic resistance. *FEMS Microbiol. Rev.* 3:3. doi: 10.1093/femsre/fux004

Donlan, R. M., and Costerton, J. W. (2002). Biofilms: survival mechanisms of clinically relevant microorganisms. *Clin. Microbiol. Rev.* 15, 167–193. doi: 10.1128/CMR.15.2.167-193.2002

Duar, R. M., Frese, S. A., Lin, X. B., Fernando, S. C., Burkey, T. E., Tasseva, G., et al. (2017). Experimental evaluation of host adaptation of *Lactobacillus reuteri* to different vertebrate species. *Appl. Environ. Microbiol.* 83:e00132-17. doi: 10.1128/AEM.00132-17

Figueiredo, L. M., Trindade, S. C., Sarmento, V. A., de Oliveira, T. F., Muniz, W. R., and Valente, R. O. (2013). Actinomycotic osteomyelitis of the mandible: an unusual case. *Oral Maxillofac. Surg.* 17, 299–302. doi: 10.1007/s10006-012-0381-2

Fojo, T. (2007). Multiple paths to a drug resistance phenotype: mutations, translocations, deletions and amplification of coding genes or promoter regions, epigenetic changes and microRNAs. *Drug Resist. Updat.* 10, 59–67. doi: 10.1016/j.drup.2007.02.002

Greisen, K., Loeffelholz, M., Purohit, A., and Leong, D. (1994). PCR primers and probes for the 16S rRNA gene of most species of pathogenic bacteria, including bacteria found in cerebrospinal fluid. *J. Clin. Microbiol.* 32, 335–351. doi: 10.1128/jcm.32.2.335-351.1994

Hyun, D. W., Sung, H., Kim, P. S., Yun, J. H., and Bae, J. W. (2021). *Leucobacter coleopterorum* sp. nov., *Leucobacter insecticola* sp. nov., and *Leucobacter viscericola* sp.

nov., isolated from the intestine of the diving beetles, *Cybister brevis* and *Cybister lewisianus*, and emended description of the genus *Leucobacter*. *J. Microbiol.* 59, 360–368. doi: 10.1007/s12275-021-0472-6

Ishikawa, T., Tojima, H., and Yamada, C. (2000). Actinomycosis in the face and neck. Report of 4 cases. *Pract. Otorhinolaryngol.* 93, 1041–1046. doi: 10.5631/jibirin.93.1041

Ju, J., Lu, X., Gao, Z., Yin, H., Xu, S., and Li, H. (2025). Genome sequencing of an antibiotic-resistant strain of *Leucobacter* sp., HNU-1 and its developmental toxicity to *Caenorhabditis elegans*. *Int J Mol Sci* 26:3673. doi: 10.3390/ijms26083673

Kaushik, M. S., Pati, S. R., Soni, S., Mishra, A., Sushmita, K., and Kateriya, S. (2020). Establishment of optogenetic modulation of cAMP for analyzing growth, biofilm formation, and virulence pathways of bacteria using a light-gated cyclase. *Appl. Sci.* 10:5535. doi: 10.3390/app10165535 IF: 2.5 Q2

Lagesen, K., Hallin, P., Rødland, E. A., Staerfeldt, H. H., Rognes, T., and Ussery, D. W. (2007). RNAmmer: consistent and rapid annotation of ribosomal RNA genes. *Nucleic Acids Res.* 35, 3100–3108. doi: 10.1093/nar/gkm160

Li, R., Hu, K., Ding, Y., Liao, X., Wang, X., Zhou, Y., et al. (2024). First report of *Leucobacter aridicollis* causes leaf spot disease on *Dendrobium officinale* in Guizhou Province, China. *Crop Prot.* 184:106779. doi: 10.1016/j.cropro.2024.106779

Liang, W., Mancl, J., Zhao, M., and Tang, W. J. (2021). Structural analysis of *Mycobacterium tuberculosis* M13 metalloprotease Zmp1 open states. *Structure* 29, 709–720.e3. doi: 10.1016/j.str.2020.12.002

Lowe, T. M., and Eddy, S. R. (1997). TRNAscan-se: a program for improved detection of transfer RNA genes in genomic sequence. *Nucleic Acids Res.* 25, 0955–0964. doi: 10.1093/nar/25.5.955

Nono, V. N., Nantia, E. A., Mutshembele, A., Teagho, S. N., Simo, Y. W. K., Takong, B. S., et al. (2025). Prevalence of katG and inhA mutations associated with isoniazid resistance in *Mycobacterium tuberculosis* clinical isolates in Cameroon. *BMC Microbiol.* 25, 1–13. doi: 10.1186/s12866-025-03816-9

Parish, T. (2003). The senX3-regX3 two-component regulatory system of *Mycobacterium tuberculosis* is required for virulence. *Microbiology* 149, 1423–1435. doi: 10.1099/mic.0.26245-0

Penttinen, R., Kinnula, H., Lipponen, A., Bamford, J. K., and Sundberg, L. R. (2016). High nutrient concentration can induce virulence factor expression and cause higher virulence in an environmentally transmitted pathogen [J]. *Microb. Ecol.* 72, 955–964.

Poullain, V., and Nuismer, S. L. (2012). Infection genetics and the likelihood of host shifts in coevolving host-parasite interactions. *Am. Nat.* 180, 618–628. doi: 10.1086/667889

Rodriguez, G. M., and Smith, I. (2006). Identification of an ABC transporter required for iron acquisition and virulence in *Mycobacterium tuberculosis*. *J. Bacteriol.* 188, 424–430. doi: 10.1128/JB.188.2.424-430.2006

Routray, S. P., Mahapatra, S., Nayak, D. S. K., Sahoo, S., Das, B. S., Subudhi, E., et al. (2025). PerSceptoMed 1.0: an advanced machine learning model for demographic-based antibiotic susceptibility prediction in *Pseudomonas aeruginosa* infections. *Eng. Appl. Artif. Intell.* 141:109773. doi: 10.1016/j.engappai.2024.109773

Ryndak, M. B., Wang, S., Smith, I., Rodriguez, G. M. (2010). The *Mycobacterium tuberculosis* high-affinity iron importer, IrtA, contains an FAD-binding domain. *J. Bacteriol.* doi: 10.1128/JB.00223-09

Scaletti, E. R., Pettersson, P., Patrick, J., Shilling, P. J., Westergren, R. G., Daley, D. O., et al. (2023). Structural and functional insights into the *Pseudomonas aeruginosa* glycosyltransferase WaaG and the implications for lipopolysaccharide biosynthesis. *J. Biol. Chem.* 299:105256. doi: 10.1016/j.jbc.2023.105256

Shin, N. R., Kim, M. S., Jung, M. J., Roh, S. W., Nam, Y. D., Park, E. J., et al. (2011). *Leucobacter celer* sp. nov., isolated from Korean fermented seafood. *Int. J. Syst. Evol. Microbiol.* 61, 2359–2363. doi: 10.1099/ijs.0.026211-0

Simpson, J. T., Wong, K., Jackman, S. D., Schein, J. E., Jones, S. J., and Birol, I. (2009). ABySS: a parallel assembler for short read sequence data. *Genome Res.* 19, 1117–1123. doi: 10.1101/gr.089532.108

Srivastava, P., and Ghosh, S. (2025). Insights into functional divergence, catalytic versatility and specificity of small molecule glycosyltransferases. *Int. J. Biol. Macromol.* 292:138821. doi: 10.1016/j.ijbiomac.2024.138821

Sturm, G., Jacobs, J., Spröer, C., Schumann, P., and Gescher, J. (2011). *Leucobacter chromiiresistens* sp. nov., a chromate-resistant strain. *Int. J. Syst. Evol. Microbiol.* 61, 927–931. doi: 10.1099/ijs.0.022780-0

Szafrański, S. P., Winkel, A., and Stiesch, M. (2017). The use of bacteriophages to biocontrol oral biofilms. *J. Biotechnol.* 250, 29–44. doi: 10.1016/j.jbiotec.2017.01.023

Takeuchi, M., Weiss, N., Schumann, P., and Yokota, A. (1996). *Leucobacter komagatae* gen. Nov., sp. nov., a new aerobic gram-positive, nonsporulating rod with 2,4-diaminobutyric acid in the cell wall. *Int. J. Syst. Bacteriol.* 46, 967–971. doi: 10.1099/00207713-46-4-967

Tamakoshi, M., Yamagishi, A., and Oshima, T. (1998). The organization of the leuC, leuD and leuB genes of the extreme thermophile *Thermus thermophilus*. *Gene* 222, 125–132. doi: 10.1016/S0378-1119(98)00482-X

Wani, A. K., Akhtar, N., Sher, F., Navarrete, A. A., Américo-Pinheiro, J. H. P. (2022). Microbial adaptation to different environmental conditions: molecular perspective of evolved genetic and cellular systems. *Arch. Microbiol.* 204:144. doi: 10.1007/s00203-022-02757-5

Xu, M., Guo, L., Gu, S., Wang, O., Zhang, R., Peters, B. A., et al. (2020). TGS-gapcloser: a fast and accurate gap closer for large genomes with low coverage of error-prone long reads. *Gigascience* 9:giaa094. doi: 10.1093/gigascience/giaa094

Zhang, Y. J., Ioerger, T. R., Huttenhower, C., Long, J. E., Sassetti, C. M., Sacchettini, J. C., et al. (2012). Global assessment of genomic regions required for growth in *Mycobacterium tuberculosis*. *PLoS Pathog.* 8:e1002946. doi: 10.1371/journal.ppat.1002946

Zhu, J., Che, J., Jiang, X., Ma, M., Guan, D., Li, L., et al. (2022). *Leucobacter chinensis* sp. nov., with plant growth-promoting potential isolated from field soil after seven-years continuous maize cropping. *Int. J. Syst. Evol. Microbiol.* 72. doi: 10.1099/ijsem.0.005417

Zhu, D., Zhang, P., Li, P., Wu, J., Xie, C., Sun, J., et al. (2016). Description of *Leucobacter holotrichiae* sp. nov., isolated from the gut of *Holotrichia oblita* larvae. *Int. J. Syst. Evol. Microbiol.* 66, 1857–1861. doi: 10.1099/ijsem.0.000957

Zwir, I., Shin, D., Kato, A., Nishino, K., Latifi, T., Solomon, F., et al. (2005). Dissecting the PhoP regulatory network of Escherichia coli and *Salmonella enterica*. *Proc. Natl. Acad. Sci. USA* 102, 2862–2867. doi: 10.1073/pnas.0408238102

frontiers | Frontiers in Microbiology

TYPE Original Research
PUBLISHED 21 January 2026
DOI 10.3389/fmicb.2025.1710390

OPEN ACCESS

EDITED BY
Lei Deng,
Chinese Academy of Agricultural Sciences, China

REVIEWED BY
Yuwen Dong,
University of Pennsylvania, United States
Yao Zhu,
Chinese Academy of Agricultural Sciences, China

*CORRESPONDENCE
Xianhui Huang
✉ xhhuang@scau.edu.cn
Lianxiang Wang
✉ imssci@126.com

†These authors have contributed equally to this work and share first authorship

RECEIVED 22 September 2025
REVISED 10 November 2025
ACCEPTED 24 November 2025
PUBLISHED 21 January 2026

CITATION
Yang D, Xu J, Hu M, Zhu J, Ren B, Huang X and Wang L (2026) Epidemiological investigation and pathogenicity of *Streptococcus suis* in eastern China. *Front. Microbiol.* 16:1710390. doi: 10.3389/fmicb.2025.1710390

Epidemiological investigation and pathogenicity of *Streptococcus suis* in eastern China

Dehong Yang[1,2†], Jingyu Xu[1,2†], Meiling Hu[1,2], Jinmei Zhu[1], Baihua Ren[2], Xianhui Huang[1*] and Lianxiang Wang[2*]

[1]College of Veterinary Medicine, South China Agricultural University, Guangzhou, China, [2]Guangdong Enterprise Key Laboratory for Animal Health and Environmental Control, Wen's Foodstuff Group Co. Ltd, Yunfu, China

Streptococcus suis (S. suis), a zoonotic gram-positive bacterium, is the etiological factor for septicemia and pneumonia in humans and pigs and poses a global public health threat. To date, epidemiological data from large-scale investigations of *S. suis* in swine populations across eastern China are still limited. This study investigated the serotypes, virulence genes, and pathogenicity of the isolates from 89 pig farms across 12 regions from 2022 to 2024. The overall infection and isolation rates were 59.59% (851/1728) and 16.1% (137/851), respectively. The infection rate was the highest in Guangdong Province (72.41%) (63/87) and the lowest in Hubei Province (43.75%) (7/16). Suckling piglets, nursery pigs, fattening pigs, and pregnant sows are susceptible to S. suis infection, with infection rates as high as 60%. The infection rates in spring, summer, autumn, and winter were 70.72% (215/304), 60.67% (344/567), 40.62% (132/325), and 68.97% (160/232), respectively. Serotype analysis of 137 isolates revealed increased serotype diversity in coastal provinces, especially in Guangdong, Jiangsu, and Shandong. Serotype 1 was detected in Liaoning. The most common serotype was serotype 2 (30.66%), especially in Guangdong, Guangxi, and Anhui, followed by serotype 7 (21.17%) and serotype 9 (10.95%). Virulence gene analysis revealed that the occurrence of *gdh*, *gapdh*, and *orf2* (>89%) was high, whereas that of 89 k and epf was low (≤ 28.47%). Serotypes 1 and 7 frequently harbored mrp and gdh but often lacked 89 k and epf. Serotype 2 and serotype NT harbored all the tested genes, withlow 89 k occurrence rates. The occurrence rates of sly and epf (≤43.75%) werelow for serotype 9. Animal challenge experiments demonstrated that Serotype 2 induced acute death in Landrace pigs aged 42 days, with a mortality rate of 100%. In contrast, Serotype 7 was associated with low mortality rates (37.5%) and induced mild pathological symptoms, including pneumonia, myocarditis, and yellow effusion in the thoracic cavity. This study provides useful insights for the prevention and control of S. suis infection on pig farms in China.

KEYWORDS

***Streptococcus suis*, epidemiological investigation, serotype, virulence gene, pathogenicity**

1 Introduction

S. suis, a gram-positive bacterium that typically appears in pairs or short chains, can infect various animals, including pigs (Mi et al., 2021), horses (Devriese and Haesebrouck, 1992), dogs, and cats (Salasia et al., 1994), as well as humans (Bamphensin et al., 2021). In pigs, *S. suis* infections cause septicaemia, pneumonia, arthritis, and endocarditis. Moreover, *S. suis*

infection can lead to symptoms such as septicemia, skin ulcers, and meningitis (Luque et al., 1998).

S. suis was initially classified into 35 serotypes on the basis of the presence of capsular antigens (Liu et al., 2013). However, advances in molecular techniques have refined the classification system. Currently, *S. suis* is divided into 29 classical serotypes (Nomoto et al., 2015). The serotype distribution of *S. suis* exhibits marked regional variation. Serotype 2, the most virulent global strain, accounts for 74.7% of human infections and dominates swine populations in Asia (44.2%) and North America (24.3%), whereas serotype 9 prevails in Europe (61%) (Haas and Grenier, 2018). Notably, South Korea shows an anomalous predominance of serotypes 3/4, and European countries such as Spain and the Netherlands display evolving serotype patterns (9/2/7) (Wisselink et al., 2000). The paucity of data regarding *S. suis* serotype patterns in the swine population of eastern China presents considerable concern and a latent risk to regional disease control efforts, underscoring the urgency of forming an interdisciplinary surveillance network to mitigate this zoonotic threat.

The pathogenicity of *S. suis* is closely related to its virulence factors. The main virulence genes of *S. suis* include *mrp*, *epf*, *sly*, *orf2*, *fbps*, *gdh, gapdh*, and *89 k*, which are involved in the pathogenic process. Among the virulence genes, *mrp*, *epf*, and *sly* are considered the key virulence factors of *S. suis* (Silva et al., 2006). In Eurasian strains, these genes are positively correlated with pathogenicity. The frequent phenotypes of diseased and healthy pigs are $mrp^{+}epf^{+}sly^{+}$ and *mrp*−*epf*−*sly*−, respectively (Petrocchi-Rilo et al., 2021). However, some highly virulent strains from Canada do not express *mrp*, *epf*, or *sly* (Gottschalk et al., 1998). Additionally, avirulent strains harboring all three of these genes have not been identified (Vecht et al., 1992). *Sly*, which encodes a cytotoxic hemolysin, may enhance pathogenicity by modulating complement deposition and promoting the penetration of *S. suis* into deeper tissues (King et al., 2001). *Epf* serves as a phenotypic marker of virulence (Wisselink et al., 1999). The scarcity of systematic data on virulence gene distributions, dominant phenotypes, and their pathogenic associations—stemming from limited *S. suis* research in eastern China-severely hinders the development of targeted interventions.

Prompted by the 2005 human outbreak in Sichuan, China, *S. suis*, a key zoonotic pathogen, has been closely monitored; however, data on its epidemiology and virulence genotypes in eastern China are sparse. This study, which was conducted from 2022 to 2024 across 89 pig farms in 12 provinces, bridges this knowledge gap by serotyping, virulence genotyping, and pathogenicity assessment of dominant serotypes, thereby providing essential evidence for evidence-based, precise control measures in China's swine industry.

2 Materials and methods

2.1 Sample collection

This study collected 1,428 samples from over 89 swine operations, including both individual farmers and large-scale commercial farms (about 5 million pigs) across 12 provinces in China (Anhui (129), Guangdong (87), Guangxi (143), Hainan (68), Hubei (16), Hunan (246), Jiangsu (119), Jiangxi (85), Liaoning (26), Shandong (98), Shanxi (119), and Shaanxi (291)) between 2022 and 2024. The samples included nasopharyngeal swabs, pleural effusion, joint fluid from the legs, lungs, brain tissue, and vaginal pus from diseased piglets, nursery pigs, fattening pigs, and breeding pigs suspected of having *S. suis* infections. These pigs presented symptoms such as fever, swollen joints, and emaciation. Post-mortem examinations revealed septicemia, polyserositis, pneumonia, myocarditis, and hemorrhaging in multiple organs. All sample collections were conducted with the informed consent of the managers of each pig farm.

2.2 Bacterial isolation and identification

The samples were inoculated on tryptic soy agar (TSA, Difco Laboratories, Detroit, MI, USA) plates containing 5% bovine serum and incubated aerobically at 37 °C for 48 h. The colonies were selected and cultured further in Todd-Hewitt broth (THB) with shaking at 37 °C for 16 to 18 h. The broth cultures were subjected to polymerase chain reaction (PCR) to identify *S. suis* through amplification of the *gdh* gene (Kerdsin et al., 2012). Positive strains were streaked onto THB plates for colony purification. The purified strains were heated in boiling water for 10 min and centrifuged at 13,000 × g for 10 min. The supernatant was stored at −20 °C until use.

2.3 Serotyping

The methods of previous studies were used (Kerdsin et al., 2014; Kerdsin et al., 2012; Liu et al., 2013; Smith et al., 1999). The serotypes of the isolated *S. suis* strains were determined using the primers listed in Table 1 (synthesized by Sangon Biotech (Shanghai) Co., Ltd.). PCR amplification was performed using 2 × Taq Quick-Load Master Mix (CW Biotech, Beijing, China) under the following conditions: 95 °C for 5 min (initial denaturation), followed by 35 cycles of 95 °C for 1 min (denaturation), 56 °C for 1 min (annealing), 72 °C for 1 min (annealing), and 72 °C for 5 min (final extension). Each sample was analyzed in triplicate. The amplicons were analyzed using 2% agarose gel electrophoresis.

2.4 Virulence gene detection

Previous methods have been used (Ju et al., 2008; Kerdsin et al., 2012; Pan et al., 2020). The virulence genes in the isolated *S. suis* strains were identified using the primers listed in Table 2 [also synthesized by Sangon Biotech (Shanghai) Co., Ltd.]. The detection method was based on previous*ly* reported PCR protocols targeting the following genes: *gdh*, *fbps*, *sly*, *orf2*, *mrp*, *89 k*, *gapdh*, and *epf*.

2.5 Animal pathogenicity experiment

The pathogenicity of isolates SS2-1 (serotype 2) and SS7-1 (serotype 7) was evaluated in 24 healthy Landrace pigs aged 42 days. These pigs tested negative for *S. suis* and other exogenous pathogens, including classical swine fever (CSF), African swine fever (ASF), porcine reproductive and respiratory syndrome (PRRS), and porcine circovirus (PCV). The pigs were randomly divided into the following three groups (seven pigs per group): the SS2, SS7, and control groups. All pigs had free access to water and food.

10.3389/fmicb.2025.1710390

TABLE 1 Primers for identifying and serotyping *S. suis*.

Serotype	Sequence (5′–3′)	Annealing temperature (°C)	PCR product sizes (bp)	Gene	Reference
All	F: TTCTGCAGCGTATTCTGTCAAACG	55	695	gdh	Kerdsin et al. (2012)
	R: TGTTCCATGGACAGATAAAGATGG				
1	F: GGCGGTCTAGCAGATGCTCG	56	440	cps1I	Smith et al. (1999)
	R: GCGAACTGTTAGCAATGAC				
2	F: CAAACGCAAGGAATTACGGTATC	56	675	cps2J	Smith et al. (1999)
	R: GAGTATCTAAAGAATGCCTATTG				
3	F: TGGGAGAAGGCAGAAAGTACGAGA	60	1,273	cps3J–cps3K	Kerdsin et al. (2012)
	R: ACCCCCAGAAGAGCCGAAGGA				
4	F: ACTTGGAGTTGTCGGAGTAGTGCT	60	783	cps4M–cps4N	Kerdsin et al. (2012)
	R: ACCGCGATGGATAGGCCGAC				
5	F: TGATGGCGGAGTTTGGGTCGC	60	166	cps5N	Kerdsin et al. (2012)
	R: CGTAACAACCGCCCCAGCCG				
6	F: TACGGTCTCCCTTGCCTGTA	60	325	cps6I	Kerdsin et al. (2014)
	R: AACTCAGCTAGTGCTCCACG				
7	F: GATGATTTATGGCACCCGAGTAAGC	60	150	cps7H	Kerdsin et al. (2012)
	R: AGTCACAATTGCTGGTCCTGACACC				
8	F: ATGGGCGTTGGCGGGAGTTT	60	320	cps8H	Kerdsin et al. (2012)
	R: TTACGGCCCCCATCACGCTG				
9	F: GGGATGATTGCTCGACAGAT	60	300	cps9H	Kerdsin et al. (2012)
	R: CCGAAGTATCTGGGCTACTG				
10	F: TTACGAGGGGATTCTGGGGT	60	153	cps10M	Kerdsin et al. (2014)
	R: CGGGACAACAGATGGAACCT				
11	F: TACAGTGCTTGCAGCCCTAC	60	896	cps11N	Kerdsin et al. (2014)
	R: CGACTTGTCGTGCCCTGAT				
12	F: TGTGGCGATAGGACAACAGG	60	209	cps12J	Kerdsin et al. (2014)
	R: ACCAAGAAGTTTCCGCCTGA				
13	F: CTGGTGCTGCAATTTCGCTT	60	1,135	cps13L	Kerdsin et al. (2014)
	R: GCAGACTAGCTGCAGTTCCA				
14	F: AATCATGGAATAAAGCGGAGTACAG	60	550	cps14J	Kerdsin et al. (2012)
	R: ACAATTGATACGTCAAAATCCTCACC				
15	F: GCAAGAAAGCTTCCGGATGGA	60	274	cps15K	Kerdsin et al. (2014)
	R: CAAGAGAGTGTGCAACCCCA				
16	F: TGGAGGAGCATCTACAGCTCGGAAT	60	202	cps16K	Kerdsin et al. (2012)
	R: TTTGTTTGCTGGAATCTCAGGCACC				
17	F: ACTTGGGTTGGAATGGCGAA	60	906	cps17O	Kerdsin et al. (2014)
	R: ACCACCGAAAGTCAGGTCAC				
18	F: CGGGGCAGTCTTACTCATGG	60	432	cps18N	Kerdsin et al. (2014)
	R: ATGACAGCGAAACGGACAGA				
19	F: AGCAGGGTTGCGTATGGCGG	60	1,024	cps19L	Kerdsin et al. (2012)
	R: ACAAGCACCAGCAAAGACCGCA				
20	F: TAATCGTTGCCTTTGAGCAT	58	938	cps20I	Liu et al. (2013)
	R: CGCTATATAAGGAAACCTCGG				

(Continued)

TABLE 1 (Continued)

Serotype	Sequence (5′–3′)	Annealing temperature (°C)	PCR product sizes (bp)	Gene	Reference
21	F: GGTGGCAAGGAGAGCAAAGT	60	325	cps21N	Kerdsin et al. (2014)
	R: ACATGGTAAGCCATTGCTGGA				
22	F: AGGATCGGTAAGTTTAGGTACA	58	158	cps22K	Liu et al. (2013)
	R: ATGCAGTAAAACACGAAAACAA				
23	F: TGCTCAACAAACGCAGCAAA	60	454	cps23I	Kerdsin et al. (2014)
	R: TGACTGGTACATCTGCAGCC				
24	F: ACCCGGAAAAACCAGGAGTT	60	500	cps24L	Kerdsin et al. (2014)
	R: ACCAATCAATGCCAAGCGAC				
25	F: GGAGGAGCTGCGGGCTCATA	60	1,211	cps25M–cps25N	Kerdsin et al. (2012)
	R: TGGCCACAACCTGGATGCGTT				
26	F: CAAAATTCCTGGATTAACGCTT	58	315	cps26P	Liu et al. (2013)
	R: CGATCTGAGGACTTATCAAGAA				
27	F: CTACGCCAATCGAAGCCAGA	60	506	cps27K	Kerdsin et al. (2014)
	R: CCAGTAAGAAGCCTGTCGCA				
28	F: GGACTTCGGTACCTTAGCGT	60	865	cps28L	Kerdsin et al. (2014)
	R: CTCCAGCACATTCCCGTACC				
29	F: GTGCGGGCGTTATTTTTGGT	60	435	cps29L	Kerdsin et al. (2014)
	R: AGCCTTGCAACCCATTTCCT				
30	F: CTTTAATTGCTTGCGCCCGT	60	170	cps30I	Kerdsin et al. (2014)
	R: ATTCGGGCTACCCATTGCAG				
31	F: GGAGTGCTCTATGCCACCTT	60	550	cps31L	Kerdsin et al. (2014)
	R: GCATTGCCCCTACAGCAAAC				
33	F: GAGTTGCGACCTATTATTCTCA	58	731	cps33K	Liu et al. (2013)
	R: GAATTGAACAACGACTGCAATA				

TABLE 2 Primers for identifying virulence genes of *S. suis*.

Gene	Sequence (5′-3′)	Annealing temperature (°C)	PCR product sizes (bp)	Reference
gdh	F: TTCTGCAGCGTATTCTGTCAAACG	55	695	Kerdsin et al. (2012)
	R: TGTTCCATGGACAGATAAAGATGG			
fbps	F: ATCGATTCATTTAAATAGGTTCCTGCTCGC	55	2,179	Ju et al. (2008)
	R: GGTACCATTGTTGGTATTTGGACACCAGAA			
sly	F: GCTTTATTGCGTGCTGAC	55	1,099	Ju et al. (2008)
	R: CTGTTCTCCACCACTCCC			
orf2	F: CAAGTGTATGTGGATGGG	56	858	Ju et al., 2008
	R: ATCCAGTTGACACGTGCA			
mrp	F: CAGATGTGGACCGTAGACC	58	316	Ju et al. (2008)
	R: GGATAATCACCAGCAGGAA			
89 k	F: TCGCCACTATGGTATCTGCTTA	56	720	Ju et al., 2008
	R: GATTGTGGACCATGCTCTTTAG			
gapdh	F: CAGTCAAAGCCCGCAACC	58	571	Pan et al. (2020)
	R: CCACCGAAGCCAAGAGGT			
epf	F: GCTACGACGGCCTCAGAAATC	55	626	Ju et al. (2008)
	R: TGGATCAACCACTGGTGTTAC			

Pigs in the SS2 and SS7 groups were intraperitoneally injected with 2 mL of 1.0×10^6 CFU of SS2-1 or SS7-1, respectively, while pigs in the control group were injected with an equal volume of sterile phosphate-buffered saline (PBS). Clinical signs and mortality were recorded daily for 14 days post-infection. Dead pigs were immediately necropsied to observe pathological changes, and lung tissues were collected for hematoxylin and eosin (H&E) staining analysis. All experiments were conducted in strict accordance with the Guidelines for the Care and Use of Laboratory Animals and were approved by the Ethics Committee of South China Agricultural University. At the end of the experiment, all surviving pigs were humanely euthanized by intravenous injection of an overdose of pentobarbital sodium following anesthesia to ensure animal welfare.

2.6 Data analysis

The analysis and mapping of *S. suis* infection rates, as well as serotype identification, were performed using Office 2021 software. Correlation analysis between serotypes and virulence genes of the isolated strains, along with the generation of related charts, was performed using the online tool https://www.chiplot.online/. The mortality rate analysis and chart creation for the animal experiments were conducted using GraphPad Prism 8 software.

3 Results

3.1 Detection and infection rate analysis of suspected *S. suis* clinical samples

To investigate the epidemiological characteristics of *S. suis* in major pig-farming regions of China, 1,428 suspected infection samples were collected from 89 pig farms across 12 provinces and tested using PCR. The distributions of the 12 provinces and the numbers of collected samples and positive test samples are shown in Figure 1.

The overall infection and isolation rates were 59.59% (851/1728) and 16.1% (137/851), respectively. The infection rates in different regions were as follows (Figure 2A): Guangdong: 72.41% (63/87); Jiangxi: 65.88% (56/85); Guangxi: 65.73% (94/143); Jiangsu: 64.71% (77/119); Shandong: 64.29% (63/98); Shaanxi: 63.92% (186/291);

FIGURE 1
Geographic distribution, sample size, and number of positive samples of suspected *Streptococcus suis* from pigs in 12 regions of China.

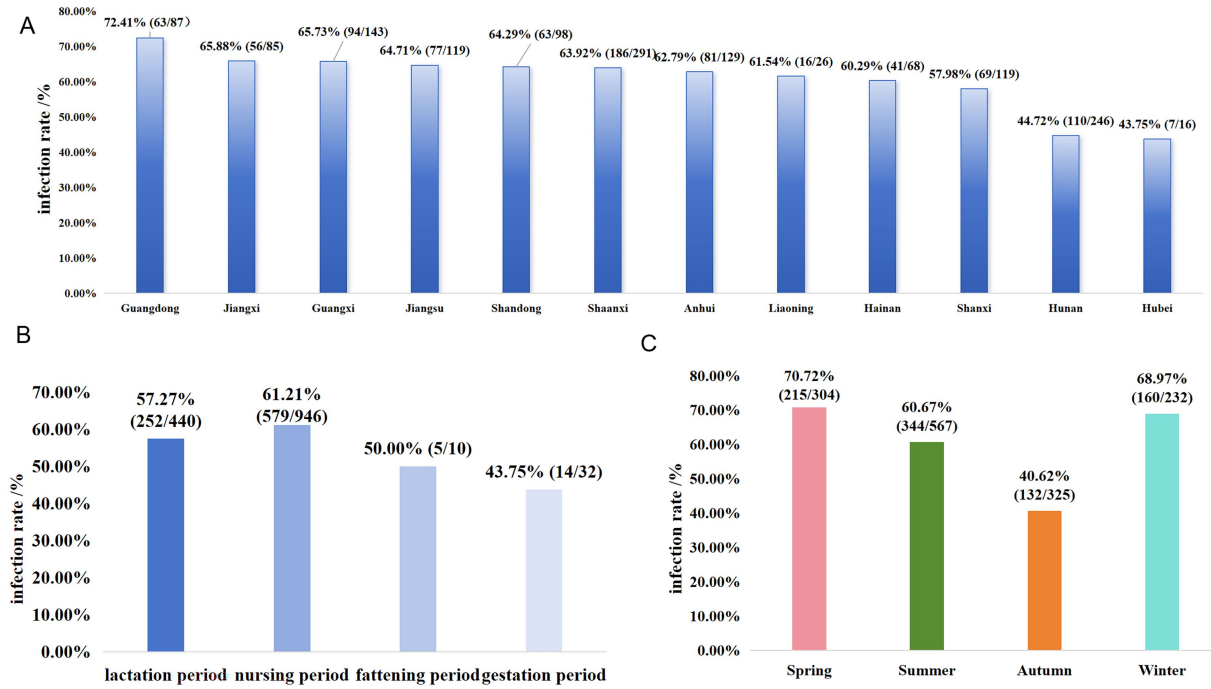

FIGURE 2
Prevalence of *S. suis* in different regions of China: **(A)** infection rates of *S. suis* in 12 regions of China; **(B)** distribution of *S. suis* infections across different growth stages of pigs; **(C)** seasonal variations in *S. suis* infection rates.

Anhui: 62.79% (81/129); Liaoning: 61.54% (16/26); Hainan: 60.29% (41/68); Shanxi: 57.98% (69/119); Hunan: 44.72% (110/246); and Hubei: 43.75% (7/16). Additionally, the infection rates in suckling piglets (aged 0–21 days), nursery pigs (aged 21–70 days), growing-finishing pigs (aged 70 days to 6 months, with weights of about 100–120 kilograms), and pregnant sows (sows in the gestation period) were 57.27% (252/440), 61.21% (579/946), 50% (5/10), and 43.75% (14/32), respectively (Figure 2B). Next, the prevalence of *S. suis* infections in spring, summer, autumn, and winter was examined. The infection rates in spring (February–April), summer (May–July), autumn (August–October), and winter (from November to January of the following year) were 70.72% (215/304), 60.67% (344/567), 40.62% (132/325), and 68.97% (160/232), respectively (Figure 2C).

3.2 Serotyping of *S. suis*

This study systematically analyzed the serotype distribution characteristics and regional differences of *S. suis* (Figure 3). In the eastern coastal provinces of China, there is a significant diversity of serotypes. In Guangdong, 9 serotypes, including serotypes 2, 5, 7, 8, 9, 16, and 33, and serotype NT were detected. In Jiangsu Province, 8 serotypes, including serotypes 2, 3, 4, 5, 7, 9, 18, and NT, were detected. In Zhejiang Province, 7 serotypes, including serotypes 2, 3, 4, 5, 7, 9, and serotype NT, were detected. The prevalence of Serotype 2 was high in Guangdong (11 cases), Guangxi (7 cases), and Anhui (6 cases). In contrast, 1–3 serotypes were detected in inland provinces, such as Hubei, Hunan, and Shaanxi. In Liaoning Province, only Serotype 1 (2 cases) was identified. This distribution pattern may be influenced by sample representation, geographic barriers, or ecological niche competition among dominant serotypes.

Further analysis of the 137 isolates revealed that Serotype 2 presented the highest occurrence rate ($n = 42$; 30.66%), followed by Serotype 7 ($n = 29$; 21.17%), Serotype 9 ($n = 15$; 10.95%), Serotype 1 ($n = 12$; 8.76%), Serotype NT ($n = 10$; 7.30%), Serotype 3 ($n = 9$; 6.57%), Serotype 4 ($n = 8$; 5.84%), and Serotype 5 ($n = 5$; 4.38%). serotypes 33 ($n = 2$; 1.46%), serotype 16 ($n = 2$; 1.46%), serotype 8 ($n = 1$; 1.46%), and serotype 8 ($n = 1$; 1.46%) (Figures 4A, B).

3.3 Detection of virulence genes in *S. suis*

This study analyzed the associations between eight virulence genes (*gdh*, *fbps*, *sly*, *orf2*, *mrp*, *89 k*, *gapdh*, and *epf*) and serotypes in 137 *S. suis* isolates. The occurrence rates of *gdh*, *fbps*, *sly*, *orf2*, *mrp*, *89 k*, *gapdh*, and *epf* were 100% (137/137), 63.5% (87/137), 55.47% (76/137), 98.54% (135/137), 100% (137/137), 2.92% (4/137), 94.89% (130/137), and 56.93% (78/137), respectively (Figure 5A). All 12 isolates of Serotype 1 harbored *mrp*. Additionally, the other tested genes, with the exception of *89 k*, were detected in all the Serotype 1 isolates. The isolates of Serotype 2 and NT harbored all the tested genes. However, for serotypes 2 and NT, the incidence rates of 89 k were 4.76% (95% CI: 13.2–15.79%) and 10% (95% CI: 17.9–40.42%), respectively. Serotypes 4 and 7 did not harbor *89 k* or *epf*. The occurrence rates of *gdh* and *orf2* in serotypes 4 and 7 were 100% and ≥ 87%, respectively. The occurrence rates of *epf* in serotypes 5 and 7 were 20% (95% CI: 36.2–62.45%) and 0% (95% CI: 0–11.7%), respectively. The frequency of occurrence of most virulence factors, except for *sly*, *89 k*, and *epf*, was high in Serotype 7, with that of *gdh*

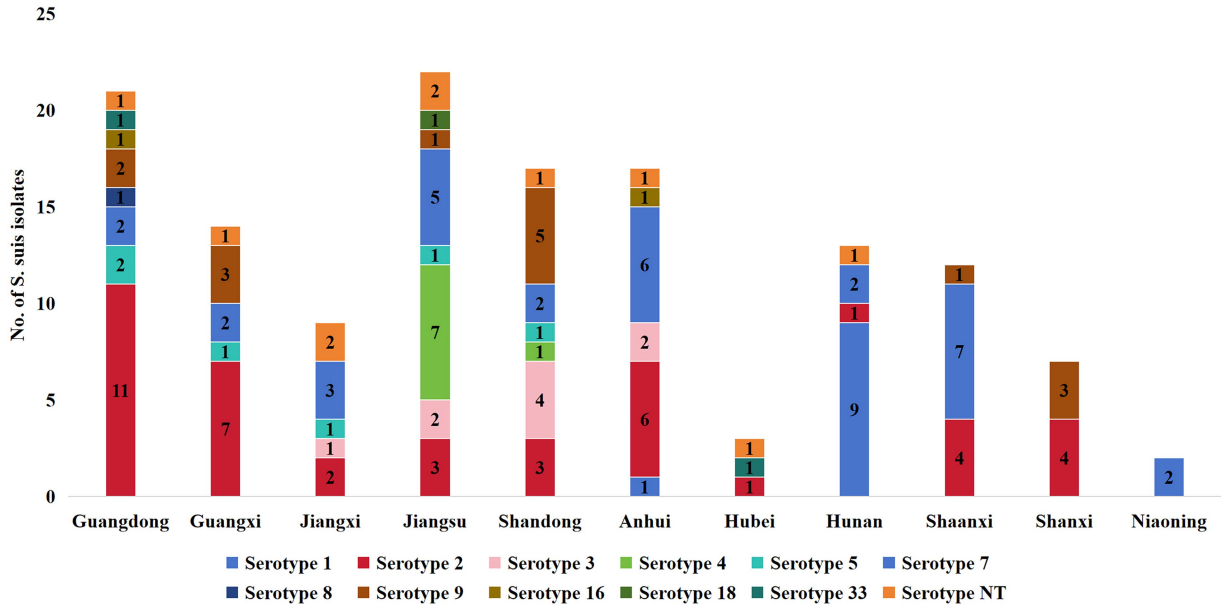

FIGURE 3
Serotype distribution characteristics of 137 *S. suis* isolates collected from 12 regions of China. NT indicates non-typeable strains.

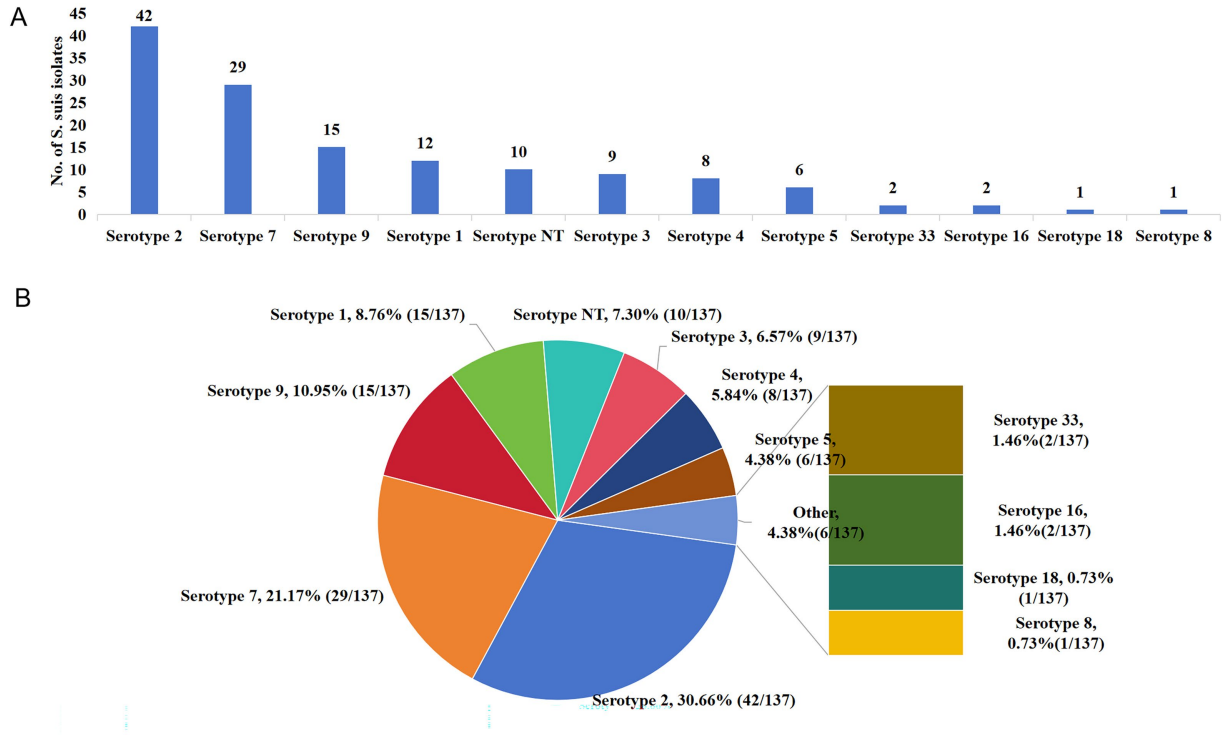

FIGURE 4
Serotype distribution patterns of 137 *S. suis* isolates. **(A)** Number of isolates corresponding to each serotype; **(B)** detailed breakdown of isolates by serotype.

and *orf2* reaching 100%. Serotype 9 did not harbor *89 k*. The occurrence rates of *sly*, *epf*, and *mrp* in Serotype 9 were ≤ 43.75%, with *epf* exhibiting a low occurrence rate (12.50, 95% CI: 35–36.02%). However, the occurrence rates of *gdh*, *fbps*, *gapdh*, and *orf2* in Serotype NT were in the range of 87.5–100%. Additionally, all Serotypes 8, 16, 18, and 33 harbored *fbps*, *orf2*, *mrp*, and *gapdh*. However, further validation is necessary, as the sample size for these isolates was small (< 3 isolates) (Figure 5B).

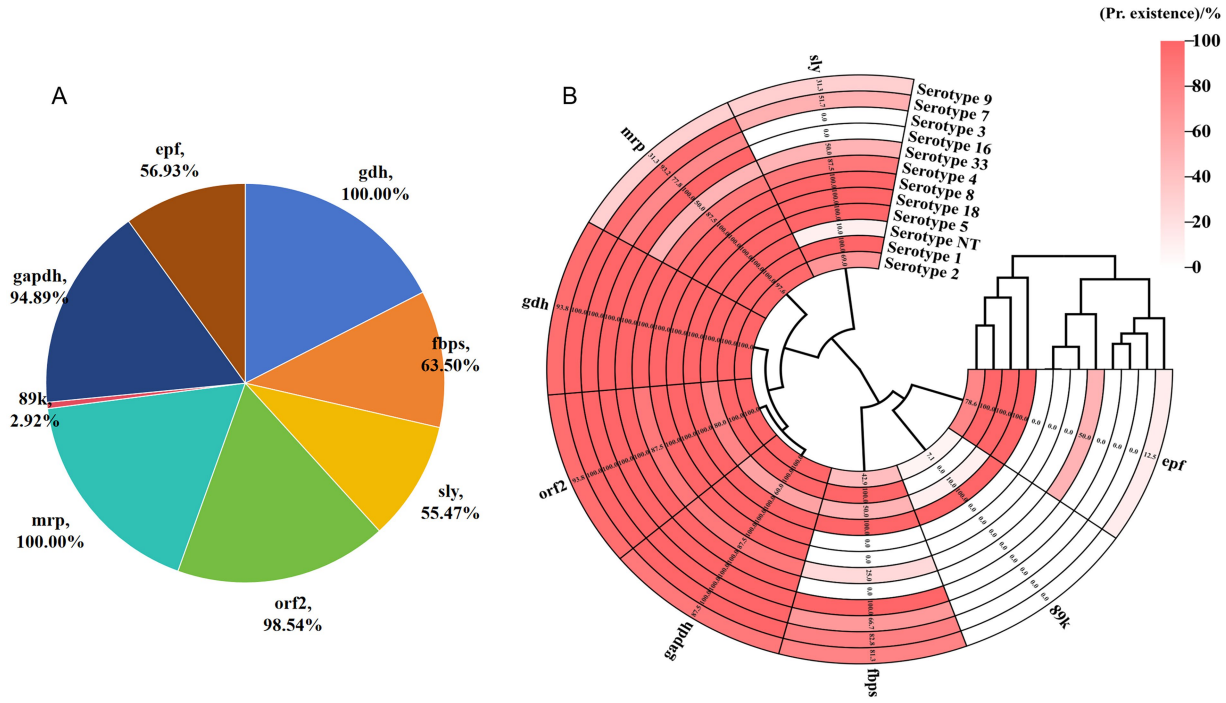

FIGURE 5
Relationships between serotypes and virulence genes in 137 *S. suis* isolates. **(A)** Positive counts of different virulence genes detected in the 137 isolates. **(B)** Heatmap showing the relationships between different serotypes and virulence genes among the isolates.

3.4 Animal experiment

To investigate the pathogenicity of the prevalent *S. suis* serotypes 2 and 7, strains SS2-1 and SS7-1 were selected for animal experimentation in 42-day-old, healthy Landrace pigs confirmed to be free of *S. suis* and other exogenous pathogens. The experimental results demonstrated that pigs in both the SS2-1 and SS7-1 challenge groups presented clinical signs such as lethargy, huddling, and a marked reduction or complete loss of appetite within 12 h post-infection (Figures 6D,G). Notably, all pigs in the SS2-1 group succumbed to acute infection by the fourth day, resulting in a mortality rate of 100% (8/8). In the SS7-1 group, no acute deaths occurred, but two pigs died on the 10th day, resulting in a mortality rate of 37.5% (3/8) (Figure 7). The surviving pigs were emaciated and exhibited slow growth, whereas no significant changes were detected in the control group (Figure 6A).

Necropsy was performed on pigs that died after infection. The results revealed the following: In the SS2-1 group, the deceased pigs exhibited typical acute fibrinous myocarditis, with yellow-brown flocculent exudates accumulating in the pericardial cavity (Figure 6E). The lungs exhibited diffuse congestion and edema, characterized by dark red congested areas along the margins of the lung lobes (Figure 6F). In the SS7-1 group, the pathological changes in the deceased pigs were similar to those observed in the SS2-1 group but were comparatively less severe. The principal findings included surface cardiac hemorrhage and enlargement, myocardial hemorrhage, and mild fibrinous myocarditis (Figure 6H). The lungs were enlarged and hemorrhagic, and a small quantity of serous or mildly fibrinous exudate was present within the thoracic cavity (Figure 6I). In contrast, no significant pathological alterations were observed in the control group during necropsy (Figures 6B,C).

Histopathological examination revealed that in both the SS2-1 and SS7-1 groups, myocardial cells exhibited disorganization, increased infiltration of inflammatory cells, interstitial edema, and erythrocyte exudation (Figures 8B,C). The alveolar structures were either disrupted or altered, with eosinophilic exudates and scattered erythrocyte leakage present within the alveolar cavities. Hemorrhage and enlargement were also prominent in the lung interstitium (Figures 8E,F). In contrast, no significant pathological alterations were observed in the control group (Figures 8A,D).

4 Discussion

S. suis is one of the most threatening bacterial infectious diseases in the global pig farming industry. Its typical clinical symptoms include purulent meningitis, septicemia, and polyarthritis, which impose substantial economic burdens on global swine production systems annually (Dutkiewicz et al., 2018). Epidemiological investigations have shown that in several regions, including Europe, North America, and Australia, the infection rate of *Streptococcus suis* has exceeded 90%. In China, the carrier rate of this pathogen on large-scale pig farms reportedly exceeds 40% (Segura et al., 2020). This phenomenon not only poses a serious threat to the health of pigs but also has a significant impact on the global agricultural economy. This study, which is based on cross-regional epidemiological surveys, revealed that the overall detection rate of *S. suis* in large-scale pig farms across 12 provinces in China reached 59.59%, which is markedly higher than the previously reported prevalence of 40.8% (Liu et al.,

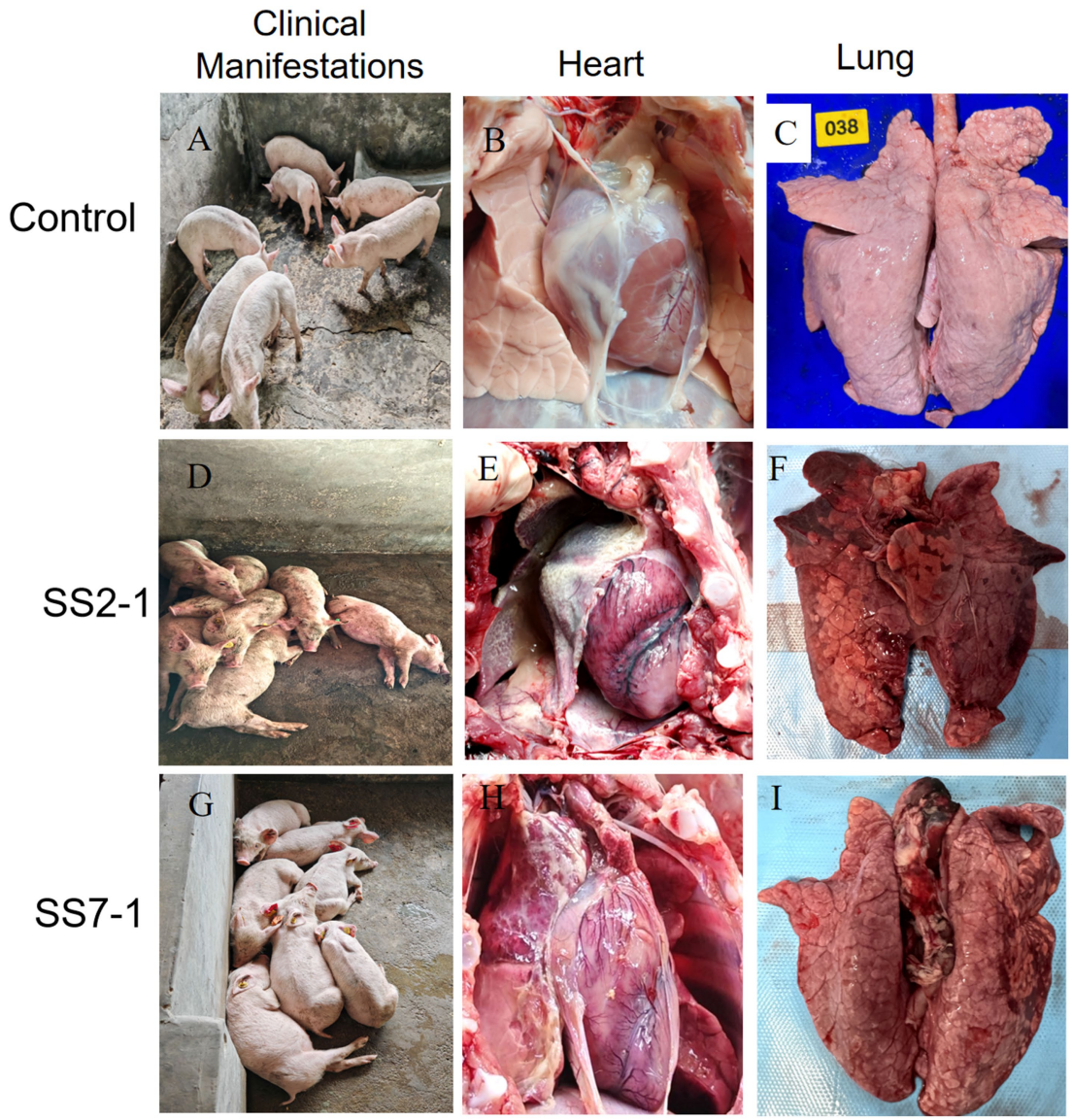

FIGURE 6
Clinical manifestations and post-mortem lesions in 42-day-old Landrace pigs after artificial infection. **(A–C)** Show the clinical status, heart, and lung lesions of pigs in the control group; **(D–F)** depict the clinical status, heart, and lung lesions in the SS2-challenged group; **(G–I)** illustrate the clinical status, heart, and lung lesions in the SS7-challenged group.

2023). Importantly, the findings also revealed the pathogen's full-cycle infection capability, with positive cases identified across all age groups of pigs, underscoring its persistent and pervasive threat within pig farming systems. The infection rates in suckling piglets (<21 days old) and nursery pigs (21–70 days old) were 57.4 and 61.21%, respectively, which is consistent with previous reports (Correa-Fiz et al., 2020). Previous studies have indicated that *S. suis* infections can occur year-round, with higher isolation rates observed during summer months, likely due to increased humidity during this season (Zhang et al., 2019). However, this study revealed that infection rates were significantly higher in winter and spring than in summer and autumn, a finding that may be associated with regional factors.

In recent years, Chinese researchers have identified several novel variants, including serotypes 21/29, NCL21-NCL26, and Chz, expanding the known diversity of *S. suis* and underscoring the evolving complexity of its epidemiological landscape (Huang et al., 2019; Pan et al., 2015). Although the prevalence of *S. suis* serotypes and genotypes varies across geographic regions and time periods, serotype 2 remains one of the most prevalent serotypes globally. Moreover, the distribution of *S. suis* serotypes shows significant regional differences: In Spain, serotypes 2 (21.7%), 1 (21.3%), and 9 (19.3%) dominate (Petrocchi-Rilo et al., 2021), whereas in North America, serotypes 2 (24.3%) and 3 (21%) prevail. In Asia, serotype 2 accounts for the highest proportion (44.2%), with a detection rate of 34.08% in Jiangxi Province, China, whereas serotypes 3 and 4 account for 12.4 and 5.6%, respectively (Tan et al., 2021). Similarly, this investigation revealed that the distribution of *S. suis* serotypes in China displays pronounced regional characteristics. For example, multiple serotypes were found to coexist within individual regions along the eastern coast, such as Guangdong, Jiangsu, and Shandong.

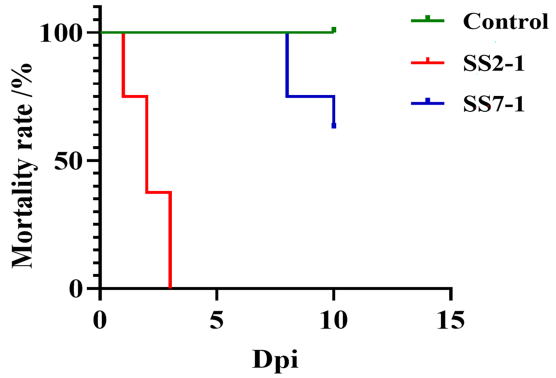

FIGURE 7
Survival curves of 42-day-old Landrace pigs after artificial infection with *S. suis*. The survival rates for the SS-2 and SS-7 challenge groups were 0 and 71.42%, respectively, whereas no deaths occurred in the control group.

Notably, serotype NT was highly prevalent in Anhui, Guangxi, and Guangdong, accounting for 65.5% of all NT isolates—a pattern seldom reported in the literature. On a global scale, the predominant *S. suis* serotypes isolated from clinical pigs, in descending order of frequency, are serotypes 2, 9, 3, 1/2, and 7, with about 15% classified as NT (Goyette-Desjardins et al., 2014). In this study, serotypes NT and 2 were dominant, followed by serotype 7, which is partially consistent with global trends. However, the higher proportion of NT (21.01%) suggests that regional characteristics or differences in detection methods may influence serotype distribution patterns. The lungs serve as the core infection site (33.33–100%), with serotypes 2, 7, 9, and NT exhibiting multiorgan invasion capabilities, indicating strong tissue invasiveness, which exacerbates disease complexity and control challenges.

The virulence of *S. suis* is closely associated with its serotypes, with notable variations in virulence factors across different serotypes. To date, over 100 virulence-associated components have been identified, including hemolysins, adhesins, and proteases, which collectively contribute to the pathogen's differential pathogenicity (Roodsant et al., 2021). Among these proteins, hemolysin *sly* (57 kDa) is recognized as a pivotal virulence factor capable of disrupting the blood–brain barrier, inhibiting complement-mediated bactericidal activity, and triggering robust inflammatory responses (Lin et al., 2019). Among the serotype 2 strains, *sly*-positive isolates were significantly correlated with increased pathogenic potential. Yin et al. (2016) reported the *89 k* pathogenicity island in serotype 2 *S. suis*, a genomic element strongly linked to severe outbreaks in Jiangsu and Sichuan and regarded as a major determinant of virulence. However, in the present study, the detection rate of the *89 k* pathogenicity island in serotype 2 strains was only 7.14% (2/28), and intriguingly, the gene was also detected in serotype 16 and NT strains, suggesting a broader distribution and variability than previous*ly* reported.

mrp, *epf*, *fbps*, and *sly* are recognized as key pathogenic marker genes of *S. suis* serotype 2 (Dong et al., 2015). Previous reports have indicated the universal presence of the *sly* gene across isolates, whereas the carriage rates of *mrp* and *epf* were notably lower, at 33 and 4%, respectively, which contrasts markedly with those of clinical isolates from North America and Europe, where the carriage rates of *mrp* and *epf* can reach 92 and 31%, respectively (Fittipaldi et al., 2009; Kim et al., 2010). In the present study, however, the carriage rates of *sly*, *mrp*, and *epf* in serotype 2 isolates were 92.85% (26/28), 96.43% (27/28), and 78.57% (22/28), respectively—levels comparable to those reported for clinical isolates from North America and Europe. Additionally, the *mrp* gene was highly prevalent in serotypes 1, 3, 4, 5, 7, 8, 9, 16, 18, 33, and NT, indicating that *mrp* might be a key virulence factor of porcine-derived *S. suis*.

The *gdh* gene of *S. suis* is a specific protein that can serve as a marker antigen for detection. About 305 porcine serum samples were found to have a *gdh* seropositivity rate of 73.1%, suggesting its potential application in diagnosing *S. suis* infections (Xia et al., 2017). This study further confirmed this finding: among 137 *S. suis* isolates, the carriage rate of the *gdh* gene was 96.35% (132/137). Except for serotype NT, where the carriage rate was 82.76%, all other serotypes carried the *gdh* gene at 100%. These findings indicate that the *gdh* gene is also a key virulence factor of porcine-derived *S. suis*, and studies on *gdh* gene deletion provide important insights for vaccine development.

gapdh is an important virulence factor closely linked to the bacterial adhesion process. Studies have demonstrated that deletion of the *gapdh* gene significantly impairs the ability of bacteria to adhere to host cells (Brassard et al., 2004). Research further indicates that the *gapdh* gene is widely distributed among various streptococcal species, including serotypes 2, 7, and 9 of *S. suis*. Only a few nonpathogenic strains lack this gene, underscoring its universality and importance (Wang et al., 2021). This study also supports this view, with the carriage rate of the *gapdh* gene being 89.78% (123/137). Serotypes 1, 2, 3, 7, 8, 16, 18, and 33 carried it at 100%, whereas serotypes 4, 5, 9, and NT had carriage rates as high as 87.5%. Thus, regardless of whether the strain is low or highly virulent, this gene is universally present. The *orf2* gene is closely related to the virulence of *Streptococcus suis*, and it is present in at least 78.3% of *Streptococcus suis* isolates (Zhao et al., 2025). This study revealed that the carriage rate of *orf2* in 137 isolates was as high as 93%, and *orf2* is widely present in different serotypes, suggesting its universality. However, its function and impact on virulence need to be comprehensively evaluated in combination with other factors.

Currently, limited research has been conducted on the pathogenicity of *S. suis* serotypes 2 and 7 in pigs, with the majority of existing studies being based on mouse models. Evidence indicates that serotype 2 is the most virulent and is capable of inducing acute mortality in pigs through septicemia and polyserositis (Lun et al., 2007). The present study corroborates this finding, which may be attributed to the high-frequency carriage of key virulence genes, including *gdh*, *fbps*, *sly*, *orf2*, *mrp*, and *gapdh*. In challenge experiments with serotype 7 in 42-day-old Landrace pigs, although no acute deaths were observed, two pigs died on the 10th day post-infection, both of which presented with leg arthritis and typical polyserositis lesions. This result is consistent with the experimental findings of Boetner AG et al., who used serotype 7 to infect 7-day-old piglets, indicating that serotype 7 has some pathogenicity in piglets of this age group (Boetner et al., 1987). Additionally, 42-day-old Landrace pigs infected with serotypes 2 and 7 presented obvious pneumonia and myocarditis symptoms, suggesting that the lungs and heart may be the primary target organs of these two serotypes.

In summary, this study revealed that the overall infection rate is markedly higher than previous*ly* reported, with pigs of all age groups demonstrating susceptibility and no evident seasonal

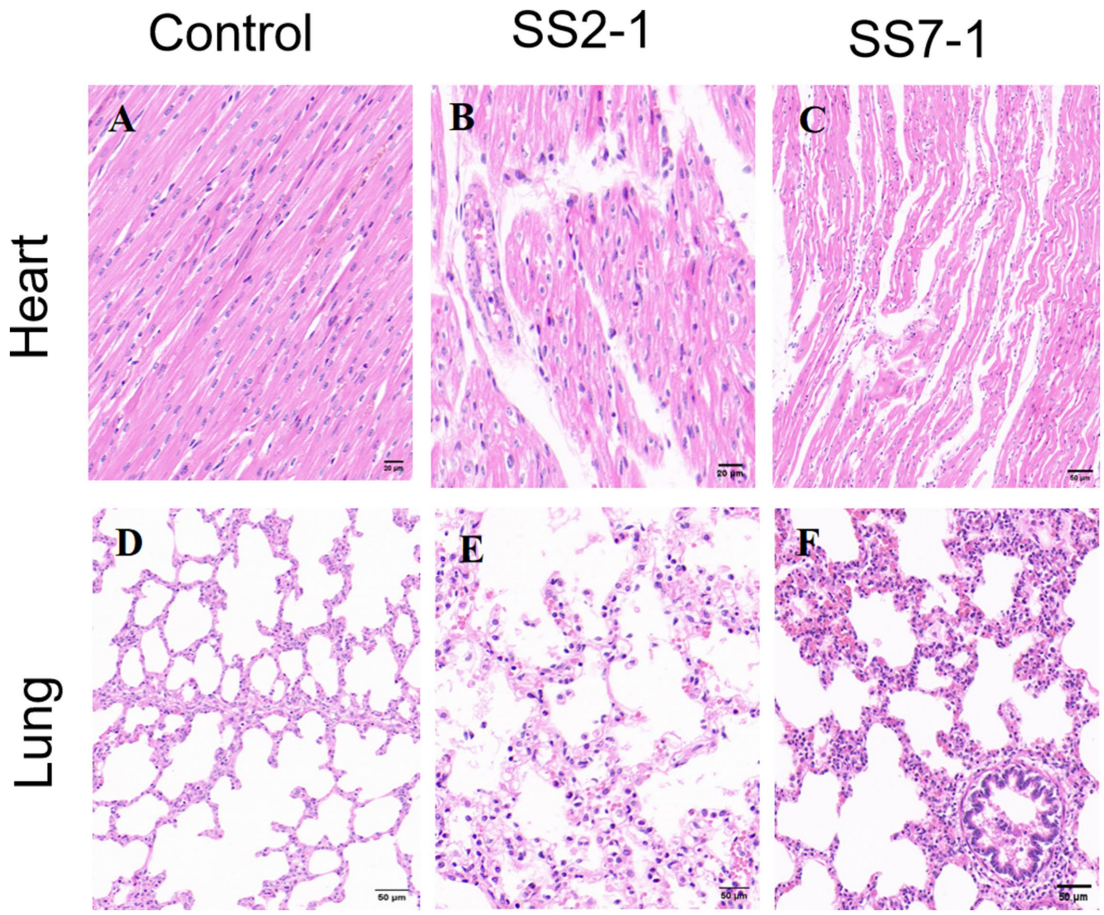

FIGURE 8
Histopathological changes in the heart and lungs of 42-day-old Landrace pigs after artificial infection. **(A–C)** Represent histopathological changes in the lungs of the control group, SS2-challenged group, and SS7-challenged group, respectively; **(D–F)** show histopathological changes in the hearts of the control group, SS2-challenged group, and SS7-challenged group, respectively.

variation. Serotypes NT and 2 emerged as the predominant strains, followed by serotype 7. While this distribution trend is partially consistent with global patterns, the elevated prevalence of serotype NT indicates that regional factors or methodological differences in detection may contribute to variations in serotype distribution. Notably, the carriage rates of virulence genes varied significantly across serotypes, with *gdh*, *fbps*, *sly*, *orf2*, *mrp*, and *gapdh* being widely detected, whereas *89 k* and *epf* were found at lower frequencies. Moreover, both serotypes 2 and 7 can cause clinical symptoms similar to those of *S. suis* disease, but serotype 2 is significantly more pathogenic than serotype 7. The absence of antimicrobial resistance profiling for the collected *S. suis* isolates constitutes a limitation of this work. Subsequent research is planned to explore this area comprehensively.

5 Conclusion

In this study, we investigated the prevalence of *S. suis* in 89 large-scale pig farms in 12 provinces in the western region of China and analyzed the serotypes and presence of virulence genes of the isolates as well as the pathogenicity of serotypes 2 and 7. The results of this study provide important baseline information on the serotype characteristics and virulence genes of *S. suis* and the pathogenicity of epidemic strains in China, which is highly important for understanding its epidemiological characteristics and the development of vaccines used to prevent *Streptococcus suis* infection in pigs.

Data availability statement

The original contributions presented in the study are included in the article/supplementary material, further inquiries can be directed to the corresponding author.

Ethics statement

The animal studies were approved by Animal infection experiments were conducted according to the Guidelines for Experimental Animals established by the Ministry of Science and Technology of China (Beijing) and were supervised and approved by the National Animal Ethics and Use Committee. The study was approved by the South China Agricultural University

(Approval No.: SYXK-2019–0136). The studies were conducted in accordance with the local legislation and institutional requirements. Written informed consent was obtained from the owners for the participation of their animals in this study.

Author contributions

DY: Conceptualization, Data curation, Formal analysis, Investigation, Methodology, Software, Validation, Visualization, Writing – original draft, Writing – review & editing. JX: Conceptualization, Data curation, Formal analysis, Investigation, Methodology, Software, Visualization, Writing – original draft, Writing – review & editing, Validation. MH: Investigation, Methodology, Validation, Writing – original draft, Writing – review & editing. JZ: Investigation, Validation, Writing – original draft, Writing – review & editing. BR: Resources, Supervision, Writing – original draft, Writing – review & editing. XH: Resources, Supervision, Writing – original draft, Writing – review & editing. LW: Funding acquisition, Investigation, Project administration, Resources, Supervision, Validation, Writing – original draft, Writing – review & editing.

Funding

The author(s) declare that financial support was received for the research and/or publication of this article. The research was funded by the Yunfu Innovation Team Project (CYRC202301).

Conflict of interest

DY, JX, MH, BR, and LW were employed by Guangdong Enterprise Key Laboratory for Animal Health and Environmental Control, Wen's Foodstuff Group Co. Ltd.

The remaining authors declare that the research was conducted in the absence of any commercial or financial relationships that could be construed as a potential conflict of interest.

Generative AI statement

The authors declare that no Gen AI was used in the creation of this manuscript.

Any alternative text (alt text) provided alongside figures in this article has been generated by Frontiers with the support of artificial intelligence and reasonable efforts have been made to ensure accuracy, including review by the authors wherever possible. If you identify any issues, please contact us.

Publisher's note

References

Bamphensin, N., Chopjitt, P., Hatrongjit, R., Boueroy, P., Fittipaldi, N., Gottschalk, M., et al. (2021). Non-penicillin-susceptible *streptococcus suis* isolated from humans. *Pathogens.* 10:1178. doi: 10.3390/pathogens10091178

Boetner, A. G., Binder, M., and Bille-Hansen, V. (1987). *Streptococcus suis* infections in Danish pigs and experimental infection with *Streptococcus suis* serotype 7. *Acta Pathol. Microbiol. Immunol. Scand. B* 95, 233–239. doi: 10.1111/j.1699-0463.1987.tb03118.x

Brassard, J., Gottschalk, M., and Quessy, S. (2004). Cloning and purification of the *streptococcus suis* serotype 2 glyceraldehyde-3-phosphate dehydrogenase and its involvement as an adhesin. *Vet. Microbiol.* 102, 87–94. doi: 10.1016/j.vetmic.2004.05.008

Correa-Fiz, F., Neila-Ibanez, C., Lopez-Soria, S., Napp, S., Martinez, B., Sobrevia, L., et al. (2020). Feed additives for the control of post-weaning *streptococcus suis* disease and the effect on the faecal and nasal microbiota. *Sci. Rep.* 10:20354. doi: 10.1038/s41598-020-77313-6

Devriese, L. A., and Haesebrouck, F. (1992). *Streptococcus suis* infections in horses and cats. *Vet. Rec.* 130:380. doi: 10.1136/vr.130.17.380

Dong, W., Ma, J., Zhu, Y., Zhu, J., Yuan, L., Wang, Y., et al. (2015). Virulence genotyping and population analysis of *streptococcus suis* serotype 2 isolates from China. *Infect. Genet. Evol.* 36, 483–489. doi: 10.1016/j.meegid.2015.08.021

Dutkiewicz, J., Zajac, V., Sroka, J., Wasinski, B., Cisak, E., Sawczyn, A., et al. (2018). *Streptococcus suis: a re-emerging pathogen associated with occupational exposure to pigs or pork products. Part ii - pathogenesis. Ann. Agr. Env. Med.* 25, 186–203. doi: 10.26444/aaem/85651

Fittipaldi, N., Fuller, T. E., Teel, J. F., Wilson, T. L., Wolfram, T. J., Lowery, D. E., et al. (2009). Serotype distribution and production of muramidase-released protein, extracellular factor and suilysin by field strains of *streptococcus suis* isolated in the United States. *Vet. Microbiol.* 139, 310–317. doi: 10.1016/j.vetmic.2009.06.024

Gottschalk, M., Lebrun, A., Wisselink, H., Dubreuil, J. D., Smith, H., and Vecht, U. (1998). Production of virulence-related proteins by Canadian strains of *Streptococcus suis* capsular type 2. *Can. J. Vet. Res.* 62, 75–79

Goyette-Desjardins, G., Auger, J. P., Xu, J., Segura, M., and Gottschalk, M. (2014). *Streptococcus suis*, an important pig pathogen and emerging zoonotic agent-an update on the worldwide distribution based on serotyping and sequence typing. *Emerg. Microbes Infect.* 3:e45. doi: 10.1038/emi.2014.45

Haas, B., and Grenier, D. (2018). Understanding the virulence of *streptococcus suis*: a veterinary, medical, and economic challenge. *Med. Mal. Infect.* 48, 159–166. doi: 10.1016/j.medmal.2017.10.001

Huang, J., Liu, X., Chen, H., Chen, L., Gao, X., Pan, Z., et al. (2019). Identification of six novel capsular polysaccharide loci (ncl) from *streptococcus suis* multidrug resistant non-typeable strains and the pathogenic characteristic of strains carrying new ncls. *Transbound. Emerg. Dis.* 66, 995–1003. doi: 10.1111/tbed.13123

Ju, A., Wang, C., Zheng, F., Pan, X., Dong, Y., Ge, J., et al. (2008). Study on molecular epidemiology of major pathgenic *Streptococcus suis* serotypes in middle part of Jiangsu province. *Chin. Epidemiol.* 29, 151–154.

Kerdsin, A., Akeda, Y., Hatrongjit, R., Detchawna, U., Sekizaki, T., Hamada, S., et al. (2014). Streptococcus suis serotyping by a new multiplex pcr. *J. Med. Microbiol.* 63:824–830. doi: 10.1099/jmm.0.069757-0

Kerdsin, A., Dejsirilert, S., Akeda, Y., Sekizaki, T., Hamada, S., Gottschalk, M., et al. (2012). Fifteen streptococcus suis serotypes identified by multiplex pcr. *J. Med. Microbiol.* 61:1669–1672. doi: 10.1099/jmm.0.048587-0

Kim, D., Han, K., Oh, Y., Kim, C. H., Kang, I., Lee, J., et al. (2010). Distribution of capsular serotypes and virulence markers of *streptococcus suis* isolated from pigs with polyserositis in Korea. *Can. J. Vet. Res.* 74, 314–316.

King, S. J., Heath, P. J., Luque, I., Tarradas, C., Dowson, C. G., and Whatmore, A. M. (2001). Distribution and genetic diversity of suilysin in *streptococcus suis* isolated from different diseases of pigs and characterization of the genetic basis of suilysin absence. *Infect. Immun.* 69, 7572–7582. doi: 10.1128/IAI.69.12.7572-7582.2001

Lin, L., Xu, L., Lv, W., Han, L., Xiang, Y., Fu, L., et al. (2019). An nlrp3 inflammasome-triggered cytokine storm contributes to streptococcal toxic shock-like syndrome (stsls). *PLoS Pathog.* 15:e1007795. doi: 10.1371/journal.ppat.1007795

Liu, P., Zhang, Y., Tang, H., Wang, Y., and Sun, X. (2023). Prevalence of *streptococcus suis* in pigs in China during 2000-2021: a systematic review and meta-analysis. *One Health.* 16:100513. doi: 10.1016/j.onehlt.2023.100513

Liu, Z., Zheng, H., Gottschalk, M., Bai, X., Lan, R., Ji, S., et al. (2013). Development of multiplex pcr assays for the identification of the 33 serotypes of *streptococcus suis*. *PLoS One* 8:e72070. doi: 10.1371/journal.pone.0072070

Lun, Z. R., Wang, Q. P., Chen, X. G., Li, A. X., and Zhu, X. Q. (2007). *Streptococcus suis*: an emerging zoonotic pathogen. *Lancet Infect. Dis.* 7, 201–209. doi: 10.1016/S1473-3099(07)70001-4

Luque, I., Tarradas, C., Arenas, A., Maldonado, A., Astorga, R., and Perea, A. (1998). *Streptococcus suis* serotypes associated with different disease conditions in pigs. *Vet. Rec.* 142, 726–727. doi: 10.1136/vr.142.26.726

Mi, K., Li, M., Sun, L., Hou, Y., Zhou, K., Hao, H., et al. (2021). Determination of susceptibility breakpoint for cefquinome against *streptococcus suis* in pigs. *Antibiotics-Basel.* 10:958. doi: 10.3390/antibiotics10080958

Nomoto, R., Maruyama, F., Ishida, S., Tohya, M., Sekizaki, T., and Osawa, R. (2015). Reappraisal of the taxonomy of *streptococcus suis* serotypes 20, 22 and 26: *streptococcus parasuis* sp. nov. *Int. J. Syst. Evol. Microbiol.* 65, 438–443. doi: 10.1099/ijs.0.067116-0

Pan, Z., Ma, J., Dong, W., Song, W., Wang, K., Lu, C., et al. (2015). Novel variant serotype of *streptococcus suis* isolated from piglets with meningitis. *Appl. Environ. Microbiol.* 81, 976–985. doi: 10.1128/AEM.02962-14

Pan, J., Zhang, H., Hen, B., Zhou, M., Wang, Z., and Xu, G. (2020). Isolation, identification and pathogenicity of *Streptococcus suis* type 2. *China J. Vet. Drug.* 54, 14–19. doi: 10.11751/ISSN.1002-1280.2020.08.03

Petrocchi-Rilo, M., Martinez-Martinez, S., Aguaron-Turrientes, A., Roca-Martinez, E., Garcia-Iglesias, M. J., Perez-Fernandez, E., et al. (2021). Anatomical site, typing, virulence gene profiling, antimicrobial susceptibility and resistance genes of *streptococcus suis* isolates recovered from pigs in Spain. *Antibiotics-Basel.* 10:707. doi: 10.3390/antibiotics10060707

Roodsant, T. J., Van Der Putten, B., Tamminga, S. M., Schultsz, C., and Van Der Ark, K. (2021). Identification of *streptococcus suis* putative zoonotic virulence factors: a systematic review and genomic meta-analysis. *Virulence* 12, 2787–2797. doi: 10.1080/21505594.2021.1985760

Salasia, S. I., Lammler, C., and Devriese, L. A. (1994). Serotypes and putative virulence markers of *streptococcus suis* isolates from cats and dogs. *Res. Vet. Sci.* 57, 259–261. doi: 10.1016/0034-5288(94)90070-1

Silva, L. M., Baums, C. G., Rehm, T., Wisselink, H. J., Goethe, R., and Valentin-Weigand, P. (2006). Virulence-associated gene profiling of *streptococcus suis* isolates by PCR. *Vet. Microbiol.* 115, 117–127. doi: 10.1016/j.vetmic.2005.12.013

Segura, M., Aragon, V., Brockmeier, S. L., Gebhart, C., Greeff, A., Kerdsin, A., et al. (2020). *Update on streptococcus suis research and prevention in the era of antimicrobial restriction: 4th international workshop on s. Suis. Pathogens.* 9. doi: 10.3390/pathogens9050374

Smith, H. E., Veenbergen, V., van der Velde, J., Damman, M., Wisselink, H. J., and Smits, M. A. (1999). *The cps genes of streptococcus suis serotypes 1, 2, and 9: development of rapid serotype-specific pcr assays. J. Clin. Microbiol.* 37, 3146–3152. doi: 10.1128/JCM.37.10.3146-3152.1999

Tan, M. F., Tan, J., Zeng, Y. B., Li, H. Q., Yang, Q., and Zhou, R. (2021). Antimicrobial resistance phenotypes and genotypes of *streptococcus suis* isolated from clinically healthy pigs from 2017 to 2019 in Jiangxi province, China. *J. Appl. Microbiol.* 130, 797–806. doi: 10.1111/jam.14831

Vecht, U., Wisselink, H. J., van Dijk, J. E., and Smith, H. E. (1992). Virulence of *streptococcus suis* type 2 strains in newborn germfree pigs depends on phenotype. *Infect. Immun.* 60, 550–556. doi: 10.1128/iai.60.2.550-556.1992

Wang, Z., Guo, M., Kong, L., Gao, Y., Ma, J., Cheng, Y., et al. (2021). Tlr4 agonist combined with trivalent protein joints of *streptococcus suis* provides immunological protection in animals. *Vaccine* 9:958. doi: 10.3390/vaccines9020184

Wisselink, H. J., Reek, F. H., Vecht, U., Stockhofe-Zurwieden, N., Smits, M. A., and Smith, H. E. (1999). Detection of virulent strains of *streptococcus suis* type 2 and highly virulent strains of *streptococcus suis* type 1 in tonsillar specimens of pigs by PCR. *Vet. Microbiol.* 67, 143–157. doi: 10.1016/s0378-1135(99)00036-x

Wisselink, H. J., Smith, H. E., Stockhofe-Zurwieden, N., Peperkamp, K., and Vecht, U. (2000). Distribution of capsular types and production of muramidase-released protein (mrp) and extracellular factor (ef) of *streptococcus suis* strains isolated from diseased pigs in seven european countries. *Vet. Microbiol.* 74, 237–248. doi: 10.1016/s0378-1135(00)00188-7

Xia, X. J., Wang, L., Shen, Z. Q., Qin, W., Hu, J., Jiang, S. J., et al. (2017). Development of an indirect dot-ppa-elisa using glutamate dehydrogenase as a diagnostic antigen for the rapid and specific detection of streptococcus suis and its application to clinical specimens. *Antonie Van Leeuwenhoek* 110, 585–592. doi: 10.1007/s10482-016-0825-z

Yin, S., Li, M., Rao, X., Yao, X., Zhong, Q., Wang, M., et al. (2016). Subtilisin-like protease-1 secreted through type iv secretion system contributes to high virulence of *streptococcus suis* 2. *Sci. Rep.* 6:27369. doi: 10.1038/srep27369

Zhang, B., Ku, X., Yu, X., Sun, Q., Wu, H., Chen, F., et al. (2019). Prevalence and antimicrobial susceptibilities of bacterial pathogens in chinese pig farms from 2013 to 2017. *Sci. Rep.* 9:9908. doi: 10.1038/s41598-019-45482-8

Zhao, X., Han, S., Zhang, F., Cui, L., Ji, G., Wang, S., et al. (2025). Identification and characterization of *streptococcus suis* strains isolated from eastern China swine farms, 2021-2023. *Sci. Rep.* 15:5677. doi: 10.1038/s41598-025-90308-5

Frontiers in Microbiology

Explores the habitable world and the potential of microbial life

The largest and most cited microbiology journal which advances our understanding of the role microbes play in addressing global challenges such as healthcare, food security, and climate change.

Discover the latest Research Topics

See more →

Frontiers

Avenue du Tribunal-Fédéral 34
1005 Lausanne, Switzerland
frontiersin.org

Contact us

+41 (0)21 510 17 00
frontiersin.org/about/contact